A PETROLOGICAL INVESTIGATION OF THE RUSTENBURG LAYERED SUITE AND ASSOCIATED MINERALIZATION SOUTH OF POTGIETERSRUS

by

LARRY JOHN HULBERT

Submitted in partial fulfilment of the requirements
for the degree of
DOCTOR OF SCIENCE
in the Faculty of Science,
University of Pretoria.

JANUARY 1983

Dedicated

to

Dr. Geoff Parslow

ABSTRACT

A sequence of 3250 m of the Rustenburg Layered Suite and its associated mineralization south of Potgietersrus was investigated. Four episodes of faulting have deformed the area. This resulted in very early differentiates, not seen elsewhere in the Bushveld Complex, to outcrop together with economic concentrations of the best metallurgical grade chromite presently being mined in the Republic.

The Mg:Fe:Ca ratio of the Ca-poor pyroxenes varies from 89,5:8,8:1,6 in the lower zone to 44,2:52,3:3,37 in the upper zone. The latter composition demarcates the Fe-rich end of the two pyroxene limit. Textural evidence implies that there is a peritectic reaction between the iron-rich Ca-poor pyroxene and the melt and that this may account for the termination of the two pyroxene field. A significantly higher mean $K_D^{opx\text{-}cpx}{}_{Mg\text{-}Fe}{}_T$ for the study area (0,822) than for the other sectors of the Bushveld Complex (0,782) suggests that the pyroxenes of similar composition crystallized at higher temperatures in the Potgietersrus limb. Examination of the Al:Si ratio in Ca-rich pyroxenes from a variety of magmatic environments confirms that this variable can be used to monitor relative changes in the $a_{SiO_2}^{melt}$. Chemical data of the Ca-rich pyroxenes suggest that this phase defines an Fe enrichment - Ca depletion trend during differentiation unlike that for most other tholeiitic intrusions.

The V_2O_5 content of the main magnetitite layer and the Cr_2O_3 and the $Cr/Fe^{2+}+Fe^{3+}$ values in the upper and lower chromitite layers in the study area are the highest encountered in the Bushveld Complex. Textural evidence in these layers show that they have been up-graded to dense monomineralic layers by postcumulus sintering.

Calculated intensive parameters for the Potgietersrus magma suggest that it crystallized over a temperature interval from 1276°C in the lower zone to 1022°C in the basal portion of the upper zone. Oxygen fugacity conditions for the lower zone ranged from $10^{-6,21}$ to $10^{-4,98}$ atm whereas lower values of 10^{-11} to 10^{-9} atm were operative in the upper zone.

The study area contains abundant concentrations of sulfides at several levels in the sequence. The separation of the sulfide liquid is related in most cases to new influxes of metal-rich magma and mixing with the residual magma in the chamber. Several definite sulfide facies occur in the layered sequence.

Sulfur isotope investigations indicate that all the sulfur in the study area is mantle derived and that the isotopic composition of the sulfur was controlled by the prevailing fo_2, which in turn controlled the partitioning of SO_2 and H_2S between sulfide melt and magma.

SAMEVATTING

'n Opeenvolging van 3250 m van die Gelaagde Suite Rustenburg en geassosieerde mineralisasie suid van Potgietersrus is ondersoek. Vier episodes van verskuiwing het die gebied vervorm en veroorsaak dat die vroeë differensiate, wat nie elders in die Bosveld waargeneem word nie, dagsoom tesame met ekonomiese konsentrasies van die beste metallurgiese graad chromiet wat tans in die Republiek ontgin word.

Die Mg:Fe:Ca verhouding van die Ca-arm piroksene varieer van 89,5:8,8:1,6 in die laer sone tot 44,2:52,3:3,37 in die bosone. Laasgenoemde samestelling merk die twee pirokseenlimiet. Teksture dui daarop dat daar 'n peritektiese reaksie bestaan tussen die Fe-ryk Ca-arm pirokseen en smeltsel en dat dit moontlik die rede vir die bestaan van die twee pirokseenlimiet mag wees. 'n Aansienlike hoër $K_{D_{Mg-Fe}}^{opx-cpx}$ in die studiegebied (0,822) as vir ander sektore van die Bosveldkompleks (0,782) dui daarop dat die piroksene van enerse samestelling by hoër temperature in die Potgietersrusgebied gekristalliseer het. Ondersoek van die Al:Si verhouding in Ca-ryk piroksene van 'n verskeidenheid van magmatiese omgewings bevestig dat hierdie veranderlike gebruik kan word om relatiewe variasies in die $a_{SiO_2}^{smelt}$ te monitor. Chemiese analises van Ca-ryk piroksene dui daarop dat hierdie fase 'n kristallisasieverloop van ysterverryking en Ca-verarming met differensiasie toon wat anders is as vir die meeste ander toleiitiese intrusies.

Die V_2O_5 inhoud van die hoof magnetitietlaag en die Cr_2O_3 en die $Cr/Fe^{2+} + Fe^{3+}$ waardes van die boonste en onderste chromitietlae in die studiegebied is die hoogstes wat in die Bosveldkompleks aangetref word. Teksturele getuienis in hierdie lae dui daarop dat hulle opgradeer is na digte, monomineraliese lae as gevolg van 'n na-kumulus sinterproses.

Berekende intensiewe parameters vir die Potgietersrusmagma dui daarop dat dit oor 'n temperatuurinterval van 1276°C in die laer sone tot 1022°C in die onderste gedeelte van die bosone gekristalliseer het. Die suurstoffugasiteit in die magma het tydens kristallisasie van die laer sone gewissel van $10^{-6,21}$ tot $10^{-4,98}$ atm, terwyl laer waardes van 10^{-11} tot 10^{-9} atm geheers het tydens kristallisasie van die bosone.

Die studiegebied bevat aansienlike konsentrasies sulfiede op verskillende hoogtes in die opeenvolging. Die afskeiding van onmengbare sulfiedvloeistof kan in die meeste gevalle in verband gebring word met die menging van nuwe, metaalryk magma met die resmagma in die kamer.

Swaelisotoopstudies dui daarop dat alle swael in die studiegebied van manteloorsprong is, en dat die isotoopsamestelling van die swael gekontroleer is deur die heersende fo_2 toestande wat op sy beurt die verdeling van SO_2 en H_2S tussen sulfiedvloeistof en magma beheer het.

CONTENTS

LIST OF FIGURES IN THE TEXT

LIST OF TABLES IN THE TEXT

1. INTRODUCTION

1.1 Purpose and Scope

The area south of Potgietersrus is unique in that it contains a sequence of ultramafic rocks and associated very high-grade chromitite layers unlike any other lower zone rocks exposed in the Bushveld Complex. Deep drilling in this area by several exploration companies over the past fifteen years has shown that, apart from chromite, a variety of different mineralized layers, essentially Ni, Cu, and platinum-group elements (PGE) are also developed. This investigation was therefore undertaken, firstly, to determine the relationship between these ultramafic rocks and their chromitite layers to the other layered rocks of the Rustenburg Layered Suite, both from a structural and a petrological point of view, and secondly, to obtain a better understanding of the controls on the variety of mineralization encountered in the sequence of layered rocks in this area.

Several periods of faulting have resulted in a complicated outcrop pattern of the rocks. This, in addition to poor outcrops over large areas, as well as localized intensive silicification of the ultramafic rocks, necessitated detailed mapping of the entire area on a scale of 1:10000. Mapping and the numerous borehole logs and core kindly made available by several exploration companies were subsequently used to reconstruct the stratigraphic column of the layered igneous rocks. This was followed by a petrological and geochemical investigation of the layered rocks, during which time special attention was focussed on the mineralized layers. The findings from these investigations were finally used, in conjunction with thermodynamic principles, to place constraints on the intensive parameters of the magma during crystallization of the whole sequence in general and the mineralized layers in particular.

1.2 Previous Work

The first documentation of the geology of the Potgietersrus area was by Molengraaff (1901) who, together with other geologists of the Geological Survey, mapped the area at that time. Kynaston and Mellor (1905), Hall (1908) and Kynaston, Mellor and Hall (1911) placed most emphasis in their repsective reports on the Bushveld granites, the Transvaal Sequence and the Waterberg Group. Scant reference in these early reports to the layered mafic rocks of the Bushveld Complex is probably due to the very poor exposure of these rocks throughout the area.

It was not until 1929 that the first significant account dealing with the mafic rocks and their associated platinum mineralization appeared in Wagner's (1929) book on the platinum mines and deposits of South Africa. Since then, no further documentation, other than brief passages in various articles, came forth until de Villiers' (1967) account of the geology of the southern portion of the Potgietersrus limb. This study evolved from the discovery by Mnr. S. P. Rautenbach in 1960 of encouraging chromite mineralization on the farms Grasvally 293KR and Zoetveld 194KR. The discovery led to the exploration for and the subsequent mining of chromite first by Amcor and at present by Samancor.

Further investigations in the southern portion of the area were based on the exploration activity by Rio Tinto during 1970-71, who discovered significant Ni-Cu and PGE mineralization, during exploration of Ni concentrations in lateritic weathering products of ultramafic rocks. The only published reference to this mineralization is by De Waal and Viljoen (1975) who conducted an electron-microprobe study of the Ni distribution in the serpentinites on the farm Volspruit 326KR.

The most significant contribution to our understanding of the regional setting and stratigraphy of the Bushveld Complex in the Potgietersrus area is by van der Merwe (1976, 1978) who, on the basis of detailed mapping of the whole Potgietersrus limb, subdivided the layered basic and ultrabasic rocks into a lower, critical, main and upper zone. From the available geological and geophysical data, van der Merwe concluded that the Potgietersrus limb is a separate entity with no obvious physical connection to either the eastern or the western lobes of the Bushveld Complex.

A gravity survey over the farm Volspruit 326KR was undertaken by Barrett et al. (1978) in an effort to interpret the structure.

1.3 Tectonic Setting and General Geology of the Potgietersrus Limb of the Bushveld Complex

The Potgietersrus limb is situated on the "Bushveld - Great Dyke lineament" (Cousins, 1959) (Fig. 1). A number of mafic igneous bodies were emplaced along this lineament, from the Great Dyke in the north to the Trompsburg Complex in the south. This lineament

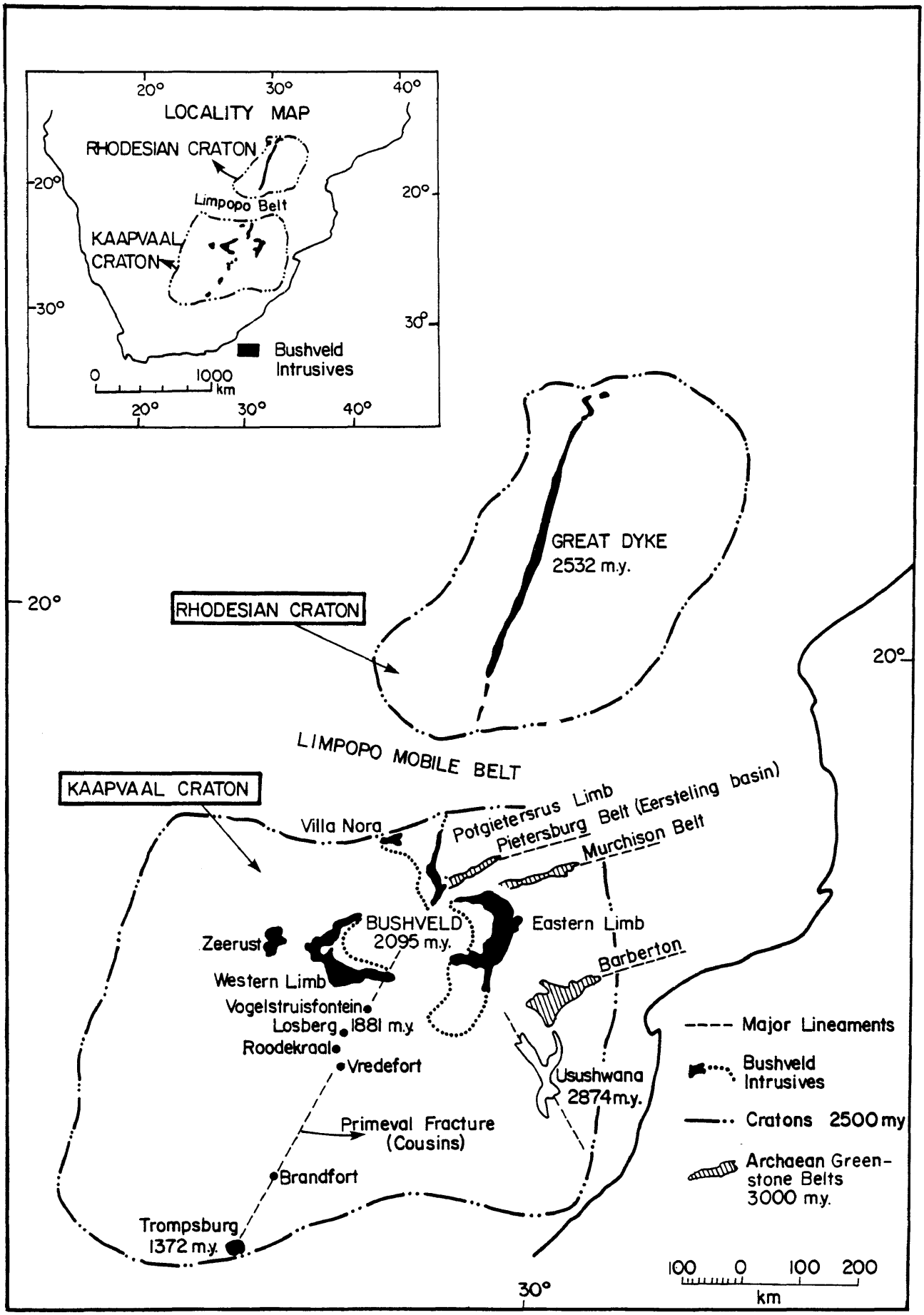

Fig. 1 Sketch map showing the setting of the Bushveld Complex on the Kaapvaal Craton in relation to some principal lineaments in southern Africa.

is believed to represent a primeval fracture that extended to the low-velocity layer in the upper mantle and along which magma was tapped from time to time (McConnell, 1974).

The mafic and ultramafic rocks of the Potgietersrus limb outcrop over a strike length of at least 110 km and a variable width of 7 to 10 km (Fig. 2A). Although the present outcrop pattern of the Potgietersrus limb defines a linear to sigmoidal shaped body in plan view, the available geophysical data (van der Merwe, 1976) suggests that the intrusion is pear-shaped, with its northwestern extremity to the west of Villa Nora (Fig. 1). The intrusive body gently plunges towards the north in the manner shown on the longitudinal section Fig. 2B). The diagram illustrates the inferred profile of the intrusion prior to the emplacement of the Bushveld granite.

The feeder of the intrusion was proposed by van der Merwe (1978) to lie at the intersection of the north-northwest trending Ushushwana lineament, the east-northeast trending Pietersburg greenstone belt (Eersteling Basin) and the "Bushveld - Great Dyke lineament" (Fig. 1). He states that the three lineaments intersect just to the west of Potgietersrus. A reconstruction of the traces of these lineaments reveal the intersection to lie approximately 8 to 10 km south of the town of Potgietersrus and to coincide with a gravity high obtained by re-contouring the gravity data of Smit et al. (1962). Forceful upward migration of mafic magma could have resulted in shallow angle Hertzian shear fractures within the Transvaal Basin about this focal point according to the model of Sharpe and Snyman (1980), and account for the apparent funnel shaped profile of the intrusion.

The mafic and ultramafic rocks of the Potgietersrus limb can be divided into four distinct zones on the basis of diagnostic mineral assemblages. The oldest rocks in the layered sequence are harzburgites, pyroxenites and chromitites of the lower zone. Rock types from this zone outcrop only in the southern portion of the Potgietersrus limb and as satellite intrusions north of this town (Fig. 2A). Critical zone lithologies which occupy the smallest volume of the intrusion are made up of spotted and mottled norites,

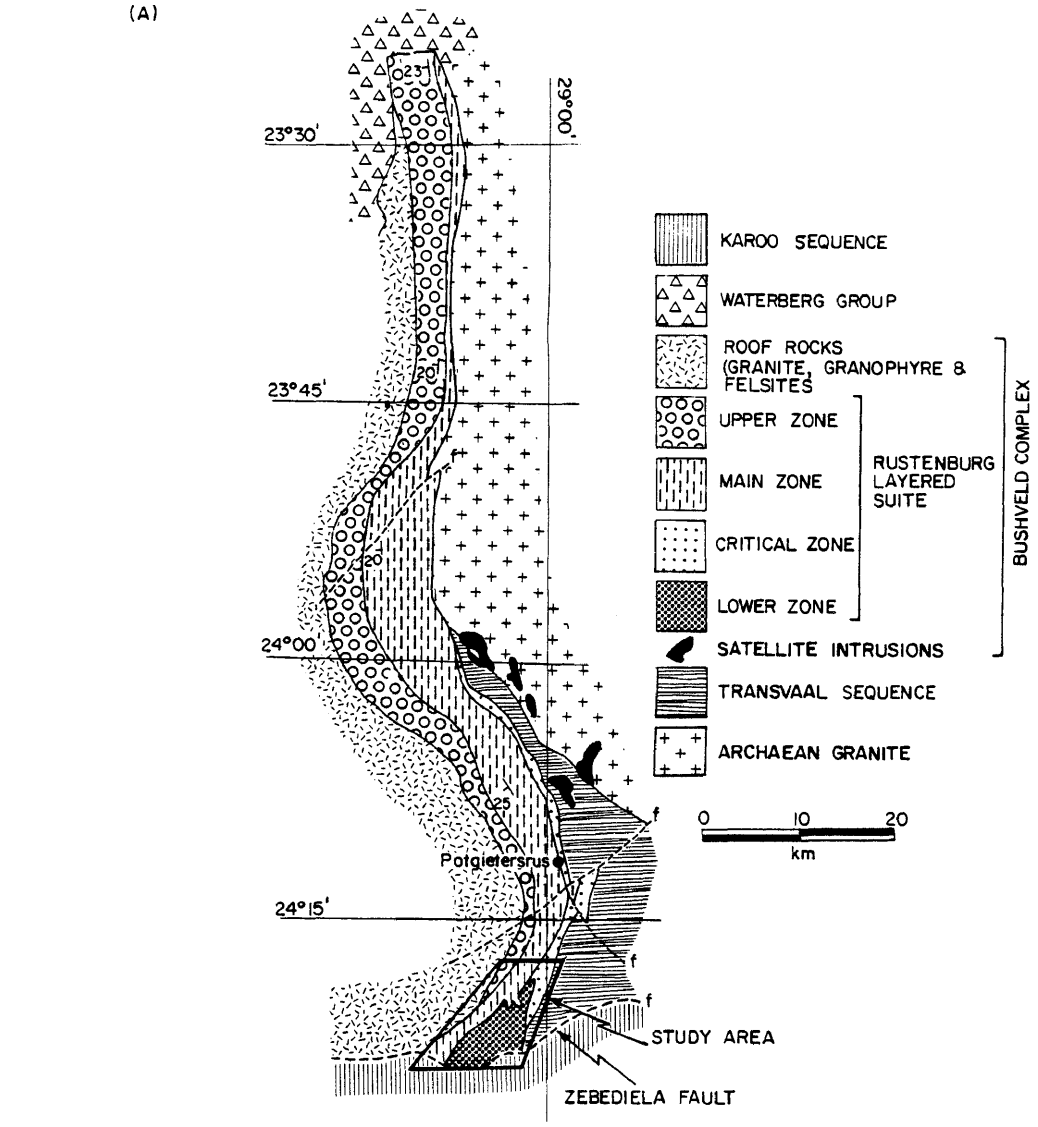

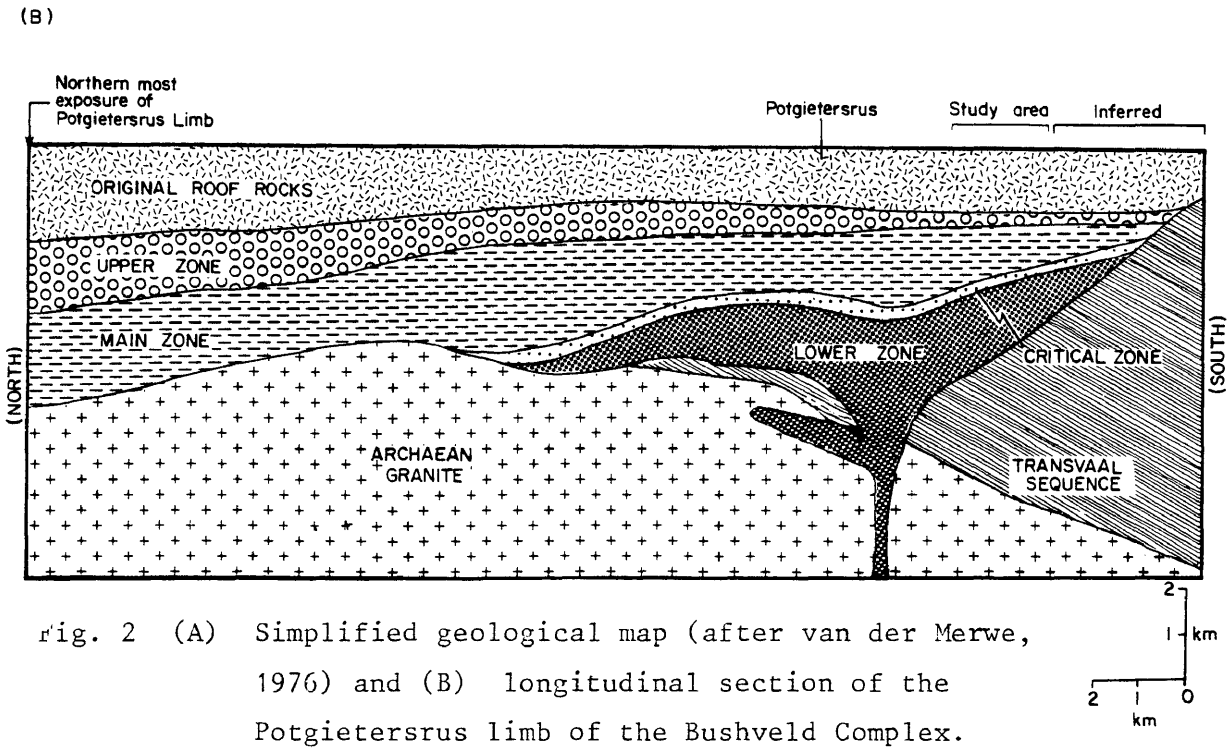

Fig. 2 (A) Simplified geological map (after van der Merwe, 1976) and (B) longitudinal section of the Potgietersrus limb of the Bushveld Complex.

anothosites, feldspathic pyroxenites and one thin chromitite layer. Surface exposures of this zone are generally poor, and exposures are usually encountered where this zone is in contact with the Transvaal Sequence. Unlike the lower and critical zone sequences which are well layered and contain a variety of rock types, the main zone consists of a fairly homogeneous sequence of rather monotonous gabbros and gabbronorites, layered only on a macro scale. The youngest rocks are the magnetite bearing gabbros, gabbronorites, diorites, olivine diorites and anorthosites, as well as the magnetitite layers of the upper zone. Small scale and micro layering can be spectacularly developed in this zone. Contact relationships between the layered mafic-ultramafic rocks and the floor as well as the roof rocks are seldom observed, due to the extremely poor exposure throughout most of the area and also because of the later intrusive granitic activity.

Along the northern 60 km of strike the base of the layered sequence is in contact with basement granite, compared to sediments of the Transvaal Sequence along the remaining 50 km of strike in the south (Fig. 2A). Although contacts are virtually nowhere exposed, the contact with the basement granite was observed in an underground exploration cross-cut on the farm Overysel 815 LR. Here the contact is a highly brecciated zone, a few metres to tens of metres wide, in which fragments of granite ranging in diameter from a few centimetres up to several metres are set in a fine-grained dark noritic matrix. In contrast, borehole intersections show the contact against sediments to manifest itself as a zone of interfingering magmatic and sedimentary rocks over a thickness of about 100 m.

In the metamorphic aureole generated by the intrusion a spectacular array of metamorphic mineral assemblages are developed in a zone that extends up to 3 km away from the contact. Original dips of 10 to 15° in the sediments have been steepened to 40° on average near the contact, and at some localities they may even be vertical and extremely contorted.

On average, the dip of the layered mafic to ultramafic rocks is about 20 to 25°W which is appreciably steeper than that of the country rock. Dips of up to 40°W have been observed in the critical zone chill and the associated marginal rocks south of Potgietersrus.

This difference in dip between the marginal rocks and the layered rocks of the intrusion indicates that the contact of the intrusion is approximately twice as steep as the layering within it. Although the contact of the lower zone rocks with the Pretoria Group country-rocks has never been observed, numerous magnetometer traverses across the contact on the farms Zoetveld 294KR and Volspruit 326KR as well as percussion drilling across the contact zone on Zoetveld 294KR by SAMANCOR indicates that it may be as steep as 70°. Such a relationship clearly suggests a funnel-shaped form (Fig. 2B) similar to that of other layered intrusions.

The layered rocks are overlain to the west by the roof-rocks of the complex which consist of felsite, granite, and granophyre, but to the northwest also by clastic sediments of the Waterberg Group. To the south the complex is terminated by the east-northeast trending Zebediela fault, which has brought the layered sequence up against basalts of the Karoo Sequence. Results of geophysical work reported by van der Merwe (1978) suggests that the Potgietersrus limb may extend a further 20 km south-southwest, as far as the town of Naboomspruit.

1.4 Age of the Potgietersrus Limb

One interesting feature of the "Bushveld - Great Dyke lineament" is the younging of the intrusives on this lineament towards the south (Fig. 1). This, as well as the striking petrological similarities between the Great Dyke and the lower zone lithologies of the Potgietersrus limb led the author to believe that the Potgietersrus limb could possibly be older than the eastern or western compartments of the Bushveld Complex, which have been dated at 2095 ±24 m.y. (Hamilton, 1977). Unpublished initial $^{87}Sr/^{86}Sr$ ratios (J. Harmer, personal communication) of quenched samples from the margin of the critical zone in the study area gave values of 0,70598 and 0,70608. These values are similar to Hamilton's (1977) values of 0,70603 ±10 for the critical zone and 0,70563 ±2 for the upper portion of the lower zone. Seeing that this new data fits on the isochron given by Hamilton, indications are that the Potgietersrus limb and the western and eastern compartments of the Bushveld Complex are contemporaneous.

1.5 The Study Area and Fieldwork

The centre of the study area is approximately 20 km south of the town of Potgietersrus (Fig. 2A). Access to the area may be gained by the national road or via numerous secondary roads.

The bulk of the field work was conducted during the second half of 1978. Detailed mapping revealed that the area has no more than ten per cent exposure and of this approximately half consists of laterized ultramafic rocks, known as "birbirite". The birbirites are highly leached and silicified harzburgites and pyroxenites of the lower zone. These rocks are altered to such an extent that distinction between the original lithologies is not possible. The only indication of the original mineralogy is the presence of small specks of ferritchromit.

The topographic expression of the more resistant granitic and psammitic lithologies was found to be a very unreliable indicator of contact relations. For this reason, the contact between the mafic rocks and the granitic roof-rocks to the west had to be inferred from available airborne radiometric and magnetometer surveys. The identification of borehole cuttings of shallow percussion holes drilled by the local farmers for underground water proved useful in delineating the contact more accurately.

The eastern contact of the intrusion with the Pretoria Group sediments could be inferred with reasonable accuracy with the aid of a magnetometer survey, the results of which were supplemented by surveys conducted by exploration companies.

In addition to surface mapping, logs and core of over 100 diamond boreholes were available for this investigation and provided valuable fresh material for petrological and geochemical studies. Ninety per cent of these holes were drilled on the farm Volspruit 326KR. Of the remainder, three holes were drilled on the farm Jaagbaan 291KR two on the farm Moorddrift 289KR and five on Grasvally 293KR. In addition to these boreholes the mine workings on Grasvally and Zoetveld 294KR, as well as old chrome exploration pits, were useful in the construction of the geological map. In certain areas mapping of soil types proved to be of value in obtaining some indication of the underlying rock type.

In an effort to obtain additional information on the distribution of the different rock types of the layered sequence Rand Mines, Samancor, and Billiton Exploration kindly sponsored an airborne infra-red survey of the area. Unfortunately the survey proved unsuccessful due to the deep soil cover.

1.6 Physiography

The morphological features of the area reflect the distribution of the principle rock units. The larger portion of the study area is situated in a broad valley which is underlain by readily weathering mafic and ultramafic rocks of the Rustenburg Layered Suite. This valley is flanked to the west and east by hills 300 to 400 metres high, composed of Bushveld granite and quartzite of the Pretoria Group respectively.

The most prominent physiographic feature of the mafic rocks of the Rustenburg Layered Suite is a gently sloping hill consisting of anorthositic and noritic rocks in the northern most portion of the area. Most of the other topographic expressions over the Layered Suite are due to resistant silicified birbirite cappings, whereas others are caused by quartzite emplaced into the mafic rocks by faulting.

The adjoining area to the south forms the northern extremities of the Springbok Flats, which are underlain by basalts and sediments of the Karoo Sequence.

2. THE RUSTENBURG LAYERED SUITE SOUTH OF POTGIETERSRUS

2.1 The Stratigraphic Column

The 3250 m thick succession of rocks that make up the Rustenburg Layered Suite has been divided into a lower, critical, main, and an upper zone on the basis of the appearance or disappearance of diagnostic cumulus phases, the compositional variations of these minerals, and on structural evidence for a major influx of new magma. The generalized stratigraphic column and the compositional variation of certain cumulus minerals indicated in Figure 3, gives some indication of the intricate crystallization history of the magma from which this sequence was derived.

The sequence has also been subdivided in accordance with the accepted system of lithostratigraphic nomenclature. On this basis the lower zone can be subdivided into three subzones referred to as the Volspruit Pyroxenite, the Drummondlea Harzburgite-Chromitite and the Moorddrift Harzburgite-Pyroxenite, whereas the critical, main and upper zones have been designated the Grasvally Norite-Pyroxenite-Anorthosite, the Rooipoort Gabbronorite and the Jaagbaan Magnetite-Gabbronorite respectively.

The lower zone consists of an alternating sequence of opx-ol-chr cumulates, ol-chr cumulates, and opx cumulates collectively also referred to as harzburgites and pyroxenites. Chromite usually contributes less than 5 vol. per cent of the rocks, except at two levels where chromitite layers are developed in olivine-rich cumulates. One of the orthopyroxene cumulates is considerably enriched in Ni-, Cu-, and PGE-bearing sulfides.

Unfortunately the base of the lower zone is not exposed, and has yet to be intersected by drilling, thus our knowledge of the basal portion of this zone must be considered as incomplete. Also at the -900 m level a gap exists in the column due to faulting.

The lower zone is separated from the critical zone by a major structural and stratigraphic, as well as petrographic, discontinuity. Here, fine-to medium-grained gabbronorites and pigeonite gabbros overlay the uppermost harzburgites of the lower zone. These fine-grained plagioclase-rich rocks contain orthopyroxenes of approximately 20 mole per cent less of the enstatite component than those of the

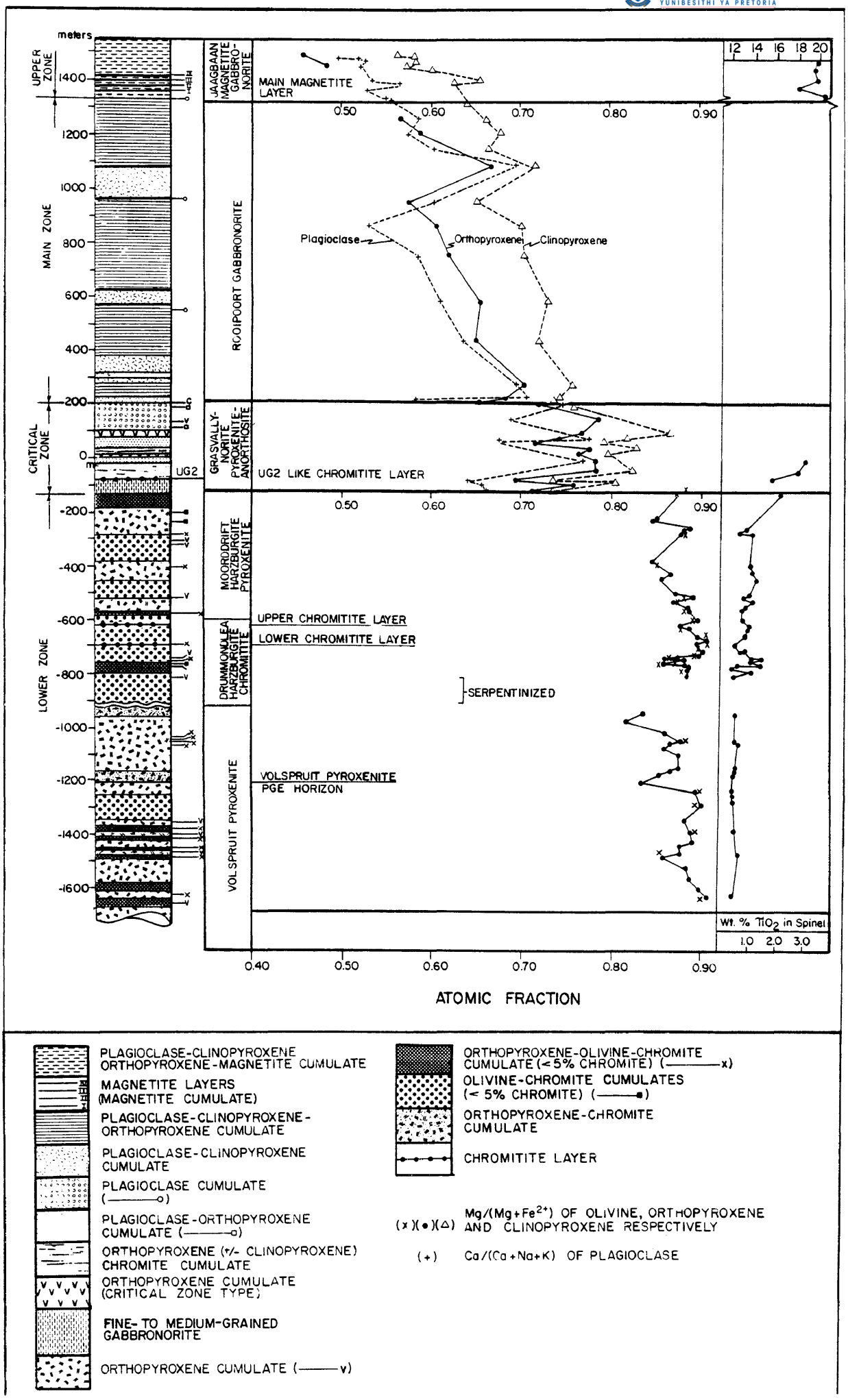

Fig. 3 Generalized stratigraphic column of the Rustenburg Layered Suite and compositional variation of the major cumulus phases of the rocks for the area south of Potgietersrus.

immediate underlying lower zone harzburgites. The layered member has been divided into two subzones (Fig.13). The more mafic early differentiates of subzone 1 consist predominantly of orthopyroxene, orthopyroxene-chromite (+/- clinopyroxene) and plagioclase-orthopyroxene cumulates with subordinate amounts of plagioclase and plagioclase-orthopyroxene cumulates. Overlying subzone 1 and making up the remaining one-third of this zone is the anorthositic subzone 2, which consists almost totally of plagioclase cumulates (mottled anorthosite). These are in turn, overlain by a thick sequence of plagioclase-clinopyroxene-orthopyroxene cumulates and plagioclase-clinopyroxene cumulates of the main zone. Due to the absence of a primary roof contact with the Rustenburg Layered Suite in the study area and the lack of deep drilling to confirm the position of the basal contact of the lower zone, a distinctive reference datum ("0") was found necessary. A platiniferous feldspathic pyroxenite with coarse sulfide blebs similar in appearance to the Merenskey Reef, with the exception of the absence of the chromitite layers, was chosen as this datum (Fig. 13).

The appearance of cumulus titaniferous magnetite near the top of the layered sequence marks the base of the upper zone, which consists mostly of plagioclase-clinopyroxene-orthopyroxene-magnetite cumulates. Four magnetite layers are developed near the base of this zone and it is the lowermost one which is the thickest and has the highest V_2O_5 content.

2.2 Field Relations

2.2.1 Lower Zone

Lower zone lithologies are confined mainly to the southern half of the area as well as to a wedge shaped horst block that bisects the northern half of the area (Fig. 4 (Folder I in back pocket)). Harzburgites and pyroxenites, or their altered equivalents, predominate in outcrop. The harzburgites are medium-to coarse-grained poikilitic or granular. The poikilitic variety is a ol-chr cumulate with large oikocrysts of intercumulus or reaction orthopyroxene. These oikocrysts are on average 2 to 4 cm in diameter and can, even in handspecimen, be seen to include chadacrysts of cumulus olivine and chromite. The granular variety appears as a fairly even grained

rock with varying proportions of cumulus olivine and orthopyroxene. When fresh, both varieties are black to brownish in colour, although the poikilitic variety is readily recognized by its distinctive pocked appearance in outcrop. Serpentinization imparts a greenish colour to these rocks in which the pseudomorphs after olivine take on a light green colour compared to the more resistent, silky greenish-brown bastite after orthopyroxene. In areas of extreme surface leaching these ultramafic rocks are completely converted to birbirites, i.e. the entire rock has been replaced by silica and iron. Chalcedony pseudomorphs after olivine can sometimes be recognized in these rocks. The original cumulus chromite is relatively unaffected by this extreme leaching process and occurs as discrete disseminated specks in the dark brown to red birbirite.

The lower zone orthopyroxenites are medium-grained green to brownish green monomineralic rocks. The coarse-grained varieties can contain up to 10 to 15 per cent intercumulus plagioclase and together constitutes a sequence of cyclic units in which the poikilitic harzburgite generally forms the base. This rock usually grades upward into granular harzburgites which in turn are overlain by the pyroxenites. The pyroxenites are more resistant to weathering and tend to form more prominent outcrops than the more readily weathering harzburgites. In areas of extreme birbirization even the pyroxenites can be leached and replaced by silica and iron hydroxides so that the original chemical and petrological character is completely destroyed. Two chromitite layers are developed in the lower zone. Although they hardly outcrop their surface position (Fig. 4 (Folder I)) has been delineated from the numerous prospecting trenches that occur in the area. Because of the oxidized nature of the chromitite and the very weathered nature of the associated harzburgite, these trenches unfortunately did not yield any information other than the location of the chromitite layers.

2.2.2 Critical Zone

The critical zone is best exposed in the northern portion of the farm Grasvally. Although this zone is in direct contact with the sediments of the Pretoria Group at this locality, the layered rocks are separated from the floor by an envelope of fine-grained gabbronorites referred to as the marginal member of the critical zone

(M.Mb./P.G.) (Fig. 4 (Folder I)). This marginal member consists of very fine-grained gabbronorites, and quartz gabbronorites in direct contact with the sediments. Away from the contact these rocks grade into medium-grained ophitic gabbronorites and finally into medium- to coarse-grained gabbronorites. This member has a variable dip averaging 40°W and a thickness that varies from 100 to 150 m.

Draping disconcordantly against this marginal member are cumulates of subzone 1 of the critical zone (Fig. 9). In the northern portion of the farm Grasvally spotted norites and anorthositic norites of the upper part of subzone 1 are in juxtaposition with the marginal member. Sulfides occur sporadically at this position of the critical zone, particularly near the top of subzone 1 where a mineralized spotted norite, approximately 44 to 50 cm thick, exists. The lower part of subzone 1 of the critical zone is exposed further south, where apart from plagioclase-bearing cumulates, feldspathic pyroxenites, chromite-bearing two pyroxene pyroxenites and a 0,80 m thick chromitite layer, analogous to the UG2, are found. Outcrops of these rocks are not particularly good in this area and their distribution was largely deduced from prospecting trenches on the UG2-like chromitite layer. Fine-to medium-grained gabbronorites, which contain considerable concentrations of sulfides, separate the critical zone from the lower zone rocks in this area. These fine-grained rocks constitute the marginal rocks of the critical zone in this area.

Subzone 2 is distinguished from subzone 1 by a marked increase in the amount of plagioclase cumulates. The predominant rock type is mottled anorthosite which contains thin intercalations of noritic anorthosite, anorthositic norite, norite, feldspathic pyroxenite and gabbronorite. Spherical aggregates of orthopyroxene 20 to 60 mm in diameter and similar to those described by Lee and Sharpe (1979) from the contact zone of the eastern Bushveld are developed in a 5 m thick mottled anorthosite layer within this subzone. Also associated with this horizon are irregular bodies of amphibole-bearing pegmatitic gabbronorite, which contain ovoid to round sulfide blebs. The overlying 20 m of mottled anorthosite contains numerous country-rock inclusions. These have been metamorphosed to a variety of assemblages

that contain minerals such as pure Al-spinel, grossularite, or diopside and plagioclase. Contamination in the mottled anorthosite around these xenoliths has given rise to pegmatitic gabbronorites that contain coarse pockets of quartz and seconary amphibole, identical to those with which sulfides are associated.

The relatively good outcrops of the critical zone and its marginal lithologies on the northern part of Grasvally assisted greatly in unravelling the field relations in the low lying areas to the south where outcrops are poor and sporadic.

2.2.3 Main Zone

The base of the main zone is taken where the mottled anorthosite makes way for a 10 m thick layer of medium-grained granular greyish white norite. It is well developed on the northern part of Grasvally and is characterized by the development of large acicular, frequently radiating, crystals of plagioclase, at the base of this layer. These crystals are on average 25 mm long and 2 mm wide. Above this norite, clinopyroxene is a dominant cumulus phase in all the exposed rocks. Because these acicular plagioclase crystals are similar to those described by Lofgren and Donaldson (1975) from supercooled magmas, their presence can be considered indicative of a new batch of magma that underwent some degree of supercooling along its base. This feature, together with the appearance of clinopyroxene and inverted pigeonite a few metres higher in the sequence were the criteria for subdividing the sequence into the critical and the main zones at this level.

The main zone consist essentially of an alternating sequence of pigeonite-free and pigeonite-bearing gabbroic rocks. The pigeonite-rich gabbronorites tend to be dark grey to almost black in colour and display a pronounced igneous lamination. These features are primarily due to the parallel alignment of platy, dark grey plagioclase crystals. The inverted pigeonites are also darker in hand specimen than primary orthopyroxene.

Even though these rocks do possess a good fabric, dips could not be measured frequently because it can be seen that the exfoliated

boulders in outcrop have undergone some rotation during weathering. Dip values on the map (Fig. 4 (Folder I)) usually represent attitudes for a particular area and are the best representative mean from a number of values.

Within the lower half of the main zone two thin layers of mottled anorthosite are developed of which the lower one is approximately 15 m thick and the upper one 8 m thick. These two mottled anorthosites are not unlike those of the critical zone, except that they are a turbid greenish-white in colour due to saussuritization of the plagioclase.

2.2.4 Upper Zone

Upper zone rocks do not outcrop in the study area, although the main magnetitite layer of the upper zone was exposed in an old prospecting trench on the farm Jaagbaan (van der Merwe, 1978). Unfortunately this trench could not be located. Information on the lower part of the upper zone was obtained from a borehole drilled by J.C.I. on the central portion of the farm Moordrifft.

2.3 Structural Deformation

After emplacement and consolidation of the Rustenburg Layered Suite, the area was subjected to four episodes of fault deformation.

The earliest generation of deformation (f_1) was an episode of north-south trending reverse faulting. This faulting resulted in a horst-like block of lower zone harzburgites and pyroxenites to be vertically displaced upwards by as much as 800 m, into the critical zone (Fig. 5). The upper and lower chromitite layers presently being mined on the farms Grasvally and Zoetveld are confined to the horst-like block. The distribution of these two chromitite layers on surface, underground and in diamond drill core, reveals that the horst-like body was not emplaced as a solid block, but as a series of imbricate faults (Fig. 6). Dykes of granitic composition, which form part of an early north-south trending dyke swarm were subsequently emplaced along these faults. Although not shown on the map (Folder I) for the sake of clarity, up to 40 per cent of the northern portion of this horst wedge consists of this granitic material.

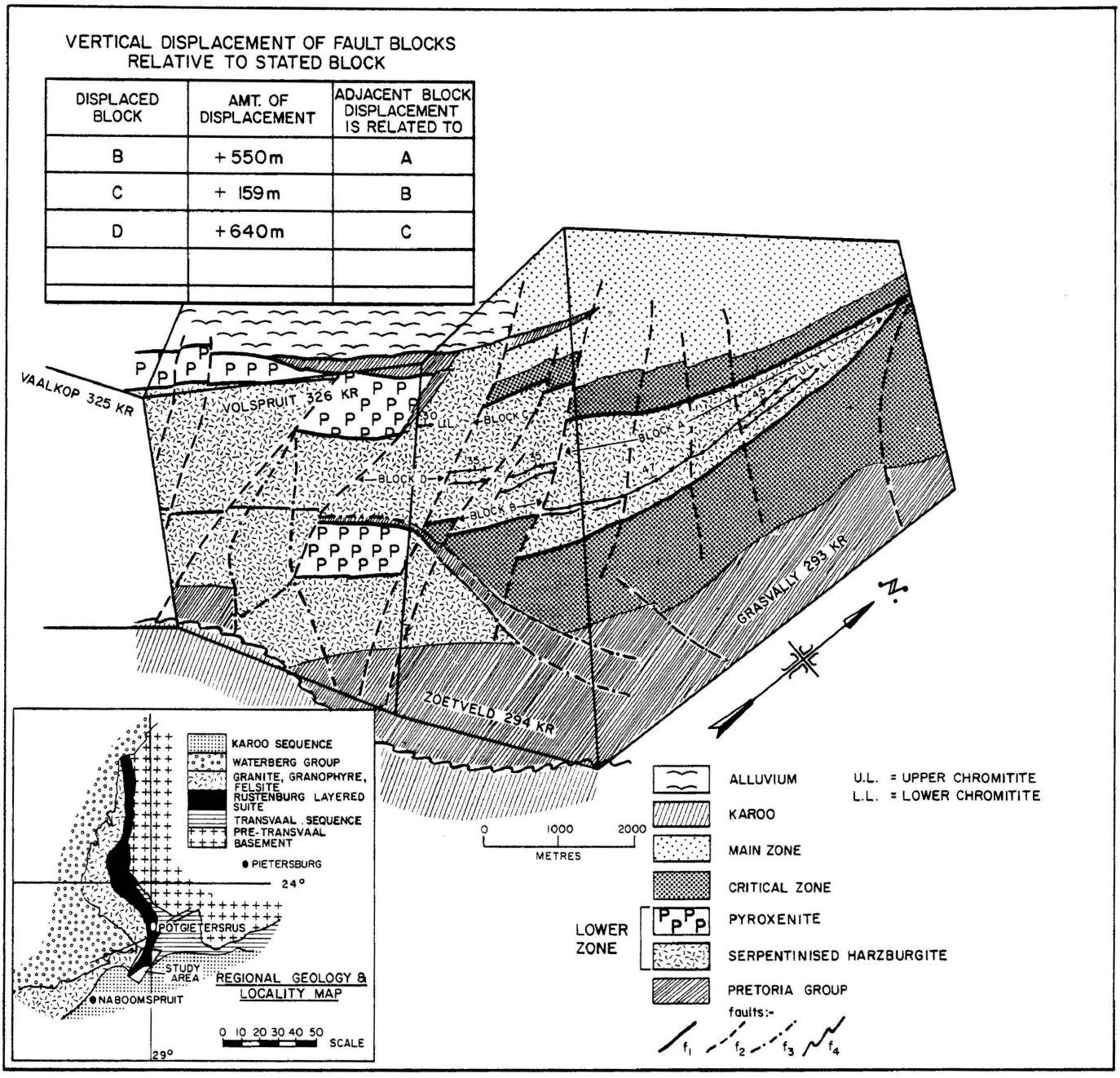

Fig. 5 Generalized geological map of the Grasvally - Zoetveld - Volspruit area showing different generations of faults.

Due to the imbricate nature of the faulting, the attitude of the shear planes are variable, both at the contact and within the horst block. Generally the shear planes dip about 70°W. The chromitite layers within the wedge have a variable dip, which decreases from 55°W in the north to 35°W in the south.

Steeply dipping slices of Pretoria Group quartzites, e.g. on the farms Zoetveld, Volspruit, Rondeboschje and Grasvally have also been upfaulted along these N-S faults.

The second generation of fault deformation (f_2) (Fig. 5) is WNW - ESE reverse block faulting. This has resulted in a step-like displacement of the Rustenburg Layered Suite towards the west. The distribution of the various blocks is best displayed by the displacement of the chromitite layers. The displacement of each of these blocks relative to the adjacent blocks is illustrated in Figure 5. The chromitite layers in the lower zone served as excellent markers for calculating displacement by these second generation faults. The minimum cumulative vertical displacement from the northern portion of block A to the southern limit of block D is about 1350 m. Chromitite layers are not present south of block D indicating an even greater vertical displacement than that observed between the other blocks, so that the upper part of the lower zone is completely absent in this area. Mineable chromitite layers last occur in block C, but as will be seen later the chromitite layer found in block D is considered to be the faulted equivalent of the upper of the two chromitite layers.

The reverse faulting in the southern part of the area (Zoetveld, Volspruit, and Vaalkop) has exposed portions of the lower zone that are from deeper stratigraphic levels than the chromitite horizons.

This second generation faulting has also modified the configuration of the contact between the lower zone and the quartzites of the Pretoria Group as seen, e.g. in the southeastern corner of the farm Volspruit where a block of quartzite is displaced 1 km to the west. This, like the other contact relations along the eastern margin of the area is based on ground magnetometer surveys.

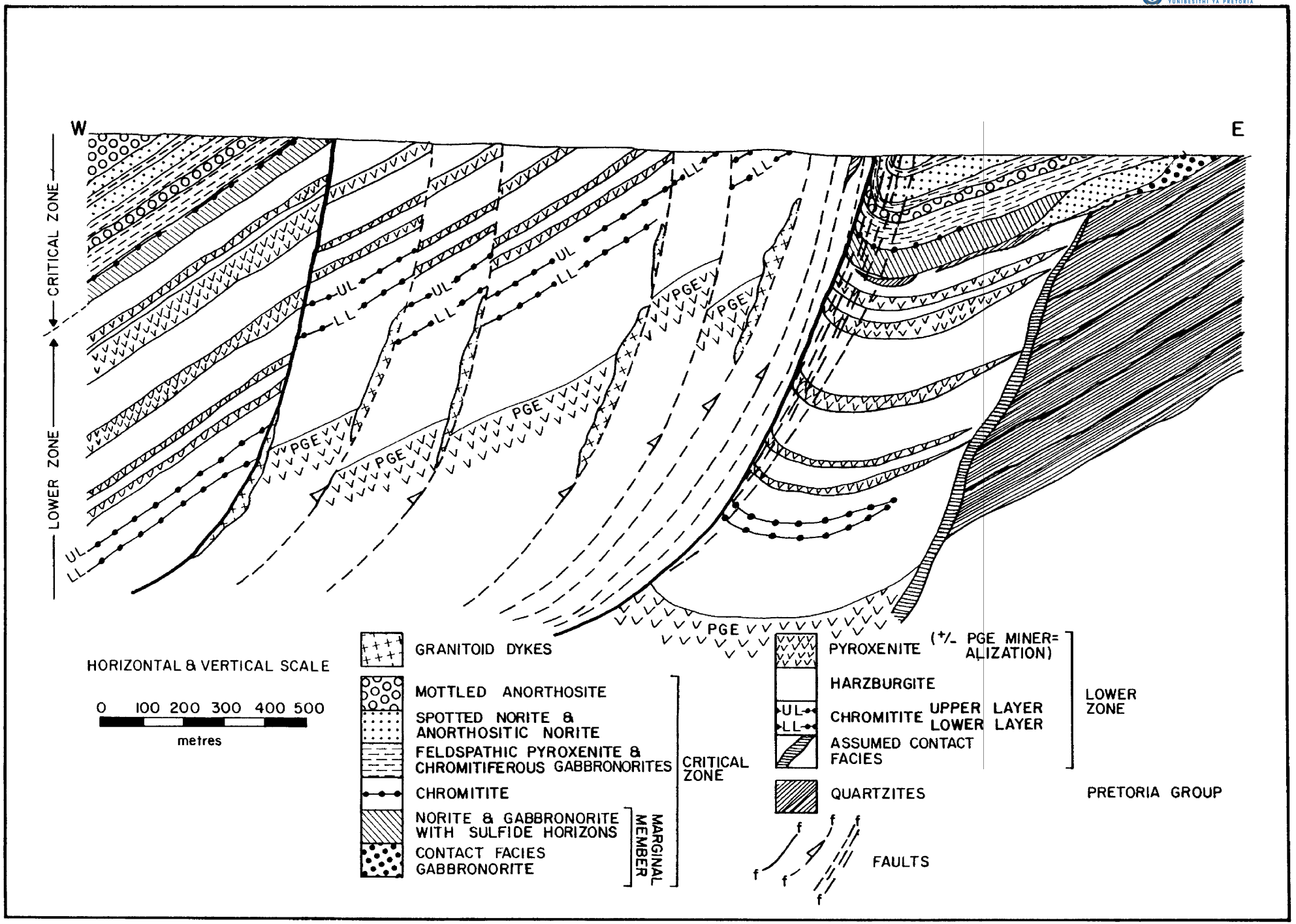

Fig. 6 Idealized cross-section of the Grasvally area. Note the horst-like nature of the lower zone block which hosts the upper and lower chromitite layers.

Third generation (f_3) faults strike NE-SW and result in the upfaulting of slices of Pretoria Group quartzites into the Rustenburg Layered Suite. Similar trending fault lineaments observed on aerial photographs cut through the farms Cyferkuil 321KR and Rondeboschje 295KR and are also present in the Waterberg Group southwest of the study area. From this it is assumed that the NE-SW faults are post-Waterberg in age.

The fourth and final period of faulting (f_4) occurred in post-Karoo times when Karoo basalts were brought into contact with the lower zone lithologies along the Zebediela fault.

3. PETROLOGY OF THE RUSTENBURG LAYERED SUITE SOUTH OF POTGIETERSRUS

Although Campbell (1978) and McBirney and Noyes (1979) have questioned the concept of gravitative settling of crystals to give rise to cumulates, the cumulate terminology for igneous rocks is well entrenched in the literature. Seeing that this terminology, as originally proposed by Wager et al. (1960) and subsequently expanded, modified and redefined by Jackson (1961 and 1967) and Irvine (1982), can be used in a purely descriptive sense without any petrogenetic connotations, this terminology is generally used throughout the text, in conjunction with the descriptive rock names suggested by Streckeisen (1967).

3.1 The Lower Zone

The lower zone south of Potgietersrus has a minimum thickness of 1600 m and consists of at least 37 cyclic units (Fig. 7A). These cyclic units change in composition and appearance upwards in the sequence which facilitated the subdivision of the lower zone into three subzones (Fig. 7A). Cyclic units consisting of opx-ol-chr and opx cumulates predominate in the Volspruit Pyroxenite subzone. The presence of one cyclic unit (No. 10, Fig. 7) with an ol-chr member at its base, in the middle of this subzone, served as a basis for subdividing the Volspruit Pyroxenite further, i.e. lower and upper Volspruit.

Olivine-rich cumulates predominate in the cyclic units (20 to 26, Fig. 7A) of the overlying Drummondlea Harzburgite-Chromitite subzone. The cyclic units in the Moorddrift Harzburgite-Pyroxenite subzone differ from those in the lower two subzones in that both ol- and opx-rich cumulates are well developed in the cycles of this subzone.

The basal layer of a fully developed cyclic unit is an ol-chr cumulate. They usually contain about 50 per cent cumulus olivine and less than 5 per cent cumulus chromite, the remainder being intercumulus orthopyroxene and plagioclase (Fig. 8A). The top of the ol-chr cumulate is marked by a phase contact where cumulus orthopyroxene joins olivine and chromite as a liquidus phase. The olivine content of these ol-opx-chr cumulates decreases upwards, however magmatic resorption of olivine prevents accurate estimate of the modal proportions in most cases. Due to the changing proportion of olivine and orthopyroxene within the middle member of such cyclic units the rock type changes upwards from ol-opx-chr cumulate to opx-ol-chromite cumulate (Fig. 8B). The chromite content usually remains below 5 per cent in these rocks.

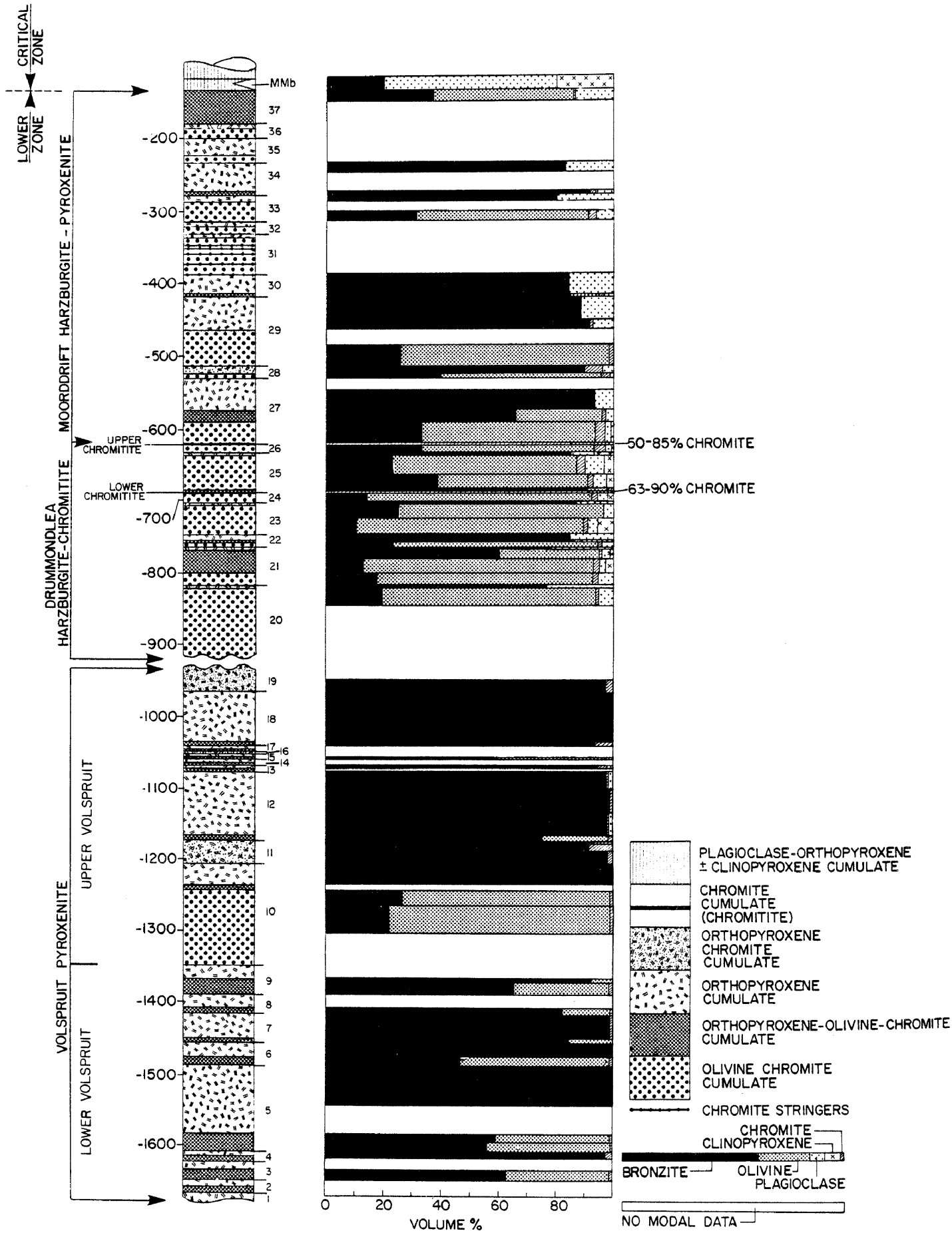

Fig. 7A Stratigraphic column and modal variation of minerals in the lower zone of the Potgietersrus limb south of Potgietersrus.

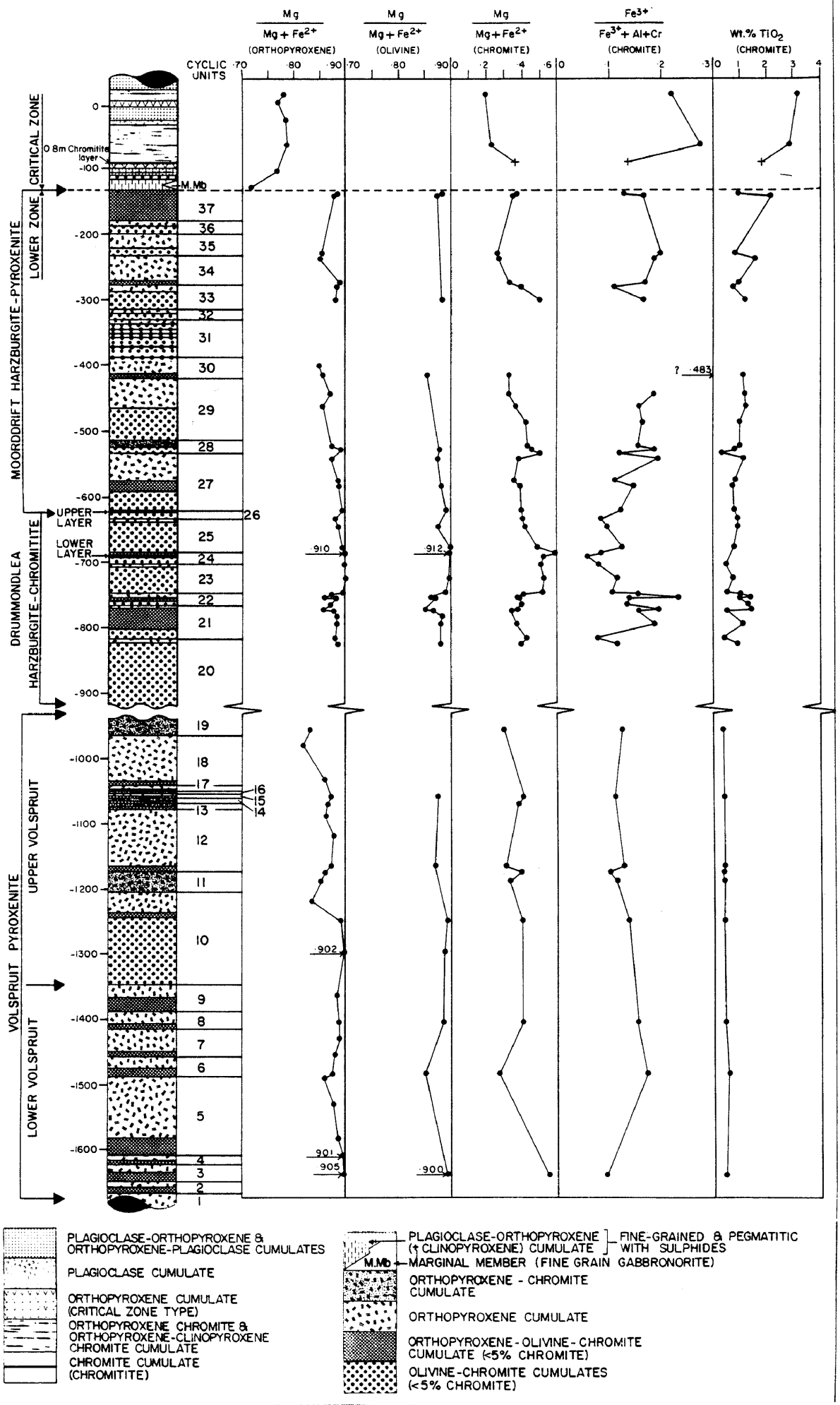

Fig. 7B Stratigraphic column of the lower zone with data on the compositions of orthopyroxene, olivine, and chromite.

Olivine disappears upwards so that the uppermost member of the cyclic unit is an orthopyroxene cumulate (Fig. 8D). The disappearance of olivine is mostly accompanied by a drop in the chromite content to levels less than 1 per cent, and by an increase in intercumulus plagioclase.

As a rule most of the cumulates have undergone varying degrees of postcumulus modification, either in the form of resorption or by adcumulus growth. Comparison of Figure 8A and 8F shows that the transformation from an ol-chr cumulate to an olivine adcumulate involves extensive overgrowth of olivine, with the elimination of as much as 50 per cent intercumulus liquid. Figure 8H is an orthopyroxene adcumulate that was probably derived from an orthopyroxene cumulate similar to that in Figure 8D. Orthopyroxene adcumulates are very common in the sequence and typically show grain boundary triple point junctions. Olivine adcumulates on the other hand are extremely rare and are only known to occur at two levels in the entire lower zone.

Olivine-chromite cumulates often display textures indicative of a reaction relationship between cumulus olivine and intercumulus liquid (Figs. 8A and 8E). In such rocks irregularly resorbed olivine crystals of cumulus origin now rest in an orthopyroxene matrix. Similar resorption features can also be seen in ol-cumulates where clinopyroxene crystallized from the intercumulus liquid (Fig. 8G).

A fully developed cyclic unit records the liquidus crystallization path, olivine-chromite, olivine-orthopyroxene-chromite, orthopyroxene. However, most cyclic units are incomplete either because prevailing conditions in the crystallizing magma prevented crystallization of the complete cycle, alternatively because certain members were subsequently eroded by convecting magma. Cyclic units 1 to 9 in the lower Volspruit subzone (Fig. 7A) are, for instance, incomplete in that these units consist of opx-ol-chr cumulates at the base and opx cumulates at the top. Cyclic unit 11 is also incomplete in that the entire unit consists only of opx-chr cumulates (Fig. 8C). This cyclic unit is unique in that it contains significant concentrations of Ni, Cu, and PGE mineralization,

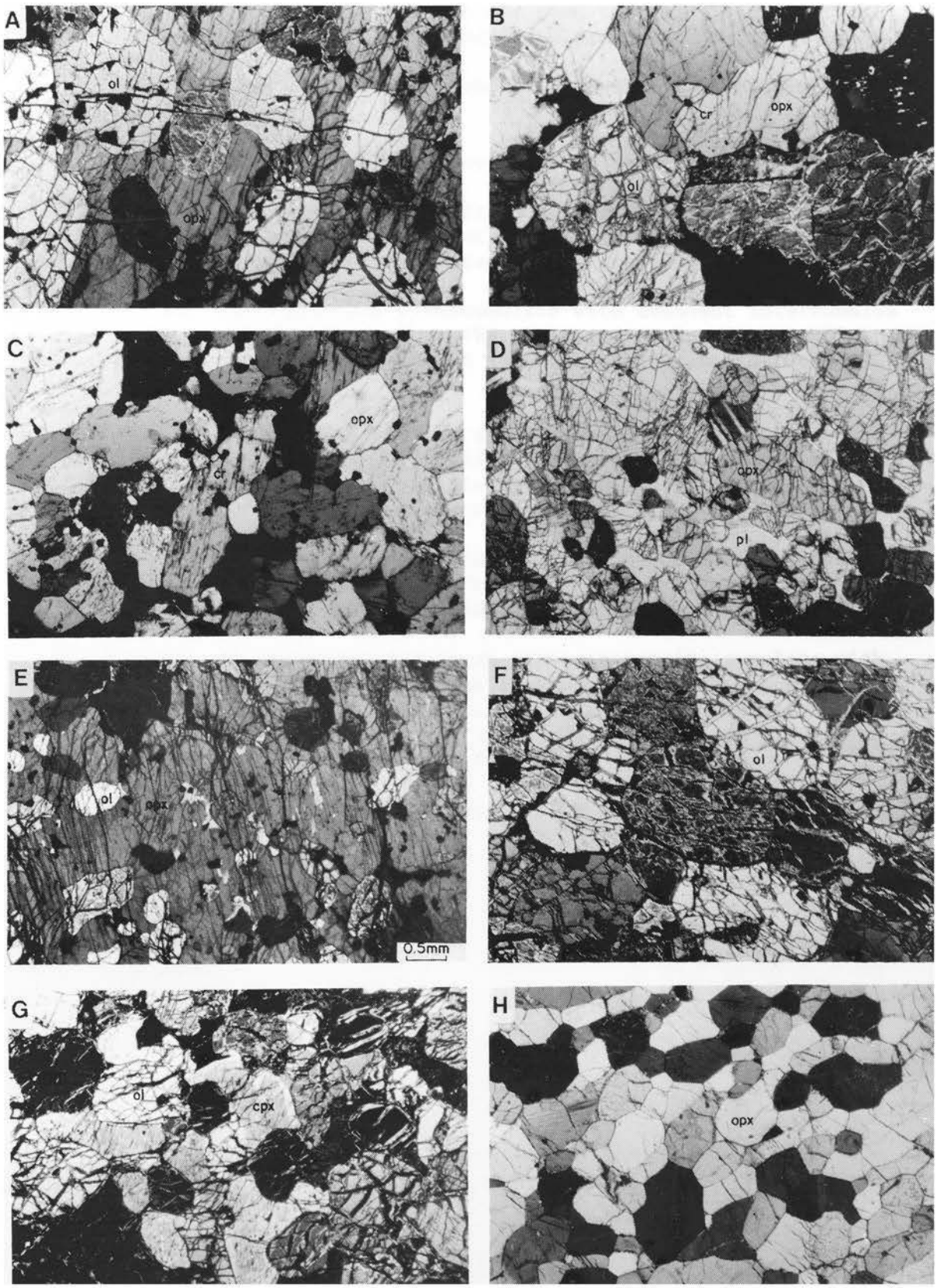

Fig. 8

Figure 8. Photomicrographs of rocks from the lower zone. ol = olivine; opx = orthopyroxene; Cr = chromite; cpx = clinopyroxene. All sections photographed with transmitted light under crossed nicols. Magnification is the same for all photomicrographs, see Fig. 8E. Sample numbers are indicated in brackets.

(A) Olivine-chromite orthocumulate from a basal member of a cyclic unit. (DR-4)

(B) Olivine-orthopyroxene-chromite mesocumulate. (6A-244)

(C) Orthopyroxene-chromite cumulate. This rather rare rock type makes up the entire thickness of cyclic unit 11 which hosts significant Ni-Cu and PGE mineralization. (X-25)

(D) Orthopyroxene orthocumulate with abundant intercumulus plagiocalse. Note the elongated orthopyroxene which imparts a pronounced igneous lamination to the rock. (X-3)

(E) Resorbed olivine in a olivine-chromite cumulate. The irregular resorbed olivine crystals have been involved in a reaction relationship with the intercumulus liquid to give rise to reaction orthopyroxene. (3-2985)

(F) Olivine adcumulate that forms the foot-wall of the lower chromitite layer. This layer was originally an olivine-chromite cumulate similar to that shown in 8A. (GV-22)

(G) Resorbed olivine in an olivine-chromite cumulate with abundant intercumulus clinopyroxene. This photomicrograph suggests that there is a reaction relationship between olivine and intercumulus liquid to produce clinopyroxene. (78-291)

(H) Orthopyroxene adcumulate with pronounced 120° triple point grain boundary junctions. (78-26)

and because of its abnormally high modal chromite content (5 to 9 per cent) in the upper part of the cycle. Cyclic unit 19, which is believed to be similar to unit 11 has been intersected by drilling; the remainder, an unknown thickness of cumulates which could include several additional cyclic units was removed by faulting and erosion.

Two other incomplete units, different from those described above, are cyclic units 24 to 26. The cumulate succession in unit 24 is ol-chr at the base followed by chromite and opx-ol-chr at the top. This cyclic unit marks the first horizon of enhanced chromite crystallization, whereas cyclic unit 26 has ol-chr cumulates at its base and a chr cumulate at its top.

The Moorddrift Harzburgite-Pyroxenite subzone is similar in many respects to that of the underlying Drummondlea Harzburgite-Chromitite, however the former can be distinguished from the latter by the marked increase in the amount of intercumulus plagioclase (Fig. 7A).

Lateral changes in the stratigraphy are mainly due to variations in the thickness of the various cyclic units, especially thickening in a down-dip direction. The most pronounced change was observed in the Ni-Cu sulfide and PGE mineralized layer on the farm Volspruit. Here the mineralized layer increases in thickness four times when measured 2000 m down-dip from a position 1000 m from the eastern intrusive contact (Fig. 82). Similarily, on the northern portion of Grasvally, the ol-chr cumulates in the hanging-wall of the upper chromitite layer increase in thickness from 24,5 cm to 27,5 cm down-dip over a distance of only 20 m. (Fig. 40). This is equivalent to a change in thickness of 0,6 per cent per metre down-dip compared to 0,15 to 0,20 per cent per metre found on the farm Volspruit.

Such a down-dip increase in thickness is not unusual in layered intrusions and can be expected in this area if the configuration of the intrusion (Fig. 2B) and the location of the study area are taken into consideration. Not only are the layers of the lower and critical zones plunging to the north but the layers are also dipping away from the eastern contact of the intrusion at a fairly steep angle, which gradually flattens with increasing thickness of the layers

towards the centre of the intrusion. An analogous, yet somewhat more extreme situation, is seen in the Jimberlana Intrusion, (Campbell, 1977). A cross section of the Norcott Complex of this intrusion (ibid., Fig. 5) shows that the layers within the upper layered series can increase in thickness at a rate of 0,80 per cent per metre down-dip.

It must be stressed that the stratigraphic column of the lower zone in Figure 7A is a compilation based on three sections along 8 km of strike. Therefore, until such time as further deep drilling confirms a general increase in thickness down-dip, the thickness of the various rock units in Figure 7A could be regarded as a minimum.

Only minor changes in the lateral continuity of the layers were observed when studying the chromitite layers over a strike length of 8 km. The only noticeable change is that the distance between the upper and lower chromitite increases towards the north and that the thin hanging-wall pyroxenite (opx-ol-chr cumulate) of the lower layer dies out on the northern portion of Grasvally. Considerably more striking lateral discontinuities were described by Jackson (1970) over similar distances in the Mountain View and Benbow areas of the Stillwater Complex.

Modal proportions based on point counting (>1000 points per section) 50 different samples from stratigraphic levels in the upper and lower Volspruit Pyroxenite reveal that the opx-ol-chr cumulates contain between 7 to 57 (average 40) volume per cent olivine, 42 to 92 (average 57) per cent orthopyroxene with 0,5 to 8,0 (average 1) per cent chromite. Intercumulus plagioclase was only observed in cyclic units 12 and 14 where it was found to range from 1 to 7 (average 2) per cent. Clinopyroxene was never observed in these rocks (Fig. 7A).

All of the opx cumulates are virtually monomineralic and contain 95 to 99,7 volume per cent bronzite, 0 to 2,5 (average 0,5) per cent chromite, 0 to 4 (average 1,0) per cent intercumulus plagioclase. The highest concentration of plagioclase occurs at the top of unit 12. The opx-chr cumulate of cyclic units 11, 13, 14, 16, and 19 differ from the opx cumulates in that their chromite content ranges from 2,0 to 9,0 (average 5,0) per cent. Their intercumulus plagioclase and clinopyroxene content never exceeds 1,0 per cent and the

remaining portion of the rock consists of small amounts of sulfides (< 3,0 per cent).

The first ol-chr cumulates in the lower zone and the only layer in the Volspruit Pyroxenite subzone is found at the base of cyclic unit 10. In places the rock is an olivine adcumulate (dunite). The olivine content ranges from 60 to 97 (average 78) per cent with 0,5 to 3,0 (average 1,25) per cent chromite. The remainder of the rock consists of between 3 to 37 (average 21) per cent intercumulus orthopyroxene.

Trace amounts of cumulus sulfides occur throughout the succession and consists mainly of pyrrhotite, pentlandite and chalcopyrite. The highest concentrations occur near the top of cyclic unit 10 and at the base of the cyclic unit 11 where concentrations of 2,0 to 3,0 per cent are present.

The Drummondlea Harzburgite-Chromitite subzone consists of cyclic units 20 to 26. It is characterized by significant quantities of ol-chr cumulates, a new cumulate sequence of ol-chr, ol-opx-chr, opx and two thick chromitite layers superior in quality to any other chromitite in the Bushveld Complex. The ol-chr cumulates contain 40 to 70 (average 55) per cent olivine and between 0 to 6 (average 2,5) per cent chromite. Intercumulus plagioclase is relatively abundant in all rock types and ranges from 0 to 8 (average 3,0) per cent in the ol-chr cumulates. Intercumulus clinopyroxene can also be abundant, ranging from 0 to 3,5 (average 1,75) per cent. The opx-ol-chr cumulates from this subzone differ from those in the underlying subzone in that they contain less olivine, on average only about 15 per cent. The levels of modal chromite are similar to those of the ol-chr cumulate. The highest concentrations of intercumulus plagioclase and clinopyroxene are found in these opx-ol-chr cumulates, in particular cyclic unit 21, where averages are 4,0 and 1,0 per cent respectively. The orthopyroxenites also differ from those of the underlying subzone in that they contain much higher concentrations of intercumulus plagioclase, from 6 up to 22,4 per cent, but on average about 15 per cent. Clinopyroxene ranges from 0 to 4 (average 1) per cent.

The chromitite layers are confined to cyclic units 24 and 26 and

contain between 50 to 90 per cent chromite, depending on the position within the layer. Although the Drummondlea subzone will be described in detail in Chapter 5.2 it should be mentioned that the harzburgites within it contain some excellent examples of mineral graded layers and a greater volume of intercumulus material than the underlying Volspruit Pyroxenite subzone. The harzburgites from this Drummondlea subzone are predominantly of the poikilitic variety with large oikocrysts of orthopyroxene poikilitically enclosing early cumulus chadacrysts of olivine and chromite. This distinquishes them from the granular harzburgites of the underlying subzone.

The ol-chr and the opx-ol-chr cumulates of the Moorddrift subzone are very similar to those found in cyclic units 20 to 26. The modal chromite content throughout the section ranges from 1 to 2 per cent except in cyclic unit 31 where four thin chromitite stringers are developed. From bottom to top they are 0,20; 0,20; 10,0; and 2,5 cm thick respectively. The most important feature is the pronounced increase in the amount of intercumulus plagioclase with increasing stratigraphic height, both in the olivine-rich and in the orthopyroxene-rich cumulates (Fig. 7A). The upward increase is from about 2 to 17 volume per cent for the orthopyroxene cumulates and from 2 to 10 per cent for the olivine-rich rocks. The concentration of intercumulus clinopyroxene remains fairly constant at about 1 per cent. Concomitantly with this upward increase in the amount of intercumulus plagioclase the orthopyroxene cumulates particularly change from adcumulates to meso or even orthocumulates, suggesting a relationship between textural type and lithostatic load. The increased lithostatic pressure may be an important factor augmenting grain boundary migration and thus the lower porosity observed in the early lower zone cumulates. Also, the predominance of plagioclase over clinopyroxene as an intercumulus phase suggests that the composition of the magma approached the boundary of the plagioclase phase volume through fractional crystallization, and that plagioclase would have become the next cumulus phase to crystallize from the magma, had it not been for an interruption of the crystallization sequence.

The lower zone sequence is abruptly terminated by an erosional and depositional unconformity at the -130 m level, where the ultramafic rocks make way for fine-to medium-grained pigeonite gabbro and

gabbronorite (Fig. 7B). The emplacements of the critical zone magma has ripped up underlying lower zone cumulates and redeposited them in the critical zone. Evidence for this can be seen at approximately the -112 m level where xenoliths of ol-chr cumulates occur in gabbronorites. The contact relationship in core from numerous boreholes also strongly suggests that the base of the critical zone rests on a highly irregular surface of eroded lower zone, as the gabbronorites can be in contact with ol-chr cumulates, opx-ol-chr cumulates or opx cumulates.

3.2 Variation of Mineral Compositions within the Lower Zone

Analyses of orthopyroxene, olivine and chromite from the lower zone are given in Appendices 1,3, and 7. The $Mg/(Mg+Fe^{2+})$ ratio or Mg* of the orthopyroxene, olivine and chromite as well as the $Fe^{3+}/(Fe^{3+}+Al+Cr)$ ratio or Fe^{3+}* and the weight per cent TiO_2 in the chromite are shown in Figure 7B. A systematic variation in the mineral chemistry of these three phases has been recorded from the 37 cyclic units of the lower zone. The sympathetic trends recorded in these three phases suggest that their chemistry can be used to interpret the crystallization history of the magma(s) that give rise to the lower zone.

The lowest recorded level from which compositional data was obtained is from the base of cyclic unit 3, where the opx and ol have a Mg* of 0,905 and 0,900 respectively. A normal iron enrichment fractionation trend is recorded from this level to the base of cyclic unit 6, from where this trend is reversed abruptly to one of magnesium enrichment up to the -1300 m level. The iron enrichment trend is likely due to normal differentiation of a single batch of magma as a result of continuous fractional crystallization. The reversed trend may be due to continuous introduction and crystallization of more magnesium-rich liquid or due to crystallization under increased fo_2 conditions up to the -1300 m level. From this level to the -1220 m level the Mg* decreases fairly rapidly and is accompanied by the appearance of sulfides, which are particularly abundant at approximately the same level as the minimum recorded Mg*. Once again, a reversal is observed which coincides with increasing amounts of chromite (3 to 8 per cent) from the base towards the top of cyclic unit 11. The trend from the base of cyclic unit 12 to the top of unit 18 is essentially one of iron enrichment, with a relatively minor reversal in cyclic units 13 and

14. Unfortunately very little is known about the compositional trends between cyclic units 18 and 21 because of the gap in the succession and the intense serpentinization of the rock units belonging to cycle 20. The pronounced Mg enrichment of the rocks in the Drummondlea subzone and their enrichment in chromite, together with trace element data on orthopyroxene and olivine which will be presented later, suggests that the Drummondlea subzone crystallized from a new, chromium-rich, magma at higher fo_2 conditions. The reversal of the Mg* at the base of cyclic unit 19 may already be a manifestation of such an influx.

Cyclic units 27 to 30 record the longest period of normal fractional crystallization as seen in the progressive iron enrichment of the differentiates. The Mg* of the orthopyroxene changes from 0,883 to 0,845 over this interval. Both olivine and chromite show the same strong iron enrichment trend.

Compositional data is lacking for units 31 and 32 due to some confusion regarding the disordered nature of the available core. However, there appears to be another magnesium enrichment trend towards the top of cyclic unit 33 and from the base of unit 35 to the top of the lower zone.

The major stratigraphic unconformity at the top of the lower zone is also recorded in a pronounced discontinuity in the composition of primary orthopyroxene in that the Mg* drops from 0,880 to 0,710 (Fig. 7B).

It should be noted that the overall fractionation trends recorded in the cumulus phases of the lower zone is that of iron enrichment. Fractionation also appears to have enriched the residual liquids in TiO_2, which was accommodated in successively higher concentrations in chromite as fractionation proceeded (Fig. 7B). The lowest values are recorded in the Volspruit Pyroxenite subzone, where values remain very constant at about 0,50 weight per cent. The TiO_2 value of chromite from successively younger cumulates increases, so that chromite in the Drummondlea subzone contains an average 1,0 per cent TiO_2, whereas those in rocks of the Moorddrift subzone contain on average 1,3 per cent. Very high TiO_2 values are recorded in the disseminated chromite from the critical zone (Fig. 7B).

The increase in the TiO_2 content of chromite in successively younger cumulates is in accordance with the findings of Evans and Wright (1972), who found that chromite precipitating at progressively later stages from the Kilauea basalts are richer in TiO_2 as a result of an increase in the ulvöspinel molecule in the more differentiated magmas. They also established that a decrease in the MgO content of the chromite is accompanied by a decrease in Al_2O_3, and Cr_2O_3 and by an increase in FeO, Fe_2O_3, V_2O_3, and TiO_2. Figure 7B illustrates a similar antipathetic relationship between magnesium and iron as well as titanium in chromite from the lower zone in the Potgietersrus area.

3.3 Critical Zone

The above discussions have strongly emphasized the presence of a major unconformity at the top of the lower zone. This unconformity is the result of a new influx of magma, the most obvious expression of which is the presence, at the contact, of a fine-grained gabbronorite with its own distinctive textures and mineralogy. It is developed as a marginal facies of variable thickness along the top of the lower zone as well as adjacent to the country rock sediments of the Pretoria Group. This new and distinctive facies is referred to as the marginal member of the critical zone and depending on its position is referred to as the marginal member adjacent the lower zone or the marginal member adjacent the Pretoria Group. The overlying cumulates of the critical zone are, in turn, referred to as the layered member.

3.3.1 The Marginal Member Adjacent to the Pretoria Group. (M.Mb./P.G.)

In the northeastern corner of the farm Grasvally a 210 m wide group of rocks consisting mainly of oxide-rich gabbronorites, with a variety of textures, is developed adjacent the Pretoria Group quartzites (Fig. 9). These rocks do not display any textures reminiscent of crystal settling and they seem to constitute a marginal unit between the layered critical zone cumulates and the floor rocks of the intrusion (Fig. 9).

The most fine-grained, possibly chilled facies of this marginal member occurs as a few loose boulders of aphanitic dark green and light green mafic rocks at the foot of the dip slope of the Pretoria

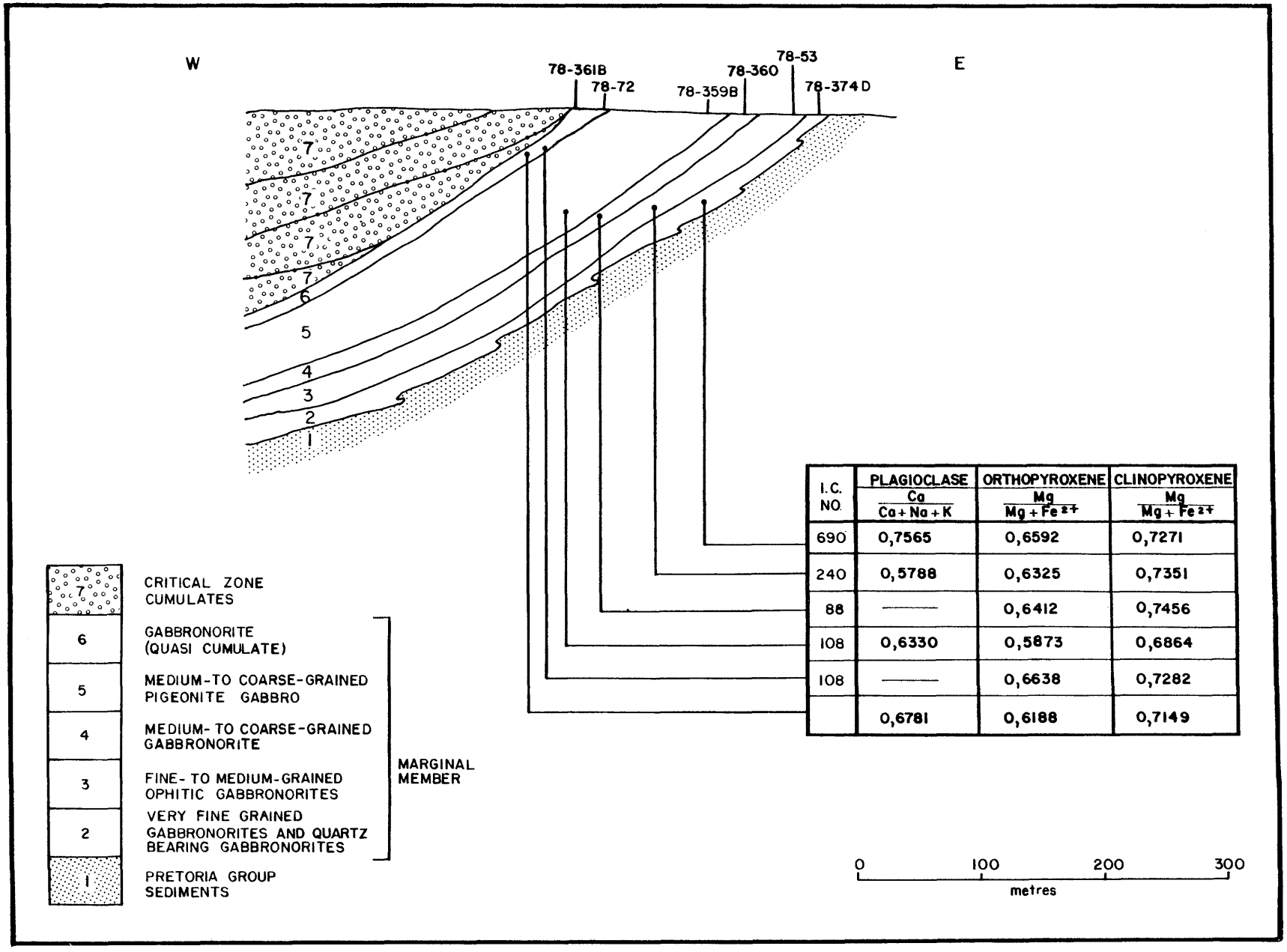

I.C. NO.	PLAGIOCLASE $\frac{Ca}{Ca+Na+K}$	ORTHOPYROXENE $\frac{Mg}{Mg+Fe^{2+}}$	CLINOPYROXENE $\frac{Mg}{Mg+Fe^{2+}}$
690	0,7565	0,6592	0,7271
240	0,5788	0,6325	0,7351
88	———	0,6412	0,7456
108	0,6330	0,5873	0,6864
108	———	0,6638	0,7282
	0,6781	0,6188	0,7149

Fig. 9 Stratigraphic relations, mineral compositions and grain size variation within the marginal member (adjacent the Pretoria Group) of the critical zone as observed in the northeastern corner of Grasvally.

Group quartzites. In thin section, the light green variety is seen to be a fine-grained allotriomorphic granular gabbronorite containing up to 11 per cent quartz. The dark green variety, on the other hand, is a very fresh magnetite-rich gabbronorite, which consists of about 53 per cent plagioclase, 15 per cent clinopyroxene, 25 per cent orthopyroxene and 7 per cent ore minerals, essentially titaniferous magnetite and ilmenite (Fig. 10A).

Away from the contact these very fine-grained rocks pass into a fine-to medium-grained ophitic gabbronorite (sample 78-53, Fig. 9 and 10C) which contains approximately 57 per cent plagioclase, 15 per cent orthopyroxene, 25 per cent clinopyroxene and 3 per cent ore minerals. The grain size can vary from fine-to medium-grained and the proportions of orthopyroxene to clinopyroxene can be variable. The next two rock types further away from the contact differ little in their macroscopic appearance, as both have roughly equal amounts of plagioclase (≈60 per cent) Fe-Ti oxides (≈0,60 per cent) and ubiqutous phlogopite (2 to 5 per cent). Microscopically these rocks differ in that the one is a gabbronorite and the other a pigeonite gabbro, i.e. samples 78-360 and 78-359B respectively (Fig. 9). In a typical pigeonite gabbro the core of the Ca-poor pyroxene consists of hypersthene rimmed by inverted pigeonite. These rocks originated as a result of the reaction: hypersthene + liquid $\rightleftharpoons$ pigeonite.
The zoned Ca-poor pyroxene may be the result primary hypersthene coming in contact with more Ca- and Fe-rich interstial liquid (Nakamura and Kushiro 1970). These two rock types characteristically contain between 3 and 5 per cent interstial quartz (Fig. 10H). The quasi-cumulates commonly have a spotted texture like the norites from the layered sequence, but they differ from these layered cumulates in that they are richer in quartz and clinopyroxene and possess a non-cumulate texture when observed in thin section. Other distinguishing features are the strongly zoned nature of the orthopyroxene and plagioclase in these rocks and the presence of phlogopite (Fig. 9).

The variation in grain size of the successively higher rock units was estimated by using the I.C. number of Chayes (1956), a method which is a measure of the grain size of a rock calculated from the

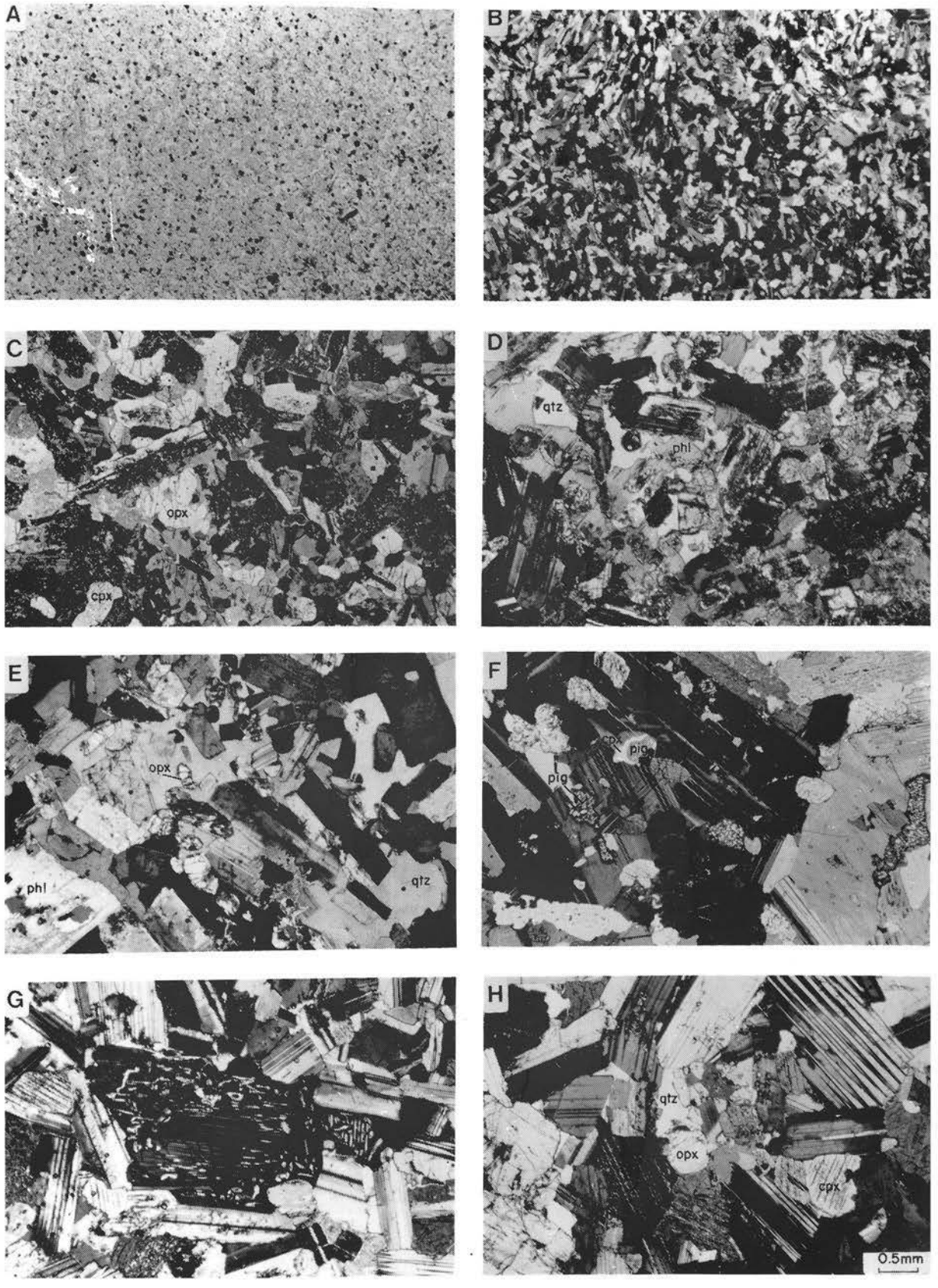

Fig. 10

Figure 10. Photomicrographs of rocks from the marginal member adjacent the Pretoria Group. opx = orthopyroxene; pig = inverted pigeonite; phl = phlogopite; qtz = quartz; cpx = clinopyroxene. All sections except A have been photographed with transmitted light under crossed nicols. Magnification is the same for all photomicrographs, see Fig. 10H. Sample numbers are indicated in brackets.

(A) Dark green gabbronorite from a chill. Note the very fine-grained allotriomorphic granular texture and the Fe-Ti oxide-rich nature of the sample. (78-374D)

(B) Fine-grained hypidiomorphic granular gabbronorite with interstitial quartz. (GR1-69)

(C) Medium-grained gabbronorite containing dark, zoned plagioclase. The cores of the plagioclase crystals are turbid as a result of rapid growth of the skeletal plagioclase and incorporation of melt. (78-53)

(D) Contaminated medium-grained gabbronorite containing large interstitial patches of quartz and phlogopite, which poikilitically encloses numerous grains of orthopyroxene, clinopyroxene, plagioclase and ore minerals. (GR1-102,5)

(E) Contaminated gabbronorite with large optically continuous interstitial quartz grains and large Fe-Ti oxide crystals with mantles of phlogopite. (GR1-100)

(F) Pigeonite gabbro with mantles of augite around partially resorbed, inverted pigeonite suggesting a reaction relationship between pigeonite and liquid. (GR1-44,8)

(G) Coarse-grained pigeonite gabbro. The Ca-poor pyroxenes in this rock type are unusual in that they contain cores of hypersthene and rims of inverted pigeonite. (78-71)

(H) Quasi-cumulate. The orthopyroxene crystals are starting to develop a spotted appearance in the rock like that of the spotted norites and anorthosites that overlie this unit of the M.Mb./P.G. Note the presence of interstitial quartz. (78-72)

number of mineral grain boundries encountered in a 40 mm traverse across a thin section. Representative samples 78-374D, 78-53, 78-359B, and 78-72 (Fig. 9) have I.C. numbers of 690, 240, 108, and 108 respectively.

The cross-section shown in Figure 9 is constructed on the basis of field relations of the mafic rocks that border the Pretoria Group sediments. On the basis of these field relations it was initially assumed that the various fine-grained units of the marginal member crystallized essentially conformable to the floor contact of the intrusion and that no pronounced incising of magma into the sediments took place, since virtually no inclusions of Pretoria Group sediments were found in outcrops of the marginal member. This earlier assumption and somewhat simplistic impression of the marginal member and its contact with the floor had to be revised subsequently, when results of a diamond drill hole intersection (DDH-GR1) drilled by Billiton Exploration Ltd. became available. This hole was collared 1500 m south of the area on which Figure 9 is based. A columnar section of borehole GR1 is shown in Figure 11B whereas 11A represents an idealized section across the contact zone, based on the relationship of the rock types intersected in the borehole.

Unlike the section to the north, the very fine-grained gabbronorites, quartz bearing gabbronorites and the fine-to medium-grained ophitic gabbronorites could be lumped into a mixed zone of gabbronorite. This mixed zone is intercalated with feldspathic quartzites and granitoids, the latter of which probably represents partial floor melts, which subsequently formed irregularly shaped masses of granitoid material.

Apart from the intimate interfingering of sediments and basic igneous material a noteable feature is the pronounced variation in grain size of the igneous rocks (Fig. 11B). For example, the sample from the 69 m level has an I.C. number of 534 whereas that at 102,5 m is more than twice as coarse-grained with an I.C. number of 262. Table 1 shows that there is, apart from phlogopite, very little difference in the modes of these two rocks, even with respect to their quartz content which may reflect similar degrees of contamination. The reason for the coarse grain size of sample GR-102,5 is considered to be due to a higher initial water content, which is reflected by

A.

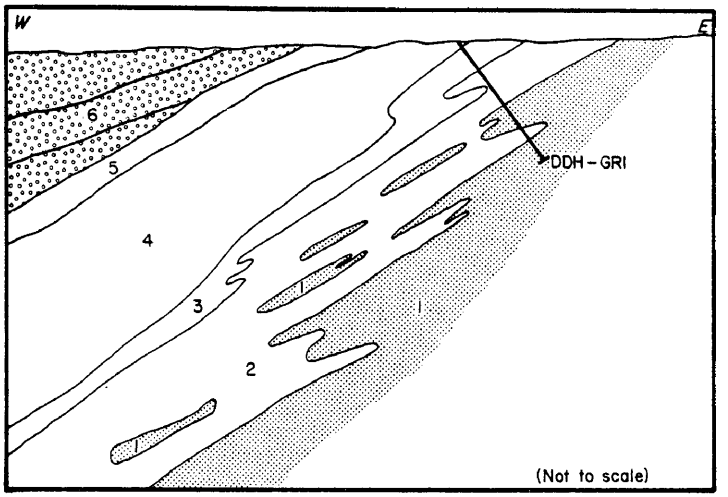

6 CRITICAL ZONE CUMULATES
5 GABBRONORITE ZONE (QUASI CUMULATE)
4 OXIDE RICH PIGEONITE GABBRO ZONE
3 OXIDE RICH GABBRONORITE ZONE
2 MIXED ZONE GABBRONORITES
1 PRETORIA GROUP SEDIMENTS

B.

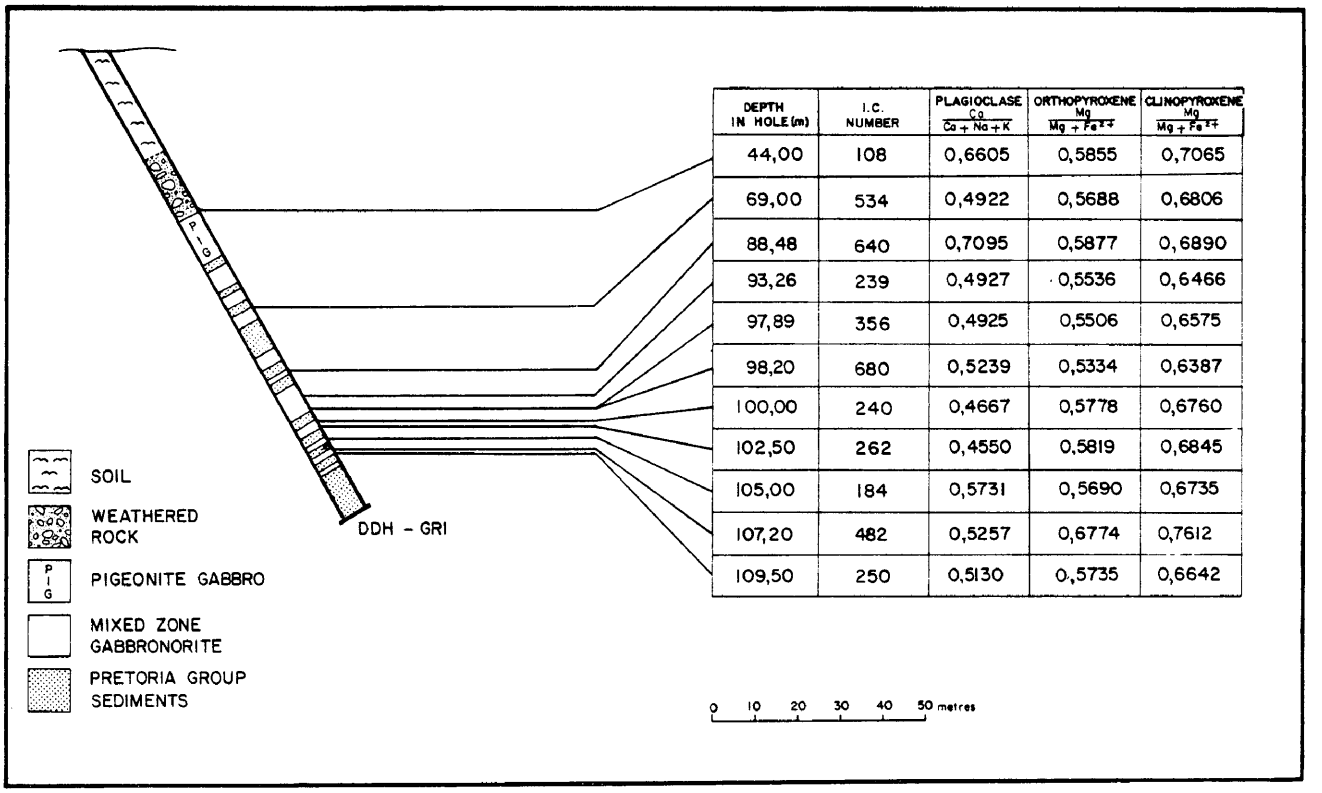

DEPTH IN HOLE (m)	I.C. NUMBER	PLAGIOCLASE $\frac{Ca}{Ca+Na+K}$	ORTHOPYROXENE $\frac{Mg}{Mg+Fe^{++}}$	CLINOPYROXENE $\frac{Mg}{Mg+Fe^{++}}$
44,00	108	0,6605	0,5855	0,7065
69,00	534	0,4922	0,5688	0,6806
88,48	640	0,7095	0,5877	0,6890
93,26	239	0,4927	0,5536	0,6466
97,89	356	0,4925	0,5506	0,6575
98,20	680	0,5239	0,5334	0,6387
100,00	240	0,4667	0,5778	0,6760
102,50	262	0,4550	0,5819	0,6845
105,00	184	0,5731	0,5690	0,6735
107,20	482	0,5257	0,6774	0,7612
109,50	250	0,5130	0,5735	0,6642

Fig. 11 (A) Idealized cross-section of the marginal member (adjacent the Pretoria Group) of the critical zone, 1500 m south of the section shown in Fig. 9.

(B) Detail of the intersected rock sequence in borehole DDH-GR1, as well as mineral compositions and grain size variation of the lower half of the M.Mb./P.G.

Table 1 MODES AND GRAIN SIZE VARIATION (I.C. NO) FOR MARGINAL MEMBER ROCKS

	Sample #	Plagioclase	Orthopyro= xene	Clinopyro= xene	Olivine	Ore Minerals	Biotite	Quartz	Amphibole	Apatite	I.C. No	Comments
*	GR1-44	54,93	17,95	26,57	-	trace	0,53	-	-	-	108	all opx=inv.pig.
*	GR1-69	61,81	12,25	13,35	-	3,86	0,99	7,72	-	-	534	
*	GR1-97,89	60,57	11,36	12,82	-	2,13	4,94	7,58	0,56	-	356	
*	GR1-98,20	61,20	14,04	10,37	-	4,02	1,22	9,00	0,12	trace	680	
*	GR1-100	61,45	12,59	6,98	-	2,88	2,88	10,16	3,03	-	240	
*	GR1-102.5	61,50	10,39	10,39	-	2,43	5,75	9,51	-	trace	262	
*	GR1-107.2	40,40	45,05	11,11	-	0,40	2,82	0,20	-	-	482	
*	H-78-72	64,58	17,36	12,15	-	0,52	1,04	4,34	-	-	108	
*	H-78-359B	60,86	13,61	15,87	-	0,56	4,15	4,91	-	-	108	opx=inv. pigeonite
*	H-78-360B	58,46	22,78	11,69	-	0,60	2,62	3,83	-	-	88	
*	H-78-53	56,94	15,50	24,76	-	2,77	trace	-	-	-	240	
*	H-78-374D	53,27	24,92	14,95	-	6,85	trace	-	-	-	690	
**	GR4-6	49,38	27,37	13,45	-	9,63	0,15	-	trace	-	80	
**	GR4-4	60,05	22,52	17,42	-	-	-	-	-	-	160	opx=inv.pigeonite
**	GR4-1	54,71	40,45	4,82	-	-	-	-	-	-	164	

* Marginal Member of Critical Zone adjacent the Pretoria Group
** Marginal Member of Critical Zone overlying the lower zone

the higher concentration of phlogopite (5,77 per cent) compared to 0,99 per cent for the sample at the 69 m level. Figures 10B and D illustrate these two contrasting textural types; sample GR1-69 being allotriomorphic granular with fine interstitial quartz, whereas the coarser variety (Fig. 10D) from the 102,5 m level contains coarse interstitial quartz and phlogopite, which poikilitically encloses numerous grains of orthopyroxene, clinopyroxene, plagioclase and ore minerals.

The plagioclase is usually extensively zoned (normal zoning) and in some cases resorbed by quartz. The plagioclase in the marginal member adjacent the Pretoria Group are unique compared with that found elsewhere in the complex in that it commonly has turbid to cloudly iron-rich cores (Fig. 10C and D). These plagioclase features reflect periods of rapid crystal growth in which melt was trapped in the skeletal crystals and subsequently crystallized as glass. Similar textures were observed by Luhr and Carmichael (1980) from the post-caldera andesites of the Colima Volcanic Complex, Mexico.

Although mica (biotite, phlogopite) may be abundant in these rocks amphibole seldom exceeds half a per cent when present, and the maximum concentration recorded is 3,03 per cent (Table 1).

At the 44 m level of DDH-GR1 (Fig. 11B) a distinctive pigeonite gabbro is developed. It lacks signs of country rock contamination and can be distinguished from the previously described pigeonite gabbro to the north in the that the grains of the inverted pigeonite are poikilitically enclosed in plagioclase (Fig. 10F). Evidence for the reaction: Pigeonite + liquid $\rightleftharpoons$ augite + tridymite (Morse 1980A) is demonstrated by the development of mantles of augite around the pigeonite (Fig. 10F).

The very fine-grained allotriomorphic granular textures seen in Figure 10A evidently developed in response to rapid cooling and may be related to the observations that nucleation rates seem to peak at lower temperatures than crystal growth rates (Carmichael et al. 1974). The magma from which the slightly coarser grained hypidiomorphic sample seen in Figure 10B crystallized seems to have cooled more slowly, due to a higher water content as recorded

by the presence of 0,99 per cent phlogopite in this sample compared to the virtual absence of this hydrous phase in the very fine-grained rocks. The extremely large poikilitic phlogopite crystals shown in Figure 10D are considered to have formed at even slower cooling rate of the magma, under conditions of much higher water pressure than in the previous cases. It is, however, not only the slower cooling rate that contributes to the growth of large crystals, but also the entropy of melting which controls to a very large extent the nucleation and growth rate of compounds in melts. Since the nucleation rate and the growth rate are known to be respectively inversely proportional and proportional to the entropy of melting, ophitic and poikilitic textures are to be expected at intermediate cooling rates (Carmichael et al. 1974).

Since the plagioclase has a significantly lower entropy of melting than pyroxene, a larger number of plagioclase nucleii are to be expected in rapidly cooled rocks. This is substantiated by the fact that rocks of the marginal member with higher I.C. numbers have a greater proportion of plagioclase to pyroxene crystals. The relatively slow growth rate of plagioclase nucleii enhances the development of ophitic textures owing to the lower nucleation rate yet faster growth rate of the pyroxenes.

Iron titanium oxides can also attain unusually large grain sizes in the marginal rocks (Fig. 10E) and can also be related to high entropy of fusion values for these two minerals (Carmichael et al., 1974, p. 167).

The general coarsening of the grain size of the marginal member rocks away from the contact also reflects a decrease in the cooling rate of the magma towards the west, caused by the thermal insulation provided by the ever thickening marginal member.

3.3.2 Variations of Mineral Compositions Within the Marginal Member Adjacent to the Pretoria Group

Atomic ratios of primary silicate phases in two sections were calculated from electron microprobe analyses and are tabulated in Figures 9 and 11. The analyses show a somewhat irregular decrease in the Mg* of the orthopyroxene in the northern section from 0,659 in the very fine-grained gabbronorite at the contact to 0,587 in the

pigeonite gabbros in the middle of the marginal member. Although the data are limited a reversal from the middle of the marginal member through to the quasi-cumulates where a value of 0,618 was recorded, is suggested. The Mg* of the coexisting clinopyroxenes suggests a similar trend. Fewer data points are available for plagioclase,nevertheless they also suggest a higher Ca/(Ca+Na+K) ratio or Ca* near the contact and the top of the marginal member than in the middle.

The iron and sodium enrichment trends from the very fine-grained gabbronorite contact to the pigeonite gabbro are accompanied by a progressive coarsening in grain size from I.C. numbers of 690 to 108 together with a change of fabric from allotriomorphic granular to ophitic and finally idiomorphic granular. These features could represent a cooling profile within a differentiating liquid. The eventual adjustment of the magma at this level to the equilibrium conditions prevailing in the layered sequence is inferred on the basis of textures observed from levels approaching the layered sequence. The somewhat asymptotic chemical profile recorded in the various mineral phases is believed to represent the temperature profile present during the evolution of the marginal member adjacent the Pretoria Group.

In the southern section (Fig. 11) the compositional variation found in the orthopyroxenes, clinopyroxenes and plagioclase differs significantly from that found in the north. Explanation of these variations in composition is extremely complicated and is believed to represent a combination of conditions not experienced to the same degree by the magma in the north. Examination of data pertinent to the pyroxenes from samples at the 98,20; 97,89; and 93,26 m level in borehole GR1 reveals that as the I.C. number drops from 680 to 356 and 239 respectively the Mg* of the orthopyroxene increases from 0,533 to 0,550 and 0,553. Also in a general way the samples from the 100,00; 102,50; and 109,5 m level all have I.C. numbers between 240 and 262 and a Mg* restricted to 0,573 - 0,581. This relationship between composition and grain size for the lower half of this diamond drill hole intersection suggests that the water content of the melt could have influenced the resulting grain size, as well as the composition. Higher water pressures would give rise to elevated oxygen fugacity conditions

and thus a higher Mg* in the pyroxenes (Luhr et al., 1980; Hill and Roeder, 1974; Hamilton et al., 1964; Irvine, 1965; Biggar, 1974; Roeder and Emslie, 1970; Sack et al., 1980; Clark and Biggar, 1972A).

The postulated high fo_2 may also explain the relatively high concentrations of clinopyroxene in the marginal member since augite accepts higher concentrations of Fe^{3+} which may stabilize its existence in the melt (Biggar, 1974). This is substantiated by the virtual absence of clinopyroxene in a sample of the critical zone chill adjacent the Archean granite from the farm Overysel 815LR north of Potgietersrus, where considerably less contamination of the magma by water from the immediate wall rocks was likely.

The composition of the plagioclase shows the most variation (Fig. 11). In theory an increase in the fo_2 due to an increase in the water content of the magma should increase the Ca* of the plagioclase. The lack of systematics with respect to the plagioclase is believed to be the result of the variable activity of Na_2O in the system and not the water content. Melting of albite-rich feldspathic quartzites to produce granitic melts could have resulted in localized contamination of the basaltic liquid. Varying degrees of contamination by sodium-rich emanations from the floor-rock is therefore considered the reason for the unsystematic Na_2O compositions of the plagioclase feldspars, and any influence the water content may have had on the composition of the plagioclase could therefore have been masked.

It is furthermore of interest that the variation in the Mg* for the orthopyroxene from the fine-grained gabbronorites of the lower half of the marginal member in the north are noticeably higher (0,59 - 0,66) than those of orthopyroxene from the correlated rock units in borehole GR1, which have values ranging from 0,53 to 0,59. Assuming that the fo_2 in the magma was approximately the same in both studied sections, then the magma to the north may be slightly less differentiated. Similar variations in compositions of minerals between the upper and lower chilled margins of the Prospect alkaline diabase sill, New South Wales were noted by Wilshire (1967). Also, similar fluctuations in the forsterite content of olivines from the same stratigraphic level have been recorded by Hoover (1978) over similar strike separations in a detailed study of the Marginal Border Group of the Skaergaard Intrusion. This also

found, as in this study, considerable irregularity in trends normal to the strike of the Marginal Border Group. His study did however reveal a better defined succession of rock units along the margin which is equivalent in composition and crystallization order to that found in the layered series than in this study area.

3.3.3 The Marginal Member Adjacent to the Lower Zone (M.Mb./L.Z.)

This member of the critical zone is approximately 50 m thick and is situated between the top of the lower zone and the foot-wall of the UG2-like chromitite layer. There is little doubt that the basal portion of this member is of the same age as the M.Mb./P.G.

Directly in contact with the lower zone is a 260 mm thick layer of fine-to medium-grained gabbronorite (Figs. 12 and 14A). This rock type is overlain by a 100 mm thick layer of fine-to medium-grained pigeonite gabbro. Overlying this gabbronorite is a 200 mm thick layer of coarse-grained to pegmatitic sulfide bearing gabbronorite with a grain size of about twice that of the underlying rock (Fig. 12). Modal analyses of the rocks intersected in DDH-GR4 (Table 1) illustrates the orthopyroxene-rich nature of the rocks at the base and their upward enrichment in clinopyroxene.

The sequence just described could be considered as a thin (580 mm) cyclic unit similar to at least five other much thicker cyclic units which constitute the bulk of the 50 metre thick M.Mb./L.Z. A more detailed description of the remaining 50 metres will be given in a later section dealing with the sulfide and PGE mineralization in this marginal member of the critical zone. It may be mentioned at this stage that each successive cycle is systematically enriched in sulfide Cu, Ni, and PGE. This upward enrichment trend, accompanied by fine-grained rocks at the base of each cycle, suggests that the marginal member crystallized from at least five influxes of magma, each of which represents the product of mixing of a new influx and the residual liquid from which the previous cycle crystallized. As a result of this mixing process the new liquid in the chamber could have become significantly undercooled to produce the fine-grained basal portion of each cycle.

Exposures, borehole information and I.P. geophysical data along the eastern portion of the area has shown that the mineralized gabbro-

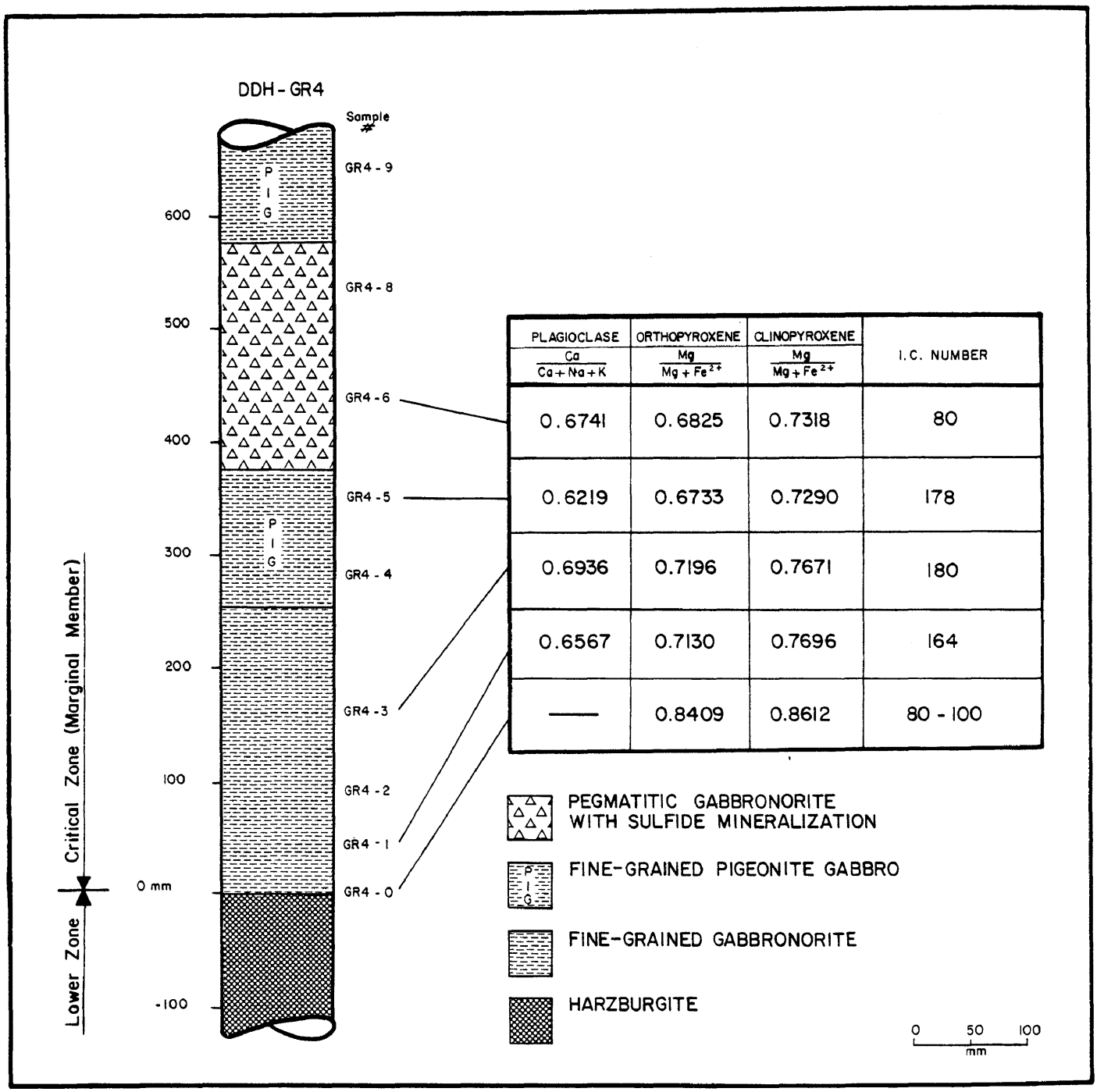

PLAGIOCLASE $\frac{Ca}{Ca+Na+K}$	ORTHOPYROXENE $\frac{Mg}{Mg+Fe^{2+}}$	CLINOPYROXENE $\frac{Mg}{Mg+Fe^{2+}}$	I.C. NUMBER
0.6741	0.6825	0.7318	80
0.6219	0.6733	0.7290	178
0.6936	0.7196	0.7671	180
0.6567	0.7130	0.7696	164
——	0.8409	0.8612	80 - 100

Fig. 12 Detailed petrological relations observed in the lowest unit of the marginal member (of the critical zone) overlying the lower zone as intersected in borehole DDH-GR4.

norites do not extend beyond the confines of the lower zone rocks.

3.3.4 Variation of Mineral Compositions within the Marginal Member Adjacent the Lower Zone

Variations in the Ca/(Ca+Na+K) of the plagioclase and the $Mg/(Mg+Fe^{2+})$ in the pyroxenes are shown in Figure 12. As mentioned earlier, the drop in the Mg* of the orthopyroxene from 0,840 at the top of the lower zone to 0,713 at this contact is the most extreme encountered in the 3250 m of cumulates in the study area. The Mg* seems fairly constant in the fine-grained gabbronorite and decreases to 0,673 in the pigeonite gabbro. Specks of sulfide become visible near the top of the layer and increase up to 9,63 weight per cent in the overlying pegmatitic gabbronorite where the Mg* of the orthopyroxenes shows a slight increase. The reason for this increase, although slight, is believed to reflect an increase in the fo_2 of the crystallizing magma. The Ca* in the plagioclase seems to vary sympathetically with the trends established for orthopyroxene.

One of the striking and distinctive features both in this section and in the two sections of the M.Mb./P.G. is the abundance of inverted pigeonite. There is, however a noticeable difference in their $Mg/(Mg+Fe^{2+})$ ratio, which is considerably higher in the rocks adjacent to the lower zone (0,673) than those adjacent to the Pretoria Group (0,585). The difference in composition of the pigeonite must be ascribed to a higher MgO content of the magma in the area adjacent to the lower zone. This early crystallization of pigeonite found in both marginal members is unique, in that it is the only occurrence of pigeonite in rocks associated with the critical zone, with the exception of one local occurrence of inverted pigeonite as an intercumulus phase in a mottled anorthosite.

Available data on the Mg* of the pyroxenes and the Ca* of the plagioclases indicates an upward increasing trend towards the UG2-like chromitite layer (Fig. 13).

3.3.5 The Layered Member

A columnar section of the critical zone as developed on Grasvally is presented in Figure 13. The stratigraphic relations seen in this Figure are those most frequently observed and it must be stressed that a few layers do vary considerably along strike.

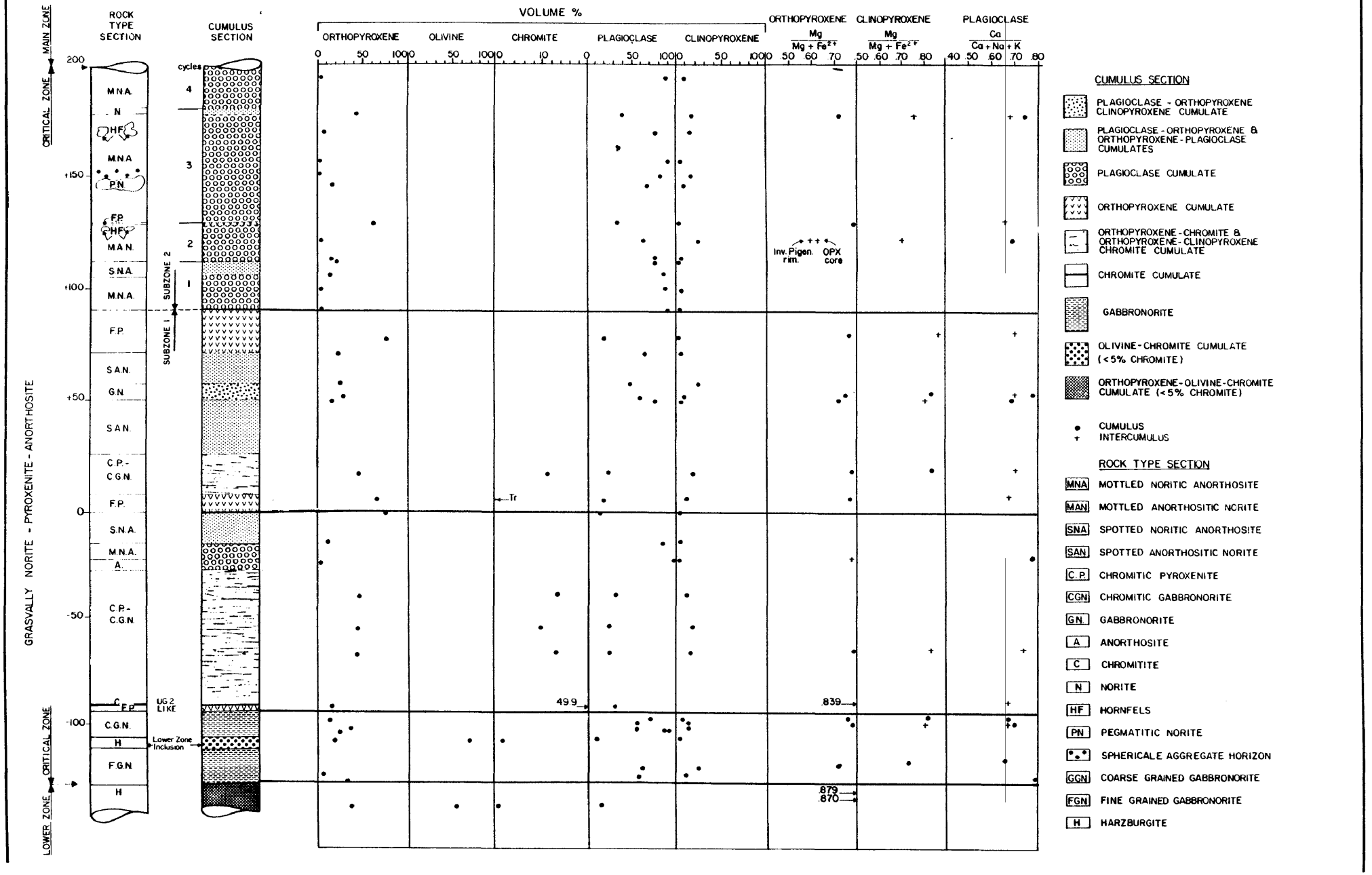

Fig. 13 Stratigraphic column, modal analyses and compositional data for orthopyroxene, clinopyroxene, and plagioclase of the critical zone.

Resting conformably on top of the fine-grained gabbronorites of the M.Mb./L.Z. is the UG2-like chromitite layer and its immediate foot-wall pyroxenite. This chromitite is a chromite orthocumulate, approximately 0,80 m thick, and contains on average 50 volume per cent chromite. The chromite is set in a matrix of varying proportions of intercumulus plagioclase, orthopyroxene, and clinopyroxene with the plagioclase and pyroxenes constituting 30 and 20 volume per cent of the rock respectively (Figure 14B). The foot-wall pyroxenite is similar to other feldspathic pyroxenites in the overlying sequence, except that it contains 3 to 4 per cent disseminated sulfide blebs.

The UG2-like chromite cumulate is overlain by medium-grained opx-chr and opx-cpx-chr cumulates. The modal proportions of both rock types are very similar, the difference being that some of the clino-pyroxene in the more subordinate opx-cpx-chr cumulate is definitely of cumulus origin. On average, these rocks contain 40 per cent orthopyroxene, 11 per cent chromite, 29 per cent plagioclase and 20 per cent clinopyroxene. Plagioclase is always intercumulus as is the clinopyroxene in the opx-chr cumulate. Initial porosities of up to 50 per cent were present in these orthocumulates (Fig. 14C).

The opx-cpx-chr cumulate (chromitic gabbronorite) seems unique to the Potgietersrus limb of the Bushveld Complex as no such rock has been described from other localities in the Bushveld Complex. Similar rocks are developed on the farm Overysel which is situated in the north-central part of the limb.

The recognition of this cumulus association has significant genetic connotations because it is generally regarded that the termination of chromite crystallization can be related to a liquid-spinel-pyroxene reaction relationship which produces a chrome-rich clino-pyroxene. Spinel crystallization in a fractionating magma is sub-sequently resumed when the concentrations of Fe and Ti increases to levels sufficient to enable titaniferous magnetite to crystallize (Irvine 1967A). However, chromite grains in contact with clinopyroxene as well as orthopyroxene show no signs of a reaction relationship. It is believed that this reaction relationship does occur, but only at lower oxygen fugacities than those which prevailed during crystal-lization of these rocks. Hill and Roeder (1974) have demonstrated

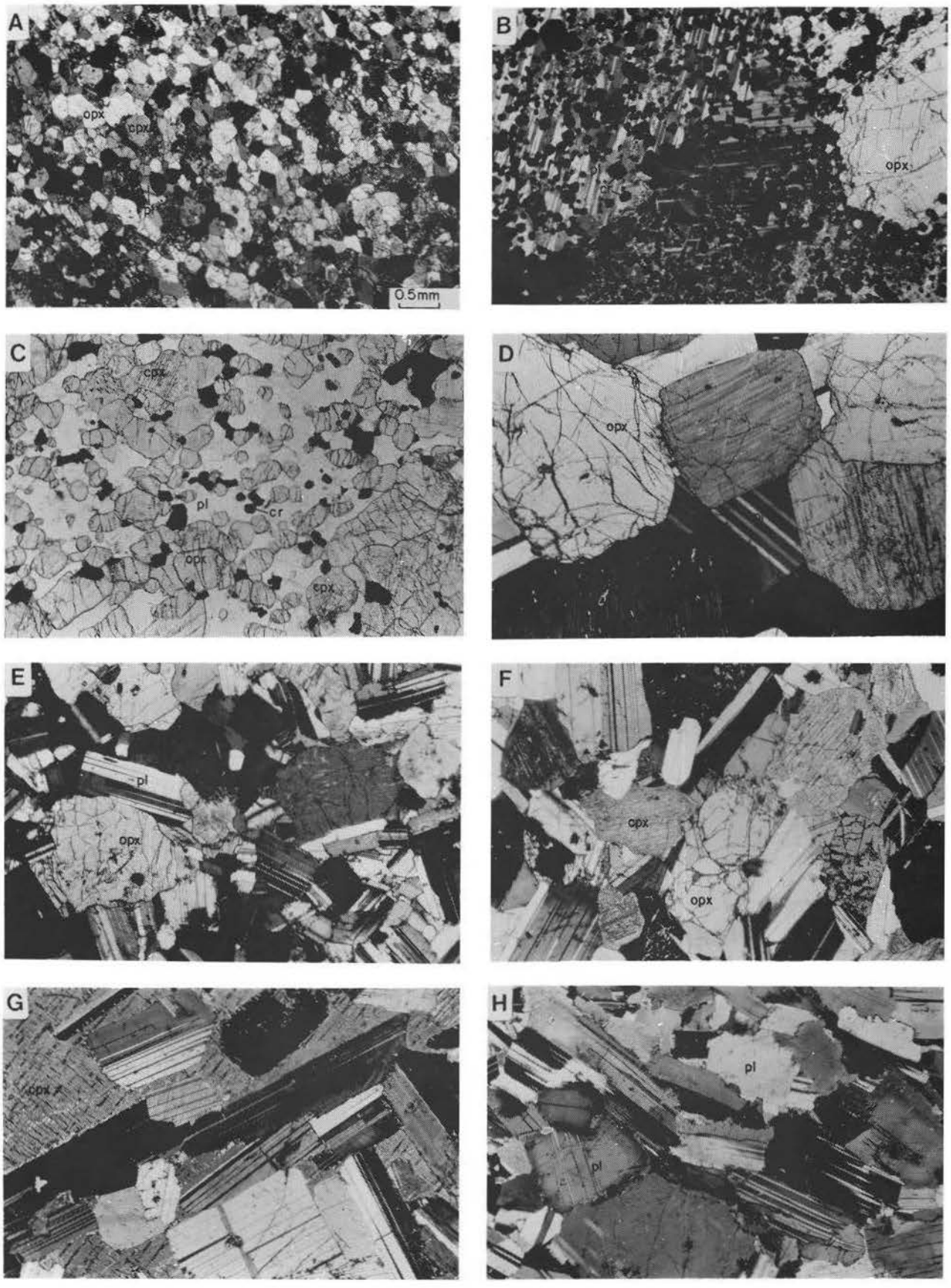

Fig. 14

Figure 14. Photomicrographs of rocks from the M.Mb./L.Z. and the layered member of the critical zone. opx = orthopyroxene; cpx = clinopyroxene; cr = chromite; pl = plagioclase. All sections except C have been photographed with transmitted light under cross nicols. Magnification is the same for all photomicrographs, see Fig. 14A. Sample numbers are indicated in brackets.

(A) Fine- to medium-grained gabbronorite of the M.Mb/L.Z. directly above the lower zone. (GR4-1)

(B) The UG2-like chromitite is a chromite orthocumulate with approximately 50 per cent chromite. Note the large quantity of intercumulus plagioclase in the section. (78-160A)

(C) Orthopyroxene-chromite orthocumulate from the hanging-wall of the UG2-like chromitite. This rock originally had a porosity of approximately 50 per cent prior to crystallization of the intercumulus plagioclase. (78-413)

(D) Orthopyroxene orthocumulate from the "O" datum. All of the plagioclase present in this sample is intercumulus. (78-405)

(E) Typical plagioclase-orthopyroxene cumulate. (78-365)

(F) The first plagioclase-orthopyroxene-clinopyroxene cumulate in the critical zone. (78-373)

(G) Plagioclase cumulate with large intercumulus patches of clinopyroxene which poikilitically enclose cumulus plagioclase laths. (78-68A)

(H) Plagioclase adcumulate with sutured grain boundaries caused by postcumulus resorption. (78-133)

that at fo_2 conditions greater than $10^{-8,6}$ atm there is no interruption in the crystallization of chromite when clinopyroxene crystallizes, because there is sufficient ferric iron in the melt to stabilize the spinel. Thus it would seem as if ferric iron plays a more important role in stabilizing the spinel than the relatively small amounts of chrome in the magma. This would also suggest that the major reason for the discontinuity in composition between chromite and magnetite in layered intrusions is due to low oxygen fugacity conditions during the middle stages of fractional crystallization of the magma.

The thickness of this composite opx-chr and opx-cpx-chr cumulate layer was found to be highly variable and only 10 m thick some 500 m south of the area from which the section on Figure 13 is based. Unfortunately it is difficult to ascertain whether the thickness of this layer indicated on Figure 13 is primary or the result of duplication due to faulting.

This rock type passes upwards into a thin plagioclase adcumulate which in turn grades into a pl-opx mesocumulate. The former consists of 95 per cent plagioclase and 5 per cent intercumulus orthopyroxene, whereas the latter consists of 80 per cent plagioclase, 15 per cent orthopyroxene and 5 per cent intercumulus clinopyroxene. No chromite is present in these plagioclase-rich cumulates. These anorthositic layers define the onset of a common cumulate cyclic sequence found here and at higher stratigraphic levels, i.e. pl cumulates grading upwards into pl-opx cumulates. This is similar to Irvine's (1970, Table II) crystallization order 11.

The base of the overlying orthopyroxene cumulate (Fig. 14D) or feldspathic pyroxenite occurs at the zero ("0") datum level. This orthopyroxene orthocumulate is 7 m thick and has 3 to 4 weight per cent sulfides near its base. It, in turn, passes upwards into a opx-chr orthocumulate and finally into a opx-cpx-chr orthocumulate similar to that in the immediate hanging of the UG2-like chromitite layer. Available modal analyses show a mineral grading from the zero datum to the +25 m level with respect to orthopyroxene, plagioclase and clinopyroxene (Fig. 13).

The succession from the +25 to +50 m level consists of pl-opx

cumulates (Fig. 14E) similar to those encountered at the -10 m level. At the +50 m level this rock grades via a phase contact into a 6 m thick pl-opx-cpx cumulate (Fig. 14F). This succession is therefore also suggestive of Irvine's (1970) crystallization order 11; pl, pl-opx, pl-opx-cpx and governed by the liquidus crystallization order pl, opx, cpx. Although basal plagioclase-only cumulates where not observed at this level, the observed order pl, pl-opx cumulates from below the zero datum suggest this crystallization sequence.

The overlying layer is again a pl-opx mesocumulate similar to those previously described, except for its spectacular enrichment in sulfides over 44-50 cm near its upper contact with the overlying feldspathic pyroxenite. It is thought that a new batch of magma was emplaced during the final stages of crystallization of the pl-opx cumulate which resulted in the separation of an immiscible sulfide liquid, followed by the crystallization of the overlying opx cumulate. The sulfide-rich pl-opx mesocumulate consists on average of 20 per cent orthopyroxene, 70 per cent plagioclase, 7 per cent clinopyroxene and 3 per cent sulfides with a high pentlandite to pyrrhotite ratio. The overlying coarse grained opx cumulate consist of about 75 per cent cumulus orthopyroxene, 20 per cent intercumulus plagioclase and 5 per cent intercumulus clinopyroxene. This pyroxenite layer forms the top of subzone 1.

With the exception of thin layers of pl-opx cumulate at the +110 m and +180 m level and a very thin opx cumulate at the +127 m level, subzone 2 consists almost entirely of plagioclase-rich cumulates like those shown in Figure 14G and H. Plagioclase is the only cumulus phase in the mottled anorthosites in which the mottles consist of large oikocrysts of clinopyroxene or orthopyroxene. Interstitial inverted pigeonite and even quartz may be present. Sutured or embayed grain boundaries are characteristic of several of the anorthosites (Fig. 14H), a feature that may have been caused by local postcumulus resorption. Identical textural features from the Skaergaard Intrusion have been referred to as plagioclase-plagioclase resorption by Maaløe (1976).

Three other horizons within this anorthositic subzone are worthy of note, because of their sulfide content. The first of these is at the

+150 metre level where spherical orthopyroxenite bodies, 20 to 60 mm in diameter, are developed over a 5 m thickness in the mottled anorthosite. The spherical bodies are similar to the spherical aggregates described by Lee and Sharpe (1979). It is envisaged that the abundant nearby country-rock xenoliths contaminated the magma to produce spherical aggregates in a similar fashion as envisaged by Lee and Sharpe (1979) and that water liberated from these xenoliths increased the oxygen fugacity in the melt and caused the precipitation of sulfides.

The other two levels where trace amounts of sulfides occur are at the +125 m and the +180 m levels and, similarly to the +150 m level, their presence is closely associated with inclusions of sedimentary material.

If Irvine's (1970) liquidus crystallization order; pl, opx, cpx is used to produce the cumulus sequence pl; pl-opx, pl-opx-cpx, four incomplete or beheaded cyclic units can be distinquished in this plagioclase-rich subzone, i.e. 1) pl; pl-opx, 2) pl; pl-opx, 3) pl; pl-opx 4) pl. Although the top of cycle 2 is indicated as a feldspathic pyroxenite or opx cumulate on Figure 13 cumulus plagioclase may be developed in this layer at various places along strike.

The sudden increase and the persistently high modal values of cumulus plagioclase as well as its consistent, high An component within this subzone may possibly be due to the assimilation of very aluminous as well as calcareous sediments. It is estimated that at least 10 per cent of this subzone is made up of highly metamorphosed xenoliths of sedimentary material. Some of these xenoliths consist of over 75 per cent aluminous spinel which contains 61 weight per cent Al_2O_3, whereas other, more carbonate-rich material, has been metamorphosed to grossularite-rich assemblages which contain 23 weight per cent Al_2O_3. Assimiliation of such carbonate rocks would have the effect of desilicifying the magma as was illustrated by Bowen (1922) with the aid of the simple equations:

1) $CaCO_3 + 2(Ca,Na)(Al,Si)_2Si_2O_8 + \frac{1}{2}Al_2O_3 \rightleftharpoons 2CaAl_2Si_2O_8 + NaAlSiO_4 + CO_2$
calcite plagioclase melt nepheline

2) $CaCO_3 + 3(Mg,Fe)SiO_3 \rightleftharpoons Ca(Mg,Fe)Si_2O_6 + (Mg,Fe)_2SiO_4 + CO_2$
calcite hypersthene augite olivine

Bowen stressed that addition of calcium enhances the precipitation of anorthite and augite and depletes the magma in the other components of these minerals not contained in the xenoliths. He also proposed that assimilation of aluminous sediments should similarily increase the enstatite and anorthite content of the final crystallization products by the proposed reaction:

$$2Al_2O_3 + SiO_2 + 2CaMgSi_2O_6 \rightleftharpoons 2CaAl_2Si_2O_8 + 2MgSiO_3$$

Alum. clay diopside anorthite enstatite

The above reactions merely serve to illustrate how additions of calcareous and aluminous material could enhance precipitation of plagioclase from a melt, however it is not implied that these reactions actually took place in the critical zone.

As stated previously, the crystallization order of the magma that produced the sequence above the +25 m level was pl, opx, cpx and the early magma may therefore have had a composition within the plagioclase volume of the system plagioclase - olivine - clinopyroxene - quartz (Irvine 1970). Extraneous calcium and alumina, added to the magma periodically, could have restricted its composition to the plagioclase volume for relatively long periods of time thus giving rise to the abnormal quantities of plagioclase in this sequence.

3.3.5.1 Variations of Mineral Compositions Within the Layered Member

Orthopyroxene is the most widely distributed cumulus phase throughout the critical zone, and its chemistry should therefore be the most informative of all the cumulus phases. The high Mg* (0,839) of interstital orthopyroxene in the UG2-like chromitite is evidently the result of subsolidus equilibriation between the orthopyroxene and the chromite (Irvine 1967A) and not an indication of the degree of differentiation of the parent magma.

In the lower part of the critical zone, at the -50 m level, the Mg* of the cumulus orthopyroxene is 0,781 and appears to define a iron enrichment trend up to the +50 m level (Mg* 0,713). Above the +50 m level a reversal in this trend sets in and a gradual magnesium enrichment in the orthopyroxene persists up to at least the +125 m level. The next cumulus orthopyroxene at the +180 m level has a considerably lower Mg* which may be ascribed to the associated sulfides in the rocks, so that this value may

not be a true reflection of the fractionation trend in the orthopyroxenes. All electron microprobe analyses of pyroxenes from mineralized horizons were, whenever possible, conducted on grains from samples barren of sulfides in order to avoid the effects of postcumulus re-equilibriation with the sulfides. The composition of the cumulus plagioclase does not display an upward sodium enrichment from the +50 m to the +180 m level. These trends could represent conditions of gradually increasing or consistently high fo_2. As stated previously such increases in the fo_2 of the magma could have been brought about by the assimilation of water from the numerous carbonate inclusions. Although increasing water content is known to increase the anorthite content of crystallizing plagioclase (Burnham 1979) the persistently high An values of the plagioclase may be due to assimilation of calcareous material according to reactions similar to those proposed by Bowen (1922). However, the absence of chromite in the sequence above the +50 m level indicates that any possible rise in the fo_2 was not sufficient to bring about the precipitation of chromite.

The composition of the intercumulus plagioclase and clinopyroxene seem to fluctuate sympathetically. Zoning in plagioclase when present as at the +50 m and +180 m level is always normal with the cores approximately 6 to 9 mole per cent richer in the anorthite molecule than the rims.

3.4. Main Zone

A petrographic study of the 1120 m of main zone lithologies has revealed that this zone is not as homogenous and unsystematic as would first appear from field observations, and that it is possible to define a crude cyclicity within this zone based on the variation and abundance of the main cumulus constituents.

Resting on the mottled anorthosite at the top of the critical zone is a 1 - 2 m thick layer of medium-grained gabbronorite. Apart from its finer grain size this rock also contains clusters of radiating blades of plagioclase. These crystals are about 25 mm long and 2 mm wide and thus have a much greater length to width ratio than other plagioclase crystals from the layered sequence. In thin section, this rock is seen to contain traces of inverted pigeonite, compared to the directly overlying cumu-

lates which contain primary cumulus hypersthene. This horizon with its distinctive texture and mineralogy as well as its setting in the sequence, suggests that it crystallized in response to a new magma influx into the chamber.

Supercooling of this magma resulted in the crystallization of this comparatively finer grained rock with its radiating acicular plagioclase crystals.

This thin layer of gabbronorite is overlain by a 10 to 12 m thick layer of pl-opx orthocumulate (Fig. 16A); the only pl-opx cumulates of the main zone. All the clinopyroxene within this layer is intercumulus but cumulus in all the overlying layers of the main zone. This norite is overlain by a pl-cpx-opx cumulate (Fig. 16B) which in turn grades into a layer of pl-cpx cumulates thus marking the end of the crystallization order pl, opx, cpx.

Onset of crystallization of plagioclase at the +285 m level marks the beginning of a new crystallization order with the resulting development of a cumulate sequence different to that of lower levels in the sequence. This new crystallization order is equivalent to crystallization order 10 of Irvine (1970) i.e. pl, cpx, opx with a predicted cumulate sequence pl; pl-cpx, pl-cpx-opx. From the +285 m level to approximately the +1330 m level three cycles of this nature are developed in the sequence (Fig. 15). Each of these cycles show an overall upward decrease in the amount of clinopyroxene as well as for plagioclase, particularly in the first and last cycle.

Textural features of the plagioclase-rich cumulates (Fig. 16C and D) show that they can consist of either abundant plagioclase with large oikocrysts of clinopyroxene (Fig. 16C) or lower proportion of cumulus plagioclase and a greater volume of intercumulus orthopyroxene. These rocks are best referred to as orthocumulates because they may occasionally contain intercumulus quartz and because the cumulus plagioclase is zoned. With the introduction of cumulus clinopyroxene the rock changes to a pl-cpx orthocumulate (Fig. 16E).

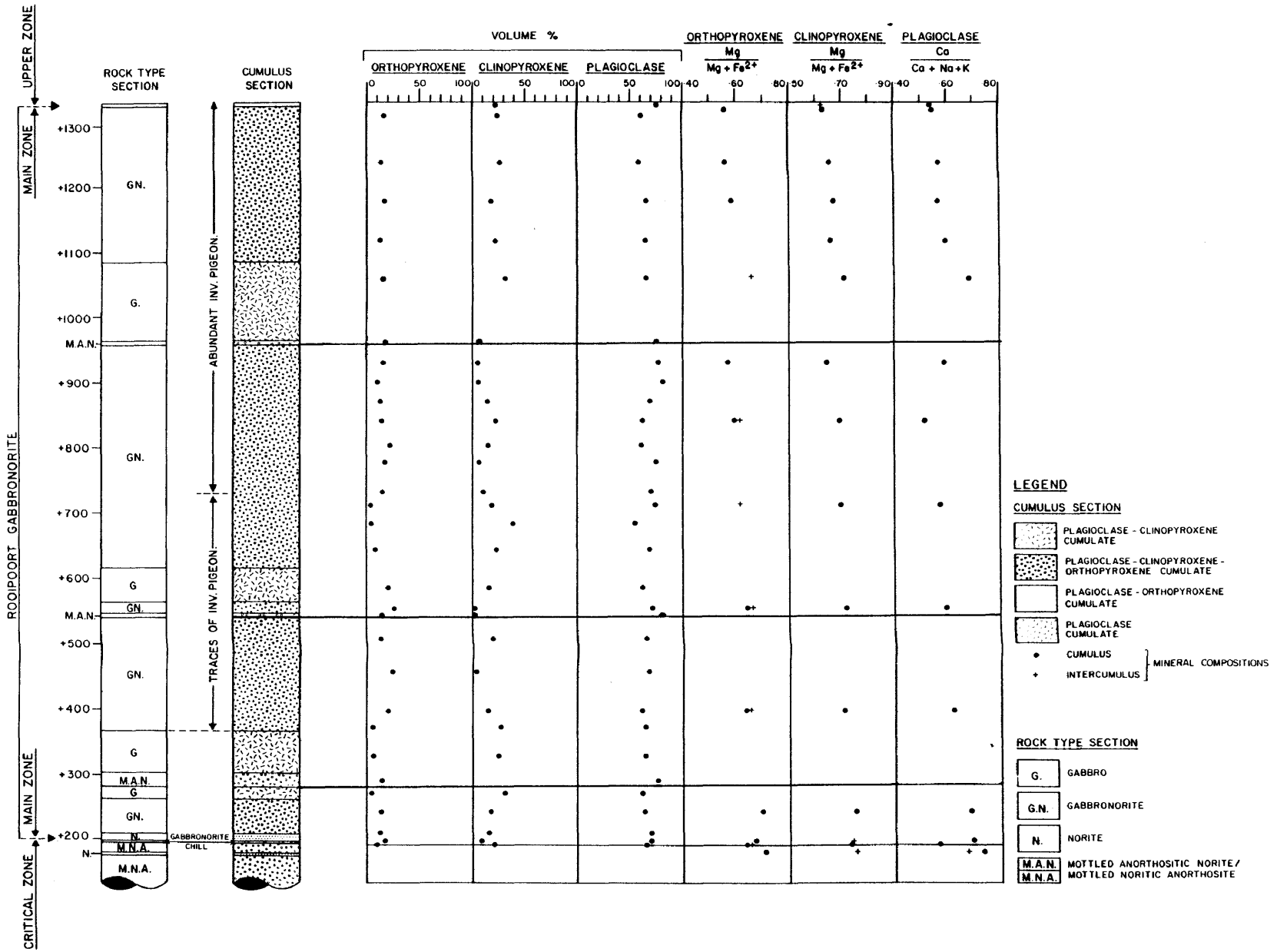

Fig. 15 Stratigraphic column of the main zone with modal analyses and data on the compositions of orthopyroxene, clinopyroxene and plagioclase.

The uppermost layers of cycles of this nature are pl-cpx-opx cumulates (Fig. 16F). In this case the Ca-poor pyroxene occurring with clinopyroxene and plagioclase is inverted pigeonite. Although the appearance of inverted pigeonite in layered intrusions is generally accepted to be a normal feature of iron enrichment, Morse (1980A) demonstrated that the crystallization sequence opx → pigeonite is also possible with increasing silica content of the magma.

The first occurrence of inverted pigeonite occurs at approximately the +375 m (Fig. 15). Here it occurs as minute resorbed cores within augite crystals, which appear as if they could be of a cumulus origin. This texture is very common up to the +725 m level where the pigeonites appear to be less resorbed. Such resorption features are very common through the entire main zone except above the +1085 m level. Also, whenever this texture is observed, small guantities of interstitial quartz are common.

It should be noted that the orthopyroxene modal column in Figure 15 represents the total volume per cent Ca-poor pyroxene present. In the pl-cpx-opx cumulates both inverted pigeonite of a cumulus origin and intercumulus hypersthene may be present.

3.4.1 Variations of Mineral Compositions Within the Main Zone

The Ca-poor pyroxene in the basal, gabbronorite "chill" of the main zone is inverted pigeonite with a Mg* of 0,652. The overlying cumulus orthopyroxene at the +205m level is hypersthene with a Mg* of 0,681 compared to 0,702 for cumulus orthopyroxene at the +250 m level. The Ca* of the plagioclase reflects a similar trend, i.e. 0,581; 0,703 and 0,696 respectively. This reversal in the composition of the silicates in quickly cooled, particularly basal portions of layered intrusions is well known (Sharpe (1980), Maske (1966)) and illustrated here. In addition, there is a well defined compositional break at the contact between the critical and the main zone which would substantiate a possible new influx of magma at this level.

The compositional data for pyroxenes and plagioclase in Figure 15 reveals a normal iron and sodium enrichment trend upwards in the main zone. This trend is however interrupted by a comparatively

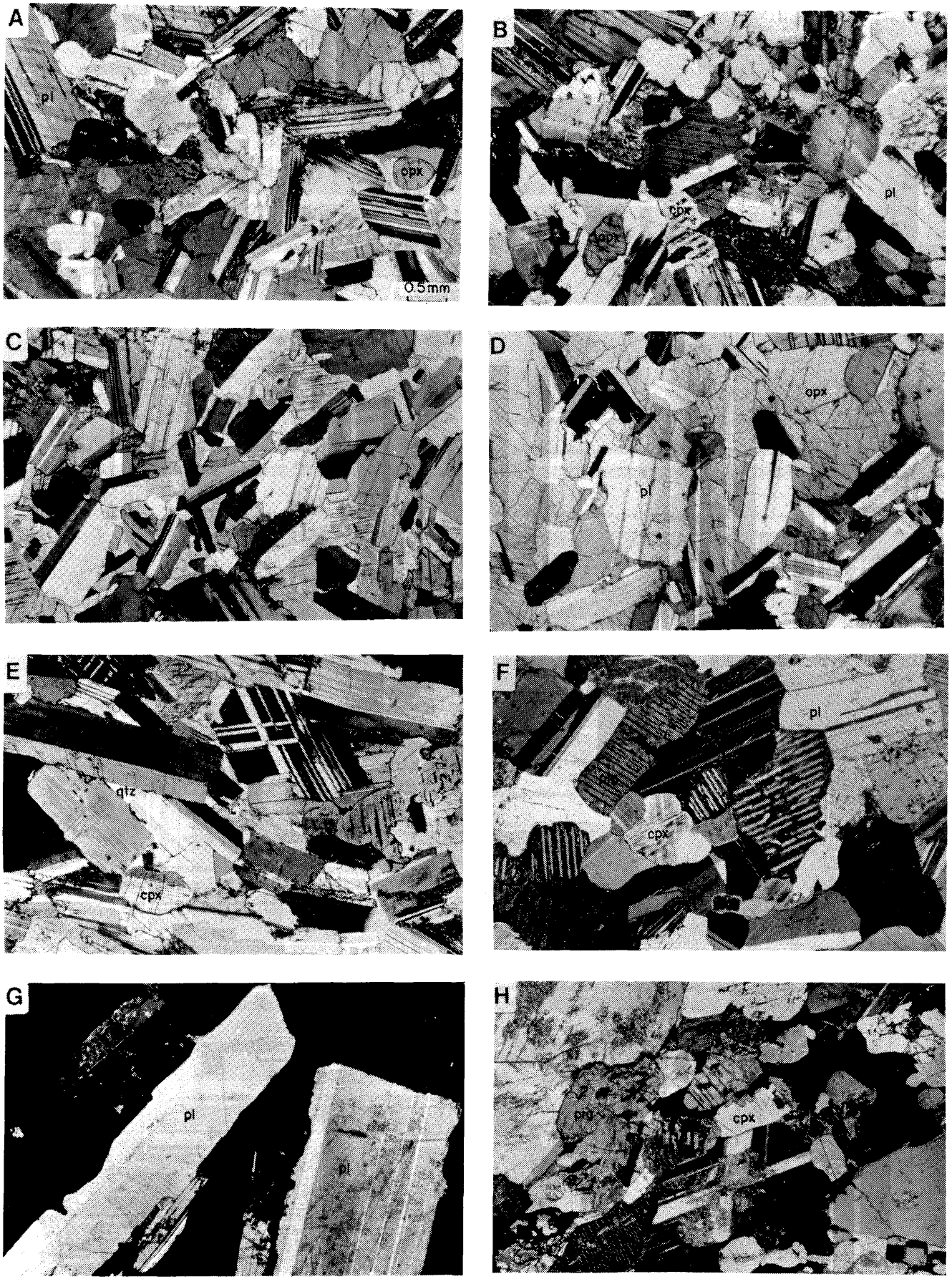

Fig. 16

Figure 16. Photomicrographs of rocks from the main and upper zone. opx = orthopyroxene; cpx = clinopyroxene; pl = plagioclase; pig = inverted pigeonite. All sections have been photographed with transmitted light under crossed nicols. Magnification is the same for all photomicrographs, see Figure 16A. Sample numbers are indicated in brackets.

(A) Plagioclase-orthopyroxene orthocumulate at the base of the main zone. (78-76B)

(B) Plagioclase-orthopyroxene-clinopyroxene cumulate in the basal portion of the main zone. (78-207)

(C) Plagioclase cumulate (mottled anorthosite) with large oikocrysts of clinopyroxene. (78-385)

(D) Plagioclase cumulate (mottled anorthosite) with large oikocrysts of orthopyroxene. (78-126)

(E) Plagioclase-clinopyroxene orthocumulate with abundant intercumulus quartz. Note the pronounced igneous lamination present in this sample. (78-127)

(F) Plagioclase-clinopyroxene-orthopyroxene (inverted pigeonite) cumulate. The inverted pigeonite has coarse exsolutions of augite parallel to the (001). This rock type typically contains a fairly well developed igneous lamination. (5-640)

(G) Magnetite-plagioclase cumulate from magnetitite layer 3. Note the resorbed edges of the plagioclase crystals. All of the opaque material is magnetite. (5-365)

(H) Plagioclase-clinopyroxene-orthopyroxene-magnetite cumulate. The orthopyroxene is inverted pigeonite. (5-233)

sudden reversal between the +960 and +1075 m levels. The reversal coincides with the position of a similar reversal, recorded by van der Merwe (1978) from the area north of Potgietersrus, for the pyroxenite marker. The interruption of such a well established fractionation trend suggests that a new influx of magma could have taken place at this level.

3.5 Upper Zone

A borehole intersection of the lower 160 m of upper zone was available from the study area.

A 9 m thick layer of plagioclase cumulates forms the base of this zone (Fig. 17). It is followed by pl-cpx-opx-mt cumulate in which the orthopyroxene is inverted pigeonite. It differs from the pl-cpx-opx cumulate at the top of the main zone in that it contains between 8 to 10 per cent titaniferous magnetite (Fig. 16H). Varying amounts (1 to 8 per cent) of biotite occurs in these cumulates and seem to have formed as a result of a postcumulus reaction between plagioclase and magnetite.

The first of four magnetitite layers, the main layer, lies 37 m above the base of the upper zone. It is 1 m thick and consists of about 95 per cent titaniferous magnetite, 3 to 5 per cent plagioclase and 2 to 4 per cent orthopyroxene. The second layer is 10 cm thick and has a plagioclase-rich foot-wall, which contains about 12 per cent disseminated magnetite. The third layer is 30 cm thick and contains approximately 60 per cent Fe-Ti oxides; 30 per cent plagioclase and 10 per cent pyroxene.

The plagioclase in this layer can be very coarse-grained and partially resorbed along the edges (Fig. 16G). The fourth layer is approximately 15 cm thick and consists of about equal amounts of plagioclase and titaniferous magnetite.

No plagioclase-rich cumulates were observed at the base of the main magnetitite layer in this borehole intersection, although van der Merwe (1978) claims that the foot-wall in the old trenches on Jaagbaan contain plagioclase-rich cumulates. The lack of plagioclase-rich cumulates is not surprising as van der Merwe found the nature and thickness of the main magnetitite and its

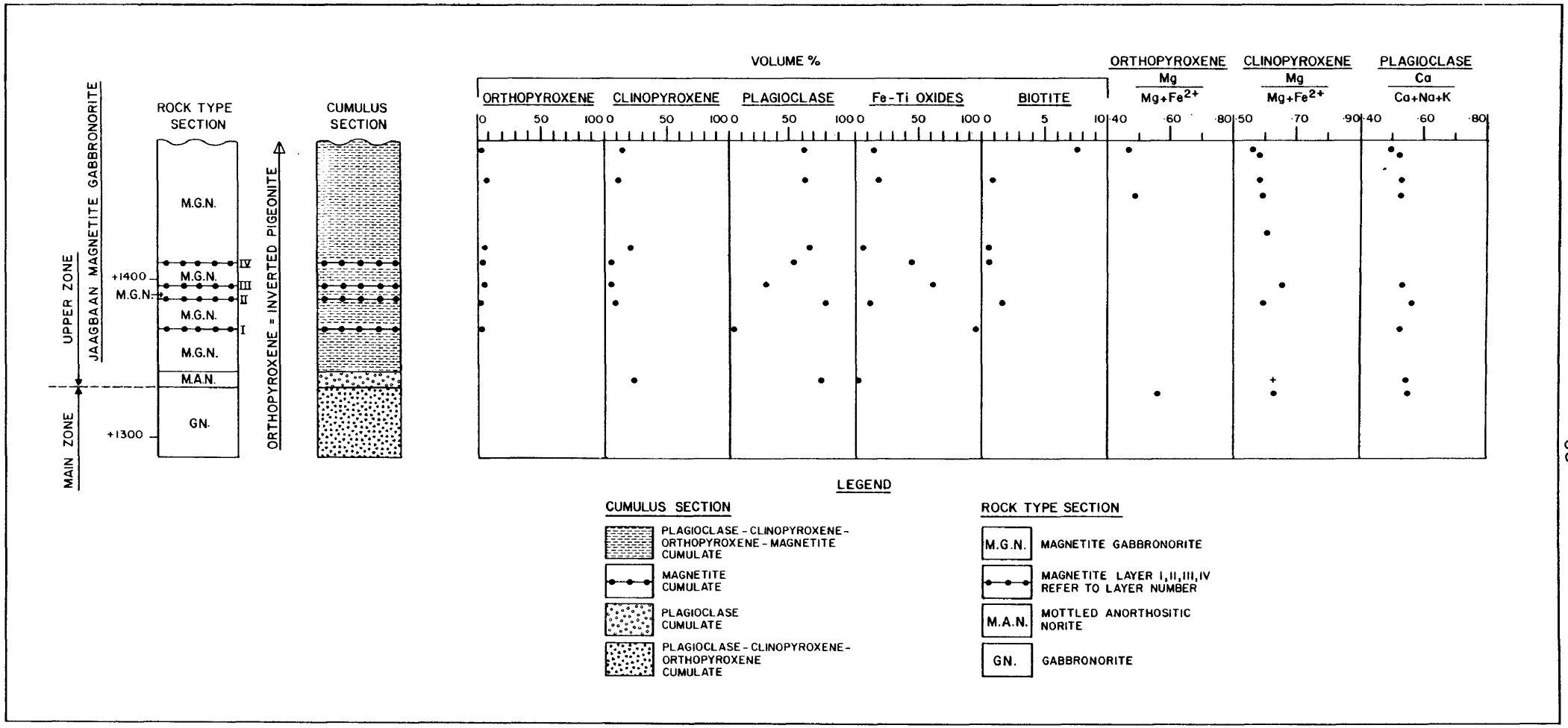

Fig. 17 Stratigraphic column of the upper zone with modal analyses and data on the compositions of the orthopyroxene, clinopyroxene, and plagioclase.

associated layers to vary considerably along strike.

3.5.1 Variations of Mineral Compositions Within the Upper Zone

From the top of the main zone and through to the highest level available for study in the upper zone a slight Na and Fe enrichment takes place in the plagioclase and pyroxenes respectively (Fig. 17). Data for the orthopyroxenes is limited because the orthopyroxene associated with or in proximity to the magnetitite layers are altered to a phase low in SiO_2, yet very high in iron and Al_2O_3 (Appendix 5). This alteration feature will be discussed in more detail in Chapter 8.

The V_2O_5 content of 2,2 weight per cent for the main titaniferous magnetitite layer on the farm Jaagbaan is the highest of any of the magnetitite layers in the Potgietersrus limb and of the Bushveld Complex (van der Merwe, 1978). The same layer further north has values ranging from 1,50 to 1,80 per cent.

4. SILICATE MINERALOGY OF THE LAYERED SUITE

In order to evaluate fractionation trends and the nature of the magma(s) that differentiated to produce the lower, critical, main and upper zones of the Rustenburg Layered Suite it was necessary to obtain accurate chemical analyses of the cumulate phases that crystallized from the respective magmas. A Joel JXA-50 electron microprobe was used for all of the analyses. The natural minerals wollastonite, corundum, rutile, hematite, chromite, sanidine, pyrolusite, albite, and trevorite were used as standards for the elements Si and Ca, Al, Ti, Fe, Cr, K, Mn, Na, and Ni, whereas synthetic periclase was used for Mg. Corrections were made for background, mass absorption, secondary fluorescence and atomic number according to the method of Bence-Albee (1968). All phases were analysed with a fine, 5 micron diameter, beam. Three to five grains per section were analysed depending on homogenuity. An interlaboratory check was made by re-analyzing 25 orthopyroxenes from the lower zone that were analysed on a ARL-SEMQ housed in the Department of Geology at the University of the Witwatersrand. With the exception of two samples that differed by more than half a mole per cent enstatite, both laboratories showed virtually identical results, and well within the analytical error of the respective instruments.

Bulk compositions of the pyroxenes were obtained by using a defocussed beam, 25 microns in diameter. The analyses are averages of step traverses representing at least ten spots per grain on two representative grains of clinopyroxene and orthopyroxene from each sample. All electron microprobe analyses reported in this study were done by the author and represent full analyses of major oxides and certain trace elements. Also all olivines, orthopyroxene, and plagioclase analyses have been checked against working curves constructed for these minerals. The curves represent compositional variation diagrams constructed from a literature search of all the best plagioclase, orthopyroxene and olivine analyses available and thus serve as a useful check on the accuracy of the analyses because of inter-element compositional relationships.

4.1 Pyroxenes

Initially, all pyroxenes were analysed with the electron microprobe by using a fine beam, in order to establish subsolidus trends and to ascertain the maximum spread in the Mg* between the lowest and highest stratigraphic levels. Subsequently the bulk composition of the heavily exsolved phases was determined by defocussing the beam.

Representative subsolidus and solidus (bulk) electron microprobe analyses and their structural formulaeare given in Appendix 1 and 2 respectively. Most analyses total between 99,00 and 100,50 and contain sufficient, Al to fill all sites of tetrahedral coordination whereas the sum of X and Y ions vary between 1,98 and 2,04 with most in the range of 1,99 and 2,02.

4.1.1 Subsolidus Mg:Fe:Ca Trends

Subsolidus compositional trends for the orthopyroxenes and clinopyroxenes from the upper, main, critical and lower zone are shown in Figure 18. The Mg:Fe:Ca ratio of the orthopyroxene vary from 89,5:8,8:1,6 in the lower zone to 44,2:52,3:3,37 in the upper zone and from 46,4:6,05:47,5 to 31,5:22,1:46,4 over the same stratigraphic interval for clinopyroxene. The orthopyroxenes contain a fairly constant 5 mole per cent wollastonite, which may, in part, be present as fine exsolutions of augite and in part in solid solution in the orthopyroxene. Slight fluctuations in the Ca (wollastonite) component is probably due to variations in the amount of exsolution beneath the electron beam.

Seeing that only material from the lowest 160 m of upper zone was available from the study area the trend for the Ca-rich pyroxenes with differentiation can only be inferred with the aid of four additional analyses from higher stratigraphic horizons in areas further to the north; i.e. two quoted by van der Merwe (1978) and two from C. Roberts (M.Sc. in preparation). One of the samples of van der Merwe (1978) has a Mg:Fe:Ca ratio of 32:28:40 and is taken from a level in the intrusion after about 71 per cent of the upper zone had crystallized, whereas the iron-rich, calcium-poor ferrohedenbergite sample has a Mg:Fe:Ca ratio of 11:62:27 and is from a pl-cpx-ol cumulate

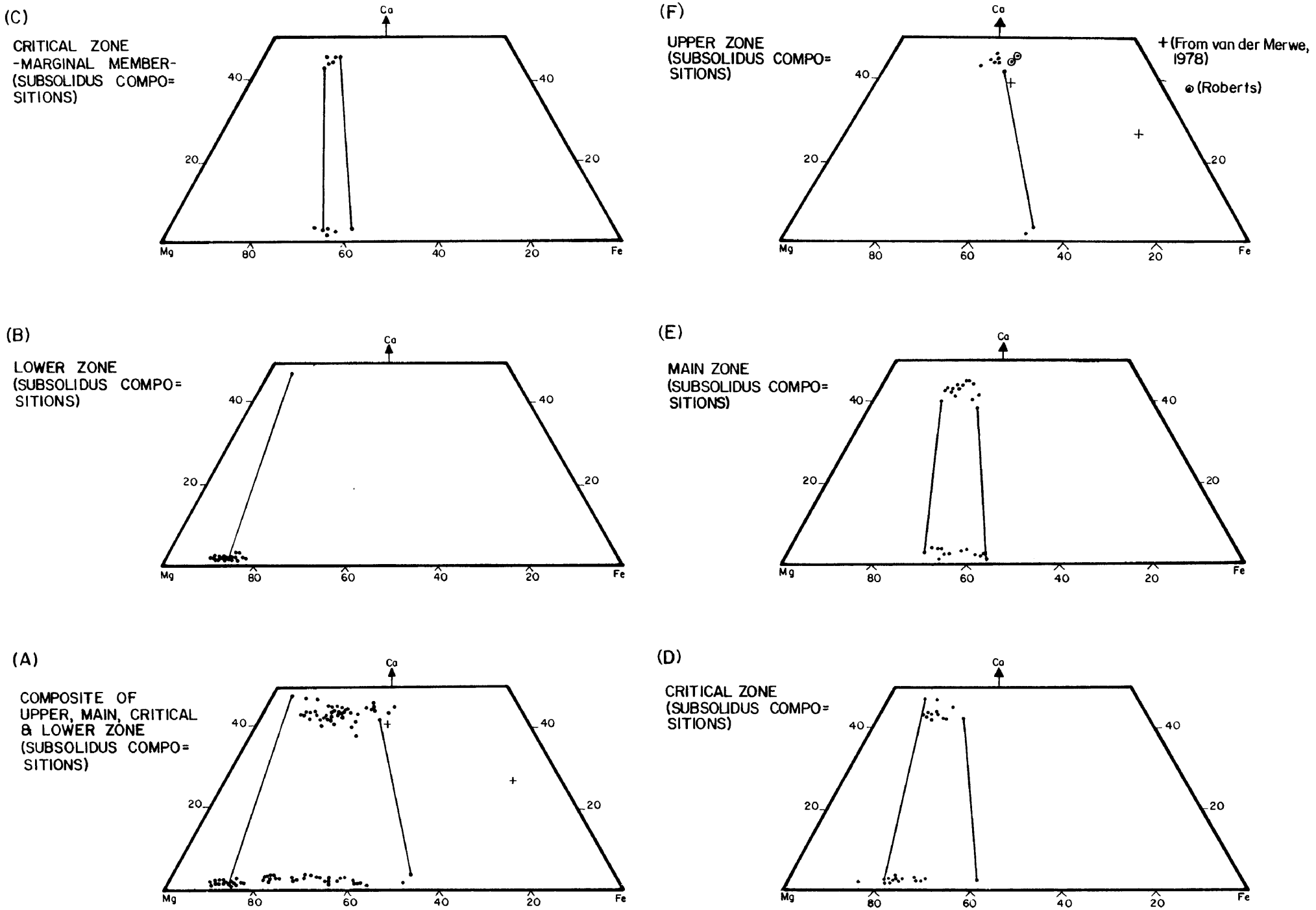

Fig. 18 Subsolidus trends and tie-line orientations of pyroxenes from the Rustenburg Layered Suite south of Potgietersrus

that crystallized after 97 per cent of the upper zone had solidified. This ferrohedenbergite coexists with olivine that has a Mg* of 0,065.

4.1.2 Solidus Compositional Trends

The compositional trends of the pyroxenes in terms of Mg, Fe, and Ca are shown in Figure 19A and 19B. Figure 19A shows the trend and the range in composition for most of the Ca-rich and Ca-poor pyroxenes in the pyroxene quadrilateral, whereas Figure 19B shows the actual bulk compositions of coexisting cumulus or intercumulus pyroxenes. With the exception of one, the orientation of all tie-lines in Figure 19B suggests equilibrium assemblages, regardless of whether both phases are cumulus or whether one is cumulus and the other is intercumulus. The cumulus orthopyroxene and intercumulus clinopyroxene assemblages are from the critical zone and do not differ in configuration from cumulus pairs in the same zone. This suggests nearly identical conditions of equilibriation regarding the partitioning of iron and magnesium.

In Figure 19A and B it can be seen that the transition from orthopyroxene to pigeonite takes place at a Mg* of about 0,657 and that the most iron-rich orthopyroxene in the study area has a Mg* of approximately 0,469. Unfortunately the limited upper zone material did not allow the observation of the limit of the two pyroxene field. However, comparision with the work of van der Merwe (1978) and Roberts (unpublished) suggests that the limit is almost exactly where it has been placed in Figure 19.

The presence of ferrohedenbergite-bearing cumulates near the top of the upper zone suggests that the Ca depletion and Fe enrichment trend of the Ca-rich pyroxenes continues into the most differentiated rocks of the upper zone of the Potgietersrus limb. Such a trend is very different to that established in the eastern and western parts of the Bushveld Complex by Atkins (1969) and Markgraaff (1976), and for this reason it is also compared with other layered intrusions (Figure 20).

Figure 20B shows the established trends for the study area in the Potgietersrus limb as well as the postulated continuation of the

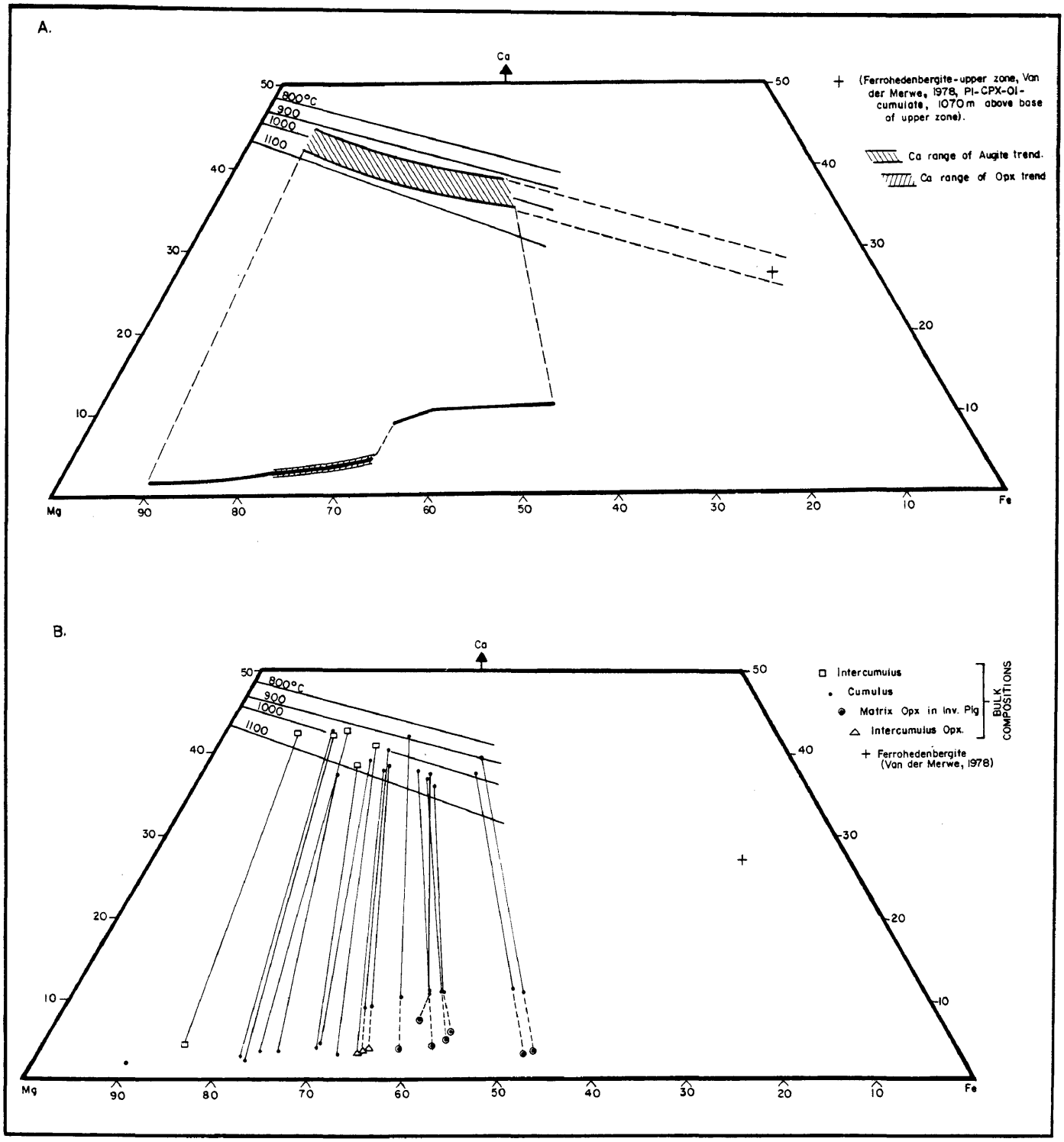

Fig. 19 Solidus trends and tie-line orientations of pyroxenes from the Rustenburg Layered Suite south of Potgietersrus.

(A) Plot illustrating the trend and range in composition of the Ca-rich and Ca-poor pyroxenes.

(B) Compositional data for coexisting Ca-poor and Ca-rich pyroxenes. Position of the solvus for Ca-rich pyroxenes at various temperatures.

trend from augite to Ca-poor ferrohedenbergite compositions in the very late differentiates. These trends show striking similarities with trends for the Dufek Intrusion both for the Ca-rich pyroxenes and for the Ca-poor pyroxenes, as well as the position of the transition from orthopyroxene to pigeonite.

The calcium depletion with fractionation of the Potgietersrus Ca-rich pyroxenes, more magnesian than ferroaugite, is less than for their counterparts in other areas of the Bushveld Complex and the Skaergaard Intrusion. For more iron-rich Ca-poor pyroxenes the Skaergaard and the Bushveld trends are one of Ca enrichment whereas the Potgietersrus trend seems to be one of Ca depletion.

Davies and Boyd (1966) and Kushiro (1969) have demonstrated that the solid solution between $MgSiO_3$ and $CaMgSiO_3$ is pressure sensitive and that it decreases with increasing pressure. Although the pressure effects on more iron-rich compositions is not known, the above work does suggest that the Potgietersrus magma could have crystallized at slightly higher pressures than that of other parts of the Complex. This is substantiated by recent investigations (Hulbert, Sharpe, Nel, research in progress) on the stabilities and element partitioning in metamorphic mineral assemblages which indicate that those from the Potgietersrus area formed at higher pressures than in other parts of the Complex.

The difference could also be ascribed to temperature, because a lowering of the temperature of crystallization would cause the solidus to intersect the solvus at a lower level and thus result in a widening of the miscibility gap.

From the literature it appears that in most complexes the trend of the Ca-rich pyroxenes in the pyroxene quadrilateral, up to the point of the two pyroxene limit, is one of a constant Ca depletion with Fe enrichment, a trend dictated by a magma that is being exhausted in calcium and enriched in iron. The continued Ca depletion and Fe enrichment trend in the Potgietersrus area therefore reflects a continuation of this normal fractionation trend of the magma up to the final stages of crystallization.

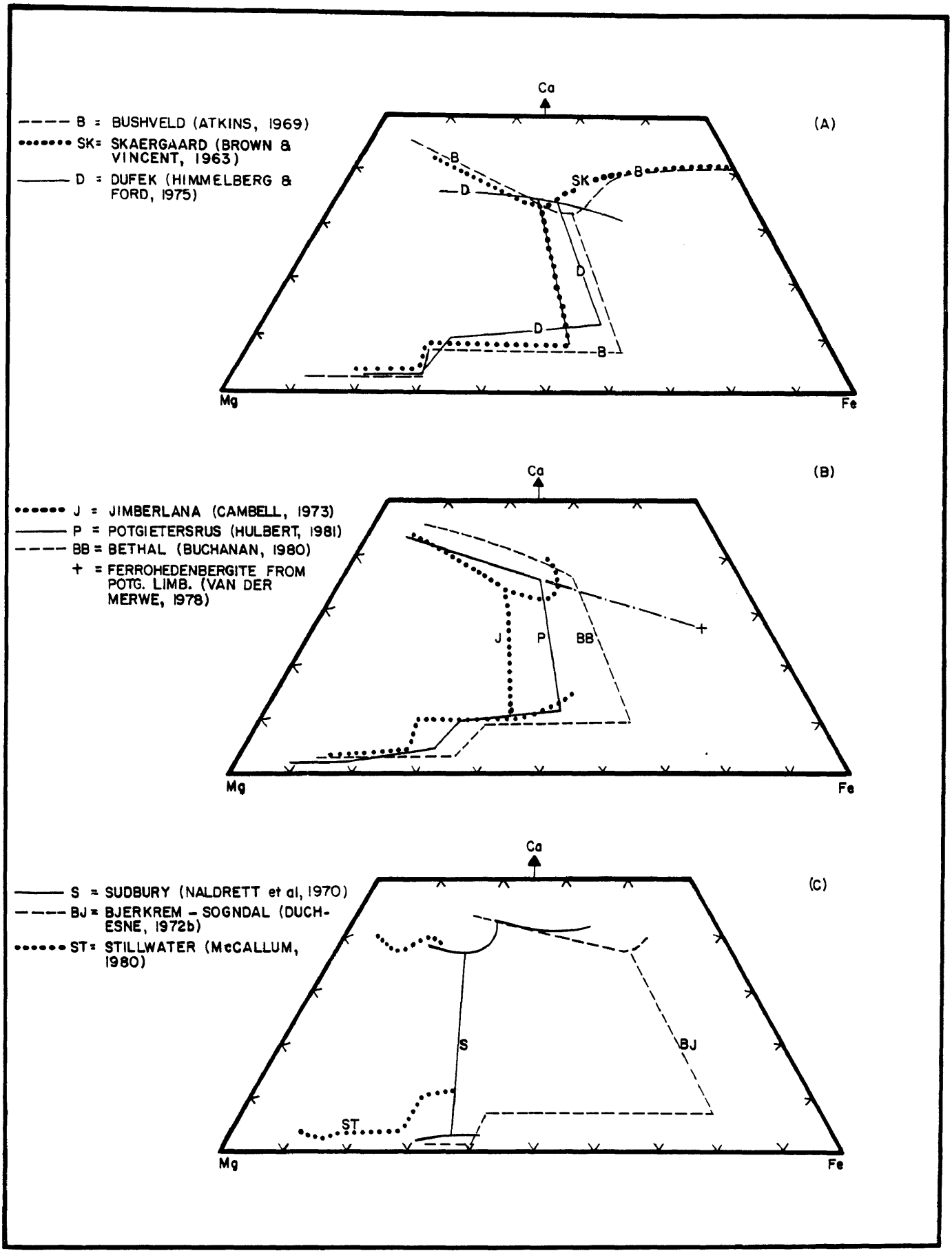

Fig. 20 Comparison of compositional trends of pyroxenes.
(A) Bushveld, Skaergaard, Dufek
(B) Jimberlana, Potgietersrus, Bethal
(C) Sudbury, Bjerkrem-Sogndal, Stillwater

The difference in the trends with continued iron enrichment of the Ca-rich pyroxenes displayed at Potgietersrus on the one hand and that established by Atkins (1969) for the eastern Bushveld Complex and by Wager and Brown (1968) for the Skaergaard Intrusion on the other hand could possibly be explained by the Ca content of the parent melt and the composition of the coprecipitating plagioclase.

At the top of the upper zone in the Skaergaard Intrusion, the most fractionated plagioclase has a Ca* of 0,33 coexisting with an olivine of Mg* of 0,21 whereas in the eastern Bushveld Complex the corresponding values are according to Atkins (1969) 0,30 and 0,00 respectively. Atkins' data also shows that, for the last 500 m of the upper zone an inverse relationship exists between the Ca content of the plagioclase and that of the coexisting clinopyroxene, and that it is this interval which defines the Ca enrichment trend of the Ca-rich pyroxenes in the pyroxene quadrilateral. A near identical situation prevails in the Skaergaard Intrusion. In the Potgietersrus limb, however, the plagioclase that coprecipitated with the ferrohedenbergite has a Ca* of 0,45 and coexists with olivine with a Mg* of 0,06 (van der Merwe 1978). The calcium-rich nature of this plagioclase in the late differentiates of the Potgietersrus limb, compared to other areas of the Bushveld Complex (Atkins 1969) and the Skaergaard Intrusion (Wager and Brown 1968) suggests that the Ca content of the clinopyroxene was controlled by the Ca content of the parent magma, which is in turn reflected by the Ca content of the coprecipitating plagioclase. It is suggested that the Na and Ca content in the respective magmas affects the distribution of Ca in coexisting clinopyroxene and plagioclase.

The higher calcium content of the plagioclase from Potgietersrus suggests that, at the equivalent stage of crystallization in all three intrusions, the Potgietersrus magma was much richer in Ca. Whole rock analyses of upper zone rocks from Potgietersrus show them to have considerably lower P_2O_5 than equivalent rocks in the Skaergaard Intrusion and other areas of the Bushveld Complex. This implies that less apatite crystallized from the Potgietersrus magma, thus leaving the residual liquids less depleted in calcium. Von Gruenewaldt(1973) demonstrated, for instance, that the appearance of cumulus apatite at the base of subzone C of the upper zone in

the eastern Bushveld coincides with the change in composition of the plagioclase from labradorite to andesine.

The Ca* of the plagioclase coexisting with the most differentiated augite in the Dufek Intrusion is 0,55. This also indicates that comparatively calcic plagioclases coexist with low Ca high Fe clinopyroxenes, as in the topmost differentiates at Potgietersrus.

4.1.3 Solidus Trends in the Marginal Members

Solidus compositions of coexisting Ca-rich and Ca-poor pyroxenes from the marginal members of the critical zone are shown in Figure 21. Also shown are the compositions of the pyroxenes from the postulated initial main zone magma (78-92) and from the harrisitic Apiesdoringdraai body. The samples designated 2 to 12 in Figure 21A are devoid of exsolution due to rapid cooling.

One of the most characteristic features of the clinopyroxenes in the marginal rocks relative to those in Figure 19B, is their calcium-rich nature. Nearly all of the phases represented in Figure 21A, except number 4 are considered to have crystallized in the presence of fairly high concentrations of water. This high water content would have lowered the crystallization temperature and would have caused the solidus to intersect the solvus at a lower level and thus widen the miscibility gap relative to a dry system. Temperature calculations based on compositions of coexisting pyroxenes reveal that the pyroxenes from the M.Mb./P.G. crystallized at temperatures 50 to 70° C lower than those with similar Mg* in samples from the relatively dry main zone magma.

The divergent tie-line configuration for sample GR1-44 represents that of an inverted pigeonite-augite pair in which the pigeonite shows a peritectic relation with the liquid. The crossing tie-lines for samples designated 1 and 3 in Figure 21B could reflect analytical error because of the close similarity in composition.

4.1.4 Distribution of Mg and Fe between Coexisting Pyroxenes

The equilibrium relations and thermal history of pyroxene pairs can be evaluated on the basis of the distribution coefficient (K_D) for Mg and Fe(total) between coexisting Ca-rich and Ca-poor

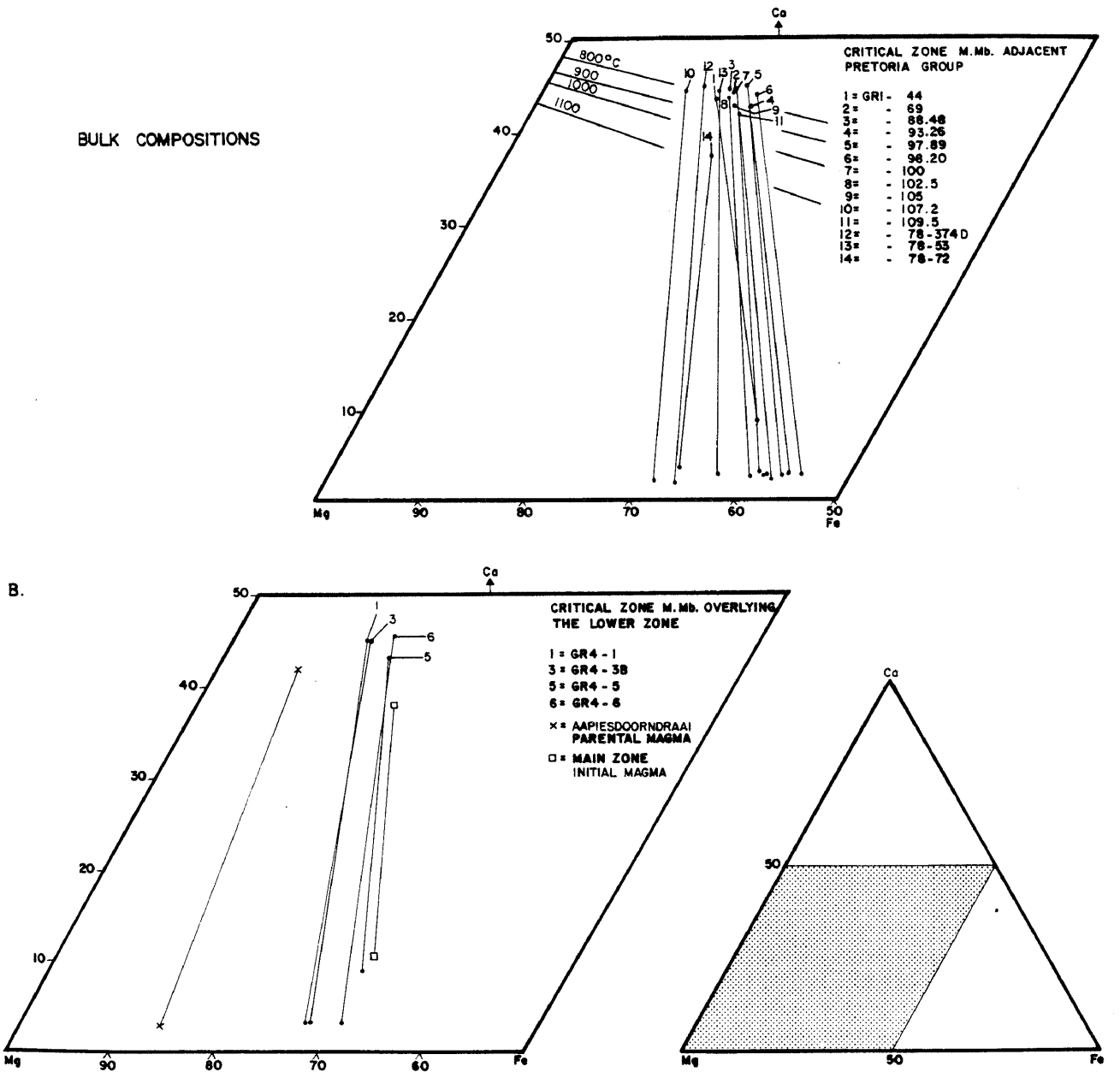

Fig. 21 Solidus compositions and tie-line orientations of pyroxenes from

(A) the marginal member adjacent to the Pretoria Group, and

(B) the marginal member overlying the lower zone. Data on pyroxenes from the postulated main zone magma quench and the Aapiesdoorndraai body are shown for comparison.

pyroxenes. Kretz (1961) suggested that the distribution coefficient varied with temperature and in 1963 he suggested a tentative diagram relating $K_D^{\frac{opx-cpx}{Mg-Fe}}$ to temperature. Fleet (1974A & B) stated that it is well known that the coefficients should tend to unity with increasing temperature of equilibriation because of the contribution of increasing thermal energy.

Figure 22A is a $K_D^{\frac{opx-cpx}{Mg-Fe}}$ plot of all previously published pyroxene data from the Bushveld Complex. The data reveals a mean K_D of 0,782 with a standard deviation of 0,075. A similar plot is shown in Figure 22Bfor pyroxene pairs from the study area as well as one sample from the Aapiesdoorndraai body. This diagram reveals that the mean K_D of 0,822 for the cumulates of the study area is much higher than that for other areas of the Complex, and that the standard deviation of 0,039 is also significantly lower. Pyroxenes from the M.Mb./P.G. have a much lower K_D of 0,651 with a standard deviation of 0,033.

The variation in K_D can be related to variations in temperature of crystallization of the pyroxene pairs of similar composition from the various areas. The lower K_D value for the critical zone chill confirms the earlier suggestion of lower crystallization temperatures. Also, the higher K_D values for pyroxenes in the cumulates from the study area, compared to those of other areas of the Bushveld Complex, may likewise be the result of equilibrium at higher temperatures as suggested earlier. Another interesting aspect of Figure 22B is that there is virtually no difference in the K_D values of pyroxene pairs, regardless of whether both phases are of a cumulus origin or whether one is cumulus and the other is intercumulus. Such an observation, in conjunction with the earlier observation relating to the orientation of tie-lines between pyroxene pairs, irrespective of their cumulus or intercumulus status, strongly suggests equilibriation under very similar conditions. If such a feature is due to re-equilibriation, the main point to be stressed is that if all solidus phases throughout the sequence re-equilibriate in a similar manner, changes recorded in the solidus chemistry should also reflect relative changes in the liquidus. Further evidence which suggests that the assemblages still reflect physiochemical conditions relatively close to those in the magmatic state is that they have much

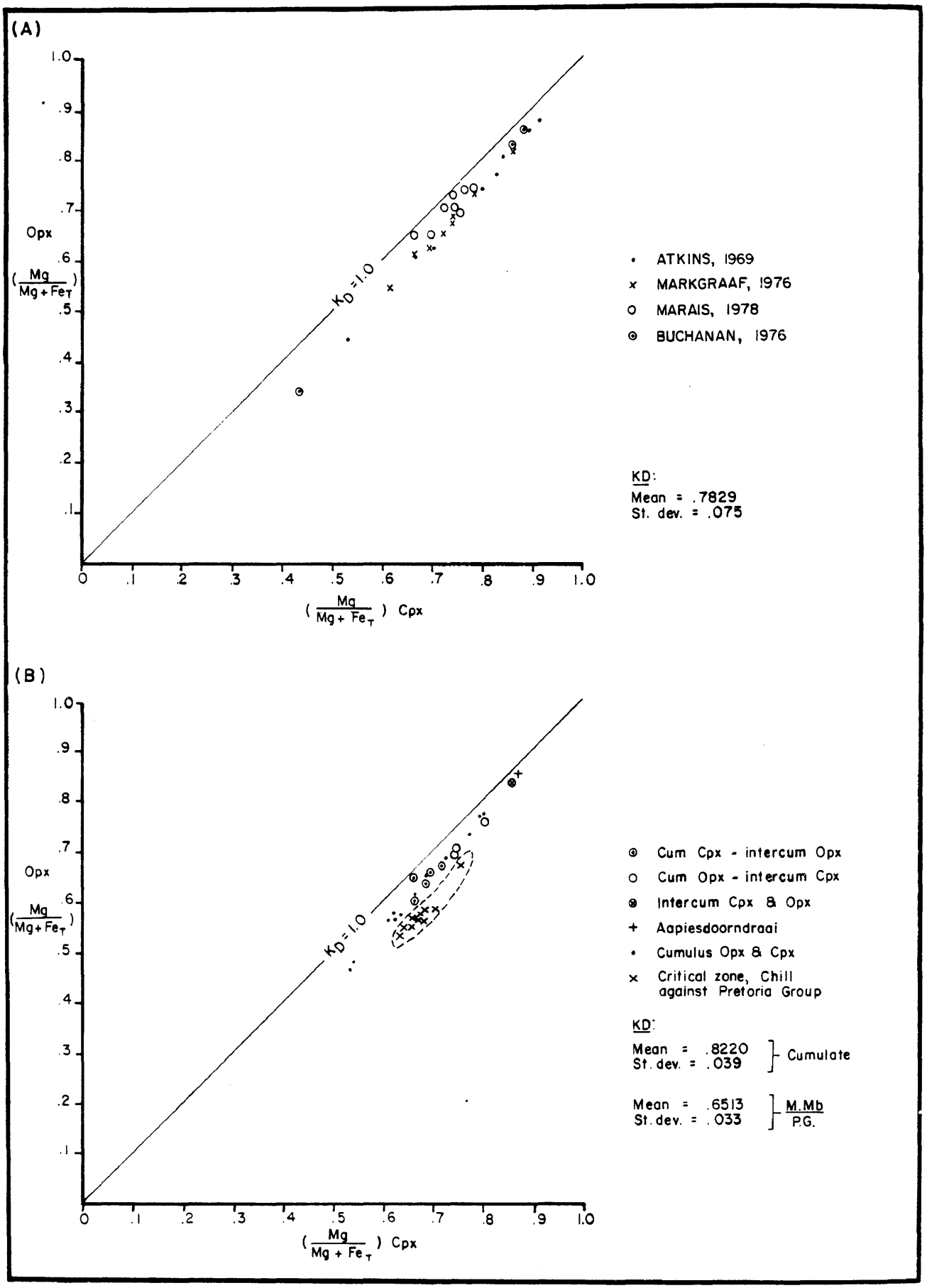

Fig. 22 Mg/(Mg+Fe$_T$) distribution plot for coexisting pyroxenes.
(A) Twenty-seven pyroxene pairs from the eastern, western and and Bethal sectors of the Bushveld Complex.
(B) Twenty-one pairs from the Rustenburg Layered Suite south of Potgietersrus, as well as ten pairs from the M.Mb./P.G.

higher K_D values than the quenched chills which crystallized at lower temperatures.

4.1.5 Silica, Alumina, and Titanium Relationship between the Pyroxenes and Parent Magma

It is well known that clinopyroxenes crystallizing from melts are fairly sensitive indicators of the concentration of Si, Al, and Ti in the magma (Le Bas, 1962; Kushiro, 1960; Gupta et al., 1973).

An Al vs Si plot similar to Figure 23 for the Bushveld clinopyroxenes was used by Kushiro (1960) in order to demonstrate differences in the composition of clinopyroxenes from tholeiites and feldspathoidal-free alkali rocks. Apart from demonstrating that most clinopyroxenes plot close to the Z saturation line (i.e. a line on the diagram on which Al+Si=2), indicating that despite plotting total Al, most of the Al is in the tetrahedral position, he found that clinopyroxenes from tholeiite magmas are confined to Si atomic proportions that range from 1,9 to 2,0 whereas those from feldspathoidal-free alkali rocks plot in the Si range 1,7 to 1,9. Le Bas (1962) pointed out that the proportion of Si to Al in the tetrahedral position of the clinopyroxene increased with fractional crystallization of the Skaergaard magma. Earlier, Brown (1957) demonstrated that Al in both the tetrahedral and octahedral sites decreased with fractionation in the same intrusion. The results of these studies indicate that magmas enriched in silica give rise to clinopyroxenes with a lower solubility of Al and Ti than those from more undersaturated melts.

The clinopyroxenes from the Bushveld Complex, including the study area, indicate a tholeiite parent magma, but this diagram (Fig. 23) can also be used to illustrate a method by which to compare the silica concentration of the host magma from which the clinopyroxenes crystallized.

Figure 23A and B represent plots based on the Si and Al proportions in the pyroxenes from Atkins (1969) and Markgraaff (1976) respectively. Markgraaff's data, although not particularly informative, does suggest that the clinopyroxenes from the upper zone in the western Bushveld could have crystallized from a more silica undersaturated magma than those from the main zone. Atkins (1969)

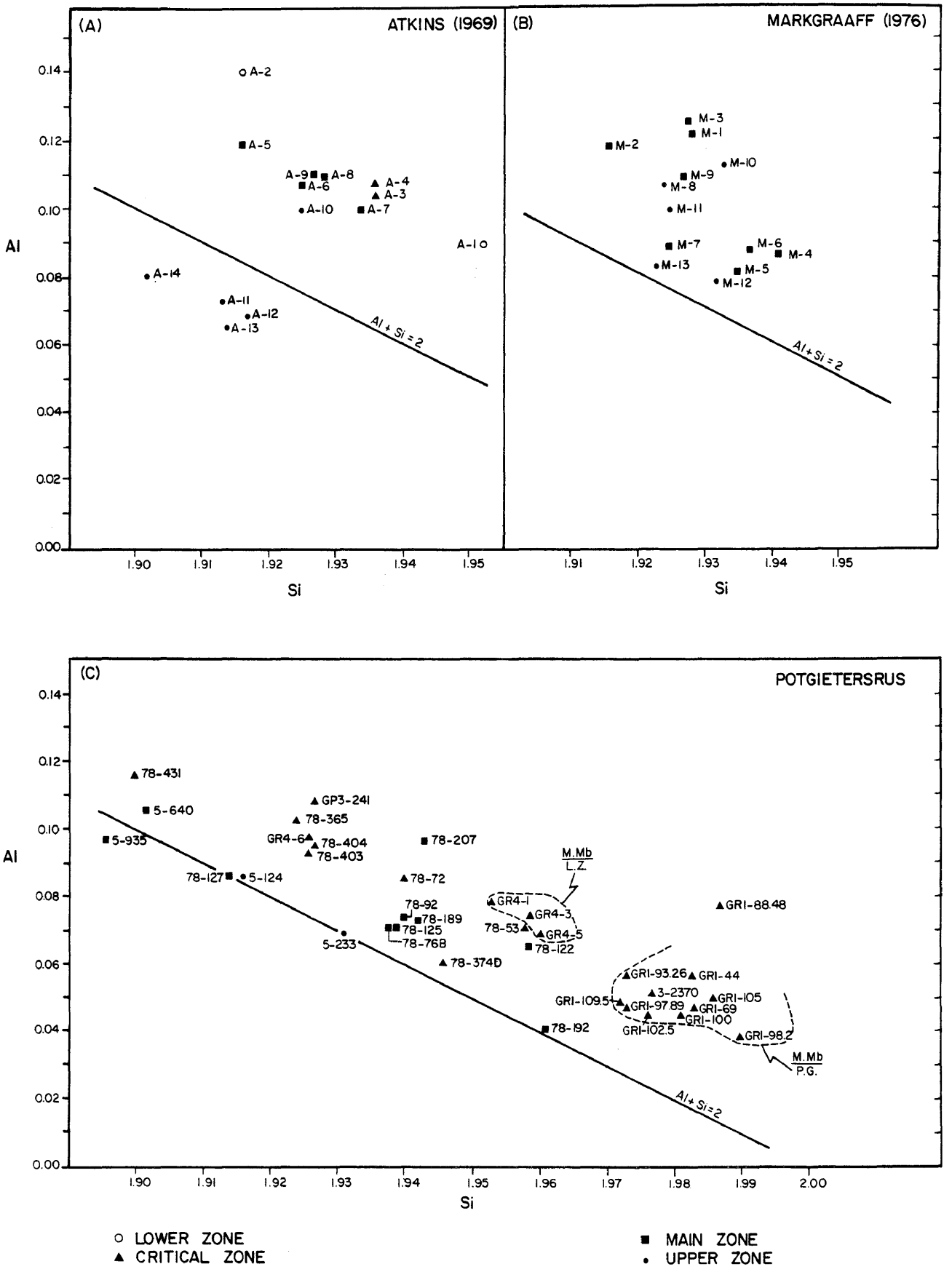

Fig. 23 A plot of the atomic proportions of Si and Al in clinopyroxenes from the data of

(A) Atkins, 1969
(B) Markgraaff, 1976 and
(C) this study.

data also suggest a more SiO_2 depleted melt from which the upper zone clinopyroxenes crystallized, yet the pyroxenes are low in Al which is not what one would expect.

A much clearer picture emerges from Figure 23C on which a variety of clinopyroxene compositions from the study area have been plotted. Clinopyroxenes from the M.Mb./P.G. in Figure 23C have the highest Si and lowest Al values. These are from rocks that contain up to 11 volume per cent quartz (Table 1), except sample GR1-44 which contains no visible quartz, although it is part of a more siliceous magmatic environment and contains inverted pigeonite with resorption textures indicative of the silica producing peritectic reaction:

pigeonite + liquid $\rightleftharpoons$ augite + tridymite (Morse, 1980A).

Samples 78-374D and 78-53 from the M.Mb./P.G. show no signs of contamination by silica and have considerably lower Si and higher Al values (Fig. 23C) than the GR1 samples. Although these two samples contain no visible quartz (Table 1) their proximity to the contact does not rule out some degree of contamination. Si and Al proportions of clinopyroxenes from the M.Mb./L.Z. (Fig. 23) are very similar to those of the uncontaminated M.Mb./P.G. (78-53, 78-374D) thus suggesting that all these clinopyroxenes crystallized from a magma with approximately the same degree of silica saturation.

A regular trend of decreasing Si and increasing Al proportions in the clinopyroxenes is seen to exist for the critical zone cumulates and their marginal members. Of interest in this regard is the fact that sample 78-72, which is the quasi cumulate from the M.Mb./P.G. falls on the critical zone trend between the cumulate field and the marginal members. Furthermore, there appears to be little difference in the Si and Al proportions between cumulus and intercumulus clinopyroxenes, for GP3-241 and 78-403 are cumulus whereas the rest are intercumulus.

The most Si depleted and Al enriched clinopyroxene is 78-431, from a sulfide enriched horizon from the M.Mb/L.Z. (sample 78-431). The position of this point suggests crystallization from

a relatively silica depleted magma or a magma with low silica activity. Because of the inverse relationship between $a^{melt}_{SiO_2}$ and fo_2, this low silica activity would indicate a high fo_2 condition (Morse 1980c), which in turn could account for the high concentration of sulfides in this rock as the higher fo_2 would have the effect of lowering the solubility of S in the melt.

Main zone samples have, except for 78-207, consistently lower (Si + Al) values than the critical zone and cluster at three different Si values (Fig. 23C). Clinopyroxenes 78-192 and 78-122 at Si values of ≈1,96 are from cumulates with visible quartz whereas those at Si ≈1,94 are from samples that contain traces of quartz, as well as pigeonites that display resorption textures which suggest the silica producing reaction:

pigeonite + liquid $\rightleftharpoons$ augite + tridymite

The remainder of the main zone samples are from higher levels where these textures and visible quartz are absent. Sample 78-127 represents a level in the intrusion equivalent to that of the pyroxenite marker were a new influx of magma is postulated. The more silica depleted Al enriched clinopyroxenes 5-640 and 5-935 are from samples near the top of the main zone. The limited data points suggest a decreasing silica, increasing alumina trend towards the upper zone from approximately the level of the pyroxenite marker. Other lines of evidence also suggest such a trend; this will be discussed in Chapter 7.3.

Samples 5-124 and 5-233 from the upper zone represent more Si enriched and Al depleted pyroxenes than 5-640 and 5-935. These samples again possess textures suggestive of a peritectic reaction involving pigeonite.

The relationship of low Si, high Al and high Ti is only observed in the clinopyroxenes from samples 5-640 and 5-935 near the top of the main zone. These pyroxenes contain on average 0,72 weight per cent TiO_2 (Appendix 2) which is about 0,10 to 0,30 weight per cent more than in other clinopyroxenes. With the appearance of cumulus titaniferous magnetite in the upper zone, the TiO_2 content in the coexisting clinopyroxene decreases to about one half the amount of that in the clinopyroxenes near the top of the main zone.

Recent calculations of the distribution coefficients $D^{cpx\text{-}liq}_{TiO_2}$ of 0,30 (Pearce and Norry, 1979) and 0,20 (Huebner and Turnock, 1980) show that TiO_2 is preferentially concentrated in the magma. If the more recent value is taken to be more correct then the critical zone liquid appears to have contained on average about 2,20 weight per cent TiO_2, the main zone liquid, up to the level of the pyroxenite marker, about 3,30 per cent TiO_2 and the liquid from this level up to the base of the upper zone about 3,60 per cent TiO_2. These values are similar to the trend and concentration levels calculated by Wager and Brown (1968) for the Middle Zone liquids of the Skaergaard Intrustion.

Similarly, an idea of the amount of Al_2O_3 in the liquid from which the clinopyroxenes crystallized can be obtained by using the $D^{cpx\text{-}liq}_{Al_2O_3}$ value of 0,13 recently determined by Huebner and Turnock (1980). These calculations gave the following values:

upper zone liquid	11,11-13,85 per cent Al_2O_3
main zone liquid (upper third)	15,70-17,33 per cent Al_2O_3
(lower two thirds)	10,74-14,37 per cent Al_2O_3
critical zone liquid	15,55-18,29 per cent Al_2O_3

4.1.6 Pigeonite Textures and Phase Relations

Pigeonite has various modes of occurrence and displays several textural features within the gabbroic rocks of the Rustenburg Layered Suite in the southern portion of the Potgietersrus limb. The first pigeonite in the sequence is partially resorbed, (Fig. 10F) and is found in the M.Mb./P.G. A second form of pigeonite, now inverted, found in the marginal member (Fig. 24A) has coarse bleb-like exsolutions of augite. The apparent lack of exsolution lamellae is according to Brown (1957) characteristic of pigeonites that crystallized at temperatures only slightly above the inversion temperature. In each case most of the augite is exsolved during rather than prior to inversion. In the same horizon large crystals of calcium-poor pyroxene consisting of cores of hypersthene surrounded by rims of inverted pigeonite are developed (Fig. 24B). This textural relationship is believed to be the reslut of replacement of hypersthene by pigeonite during crystallization as a result of the reaction: hypersthene + liquid $\rightleftharpoons$ pigeonite (Nakamura and Kushiro, 1970). The liquid which reacts with the

Fig. 24

Figure 24 Photomicrographs of pigeonite textures observed in the study area. opx = orthopyroxene; cpx = clinopyroxene, pig = pigeonite. All sections photographed with transmitted light under crossed nicols. Magnification is the same for all photomicrographs, see Figure 24A. Sample numbers are indicated in brackets.

(A) Inverted pigeonite (in the extinction position) from the M.Mb./P.G. containing plates and irregular blebs of augite primarily oriented parallel to (100). (78-74)

(B) Large poikilitic inverted pigeonite grain with a core of hypersthene (M.Mb./P.G.). The mantle of inverted pigeonite, about hypersthene, contains rods and patches of exsolved augite. (78-55)

(C) A similar poikilitic inverted pigeonite grain with a core of hypersthene in mottled anorthosite from the critical zone. (78-128)

(D) Postcumulus reaction. A thin reaction rim of Ca-poor (pigeonitic) pyroxene between plagioclase and clinopyroxene probably produced by reaction in the presence of intercumulus liquid. (78-75)

(E) Plumose to vermicular exsolution of augite in inverted pigeonite from the main zone. Hypersthene is in the extinction position. (78-125)

(F) Resorbed cumulus pigeonite from the main zone. Note the resorbed grain margin and the extensive development of a clinopyroxene mantle about the primary pigeonite. (78-350)

(G) Herringbone patterned exsolution lamellae of augite in inverted pigeonite from the main zone. (5-640)

(H) Resorbed inverted pigeonite from the upper zone. Note the extensively resorbed grain margin and the prominent development of a clinopyroxene mantle about the relict core of inverted pigeonite. (5-233)

hypersthene must be more iron- and calcium-rich than that which gave rise to the hypersthene. The Mg* of the inverted pigeonite in this case is 0,587 and that of the hypersthene core is approximately 0,620. A similar texture is shown in Fig. 24C, except that this sample is derived from the +123 m level of the critical zone. This large Ca-poor pyroxene has a core of hypersthene and a rim of inverted pigeonite and represents one of the larger oikocrysts from a mottled anorthosite. In this particular sample the hypersthene core has a Mg* of 0,623 and the inverted pigeonite rim has a value of 0,589. The higher iron content in the rim and the abundant blebs and lamellae of augite confirm the early suggestion that it resulted from reaction with more Ca- and Fe-rich liquid than that from which the hypersthene crystallized.

Within certain mottled anorthosites of the critical zone thin reaction rims of inverted pigeonite have developed, seemingly as a result of postcumulus reaction between plagioclase and clinopyroxene. Figure 24D shows such a texture, however the exsolved Ca-rich component is difficult to resolve in the photomicrograph.

Plumose to vermicular exsolution of augite in inverted pigeonite (Fig. 24E) is considered to be due to exsolution of augite synchronous with inversion.

Resorbed pigeonite like that shown in Figures 24F and H is a common feature in many main and upper zone lithologies. In contrast, the pristine, unresorbed inverted pigeonite (Fig. 24G) shows well developed twinning of the original pigeonite and coarse lamellae of exsolved augite parallel to the original (001) of the pigeonite. The resorbed inverted pigeonite occurs mostly as isolated cores in what appears to be cumulus augite. It is not always evident at what stage the replacement, and thus the rimming and embaying of the pigeonite, has taken place. There is little indication whether this texture formed after the settling of the crystal from the magma or whether the reaction has taken place whilst the crystal was still suspended in the melt. The resorbed pigeonite shown in Figure 24H gives the impression the resorption occurred whilst the pigeonite was suspended in the magma, and that it is not the result of a reaction with the intercumulus liquid. Similar textures are found in sample GR1-44, a noncumulate rock of the M.Mb./P.G., suggesting that this texture is

derived as a consequence of reaction with the melt.

Within the layered rocks, this replacement feature is especially noticeable in three different environments, viz.

a) the lower part of the main zone, from the +370 to +730 m level, where traces of pigeonite, surrounded by augite coexist with large intercumulus patches of hypersthene.

b) at the +900 m level in the main zone, i.e. in the rocks below the postulated level of the pyroxenite marker in which interstitial quartz is a noticeable intercumulus component, and

c) in the upper zone.

The textural and compositional relationship between the coexisting pyroxenes is difficult to explain and although the replacement textures look similar in all three above-mentioned environments, no single explanation can be suggested to explain the feature satisfactorily. It is, therefore, necessary to resort to a different process to explain the texture in each of the three environments.

The textural and compositional relationships in the lower part of the main zone, where cumulus orthopyroxene disappears in the sequence and where traces of inverted pigeonite, enclosed in augite, make their appearance, are similar to those described by von Gruenewaldt and Weber Diefenbach (1977) from main zone rocks in the eastern Bushveld. These authors consider pigeonites enclosed in augite to be a relict texture, i.e. pigeonites crystallizing only a few degrees above the pigeonite-orthopyroxene inversion, at e.g. D (Fig. 26). Upon slight cooling to below the pigeonite-orthopyroxene inversion temperature it is isolated in a liquid in equilibrium with orthopyroxene. This early pigeonite would, depending on the temperature interval between crystallization and inversion, either be resorbed by the liquid from which hypersthene would subsequently crystallize, or react with the liquid to form hypersthene. Some of these early pigeonite grains evidently acted as crystallization nucleii for augite and were thus

effectively shielded from reaction with liquid. Von Gruenewaldt and Weber Diefenbach (1977) found the relict inverted pigeonite grains to have lower Mg/(Mg+Fe) ratios than the later hypersthene. This was also found to be the case in the main zone rocks from the Potgietersrus area and is in accordance with the findings of Nakamura and Kushiro (1970) who have demonstrated that the pigeonite-orthopyroxene inversion illustrated by a thick dashed line in Fig. 26 is in fact a narrow field where the three pyroxene assemblage orthopyroxene + pigeonite + augite is stable.

As suggested earlier mantled pigeonites in rocks with visible quartz from levels below the pyroxenite marker could have formed by the reaction:

$$\text{pigeonite} + \text{liquid} \rightleftharpoons \text{augite}_{ss} + \text{tridymite}$$

Apart from the presence of free quartz in these rocks, there are other indications that the magma from which these rocks crystallized were fairly differentiated liquids close to oversaturation in SiO_2. These include a high calculated a_{SiO_2} for the magma during crystallization of these rocks and a fairly high concentration in incompatible trace elements. Both aspects will be dealt with more fully in subsequent chapters. It is therefore suggested that the main zone liquid, prior to the the major replenishment which resulted in the pyroxenite marker elsewhere, had a composition close to or at a point equivalent to S in the forsterite-diopside-SiO_2 system (Fig. 25). As was pointed out by Morse (1980A), S is an invariant point because it lies outside the triangle Di_{ss} - Pigeonite - SiO_2 and the pigeonite therefore will react with liquid to produce Di_{ss} and tridymite. Evidently, this reaction will only take place under conditions of equilibrium crystallization, however early formed pigeonites crystallizing along R S but close to S could, e.g. after settling and limited fractional crystallization of the intercumulus liquid, become isolated in a liquid of composition S and in this way become partially replaced by augite with the simultaneous crystallization of quartz.

The same textural feature in the uppermost available rocks of the upper zone in this area can probably be related to proximity of the two pyroxene limit. As was pointed out earlier, available data from the work of van der Merwe (1978) and Roberts (reseach in

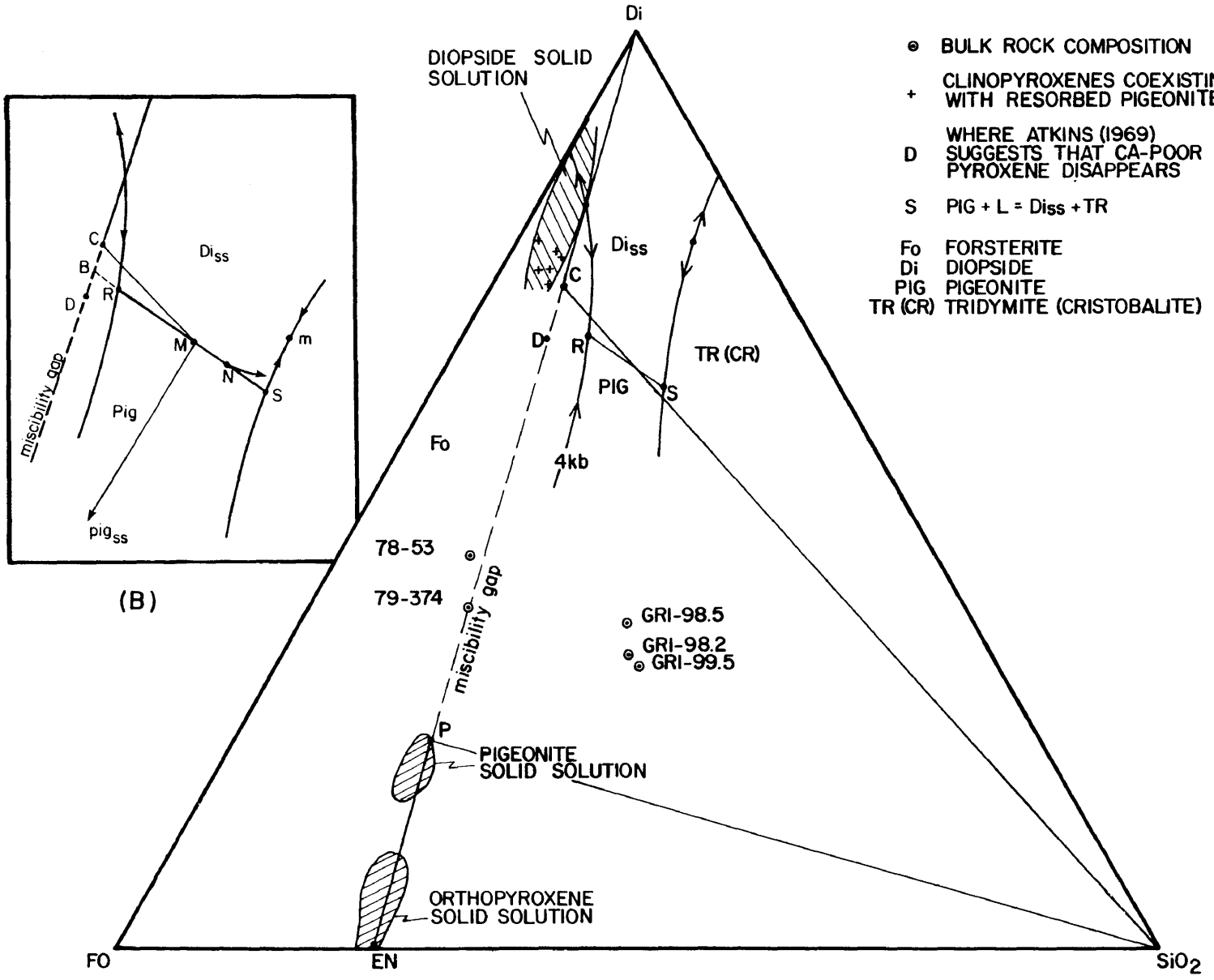

Fig. 25 (A) Phase relations for Ca-rich and Ca-poor pyroxenes in the system forsterite-diopside-quartz (SiO_2) at 4kb pressure, and compositional fields of pyroxenes from the area south of Potgietersrus.
(B) Detail of part of Figure 25A to illustrate the crystallization paths of highly fractionated liquids and the possible reason for the two pyroxene limit.

progress) shows that the most iron-rich coexisting pyroxenes in the available upper zone section south of Potgietersrus, have a composition close to the two pyroxene limit. The limited amount of data from the Potgietersrus area therefore seems to indicate that the cessation of crystallization of Ca-poor pyroxene may be due to the peritectic reaction: pigeonite + liquid $\rightleftharpoons$ augite as was proposed by Muir (1954) and Nwe and Copley (1975) for the Skaergaard Intrusion.

The crystallization relationship at the two pyroxene limit are not fully understood, and various other explanations have been proposed in the past to account for the disappearance of the Ca-poor pyroxene during fractional crystallization (Brown, 1957; Campbell and Nolan, 1974; Walker, 1969A&B; Morse, 1980A). If, however the phase relations in more Fe-rich systems are broadly similar to those in the forsterite-diopside-SiO_2 diagram (Fig. 25), then the cessation of crystallization of the Ca-poor pyroxene could possibly be related to the narrowing of the miscibility gap between the coexisting pyroxenes. This can be explained with the aid of Fig. 25B. Assuming a fractionating liquid has a composition on the diopside-pigeonite boundary, a pigeonite will crystallize together with a relatively magnesian Di_{ss} of composition C. With fractional crystallization the composition of the liquid will change from M towards N and at the same time it will become gradually enriched in iron. Simultaneously the width of the miscibility gap between diopside and pigeonite decreases mainly because of the decreasing Ca-content of the crystallizing augite. The extent of the diopside solid solution in Fig. 25B will therefore increase in the direction of B. If with continued fractional crystallization the extent of the Di_{ss} increases to beyond B, pigeonite will cease to crystallize. Further fractional crystallization will cause a Di_{ss} of composition between B and D to separate with the result that the composition of the liquid will leave the boundary curve RS and will follow a curved path into the Di_{ss} field, as the composition of the separating Di_{ss} changes towards D with continued iron enrichment. It is of interest in this regard that the inferred composition of the clinopyroxene at the limit of the two pyroxene field in the eastern Bushveld (Atkins, 1969), plots at D in Figure 25A.

The trend of the Ca-rich clinopyroxenes after cessation of crystallization of Ca-poor pyroxene varies considerably from one intrusion to the next (Fig. 20). Continued Fe enrichment and Ca depletion as proposed for the Potgietersrus intrusion would imply that the liquid composition maintains a path away from RS towards the Di_{ss}-tridymite boundary. In the majority of the other intrusions, except Dufek, the compositions of the Ca-rich pyroxenes seem to display a Ca enrichment trend with further iron enrichment. If, as has been assumed all along, the configuration of the phase boundaries for the Fe-rich pyroxenes is similar to that for the Mg-rich varieties as shown in Figure 26B, then it would be difficult for a liquid to return to the pigeonite-diopside boundary once it has left this curve. It must be borne in mind that the two pyroxene limit is reached in a fractionating magma after about 85 per cent crystallization. This imples that N in Figure 25B is close to point S, and any reduction of the extent of the Di_{ss} from a point between BD back towards C upon further fractional crystallization will tend to drive the composition of the residual liquid more or less parallel to NS towards the boundary curve SM. The configuration of the boundary curves, especially RS with respect to the Di_{ss} composition shows that a very drastic reduction in the extent of the Di_{ss} composition would be required to drive the liquid back to the pigeonite-diopside boundary curve.

In Figure 25 the compositions of Ca-rich pyroxenes that coexist with resorbed pigeonite are shown, as well as the compositional fields of the Ca-rich and Ca-poor pyroxenes from the study area. It should be borne in mind that, apart from resorbed pigeonite associated with free quartz in the main zone, it is also developed in sample GR1-44 from the M.Mb./P.G. which is associated with contaminated rocks like those represented by samples GR1-98,5; 98,2 and 99,5 in Figure 25A. Similar uncontaminated rocks of the M.Mb./P.G., e.g. 78-53, and 78-374 plot further away from SiO_2 in this figure. This tends to suggest that the resorption of the pigeonite in the marginal rocks may also be the result of the reaction: pigeonite + liquid $\rightleftharpoons$ augite + tridymite. Rapid simultaneous crystallization of pigeonite and quartz from a liquid represented by the GR1 points in Figure 25A, would have driven the residual interstitial liquid composition towards S, to produce diopside at the expense of pigeonite by the above-

mentioned reaction, and as described earlier for quartz bearing gabbroic rocks of the main zone.

If the change in crystallization order from augite-orthopyroxene to to augite-pigeonite is the result of the intersection of the solidus of the Ca-poor pyroxenes with the three pyroxene volume, as proposed by Ross and Huebner (1975) and Huebner and Turnock (1980), then it becomes possible to infer the crystallization temperature and the orthopyroxene-pigeonite phase relations from a temperature-composition diagram such as Figure 26, which is based on the data of Brown (1957, 1967) and Huebner and Turnock (1980). The sample BA4 represents an inverted pigeonite grain from the Bushveld Complex with a composition $Wo_{8,9}\,En_{48,2}\,Fs_{42,9}$ in which the inversion temperature was experimentally determined by Brown (1967) as being 1025°C at 4Kb pressure. By using this as control and the slope of the very narrow stability field of coexisting orthopyroxenes + pigeonite + augite from Huebner and Turnock (1980), the broken line on Figure 26 was constructed to demarcate the stability fields of orthopyroxene + augite and pigeonite + augite.

The suggested crystallization temperature of pigeonite BA4 (Brown, 1967) was used to construct the solidus curve. The curve designated S in Figure 26 represents the pyroxene solidus whereas L_1 and L_2 are liquidus curves for the magma.

Sample G and F (Fig. 26) represent the whole rock $Mg/(Mg+Fe^{2+})$ ratio of the uncontaminated initial magma of the M.Mb./P.G. with sample G probably being the more representative of the two. With supercooling of this magma the liquid at G should crystallize Ca-poor pyroxene of approximately the same Mg* which in fact it did, since a value of 0,618 was found in the orthopyroxenes from this sample. However, with slow cooling, the liquid G could be in equilibrium with a orthopyroxene of composition H at the same temperature, assuming L_1 represents the position of the liquidus. If L_2 represents the position of the liquidus as shown by Brown (1957) it would mean that liquid G would be in equilibrium with orthopyroxene with a Mg* of approximately 0,710 rather than 0,800. Although the position of the liquidus relative to the solidus is

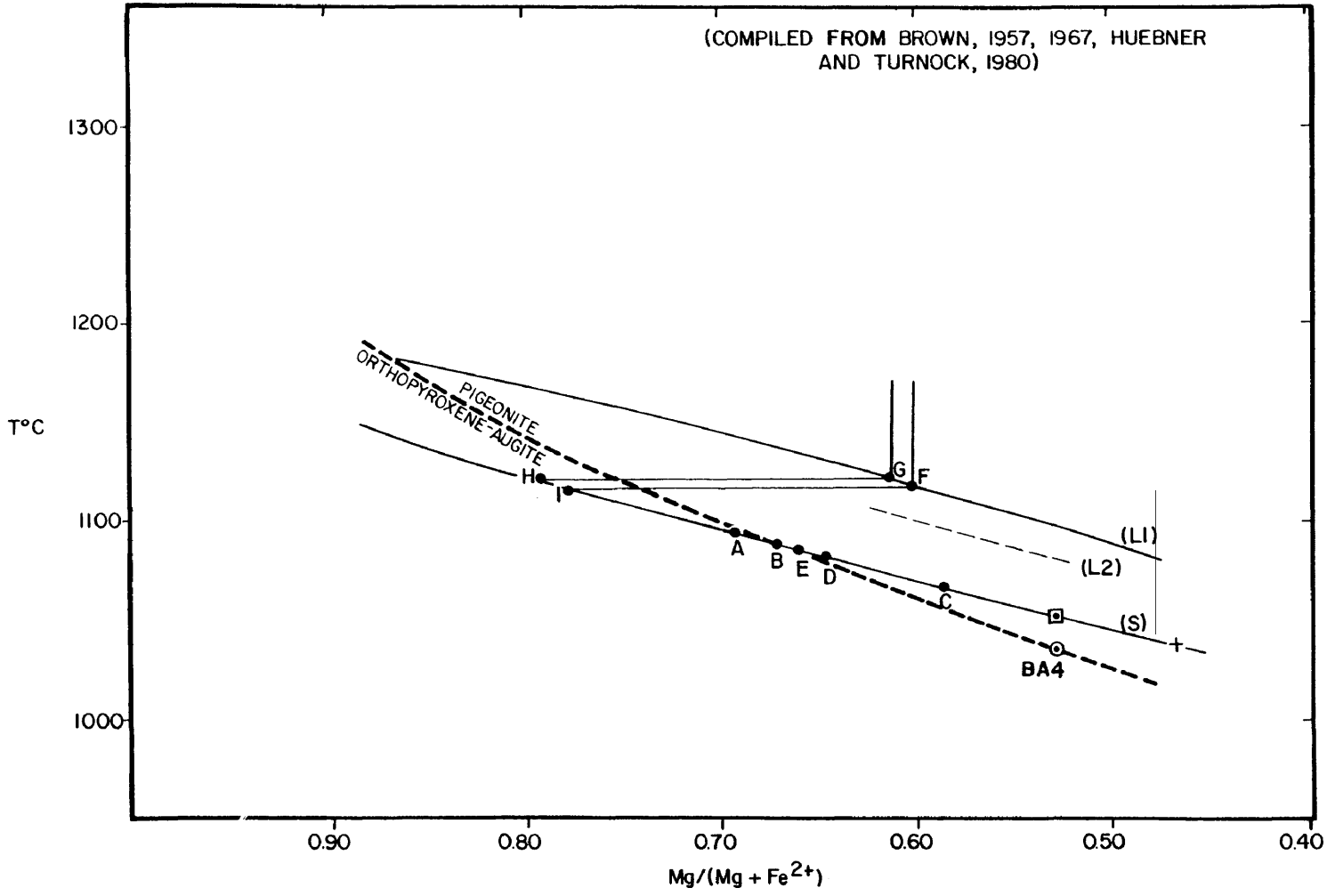

A = 78-207 (LAST CUMULUS HYPERSTHENE IN MAIN ZONE)
B = GR4-5-C (INVERTED PIGEONITE M.Mb/L.Z.)
C = GRI-44 (INVERTED PIGEONITE M.Mb/P.G.)
⊡ = SUGGESTED CRYSTALLIZATION TEMPERATURE OF BA4, BROWN, 1967
\+ = LAST INVERTED PIGEONITE IN UPPER ZONE (STUDY AREA)
D = 78-189 (FIRST CUMULUS PIGEONITE IN MAIN ZONE)
E = 78-92 (PRIMARY INVERTED PIGEONITE IN MAIN ZONE CHILL)
F = 79-374] CRITICAL ZONE CHILLED MAGMA
G = 78-53]
⊙ = INVERSION OF BA4, BROWN 1967.

Fig. 26 Schematic representation of possible phase relations between Ca-poor pyroxenes and temperature in the study area.

uncertain the position of the liquidus is not of importance in explaining the observed orthopyroxene-pigeonite relations.

As the liquid fractionates to more iron-rich compositions during crystallization, similarily the crystallizing orthopyroxene changes along the solidus from point H to more iron-rich compositions. Point A, which represents the last cumulus orthopyroxene that precipitated together with augite in the main zone, is still within the stability field of orthopyroxene. With continued fractional crystallization, the solidus for the Ca-poor pyroxenes, entered the statility field of pigeonite at about B in Figure 26. The first cumulus inverted pigeonite in the main zone has a Mg* of 0,657 and is represented by point D in the diagram. Pigeonite remained as the sole precipitating cumulus Ca-poor pyroxene down to a Mg* of 0,469 which marks the point at which it is believed that the two pyroxene field is terminated.

By using the pyroxene geothermometers of Wood and Banno (1973) and Ross and Huebner (1975), Himmelberg and Ford (1976) calculated that the phase change from orthopyroxene to pigeonite took place at 1074° C in the Dufek Intrusion, and that pigeonite ceased to crystallize at the limit of the two pyroxene field at 1040° C. According to Figure 26 the first cumulus pigeonite in the Potgietersrus intrusion crystallized at 1085° C and the termination of the two pyroxene field was at 1032° C. These graphically determined values are in good agreement with the values calculated by Himmelberg and Ford for the Dufek Intrusion and also agree fairly well with temperatures calculated by the author by using the Wells (1977) modification of the Wood-Banno geothermometer, as as well as the pigeonite thermometer of Ishii (1975). The two thermometers respectively yield values of 1111° C and 1132° C for the appearance of the first cumulus pigeonite and 1022° C and 1045° C for the last inverted pigeonite in the sequence. All other points on Figure 26 plot within approximately 30° C of the values calculated using the above mentioned geothermometers.

A variety of exsolution textures of augite within inverted pigeonite are shown in Figure 24. Boyd and Brown (1969) examined the chemical composition of the Bushveld pyroxenes, and because of the close similarity in composition between the primary and ex-

solved Ca-rich phases in the same rock on the one hand and between the primary and exsolved Ca-poor phases on the other they concluded that the Bushveld pyroxenes have maintained subsolidus equilibriation over a substantial period during cooling. A similar exercise was attempted on pyroxenes from the main and upper zone, but unfortunately the exsolved Ca-poor lamellae in the Ca-rich pyroxene were too thin (less than 5 microns) to be analysed with the electron microprobe. Buchanan (1979) conducted a similar study on Bushveld pyroxenes with the aid of a transmission electron microscope and found that the thin, Ca-poor lamellae can contain a large number of very fine exsolution lamellae less than 0,1 microns wide.

No difficulty was experienced in analyzing the exsolutions of augite in inverted pigeonite wider than 10 microns (Appendix 1). These analyses show that the composition of the exsolved augite in inverted pigeonite is virtually identical to the subsolidus composition of the cumulus clinopyroxene (Fig. 27). This suggests that the solidus compositions of the Ca-rich and Ca-poor pyroxenes have maintained equilibrium with each other, an observation noticed earlier on the basis of the configuration of the tie-lines between coexisting pyroxenes and also on the basis of the high $K_D^{opx\text{-}cpx}_{Mg\text{-}Fe}$ values with a low standard deviation.

4.2 Olivine

Olivine is found as a cumulus phase only in the lower zone, where it forms an integral part of the ol-chr cumulate and the opx-ol-chr cumulates. It occurs as euhedral crystals when found in its original state (Fig. 8A), whereas reaction with the intercumulus liquid caused resorption of the olivine (Fig. 8E). Although this reaction relationship is very common, the cores of these resorbed grains still possess their original cumulus chemistry. When the orthopyroxene : olivine ratio is fairly high, like in the opx-ol-chr cumulate (Fig. 8B), olivine is moulded against bronzite due to interference between both growing phases.

The Mg* of the olivines varies from 0,845 to 0,946 (Appendix 3), the latter value being obtained from olivine coexisting with approximately 50 per cent chromite. However, values typical of cumulus olivine not in association with abnormal concentrations

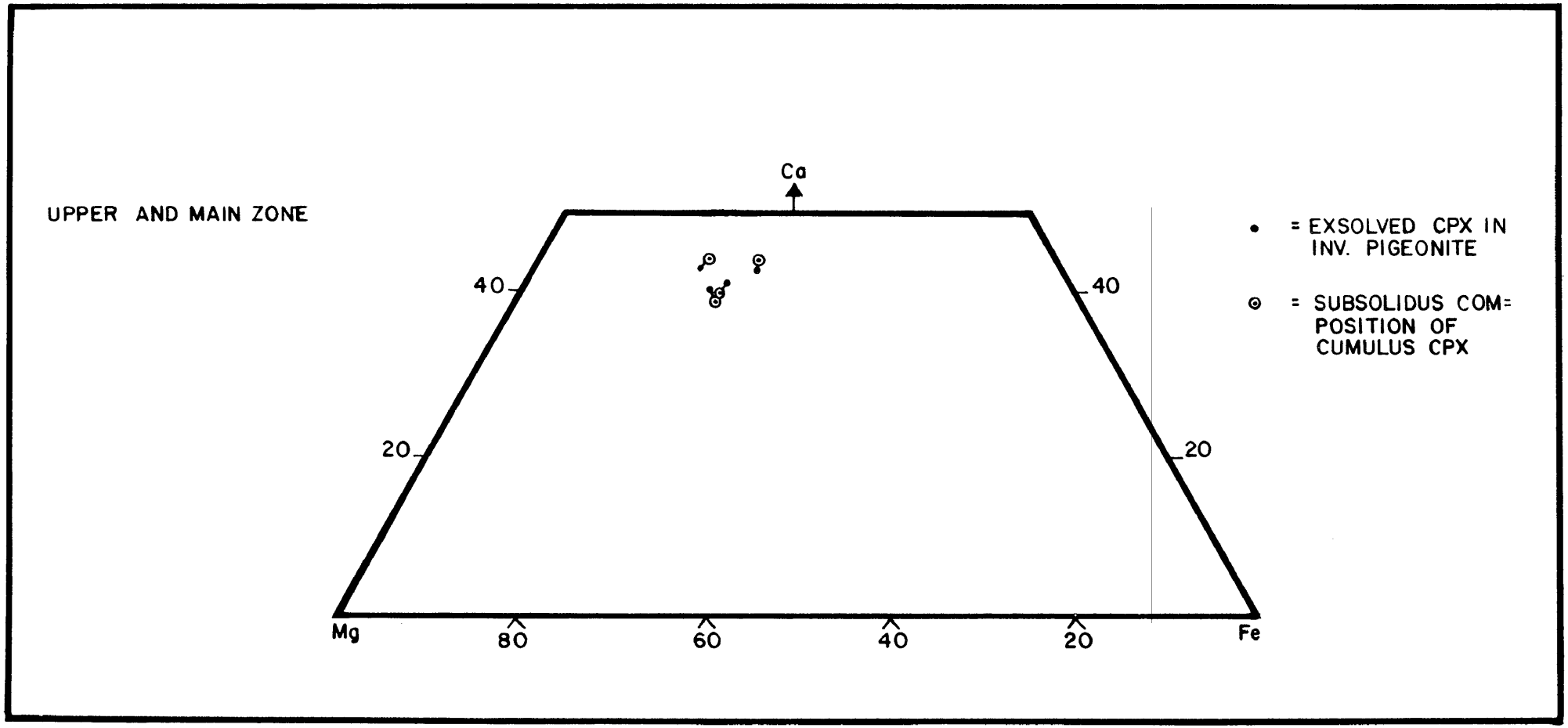

Fig. 27 A Ca-Mg-Fe plot showing the close compositional similarity between the subsolidus composition of cumulus clinopyroxene and that of exsolved clinopyroxene in the coexisting inverted pigeonite.

of chromite (<5 per cent) range from 0,845 to 0,900.

The MnO content ranges from 0,10 to 0,28 weight per cent whereas the CaO content ranges from 0,02 to 0,11 per cent. NiO is seen to range from 0,10 to 0,32 per cent with the highest value occurring about 33 m above the upper chromitite layer in cyclic unit 27, which is believed to have crystallized in response to a new influx of magma. The lowest value occurs at the -1250m level and is due to a Ni depletion in the magma caused by the precipitation of up to 1,1 weight per cent Ni-Fe-Cu sulfides in the ol-chr cumulate preceeding this level. A low value was also recorded for the last cumulus olivine (3-2395, Appendix 3) to form in the lower zone. Cr_2O_3 was found to range from 0,02 to 0,13 per cent, with the highest values occurring in samples associated with the upper chromitite layer.

Samples UGC-1A, 1B, 1C and GV-22 all contain olivines with abnormally high Mg* (Appendix 3). Of these, UGC-1A and 1B are olivine-chromite cumulates in which the olivines coexist with about 50 per cent chromite. The high Mg* in both these samples is considered to be due to postcumulus re-quilibriation of the two cumulus phases. Olivine UGC-1C is from an olivine vein that cuts the ol-chr cumulate UGC-1A (Fig. 44C and D), whereas GV-22 is olivine from an olivine adcumulate directly underlying the lower chromitite layer. These modified olivines, as well as the Cr_2O_3 content of the olivine, will be discussed in more detail in the section dealing with the petrogenesis of the chromite mineralization.

A plot of the $Mg/(Mg+Fe^{2+})$ of olivine against the same ratio of the coexisting orthopyroxene (Fig. 28) shows that the spread for cumulus olivine-intercumulus orthopyroxene assemblages is no greater than the spread for coexisting cumulus phases. This is analogous to the previously mentioned coexisting cumulus and intercumulus ortho- and clinopyroxene pairs, and suggests equilibration or re-equilibration under similar physiochemical conditions. A correlation coefficient of 0,921 suggests a strong compositional relationship between olivine and orthopyroxene, regardless of whether it is of a cumulus or intercumulus origin.

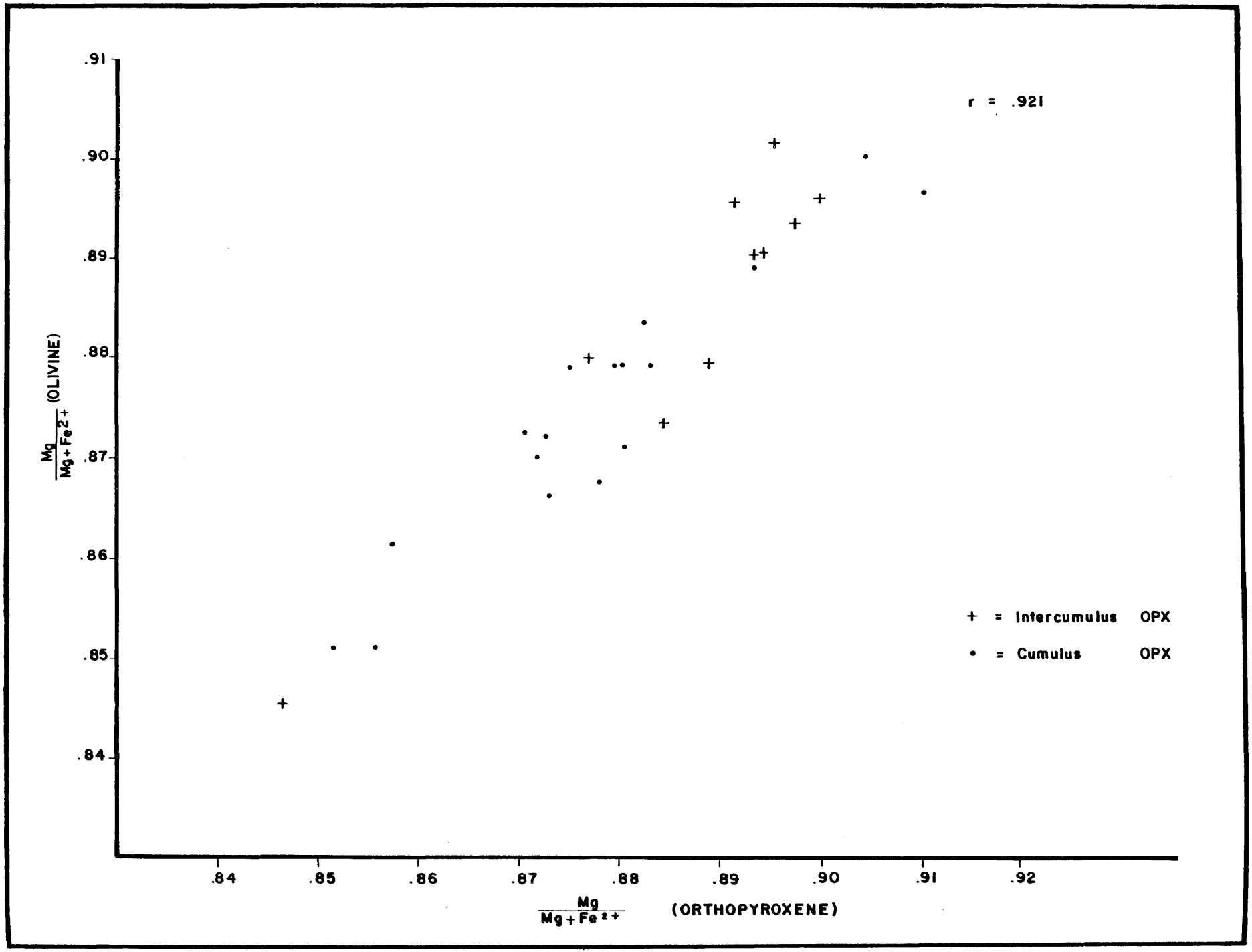

Fig. 28 $Mg/(Mg+Fe^{2+})$ plot of orthopyroxene-olivine pairs from the lower zone.

4.3 Plagioclase

Plagioclase is by far the most abundant mineral in the critical, main, and upper zones of the Rustenburg Layered Suite. It typically occurs as elongated, tabular crystals with length to width ratios of approximately 2,5:1. Although the cumulus feldspars are typically tabular, plagioclase grains in the non-cumuluate rocks of the marginal members have both skeletal as well as acicular growth cluster morphologies.

Skeletal crystals are well developed in the M.Mb./P.G. as is seen in Figure 10C and D. The cores of the plagioclase appear under the microscope as clouded dark brown to black, almost unresolveable opaque to translucent material. The intensity of the clouding varies within the cores. In some places it is similar in appearance to devitrified glass, and in other places it appears to consist of small, randomly oriented mineral inclusions of opaque iron- and iron-titanium oxides. A few grains were examined with the electron microprobe and it was found that the optically relatively homogenous portions are very rich in Fe and Ti.

The Fe-Ti oxide-rich nature of the M.Mb./P.G. samples, coupled with the devitrified glass-like character and volatile-rich nature of the turbid material, leaves little doubt that this feature is the result of fast crystal growth due to supercooling and that the enclosed material represents trapped microlites and melt. Armbrustmacher and Banks (1974) describe similar clouded feldspars with inclusions of microscopic opaque iron oxides and pyroxenes from dolerite dikes in the Bighorn Mountains of Wyoming. Similar glass-riddled cores have also been described by Luhr and Carmichael (1980) from the Colima Volcanic Complex, Mexico, and they believe it to reflect a period of skeletal crystal growth and melt incorporation under supercooled conditions. Kuno (1950) also noted plagioclase with included glass in samples from the Hakone Volcano, Japan. Bottinga et al. (1966) describe similar clouding as being due to inclusions of crystallites of hematite, magnetite, ilmenite, biotite, pyroxene and olivine. They consider the texture to be due to enrichment in iron and magnesium at the boundary layer adjacent to rapidly growing crystals.

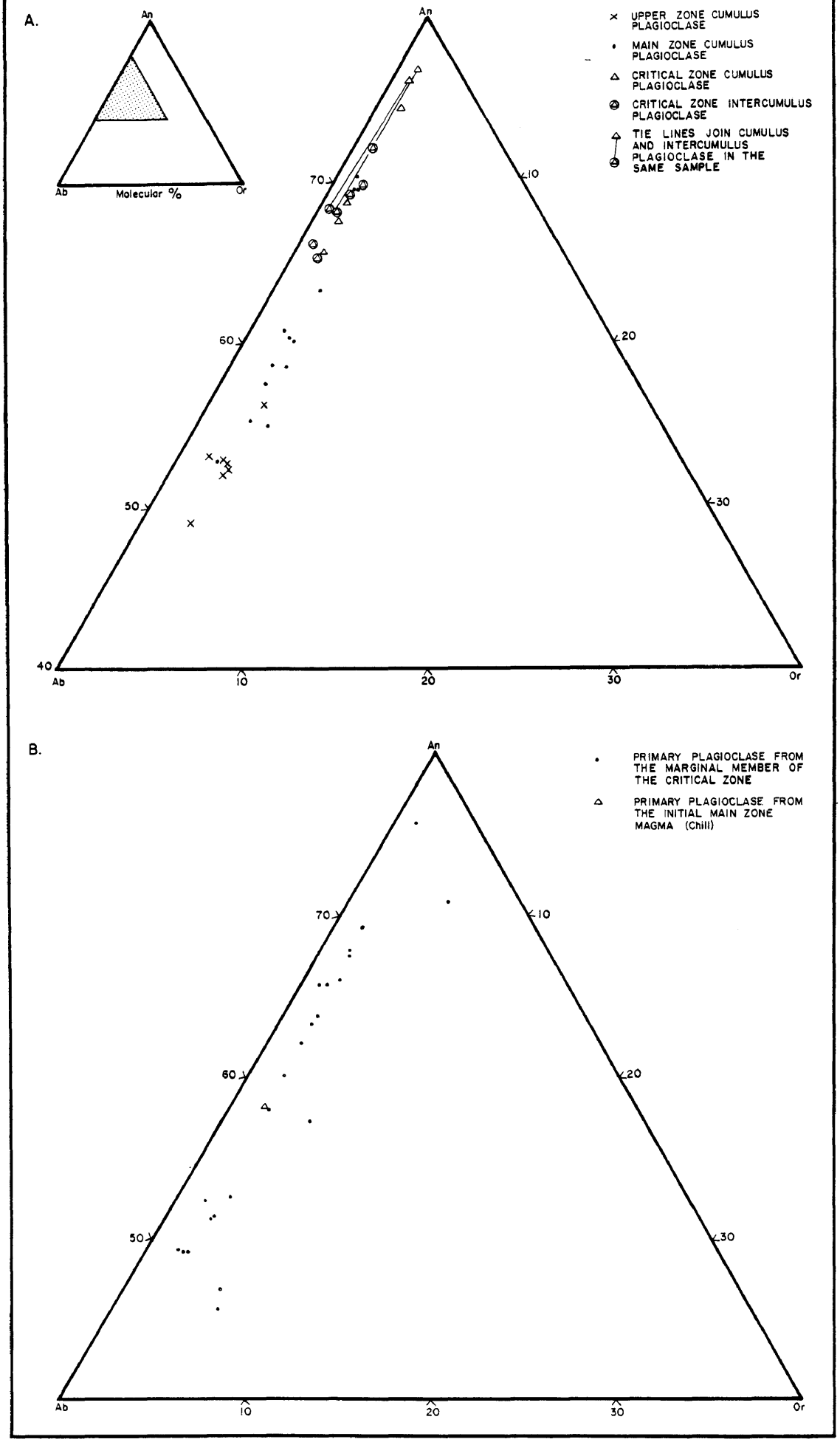

Fig. 29 Compositional variations of plagioclase from
(A) cumulates of the Rustenburg Layered Suite and
(B) the marginal member of the critical zone as well as a sample from the chill of the postulated initial main zone magma.

Kirkpatrick (1975) and Lofgren (1974) describe the development of skeletal plagioclase morphologies very similar to those seen in Figure 10. Lofgren (1974), by using plagioclase of similar composition to that described from DDH-GR1, produced skeletal plagioclase under 5kb water pressure at ΔT (supercooling) = 100° C, whereas the tabular variety required values of ΔT = 50° C. From this it can be assumed that the skeletal plagioclase with the glass-riddled cores developed in response to about 100° C supercooling. In contrast, the elongated and radiating clusters of plagioclase crystals in the basal, fine-grained layer of the main zone could have crystallized at a cooling rate of about 16° C/hr, if they crystallized under conditions similar to those described by Lofgren and Donaldson (1975).

The Ca/(Ca+Na+K), or the Ca*, of the plagioclases ranges from 0,455 to 0,769 (Appendix 4). The lowest values were recorded from plagioclase in the contaminated M.Mb./P.G., whereas the lowest values in the layered sequence is 0,490, which is of plagioclase from the highest available stratigraphic level of the upper zone in this area. All of the feldspars from the lower zone are highly altered. The compositional variations of the plagioclase in terms of their three end-members are shown in Figure 29A and B. This diagram shows that there is a definite increase in the Or component of the cumulus plagioclase from the critical zone to the upper zone. Also shown is the spread in An contents from the core to the rim in the cumulus plagioclases from the critical zone. The maximum spread of 8,9 mole per cent An occurs in pl-opx-cpx cumulates of the critical zone, and the zoning is of the normal variety.

Figure 29B represents the plagioclase from the M.Mb./P.G. and M.Mb./L.Z.. It is apparent that the feldspars have a considerable spread in An content and the more albitic samples have the highest orthoclase component. These latter samples are from rocks which were evidently contaminated by Na and K through assimilation of Pretoria Group sedimentary material.

By using the published temperature dependent partition coefficients between plagioclase and melt from Drake (1976), the calculated crystallization temperatures based on pyroxene geothermometry as

well as the plagioclase compositions, it is possible to calculate the Al_2O_3 and Na_2O content of the parent melt from which the pl-opx-cpx cumulate of the critical zone crystallized. Values of 17,29 and 2,01 per cent were obtained for Al_2O_3 and Na_2O respectively for sample 3-241, whereas similar calculations for a magnetite gabbronorite from the upper zone (sample 5-124) yield values of 12,66 and 2,91 per cent Al_2O_3 and Na_2O respectively. Earlier calculations (Chapter 4.1.4) of the Al_2O_3 content of the magma based on the $D_{Al}^{cpx-liq}$ data gave values of 18,29 per cent for sample 3-241 and 13,85 per cent for sample 5-124. Temperatures of 1154° C for the critical zone and 1045° C for the upper zone, both based on the two pyroxene geothermometer, were used for the D_{Al}^{pl-liq} calculations. The similarity of the values calculated by the two methods does indicate that the critical zone magma was in fact very aluminous and that the upper zone magma was depleted in alumina but enriched in sodium.

4.4 Other Silicates

4.4.1 Micas

The distinction between biotite and phlogopite is made on the basis of the Mg/Fe ratio of the mica as proposed by Deer, Howie, and Zussman, 1966. They proposed that if the ratio is >2:1 it is phlogopite and if <2:1 it is biotite.

Using this criteria it was found that both phlogopite and biotite occur in the rocks within the study area. Biotite is common as a reaction product between feldspar and Fe-Ti oxides in the upper zone. Both biotite and phlogopite are present in the M.Mb./P.G. where the later commonly occurs as kelyphitic rims surrounding Fe-Ti oxides. In these cases the mica is considered to be the result of reaction between the early oxides and interstitial liquids. Because the reaction involves a titanium-rich phase, the resulting mica is also rich in TiO_2 (Appendix 5, column 2).

Not all the mica in the M.Mb./P.G. is considered to be a product of the above reaction. The large poikilitic crystals (Fig. 10D) clearly are not a reaction product, but have crystallized directly from the interstitial liquid. Although only traces of K- feldspar have been found in these rocks, it may have been sufficient to pro-

mote the following reaction:

$KMg_3AlSi_3O_{10}(OH)_2 + nSiO_2 + mKAlSi_3O_8 + XH_2O \rightleftharpoons melt$

phlogopite quartz sanidine gas liquid

which Wones and Dodge (1977) found not to be stable above 850° C at 500 bars P_{H_2O}.

4.4.2 Amphibole

The only occurrence of amphibole other than trace amounts in the M.Mb./P.G., is found in the mottled anorthosite at the base of the upper zone. Here green hornblende is seen to be replacing intercumulus augite. A representative analyses is given in Appendix 5, column 3. The amphibole is thought to be a deuteric alteration product of the intercumulus augite.

4.4.3 Fe-Rich Alteration Products

Some very peculiar alteration products are associated with the magnetitite layers in the upper zone and the ferritchromit-magnetitite layer in the lower zone (Appendix 5). In almost all of the cases, the alteration products are very aluminous and iron-rich. In the upper zone samples these alteration products commonly replace orthopyroxene pseudomorphously, yet coexisting clinopyroxene is not affected. This alteration will be discussed more fully in Chapter 8.3.

4.4.4 Chalcedony Pseudomorphs

An interesting sample of chalcedony replacing cumulus olivine has been found along the boundary between the farms Volspruit and Zoetveld. Here the upfaulted equivalent of the upper chromitite layer, that has resisted weathering for a prolonged period of time, has been exposed in an old cutting. The chain-textured chromite has been unaffected by the weathering except for some marginal alteration to ferritchromit, yet the olivine, which originally had a Mg* of 0,930; is now completely replaced to an impure chalcedony with approximately 4,78 per cent impurities (Appendix 5, column 10). It is amazing that the silicate can be subjected to such extreme modification, yet the chromite remains relatively unaffected and still retains its primary chemistry (Appendix 7, sample 78-257).

5 MINERALOGY AND PETROGENESIS OF THE OXIDE MINERALS

Significant concentrations of vanadiferous titanomagnetite and chromite occur within the study area. The magnetitite layers in the upper zone contain amongst the highest levels of V_2O_5 reported from the Bushveld Complex (van der Merwe, 1978), whereas the chromitite mineralization from the lower zone is the best metallurgical grade chromitite being mined in the Republic.

5.1 (Vanadiferous) Titanomagnetites

Titaniferous magnetite is a common constituent of the upper zone lithologies, either as disseminations in the gabbronorites or as massive concentrations in the magnetitite layers. It also occurs in accessory amounts in gabbronorites from the marginal member of the critical zone adjacent to the Pretoria Group.

5.1.1 Textural Features

5.1.1.1 Morphology

The morphology of the primary titaniferous magnetite crystals is usually very difficult to define, particularly in the upper zone samples. In some samples containing disseminations of oxides, the oxides form large patches of poikilitically enclosing cumulus inverted pigeonite and augite (Fig. 30A). Microscopic investigations show these poikilitic patches to consist of several titanomagnetite grains of different orientation that have coalesced to form this texture. In other samples (Fig. 30B) the outlines of the original titaniferous magnetite grains are well preserved. The primary spinel morphology in the magnetitite layers cannot be descerned because spinel grain boundaries are usually smooth and have triple point junctions, indicative of postcumulus annealing.

Discrete cumulus ilmenite grains are very rare in both the silicate-rich and the spinel-rich layers of the upper zone. Discrete primary ilmenite and primary titaniferous magnetite grains do however occur in rocks of the M.Mb./P.G., especially in quenched rocks with high I.C. numbers (Fig. 30F).

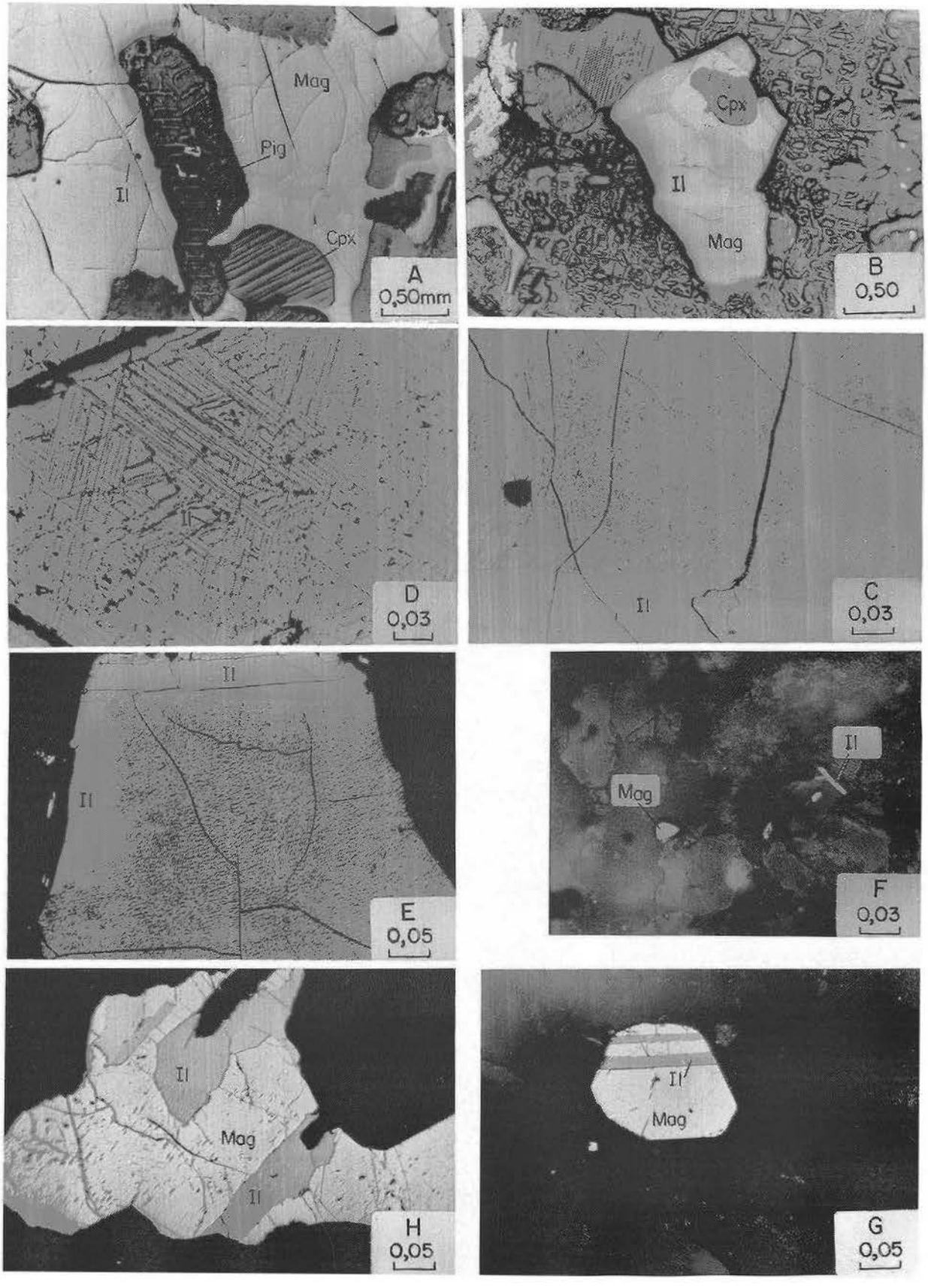

Fig. 30

Figure 30. Textural relations of Fe-Ti oxides from the study area. pig = inverted pigeonite; cpx = clinopyroxene; Mag = magnetite; Il = ilmenite. All sections have been photographed with reflected light under oil immersion. Sample numbers are indicated in brackets.

(A) Large Fe-Ti oxide grain poikilitically enclosing cumulus pigeonite and clinopyroxene (augite). (5-195)

(B) A cumulus titaniferous magnetite grain which has subsequently exsolved into a coarse granular ilmenite and magnetite fraction. Note the inclusion of cumulus augite. (5-138)

(C) Cloth textured ulvöspinel exsolution in a magnetite grain adjacent granular ilmenite. (5-124)

(D) Trellis textured exsolution of ilmenite parallel to (111) of magnetite. (5-315)

(E) Dark coloured exsolution of ulvöspinel and Mg-Fe-Al spinels in magnetite. Also present are coarse exsolutions of ilmenite along the margin of the composite titanomagnetite grain. (5-138)

(F) Discrete, unexsolved primary ilmenite and magnetite grains from a very fine-grained (I.C. # ≈650) gabbronorite in the M.Mb./P.G. (78-374D)

(G) Magnetite grain with exsolved ilmenite in a comparatively coarser-grained (I.C. # ≈350) rock from the M.Mb./P.G. (GR1-97,89)

(H) Exsolutions of ilmenite in magnetite from an even coarser-grained (I.C. # ≈240) rock of the M.Mb./P.G. (78-53)

5.1.1.2 Exsolution Textures

Coarse granular exsolution of ilmenite to form composite grains of titaniferous magnetite and ilmenite are common in the magnetitite layers and silicate rich rocks of the upper zone (Fig. 30B). The ilmenite grains occur frequently as large lobate crystals near the edge of the composite grains. These ilmenites are homogeneous and contain no exsolution of hematite. The titaniferous magnetite, adjacent to the granular ilmenite contains "cloth texture" exsolutions of ulvöspinel parallel to the (100) planes of the host magnetite. The trellis exsolution of ilmenite parallel the (111) direction of the host magnetite (Fig. 30D) could be the result of either exsolution of the Ti-component as ilmenite at relatively oxidizing conditions during cooling or to oxidation of early exsolved ulvöspinel to ilmenite and migration of the ilmenite to the (111) direction.

Exsolutions of Mg-Fe-Al spinel occur sporadically in the titanomagnetite grains. Where they are intimately associated with ulvöspinel exsolutions they impart a dark colour to the exsolution lamellae (Fig. 30E)

Exsolution textures within the Fe-Ti oxides are also observed in the M.Mb./P.G.. Although exsolution textures were not observed in the Fe-Ti oxides of the very fine-grained rocks within this member, the Fe-Ti oxides in their coarser grained equivalents, with I.C. numbers of approximately 400, contain the odd exsolution lamellae of ilmenite (Fig. 30G). Coarser grained rocks from the M.Mb./P.G., (with I.C. numbers of 240) can contain large Fe-Ti oxide grains with a greater proportion of exsolved ilmenite (Fig. 30H) than the titanomagnetite of the finer-grained lithologies.

Buddington and Lindsley (1964) suggested that with increasing degrees of oxidation and diffusion a systematic series of oxide mineral textures will result. From the described exsolution textures, there is little doubt that the cooling rate also has an influence on the type of texture, as both the cation mobility and the degree of oxidation decrease on cooling. The first generation of exsolution in the upper zone samples is that of the segregation of granular ilmenite. This granular ilmenite ex-

solved at high temperatures allowing the cations to move relatively freely within the titaniferous magnetite. Any subsequent exsolution of ilmenite as lamellae formed when the cations were less mobile. These very fine 3-8 micron wide trellis lamellae were produced when the cation mobility was further reduced with decreasing temperature. Also, the smaller grained cumulus phases and the presence of well developed ulvöspinel exsolution compared to Figure 30A, may have resulted from a larger degree of undercooling of the magma than that which produced the latter.

The oxidation process critical to the development of ilmenite can be respresented by the equation proposed by Vincent (1960):

$3Fe_2TiO_4$	+	$O \rightleftharpoons 3FeTiO_3$	+	Fe_3O_4
Usp. in Usp-Mag. solid solution		Ilm. in Ilm.-Hem. solid solution		Mag. in Mag.-Usp. solid solution

Controls on this subsolidus oxidation reaction could be the composition of the Fe-Ti oxide phases, the coexisting ferromagnesium silicate phases and volatiles present like H_2O and SO_2. The oxygen required for this oxidation could be derived from the dissociation of water. It was noticed that titanomagnetite in samples containing sulfides seldomly display the fine trellis ilmenite lamellae exsolution features. This may be due to SO_2 having the opposite effect as the dissociation of H_2O and thus cause the oxidation of magnetite to cease at a higher temperature. Mathison (1975) found that a marked parallelism exists between the modal proportions of the sulfides in each rock and the ulvöspinel content present in the magnetite.

5.1.1.3 Unusual Textural Features

Vermicular intergrowths between granular ilmenite and an unusual iron-rich silicate phase (Fig. 31A and B), and between magnetite and a similar iron-rich silicate (Fig. 31C), have been observed in the magnetite gabbronorites of the upper zone. The iron-rich silicate phase which contains about 30, 15, 9, and 35 per cent SiO_2, Al_2O_3, MgO, and total iron as FeO respectively, as well as small amounts of TiO_2, MnO, CaO, Na_2O, and K_2O (Appendix 5, columns 5-9), only seems to replace orthopyroxene. Coexisting clinopyroxene and plagioclase show no signs of alteration. Evidence for this can be seen in Figure 30A where pseudomorphs of the iron-rich silicate phase after inverted pigeonite (Appendix

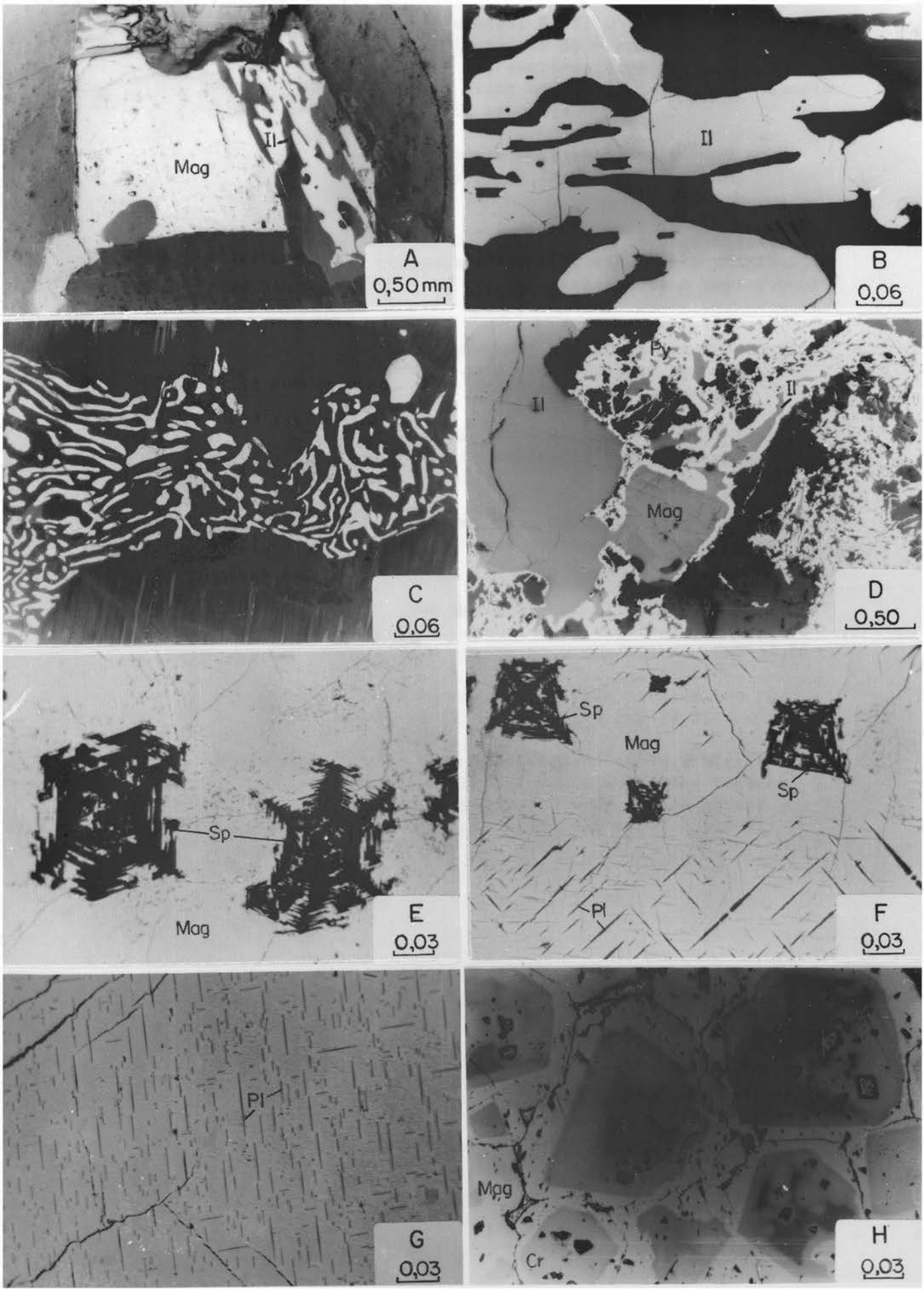

Fig. 31

Figure 31 Textural relations of unusual Fe-Ti oxides and spinels. Mag = magnetite; Il = ilmenite; Sp = spinel; Pl = pleonaste; Cr = chromite. All sections have been photographed with reflected light under oil immersion. Sample numbers are indicated in brackets.

(A) Vermicular intergrowth between ilmenite and an iron-rich silicate phase in the upper zone. (5-440)

(B) Enlarged view of the intergrowth seen in Figure 31A. The irregular embayment within the original, granular ilmenite is considered to be a replacement feature. (5-440)

(C) Vermicular intergrowth of magnetite and an iron-rich silicate phase in an altered Ca-poor pyroxene. (5-195)

(D) Replacement of granular ilmenite and, to a lesser extent, magnetite by pyrite during postcumulus sulfidation. (5-124)

(E) "Multiple cross-arm" type Mg-Fe-Al spinel within magnetite from the base of the main magnetitite layer, Molendraai. (M5-39,4)

(F) "Cruciform" type Mg-Fe-Al spinel within magnetite. Note the Mg-Fe-Al spinel rods exsolved parallel to the (100) planes of the host magnetite. (M5-39,4)

(G) Exsolution of pleonaste lamellae parallel to the (100) of the Fe-Ti oxide host. (M5-39,4)

(H) Ferritchromit from the Drummondlea Harzburgite-Chromitite. The lighter zones of higher reflectivity consist of magnetite whereas the darker areas are enriched in Cr_2O_3 and Al_2O_3. (2A-47)

5, columns 6,7,8) still contain the original exsolution lamellae of augite.

From microscopic investigations it would seem that some of the ilmenite of the composite magnetite-ilmenite grains was also replaced during formation of the Fe-rich silicates (Fig. 31A). This is also suggested by the fact that replacement of the orthopyroxene is restricted to those portions of the rock where ilmenite could also have been involved in the reaction. Furthermore, the fact that intercumulus orthopyroxene may also be replaced, leads to the conclusion that a late stage iron- and alumina-rich liquid is involved in the reaction. The vermicular texture in Figure 31C appears very similar to that described by McSween and Nystrom (1979) for vermicular orthopyroxene-magnetite intergrowths in the Dutchmans Creek gabbroic intrusion of South Carolina. They also attributed this texture as being due to a reaction between orthopyroxene and the residual melt in the crystal mush.

A similar type of texture is seen in Figure 31D, where pyrite seems to replace granular ilmenite and magnetite. The pyrite-rich areas contain slender, worm-like inclusions and lobate patches of ilmenite. Such features strongly suggest a postcumulus sulfidation process in these rocks.

Another interesting texture is formed by skeletal, and cruciform Mg-Fe-Al spinels at the base of the main magnetitite layer (Fig. 31E and F). The spinel in Figure 31E is best referred to as "Multiple cross - arm type" whereas that in Figure 31F is the cruciform type, using the nomenclature of Haggerty (1976). Previously, this spinel morphology has only been described from magnetites and chromites in rapidly cooled environments, and as Haggerty points out, the systematics for these growth habits has yet to be established. Textures such as those seen in Figure 31E and F are usually destroyed in part by the sintering or annealing of the magnetite grains.

From its geological setting it is obvious that these cruciform and multiple cross-arm spinels could not have originated as a result of rapid cooling, as is the case for similar textures

developed in magnetite from lavas. Consequently, this cruciform texture is considered to be a combination of what is referred to as synchronous dendritic growth (Spry,1969) and subsolidus exsolution due to the expulsion of high concentrations of Al and Mg that could not be accommodated in the Fe-Ti oxide lattice on cooling. Dendritic growth occurs when successive layers of a crystal are added to a nucleus at a high-energy projection to give rise to a tree like structure. Crystallization may begin with a slight departure from normal or layer crystallization when a random proturberance is formed. Accelerated growth may take place on this protuberance as it grows along local concentration paths if the energy gradient is large enough and the strong supersaturation gradients are limited around a number of nucleii (Spry, 1969).

In the case on hand, the cruciform spinel was controlled by the crystal structure of the host, high energy surfaces, and high Al-Mg concentration gradients developed within the host on a localized scale. The control exerted by the host Fe-Ti spinel can be seen by the abundance of Mg-Fe-Al spinel rods exsolved parallel to the (100) planes of the host (Fig. 31F, bottom). These exsolutions are parallel to the primary arms of the cruciform spinel and the acute arms joining the primary orthogonal arms are oriented parallel to the (111) planes (Fig. 31F). It is envisaged that higher than normal surface energy existed at the intersection of some of the (100) planes. As a result of this nucleation, dendritic growth occurred on a localized scale. The area surrounding the cruciform spinels is devoid of exsolved spinel rodlets (Fig. 31F), suggesting that growth of the cruciform spinels depleted the local environment in Mg and Al.

The multiple cross arm type of spinel (Fig. 31E) probably represents a different orientation of the cruciform type. Exsolution of sphalerite stars in chalcopyrite is a related phenomena; a small star shaped spinel occurs in the top-centre portion of Figure 31F.

The most commonly observed form of this Mg-Fe-Al spinel, probably pleonaste, is as exsolution lamellae exsolved parallel to the (100) plane of the Fe-Ti host (Fig. 31G).

5.1.2 Chemistry of the Fe-Ti Oxides

For the analysed Fe-Ti oxides the amounts of Fe_2O_3 and FeO were determined from the total iron by assuming stoichiometry and by employing the program "Ferric" designed by Finger (1972). The method of Powell and Powell (1977) was used to calculate the proportions of ulvöspinel, magnetite, ilmenite and hematite in the respective oxide phases, although their method of calculating the T-fo_2 conditions was not used.

An electron microprobe beam of approximately 2 to 3 microns in diameter was used to analyse fine ilmenite exsolutions as well as variations in composition of the magnetite within the titaniferous magnetite. A broad beam, 25 microns in diameter, was used in a step traversing manner in an effort to obtain the bulk composition of the titaniferous magnetite grains from the upper zone. In order to obtain the pre-exsolution bulk composition of the original cumulus titaniferous magnetite, it was found necessary to measure the proportions of coarse granular ilmenite, trellis ilmenite and host titaniferous magnetite with an integrated ocular. By using the proportions of the various phases and the appropriate compositions, the primary pre-exsolution, bulk composition of the titaniferous magnetite was obtained (Appendix 6). Also indicated in Appendix 6 is the composition of the primary ilmenite and primary titaniferous magnetite in samples of the marginal member adjacent to the Pretoria Group.

5.1.2.1 Titaniferous Magnetite

The samples from the M.Mb/P.G. are very homogeneous in composition (Appendix 6). The exsolved magnetite fraction of the titaniferous magnetite grains are extremely depleted in the ulvöspinel component and have average mole fraction values of between 0,020 and 0,025. The depleted nature is likely due to the greater mobility of the diffusing cations at high temperatures in this rather oxidizing environment. The mean ulvöspinel component for the recast primary titaniferous magnetite (pre-exsolution) is 0,511. These titaniferous magnetites contain very little vanadium compared to their upper zone counterparts.

The primary Cr_2O_3 content is typically between 0,45 and 0,70 weight

per cent, yet samples with values of 2,72-3,27 per cent were recorded (Appendix 6). The latter values were obtained from a sample about four times as coarse as the others and also further from the contact, indicating a slower cooling rate than for the finer grained rocks. The lower Cr_2O_3 content of the magnetite in the finer-grained rocks is probably the result of fast cooling and crystal growth which prevented diffusion of Cr_2O_3 to the crystals. Gasparrini and Naldrett (1972) described a similar situation in the magnetites from Sudbury.

The low MgO, Cr_2O_3, and Al_2O_3 content and the high TiO_2 of the M.Mb/P.G. titaniferous magnetite indicate that they crystallized at pressures lower than 10 Kb, as Osborne and Watson (1977) have shown that magnetites that have crystallized at higher pressure are considerably enriched in MgO, Cr_2O_3 and Al_2O_3.

Analyses of exsolved magnetites and recast compositions of cumulus titaniferous magnetite of the upper zone are given in Appendix 6. The position of the microprobe analyses within the various grains and with respect to the other Fe-Ti oxides is illustrated in Figure 32. The respective analyses show a large intragranular chemical variation if a 2-3 micron diameter beam is used; for example analyses 5-195-2 and -9 reveal variations of 6,02 per cent TiO_2, 4,58 per cent FeO, and 12,84 per cent Fe_2O_3. A step-traverse analysis of the same grain with a 25 micron diameter beam (5-195-7) gave almost exactly the same result as the average of numerous analyses on randomly selected spots on the exsolved titanomagnetite grain with a focused beam (Appendix 6). Step-traverse analyses, using a 25 micron diameter beam across a grain are therefore considered to be a reasonable indication of the bulk composition of the titaniferous magnetite.

Some samples, e.g. 5-138-2, contain higher than normal concentrations of Al_2O_3 and SiO_2 concentrations. Some analyses from this sample (5-138) recorded high concentrations of CaO, i.e. 5,42 per cent, and this, in conjunction with the higher SiO_2 and Al_2O_3 content, seems to indicate that not only has fine aluminous spinel been exsolved but also that it contains some sphene. The "sphenitization" process is considered by Haggerty (1976) to be a product of auto-

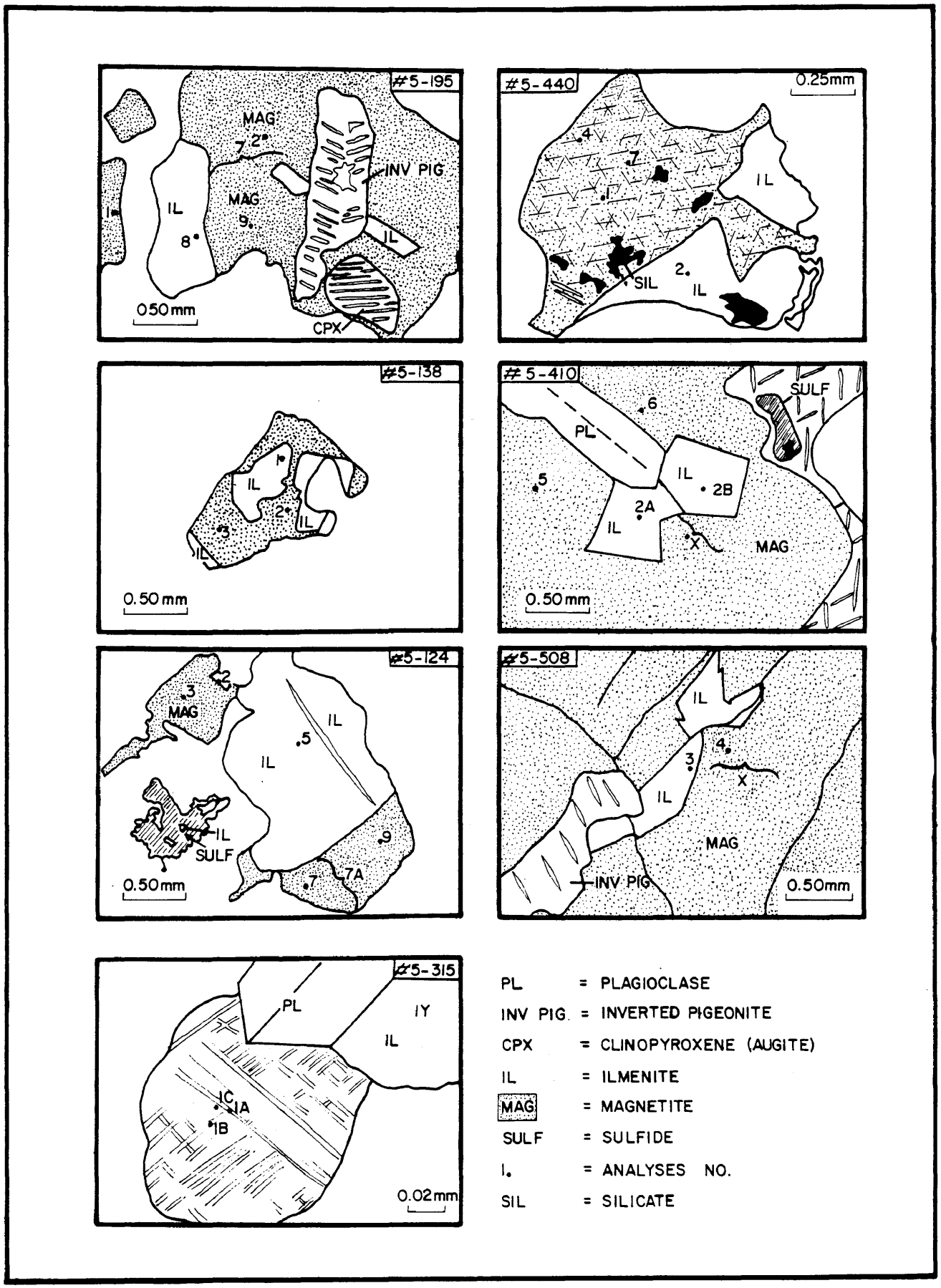

Fig. 32 Textural relationships of some coexisting magnetite and ilmenite analysed by electron microprobe. For explanation see the text.

metasomatism by reaction of residual liquids with early formed Fe-Ti oxides.

The recast upper zone titaniferous magnetites contain a mean primary mole fraction of ulvöspinel of 0,568 which is on average about 0,057 units higher than that found in the titaniferous magnetites from the M.Mb./P.G. The higher ulvöspinel content is evidently due to the titanium enriched nature of the more fractionated upper zone magma from which the primary titaniferous magnetites crystallized. Slower cooling of the upper zone liquid would also allow diffusion of TiO_2 over greater distances in the crystallizaing magma.

The upper zone titanomagnetites also differ from M.Mb./P.G. samples in that they contain considerably less Cr_2O_3, yet show a marked enrichment in Al_2O_3. The lower Cr_2O_3 content is probably due to the considerably more fractionated nature of the upper zone liquid. The higher alumina content of the upper zone titaniferous magnetite is reflected by the abundance of exsolved aluminous spinel in some of the magnetites relative to those of the M.Mb./P.G. . The low totals in these analyses (Appendix 6) indicates the presence of a significant amount of vanadium in the sample, as is also suggested by the high V_2O_5 content, of the magnetitite layers (up to 2,2 per cent; van der Merwe, 1978). Vanadium was not analysed because of the lack of a suitable standard and because of the masking of $V_{K\alpha}$ and $_{K\beta}$ radiation by $Ti_{K\beta}$ and $Cr_{K\alpha}$ respectively.

At present only semi-quantitative energy dispersive analyses are available of the Mg-Fe-Al spinels. The cruciform and rod shaped spinels (Fig. 31F) were found to contain 27 per cent MgO, 39 to 42 per cent Al_2O_3, 8 to 9 per cent Cr_2O_3 and 19 to 22 per cent FeO. It is thought that these pleonaste rods result from a higher temperature solvi intersection than the ulvöspinel - magnetite solid solution. Haggerty (1976) states that the maximum solubility of $FeAl_2O_4$ in Fe_2TiO_4 is approximately 20 mole per cent hercynite at 1000° C.

Unfortunately it is not possible to comment on the fractionation of elements within the upper zone primary titaniferous magnetites as only the lower 160 m of this zone was available for investigation.

5.1.2.2 Ilmenite

The primary ilmenite crystals and the ilmenite exsolved from titanomagnetite of the M.Mb./P.G. are chemically homogenous yet distinctly different in composition. The exsolved ilmenite is always found to be richer in TiO_2, MnO and FeO than its primary counterpart, and it consistently has a lower R_2O_3 content than the primary ilmenite. Mathison (1975) also documented similar consistent compositional differences between primary ilmenite and exsolved ilmenite from the Somerset Dam Intrusion, Australia.

What is most intriguing is the very high MnO content of the ilmenite from the M.Mb/P.G. Values range from 1,34 to 4,66 per cent with a mean value of 2,68 per cent (Appendix 6). Comparison with other layered complexes reveal that these samples are amongst the highest values ever recorded with the only other high MnO ilmenites being found in the Sudbury Nickel Iruptive (Gasparrini and Naldrett, 1972). Himmelberg and Ford (1977) reported that over half of the ilmenites exsolved from host titaniferous magnetites in the Dufek Intrusion contain approximately 2,20 per cent MnO. Morse (1980C) gives an average value of 0,46 per cent MnO for the Kiglapait ilmenites whereas Bowles (1976) reports values that range from 0,46 to 0,73 per cent MnO from ilmenites of the Freetown layered body. Mathison (1975) reports 53 ilmenite analyses from the Somerset Dam layered intrusion that range from 0,66 to 2,88 with a mean of 1,12 per cent MnO. In comparison, ilmenites from the Bjerkrem-Sogndal Massif contain less than 1,0 per cent MnO with an average of approximately 0,70 per cent (Duchesne, 1972A). Sharpe (Pers. Commun.) found that ilmenites from rapidly cooled uncontaminated marginal member rocks of the eastern Bushveld contain between 0,98 to 1,40, with a mean of 1,13 per cent MnO.

From the above it appears that most layered intrusions have ilmenites with MnO concentrations that seldom exceed 1,0 per cent and the question arises as to the high MnO content of the ilmenites from the M.Mb./P.G. Lindsley (as quoted in Himmelberg and Ford, 1977) stated that an increasing MnO content of the ilmenite is consistent with experimentally determined distributions of MnO between magnetite and ilmenite with decreasing temperature. That temperature is a factor for this relationship has also been suggested

by Buddington and Lindsley (1964), Neumann (1974), Tsusue (1973), Czamanske and Mihalik (1972) and Lipman (1971).

It is widely known that certain igneous suites can be characterized by the MnO contents in the ilmenites. Suites of acid intrusives and extrusives can characteristically have high MnO ilmenites, whereas ilmenites of higher temperature suites of basic intrusives and extrusives contain less MnO. Lipman (1971) showed a good correlation between SiO_2, temperature, MnO, and Al_2O_3 contents of ilmenite in a suite of samples ranging from latites to rhyolites. He found that the MnO content increased with increasing SiO_2 content of the parent magma, and that increasing temperature is accompanied by a decrease in the MnO content of the ilmenite.

It is interesting to note that the ilmenites in samples 78-374 and 78-360 have the lowest MnO content. These rocks are devoid of free quartz, yet are associated with a fairly siliceous environment. In contrast contaminated M.Mb./P.G. samples such as GR1-100 and GR1-102 with 9,00 and 10,16 per cent free quartz respectively, contain ilmenite with MnO values of 3,29 and 4,66 per cent. Sample GR1-69, on the other hand, contains 7,7 per cent quartz and the ilmenite 2,93 per cent MnO. It is of interest that the lowest temperatures were calculated from these rocks by using various geothermometers, and that the orthopyroxenes in these rocks contain about 0,70 per cent MnO which reflects a very high rhodonite component for an igneous pyroxene.

This strong correlation between MnO content of ilmenite and the SiO_2 content of the parent melt can also be demonstrated with the aid of data from the Sudbury Nickel Irruptive (Gasparrini and Naldrett, 1972). Although no systematic variation of the MnO content of the ilmenites was observed by these authors, variation between 1,5 and 3,9 per cent in samples from the north range and between 0,6 and 5,6 per cent in samples from the south range, a definite relationship seems to exist between the amount of quartz and micrographic intergrowth on the one hand and MnO content of the ilmenites on the other hand. Reference to their diagram (ibid, p. 607) shows that the south range norite contains significantly less quartz and micrographic intergrowth than the norite from the north range, and that the ilmenites contain on average 1,71 per

cent MnO, whereas the ilmenites of the very quartz- and micrographic-rich north range contain on average 2,57 per cent MnO.

The upper zone ilmenites (Appendix 6 and Figure 32) are extremely rich in TiO_2 and low in R_2O_3. TiO_2 values are limited to the range 52,25 to 53,01 per cent, values that are higher than those from the M.Mb./P.G. This is evidently due to the TiO_2 enriched nature of this more fractionated liquid from which the upper zone titanomagnetites crystallized, and the fact that the TiO_2 does not have to be distributed into as much primary ilmenite, which is only present in trace amounts in the upper zone, but an abundant primary phase in the M.Mb./P.G.

The ilmenites are extremely homogenous in composition (Appendix 6) and reference to Figure 32, samples 5-410-2A and 2B and samples 5-315-1A and 1B show that early, as well as late, exsolutions have nearly identical compositions, suggesting that equilibrium was maintained over a considerable period during cooling.

The MnO content of the exsolved ilmenites from the upper zone is also fairly high and values range from 1,10 to 1,93 per cent, with an average of 1,48 per cent. The high MnO and low R_2O_3 component suggests that exsolution took place under relatively reducing conditions.

The variation in the composition of the coexisting titaniferous magnetite and ilmenite of the upper zone is shown in Figure 33A. This figure illustrates the constancy in composition of the ilmenite and the considerable spread in composition of the coexisting titaniferous magnetite, all of which represents subsolidus exsolution compositions. The recast bulk composition of the titaniferous magnetite plot towards the more ulvöspinel rich end member and represent the composition of the cumulus titaniferous magnetite prior to exsolution.

The marginal member samples are shown in Figure 33B. Here, both the subsolidus compositions representative of exsolved phases, and the calculated composition of the primary magmatic titaniferous magnetite are shown. Note how depleted the exsolved magnetite is in the ulvöspinel component relative to the upper zone samples.

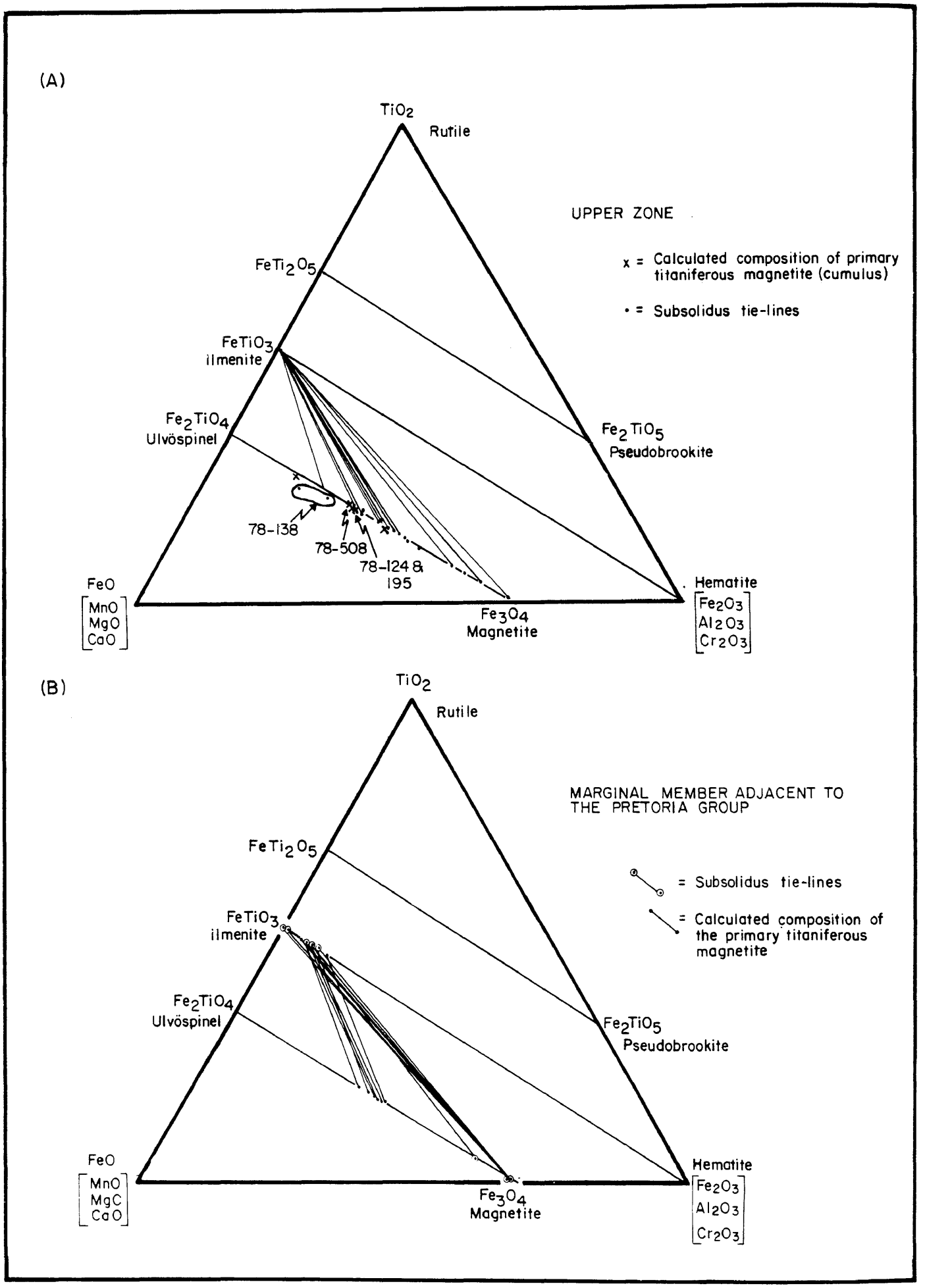

Fig. 33 Triangular variation diagram showing the composition of coexisting Fe-Ti oxide pairs for: (A) upper zone and (B) M.Mb./P.G. samples.

5.1.3 Crystallization Conditions

The conditions during crystallization of the magma that gave rise to the upper zone can best be explained with the aid of the system $MgO-SiO_2-FeO-Fe_2O_3-Cr_2O_3$ and the relevant subsystem $MgO-SiO_2-Fe_3O_4$. Figure 34A is taken from the work of Arculus et al. (1974) whereas Figure 34B is that part of the phase diagram of immediate interest. The phase relations in this subsystem have been modelled by Osborn and Watson (1977) for subalkaline volcanic rocks.

Under low fo_2 conditions (Figure 34B) a liquid of composition m will fractionate along a course m-n-o-e-f. Along path m-n-o olivine will crystallize and SiO_2 will remain fairly constant, whereas the ratio of Fe:Mg will increase rapidly. Olivine and magnetite will crystallize together along curve o-e whereas along e-f pyroxene and magnetite coprecipitate. Simultaneously the liquid becomes richer in SiO_2 while the Fe:Mg ratio remains fairly constant.

Higher fo_2 conditions result in an enlargement of the stability field of magnetite with the result the magnetite will crystallize from the liquid at considerably lower Fe:Mg ratios. The early separation of magnetite results in a strong SiO_2 enrichment trend such as indicated by m-n-c-d (Fig. 34B).

With these different possible crystallization courses in mind the possible liquidus paths followed by the upper zone magma to produce the magnetite-rich layers can be investigated. In order to do this the phase diagram in Figure 35 was constructed, based on average compositional data of whole rocks from the study area, as well as analytical data of van der Merwe (1978), Von Gruenewaldt (1971), and Buchanan (1976). By using the average rock compositions in conjunction with the cumulate phases present in the rocks, the boundary curves in Figure 35 were established. The outline of the field for average main zone rocks from the Potgietersrus limb is also shown, along with designations indicating the composition at the top and bottom of this zone. The trend indicates a path of continued increase of the Fe/Mg ratio with accompanied SiO_2 depletion as the liquid fractionated towards the pyroxene-magnetite boundary curve. Petrographic studies of the upper zone sequence available for investigation indicate that the magma composition was essentially confined to the pyroxene-magnetite boundary curve and during crystallization of the magnetitite layers in the magnetite field. From

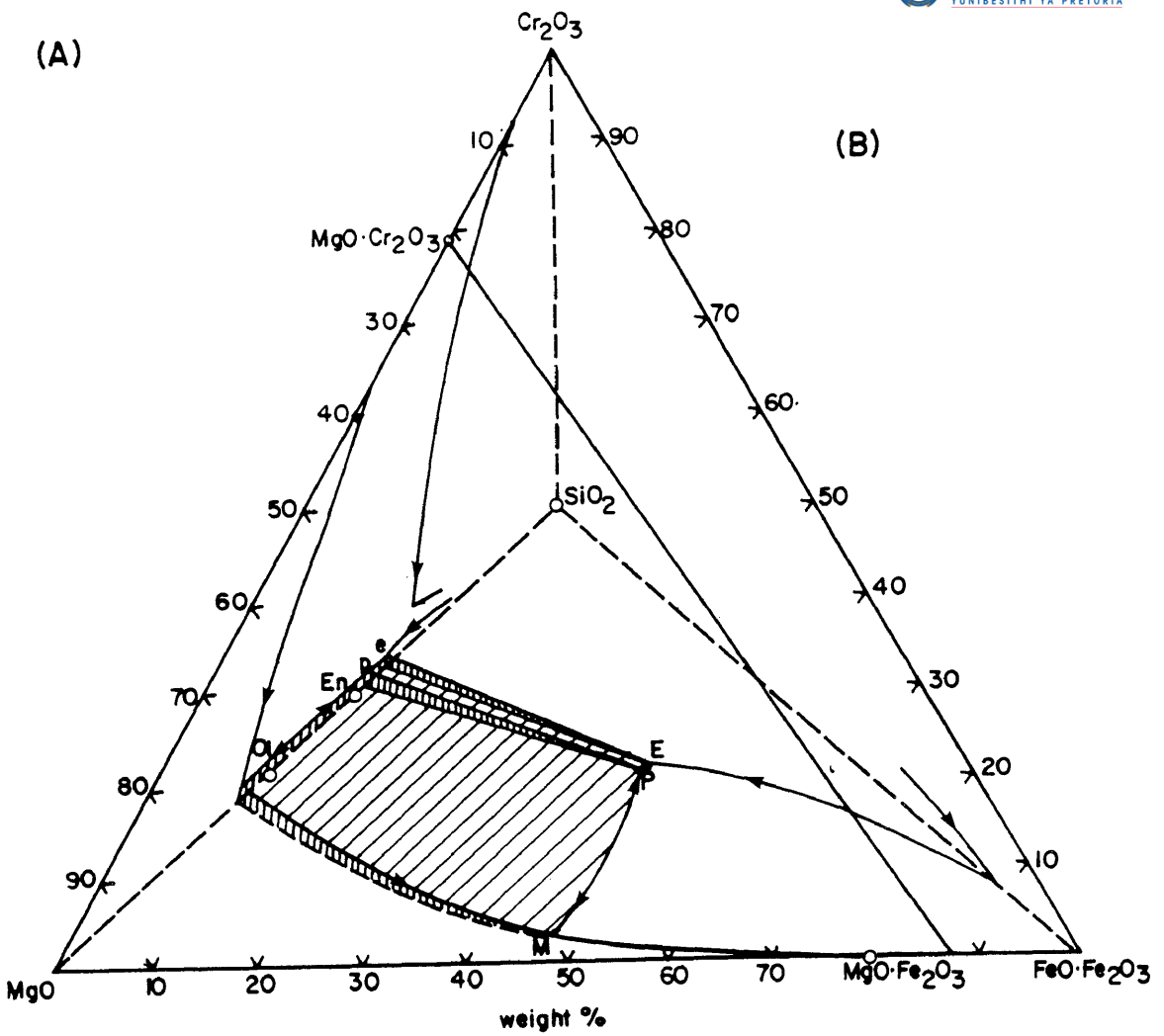

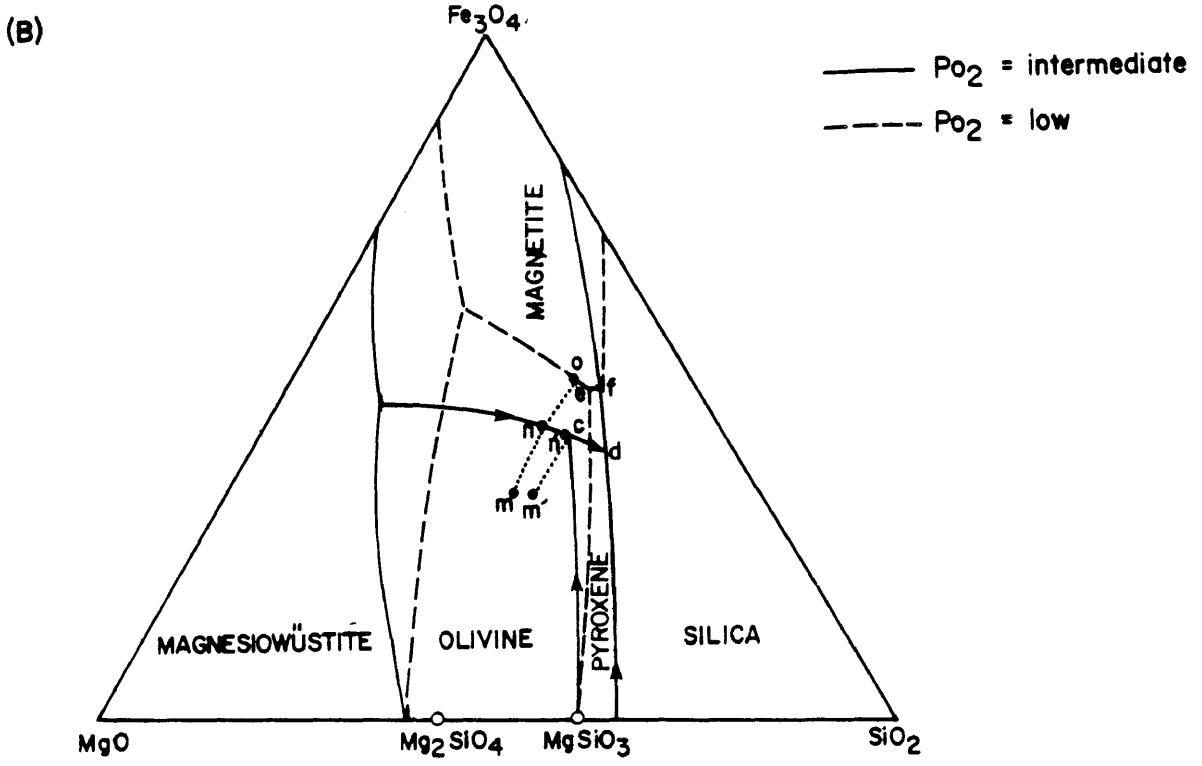

Fig. 34 Liquidus phase relations in
(A) the system $MgO-SiO_2-FeO \cdot Fe_2O_3-Cr_2O_3$
(B) the relevant subsystem $MgO-SiO_2-Fe_3O_4$ under varying fo_2 conditions
(After Arculus et al., 1974 and Osborn and Muan, 1970)

Figures 34 and 35 it is also evident that the suppression of magnetite crystallization during the development of the main zone has resulted in an iron enrichment (Fenner) fractionation trend rather than a silica enrichment (Bowen) trend.

Once the liquid fractionated to point g in Figure 35B it should fractionate along g-h to more siliceous compositions with only a slight decrease in the Fe:Mg ratio. If such a situation did exist, as it appears to have done here and elsewhere in the Bushveld Complex, then some mechanism is needed to explain the association of mottled anorthosites with the opx-mag (±pl) cumulates in the lower portion of the upper zone and the change in the cumulate sequence to ol-mag and ol-pl cumulates at higher levels in the upper zone. The change from opx-mag to ol-mag cumulates also suggests a change to more silica undersaturated conditions. Such a decrease in silica activity would give rise to increased fo_2 conditions within the evolving melt and thus the phase relations observed in the upper zone. Roeder and Osborn (1966) have demonstrated experimentally that the phase relations in the system $MgO-FeO-Fe_2O_3-CaAl_2Si_2O_8-SiO_2$ are a function of the prevailing fo_2. For example in Figure 35C the inferred liquid composition would give rise to the observed phase relations opx-mag cumulates at 10^{-9} atm. A decrease in fo_2 to 10^{-11} atm (Fig. 35D) would cause a contraction in the size of the magnetite field and an expansion of the anorthite field such that the liquid composition would now be confined to this field. The more silica undersaturated assemblage ol-mag, at higher stratigraphic levels, could have crystallized at fo_2 conditions between 10^{-7} and 10^{-9} atm (Fig. 35E) from a liquid of similar composition as was used in Figure 35C and D. Such fluctuations in the fo_2 could, therefore, produce the rock sequence and types observed in the upper zone.

The intensive parameters of this limited portion of the upper zone magma will be discussed in more detail in Chapter 7, but it is appropriate to mention at this stage that calculations indicate that crystallization of this upper zone liquid along the magnetite-pryoxene boundary took place at a temperature between 1064 to 1080° C at fo_2 conditions of $10^{-9,26}$ to $10^{-9,01}$ atm. It will also be shown with the aid of sulfur isotope data (Chapter 8) that the foot-wall mottled anorthosite, north of

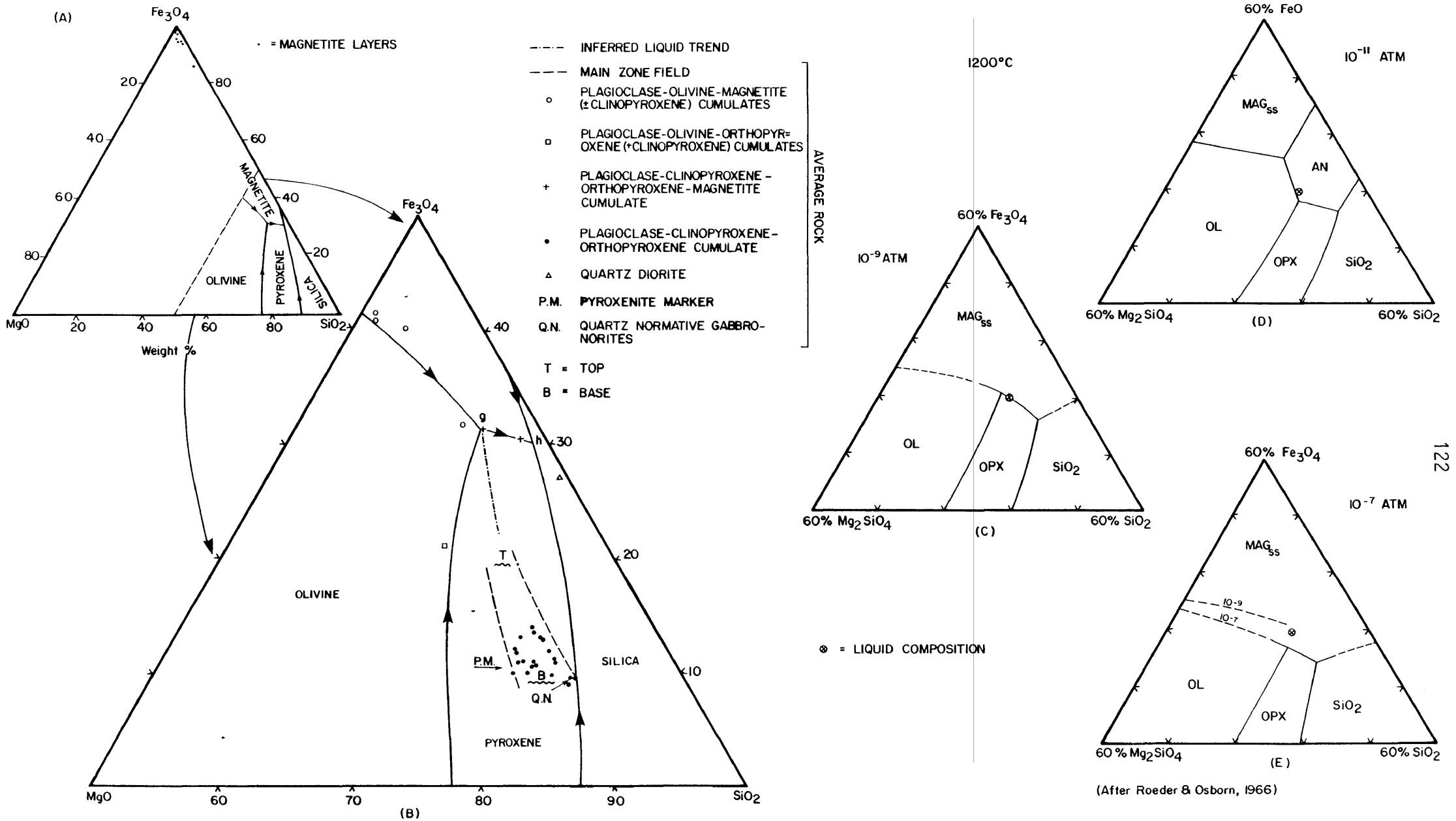

Fig. 35A and B. Proposed liquidus phase relations in the system $MgO-SiO_2-Fe_3O_4$ for the magnetite-rich layers of the upper zone.
C, D and E. Liquidus phase relations in the system $MgO-SiO_2-Fe_3O_4$ at different fo_2 conditions at 1200°C.

the study area, crystallized under fo_2 conditions of approximately 10^{-11} atm. These calculations are in good agreement with the experimental data of Roeder and Osborn (1966) and thus suggest that slight fluctuations in fo_2 could have given rise to the observed variation in rock types in the lower portion of the upper zone.

5.2 Chromite

Chromite is an accessory mineral in most of the rocks of the lower zone and the bottom half of the critical zone. It is present in concentrations that seldom exceed 5 per cent and commonly average 2 per cent by volume. Significant concentrations of chromite occur as chromitite layers at the -690, -620, and -86 metre levels (Fig. 7A). The lower and upper chromitite layers of the Drummondlea subzone are developed at the former two levels respectively, whereas the UG2-like chromitite layer of the critical zone occurs at the -86 m level of the intrusion.

The mineral chemistry of the chromite was determined with a Joel JXA-50 electron microprobe. The ferric iron content of the analysed chromite was calculated according to the method of Finger (1972).

5.2.1 The Drummondlea Harzburgite Chromitite

The Drummondlea Harzburgite-Chromitite subzone consists of the olivine-rich cyclic units 20 to 26 and hosts the upper and lower chromitite layers (Fig. 36), from which the best metallurgical chromite is mined in the Republic at present.

The material for the investigation of the Drummondlea Harzburgite-Chromitite was obtained from a continuous diamond drill hole DC-1A. Unfortunately the upper and lower chromitite intervals were used for assay purposes by the exploration company. In order to complete the section, material from the chromitite layers was obtained from the G66, 6 level of the Grasvally Chrome Mine.

5.2.1.1 Stratigraphy and Petrology

A complete cyclic unit within the Drummondlea Harzburgite-Chromitite subzone consists of an ol-chr cumulate at the base which passes

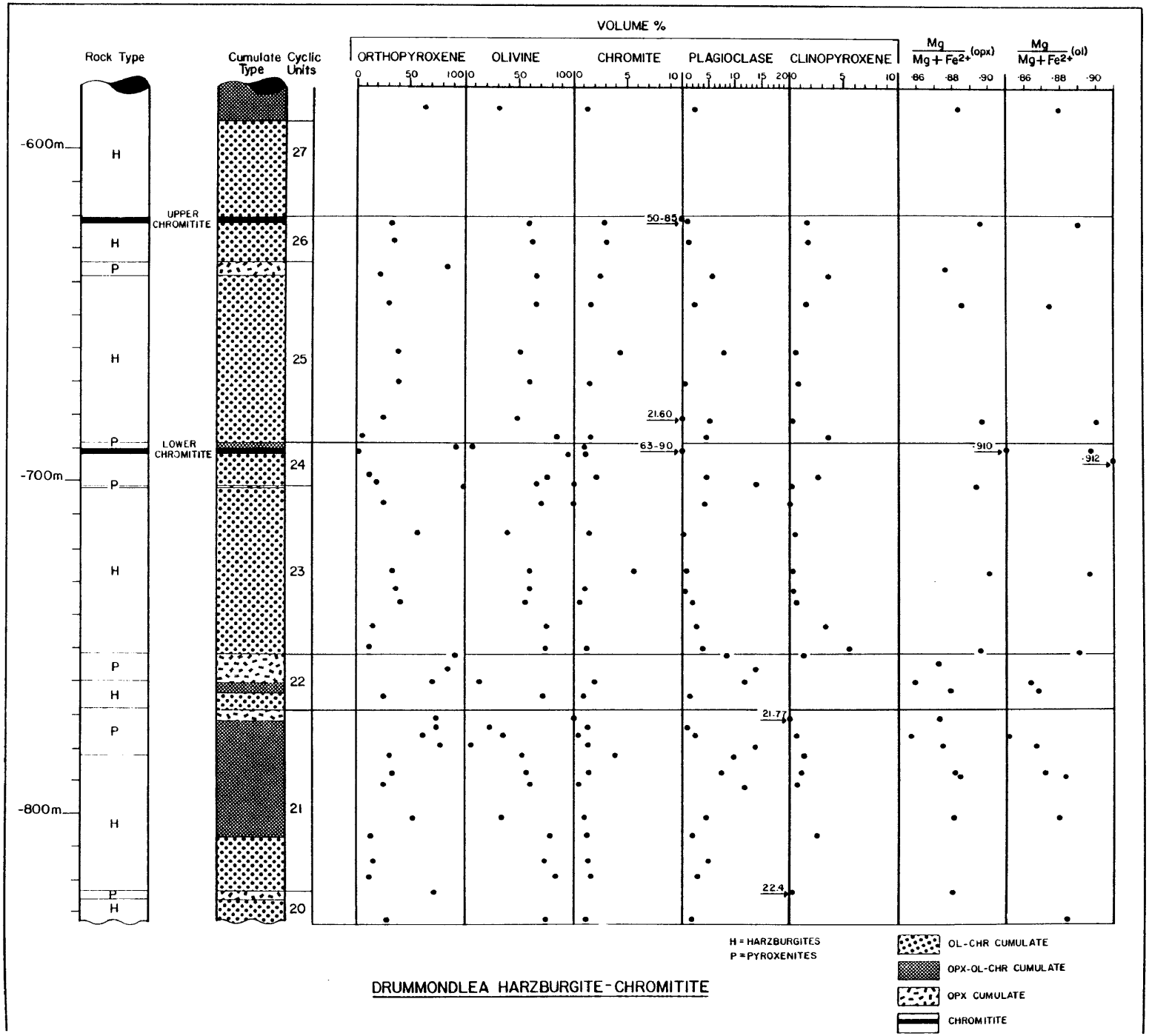

Fig. 36 Stratigraphic column of the Drummondlea Harzburgite-Chromitite showing the modal proportions of the major components and the $Mg/(Mg+Fe^{2+})$ ratios of orthopyroxene and olivine.

upwards into a opx-ol-chr cumulate layer, which in turn is capped by a opx cumulate. Cyclic units 21 and 22 are examples of such fully developed units (Fig. 36). However, not all units are complete since certain members may not always be present. Examples of such incomplete units are 23 and 25 in which the opx-ol-chr cumulate member is not developed. Cyclic units 24 and 26 on the other hand, which host the lower and upper chromitite layers, are beheaded cyclic units because the orthopyroxene-rich members are absent.

Cyclic unit 21 displays excellent examples of mineral graded layers, as the modal proportion of olivine and chromite decrease fairly systematically from the base to the top of the unit with a concomittant increase in the orthopyroxene content (Fig. 36). The other units do not display such regular variations in the modal compositions of the layers, although trends are, apart from a few exceptions, in general agreement with these observed for cyclic unit 21.

Cyclic unit 25 also shows an upward increasing orthopyroxene and decreasing olivine trend for the lower half of the unit, however a reversal in the middle of the unit reveals a trend towards decreasing orthopyroxene and increasing olivine. There is also a suggestion of upward increasing chromite with this reversal in the modal trend. Cyclic unit 24 tends also to show a similar reversal in that the orthopyroxene content decreases and the olivine increases from the base of the unit toward the chromitite layer.

Both the upper and the lower chromitite are underlain by ol-chr cumulate layers of similar thickness. The two chromitite layers have a stratigraphic separation of approximately 70 m in the northern portion of Grasvally (Fig. 36) whereas the separation is about 55 m in the southern part of Grasvally and on Zoetveld.

Other minerals present in rocks throughout this subzone are intercumulus plagioclase and clinopyroxene. In the ol-chr cumulates of cyclic unit 23 and 25 there appears to be a systematic decrease in the plagioclase and clinopyroxene content through the lower half of the unit. The highest concentration of plagioclase occurs in the orthopyroxene cumulates where concentrations up to 22,4 per

cent have been recorded. The highest concentration of intercumulus clinopyroxene (6 per cent) occurs in the ol-chr cumulates. The only other minerals present in this subzone are phlogopite which is generally present in small amounts (< 1 per cent) and pseudomorphs of antigorite and lizardite after olivine. As a rule virtually all of the olivine bearing rocks have been serpentinized to some degree. The available intersection of the lower part of cyclic unit 27 is intensely serpentinized which prevented determination of the mineral compositions and made the delineation between cyclic units 26 and 27 difficult.

The Mg* of olivines in this subzone range from 0,850 to 0,946 with the latter value being derived from a sample which contains 50 per cent chromite. Typical values in silicate-rich rocks vary between 0,850 and 0,895 for olivine and 0,857 to 0,900 for orthopyroxene indicating a fairly primitive parent magma from which these cumulates crystallized.

5.2.1.2 The Upper and Lower Chromitite

A schematic representation of the upper and lower chromitite as found on the farms Grasvally and Zoetveld is presented in Figure 37. The upper chromitite consists of four members, i.e. the 4" marker layer, the disseminated hanging-wall layer, the chromitite layer, and the disseminated foot-wall layer. A thin chromitite, known as the 1" stringer, occurs above the 4" marker layer and, as the name implies, it is approximately 2,5 cm thick. It is not unlike the 5 foot and 12 foot stringers which occur approximately 1,52 m and 3,65 m stratigraphically below the chromitite layer respectively (Fig. 46). The cumulate layers are continuous along strike from the northern portion of Grasvally to the southern portion of Zoetveld.

The lower chromitite consists of three members, the uppermost of which changes along strike from an opx-ol-chr cumulate in the southern portion of Grasvally and Zoetveld to an ol-chr cumulate in the northern portion of Grasvally. The remaining members, i.e. the chromitite layer and the disseminated foot-wall layer, remain constant along strike. The facies change of the uppermost member may also be related to the absence of the lower chromitite layer in the central portion of Grasvally. The absence of this layer at this particular locality could possibly

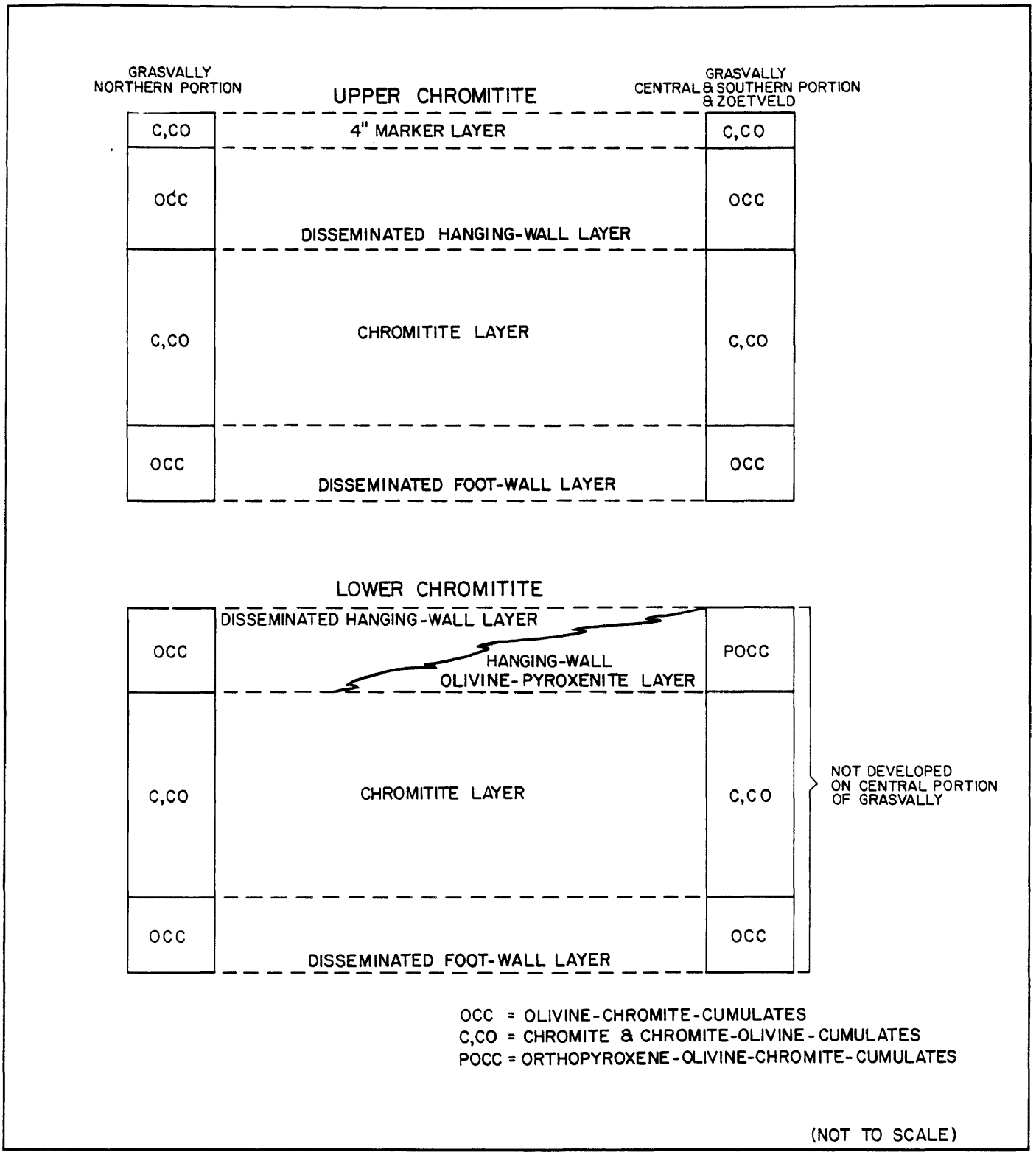

Fig. 37 Schematic representation of the upper and lower chromitite and associated rocks on Grasvally 293KR and Zoetveld 294KR.

be due to the existence of a topographic high on the magma floor during crystallization of the chromite layer. A topographic high or rise could have prevented effective mixing of the magma for a short period during crystallization, so that the opx-ol-chr cumulate in the south could represent the crystallization product of a magma slightly more siliceous than that to the north from which the ol-chr cumulate crystallized.

Figure 38, 39, and 40 are schematic representations of typical intersections of the chromitite intervals, as encountered in boreholes drilled by the Drummondlea Chrome Corporation on the northern portion of Grasvally. These diagrams show the characteristics of each chromitite with respect to cumulate rock type, chemical composition, PGE content, Cr:Fe ratio, specific gravity and true thickness of the various members.

The nature and chemical composition of the upper chromitite are illustrated in Section 2 of Figure 38. The three chromite-rich intervals all have disseminated foot-wall layers, which grade upward into the chromitite layer. The upper contact of the upper chromitite layer is also gradational and passes into an olivine-chromite cumulate which is capped by the 4" marker layer. Above the 4" marker layer is another thin chromitite, commonly referred to as the 1" stringer. This 1" marker is frequently seen in the area and is separated from the 4" marker layer by a thin layer of olivine cumulates and olivine-chromite cumulates (Fig. 38). Of interest is also that the lower chromitite layer is considerably richer in Cr_2O_3 (Fig. 38, Section 4) yet higher in iron than the upper chromitite layer. This is also borne out by the higher Cr:Fe ratio of the upper layer (Fig. 38, Section 2).

A peculiar spinel-rich layer was intersected in DDH-DC-2A (Fig. 38, Section 1). It is a 53 cm thick layer of highly magnetic, steel-blue to grey ferritchromit-magnetite. In reflected light (Fig. 31H) the spinels are seen to be zoned and subsequent microprobe analyses have shown the Cr_2O_3 content to vary from 41,58 to 0,49 per cent in the same grain. This layer is of a localized extent and lenticular in shape.

Although the chromitite layers are, apart from the lower layer on

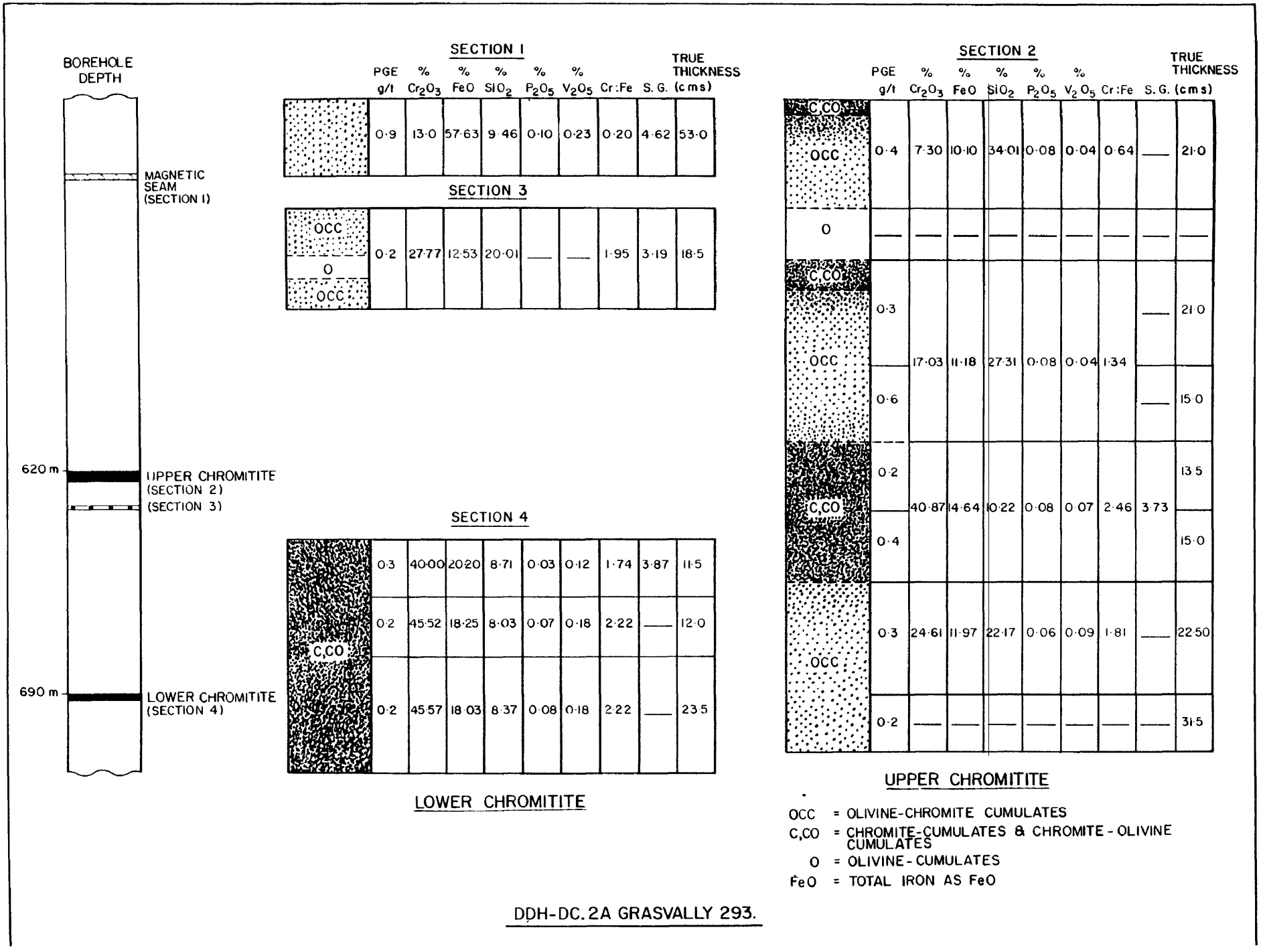

Fig. 38 Characteristic features and chemical composition of chromitite layers and associated rocks intersected in borehole DDH-DC-2A, northern Grasvally. Total iron is expressed as FeO. Analytical data taken from company records.

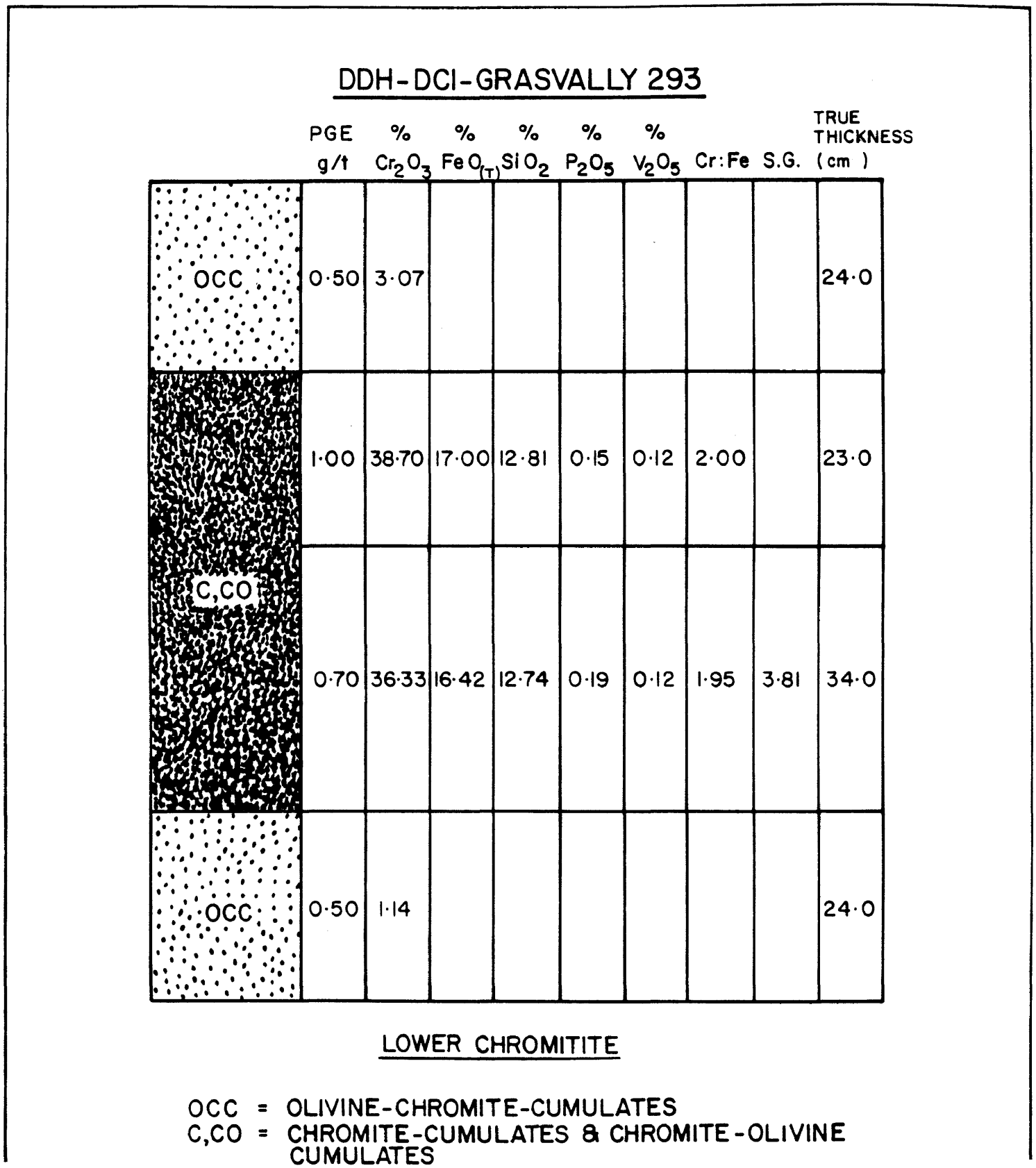

Fig. 39 Schematic representation of the nature and chemical composition of the lower chromitite from borehole DDH-DC-1, northern Grasvally.

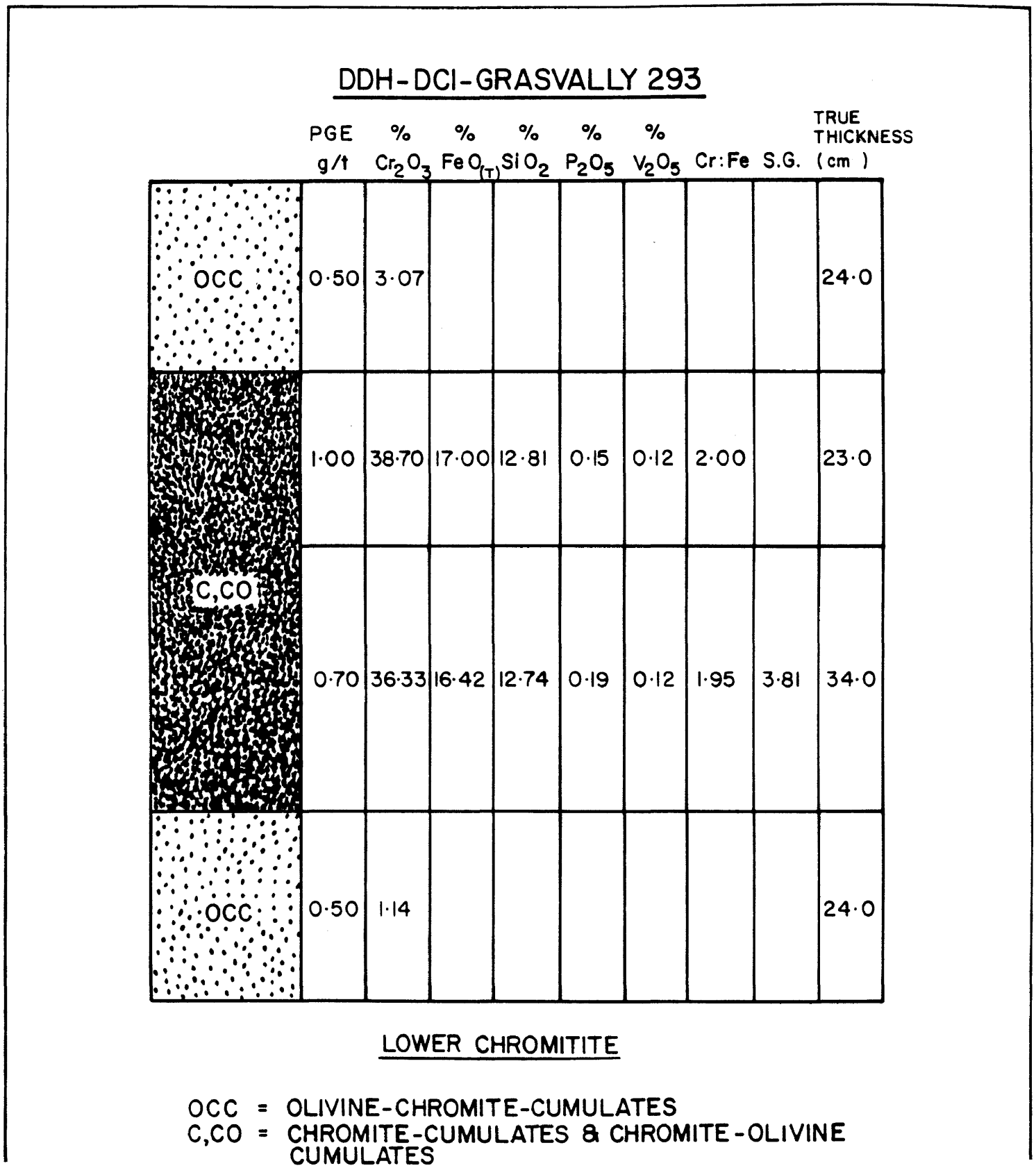

Fig. 39 Schematic representation of the nature and chemical composition of the lower chromitite from borehole DDH-DC-1, northern Grasvally.

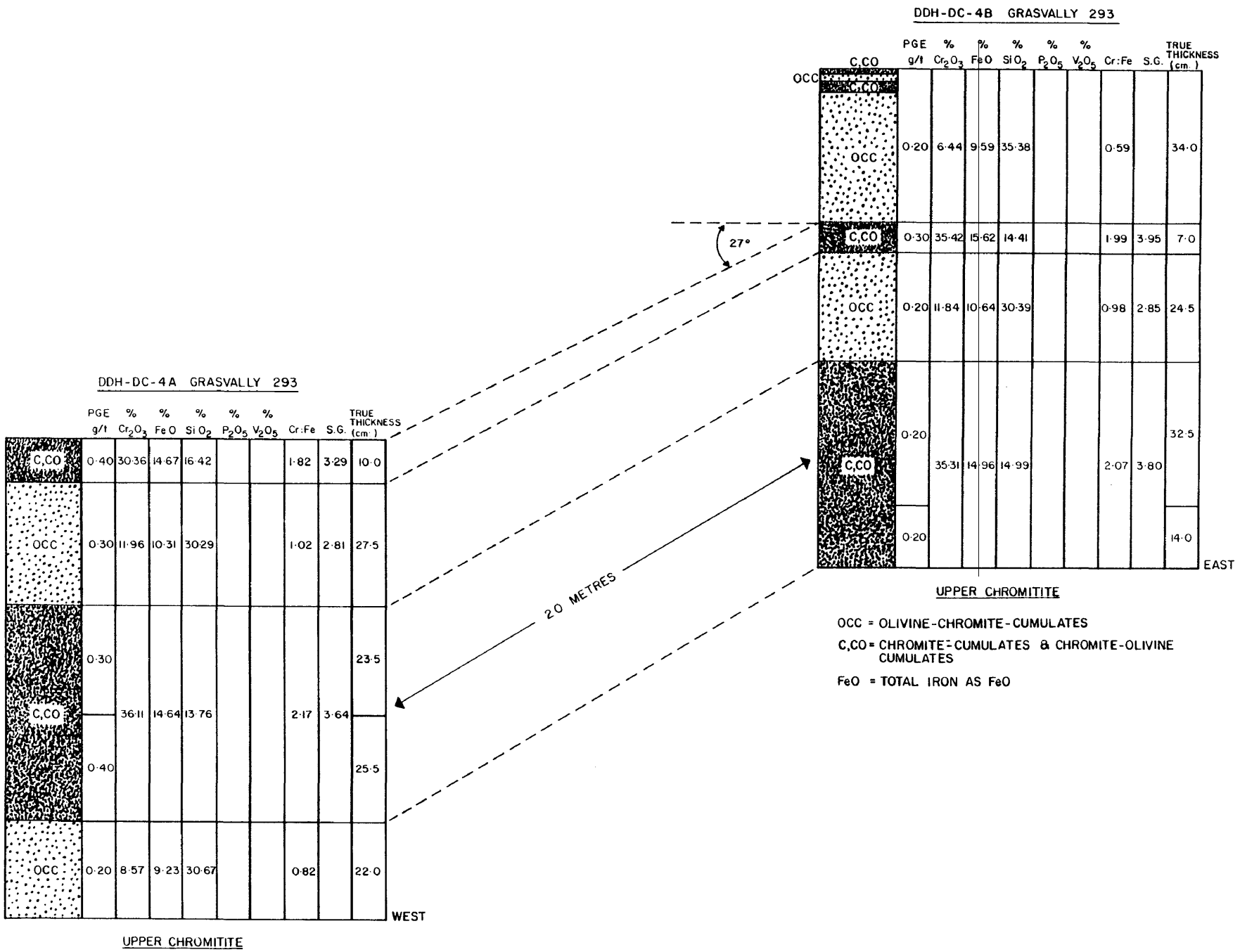

Fig. 40 Lateral variation in composition and physical features of the upper chromitite layer in a dip section on northern Grasvally.

central Grasvally, continuous along strike, they display some pronounced lateral variations in thickness and grade. This can be illustrated by comparing the intersections of the lower chromitite layer in boreholes DC-2A (Fig. 38, Section 4) and DC-1 (Fig. 39) which are separated about 100 m along strike. The lower chromitite layer of DC-2A has a true thickness of 47 cm compared with 57 cm in DC-1, whereas the respective average grades are 44,17 and 37,28 per cent Cr_2O_3. In DC-2A the Cr:Fe ratio varies from 1,74 in the top 11,5 cm to 2,22 for the remaining 35,5 cm; whereas for DC-1 the Cr:Fe ratio is 2,00 for the top 23 cm and 1,95 for the remaining 34 cm. It is interesting to note that a decrease in the thickness of a layer is always accompanied by an increase in the grade, which in turn is associated with the development of hard lumpy ore. For example, the change in the chromitite layer from DC-1 to that of DC-2A represents a decrease in thickness of 17,5 per cent, accompanied by a 18,4 per cent increase in the Cr_2O_3 content.

The physical and chemical character of the layers do not only vary along the strike but also down-dip. The sections in Figure 40 are based on borehole DC-4A which intersected a reverse fault that duplicates the upper chromitite on the northern portion of Grasvally. Although the down-dip separation is only about 20 m, some noticeable changes occur in the chromitite and its associated layers. The thickness of the 4" marker layer, for instance, changes down-dip from 7 cm to 10 cm. This increase in thickness is accompanied by a decrease in density from 3,95 to 3,29 $g.cm.^{-3}$ and by a 16,66 per cent decrease in the Cr_2O_3 content of the layer. This densification with decreasing thickness and the associated development of hard lumpy ore is a feature of the chromitite layers both along strike and down-dip. Changes of the same magnitude do not occur in associated silicate-rich layers.

The lateral variability of the chemical and physical character of the layers is not considered to be a primary magmatic feature, but to be due to postcumulus processes. This is also reflected in the modal chromite content of the layers which may vary from 50 to 88 per cent in the upper chromitite layer and from 63 to 90 per cent in the lower chromitite layer. The lower values probably reflect

TABLE 2A CHARACTERISTIC FEATURES OF THE UPPER CHROMITITE

LOCALITY	MEMBER	FOOT-WALL CONTACT	HANGING-WALL CONTACT	THICKNESS (cm)	GRADE $\%Cr_2O_3$
GRASVALLY CENTRAL & SOUTHERN PORTION & ZOETVELD	4" MARKER	SHARP	SHARP	10.0	40-42
	DISS. HANGING-WALL	SHARP	GRADATIONAL	43.0	12-15
	UPPER LAYER	GRADATIONAL - SHARP	SHARP	36-41	43-46
	DISS. FOOT-WALL	GRADATIONAL	GRADATIONAL - SHARP	25-30	25-28
GRASVALLY NORTHERN PORTION	4" MARKER	SHARP	SHARP	7-10	30-35
	DISS. HANGING-WALL	SHARP	GRADATIONAL	25-29	12-14
	UPPER LAYER	SHARP	SHARP	29-79	35-41
	DISS. FOOT-WALL	GRADATIONAL	SHARP	22	9-25

TABLE 2B CHARACTERIC FEATURES OF THE LOWER CHROMITITE

LOCALITY	MEMBER	FOOT-WALL CONTACT	HANGING-WALL CONTACT	THICKNESS (cm)	GRADE $\%Cr_2O_3$
GRASVALLY CENTRAL SOUTHERN & ZOETVELD PORTIONS	HANGING-WALL OLIVINE-PYROXENITE (POCC)	SHARP	SHARP	150	.5-.8
	LOWER LAYER	SHARP	SHARP	38-43	42-45
	DISS. FOOT-WALL	GRADATIONAL	SHARP	25-48	12-18
GRASVALLY NORTHERN PORTION	DISS. HANGING-WALL	SHARP	GRADATIONAL	24	3-5
	LOWER LAYER	SHARP	SHARP	47-57	37-44
	DISS. FOOT-WALL	GRADATIONAL	SHARP	24-30	1.14

the original amount of cumulus chromite present in the layers.

Lateral changes in the thickness, grade, and the contact relationships of the chromitite layers on the northern portion of Grasvally, the central and southern portions of Grasvally, as well as on Zoetveld, are summarized in Table 2. Data on the thickness and grades from the southern portion of Grasvally and for Zoetveld are from De Villers (1970).

5.2.2 The UG2-Like Chromitite

The UG2-like chromitite layer is highly variable along strike. A typical intersection of this layer is shown in Figure 41. The layer is underlain by a opx cumulate (feldspathic pryoxenite), which contains on average 0,38 weight per cent Cr_2O_3. The lower half of the chromitite layer consists of about 50 per cent cumulus chromite, cemented together by intercumulus pyroxene and plagioclase. The grade of this semi-massive portion of the layer averages 20 per cent Cr_2O_3 (Fig. 41). Other Cr_2O_3 values recorded along strike are also shown in Figure 41. The upper half of the chromite layer contains between 32 and 35 per cent chromite and averages about 14 per cent Cr_2O_3. This portion also contains a higher TiO_2, CaO, SiO_2, and Al_2O_3 content which reflects the higher proportions of silicates. The top contact is fairly sharp and the chromite cumulate passes rapidly into an opx-chr cumulate, which contains intercumulus plagioclase and clinopyroxene. This rock type has been referred to as a chromitic pyroxenite to gabbronorite depending on how much intercumulus plagioclase and clinopyroxene are present.

The chromite in this chromitite layer has a higher Cr_2O_3 (42,15 per cent) content and $Cr/(Fe^{2+}+Fe^{3+})$ ratio (1,21) than the chromite of the hanging-wall unit which in comparison contains 35,03 per cent Cr_2O_3 and has a $Cr/(Fe^{2+}+Fe^{3+})$ ratio of 0,73.

The Mg* of the orthopyroxenes from the hanging and foot-wall cumulates is 0,762 and 0,781 respectively, whereas the intercumulus orthopyroxene within the chromitite layer has a Mg* of 0,839. Intercumulus plagioclase in the chromitite has a Ca* of 0,652 and that from the hanging-wall unit a Ca* of 0,720.

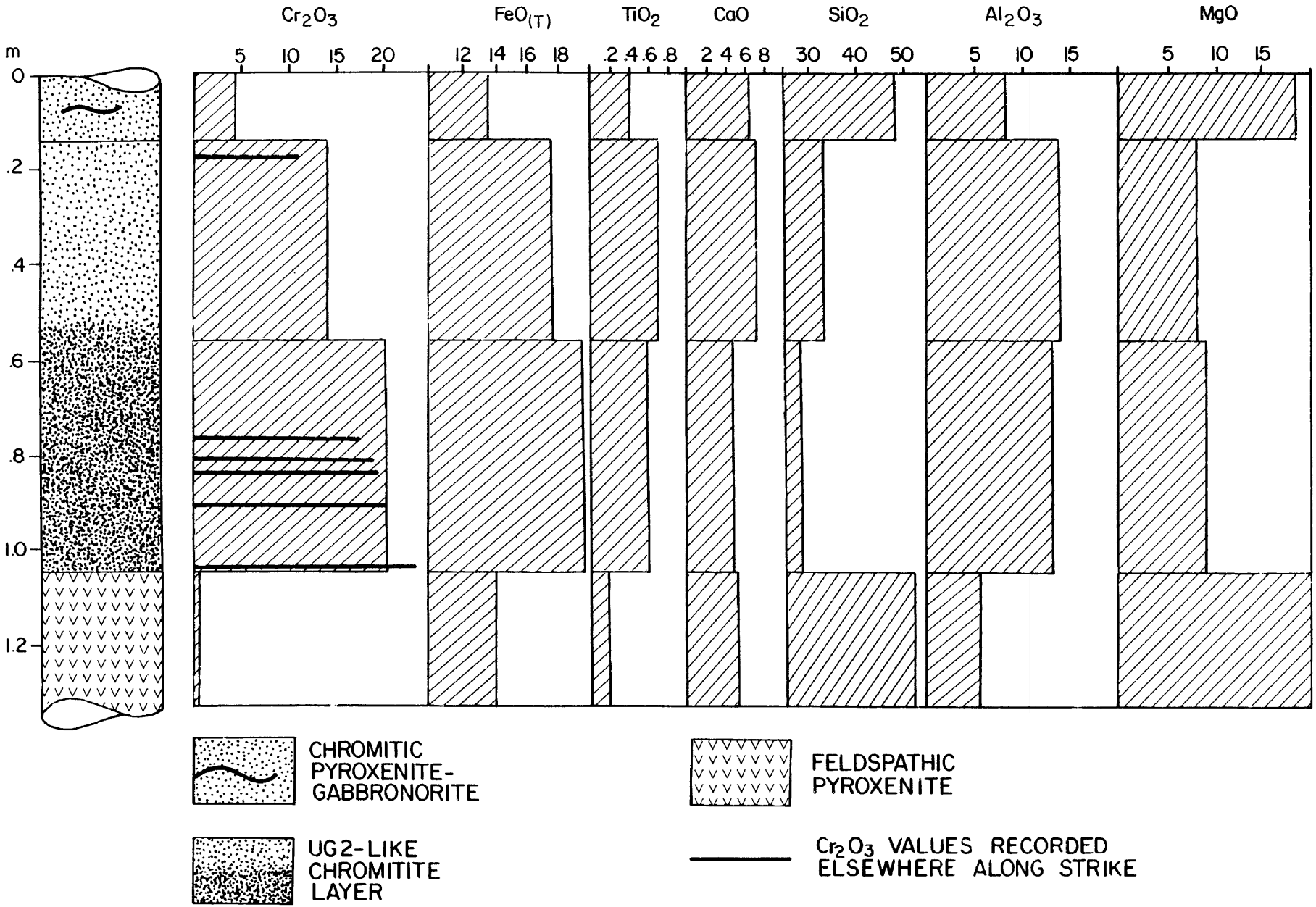

Fig. 41 Compositional variation of the UG2-like chromitite, northern Grasvally.

5.2.3 Textural Features of Chromite in Chromitite and Chromite Bearing Horizons

Typical textures encountered in the chromitite layers of the lower zone are illustrated in Figure 42, which represents a section through the lower chromitite layer as seen on the G66,6 level of the Grasvally Chrome Mine. The foot-wall of the lower chromitite is a 2 m thick olivine adcumulate (Figures 42A and 43F). Olivine adcumulates are very rare and only found to be associated with the chromitite layer. Elsewhere in the sequence the olivine-rich rocks are ol-chr cumulates such as illustrated in Figure 43G. This adcumulate is overlain by a massive chromitite, the lower half of which consists of approximately 90 per cent chromite (Fig. 42B). The massive hard lumpy portion of the layer passes into a mottled chromitite parting (Fig. 42C) in the middle of the layer which contains approximately 50 to 60 per cent chromite. The small chromite grains in the silicate-rich portion are in most cases 50 to 100 times smaller than the chromite grains of the over- and underlying massive chromite. These small grains can frequently be seen to consist of three to four discrete chromite grains indicating that the original chromite grains could have had a grain size of as little as 0,007 to 0,009 mm in diameter.

The mottled parting passes upward into massive chromitite (Fig. 42D), similar to that in the lower half of the layer, except for the presence of discrete spherical inclusions of olivine within the large chromite grains. The olivine inclusions increase both in size and in abundance towards the top of the layer where mantle chromite (Fig. 42E) is a common feature. Here, some of the olivines, now serpentinized, are only partially mantled, whereas other are completely mantled and typically occur as spheres inside the large irregular chromite grains. Mantled, spherical and especially the atoll type of chromite growth texture from near the top of the chromitite layer (Fig. 43A) suggests two generations of chromite growth. Spherical and mantled chromite have only been observed in the top portion of the chromitite layer.

Well developed chain textured chromite surrounding cumulus serpentinized olivine occurs in the 4" marker layer (Fig. 43C). The polygonal chromite grains all have straight to slightly curved

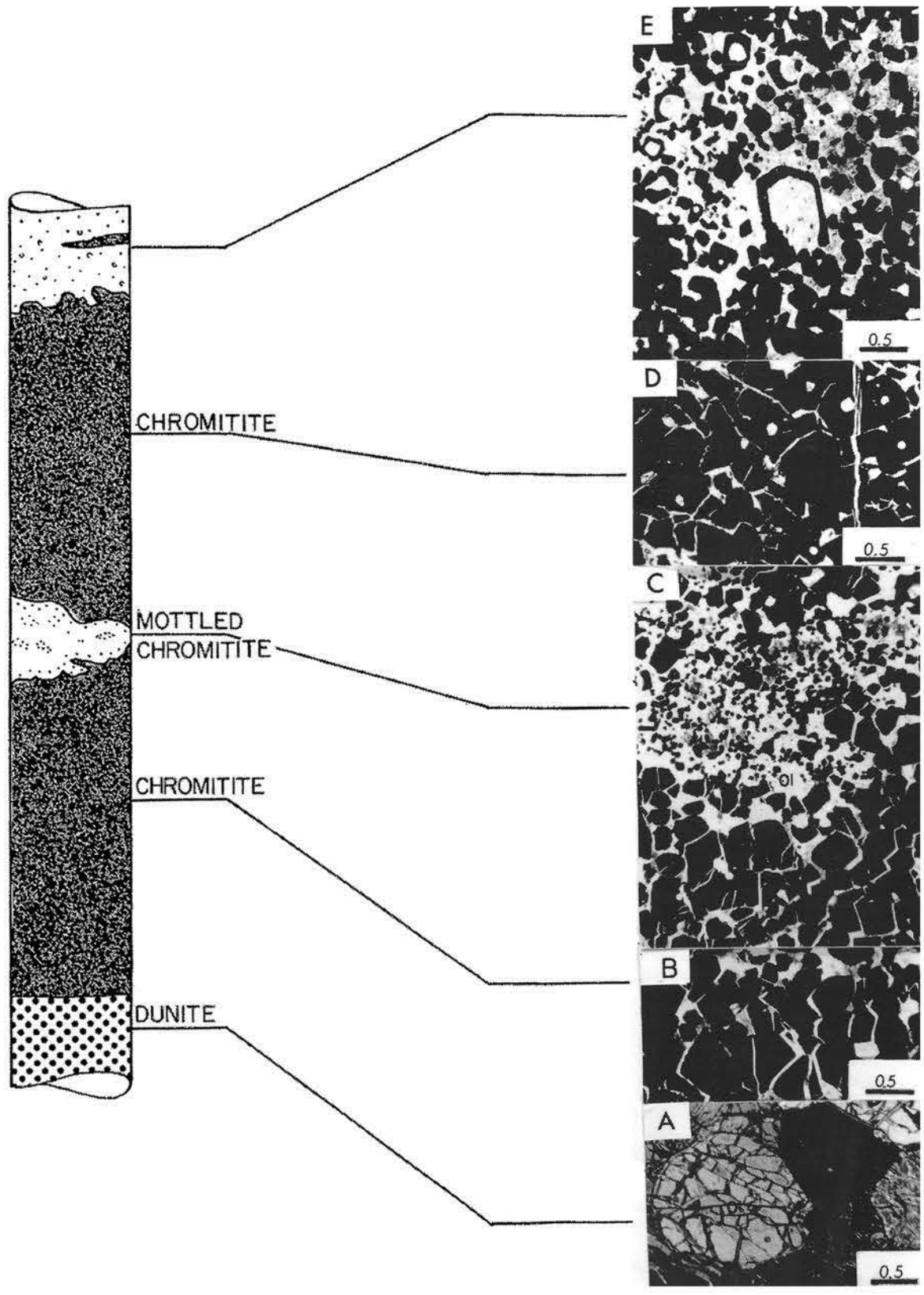

Fig. 42

Figure 42 Textural characteristics of the lower chromitite layer:

(A) foot-wall dunite

(B) coarse, massive hard lumpy chromitite consisting of large polygonal chromite grains.

(C) mottled chromitite

(D) coarse, massive chromitite consisting of large polygonal chromite grains characterized by spherical inclusions of olivine.

(E) mantle chromites.

Idealized columnar section on the left is approximately 50 cm (B, C, D and E - plane light; A - crossed nicols).

boundaries. Figure 43D also shows these same chromite-chromite boundary relations from the lower part of the lower chromite layer. The granoblastic-polygonal texture of the chromite in the chain-textured and massive chromite is very similar.

With the massive chromitite small mottled patches of serpentinized olivine are occasionally developed (Fig. 43E). These mottles are much smaller than the mottled parting referred to earlier (Fig. 42C). The centre of these mottles is devoid of chromite but disseminated chromite is abundant along their margins. Within the disseminated margins the grain size of the chromite increases towards the massive chromite. As in the parting, in the middle of the lower layer, the chromite grains along the margins of the mottles were evidently entrapped by the faster growing olivine. This texture again illustrates the smaller size of the chromite grains within the chromite-silicate fabric compared to the large polygonal grains in the massive part of the chromite layer.

The preservation of the remarkable mantle and spherical textures displayed by the chromite in the chromitite layers (Fig. 43H) is very fortunate in that they provide an indication of the postcumulus transformation, especially enlargement of chromite grains that have occurred within the chromitite layers.

Numerous other examples of postcumulus reaction and grain boundary adjustment between chromite grains as well as between chromite and silicate grains have been observed in the lower and critical zones. Figure 44A is an illustration of a chromite-orthopyroxene cumulate in which some of the orthopyroxene grains have been considerably elongated due to exaggerated grain growth within the plane of the layering. Boundaries of these crystals are irregular and tapered as a result of secondary enlargement in an environment of impinging chromite grains. There is little doubt that the chromite and the orthopyroxene crystals were enlarged in place. Note the orthopyroxene sphere inside the chromite beneath the enlarged crystal.

The reaction relationship between cumulus olivine and intercumulus liquid to produce reaction orthopyroxene is well illustrated in

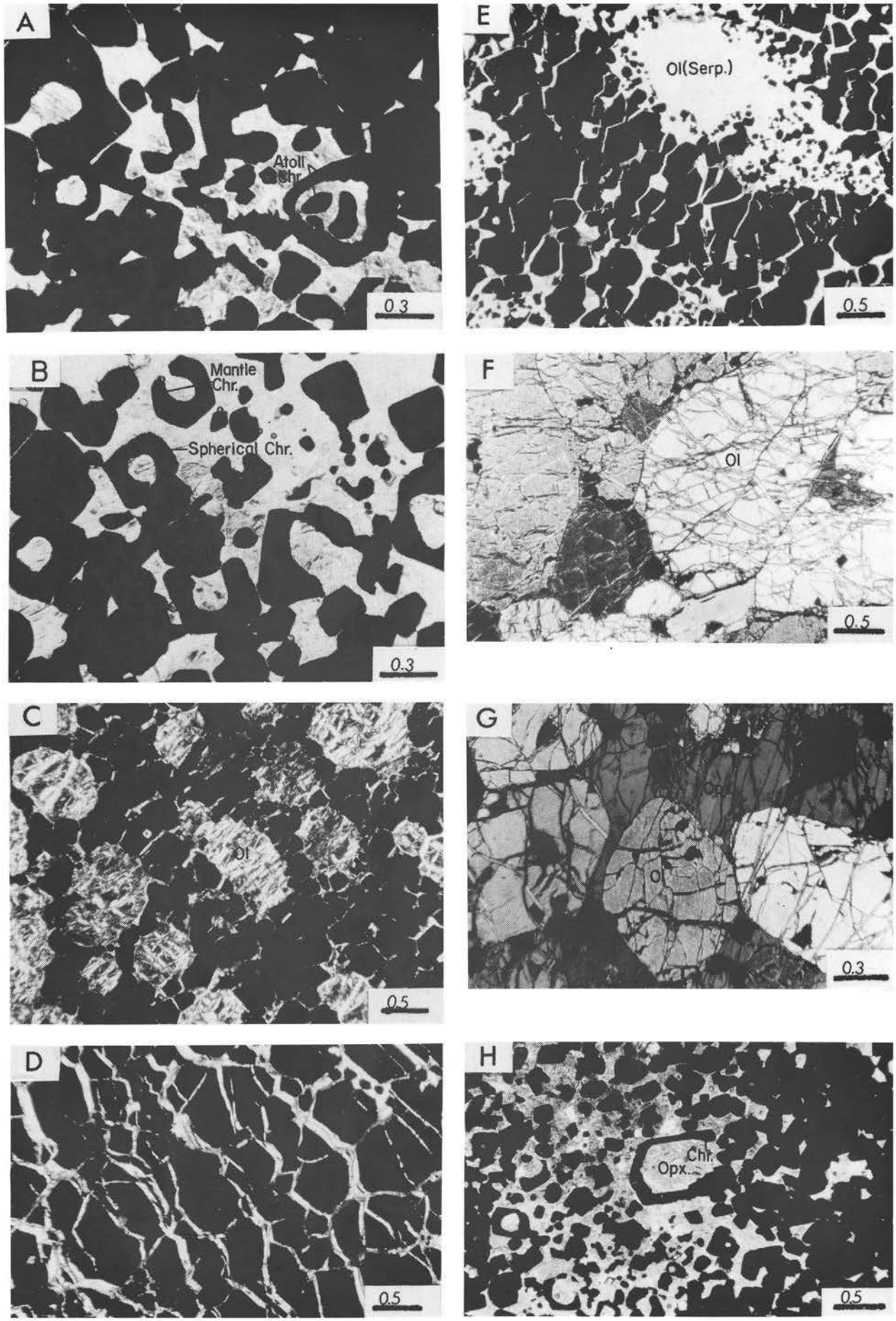

Fig. 43

Figure 43 Postcumulus crystal growth features within and adjacent to the upper and lower chromitite layers. chr = chromite, ol = olivine; opx = orthopyroxene. All sections have been photographed with transmitted light (A, B, C, D, E, and H - plane light; F and G - crossed nicols).

(A) Mantle and atoll-type chromite. Top of lower layer. (GV-20)

(B) Mantle and spherical inclusion-type chromite. Top of lower layer. (GV-20)

(C) Chain textured chromite defined by continuous polygonal aggregates of chromite grains around cumulus, serpentinized, olivine. 12' stringer (3,6 m below upper chromitite layer). (GV-18)

(D) Massive compact aggregates of polygonal chromite grains in hard lumpy chromitite (veined by serpentine material). Bottom of lower chromitite. (GV-19)

(E) Coarse-grained polygonal aggregates of chromite grains enclosing a serpentine pseudomorph after olivine. Middle of lower chromitite layer. (GV-10)

(F) Olivine adcumulate, foot-wall of lower chromitite. (GV-22)

(G) Typical olivine-chromite cumulate. 5 m below the lower chromitite layer. (DR-4)

(H) Well preserved mantle chromite. Top of lower chromitite. (GV-20)

certain of the ol-chr cumulates (Fig. 44B). As a result of the reaction orthopyroxene now separates the chain textured chromite from the olivine with which it was originally in contact. A similar texture without the reaction orthopyroxene is illustrated in Fig. 44C. It is evident that considerable enlargement of the chromite grains must have taken place in this case to give rise to the massive nature of the chain textured chromite. It is again felt, that the size of the chromite grains shown in Figure 44B reflect the size of the original cumulus chromite grains.

Another unusual texture, only observed twice, in opx-chr orthocumulates, involves cumulus chromite grains surrounded by a thin reaction zone of plagioclase and enclosed by secondarily enlarged cumulus orthopyroxene (Fig. 44E). The subsolidus reaction of chromite with orthopyroxene to produce plagioclase would deplete the chromite in Al and should give rise to a higher Cr/(Cr+Al) ratio in the chromite. This is the opposite of the postcumulus reaction between plagioclase and Cr-rich chromite to form an Al-rich chromite (Henderson and Suddaby, 1971).

Chromite grains with perfect spheres of plagioclase of an unquestionable intercumulus origin have been observed in the UG2-like chromitite layer (Fig. 44F). Both the included and the surrounding plagioclase are optically continuous (Fig. 44G) which leaves little doubt that this, as well as other silicate spheres within and mantled by chromite are due to a postcumulus growth process. In other parts of the UG2-like layer where intercumulus orthopyroxene predominates, spheres of orthopyroxene are included in chromite. This process must have taken place just before the intercumulus liquid crystallized. Had it taken place after crystallization of the plagioclase the plagioclase within and surrounding the chromite grain would have been fractured, which is not seen to be the case. Also note the contrast in grain size of the chromite grains shown in Figure 44F. Another example of the contrast in the chromite fabric in the UG2-like chromitite is shown in Figure 44H, where chromite ranges from discrete octahedral crystals set in intercumulus plagioclase and orthopyroxene to a concentration forming a solid chromitite band of large polygonal chromite grains.

Numerous descriptions of silicate inclusions within chromite appear

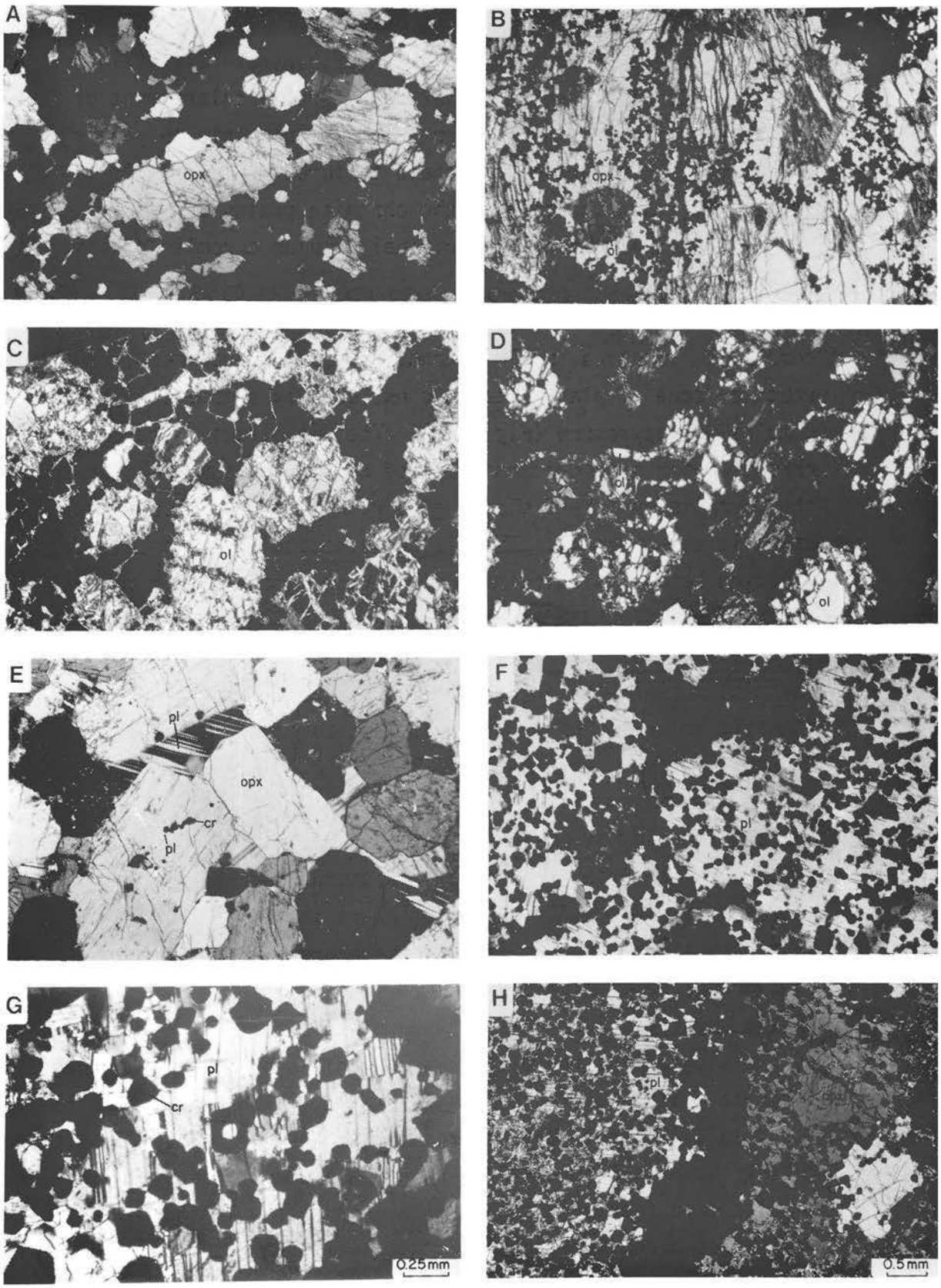

Fig. 44

Figure 44 Further examples of postcumulus reaction and grain boundary adjustment involving chromite in the lower and critical zone. ol = olivine; opx = orthopyroxene; pl = plagioclase. All sections have been photographed with transmitted light under crossed nicols. The scale on Figures 44A, B, C, D, E, and F is the same as on Figure 44H.

(A) Grain boundary adjustment between chromite-chromite and chromite-orthopyroxene crystals. Note the elongated growth of the orthopyroxene grain along the bedding defined by parallel trains of chromite. Also, note the sphere of orthopyroxene in chromite in the centre of the photomicrograph. (6A-130A)

(B) Chain-textured chromite in olivine-chromite cumulate. Note the reaction halo of orthopyroxene around the olivine grain. (1-123)

(C) Modified olivine-chromite chain texture. The smooth to slightly curved polygonal chromite - chromite grain boundaries have evidently resulted from postcumulus enlargement of chromite grains. (UGC-1A)

(D) Vein- or channel-type olivine in chromitite. Channels of slightly more magnesian olivine are connected with the cumulus olivine in the specimen and may represent a postcumulus plumbing system with overlying magma. (UGC-IC)

(E) Thin film of plagioclase surrounding chromite enclosed in cumulus orthopyroxene. The plagioclase formed by subsolidus reaction between chromite and orthopyroxene. (X-11)

(F) Grain size variation of chromite in the UG2-like chromitite. Note the small chromite grain with a spherical inclusion of plagioclase in the centre of the photomicrograph. (78-160B)

(G) Enlarged view of the above showing the sphere of plagioclase in the chromite grain. (78-160B)

(H) Contrast in the fabric and grain size of the chromite in the UG2-like chromitite. The solid, continuous band of chromitite within the silicate-rich matrix consists of large polygonal chromite grains. (78-160B)

in the literature. Kruparz and Van Rensburg (1965) describe drop-like inclusions of silicates, 20 micron in diameter, in chromite of the chromitite deposits at Nietverdiend, Marico District, western Transvaal. McDonald (1965) also described rounded to subrounded silicate inclusions, ranging in diameter from 0,05 to 0,20 mm, in chromite from the chromitite layers of the lower critical zone on the farm Ruighoek in the western Bushveld. He observed that all the silicate minerals forming inclusions in the chromite, with the exception of orthopyroxene, occur elsewhere only as intercumulus minerals. The minerals found in these inclusions are orthopyroxene, clinopyroxene, biotite, plagioclase and chromite. Biotite and clinopyroxene are always intercumulus constituents in the lower zone and the lower part of the critical zone, and for this reason it is felt that the silicate inclusions developed as part of a postcumulus enlargement of chromite. Jackson (1966) also noticed these inclusions in the chromitite layers of the Stillwater Complex and referred to them as his "type 2" inclusions. Although he could not substantiate it, Jackson believed that the spherical inclusions, including those described by McDonald, to be overgrowth features. He suggested that postcumulus enlargement occurred either at the surface of the crystal mush, or within a few inches of it, whilst the chromite still was in contact with a magma saturated with respect to and crystallizing chromite.

These spherical silicate inclusions should not be confused with the mono- and bimineralic assemblages described by Irvine (1975). These tend to be more granitic in composition and are probably related to a different mechanism than that which will be described below.

5.2.4 The Postcumulus Enlargement of Chromite

One of the major problems concerning the origin of chromite layers is how a chromite cumulate with a calculated and experimentally determined porosity of 30 to 45 per cent (Jackson, 1961; Cameron and Desborough, 1969) became "densified" to massive chromite layers containing less than 10 per cent intercumulus silicates. Various hypothesis have been proposed to account for this feature. Cameron and Emerson (1959) have, for instance, proposed partial

remelting of cumulus chromite, whereas McDonald 1965, 1967A, 1967B, suggested the existence of a chromite-rich liquid. Both theories have been rejected by Jackson (1966) because chromite-rich liquids would require a temperature of 1700 to 2000° C. Cameron (1969) subsequently also rejected the concept of a chromite-rich liquid to account for massive chromitite layers in stratiform intrusions. Henderson and Suddaby (1971) proposed an increase in volume of chromite within the layers by post-cumulus reaction of chromite with plagioclase and liquid to form Al-rich chromite. Such a mechanism is not possible in most chromite deposits from the Bushveld because of the lack of plagioclase especially in the Potgietersrus area. In situ overgrowths of cumulus chromite grains are unlikely because of the very low concentration of chromium in the interstital liquid. Similarily, diffusion of chrome from the overlying magma is difficult to envisage because of the large amount of chromium involved.

The numerous examples of postcumulus modification features documented earlier, together with the observation that a lateral thinning of chromite layers is accompanied, apart from the development of hard lumpy ore, also by a proportional increase in the Cr_2O_3 content suggests that the layers were densified by a process analogous to sintering. Spry (1969) points out that one of the simplest examples of growth enlargement of crystals is by annealing or sintering of fine-grained aggregates of strained grains to give a coarse-grained aggregate of unstrained grains. The driving force for the growth is the lattice strain energy plus grain boundary energy. As a result of this, coarse polygonal textures, such as those in Figures 43C, D and E, will develop. The grain boundaries will tend to be fairly straight because the surface energy decreases with decrease in radius of curvature.

This process of sintering has been mentioned in connection with the densification of chromite by Golding (1975), who described relict textures in podiform chromitite from the Coolec Ultramafic Belt in New South Wales.

Sintering is a term used in the ceramics industry to describe a process that results in the densification of a porous aggregate

of similar material by the application of heat not sufficient to melt the material. Sintering is accompanied by a change in the number and size of the pores, and an increase in the grain size. The pores between the grains initially change shape by becoming channels or isolated spheres and as the process continues, the shape and the size of the pores change with the pores becoming more spherical and smaller in size. If the original material consisted of a loosely packed aggregate of small particles the surface energy will be lowered by the formation of a number of larger particles. The driving force for sintering is universally considered to be the excess surface energy within a given amount of material in the form of fine particles, relative to the surface energy of the same amount of material in a solid lump. Numerous other factors also contribute to the driving force of this sintering process (Kingery et al., 1976; Budworth, 1970 A&B).

Sintering is initiated at points of grain contact and the interaction between the two adjacent particles occur in what is called the neck zones or the junction between the two particles. These contact points between particles act as bridges and set up high local stress which lead to plastic deformation or creep by the Nabbaro-Herring mechanism (Kingery et al., 1976). This deformation is a diffusional flow within each grain away from boundaries where there is compressive force towards boundaries having normal tensile stresses, because tensile stresses on a grain boundary increases the site vacancy concentrations, whereas a compressive stress reduces the concentration. Thus, the specimen yields to an applied stress even if the loads are not great enough to deform it mechanically.

The sintering process can be greatly enhanced by the presence of a capillary fluid and pressure for the liquid phase can rearrange the particles in the aggregate to get the most effective packing and thus the maximum number of grain boundary contacts. The capillary pressure can be most effective because it can build up considerably, for example 0,1 and 1 micron diameter capillaries can develop pressures of 1750 p.s.i. and 175 p.s.i. in silicate melts and pressures of 9750 p.s.i. and 950 p.s.i. for metal-rich liquids like liquid cobalt etc. (Kingery et al., 1976). When

particles in the aggregate are penetrated by the liquid the increased pressure at the contact points lead to an increased solubility and material transfer away from the contact area so shrinkage results since the particle centres approach each other. Thus, during the sintering and densification process there is a solution of smaller particles and growth of larger grains by material transfer through the liquid, for example as seen in Figures 42C, 45E, and 46F and H. However, the need for the capillary pressure as an additional driving force for sintering is eliminated if an external pressure is applied at elevated temperatures and it also eliminates the need for very fine particles. Such a process is referred to as pressure sintering and hot pressing if the process takes place at elevated temperatures. Not only does the applied pressure improve the packing but it also enhances the bulk diffusion and plastic flow.

Solid state sintering without the presence of a liquid can and does occur, however its progress is minimal when compared to that of sintering in the presence of a reactive liquid at elevated temperatures. The effect of pressure in the presence of a reactive liquid is manifest in the chromite textures by the zig-zag pattern of the silicate films (now serpentinized) as seen in the massive as well as chain textured chromitite (Figure 42B and D as well as Figure 43C, D and E). This texture resembles that of intergranular slip and fracture which is induced in metals (Conrad, 1961) and ceramics (Day and Stokes, 1966) stressed at high temperatures and low strain rates. Under pressure, this silicate fluid would probably weaken the chromite aggregate and facilitate somewhat similar slip and fracture during extension of this aggregate.

The silicate magma, in particular when MgO- and NiO-rich, can be very effective as natural reactive agent to control the grain growth. It is well known that small amounts of magnesia can be used to control grain growth of alumina, as well as other substances, as was shown by Coble (1961), who successfully sintered alumina to a pore-free condition, something that had never been done before. Magnesia, when added in amounts of only 0,25 weight per cent to alumina can distribute itself very readily through the initially porous specimen. NiO, and ZnO have been found to be as effective as MgO as a grain growth control additive in that

it ends up distributing itself as a grain boundary film that wets the loose aggregate (Budworth, 1970A&B).

The most common shape of sintered grains when the system is in thermodynamic equilibrium, is polygonal where grains meet at triple junctions (120°) with straight to slightly curved crystal faces. More comprehensive explanations of sintering are provided by Budworth (1970A) and Kingery et al. (1976).

The numerous examples of silicate (olivine, orthopyroxene and plagioclase) inclusions within chromite and chromite grains that mantle olivine are considered to be postcumulus textures related to the sintering process. This can be explained with the aid of Figure 45, an idealization of the sintering process as it could have occurred in the UG2-like chromitite immediately following the deposition of cumulus chromite. Figure 45A represents an accumulation of fairly well sorted chromite crystals, surrounded by intercumulus liquid from which orthopyroxene and plagioclase subsequently crystallized (Fig. 45B). Four grains, encircled in Figures 45A and B, have been chosen to illustrate the sintering process, but many more grains could have been involved to produce one larger grain. At the points of contact of the grains high local stresses will lead to plastic deformation and creep, thereby initiating sintering (Fig. 45C). All other factors previously mentioned in the discussion on sintering will come into effect, i.e. reactive liquids, capillary pressure etc. and thus enhance the transfer of material to the neck region between the grain contacts, either by solution and re-deposition of material or by diffusion via the Nabbaro-Herring mechanism. As a result of this transfer of material, grain boundaries will be readjusted to a lower energy curvature which will also modify the shape of the composite (four) grains as a whole. As the process continues, both the size and shape of the pores change, with the pores becoming smaller in size and more spherical in shape. Eventually, the form seen in Figure 45D will be transformed into that seen in Figure 45E. Here the smooth straight grain boundaries represent the form with the lowest surface energy, whereas the shape of the inclusion tends to be spherical because a sphere has the lowest surface area for any given volume and therefore also the lowest surface energy (Spry, 1969). Subsequent crystallization

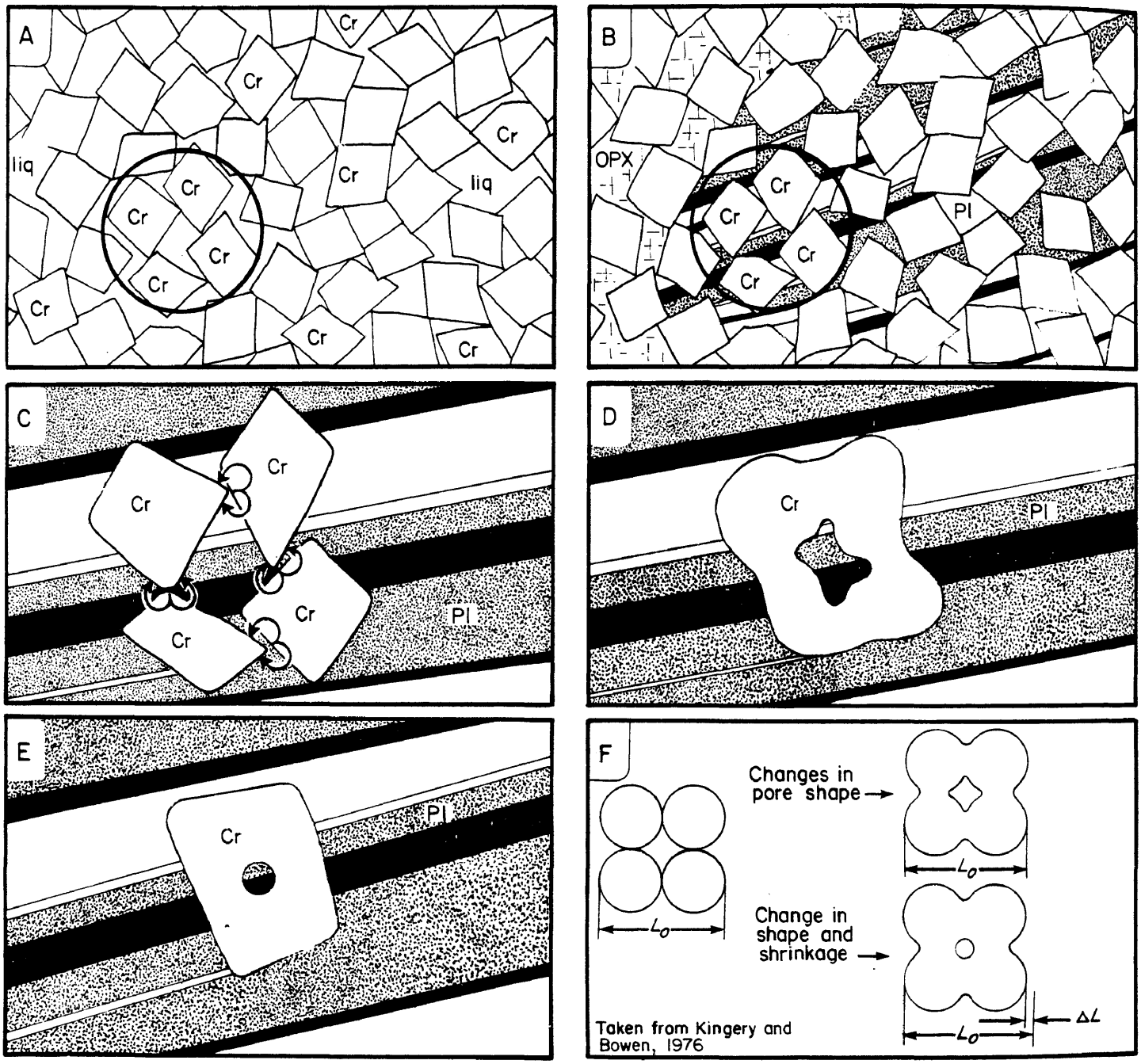

Fig. 45 Schematic representation of the sintering process as it appears to have occurred in the UG2-like chromitite to give rise to spherical silicate inclusions in chromite. For further details see text.

of the trapped intercumulus liquid results in a sphere of plagioclase of similar optical orientation to that outside of the grain. This similarity was probably the result of this liquid being polymerized. Figure 45F taken from Kingery et al (1976) illustrates the same principle except that the particles are four spheres. Note the development and extensions of necks at the sphere contacts and how the shape and size of the pore changes. As the process goes towards completion the spherical inclusions will get successively smaller and smaller until they disappear completely, e.g. in the lower massive portions of the lower chromitite layer (Fig. 42B) no spherical inclusions are present, whereas in the massive upper portion of the same layer (Fig. 42D) the odd olivine spheres are retained. The presence of abundant spheres and mantles of chromite near the top of the lower chromitite layer (Fig. 42E) suggests that the sintering process was either arrested at a relatively early stage or that the upward decrease in the amount of cumulus chromite prevented formation of massive chromitite, so that the process could not be brought to completion. Important in the understanding of sintering was the discovery that pores will continue to shrink and thus enhance densification only as long as they are situated on grain boundaries. Should a mutual grain boundary be removed from a pore, the pore will stop shrinking because the grain boundary acts as a vacancy sink for material to diffuse to. The removal of grain boundaries from pores during the densification of the layer may have given rise to the arrested textures observed at the top of the layer.

D. Kotze (person. commun.) who has been involved with experiments on sintered products containing Transvaal chromite agrees that the observed chromite textures in Figures 42, 43, and 44A, C, D, F, G, and H are the products of sintering.

In conclusion, it is felt that the sintering process could adequately explain densification of chromitite layers to concentrations of 90 per cent and higher from an original chromitite crystal mush containing between 55 and 70 per cent chromite. The process also explains how original chromite grains, as small as 0,007 mm in diameter, can get enlarged to grains 0,75 mm or more in diameter. It also accounts for the tremendous contrast in grain size observed

in the layers.

5.2.5 Chromite Chemistry

5.2.5.1 Chromitite Layers

A detailed study of the chromite chemistry of the upper and lower chromitite was undertaken in the hope that it would shed some light on the controls governing the precipitation of chromitite layers from the magma. The results of the study are shown in Figure 46 together with the modal per cent chromite present in each layer. Unfortunately, due to varying degrees of postcumulus modification processes and the variations in the proportions of cumulus olivine, now serpentinized, and chromite, no meaningful deductions on the genesis of the layers can be made other than the fact that the chromite of the chromitite layers contain more Cr_2O_3 ($\approx$10 per cent) and have a higher $Cr/(Fe^{2+}+Fe^{3+})$, $Cr/(Cr+Al+Fe^{3+})$ and Mg* than the disseminated chromite in silicate-rich rocks (Appendix 7). The higher Mg* of the chromite in the chromitite is probably the result of crystallization under higher fo_2 conditions or the result of sintering in a MgO-rich environment.

Although most of the chromitites have been sintered an understanding of the chromite genesis may be gleaned from a very detailed study of the 1" stringer and its immediate foot-wall, where regular systematic trends have been observed as this thin chromitite layer is approached. This will be dealt with in more detail in section 5.2.6.2.

5.2.5.2 Compositional Variations of Chromite and Coexisting Silicates in the Drummondlea Harzburgite-Chromitite

The chemical trends observed in chromite, olivine and orthopyroxene from the various cyclic units can be most informative in interpreting the conditions of crystallization of the magma that gave rise to the various cyclic units. For this reason the chemical parameters for chromite (Fig. 47) must be discussed in conjunction with the Mg* of the olivine and orthopyroxene (Fig. 36).

It was pointed out earlier that cyclic unit 21 was mineral graded. This mineral grading is accompanied by a chemical grading

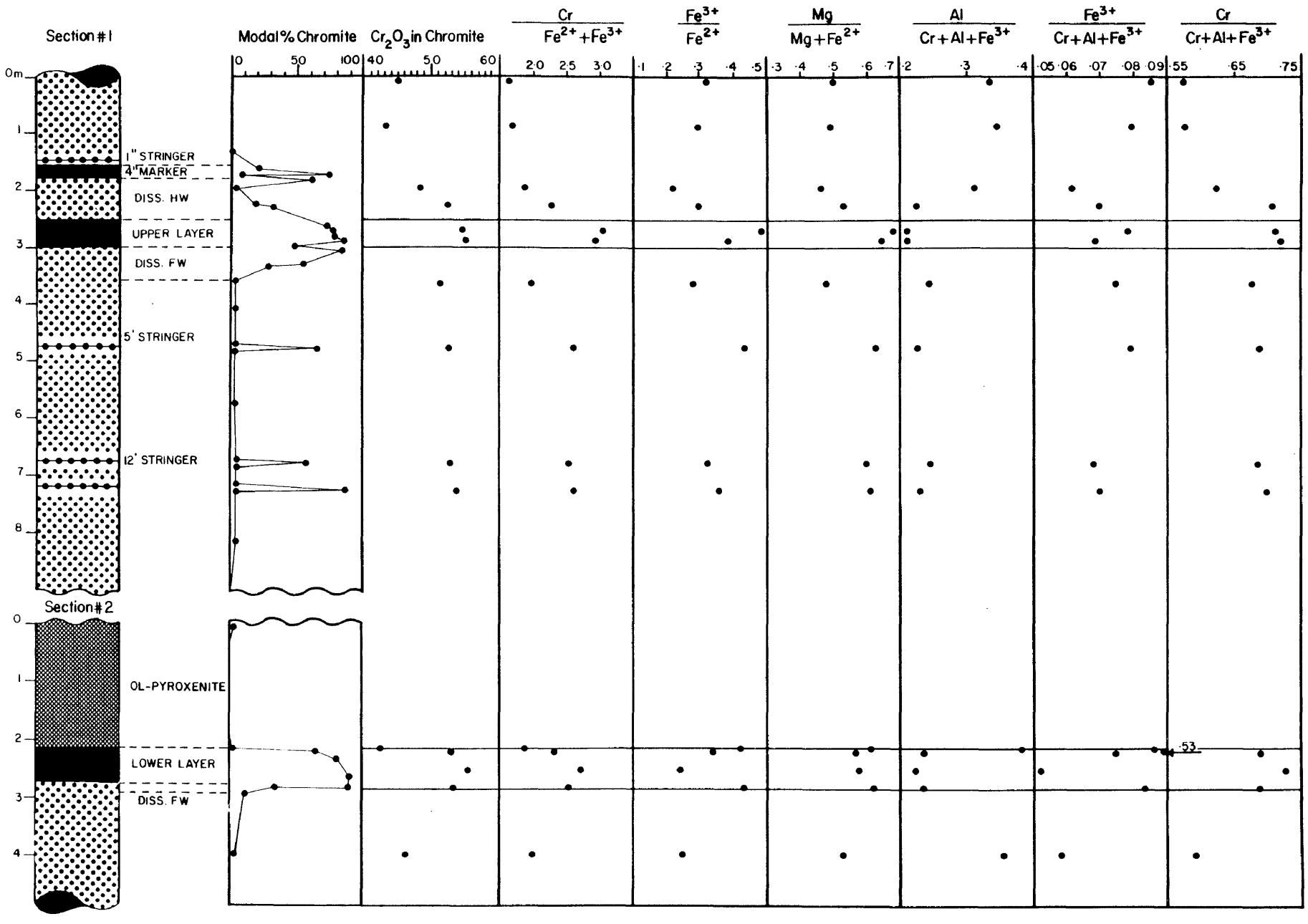

GRASVALLY CHROME ORE SECTION G66, 6TH LEVEL

Fig. 46 Modal per cent and crystal chemistry of chromite from the G66,6 level, Grasvally Mine. For legend of columnar section see Figure 36.

of the cumulus phases in that the Mg* of the silicates decreases with increasing stratigraphic height. Such a normal Fe enrichment with differentiation, accompanied by a decrease in temperature of crystallization of successive cumulus phases has been documented from many layered intrusions. Figure 47 reveals that the Fe^{3+}/Fe^{2+} ratio and to a lesser extent the Mg* of the chromite decreases with stratigraphic height. Arculus et al. (1974) have shown that the Fe^{3+}/Fe^{2+} ratio in chromites tend to decrease with decreasing temperature. Fisk and Bence (1980), on the other hand, have shown that the Mg* of chromite also decreases with decreasing temperature and that this probably reflects the decrease in the Mg content of the melt due to crystallization of Mg-rich silicates. Similarily, Hill and Roeder (1974) pointed out that at constant partial pressure of oxygen the Mg*, $Cr/(Fe^{2+}+Fe^{3+})$ and Al_2O_3 content of the spinel decreases with decreasing temperature. Therefore, although the available evidence is not conclusive, it would appear from the decreasing Mg* of the silicates and the concomittant decrease of the Fe^{3+}/Fe^{2+} of the chromite that a slight drop in temperature of the magma during crystallization of cyclic unit 21 took place.

It should be pointed out that chromite chemistry depends to a certain extent on the nature of the coprecipitating silicates. The chemistry of the chromites should therefore be viewed in conjunction with the Mg* trends observed for the associated silicate. Fisk and Bence (1980) have also shown that the $Cr/(Cr+Al+Fe^{3+})$ ratio of the chromite coprecipitating with olivine decreases with a decrease in temperature and that this is probably due to the combined effect of a decrease in the Cr content of the magma caused by continued spinel crystallization. However, when the crystallizing phases are joined by plagioclase or another phase that competes for Al from the melt, the $Cr/(Cr+Al+Fe^{3+})$ ratio increases and the trends become more difficult to interpret.

Cyclic unit 22 is difficult to comment upon because of its restricted thickness and the limited number of available data points. Nevertheless, the Mg* of the chromite suggests a drop in the temperature from the ol-chr cumulate to the opx-ol-chr cumulate but an increase at the top towards the base of the next unit, suggesting an increase in the fo_2 in the magma at this level.

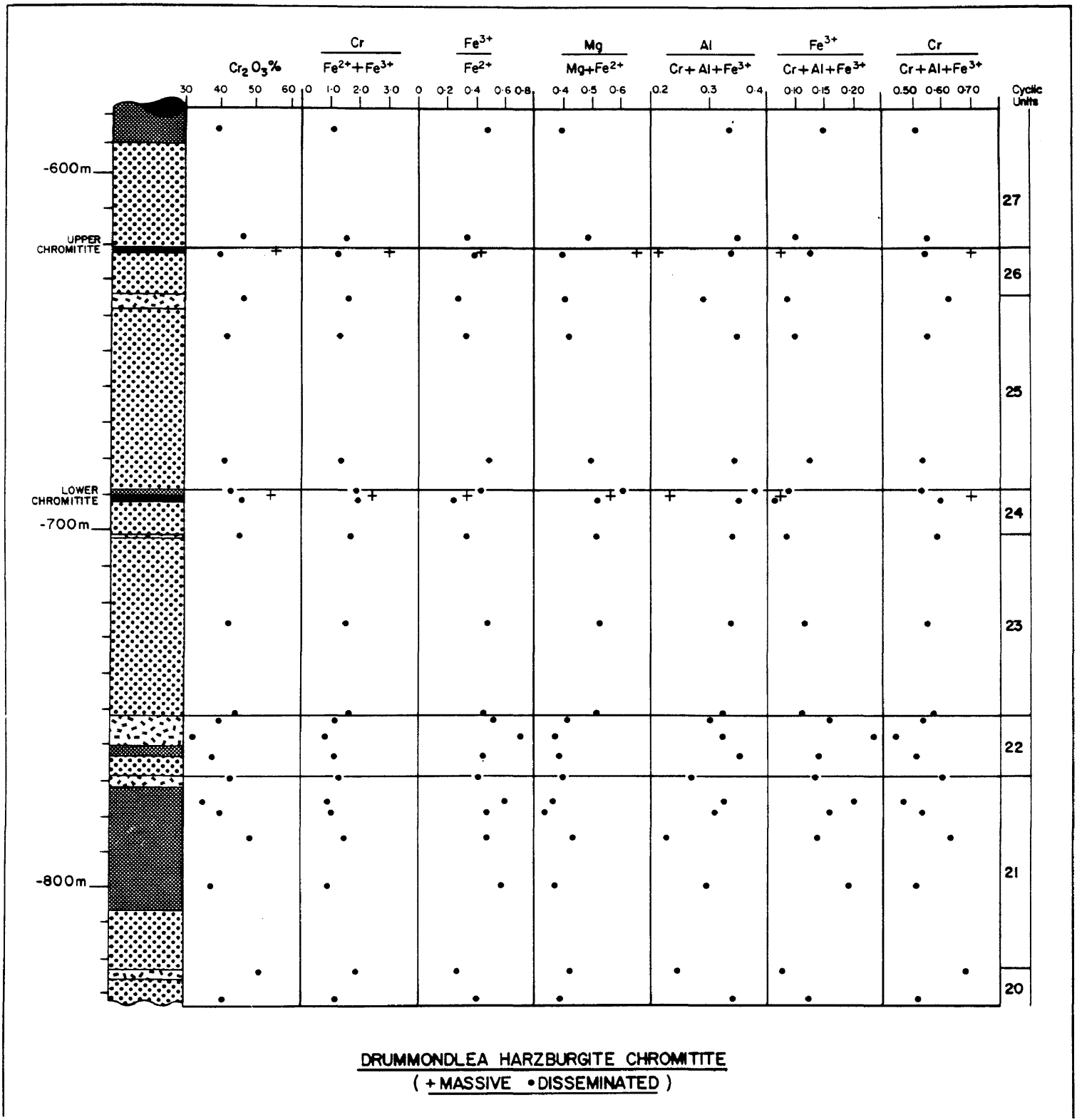

Fig. 47 Compositional variation of chromite in the Drummondlea Harzburgite-Chromitite. For legend of columnar section see Figure 36.

The $Cr/(Fe^{2+}Fe^{3+})$ and the $Cr/(Cr+Al+Fe^{3+})$ ratios also suggest an initial drop in temperature, whereas the reversal near the top of the opx-rich cumulates suggest a rise in temperature and fo_2 conditions during crystallization. The compositional trends of chromite near the top of cyclic unit 22 and at the base of the overlying cyclic unit 23, as well as the compositional reversals of the coexisting olivine and orthopyroxene as indicated by their respective Mg* (Fig. 36), therefore suggest the influx of fresh magma into the chamber. This magma had a higher temperature and higher fo_2 than the residual melt in the chamber.

The data points for chromite through the olivine-rich rocks of cyclic units 23 and 24 (Fig. 47) show an initial trend of decreasing Mg* and increasing $Al/(Cr+Al+Fe^{3+})$ ratio (hereafter referred to as Al*). The gradual decrease in the Fe^{3+}/Fe^{2+} ratio and concomittant increase in the $Cr/(Cr+Al+Fe^{3+})$ ratio in the ol-chr and opx-ol-chr cumulates, followed by a subsequent increase and decrease in these values respectively near the chromitite layers suggests that the temperatures of the melt was dropping with increased fractionation from above the base of cyclic unit 23. The reversal near the chromitite layers does again suggest an increase in the fo_2 and temperatures of the melt. In all likelihood, this increase in fo_2 is the reason for the enhanced precipitation of chromite at this horizone.

Evidence that this new impulse was of a more chrome-rich nature is seen in the olivine cumulates at the base of cyclic unit 23. Here, the olivine contains 0,08 per cent Cr_2O_3, whereas the olivine of the underlying olivine bearing cumulates in cyclic unit 22 contain only 0,05 per cent Cr_2O_3. In contrast the olivine in the olivine-rich rocks in the foot-wall of the lower chromitite layer contains 0,09 per cent Cr_2O_3 whereas olivine in the opx-ol-chr cumulate in the hanging-wall of the lower chromitite contains only 0,05 per cent Cr_2O_3 and therefore reflects the depletion of chrome in the magma after crystallization of the lower chromitite layer. The fact that the Cr_2O_3 content of olivines could be interpreted in such a manner was demonstrated by Akella et al. (1976) on the basis of controlled cooling experiments, that the Cr_2O_3 content of olivines do not re-equilibriate

upon cooling and consequently the Cr_2O_3 content of olivines can be used to calculate Cr_2O_3 content of the melt from which they crystallized. Based on a $D_{Cr}^{ol-liq.} \approx 0,85 \pm 0.15$ (Huebner et al., 1976) the new magma from which cyclic unit 23 crystallized probably contained 0,09 per cent Cr_2O_3, whereas the magma that gave rise to the olivine-rich cumulates of the cyclic unit 22 probably contained about 0,06 per cent Cr_2O_3.

The $Fe^{3+}/(Cr+Al+Fe^{3+})$ ratio shows variations similar to that of the Fe^{3+}/Fe^{2+} ratio. The ratio drops from 0,13 - 0,06 from the base of cyclic unit 23 to the lower chromitite layer then rises fairly rapidly to a value of 0,13 above the lower layer and then decreases steadily towards the upper chromitite layer to a value of about 0,06 once more. Subsequently, at 1,5 m above the upper layer the ratio rises to 0,13 and increases to 0,15 thirty stratigraphic metres above the upper chromitite layer. It appears that a value of $Fe^{3+}/(Cr+Al+Fe^{3+})$ of $\leq 0,08$ is indicative of chromite enrichment whereas values of $> 0,08$ are associated with silicate-rich lithologies.

Cyclic units 25 and 26 are more difficult to interpret with respect to the ratios $Mg/(Mg+Fe^{2+})$, $Cr/(Cr+Al+Fe^{3+})$, and $Cr/(Fe^{2+}+Fe^{3+})$. The $Cr/(Fe^{2+}+Fe^{3+})$ and the $Cr/(Cr+Al+Fe^{3+})$ ratio remains fairly constant over this interval but the $Mg/(Mg+Fe^{2+})$ ratio of the chromite and the olivine and orthopyroxene decrease. The decreasing $Cr/(Fe^{2+}+Fe^{3+})$, $Mg/(Mg+Fe^{2+})$ and $Cr/(Cr+Al+Fe^{3+})$ ratios with increasing stratigraphic height above the upper chromitite layer suggest decreasing fo_2 conditions subsequent to the formation of this chromitite.

5.2.5.3 Compositional Trends within the Lower and Critical Zone

Although the chemistry of the chromite in the Drummondlea Harzburgite-Chromitite subzone was studied in detail the investigation was extended to the Volspruit Pyroxenite and the Moorddrift Harzburgite-Pyroxenite subzones of the lower zone and to the lower half of the critical zone (Grasvally Norite-Pyroxenite-Anorthosite) in order to evaluate trends in the composition of chromite with differentiation and increasing stratigraphic height (Figs. 7B and 48).

It was established that the Mg* of chromite varies very sympathetically with the Mg* of coexisting orthopyroxene and olivine (Fig. 7B).

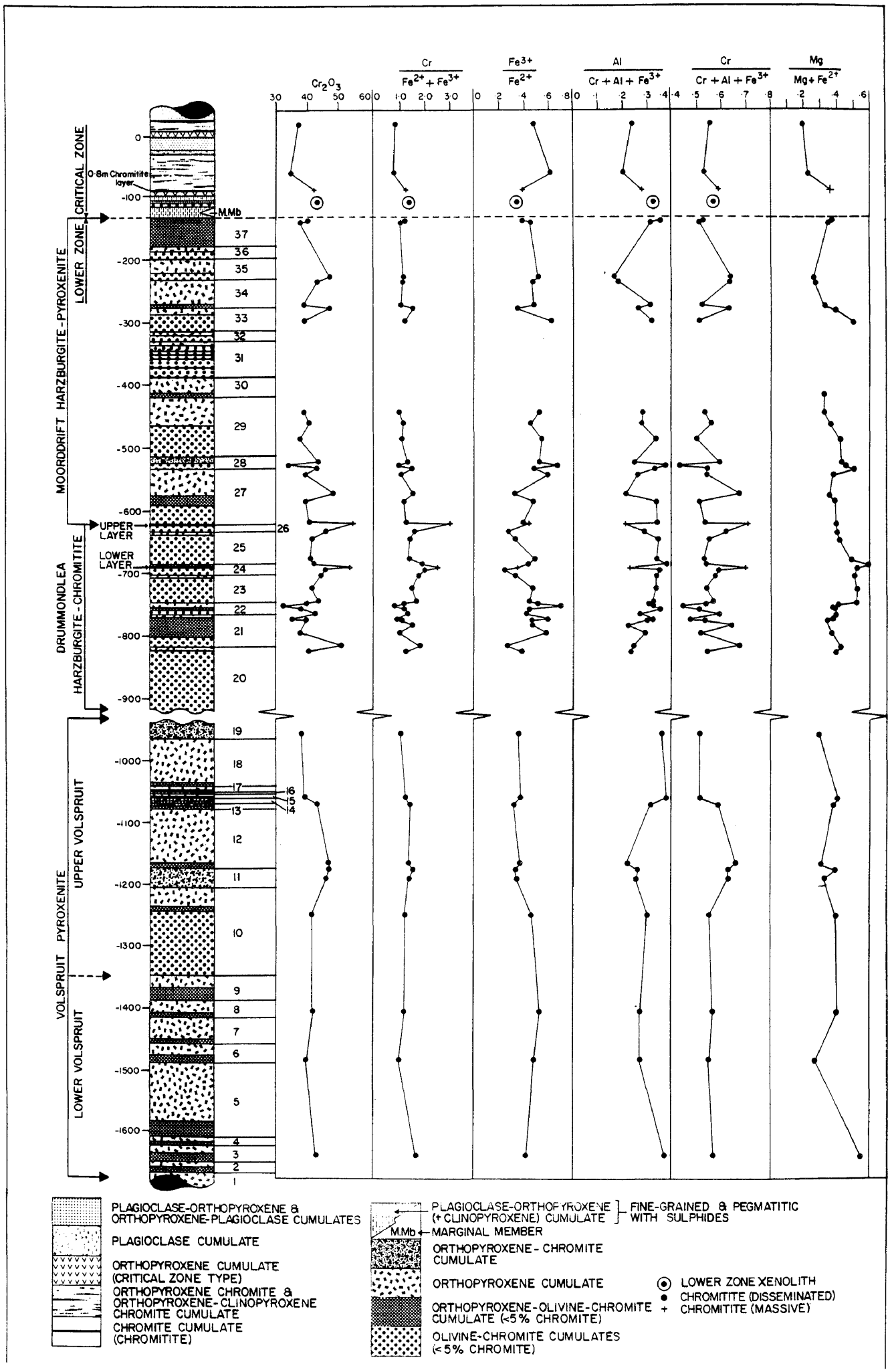

Fig. 48 Compositional variation of chromite in the lower and critical zones south of Potgietersrus.

The overall trend in the Volspruit Pyroxenite is a decrease of the Mg* from approximately 0,559 to 0,303. A similar trend is recorded by the Mg* of the orthopyroxenes, thus suggesting a decrease in both temperature and fo_2 with differentiation. Local irregularities do occur, for example relatively low values occur at the -1480 and -1190 metre levels, although further microprobe data on the chromite are necessary to define more precisely the horizons at which these breaks occur. The breaks do tend to suggest short lived decreases in the temperature and possibly fo_2. The two observed decreases in the Mg* are associated with some sulfide enrichments.

The general trend of the Mg* of the disseminated chromite increases to a maximum at the lower chromitite layer from where it decreases gradually up to the -420 m level in the Moorddrift Harzburgite-Pyroxenite. A similar increase in the Mg* is also seen in a detailed study of the silicate-rich 10 mm interval in the immediate isomodal foot-wall layer of the 1" chromite stringer where the Mg* steadily increases from 0,526 to 0,617 as the chromitite layer is approached. Although the trends in the Mg* can change very rapidly, the trends shown in Figure 7B and 48 reveal that a major change in the oxidation state and temperature of the crystallizing magma must have taken place as the chromite-rich intervals were approached. Since most authors, e.g. Buddington and Lindsley (1964) and Bowles (1977) believe that the cooling curve of a magma normally follows a buffer curve, any increase in temperature would, under normal conditions, give rise to an increase in fo_2 and vice-versa.

In cyclic unit 28 the localized increase in the Mg* probably reflect enhanced fo_2 conditions which gave rise to the accompanying chromite mineralization. The Mg* decreases from cyclic units 33 to 35 and increase again in unit 37 and in the xenolith of lower zone material in the critical zone. The Mg* of the UG2-like chromitite layer is similar to that at the top of the lower zone but the disseminated chromite in the opx-chr and opx-cpx-chr cumulate is lower.

The $Fe^{3+}/(Fe^{3+}+Al+Cr)$ ratio, or Fe^{3+*}, of chromite is antipathetic to the Mg*. The increasing Fe^{3+*} with decreasing Mg* may be due to a drop in temperature with differentiation under fairly constant fo_2 conditions. As a result of early chromite crystallization

the Fe^{3+} in the spinel should increase and the Cr decrease because of a depletion of the crystallizing magma in chromium (Hill and Roeder, 1974).

One of the most informative chemical parameters regarding differentiation is the TiO_2 content of chromite. From Figure 7B it is apparent that the TiO_2 content of the disseminated chromite increases from the lowest to the highest stratigraphic horizons. The average TiO_2 content of chromite from the Volspruit Pyroxenite is 0,47 weight per cent, the Drummondlea Harzburgite Chrometite contains 0,87 per cent and the Moorddrift Harzburgite-Pyroxenite 1,00 per cent TiO_2, whereas the TiO_2 content of the disseminated chromite in the lower half of the critical zone is 2,98 per cent. Reference to Appendix 7 shows that one of the rocks (78-360) from the M.Mb./P.G. contains a low chrome chromite with 3,78 weight per cent TiO_2 (78-360-1) which coexists with primary magnetite (78-360-2). Cameron (1977) also noted that the TiO_2 and V_2O_5 content of the chromitite layers increase upwards in the critical zone in the eastern Bushveld Complex. It is furthermore well known that the TiO_2 content of the magnetitite layers from the upper zone also increases upward in the succession (Molyneux, 1970; van der Merwe, 1978). Evans and Wright (1972) showed that the more fractionated the host basalt the more TiO_2-rich are its chrome spinels. The higher TiO_2 content of the chromite is probably due to the higher concentration of ulvöspinel molecule in successive liquids. Hill and Roeder (1974) showed that under decreasing temperature conditions at fixed fo_2 the successive chromite from more fractionated liquids are richer in TiO_2. El Goresy et al. (1976) also found that later generations of lunar chromites are enriched in Ti and Fe yet have a fairly constant Cr/(Cr+Al) ratio.

Since the octhahedral site preference energy of Ti^{4+} is considerably lower than elements such as Cr^{3+}, (Burns, 1970) it should, by virtue of its lower distribution coefficient become enriched in the melt relative to the solid phase during crystallization (Eales and Reynolds, 1981). Therefore, there appears to be little doubt that the more TiO_2-rich chromites in the Rustenburg Layered Suite south of Potgietersrus are derived from successively more fractionated magmas. In fact, the TiO_2 content of the spinels is the most reliable cryptic indicator in the lower zone regarding

the chronological order of the rocks, because high Mg* in the silicates can be the result of more fractionated liquids crystallizing in a more oxygenated environment, whereas the TiO_2 content of chromite at 1200° C is virtally unaffected by increases in fo_2 (Hill and Roeder, 1974). This cryptic indicator also substantiates the structural interpretation that the Volspruit Pyroxenite subzone is an earlier cumulate sequence than the Drummondlea Harzburgite-Chromitite subzone.

The Cr_2O_3 content and the $Cr/(Fe^{2+}+Fe^{3+})$ ratio of chromite vary in a sympathetic manner through the lower and critical zone (Fig. 48), therefore, a satisfactory interpretation for the variation in the Cr_2O_3 could also apply for the $Cr/(Fe^{2+}+Fe^{3+})$ ratio, hereafter referred to as the Cr/Fe ratio. Apart from a few exceptions and for a larger fluctuation of the Cr/Fe ratio, the trend is similar to that of the Mg* for disseminated chromites (Fig. 48 and 7B). The ratio decreases from 1,75 to 1,07 from the lower to upper stratigraphic levels of the Volspruit Pyroxenite subzone, with a small localized break at the -1190 m level. In the Drummondlea Harzburgite-Chromitite subzone the Cr/Fe ratio decreases up to approximately the -765 m level, as is the case for the Mg*, whereupon it jumps to a higher value and steadily increases toward the lower chromitite layer. Excluding the high values for the massive upper chromitite, the Cr/Fe ratio drops off from the lower chromitite up to the -440 m level. Greater density of analyses would probably also have shown an increase in the Cr/Fe ratio towards the upper chromitite.

There is compelling evidence that the Cr/Fe ratio is controlled by the prevailing fo_2 and temperature of the system. Hill and Roeder (1974) pointed out that, at a fixed fo_2, the Cr_2O_3 content and the Cr/Fe ratio of the chromite drops with decreasing temperature. Schreiber and Haskins (1976) deduced from experimental investigations that the chromium-redox equilibria was controlled by the composition of the silicate melt, the temperature and the partial pressure of oxygen. They furthermore showed that the oxidation state of chromium, i.e. the proportion of Cr^{3+} and Cr^{2+} in the liquid, is dependent on the prevailing fo_2. This they illustrated with the aid of the system Forsterite-Anorthite-Silica where they could demonstrate that at 1500° C and and fo_2

of 10^{-7} atm, 35 per cent of the chromium was trivalent whereas 65 per cent was divalent. At the same temperature but at an fo_2 of 10^{-5} atm the proportions were 64 per cent Cr^{3+} and 36 per cent Cr^{2+}. They also showed that 90 per cent of the total chromium is in the divalent state over a wide range of melt compositions and temperatures at oxygen partial pressures between 10^{-9} to 10^{-11} atm. Since chromite can only accept Cr^{3+} in its structure the oxidation state of the system will control the amount of chromium in the chromite. Schreiber and Haskins could, in fact, demonstrate that an increase in fo_2 by two log units doubled the amount of chromium available to be taken up by chromite. This would corroborate the earlier deduction that an increase in the Mg* of the spinels and silicates is in response to an increase in fo_2 of the system as this would also cause the oxidation of chromium from the Cr^{2+} state to the Cr^{3+} state and the resultant sympathetic increase in the Cr/Fe ratio and the Cr_2O_3 content of the chromite.

Crystallization experiments by Fisk and Bence, (1980) on a primitive "Famous basalt" with a Mg* of 0,68; a Cr content of 510 ppm (0,075 per cent Cr_2O_3) and coexisting with olivines (Fo_{86-89}) showed that chrome spinel would not crystallize below an oxygen fugacity of $10^{-9,5}$ atm. They assumed that most of the chromium in the melt was reduced to the Cr^{2+} state, and showed that as the conditions of their experiments became more reducing, the Cr^{3+} and Fe^{3+} in the melt were reduced to Cr^{2+} and Fe^{2+} until at an fo_2 of about 10^{-9} atm the concentration of trivalent cations was so low that spinel no longer crystallized.

The Fe^{3+}/Fe^{2+} ratios of the chromite are more difficult to interpret. Arculus et al., (1974) stated that an increase in the Fe^{3+}/Fe^{2+} ratio occurs with decreasing temperature whereas Hill and Roeder (1974) also report that at a fixed fo_2 the Fe_2O_3/FeO ratio increases with decreasing temperature. Since the Fe^{3+} values in this study are calculated and based on the assumption of stoichiometry of the chromite, any interpretation should be weighed against the trends of other variables for chromite and mafic silicates. In the samples from the Drummondlea Harzburgite-Chromitite subzone and the Moorddrift Harzburgite-Pyroxenite subzone a fairly antipathetic relationship can be seen between the Fe^{3+}/Fe^{2+} ratio and the Mg* and Cr/Fe ratio of chromite therefore interpretations

for these latter ratios should also apply for the explanation of the Fe^{3+}/Fe^{2+} ratio.

The $Cr/(Cr+Al+Fe^{3+})$ and $(Al/(Cr+Al+Fe^{3+})$ ratio (Fig. 48) in chromite display an antipathetic behaviour. Due to the variety of rock types the trends are difficult to interpret. However, the overall decreasing $Cr/(Cr+Al+Fe^{3+})$ and increasing $Al/(Cr+Al+Fe^{3+})$ ratio with differentiation within the lower zone are probably the result of the effects of decreasing temperature, i.e. decrease in Cr, and an increase in Al and Fe^{3+} in the magmas.

5.2.5.4 Intergrain Variation

Although only the cores of chromite enclosed in either cumulus olivine or orthopyroxene were analyzed, it was important to establish whether the chemical variations reflect primary magmatic or postcumulus conditions. A better understanding of this problem was obtained by monitoring the chemical variation of the chromite in various silicate environments within the same sample. It was found that the intergrain compositional variation between chromite included in olivine and that in cumulus orthopyroxene was very small.

The most extreme example encountered was an ol-chr cumulate (harzburgite) in sample 1-123, Fig. 49, Table 3. Comparison of the Cr_2O_3 and Al_2O_3 content reveals little variation between chromite included in olivine (1C) and that in feldspar (5A, B, C). Although the chromite in the intercumulus plagioclase was expected to be enriched in Al_2O_3 this was not found to be the case and little re-equilibriation seems to have taken place between these two phases. The most pronounced differences in the chromite chemistry was found between the above-mentioned compositions (i.e. 1C, 5A, and 5C) on the one hand and chromite enclosed in reaction orthopyroxene. Where olivine has been completely replaced by orthopyroxene, like that which hosts grain 4, the chromite chemistry has changed significantly as can be seen by comparing the Mg*, $Cr/(Cr+Al)$, Al*, Cr*, Fe^{3+}/Fe^{2+}, Fe^{3+*} and the Cr/Fe ratios with those of analyses 1C and 5 (Table 3). Chromite grains enclosed partially by cumulus olivine and reaction orthopyroxene have intermediate compositions (i.e. 1A, Fig. 49, Table 3). Thus chromite enclosed in reaction orthopyroxene was excluded from any interpre-

Fig. 49 Intergrain chemical variation encountered in sample 1-123, an ol-chr cumulate, from the Drummondlea Harzburgite-Chromitite.

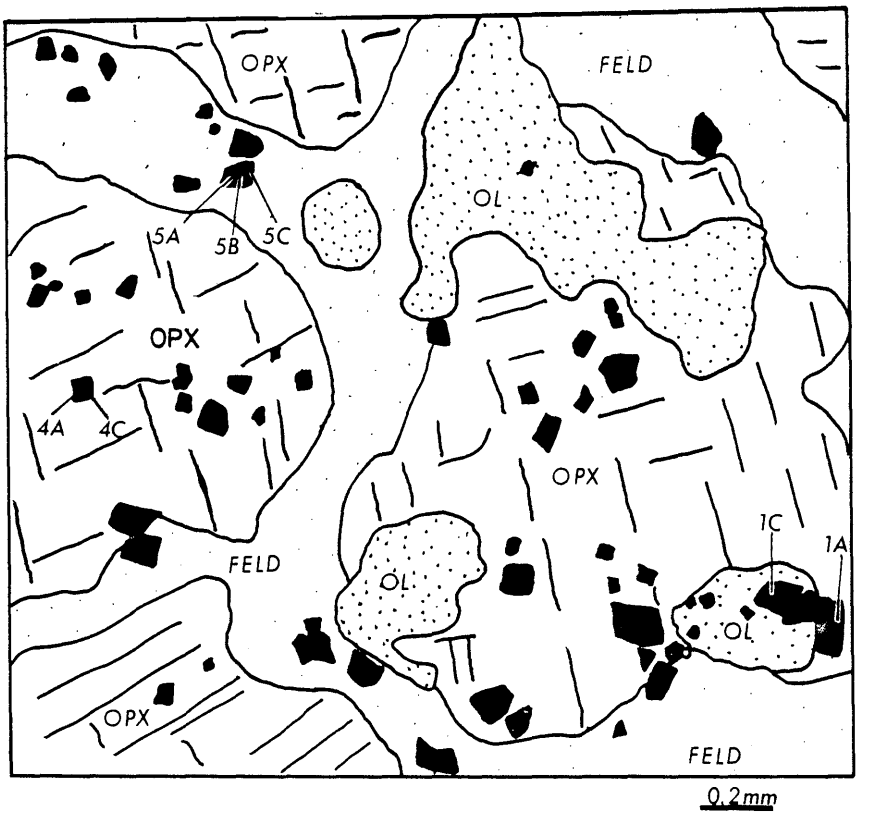

Table 3

CHROMITE ANALYSES FROM SAMPLE 1-123

Sample #	1A	1C	4A	4C	5A	5B	5C
TiO_2	0,75	0,77	0,85	0,88	0,83	0,79	0,85
Al_2O_3	18,51	18,83	17,95	18,44	18,75	18,56	18,84
Cr_2O_3	42,41	41,88	42,00	42,84	41,37	41,09	41,35
Fe_2O_3	9,03	8,79	9,34	8,55	9,25	9,86	8,85
FeO	19,38	20,46	18,01	18,47	20,47	20,00	20,89
MnO	0,37	0,37	0,35	0,36	0,44	0,44	0,44
MgO	10,50	9,84	11,13	11,11	9,85	10,03	9,52
Total	100,94	100,94	99,63	100,65	101,09	100,77	100,73
CATIONS BASED ON 32 OXYGEN							
Ti	0,147	0,151	0,168	0,172	0,163	0,155	0,167
Al	5,521	5,633	5,405	5,492	5,638	5,562	5,658
Cr_{3+}	8,485	8,405	8,484	8,559	8,291	8,261	8,330
Fe^{2+}	1,722	1,682	1,798	1,628	1,768	1,889	1,700
Fe^{3+}	4,109	4,351	3,856	3,912	4,349	4,261	4,459
Mn	0,084	0,084	0,080	0,082	0,099	0,099	0,099
Mg	3,901	3,720	4,241	4,187	3,724	3,804	3,618
CATION RATIOS							
$Mg/(Mg+Fe^{2+})$	0,491	0,461	0,524	0,517	0,461	0,472	0,448
$Cr/(Cr+Al)$	0,606	0,599	0,611	0,609	0,595	0,598	0,596
$Al/(Al+Fe^{3+}+Cr)$	0,351	0,358	0,345	0,350	0,359	0,354	0,361
$Cr/(Cr+Fe^{2+}+Fe^{3+})$	0,593	0,582	0,600	0,607	0,576	0,573	0,575
$Cr/(Cr+Fe^{3+}+Al)$	0,540	0,535	0,541	0,546	0,528	0,526	0,531
Fe^{3+}/Fe^{2+}	0,419	0,387	0,466	0,416	0,407	0,433	0,381
$Fe^{3+}/(Fe^{3+}+Al+Cr)$	0,110	0,107	0,115	0,104	0,113	0,120	0,108
$Cr/(Fe^{2+}+Fe^{3+})$	1,455	1,393	1,500	1,545	1,355	1,343	1,353

tation concerning the intensive parameters of the magma that gave rise to that horizon.

5.2.5.5 Ferritchromit

A most interesting iron-rich chromitite layer, 53 cm thick, was intersected in borehole DDH-DC2A approximately 90 metres above the upper chromitite layer (Fig. 38). As mentioned previously, it occurs in serpentinite, is steel-blue in colour, and is strongly magnetic. This layer has only been intersected by this one borehole, and it could possibly represent an extremely altered and up-faulted equivalent of the upper chromitite layer. Petrographical and electron microprobe investigations have revealed the chromite in the layer to be strongly zoned, both with respect to reflectivity (Fig. 31H) and composition (Fig. 50 and Table 4).

A chromite grain in sample 2A-47 was investigated in detail. It consists of sharp to diffuse zones of low reflectivity chromite with a core of ferritchromit surrounded by magnetite of a higher reflectivity. The term "ferritchromit" was coined by Spangenberg (1943) to describe an opaque substance which physically and chemically is intermediate between chromite and magnetite. The core of the composite grain in Figure 50 has a Cr_2O_3 content of between 9,88 to 11,79 per cent, but differs from the ferritchromit described by Spangenberg in that it is extremely depleted in Al and Mg. This core is surrounded by an irregular zone of chromite which contains between 30,89 to 41,58 per cent Cr_2O_3 and has an Al_2O_3 content that varies between 1,47 and 16,79 per cent. This is surrounded by a well defined zone of low-Cr chromite which contains approximately 22 per cent Cr_2O_3 and 1,0 per cent Al_2O_3, whereas the outermost zone is highly reflecting, pure magnetite with 0,49 per cent Cr_2O_3, 0,30 per cent Al_2O_3 and 0,19 per cent MgO. Most surprising is the extremely low MgO content of the various zones; even the high Cr_2O_3 (41,58 per cent) spinels only contain 0,53 per cent MgO. In fact, the entire range of MgO is from a maximum of 0,63 to a low of 0,15 per cent.

The reflectivity of the various zones can be directly related to the composition. It is a function of the Fe,Al, and Cr content, in such a way, that Cr and Al decrease with increasing Fe content and reflectivity. Some of the zones are irregular and appear

Fig. 50 Compositional zoning within a ferritchromit grain from a chromitite layer encountered in a serpentinite from the Drummondlea subzone.

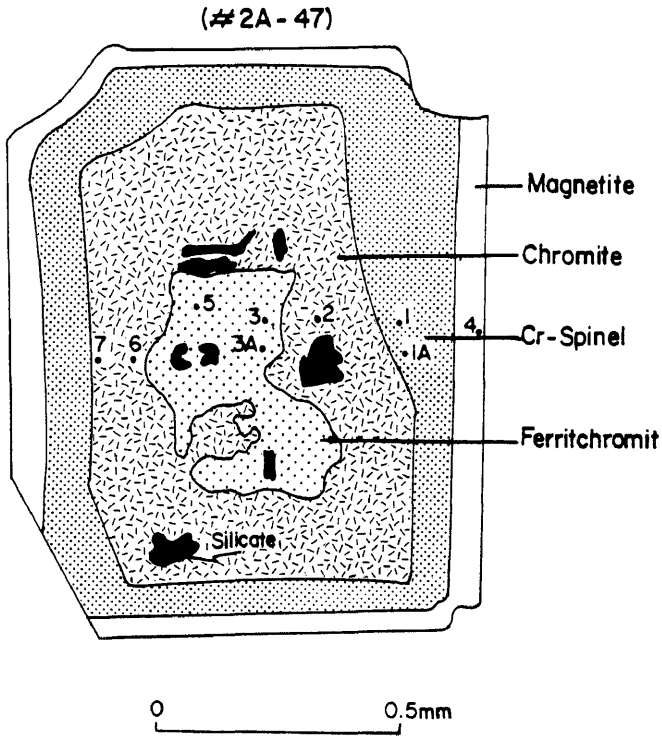

Table 4

CHROMITE - MAGNETITE ANALYSES FROM SAMPLE 2A - 47

Sample #	7	2	6	1A	1	3	5	3A	4
TiO_2	0,58	0,82	1,05	1,06	0,93	0,43	0,56	0,51	0,35
Al_2O_3	16,55	16,79	1,47	1,04	1,04	0,51	0,50	0,51	0,30
Cr_2O_3	41,58	40,49	30,89	22,32	22,06	11,79	10,97	9,88	0,49
Fe_2O_3	6,80	6,98	33,02	44,46	43,87	55,97	56,72	57,87	67,88
FeO	34,21	33,54	31,56	32,29	31,63	31,14	31,40	31,27	31,03
MnO	0,21	0,86	0,20	0,49	0,49	0,34	0,34	0,34	0,19
MgO	0,53	0,63	0,32	0,20	0,22	0,20	0,15	0,18	0,19
Total	100,46	100,12	98,51	101,87	100,24	100,36	100,65	100,55	100,42
CATIONS BASED ON 32 OXYGEN									
Ti	0,124	0,174	0,245	0,241	0,215	0,103	0,132	0,121	0,085
Al	5,350	5,435	0,532	0,368	0,374	0,187	0,183	0,187	0,113
Cr_{3+}	9,017	8,793	7,437	5,241	5,263	2,836	2,634	2,375	0,123
Fe_{2+}	1,407	1,447	7,564	9,931	9,955	12,794	12,941	13,218	15,617
Fe	7,859	7,716	8,048	8,029	7,991	7,925	7,977	7,952	7,949
Mn	0,053	0,204	0,056	0,128	0,130	0,092	0,092	0,092	0,054
Mg	0,221	0,262	0,150	0,093	0,103	0,095	0,072	0,086	0,091
CATION RATIOS									
$Mg/(Mg+Fe^{2+})$	0,027	0,033	0,018	0,012	0,013	0,012	0,009	0,011	0,011
$Cr/(Cr+Al)$	0,628	0,618	0,933	0,934	0,934	0,938	0,935	0,927	0,522
$Al/(Al+Fe^{3+}+Cr)$	0,339	0,347	0,034	0,024	0,024	0,012	0,012	0,012	0,007
$Cr/(Cr+Fe^{2+}+Fe^{3+})$	0,493	0,490	0,323	0,226	0,227	0,120	0,112	0,101	0,005
$Cr/(Cr+Fe^{3+}+Al)$	0,572	0,561	0,479	0,337	0,338	0,179	0,167	0,151	0,008
Fe^{3+}/Fe^{2+}	0,179	0,188	0,940	1,237	1,246	1,615	1,622	1,662	1,965
$Fe^{3+}/(Fe^{3+}+Al+Cr)$	0,089	0,092	0,487	0,639	0,638	0,809	0,821	0,838	0,985
$Cr/(Fe^{2+}+Fe^{3+})$	0,973	0,960	0,476	0,292	0,293	0,137	0,126	0,112	0,005

mottled and can probably be related to diffuse reaction contacts (Haggerty, 1976).

The analyses given in Table 4 shows the complete chemical range between chromite and magnetite and thus suggests complete solid solution between these two spinels.

In a study of chromite alteration Weiser (1966) found that the alteration products could be devided into two groups. The first of these shows an increase in Fe and Cr at the expense of Mg and Al, whereas the second group shows a decrease of Cr, Al, and Mg with an increase in Fe. It is obvious from Figure 50 and Table 4, that the example at hand falls into Weiser's second group. During the alteration process a considerable amount of ferric iron must have been introduced into the chromitite layer, thereby replacing large quantities of Mg, Cr, and Al. The most likely source of this ferric iron is that released during serpentinization, as thin and polished sections show the serpentinites to contain abundant secondary magnetite.

The non-opaque phases in this sample are serpentine, dolomite, and an unknown Fe-Na-Mn silicate. Analyses of this Fe-rich alteration phase is given in Appendix 5, sample number 9.

Ferritchromit-magnetite reaction zones about chromite are extremely rare in stratiform intrusions (Beeson and Jackson, 1969). These authors state that, to their knowledge, ferritchromit alteration zones have never been described for any stratiform intrusion other than the Stillwater Complex. The zoning and the compositional variation within the chromite from the layer in the Potgietersrus area is more spectacular than that described by Beeson and Jackson (1969) and thus makes it rather unique. Their samples came from a thin chromitite layer sandwiched between serpentinite in the West Fork and Chrome Mountain areas of the Stillwater Complex. It would therefore seem as if serpentinization in both areas is responsible for the alteration of the chromite.

5.2.5.6 Comparison of Chromite Compositions

The composition of the chromite is strongly influenced by the mineralogical composition of the host rock and a clear distinction

seems to prevail between harzburgite and pyroxenite hosted chromites (Fig. 51B and C). The distinction between the two types is particularly evident for the Moorddrift and Drummondlea subzones, and not quite as evident for the Volspruit subzone (Fig. 51E). The difference may be related to the fact that the harzburgites of the Volspruit subzone are opx-ol-chr cumulates whereas those in the other two subzones are predominantly ol-chr cumulates. Chromite in pyroxenites can be distinguished from chromite in harzburgites by its higher Cr/Al ratio. In the chromite-rich successions, chromite from ol-chr and chr-ol cumulates (dunitic rocks) have a lower Cr/Al ratio than chromite from the chromitite layers (Fig. 51D). The sample designated Z in Figure 51D is a massive chromitite from a surface pit near the farm boundary between Volspuit and Zoetveld. The sample GV-1 is chromite from the opx-ol-chr cumulate in the hanging-wall of the lower chromitite.

Although available data for the critical zone are limited, it does indicate that the chromite from the gabbronorite of the layered member is much richer in Fe^{3+} than chromite from the UG2-like chromitite. Chromite coexisting with magnetite in the sample from the M.Mb./P.G. has an even higher Fe^{3+} content (Fig. 51F).

A binary plot of Cr/(Cr+Al) against Mg/(Mg+Fe^{2+}) also differentiates chromite from different rock types (Fig. 52). The range in the Mg* for both pyroxenite and harzburgite is about the same but their Cr/(Cr+Al) ratios are significantly different, with much higher values being found in the pyroxenites than in the harzburgite. Chromite in the chromitic gabbronorites are distinct in that they have the lowest Mg* yet have a relatively high Cr/(Cr+Al) ratio. A distinction can also be made between the disseminated chromite from the ol-chr and chr-ol cumulates associated with the upper and lower chromitite layers and chromite from other ol-chr and opx-ol-chr cumulate horizons. Even though both are fairly olivine-rich environments the chromite in the former has a much higher Mg* and Cr/(Cr+Al) ratio. Chromites from the upper and lower chromitite layers have considerably higher Mg* and Cr/(Cr+Al) values.

Indications are, therefore, that the Cr/(Cr+Al) ratio in chromite is a function of the type of coexisting cumulus phase. If the chromite crystallizes in the presence of orthopyroxene, which can accommodate comparatively more Al in its lattice than olivine, the

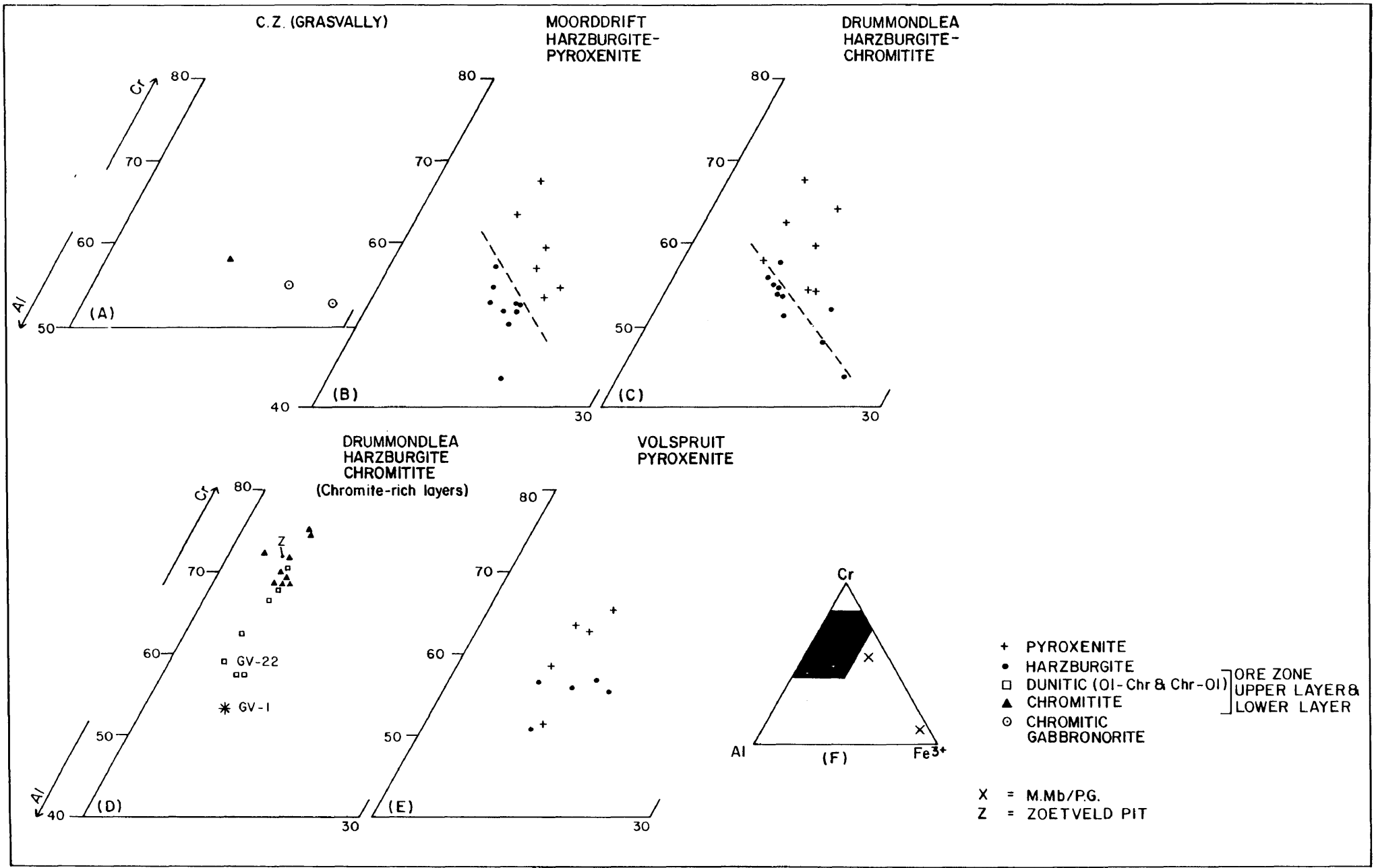

Fig. 51 Cr-Al-Fe^{3+} plot of chromite from different subzones and in different lithologies of the lower and critical zones south of Potgietersrus.

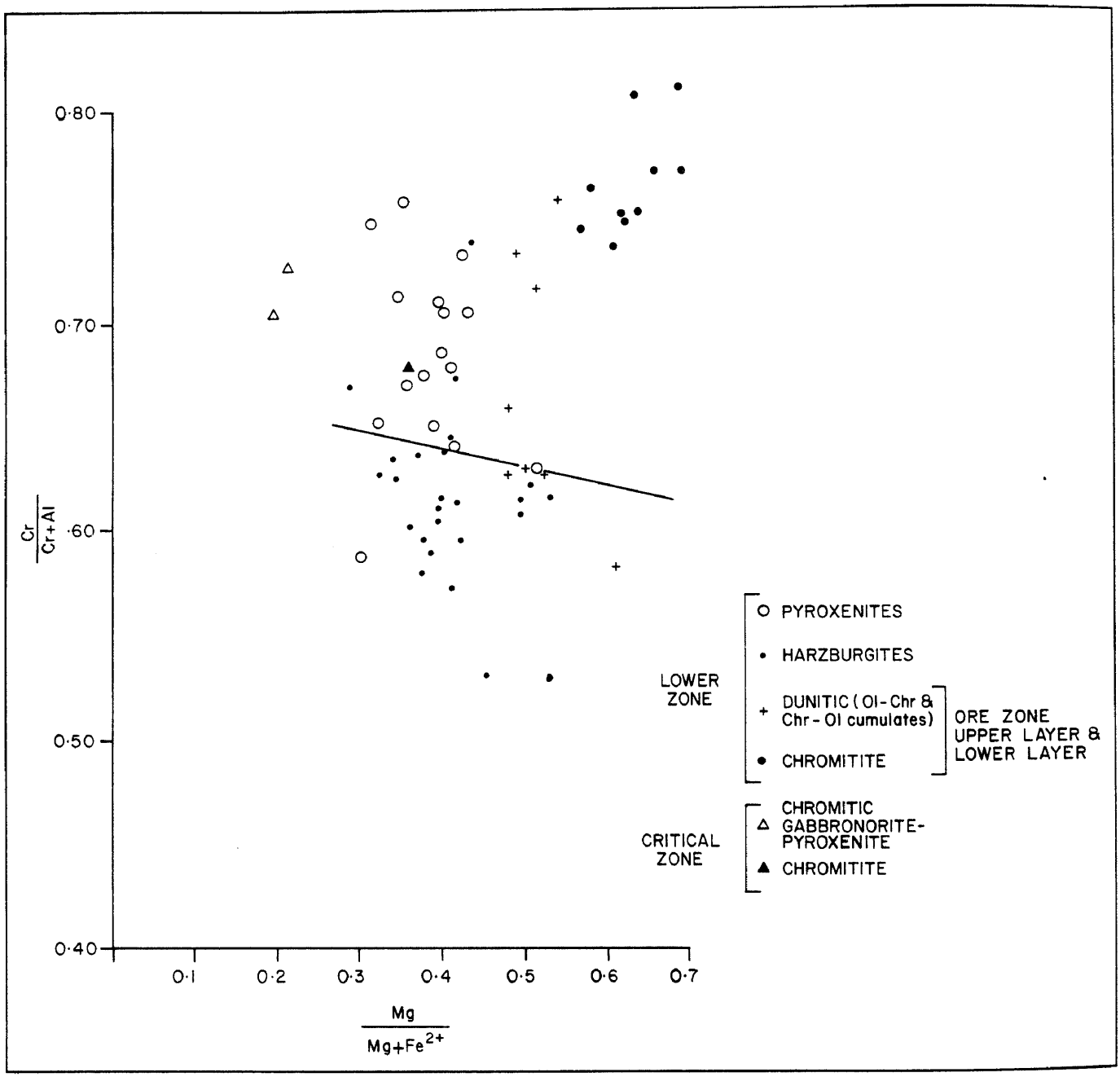

Fig. 52 Cr/(Cr+Al) vs $Mg/(Mg+Fe^{2+})$ plot of chromite compositions from different lithologies in the lower and critical zone.

coexisting chromite will have a higher Cr/(Cr+Al) ratio than chromite crystallizing together with olivine. The higher Mg* of chromite in the reaction orthopyroxene may be due to the chromite reacting (equilibrating) with a magnesium-rich environment, which in this case would be the local peritectic environment where olivine was consumed by the intercumulus liquid to produce orthopyroxene. Kotze (1968) has shown that the MgO-content of chromite, in chrome-magnesite refactories, increases considerably where it is in contact with magnesite. The chemistry of the reactive environment seems, therefore, to have a considerable influence on the resulting composition of the chromite. Similarly the high Mg* of the massive chromitite layer could be due to sintering of chromitite in the presence of Mg-rich interstitial liquid.

With the exception of the analyses in Table 3 and 4, the composition of all chrome spinels have been plotted in the spinel prism (Fig. 53). Samples from the lower chromitite (G66,6 level) plot near the base of the prism and are rich in the $MgCr_2O_4$ component, whereas the disseminated chromite from the other subzones, as well as the Drummondlea Harzburgite-Chromitite, display a trend of decreasing $MgCr_2O_4$ component with a concomitant increase in Fe_3O_4 (Fe_2TiO_4). The upward sweep of the trend towards Fe_3O_4(Fe_2TiO_4) does not necessarily indicate increasing fo_2 conditions during crystallization of these samples. As has been shown previously, a decrease in temperature during fractional crystallization at fixed fo_2 will enrich the residual magma in Fe_2O_3 relative to FeO and in TiO_2 (Hill and Roeder, 1974; Eales and Reynolds, 1981; El Goresy et al., 1976; Cameron, 1977).

The high Fe_3O_4(Fe_2TiO_4) spinel (78-360-1) from the M.Mb./P.G. projects approximately midway up the Fe_3O_4-$FeCr_2O_4$-$FeAl_2O_4$ face and has the lowest Cr_2O_3 content (19,43 per cent) of all the primary Cr-spinels. Low chrome high Fe and Ti spinels also occur as chromite from the layered member of the critical zone. The spinel with the highest Fe_3O_4 and lowest Cr_2O_3 content (78-360-2) in Figure 53 is a magnetite which occurs in the same sample as the chromite with 29,43 per cent Cr_2O_3. The presence of chromite in this rock is very unusual. It does not appear to be a foreign inclusion and would seem to be a reaction type that is frequently found in contaminated rocks of the Bushveld Complex (Lee and Sharpe, research in progress). This sample as well as others

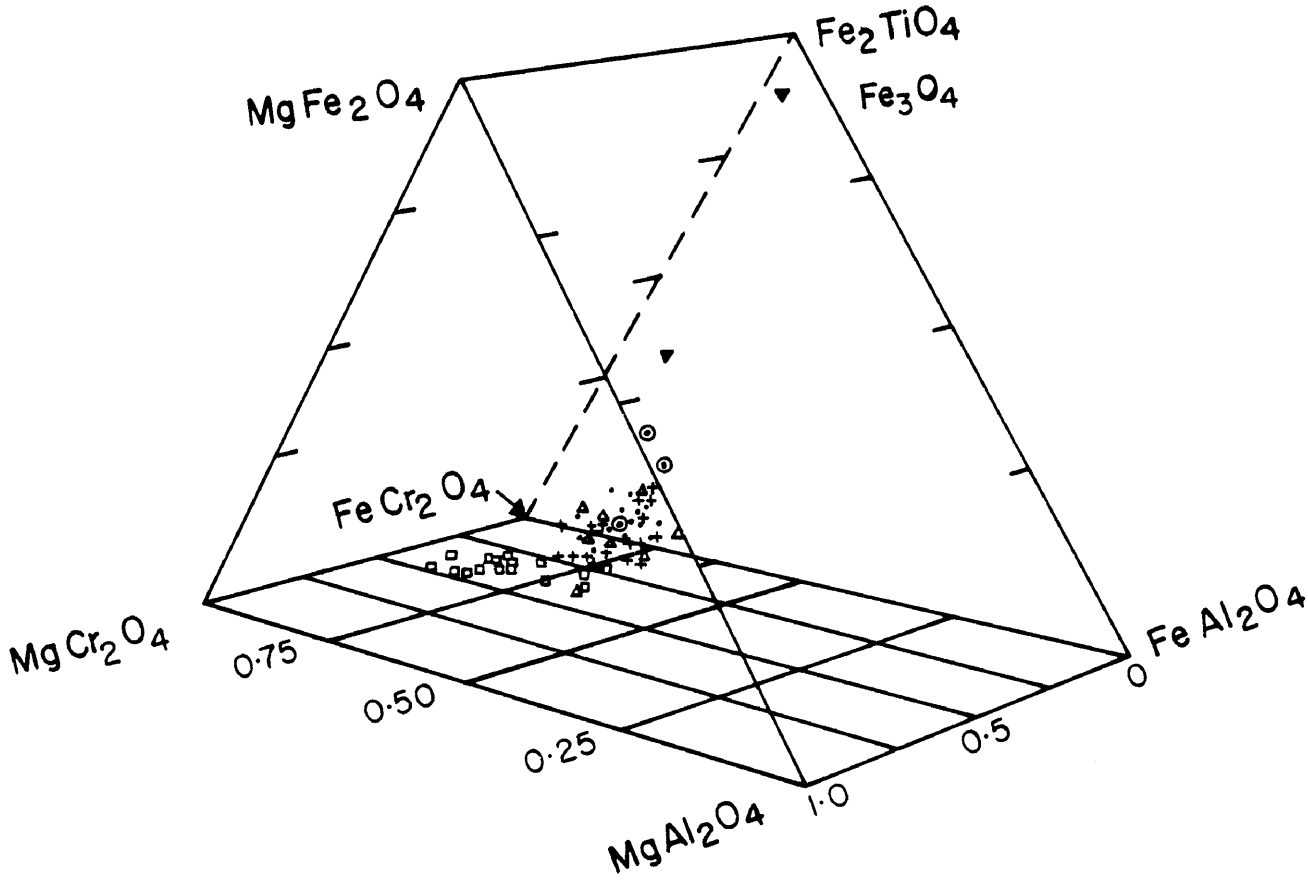

- MOORDDRIFT HARZBURGITE-PYROXENITE
+ DRUMMONDLEA HARZBURGITE-CHROMITITE
△ VOLSPRUIT PYROXENITE
□ G66,6 LEVEL CHROME MINE
▼ CRITICAL ZONE CHILL
⊙ CRITICAL ZONE LAYERED MEMBER

Fig. 53 The spinel compositional prism illustrating chemical variations encountered in spinels from the lower and critical zone.

suggest that the solubility of Cr in spinel is over a considerable compositional range.

Analytical data of the composition of the chromite in the critical zone of the eastern Bushveld (Cameron, 1977) shows the Mgx100/(Mg+Fe^{2+}) values of chromite to be between 14 to 54 in chromite from the chromitites confined to more magnesium-rich intervals than the disseminated chromite in silicate-rich rocks (Fig. 54A). The higher Mg values of the chromites in and near the chromitites are considered to indicate higher fo_2 and temperature conditions during their formation (Arculus, 1974; Ulmer, 1969; Muan and Osborne, 1956). The Crx100/(Cr+Al) values are more difficult to interpret due to the diverse nature of the coexisting silicates. Nevertheless, Cameron has shown that with increasing height, and thus fractionation, the Al* and the Fe^{3+*} of the chromite within the chromitites increase whereas the Cr* decreases. A similar, yet somewhat more diffuse trend is seen for the chromite in silicate-rich rocks. From this one could deduce that the chromite in the chromitites with the high Crx100/(Cr+Al) ratios formed early, in an environment where mafic silicates were the coexisting cumulus phases, whereas samples with lower ratios formed from more fractionated magma enriched in Al. Irvine (1977) has shown experimentally that with differentiation and falling temperatures the Cr/(Cr+Al) in the chromite decreases rapidly as the plagioclase liquidus is approached, because the composition of the melt is moving towards the liquidus volume of $MgAl_2O_4$. Upon crystallization of plagioclase, the composition of the melt turns away from this volume, with the result that the Cr/(Cr+Al) in chromite can rise again due to incorporation of Al in plagioclase (see Fig. 56). The extremely high Crx100/(Cr+Al) ratios for disseminated chromites in the eastern Bushveld (Fig. 54A) are the result that plagioclase crystallized together with chromite which depleted the melt in Al. Analyses of chromite from UG1, UG2, and UG3 chromitite layers on the farm Maandagshoek (Gain, 1982) shows that the chromite from the UG1 (Fig. 54C) chromitite has a slightly higher Crx100/(Cr+Al) ratio than the other two layers. This confirms the suggestion that Al depletion in the melt due to coprecipitation of plagioclase, as the UG1 chromitite layer occurs in an anorthositic enviornment compared to the UG2 and UG3A layers which are associated with harzburgite and pyroxenite.

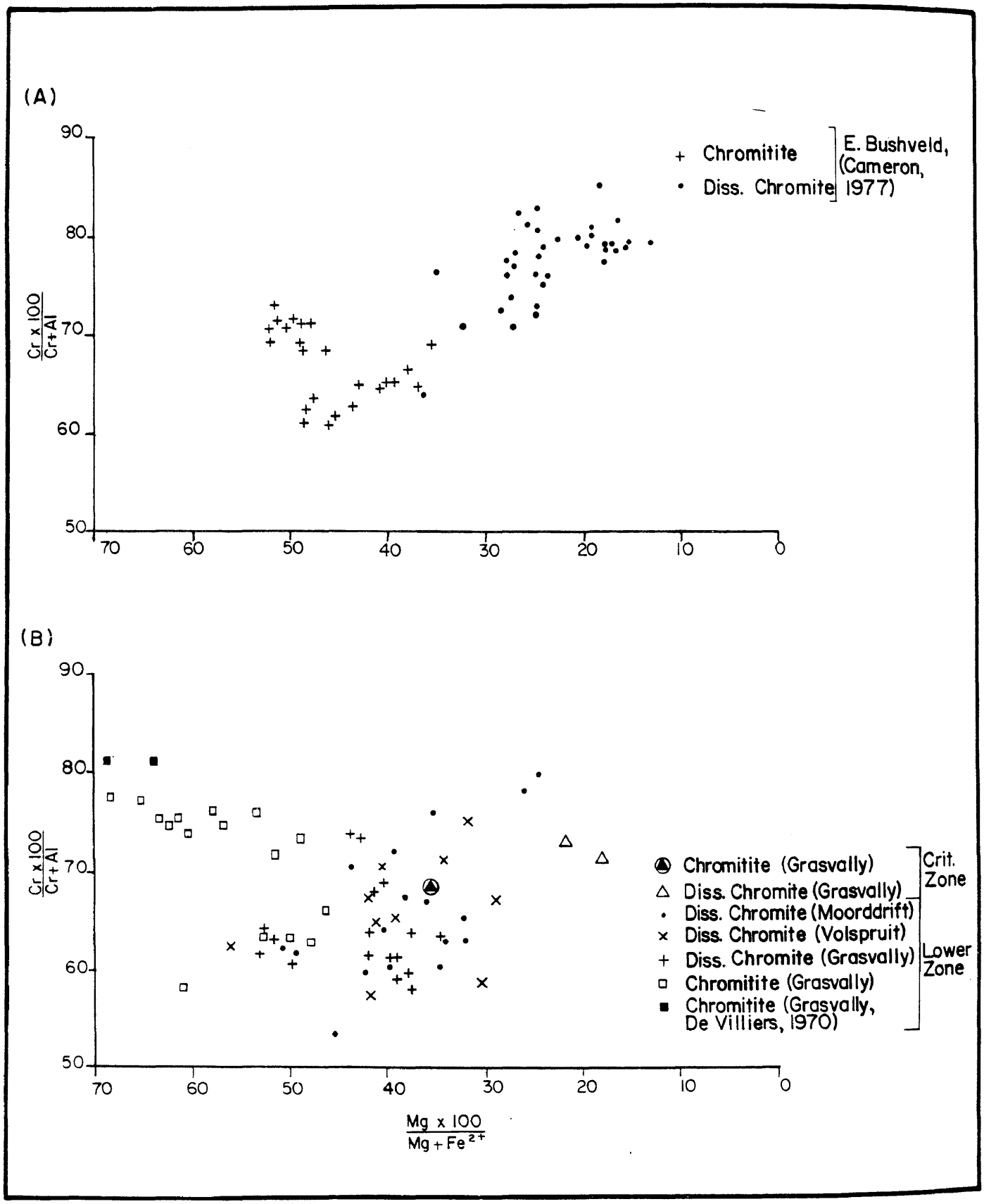

Fig. 54 Mg x 100/(Mg+Fe^{2+}) vs Cr x 100/(Cr+Al) plot of chromite from major stratiform intrusions: (A) eastern portion of Bushveld Complex (Cameron, 1977); (B) southern portion of the Potgietersrus limb; (C) Muskox, Duke Island, Union Bay and Tulameen Intrusion (Irvine, 1967), including data from the Merensky Reef (Brynard et al., 1976; Vermaak and Hendriks, 1976) as well as the UG1, UG2, and UG3 chromitite layers (Gain, 1982); and (D) the Great Dyke (Worst, 1960).

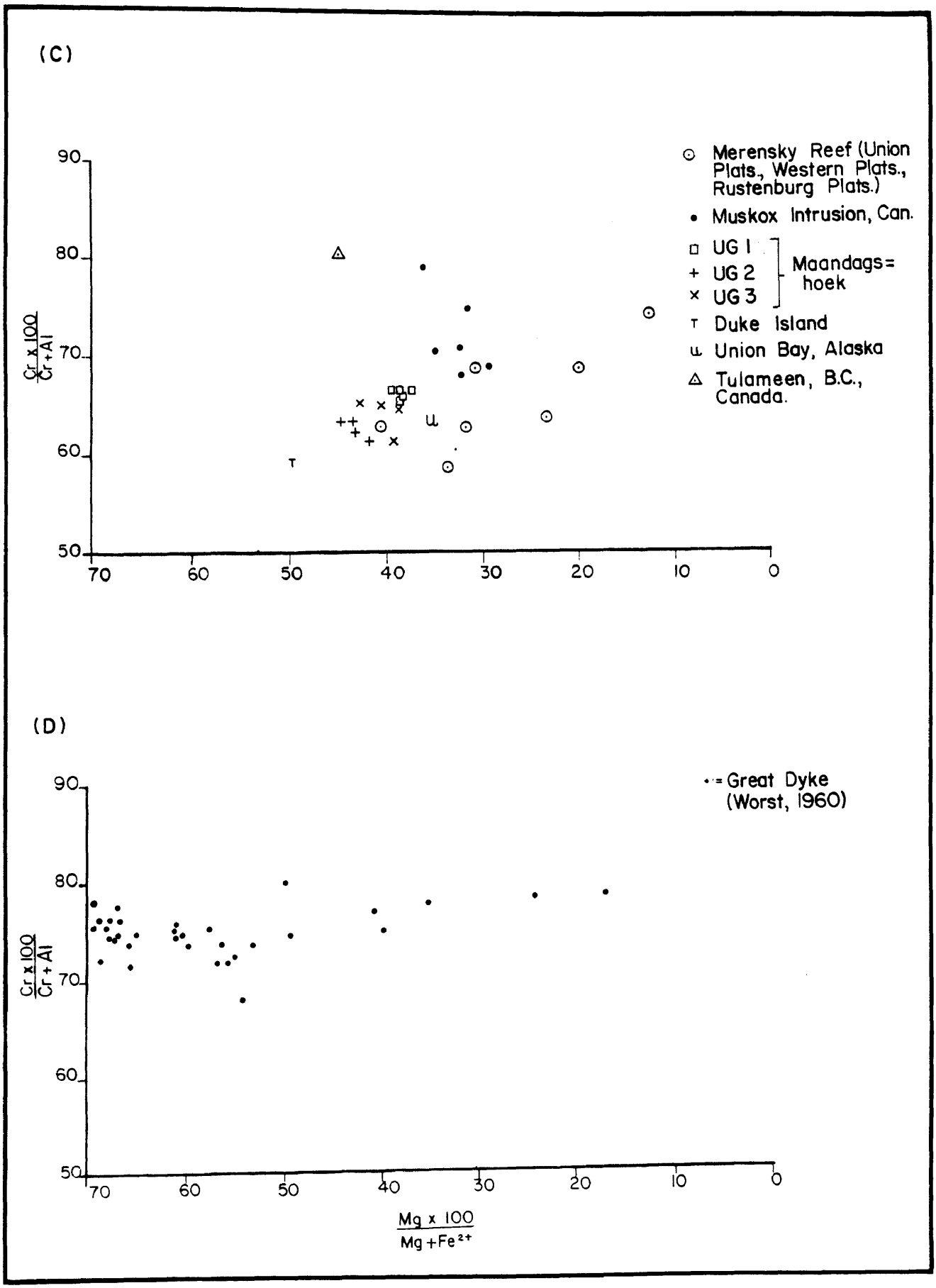

Fig. 54 (Continued)

Comparison of the composition of chromite from the Potgietersrus limb (Fig. 54B) with that of other areas of the Bushveld Complex (Fig. 54A and C) shows the Potgietersrus chromites to have a much larger range in $Mgx100/(Mg+Fe^{2+})$ values. Chromites from silicate rich environments display a large spread in the $Crx100/(Cr+Al)$ ratio which may be due to the type of coexisting cumulus phases. Note that the chromite from the Grasvally chromitite layers plot at the magnesium-rich end of the diagram and that their composition is very similar to chromite of the Great Dyke (Fig. 54D). Apart from the Great Dyke, no other layered intrusion contains chromite with such high $Mgx100/(Mg+Fe^{2+})$ values. Although the Muskox chromitite also occurs in an olivine-rich environment, its chromite has $Mgx100/(Mg+Fe^{2+})$ values ranging between 29 to 36 (Irvine, 1967A). The chromite from the G and H chromitite of the Stillwater Complex has higher $Mgx100/(Mg+Fe^{2+})$ values, average of about 47 with a maximum of 59 (Jackson, 1969).

The reason for the extreme Cr_2O_3 and MgO enrichment of the Great Dyke and Grasvally chromitites is not yet fully understood. It was mentioned earlier that the Mg* and the Cr_2O_3 content of chromite may increase if it crystallized under higher fo_2 conditions, but it is doubtful whether an increase in fo_2 alone can account for the observed high values. It is therefore considered, as mentioned perviously, that the Cr_2O_3 and Mg* of the chromite in these layers could have increased during sintering of the crystal mush, especially since the chromitite layers from both these intrusions are chracterized by the abundance of hard lumpy ore. One of the most important controls on the Mg* of the chromite could have been the composition of the coexisting cumulus silicate phase, as well as that of the intercumulus liquid present during the sintering process. In this regard Zubakov and Yusupova (1964) made the interesting observation that chromite in chrome-magnesite refractory bricks was enriched by up to 50 per cent in MgO as a result of reaction with periclase. Kotze (1968) observed a similar enrichment in the MgO content of chromite during heating of chrome-magnesite refractory bricks. He could show that the Al_2O_3 content of chromite in direct contact with the magnesite remained constant, but that the FeO and Fe_2O_3 content decreased with a concomitant increase in the MgO content from 9,44 to 19,80 per cent. Simultaneously the Cr_2O_3 content increased from 45,60 to 48,89 per cent.

A MgO-rich liquid overlying the cumulus chromite pile could result from the enhanced precipitation of chromite from a melt that previously crystallized olivine and chromite. The crystallization of abundant chromite only to produce the chromitite layer would leave the overlying liquid enriched in the olivine components and thus MgO. If bottom crystallization was the process by which the chromitite layers formed, then one would expect both the interstitial liquid and the directly overlying magma to be enriched in MgO. The interstitial liquid of the chromitite layer would, therefore not be in equilibrium with the intercumulus liquid of the immediately underlying olivine cumulate. In order to attain equilibrium between the two intercumulus liquids, diffusion would set in resulting in a Mg enrichment of the intercumulus liquid of the olivine cumulate. The olivine of this cumulate would, in turn, have to re-equilibrate, resulting in the observed abnormally high Mg* of 0,91 in this layer. Any Mg loss from the intercumulus liquid of the chromitite-layer to the underlying intercumulus liquid of the olivine cumulate would be replenished by diffusion of Mg from the Mg-rich liquid directly overlying the chromitite layer along a concentration gradient. A relatively high Mg content could therefore, have been maintained in the intercumulus liquid of the chromitite cumulate, so that subsequent sintering could have taken place in the presence of a Mg-rich reactant. A small temperature gradient, if present, would also have enhanced this diffusion process.

Calculations of thermal gradients in crystallizing magmas led Hess (1972) to conclude that diffusion between intercumulus liquid and magma is not a feasible process to give rise to adcumulates. Freer (1981) presented new data on the factors controlling diffusion, from which it becomes evident that diffusion is much more rapid than previously thought. By using a diffusion coefficient Do of $1{,}74 \times 10^{-6} m^2 s^{-1}$; a temperature of 1474°K, an activation energy Q of 242,9 KJ $mol.^{-1}$ and a fo_2 of $1og_{10}^{-12}$ atm, in conjunction with the conventions of Freer (1981), it was calculated that it would take 29,55 years for Mg and Fe to diffuse 2 mm in a solid state environment like that of olivine, on which the diffusion data is based. If it is assumed that diffusion of Mg and Fe in the melt was at a faster rate to that in pure olivine, it would require a maximum of 14775 years to convert an olivine chromite cumulate to an

(continued overleaf)

olivine adcumulate. This is far too long a period of time, considering that chromite with a radius of 0,05 cm and a density of 4,5 g.cm.$^{-1}$ would settle approximately 45 m per year in a basic magma. However, Buening and Buseck (1973) showed that the diffusion coefficient for Mg and Fe in olivine (parallel to the c-axis) increases by a factor of approximately 2,5 if the fo_2 changes from 10^{-14} to 10^{-12} atm at 1000° C. Calculations have shown that the lower chromitite layer crystallized at an fo_2 of approximately 10^{-5} atm at 1243°C. Therefore, if Buening and Buseck's (1973) observation that the diffusion increases linearly with increasing fo_2 is correct, then 1 m of olivine adcumulate could have formed in 4925 years. Likewise, an increase in temperature of 73° C over that calculated would increase the diffusion rate by a factor of 3,2; i.e. a time of 1539 years, provided that a Mg and Fe source is within a metre or so from the adcumulates forming by this process. The above calculations are based on diffusion in the solid state and diffusion of Mg and Fe in a melt would be considerably faster. The above values, therefore, provide an upper limit on the time required for the diffusion process.

The process of adcumulus growth would be even more likely if a break in the sedimentation occurred following crystallization of the lower chromitite, for this would possibly provide sufficient time for the Mg and Fe to diffuse through the unconsolidated chromite layer.

Evidence that an overlying Mg-rich liquid did exist can be seen in Figure 44D where it is shown that veins of olivine are connected to cumulus olivine in this olivine-chromite cumulate. The sample (Fig. 44D) is taken from diamond drill core and sectioning revealed that the veins are oriented normal to the plane of the layering. This evidence strongly suggests that these so-called veins actually represent a postcumulus "plumbing" system which was in "communication" with the overlying Mg-rich liquid. It is also interesting to note that the cumulus olivine in this layer has a Mg* of 0,939 whereas the olivine in the veins or channels has a value of 0,946 which further suggests a more Mg-rich overlying liquid was permeating through this portion of the chromitite layer.

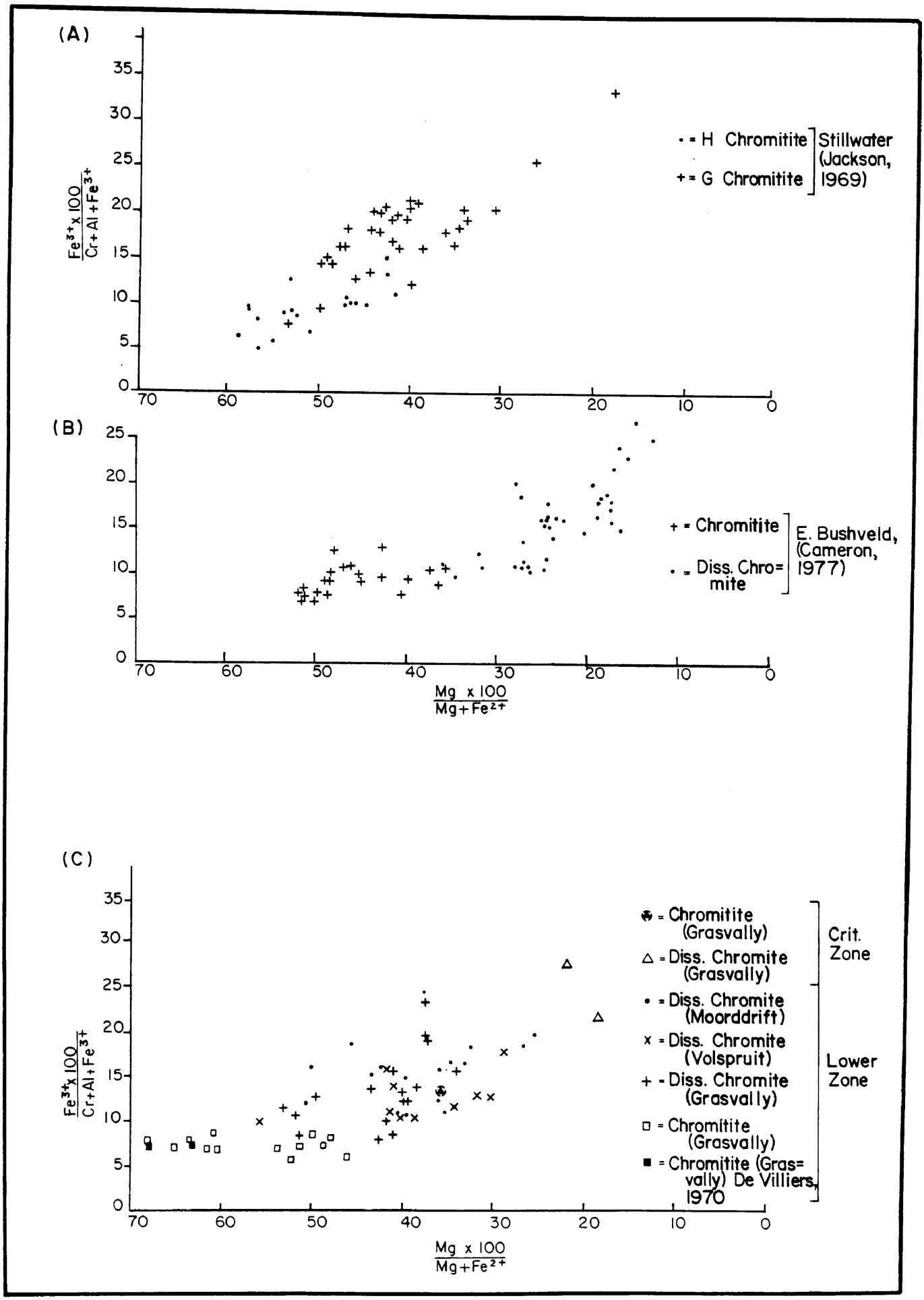

Fig. 55 $Mg \times 100/(Mg + Fe^{2+})$ vs $Fe^{3+} \times 100/(Cr+Al+Fe^{3+})$ plot of chromite from major stratiform intrustions: (A) Stillwater Complex (Jackson, 1969); (B) eastern portion of the Bushveld Complex (Cameron, 1977); (C) southern portion of the Potgietersrus limb;

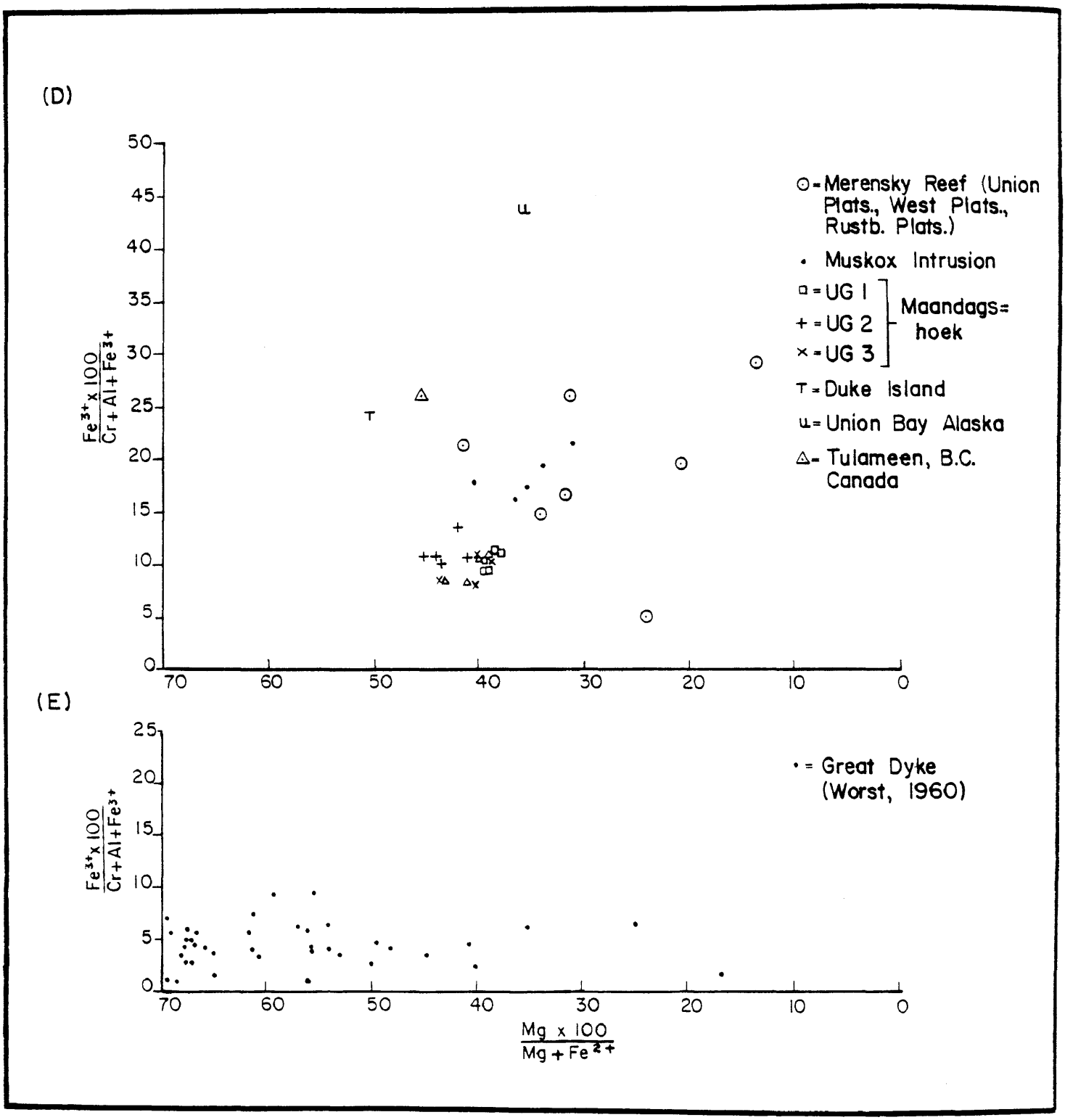

Fig. 55 cont'd
(D) Muskox, Duke Island, Union Bay, and Tulameen Intrusions (Irvine, 1967) including data from the Merensky Reef (Brynard et al., 1976; Vermaak and Hendriks, 1976) as well as the UG1, UG2, and UG3 chromitite layers (Gain, 1982); and (E) the Great Dyke (Worst, 1960).

Any trends shown in Figure 55A, B, C, D, and E can probably be related directly to the degree of fractionation of the magma from which the chromite crystallized. The slope of the trends in Figure 55 could indicate the relative rate at which the magmas were fractionating. The steeper trends from the G and H chromitite from the Stillwater Complex would, for instance, imply a rapid fractionation of the magma. All the information at hand, including calculated oxygen fugacity values for various horizons, suggests that the $Fe^{3+}/(Cr+Al+Fe^{3+})$ is not a reliable measure of the fo_2 of the system, but is rather an indicator of the degree of fractionation of the magma.

5.2.6 Chromite Crystallization

5.2.6.1 The Liquidus Path

The crystallization of chromite from basaltic and picritic melts has long puzzled researches because of the various inconsistencies reported from melting experiments and from field observations on apparently similar rock types. It was not until Irvine's (1977) experimental work in the join Mg_2SiO_4-$CaMgSi_2O_6$-$CaAl_2Si_2O_8$-$MgCr_2O_4$-SiO_2 that many of the problems concerning chromite crystallization were removed from the rather conflicting existing information. His experiments were designed to show the position of the olivine-chromite cotectic in the Fo-Di-An-Qtz system, the liquidus relations of which closely resemble those of subalkaline basic and ultrabasic magmas.

In Figure 56A and B, crystallization path 1 is similar to that of abyssal tholeiites, path 2 corresponds to the Kilauean trend, as it intersects the plagioclase liquidus at the olivine-clinopyroxene-plagioclase cotectic, path 3 is similar to the early trend of the Muskox magma, whereas path 4 approximates that of the Great Dyke, Sillwater and Bushveld trends. Irvine (1977) could demonstrate from this work that the amount of Cr_2O_3 necessary to saturate the melt with chromite at any given temperature increases from path 1 to 6. This required increase in Cr_2O_3 corresponds to a decrease in the Al_2O_3 content of the respective melts. He could, therefore, show that the chrome content required to saturate a melt with chromite is dependent on the type of liquid and its degree of fractionation. An abyssal tholeiite, for instance, is saturated with Cr_2O_3 at much lower levels of chromium than a magma like

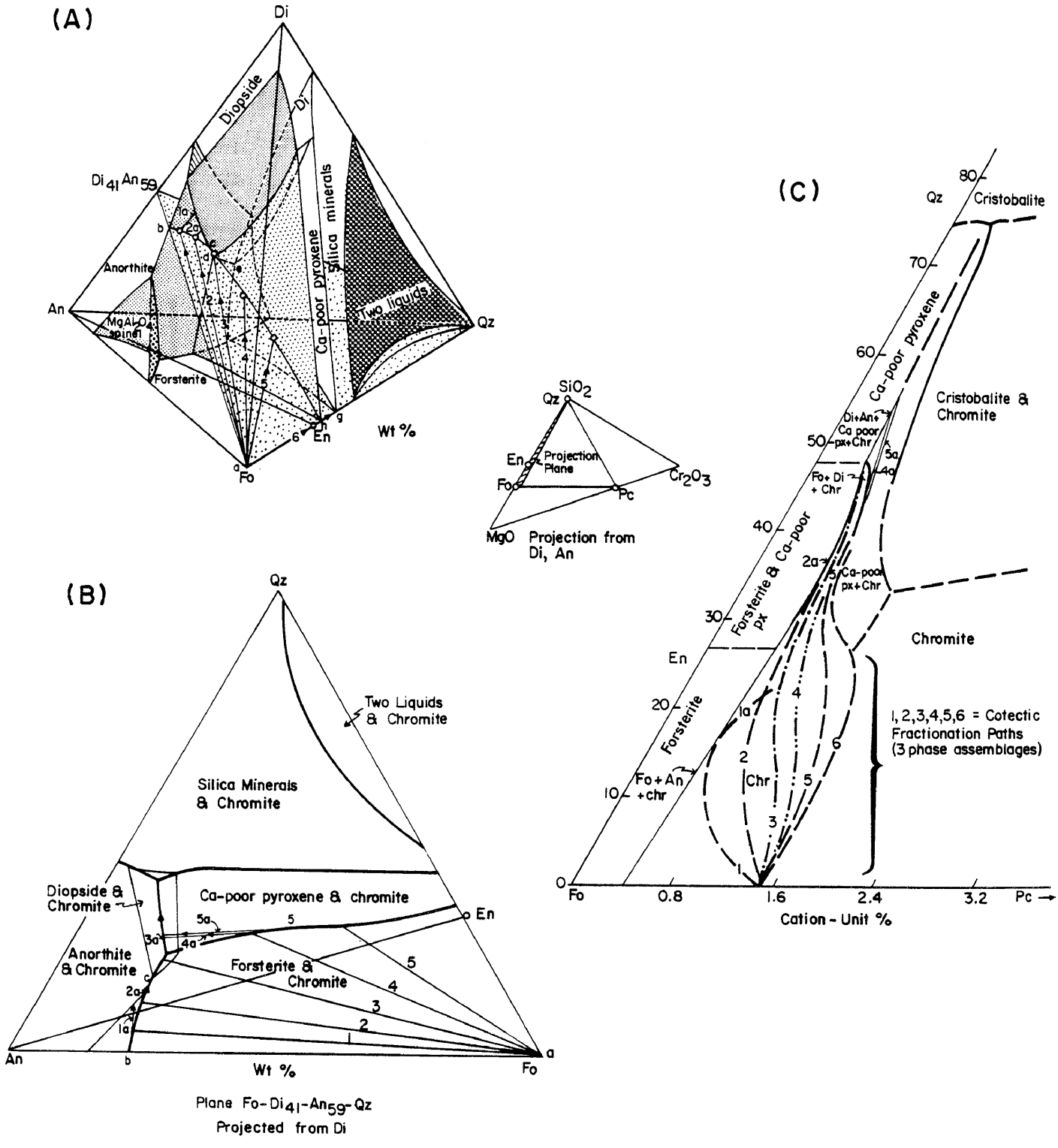

Fig. 56 Liquidus phase relations in the system Fo-Di-An-Qz and relevant subsystems after Irvine, 1977.
(A) crystallization paths of melts 1-6 in the system Fo-Di-An-Qz;
(B) silicate phase relations projected on the Fo-An-Qz plane from Di and Pc;
(C) melt compositions 1-6 projected from Di and An onto the plane Fo-Pc-Qz, showing the variation of the olivine-chromite cotectic with chromium content and their configuration.

that which gave rise to the chromite bearing horizons in the Great Dyke or the Bushveld Complex. Many of the normal abyssal tholeiites have Al_2O_3 contents of 14,5 to 15,5 per cent (Carmichael, et al., 1974) whereas others typically contain about 16,5 per cent Al_2O_3 (Fisk and Bence, 1980). This contrasts significantly with calculated Al_2O_3 content of the magma that produced the ol-chr cumulates in the Drummondlea Harzburgite-Chromitite. By employing a $D_{Al}^{spinel-liq}$ of 1,8 (Fisk and Bence, 1980), at a fo_2 of 10^{-5} to $10^{-5,5}$ atm, it was calculated that the liquid had an average Al_2O_3 content of 9,01 per cent, based on chromite with 16,23 and 17,81 per cent Al_2O_3 respectively.

Irvine's (1977) experimental results also showed that the ol-chr cotectic is curved, and that the nature of the curvature depends on the Cr_2O_3 content of the melt. A projection of the experimental data onto the plane Fo-Pc-Qtz from Di and An (Fig. 56C) shows the change in the olivine-chromite cotectic for different types of liquids. The positions of the curves are determined by the amount of chromium necessary to saturate the respective liquid. If a tangent is drawn from the liquid on the cotectic to the Fo-Pc join it is apparent that when crystallization paths are convex, the amount of Pc that crystallizes together with olivine gradually increases with fractionation, and decreases during crystallization along the concave part of the cotectic.

It was previously pointed out that the magma that gave rise to cyclic unit 23 and possibly 24 (Fig. 36) is believed to have been more Cr_2O_3-rich and more primitive than the magma from which unit 22 crystallized, i.e. 0,094 and 0,058 per cent Cr_2O_3 respectively. Assuming crystallization along path 4 (Fig. 56C) the magma that gave rise to cyclic unit 23 and 24 should crystallize successively more Pc with fractionation due to the configuration of the cotectic. It can be seen from Fig 36 that, with the exception of one point, there is an upward increasing trend, although only slight, in the amount of modal chromite through cyclic unit 23 and 24, suggesting that the cotectic followed by the liquid during the course of crystallization towards the lower chromitite layer was in fact slightly convex.

Irvine also found that chromites crystallizing along paths 1 to 6

have successively lower Al_2O_3 contents and greater Cr/Al ratios. Those that crystallized between paths 3 and 4 have high Cr/Al ratios similar to those from the Great Dyke and the upper and lower chromitite layers in this study. Also, with falling temperature along path 1, the Cr/(Cr+Al) ratio in the chromite decreases as the plagioclase liquidus volume is approached (Fig. 56A and B), because the melt is moving towards the $MgAl_2O_4$ spinel liquidus volume. However, upon crystallization of plagioclase the melt turns away from the spinel volume along path 1A and the successive chromites have higher Cr/(Cr+Al) values. This experimental work therefore suggest that the larger proportions of Cr_2O_3 in parental magmas of the Great Dyke, Bushveld and Stillwater intrusions may be the underlying factor for the abundance of chromite mineralization.

5.2.6.2 Controls on Chromitite Formation

A detailed study of compositional variation of the chromite in the foot-wall of the 1" chromitite (Fig. 57, Appendix 7) was undertaken in an effort to obtain information on the changes of the conditions in the crystallizing magma that resulted in the precipitation of the chromitite layers. As the chromite distribution in the immediate foot-wall of the lower and upper chromitite layer is similar to that of the 1" stringer, the controls that governed the crystallization of this layer can probably be extrapolated to other layers which have undergone considerable postcumulus modification. The foot-wall consists of olivine-chromite cumulates in the approximate proportion ol(96):chr(4) which passes into a massive chromitite layer with ol(30):chr(70).

The disseminated foot-wall is only very weakly mineral graded and the proportion of modal chromite does not increase by more than 2 per cent from the -17 mm to -6 mm level. The upper 5 mm of the section constitutes the lower fifth of the 1" stringer which is a massive chromitite layer.

The systematic upward increase in the Cr/(Cr+Al) ratio is believed to represent an increase in the crystallization temperature from the disseminated foot-wall to the chromitite, because both Irvine (1977) and Jaques and Green (1980) showed that a drop in Cr/(Cr+Al) ratio usually reflects a drop in temperature within

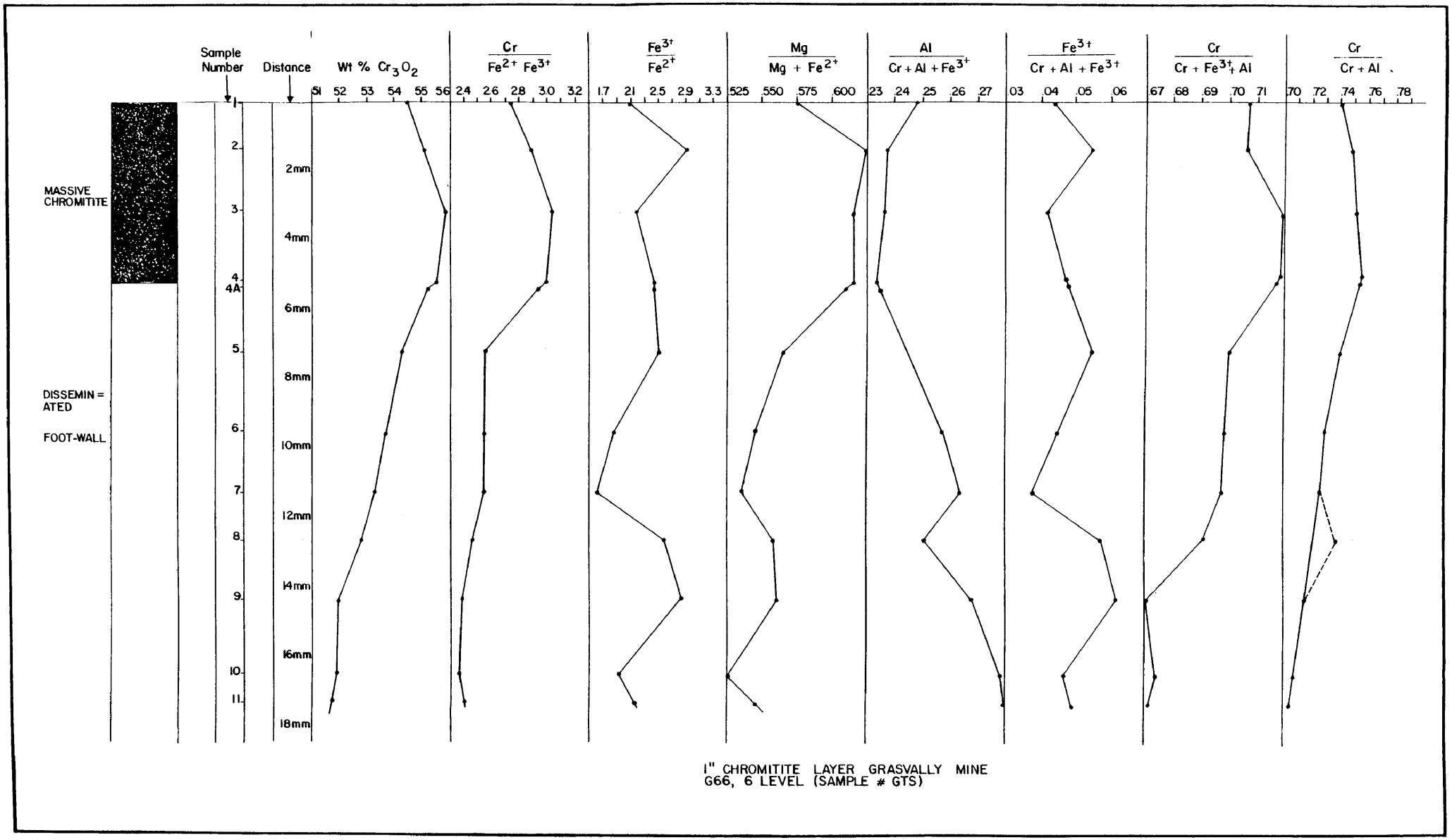

Fig. 57 Compositional variation of chromite across an 18 mm vertical section through the foot-wall contact of the 1" chromitite stringer in the Drummondlea Harzburgite-Chromitite.

the system. Jaques and Green (1980) showed in anhydrous melting experiments on systems equivalent in composition to Hawaiian pyrolite that the Cr/(Cr+Al) ratio drops 0,01 units per 3,33° C at a pressure of 5kb in the temperature interval from 1300 to 1200° C. In terms of their experiment, the increase in the Cr/(Cr+Al) from 0,695 to 0,753 from the -17 mm to -5 mm level (Fig. 57) would be equivalent to an increase of 19° C. This small increase in temperature may have been sufficient to move the composition of the melt from the ol-chr stability field to the spinel (chromite) field (Hill and Roeder, 1974; Fisk and Bence, 1980).

Jaques and Green (1980) also demonstrated that a decrease in the Cr/(Cr+Al) is accompanied by a decrease in the Mg* of coexisting olivine and pyroxene. Akella et al. (1976) also noted from their melting experiments that the Cr/(Cr+Al) and the $Mg/(Mg+Fe^{2+})$ ratio of the spinel decrease sympathetically with a lowering of the temperature of crystallization. Therefore, increasing temperature and fo_2 of the melt should result in a increase of both the Cr/(Cr+Al) and $Mg/(Mg+Fe^{2+})$ ratio of the crystallizing spinels.

Hill and Roeder (1974) found that at a fixed fo_2 of 10^{-7} atm the Cr_2O_3 content and the Cr/Fe ratio of crystallizing chromite drop with a decrease in temperature which would suggest that Cameron's (1977) recorded trend of decreasing Cr/Fe, Cr_2O_3 content, and Mg* of chromite with increasing stratigraphic height in the eastern Bushveld is primarily controlled by a drop in temperature and probably also fo_2, because Hill and Roeder demonstrated that the $\log_{10} fo_2$ falls by about 1,5 units for each 100° C drop in temperature at a constant oxygen content. The increase in the Cr/Fe ratio and the Cr_2O_3 content of the chromite at the lower contact of the 1" stringer would thus also suggest an increase in the temperature at a fixed fo_2, but more likely also an increase in the fo_2 in the magma towards the massive chromitite part of the 1" stringer. Such an increase in the fo_2 of the magma would have the additional affect of oxidizing Cr^{2+} to Cr^{3+} which would be incorporated by the spinel.

In an isothermal intrinsic oxygen fugacity study of the LG4 chromitite layer at the Zwartkop Chrome Mine Snethlage and Von Gruenewaldt (1977) showed the Cr_2O_3, MgO, Mg* to increase,

whereas the Al_2O_3 and total Fe of the chromite decrease with increasing fo_2. Such findings also suggest an increase of the fo_2 in the magma as the 1" stringer is approached.

Although the Mg* of the spinel is usually found to decrease with decreasing temperature of crystallization (Fisk and Bence, 1980; Hill and Roeder, 1974) an increase could therefore imply an increase in temperature. It was shown by Arculus et al. (1974); Muan and Osborn (1956) and Ulmer (1969) that an increase in fo_2 raises both the Mg* of the mafic silicates and the spinel. In conjunction with this increase in the Mg* of the spinel towards the chromitite, the Al* and the Al_2O_3 content decreases (Fig. 57, GTS analyses Appendix 7). Although Muan (1957) could show that an increase in fo_2 causes a decrease in the Al_2O_3 content of the spinel in the system $FeO-Fe_2O_3-Al_2O_3-SiO_2$, it must be kept in mind that an increase in temperature at a fixed fo_2 will also result in an increase of the Al_2O_3 content of the crystallizing spinel (Hill and Roeder, 1974).

By using the 1" stringer and its foot-wall as a model, it is envisaged that a liquid with a composition on the olivine-chromite cotectic fractionated to a level approximately 50 mm below the base of the 1" chromitite. At this level the chromite with a Cr_2O_3 content of about 42-45 per cent crystallized; a chrome content typical for olivine-rich rocks in the Drummondlea Harzburgite-Chromitite. At this stage a more Cr_2O_3-rich, primitive and probably also hotter, liquid was introduced into the system and blended with the residual, more fractionated liquid. As a result of blending of these two liquids the temperature in the crystallizing lower portion of the magma was gradually increasing, because larger volumes of new liquid were mixing with successively smaller portions of the residual liquid. Since most authors believe that the crystallization temperature of a magma normally parallels the buffer curves, an increase in temperature is believed to result in an increase in fo_2 of the crystallizing magma. The increased fo_2 need only be small, because Snethlage and Von Gruenewaldt (1977) have shown that an increase of as little as 0,5 to 1,0 log units is sufficient to enhance crystallization of chromite to form chromitite layers. The effect of increasing fo_2 at constant Cr concentration in the

liquid, would be to promote the precipitation of spinel since increasing the fo_2 results in an increase in Cr^{3+}/Cr^{2+} and Fe^{3+}/Fe^{2+}. If the Cr_2O_3 content of the new magma is considerably higher than that of the fractionated magma, it would have the same affect as "spiking" a basaltic magma with Cr_2O_3 which, in turn, lowers the required fo_2 necessary to precipitate chromite (Hill and Roeder, 1974). The increase in Cr_2O_3 and fo_2 may drive the crystallizing liquid from the ol-chr cotectic into the chromite volume so that only chromite crystallizes to give rise to a chromitite layer.

5.2.6.3 Olivine-Chromite Crystallization Temperatures

Irvine (1965) has shown that the relative distribution of ferrous iron and magnesium between olivine and spinel may be expected to vary significantly with temperature. The equilibrium distribution of Fe^{2+} and Mg between olivine and chromite can be expressed as follows:

$$1/2Fe_2SiO_4+Mg(Cr_\alpha Al_\beta Fe^{3}_{\gamma})_2O_4 \rightleftarrows 1/2Mg_2SiO_4+Fe(Cr_\alpha Al_\beta Fe^{3}_{\gamma})_2O_4$$

where α, β, and γ are the atomic fractions of the respective trivalent cations. Jackson (1969) used a thermodynamic appraoch similar to that of Irvine and formulated from the above equilibrium reaction the following equation to estimate the equilibrium temperature of coexisting olivine and chromite:

$$T = \frac{5580\alpha+1018\beta-1720\delta+2400}{0,90\alpha+2,56\beta-3,08\delta-1,47+1,987 \ln K_{D_{Mg-Fe^{2+}}}}$$

By using Jackson's formula and the olivine and chromite compositions given in Table 5, equilibrium temperatures, based on coexisting olivine-chromite pairs, were calculated from the lower zone samples. The temperatures were found to vary from 918° C to 1399° C (excluding the 1528° C value) with a mean value of 1111° C. A mean temperature of 1146° C was calculated for the Drummondlea Harzburgite-Chromitite subzone which is approximately mid-way between Jackson's calculation of the mean temperature for the H zone (1284° C) and the G zone (1036° C) of the Stillwater Complex. Jackson's equation was applied to other ultramafic bodies, i.e. the Red Mountain Complex of New Zealand where temperatures were found to range from 930 to 1140° C with a mean of 1060° C (Sinton, 1977) Medaris (1972) calculated temperatures between 1200 to 1400° C for high pressure peridotites from southwestern Oregon where the O'Hara (1967) grid gave temperatures of 1075 to 1175° C. These

Table 5 CATION RATIOS, DISTRIBUTION COEFFICIENT, AND TEMPERATURE CALCULATIONS* FOR OLIVINE-CHROMITE PAIRS FROM THE LOWER ZONE SOUTH OF POTGIETERSRUS

		CATION RATIOS									
Sample #	Modal % Chromite	$\frac{Mg}{Mg+Fe^{2+}}$ Olivine	$\frac{Fe^{2+}}{Fe^{2+}+Mg}$ Olivine	$\frac{Mg}{Mg+Fe^{2+}}$ Chromite	$\frac{Fe^{2+}}{Fe^{2+}+Mg}$ Chromite	$\frac{Cr}{Cr+Al+Fe^{3+}}$ Chromite	$\frac{Fe^{3+}}{Cr+Al+Fe^{3+}}$ Chromite	$\frac{Al}{Cr+Al+Fe^{3+}}$ Chromite	K_D $\frac{Ol-Chr}{Mg-Fe^{2+}}$	TEMP. °C (JACKSON) *	Suggested Temp.range°C (N.V.K.) **
3-2395	1,63	0,845	0,155	0,403	0,597	0,571	0,107	0,323	8,07	1 280	1204-23
3-2485	2,05	0.879	0,121	0,359	0,641	0,527	0,125	0,348	12,97	918	1225-56
3-2500	0,64	0,870	0,130	0,343	0,657	0,523	0,164	0,313	12,81	956	1221-47
3-3027	1,99	0,879	0,121	0,494	0,506	0,514	0,164	0,322	7,44	1 338	1224-57
3-3766	2,99	0,879	0,121	0,453	0,547	0,432	0,187	0,381	8,77	1 070	1231-56
3-3819	trace	0,872	0,128	0,378	0,622	0,543	0,195	0,262	11,20	1 108	1220-50
3-4002	1,13	0,879	0,121	0,396	0,604	0,516	0,148	0,337	11,08	1 011	1227-56
1-50	3,80	0,890	0,110	0,397	0,603	0,537	0,122	0,341	12,28	958	1233-67
UGC-1	52,75	0,939	0,060	0,616	0,384	0,699	0,071	0,230	9,58	1 322	1314 ?
1-80,5	1,85	0,873	0,127	0,417	0,583	0,553	0,099	0,348	9,61	1 107	1228-51
1-123	21,60	0,901	0,099	0,496	0,504	0,532	0,126	0,343	9,24	1 131	1234-78
GV-1	1,12	0,896	0,104	0,609	0,391	0,533	0,086	0,381	5,53	1 528?	1242-73
GV-22	6,16	0,912	0,088	0,523	0,477	0,591	0,058	0,351	9,45	1 130	1288 ?
1-179	5,69	0,895	0,105	0,529	0,471	0,545	0,115	0,340	7,58	1 296	1237-72
1-209	6,84	0,890	0,110	0,520	0,480	0,573	0,107	0,320	7,46	1 353	1233-67
1-219	2,00	0,862	0,138	0,375	0,625	0,444	0,233	0,323	10,41	1 029	1213-40
1-223	3,91	0,867	0,133	0,386	0,614	0,508	0,139	0,353	10,36	1 031	1224-45
1-240,9	3,10	0,850	0,150	0,377	0,623	0,478	0,197	0,325	9,36	1 121	1212-28
1-244	1,21	0,865	0,135	0,341	0,659	0,535	0,156	0,309	12,38	984	1222-43
1-253,5	1,61	0,870	0,130	0,435	0,565	0,640	0,133	0,227	8,69	1 399	1226-48
6A-259	0.92	0,879	0,121	0,372	0,628	0,516	0,190	0,295	12,26	996	1226-56
6A-296,7	1,14	0,883	0,117	0,397	0,603	0,542	0,119	0,339	11,46	1 002	1260
X-10	2,28	0,879	0,121	0,416	0,584	0,510	0,112	0,379	10,19	1 014	1223-56
X-21	1,66	0,871	0,129	0,317	0,683	0,651	0,129	0,220	14,54	1 041	1221-49
X-31	0,95	0,895	0,105	0,408	0,592	0,556	0,139	0,305	12,36	1 000	1232-72
A-3	0,55	0,889	0,111	0,417	0,583	0,568	0,158	0,275	11,19	1 102	1230-66
A-9	1,15	0,853	0,147	0,287	0,713	0,553	0,177	0,270	14,41	947	1223-32
A-16	0,75	0,900	0,100	0,559	0,441	0,564	0,099	0,337	7,10	1 366	1239-76 opx ol

* TEMPERATURE CALCULATIONS BASED ON THE METHOD OF JACKSON, 1969.

** TEMPERATURE CALCULATION BASED ON THE METHOD OF NATHAN AND VAN KIRK, 1978.

temperature calculations are reasonable if one assumes crystallization from a basaltic liquid at temperatures between 1000°C and 1300°C (Roeder et al., 1979). The temperature variation from sample to sample is, however, far too large to be of significance.

The range in $K_D^{\text{ol-chr}}_{\text{Mg-Fe}^{2+}}$ in Table 5 has a strong influence on the calculated temperatures. The slopes of the tie-lines for each ol-chr pair is shown in Figure 58 and represents the $K_D^{\text{ol-chr}}_{\text{Mg-Fe}^{2+}}$ value for each pair. The large spread of $Mg/(Mg+Fe^{2+})$ ratio for chromite relative to olivine can be explained in three different ways. Firstly, that the chromite composition deviates from ideality in end member components; secondly, that the variations in K_D values represent differences in liquidus temperatures of the cotectically crystallizing pairs; and thirdly, the most likely explanation for the spread in the variation in the calculated K_D, re-equilibriation of some of the olivine-chromite pairs at lower temperatures in the cumulate pile.

On re-examination of Jackson's equation, Roeder et al. (1979) found that by changing the free energy value of $FeCr_2O_4$, the revised geothermometer yields values of 500 to 800°C for basic plutonic rocks and 1100-1300°C for the Kilauea volcanics. Although the volcanic temperatures are acceptable the plutonic values are considerably lower than Jackson's values, with the result that the application of this geothermometer is questionable.

A more realistic crystallization temperature is obtained by using the crystallization model of Nathan and van Kirk (1978), in which the crystallization temperature and the composition the olivine and orthopyroxene are calculated as a function of the composition of the magma. This compositional relationship was obtained by fractionating a proposed parental magma composition which is believed to be the initial lower zone magma (see Chapter 6). The first set of values in the N.& V.K. temperature column, Table 5, are based on the composition of orthopyroxene, whereas the second is based on the composition of olivine. In nearly all cases the two values are within 39°C of each other which agrees well with the acceptable error of other geothermometers.

It will be shown in the next chapter that the Mg-Fe of the postu-

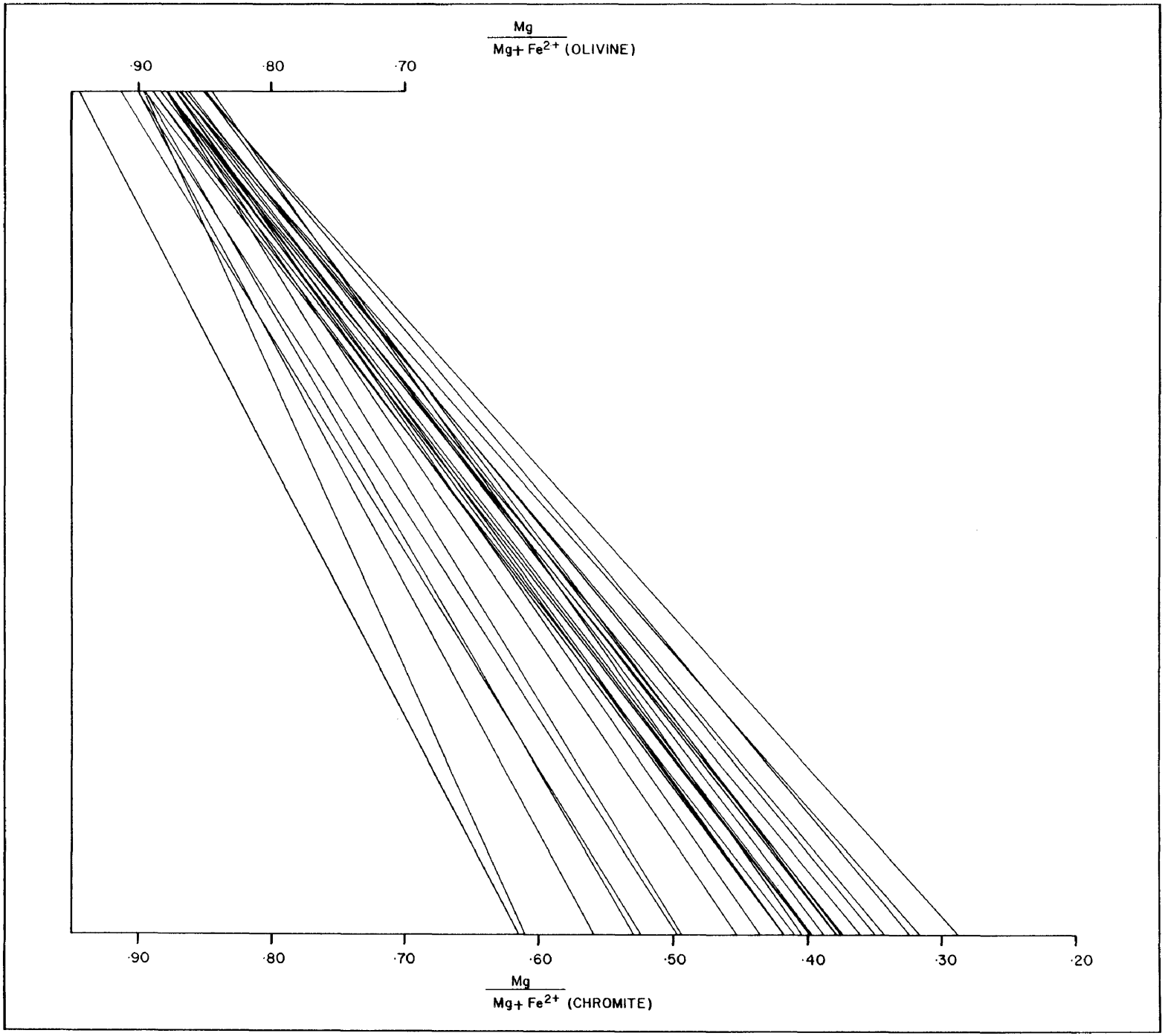

Fig. 58 Compositional relations between coexisting olivine and chromite in the lower zone south of Potgietersrus.

lated parent magma and the composition of the chromite and olivine in the lower zone are very similar to those described by Evans and Wright (1972) from the Kilauea volcanoes. The data of Evans and Wright (1972) can therefore be used to test the validity of the Nathan and van Kirk method to define crystallization temperatures. The Kilauea olivine with a Mg* of 0,863 quenched at 1225°C, whereas this same sample was calculated by the N.V.K. method to have crystallized at 1240°C. Similarly, a sample from Makaopuhi with a Mg* of 0,816 for olivine was calculated to have crystallized at 1194°C, whereas this sample was known to have quenched at 1170°C.

Based on the composition of the olivine the lower zone is inferred to have crystallized over a range in temperature from 1223 to 1273°C. A slightly lower temperature range is obtained from the composition of the opx. A temperature of 1240°C was calculated for the opx-ol-chr cumulate, which formed immediately after crystallization of the lower chromitite layer. This sample GV-1 was taken 2 cm above the top of the lower chromitite layer and contains only 1,12 per cent chromite, which could not have influenced the composition of the olivine or orthopyroxene through postcumulus re-equilibriation. The Mg* of the cumulus silicates in chromite poor rocks (i.e. 5 per cent) should, therefore, monitor conditions in the magma immediately following the formation of the lower chromitite. It is of little value to equate the Mg* of the olivine where it coexists with large proportions of chromite to temperatures of crystallization, because the $K_D \frac{ol\text{-}chr}{Mg\text{-}Fe^{2+}}$ is a function of the proportion of coexisting chromite (Jackson, 1969; Irvine, 1967).

Although the stability of chromite in a liquid of olivine tholeiite composition depends on many physical and compositional parameters, it will normally be a stable phase on the liquidus at 1200°C at an fo_2 of 10^{-8} atm (Hill and Roeder, 1974). Fisk and Bence have shown that a "Famous" olivine tholeiite with a Mg* of 0,68; a chrome content to 510 ppm and olivine of Mg* 0,86 - 0,89; will crystallize chromite at temperatures of 1230 to 1250°C at fo_2 of 10^{-9} atm, whereas at $10^{-8,5}$ atm chromite would crystallize at 1200°C. The stability field of spinel can be extended by spiking the sample with Cr. This was demonstrated by Hill and Roeder who have shown that spinel crystallized at 1200°C and $10^{-6,5}$ atm when the sample

contained 80 ppm Cr, whereas the same sample with 770 ppm Cr crystallized spinel at 1200° C, but at an fo_2 of 10^{-11} atm.

A sample of a fine-grained marginal rock considered by Cawthorn et al. (1979) as being representative of the initial lower zone magma contains 970 ppm Cr. Cawthorn et al. melted this sample at controlled oxygen fugacities and found that at $10^{-9,2}$ atm olivine plus chromite crystallized at 1250° C, whereas olivine and spinel crystallization commenced at 1310° C at an fo_2 of $10^{-5,5}$ atm.

Calculations based on the Wood-Banno (1973) geothermometer suggested that the temperature of crystallization for the opx-cpx-chr and opx-chr cumulates of the critical zone was approximately 1166° C. Since similar values are obtained from samples situated in the immediate hanging-wall of the UG2-like chromitite layer it is assumed that crystallization of this layer occurred at a similar temperature.

5.2.6.4 Chrome Spinel as an Indicator of Oxygen Fugacity

Apart from the Cr_2O_3 and Al_2O_3 content of the magma, the prevailing oxygen fugacity is considered to be a major factor governing the crystallization of chromite. Snethlage and Von Gruenewaldt (1977); Snethlage and Klemn (1978); Irvine (1965, 1967A); Ulmer (1969); Hill and Roeder (1974) and Fisk and Bence (1980) have experimentally or theoretically shown that the stability and composition of the chrome spinel is dependent on the fo_2 of the system. For this reason analyses of the oxygen fugacity sensitive assemblage opx-ol-chr was used in a thermodynamic approach, based on the principles outlined by Irvine (1965), to calculate the fo_2. Irvine (1965) showed that the fo_2 may be defined if chromite coexists with primary orthopyroxene and olivine by the reaction:

$$\underset{ol}{6Fe_2SiO_4} + O_2 \rightleftharpoons \underset{mt}{2Fe_3O_4} + \underset{opx}{6FeSiO_3}$$

$$\text{then } fo_2 = \frac{(a^{sp}_{mt})^2 \, (a^{opx}_{Fs})^6}{Km \quad (a^{ol}_{Fa})^6}$$

Using a similar approach and the latest available thermodynamic data in conjunction with the composition of olivine, orthopyroxene

and chromite the reaction:

$$\underset{\text{opx}}{3FeSiO_3} + \underset{\text{mt}}{Fe_3O_4} \rightleftharpoons \underset{\text{ol}}{3Fe_2SiO_4} + \underset{\text{gas}}{1/2O_2}$$

was used to calculate the oxygen fugacity from the following equation:

$$\log_{10} fo_2 = 2\left[\frac{-11411}{T°K} + 3{,}54 + \frac{0{,}0227(P-1)}{T} - \log\left(a^{ol}_{Fe_2SiO_4}\right)^3 + \log\left(a^{opx}_{FeSiO_3}\right)^3 + \log\left(a^{mt}_{Fe_3O_4}\right)\right]$$

where T = °K, P = bar, and $(a^{Sp}_{Fe_3O_4}) = X^{mt}_{Fe_3O_4}$
(Williams, 1971A and Arculus and Wills, 1980).

With the aid of the above equation it was calculated that the lower zone opx-ol-chr cumulates crystallized over an oxygen fugacity interval of $10^{-6,21}$ to $10^{-5,02}$ atm, with a mean value of $10^{-5,48}$ atm. Because the chromite-rich horizons are all in ol-chr cumulates, a direct calculation in these chromite-rich rocks could not be made. Nevertheless, in an attempt to record as closely as possible the effective oxygen fugacity at the end of the development of the lower chromitite layer, the fo_2 was calculated from an opx-ol-chr cumulate 2 cm above the upper contact of this layer. A value of $10^{-4,98}$ atm was obtained at a temperature of 1242° C. This calculation suggest that an increase of about 0,50 log units over the average value is necessary to enhance chromite formation, which agrees well with the experimental intrinsic oxygen fugacity measurements of Snethlage and Klemm (1978) on chromite from the Bushveld Complex.

Snethlage and Von Gruenewaldt (1977) conducted intrinsic oxygen fugacity studies on chromite and olivine from the LG4 chromitite at the Zwartkop Chrome Mine in the Western Bushveld. This study can be used to varify the previous fo_2 calculation for the lower chromitite, since the LG4 chromitite is very similar to the lower chromitite both as far as mineralogy and composition are concerned. Both layers occur in olivine-rich rocks with high $Mg/(Mg+Fe^{2+})$ ratios and consist of chromite with high $Mg/(Mg+Fe^{2+})$ ratios and Cr_2O_3 content. They found that at 1200° C the measured fo_2 increased from 10^{-7} to 10^{-6} atm from the disseminated base to the massive top of the layer, whereas at 1300° C the respective values would have been $10^{-6,10}$ and $10^{-5,80}$ atm. These values are fairly close to those obtained by the author for the lower chromitite.

Unfortunately the method of intrinsic oxygen fugacity has the disadvantage that postcumulus re-equilibriation effects cannot be eliminated and thus the results tend to incorporate reducing postcumulus effects, which may account for the slightly lower values.

The fo_2 in the hanging-wall opx-ol-chr cumulate above the lower chromitite layer was also calculated by using the method of Schreiber and Haskins (1976, Fig. 14) which is based on the $D_{cr}^{px\text{-}ol}$. From their forsterite-anorthite-silica curve at 1300° C and a calculated $D_{cr}^{px\text{-}ol} = 6{,}41$; an operative oxygen fucacity of 10^{-5} atm was calculated for the magma during crystallization of this layer, which agrees surprizingly well with the previously calculated value of $10^{-4{,}98}$ atm at 1242° C.

From the many experimental investigations in the system MgO-Iron Oxides - Cr_2O_3-Al_2O_3 at 1300° C it was found that the stability field of spinels is very sensitive to the prevailing oxygen fugacity. Ulmer (1969) summarized the data diagramatically (Fig. 59) and could show with the aid of these diagrams that spinel has its maximum stability in the fo_2 range of 10^{-5} to 10^{-7} atm. These values agree well with those calculated for the lower zone, as well as for the lower chromitite layer.

Unfortunately fo_2 for the opx-chr, opx ± cpx-chr cumulate and UG2-like chromitite of the critical zone could not be calculated directly due to the lack of suitable mineral assemblages. Nevertheless, an estimate of the oxygen fugacity can be made if the nature and abundance of the cumulus phases is known as well as the temperature at which they crystallized, and this information is used in conjunction with the diagram of Hill and Roeder (1974, Figure 9). A crystallization temperature of 1166° C was calculated for two samples (78-403 and 78-413) of opx-cpx-chr cumulate. Both samples contain approximately 13 per cent chromite. Since sample 78-413 is from the hanging-wall of the UG2-like chromitite layer, a similar temperature was assumed for crystallization of this chromite cumulate. Projection from a temperature of 1166° C to the maximum spinel precipitation on the liquidus diagram of Hill and Roeder (1974) suggests a fo_2 of $10^{-7{,}3}$ atm. The presence opx-cpx-chr cumulates in the immediate hanging-wall of the chro-

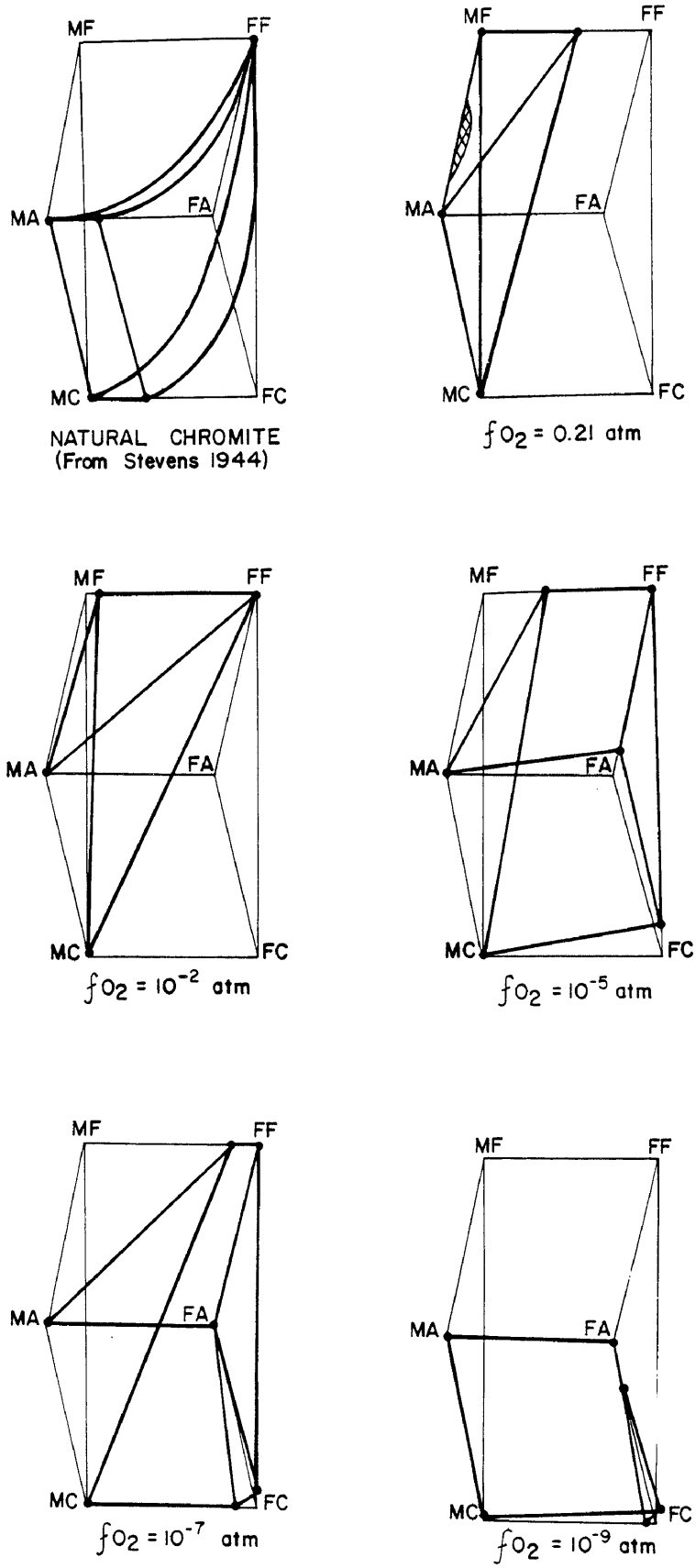

Fig. 59 The spinel compositional prism showing the spinel solid solutions at 1300°C and various oxygen fugacities.

mitite layer places further constraints on the conditions in the magma during onset of crystallization of cumulus clinopyroxene in chromite bearing assemblages, as this coincides with the T-fo_2 conditions where clinopyroxene becomes stable in the phase diagram of Hill and Roeder. Furthermore, if crystallization at a constant oxygen content is assumed, the fo_2 falls 1,5 units per 100° C (Hill and Roeder, 1974) and a drop in crystallization temperature from 1242° C in the chromitite layer to 1166° C for the UG2-like chromitite would suggest a drop in fo_2 of 1,14 log units to yield an fo_2 value of $10^{-6,14}$ atm for the UG2-like chromitite layer. Indications are, therefore, that the UG2-like chromitite layer crystallized in the fo_2 range of $10^{-6,14}$ to $10^{-7,30}$ atm at about 1166° C.

One of the most perplexing aspects of chromite mineralization in the Bushveld Complex is the lack of chromite in the quenched parental liquid, even though these samples are rich in Cr_2O_3. The proposed initial lower zone liquid contains 970 ppm Cr yet no visible chromite is present (Cawthorn et al., 1979), a feature also observed in lunar basalts (Taylor, 1975). The reason for the lack of chromite in these rocks may be found in the experimental work of Schreiber and Haskins (1976); Hirashimaet al., (1974); Frohberg and Richter (1968) and Healy and Schottmiller (1964); who presented graphs of the Cr^{3+} - Cr^{2+} redox equilibria for a variety of different liquid compositions. From their experimental work it can be seen that 90 per cent of the total chromium is Cr^{2+} over a wide range of melt compositions and temperatures if the partial pressure of oxygen is below 10^{-9} atm. These authors emphasize that it is the Cr^{3+} concentration of the melt and not the total Cr content that determines the solubility of spinel and therefore whether chromite will crystallize.

Melting experiments by Cawthorn et al. (1979) on the lower zone chilled material at 1250° C, showed that chromite only crystallized from the liquid at an fo_2 of greater than $10^{-9,2}$. The inferred low fo_2 at the time of intrusion, in addition to the relatively low Al_2O_3 content of 12,7 per cent, would have the effects of increasing the solubility of spinel and thus inhibit the crystallization of chromite.

An explanation of the low fo_2 of the initial lower zone magma and the lack of chromitites in the lower levels of stratiform intrusions may be explained on the basis of the recent intrinsic oxygen fugacity measurements by Arculus and Delano (1980) on spinels from Kimberlites, peridotites and from megacrysts in nodules within Hawaiian basalts. From these studies they concluded that the fo_2 - T conditions in the upper mantle are close to the iron-wustite (I-W) buffer. With the aid of a survey of common basic rocks they show that there is a difference of approximately four log units between the oxidation state of the investigated peridotitic rocks and igneous rocks from near surface environments. They ascribe this difference in oxidation of the igneous rocks to H_2 loss at shallow depths as a result of the dissociation of water. Similarly, the low fo_2 conditions reflected by Fe-wustite bearing assemblages in lunar basalts is probably also the result of an oxygen deficient environment.

Sharpe (personal communication) has calculated the fo_2 for the critical zone chill to be $10^{-10,5}$ atm at 1050° C, by using the Fe-Ti oxide method of Buddington-Lindsley (1964). This low oxygen fugacity in marginal rocks adjacent to the critical zone and the absence of chromite in Cr-rich quenched martinal rocks of the lower zone indicates that the parental magmas of the Bushveld Complex had low fo_2 values outside the stability field of chromite.

Therefore, although rich in Cr the initial parental magma(s) were too low in Cr^{3+} to stabilize chromite during its early stages of crystallization and it was only through subsequent H_2 loss and accompanying oxidation that crystallization of the magma gave rise to chromite and chromitite formation.

The position of the chromitite layers in many stratiform intrusions may also be related to this hypothesis of belated oxidation of the magma through H_2 loss and build up of oxygen with fractional crystallization. At Potgietersrus the upper and lower chromitite layer developed after at least 66 per cent of the lower zone had crystallized, the most significant chromitite layers (G and H) in the Stillwater Complex developed after about two thirds crystal-

lization of the peridotite member, the chromitite layers of the Muskox Intrusion developed after 83 per cent of the intrusion had crystallized, whereas most of the chromitite in the Bushveld Complex, with the exception of Potgietersrus, occurs in the critical zone after crystallization of at least 1500 m of ultramafic rocks.

6. CHEMISTRY OF THE LAYERED SUITE

This investigation was undertaken in order to study the whole-rock chemical variation within the intrusion, to characterize the various rock types on the basis of their chemical composition, to establish trends which may be compared with petrochemical data from other stratiform intrusions, and to establish whether significant within and inter-group element correlations exist.

All samples were prepared and analysed by the author in the Department of Geology at the University of Pretoria. Most of the samples were taken from diamond drill core and the remainder from surface outcrops. After primary crushing in a jaw-crusher the samples were powdered in a tungsten carbide swing mill and analysed in duplicate on a semi-automated Siemens SRS-XRF spectrometer. The major elements SiO_2, TiO_2, Al_2O_3, total iron as FeO, MnO, MgO, CaO, K_2O, and P_2O_5 were determined on glass discs, using a method developed by the University of Cape Town, based on the method by Norrish and Hutton (1969). The trace elements Co, Cr, V, Zn, Cu, Ni, Nb, Zr, Y, Sr, and Rb, as well as Na_2O were determined on compressed powder pellets. Sulfur was analysed commercially with a Leco titration analyser by McLachlan and Lazar. Average errors in accuracy between ten calibrations and the values given by Flanagan (1969) relative to 11 standards were as follows. Using standards AGV-1, BCR-1, G-2, GSP-1, JB-1, JG-1, MRG-1, NIM-D, N1M-N, N1M-P and PCC-1 errors were at maximum levels of: SiO_2 ± 0,204; TiO_2 ± 0,010; Al_2O_3 ± 0,111; Fe_2O_3 ± 0,104; MnO ± 0,002; MgO ± 0,032; CaO ± 0,032; Na_2O ± 0,073; K_2O ± 0,025; P_2O_5 ± 0,010; Cr_2O_3 ± 0,004; NiO ± 0,012. Trace elements were: Co ± 3; Cr ± 2; V ± 4; Zn ± 2; Cu ± 2; Ni ± 3; Nb ± 2; Zr ± 4; Y ± 2; Sr ± 3; Rb ± 4 ppm respectively. Precision in all cases is better than ± 25 per cent of the absolute error.

The Fe_2O_3 was calculated as TiO_2 + 1,5 (Irvine and Baragar, 1971).

The cation norm (Appendix 8) is based on the convention of Irvine and Baragar (1971) and was calculated with the computer program "Regnorm" obtained from the Geological Survey of Canada.

6.1 Major Element Variation

The major and trace element data for the cumulates are given in Appendix 8 and presented diagrammatically in Figure 60 (Folder II). Although the composition of adjacent rock types can differ greatly, e.g. where norite overlies bronzitite or norite overlies anorthosite, the range in composition exhibited by each rock type is comparatively limited. The relatively constant trends of certain elements in the main zone and the close relationship between the normative mineral compositions and the modal composition of these rather isomodal rocks, suggests a close relationship between the solidus and the liquidus for this portion of the layered suite.

All analyses shown in Figure 60 have been recalculated on an anhydrous basis to facilitate comparison, although this has only modified the serpentinized olivine bearing cumulates.

6.1.1 SiO_2

An erratic distribution pattern for SiO_2 in the lower zone is due to the varying proportions of olivine and orthopyroxene in these ultramafic cumulates. Values as low as 40,5 per cent are found in the ol-chr cumulates whereas the highest value of 57,7 per cent was recorded in an opx cumulate of the Volspruit Pyroxenite. Average values of 53 to 55 per cent are typical of these lower zone pyroxenites.

The critical and main zones contain a fairly constant SiO_2 content, with a mean value of approximately 52 per cent. At the base of the upper zone a marked decrease in SiO_2 to 47 per cent is observed.

6.1.2 FeO (Total Fe)

The FeO content of the lower zone rocks is fairly constant, with a mean value of about 9 per cent. In contrast, the diversity of rock types in the critical zone gives rise to a considerable scatter, whereas the main zone rocks display a gradually increasing iron trend from 7 per cent at the base to about 10 per cent at the top. The upper zone pl-cpx-opx-mag cumulates contain on average about 18,5 per cent FeO. This increase in FeO from the base of the main zone to the lower part of the upper zone is due to an increase in the ferrosilite and hedenbergite components in the

pyroxenes. The marked increase at the base of the upper zone is due to the appearance of magnetite as a cumulus phase. The comparatively high FeO values of the lower zone rocks is due to the high mafic index, even though the mafic minerals have a low fayalite and ferrosilite component.

6.1.3 Al_2O_3

This oxide displays a well defined trend of increasing concentration towards higher stratigraphic levels. Minimum values in the order of 1 per cent were recorded in the lower Volspruit pyroxenites from where values gradually increase to about 5 per cent at the top of the lower zone. Although the increase is small it records the successively increasing amounts of intercumulus plagioclase found in these rocks.

The introduction of cumulus feldspar in the critical zone marks an abrupt increase in the concentration of Al_2O_3. The highest Al_2O_3 content of about 32 per cent is found in the plagioclase cumulates or anorthosites. The antipathetic relationship between Al_2O_3 and MgO and to a lesser extent FeO in the critical and main zone rocks reflect the modal proportions of plagioclase and mafic minerals. Apart from the anorthosite at the base of the upper zone the average upper zone rocks appear to contain about the same amount of Al_2O_3, i.e. about 17,5 per cent, as the main zone cumulates.

6.1.4 MgO

This oxide falls from extremely high values of up to 45 per cent in the ultramafic lower zone cumulates to surprisingly low values of between 3,01 and 1,31 per cent in the normal upper zone cumulates. This overall decrease (Fig. 60) is to be expected with differentiation, but some rather interesting localized trends can be observed. For instance, the very systematic drop in the MgO content of the monomineralic orthopyroxene cumulates from the -1250 m level towards and slightly into the overlying mineralized opx-chr cumulate at -1200 m, and the subsequent increase through and out of this mineralized zone towards the alternating succession of opx-chr and opx-ol-chr cumulates at the -1075 to -1032 m level. This trend is very similar to that previously established for the olivines and orthopyroxenes with the electron

microprobe, but in this case the compositional trends can be observed in more detail. Because of the larger number of whole rock analyses than microprobe analyses over this section, it is possible to demonstrate that the systematic drop occurs not only up to but also into the mineralized horizon. The drop in the MgO is associated with an increase in the FeO content of the rocks and thus reflects the drop in the Mg* of the mafic silicates, which is believed to be due to a drop in temperature during crystallization of the host magma.

The systematic increase in MgO in the upper half of the lower Volspruit Pyroxenite defines a reverse fractionation pattern, whereas the increase of the MgO content at the top of cyclic unit 22 in the lower part of the Drummondlea Harzburgite-Chromitite may be related to an influx of fresh undifferentiated magma into the magma chamber, as was previously deduced from miroprobe analyses of the silicates. The MgO content of the rocks in the main zone is fairly constant but decreases fairly abruptly at the base of the upper zone.

6.1.5 Na_2O, K_2O, and CaO

Na_2O and CaO will be dealt with together since they are found mainly in plagioclase and clinopyroxene relative to the other cumulus minerals in the layered suite. Both Na_2O and CaO vary sympathetically with the Al_2O_3 content of rocks in the lower zone and again reflects the upward increase in the amount of intercumulus plagioclase and to a lesser extent clinopyroxene.

The introduction of cumulus plagioclase in the critical zone and cumulus clinopyroxene in the main zone, give rise to a marked increase in the Na_2O and CaO content of the rocks in the critical, main, and upper zone.

The K_2O content of the rocks was found to increase from the lower zone to the upper zone. The trends seen within each zone tend to follow that of Na_2O, suggesting that this element is also controlled by the modal amounts of plagioclase and the degree of differentiation.

6.1.6 MnO

MnO is contained in decreasing amounts in the following minerals of the layered sequence: ilmenite, magnetite, orthopyroxene, olivine, chromite, clinopyroxene and plagioclase. Wager and Brown (1968) found the MnO content to increase in each of these minerals with differentiation in the Skaergaard Intrusion. This was also found to be the case for orthopyroxene in this study.

The MnO content throughout the layered squence averages about 0,17 per cent and its proportion in the rocks of the lower, critical, and main zone is essentially controlled by the amount of orthopyroxene in the rock. The most significant local MnO anomaly is in the opx cumulates below the sulfide enriched opx-chr cumulate of cyclic unit 11. The MnO content, which increases well into the mineralized layer, suggests that a more fractionated, lower temperature magma gave rise to this interval. The low MnO content of the upper zone is enigmatic and reflects the low MnO contents of the ilmenites and magnetite relative to these two minerals in the M.Mb./P.G. (Appendix 6).

6.1.7 TiO_2

It was previously mentioned that this oxide preferrentially partitions into the melt because of its low D value in basic magmas. Watson (1976) and Pearce and Norry (1979) showed in experimental investigations on the partitioning of trace elements that ions with high field strengths (charge / radius ratio) were partitioned more strongly, 2,9 and 2,3 fold for Ti and Zr respectively, into basic melts. This is ascribed by these authors to a lower degree of polymineralization of basic melts so that more low energy sites for these ions are provided for in such melts. A solid phase crystallizing from a basic melt will therefore contain lower abundances of Ti, Zr, Y, and Nb than the same phase crystallizing from a more fractionated acidic melt.

Bowes et al., (1973) showed in a petrochemical study of the Stillwater Complex that the TiO_2 content of the rocks weakly increased with differentiation. The later differentiates of this intrusion are unfortunately not exposed. Wager and Brown (1968) have, however, shown that the TiO_2 content of the Skaergaard magma increased with differentiation up to the point at which titani-

ferous magnetite crystallized as a cumulus phase. This occurred when the TiO_2 content of the melt was about 2,8 per cent and the FeO and Fe_2O_3 content was 14,0 and 3,5 per cent respectively. Therefore, due to the low $D_{Ti}^{solid\text{-}liquid}$ values in the lower zone the TiO_2 content of the rocks can be used as a indirect measure of the degree of fractionation of the magma from which they crystallized, because the more fractionated the magma, the higher the TiO_2 concentration in the crystallizing cumulates. The least differentiated rocks are, therefore, those of the Volspruit Pyroxenite subzone, because they contain the lowest mean TiO_2 content of 0,04 per cent. Rocks of the Drummondlea Harzburgite-Chromitite contain on average 0,07 per cent TiO_2, and the uppermost Moorddrift Harzburgite-Pyroxenite contains 0,10 per cent TiO_2. The upward increase in the whole-rock TiO_2 content is paralled by a similar trend observed for TiO_2 of chromite in the lower zone.

The TiO_2 content of the critical zone samples is, on average, slightly higher than that of the rocks in the upper part of the lower zone, whereas the rocks of the main zone contain about 0,25 per cent TiO_2. It is interesting to note that the plagioclase cumulate at the base of the upper zone contains 1,17 per cent TiO_2, which is mainly contained in the intercumulus Fe-Ti oxides. The average rocks in the upper zone contain over 3 per cent TiO_2. The TiO_2 content of the upper zone liquid must have been maintained at a very high level in order to account for the progressive increase in the TiO_2 content of the magnetitite layers upwards in the sequence (Molyneux, 1970; van der Merwe, 1978).

6.1.8 P_2O_5

Like TiO_2, the concentration of P_2O_5 increases in the liquid until apatite precipitates (Wager and Brown, 1968; Morse, 1969; and Maske, 1966). Consequently the lowest levels of P_2O_5 are found in rocks of the Volspruit Pyroxenite subzone where virtually all samples contain 0,01 per cent P_2O_5. Higher values ranging from 0,01 to 0,03 per cent are found in rocks of the Drummondlea Harzburgite-Chromitite and in the Moorddrift Harzburgite-Pyroxenite.

The P_2O_5 levels remain fairly low through the lower portion of the critical zone but rise to an average of approximately 0,05 per cent in the plagioclase cumulates in the upper part of the critical zone. A fairly constant level of 0,04 per cent P_2O_5 is contained in the rocks of the main zone, but this value increases to 0,08 per cent in the upper zone pl-cpx-opx-mag cumulates. According to van der Merwe (1978) the P_2O_5 content of the upper zone cumulates remains at about 0,10 per cent until apatite becomes a cumulus phase whereupon the P_2O_5 content rises suddenly to 1,13 per cent.

Morse (1969) calculated that apatite became a cumulus phase in the upper zone of the Kiglapait Intrusion after 94 per cent of the intrusion had crystallized. Although the rocks contain on average 1 per cent or less apatite, local concentrations of up to 7 per cent may be found. He calculated that rocks which contain 1,60 per cent P_2O_5 crystallized from liquids which should have contained 1,40 per cent P_2O_5. Huntington (1979) estimated that the magma which gave rise to the Kiglapait Intrusion contained 900 ppm P_2O_5. Similarily Wager and Brown (1968) found that the Skaergaard magma precipitated apatite after approximately 97 per cent solidification, at which stage the liquid is considered to have contained about 1,75 per cent P_2O_5. These rocks that crystallized from this liquid contain about 2,30 per cent P_2O_5. From the above values for the Skaergaard and Kiglapait Intrusions it can be estimated that the upper zone magma at Potgietersrus must have contained about 0,90 per cent P_2O_5 on saturation to give rise to apatite bearing cumulates containing 1,13 per cent P_2O_5.

The rock analyses have been plotted on a AFM diagram (Fig. 62) to show the respective fields of each rock type.

6.2 Trace Element Geochemistry

6.2.1 Sulfur

The distribution of sulfur is very irregular in the lower zone due to an irregular distribution of sulfides, as well desulfurization in rocks which are serpentinized. The S, Ni, and Cu content of the lower and critical zones will be dealt with in more detail in Chapter 8 which deals with sulfide mineralization.

Within the main zone, the mean sulfur content of the pl-cpx-opx cumulates is 54 ppm. In the topmost 257 metres of the main zone the sulfur content increases from 20 to 50 ppm. The mottled anorthosite at the base of the upper zone contains 530 ppm whereas the average upper zone pl-cpx-opx-mag cumulates contain in excess of 1000 ppm S. The abrupt and substantial increase in S content of the rocks of the upper zone would seem to indicate that the crystallization of abundant magnetite in conjunction with Fe-rich pyroxene lowered the S carrying capacity of the magma and resulted in the separation of small quantities of sulfide liquid.

6.2.2 Copper

Like sulfur, the copper content of rocks is highly variable since both elements are tied up in the sulfides. The most significant concentrations of sulfides and therefore also Cu occur in the sulfide and PGE-rich opx-chr cumulate of the Volspruit Pyroxenite and in the hanging-wall opx-ol-chr cumulate overlying the lower chromitite layer. Noteable Cu concentrations also occur in well mineralized horizons within the critical zone.

Copper values increase towards the top of the main zone as well as in the lower portions of the upper zone.

6.2.3 Zinc

Inspection of the Zn and MnO columns in Figure 60 (Folder II) shows a sympathetic behavior of these two elements with fractionation. A correlation matrix constructed for all the available analyses revealed a correlation coefficient of 0,642 between Zn and MnO and 0,531 between FeO and Zn. Buchanan (1976) also found a very high correlation between Zn and MnO in the Bushveld rocks from the Bethal area. The reasonably high correlation coefficients and the sympathetic trends indicate the ease with which Mn and Zn can substitute for iron in mafic silicates and oxides.

The whole rock analyses show that the Zn content of the rocks from the lower zone to the upper zone remains fairly constant. This may be ascribed to the balancing effect of a general decrease in the volume proportion of pyroxenes upward, coupled with a general increase in the FeO, MnO, and Zn concentrations of the

pyroxenes.

The systematic upward increase in MnO and Zn with accompanying decrease in MgO in the foot-wall sequence of the sulfide mineralization in the Volspruit Pyroxenite subzone is indicative of cumulates that crystallized from a more differentiated magma than the over- and underlying layers. The comparatively Fe-rich monomineralic cumualtes must have crystallized from a more Fe-rich liquid which could therefore also have been enriched in Mn and Zn component which would enter the lattice of the precipitating pyroxenes.

6.2.4 Nickel

Due to varying proportions of olivine and sulfide in the rocks of the lower and critical zone, considerable scatter occurs with respect to this element. In contrast, a gradual depletionary pattern is evident in the main and upper zones with fractionation.

High silicate Ni values occur in the olivine adcumulate (dunite) at the -1250 m level in rocks that contain 10 ppm S. The lowest Ni values of 37 ppm was recorded for an anorthosite at the -22 m level.

Correlation coefficients between Ni and MgO of 0,121, Ni and S of 0,688, and Ni and Cu of 0,902 suggests that the bulk of the Ni in the layered suite is related to the amount of sulfides and not the silicates. A statistical evaluation of the lower zone lithologies, however, reveals that the correlation coefficient between Ni and MgO is 0,802 in ol-chr cumulates, 0,163 in opx-ol-chr cumulates and 0,237 in the opx cumulates. This indicates that virtually the bulk of the Ni in the ol-chr cumulates is contained in olivine.

6.2.5 Chromium

The chromium content in the lower zone is primarily controlled by the modal chromite content of the rocks. Any fluctuations in these rocks are, therefore, in most cases due to changing proportions of olivine and chromite and, to a lesser extent, between orthopyroxene and chromite. The highest values in the layered suite are associated with the chromitite layers and the lowest values of 2 ppm Cr are found in the plag-opx-mag cumulates of the upper zone.

The magma that gave rise to these cumulates must have been extremely depleted in Cr_2O_3. This is also substantiated by van der Merwe (1978) who gives values as low as 23 ppm Cr for the similar upper zone cumulates. The depletion of Cr through the main zone to the +850 m level where it increases abruptly to peak values at the +1067 m level agrees with other evidence for an influx of fresh magma at this level in the intrusion to give rise to the pyroxenite marker found elsewhere in the Bushveld Complex (Von Gruenewaldt, 1973). The increase in the Cr values at the +850 and +940 m levels of the main zone is not related to an increase in the clinopyroxene content of the rock as both the modal orthopyroxene and clinopyroxene content of these rocks decrease over this stratigraphic interval.

6.2.6 Vanadium

The geochemical behaviour of V is very similar to that of Mn, Fe, and Zn as is seen by the sympathetic trends of these elements. The vanadium content of the liquid appears to increase with differentiation as is shown by a very gradual increase from the lower zone to the top of the main zone. The successive build up of V with differentiation is probably due to low $D_V^{solid\text{-}liq}$ values of the early coprecipitating phases. Crystallization of cumulus Fe-Ti oxides will scavenge V from the magma so that a vanadium depletion trend develops with continued differentiation of upper zone liquid (Molyneux, 1970).

6.2.7 Rubidium

This element is present only in very low concentrations throughout the layered suite (Fig. 60, Folder II). Rubidium correlates strongly with K_2O ($r = 0{,}862$) and weakly with Na_2O ($r = 0{,}287$) and thus it is assumed, as is generally believed, that Rb is tied up in the orthoclase component of the rock. A correlation matrix conducted on the ol-chr cumulates reveals coefficients of 0,555; 0,956; and 0,958 for Rb with CaO, Na_2O, and K_2O respectively leaving little doubt that most of the Rb is tied up in the intercumulus plagioclase. This is furthermore indicated by the high correlation coefficients of 0,782 and 0,708 for Rb:Zr and Rb:Y respectively. Correlation coefficients for Rb on the one hand and CaO, Na_2O, K_2O, FeO, as well as Fe_2O_3 on the other hand for plagioclase cumulates are -0,791; 0,338; 0,975; 0,791, and

0,792 respectively, which indicates that the Rb in these rocks is restricted to the intercumulus components. The high correlation with iron is due to the fact that the ferromagnesium minerals are all intercumulus in these rocks.

The lowest Rb values occur in the lower zone where values are frequently below the detection limit, whereas the highest values of up to 44 ppm occur in upper zone rocks.

6.2.8 Strontium

From Wager and Brown's (1968) data on the Skaergaard intrusion it can be seen that strontium most readily enters plagioclase and, to a lesser extent, apatite, whereas small quantities can replace the calcium in augite. The $D_{Sr}^{plag-liq}$ = 1,4 (Drake and Weill, 1975) whereas $D_{Sr}^{opx-liq}$ =0,01 (Philpotts and Schnetzler, 1970) and $D_{Sr}^{cpx-liq}$ = 0,10 (Hart and Brooks, 1974). The low $D_{Sr}^{opx-liq}$ indicates that the Sr content of the residual magma increased during crystallization of thelower zone. Consequently, the increase in Sr with height in the lower zone (Fig. 60) is both the result of factionation and an increasing proportion of intercumulus plagioclase towards the top of the lower zone.

The high Sr content in the rocks of the critical and main zones reflect the high modal proportion of plagioclase present, whereas the upward increasing Sr content in these rocks indicate a preferential replacement of Na in plagioclase rather than Ca. The Sr:Ca and Sr:Na correlation coefficients are 0,133 and 0,600 in these plagioclase cumulates, whereas in the main zone pl-cpx-opx cumulates the values are 0,460 and 0,672 respectively. Further evidence of a preferential replacement of Na over Ca by Sr in the feldspars is shown in the upper zone rocks, where the Sr content increases by about 30 per cent over the underlying rocks of the main zone. Duchesne (1978) found a similar relationship and showed that the $D_{Sr}^{plag-liq}$ does not equal 1,4 as was proposed by Drake and Weill (1975), but that it changes with the anorthite content of the plagioclase from 2,0 at An_{50} to 3,9 at An_{31}. Wager and Brown (1968) also showed that the Sr content of the plagioclase increases from early cumulus plagioclase (An_{60}) to a maximum in plagioclase (An_{40}) of the UZa cumulates.

6.2.9 Cobalt

This element has been shown by Wager and Brown (1968) to enter pyroxenes, olivine, magnetite, ilmenite, and sulfides. When the silicate liquid coexists with a sulfide liquid the $D_{Co}^{sulf-liq} = 7$ and is thus not as effectively scavenged by the sulfide as is Ni and Cu (Maclean and Schimazaki, 1976). A correlation matrix conducted on all the samples from the layered suite yields coefficients of 0,435; 0,518; 0,658; and 0,089 with Ni, Cu, S, and MgO respectively, suggesting that throughout the layered suite Co tends to be related to the sulfide content of the host rock. However, one would also expect a positive correlation between the modal olivine and cobalt content of the lower zone rocks yet a correlation based on the Co and MgO in the olivine-chromite cumulates suggest no relationship (r = -0,069), whereas the correlation coefficient for Co and Ni in the same rocks is negative. In the main zone the pl-cpx-opx cumulates show a very weak positive correlation of 0,264 and 0,281 for Ni and MgO respectively. Whereas coefficients as low as 0,002 and -0,408 for S and Cu respectively suggest little relationship between Co and sulfides in these rocks.

Inspection of the Co trend in Figure 60 (Folder II) is most informative, in that it picks out local sulfide anomalies in the lower zone, yet is not scattered by the alternating olivine-rich and olivine-poor nature of the rock types as is the case for Ni. The first anomaly occurs at the PGE mineralized layer between -1250 and -1180 m. The next anomaly from the -820 to the -770 m level coincides with weak sulfide mineralization in cyclic unit 21.

Apart from these two anomalies and high Co values in the sulfide bearing rocks associated with the chromitite layers which are not shown, the overall cobalt trend in the lower zone seems to be one of weak depletion towards higher stratigraphic levels. The best explanation for this trend is that cobalt was continually extracted from the magma by small quantities of sulfide liquid separating from the melt. Investigation of hundreds of polished sections examined during the course of the mineralogical investigation of the lower zone cumulates showed traces of sulfides to be

present in virtually every section.

Seeing that the Co is essentially contained in the sulfides, its distribution should correlate with the sulfide distribution. However Co does not appear to be remobilized during serpentinization as does Ni and S, but instead appears to have remained in the rock in secondary pentlandite. A survey of cobaltian pentlandite and cobalt penlandites by Harris and Nickel (1972) and Riley (1977) revealed that the more cobalt-rich pentlandites are commonly associated with serpentinized environments which suggests that the cobalt was not removed during serpentinization. Assuming this to be the case, the Co trend in Figure 60 should reflect the original cobalt content of the rocks and a weak decrease in the trend towards the top of the lower zone could be due to a depletion of the magma during fractionation. From this it appears as if Co is a comparatively immobile element and it could therefore be useful in geochemical exploration for picking out mineralized horizons, particularly in bodies with rapidly alternating rock types as well as in rock types susceptible to serpentinization.

The high Co values in the critical zone are due to localized enrichment of sulfides at particular horizons. The rather sulfide deficient main zone rocks suggest that the cobalt is contained in orthopyroxene and to a lesser extent in clinopyroxene. The Co depleted nature of the rocks near the top of the main zone is possibly the result of depletion due to fractionation.

The sudden rise in the cobalt content in the upper zone is due to an increase in the amount of sulfides in the rocks, but also due to the Fe-Ti oxides which can accommodate some Co. The high content of Fe-Ti oxides and the presence of pyrite-rich sulfides in the normal upper zone cumualtes seem to control the levels of cobalt in these rocks as they can contain as much, if not more, Co than the well mineralized layers in the critical and lower zones.

6.2.10 Niobium

This element is present in concentrations below the analytical

detection limit in all the cumulates even though levels that range from 3 to 8 ppm were detected in the M.Mb./P.G. The difference in the Nb content between the marginal member and the layered rocks may be due to the former being weakly contaminated by the feldspathic quartzites which could have been derived from the Archean granite.

6.2.11 Yttrium and Zirconium

These two trace elements can be discussed together because of similarities in their geochemical behaviour. In basic magmas olivine, plagioclase, clinopyroxene and orthopyroxene have $D_Y^{solid-liq}$ values of 0,01; 0,03; 0,50; and 0,20 respectively, whereas the $D_{Zr}^{solid-liq}$ is 0,01; 0,01; 0,1; and 0,03 respectively (Pearce and Norry, 1979). The distribution coefficients determine that these two elements should increase in the residual liquids with fractionation. This seems to have been the case in the Bushveld magma (Fig. 60). According to the higher D values for Y, the Y content in the cumulates should be higher than Zr. Zr is, however, present in higher concentrations than Y which indicates that the Zr content of the initial magma must have been higher than the Y content. The fine-grained marginal rocks representative of uncontaminated magma, emplaced after consolidation of the lower zone, contain between 1,57 and 3 times more Zr than Y.

The Y and Zr content in the rocks increase from the lowest portion of the lower zone up to approximately the +724 m level from where they decrease gradually up to the top of the main zone.

The increase in the Zr and Y concentration in the upper half of the lower zone is considered to be due to the more fractionated nature of the successive intercumulus material. The increase up to the +724 m level indicates a gradual enrichment of cumulus phases in Y and Zr, due to higher concentrations in the successively more fractionated melt. A correlation matrix of all the analysed samples indicate correlation coefficients of 0,545; 0,623; 0,601; and 0,781 between Zr and SiO_2, TiO_2, Fe_2O_3, and P_2O_5 respectively, and 0,412; 0,773; 0,730; and 0,838 between Y and these elements respectively. There seems little doubt, therefore, that both Y and Zr increase in the residual liquid with fractional crystallization.

The rocks at about the +700 m level are fairly fractionated, on the basis of the amount of quartz present and mineral compositions. The drop in Zr and Y towards the top of the main zone could therefore be due to the postulated influx of more basic magma and its mixing with the residual liquid in the chamber.

Although most of the obvious chemical trends and correlations were discussed numerous other less pronounced yet informative relations exist. This statistical data is presented in Appendix 9 and 10.

6.3 Composition of the Initial Magmas

It is believed that the Rustenburg Layered Suite in the Potgietersrus limb of the Bushveld Complex crystallized from at least three major emplacements of magma. Field evidence and petrological studies indicate that influx of new magma took place before onset of crystallization of the critical zone and the main zone - sample 78-92 and 78-53 (Appendix 8) are representative of the initial main zone and critical zone magmas respectively. Influx of magma during crystallization of the lower zone, the main zone and possibly also the upper zone can only be inferred from the mineralogical and geochemical trends within these zones.

The composition of the prostulated magmas of the Potgietersrus complex as well as other layered intrusions are plotted on an alkali-silica variation diagram in Figure 61A and B. The composition of both the critical and main zone chills plot in the tholeiite field, although there is some evidence, based on the distribution coefficients for Al, that the magma from which the plagioclase-rich cumulates of the critical zone evolved had a high alumina content.

The chemistry of the parental magmas that gave rise to the lower, critical, and main zones will be discussed separately. It must be emphasized that the composition of the quenched liquids do not necessarily represent the true composition of the parental magma that differentiated and gave rise to the layered suite as it is now seen. Nevertheless, the recognition of these marginal facies is of importance in our understanding of the intrusion,

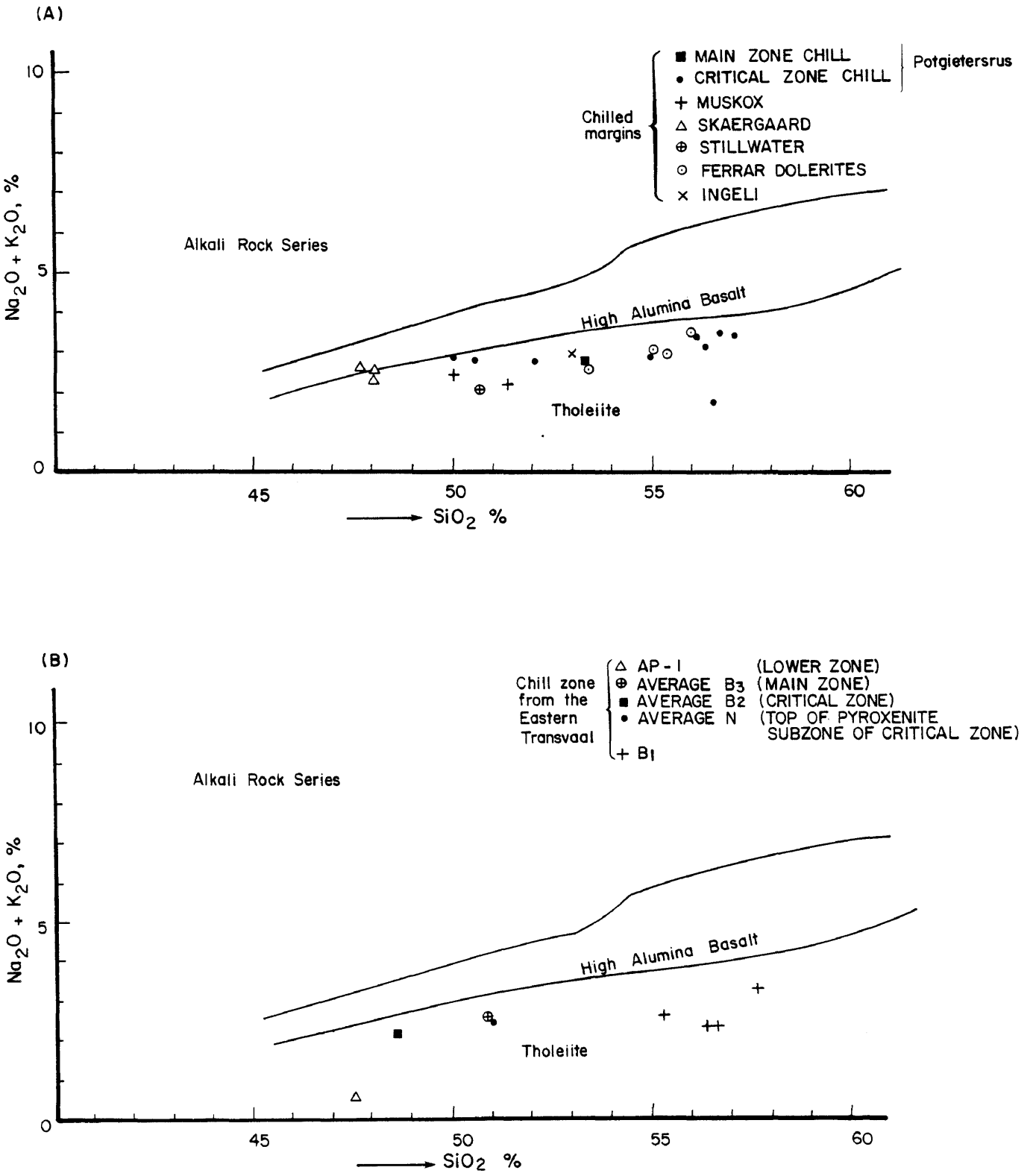

Fig. 61 Alkali-silica diagram for various initial magmas of

(A) the main and critical zone of the Potgietersrus limb, as well as for the Muskox, Skaergaard, Stillwater Intrusions and the Ferrar dolerites (Irvine, 1970) and the Ingeli Intrusion (Maske, 1966);

(B) the various chills or postulated initial magmas for the Bushveld Complex in the eastern Transvaal as reported by Sharpe, 1980.

as these, in conjunction with marked stratigraphic and textural discontinuities, provide us with the only convincing evidence that periodic new injections of magma played a major part in the evolution of the liquids from which the layered sequence crystallized.

6.3.1 Lower Zone

Many authors have speculated on the composition of the initial Bushveld magma from which the lower zone of the Complex crystallized. Hamilton (1977) proposed a high magnesium and silica saturated magma with a minimum of 22 per cent MgO and 53 per cent SiO_2. Vermaak (1976) also proposed a similar high MgO (approximately 30 per cent) magma for the lower zone. On the basis of the observed stratigraphic column for the lower zone, van der Merwe (1978) calculated that the parental magma to the lower zone at Potgietersrus contained 27,87 per cent MgO and 54,59 per cent SiO_2.

The most serious objection to any suggestion that the parental magma of this zone was ultramafic lies in the composition of the cumulus phases, particularly olivine, in the lower zone. Roeder and Emslie (1970) conducted experiments on several basaltic compositions over a temperature range of 1150 to 1300° C at oxygen fugacities of $10^{-0,68}$ to -12 atm. From the numerous analyses of early olivines and the coexisting glass, they related the partitioning of Fe^{2+} and Mg between the olivine and liquid by the distribution coefficient:

$$K_D = \frac{(X^{L}_{Mg} / X^{L}_{Fe^{2+}})}{(X^{ol}_{Mg} / X^{ol}_{Fe^{2+}})}$$

where $X_{Mg} = Mg/(Mg + Fe^{2+})$

$X_{Fe^{2+}} = 1 - X$

The experimentally determined equilibrium coefficient appears to be practically independent of temperature and pressure and is equal to 0,30 with a standard deviation of 0,03. Subsequent experimental work by Duke (1976) confirmed this $K_D^{ol\text{-}liq}{}_{Mg\text{-}Fe^{2+}}$ to be 0,30 with a standard deviation of 0,04. Numerous other studies have confirmed that the value of the $K_D^{ol\text{-}liq}{}_{Mg\text{-}Fe^{2+}}$ is in the range 0,30 to 0,36, i.e. Walker et al. (1976); Roeder (1974); Bender et al. (1978); Le Roex et al (1981); Irvine (1976); Longhi

and Walker (1975); O'Hara et al. (1975). Therefore, if one uses the method of computing the bulk composition of this zone by employing the lower zone stratigraphic column as was done, e.g. by Cameron (1978), a bulk composition of 31,72 per cent MgO is obtained. The Mg* of such a parental liquid would be 0,855. A primitive magma with such a high MgO content would have precipitated olivines with a Mg* of 0,966, based on a $K_D^{ol\text{-}lig}_{Mg\text{-}Fe^{2+}}$ of 0,30. Cameron's(1978) analyses however show that the lower zone olivines have a Mg* that ranges from 0,848 to 0,872, with a mean value of 0,865; which indicates that the olivines crystallized from a magma with a Mg* that ranged from 0,63 to 0,67. Therefore, a ultramafic parental magma to the lower zone must be ruled out.

Recently, a most unusual spinifex textured ultramfic rock was recognized by the author from the Aapiesdoorndraai ultramafic body in the eastern Bushveld. This spinifex-textured rock (AP-1) contains 31,27 per cent MgO and 7,53 per cent FeO. The olivine is skeletal as well as dendritic and constitutes about 40 per cent of the volume of the rock. The rock also contains chromite with a Mg* that ranges from 0,283 to 0,347 and a Al_2O_3 content that ranges from 16,74 to 22,17 per cent. The Mg* of the olivine, orthopyroxene and clinopyroxene are 0,850; 0,855 and 0,877 respectively (Table 6B). The rock is characterized by abundant blebs of sulfides with the highest pentlandite to pyrrhotite ratio of all known sulfide occurrences from the Bushveld Complex (Liebenberg, 1970) which suggests that this rock crystallized from a primitive parent. The rock furthermore has an initial $^{87}Sr/^{86}Sr$ ratio of 0,70423 which is the lowest ratio obtained for Bushveld rocks so far.

A comparison of the composition of this rock with harrisitic rocks from Rhum (Donaldson, 1977) shows them to be chemically different (Table 6A). It is, however, very similar in composition to ultramafic sillsin the floor of the Bushveld Complex on the farms Zwakwater and Wimbledon (Table 6A). This similarity in composition to ultramafic sills, the texture, the primitive nature of the sulfides and the low initial $^{87}Sr/^{86}Sr$ isotopic ratio strongly suggests the presence of an ultramafic magma in early Bushveld times, yet the $K_D^{ol\text{-}lig}_{Mg\text{-}Fe^{2+}}$ relationship dictates that olivines with a Mg* of 0,96-0,97 should have crystallized from such a magma. This is approximately 0,10 units higher than the average value for the

Table 6A CHEMICAL ANALYSES OF ULTRAMAFIC ROCKS FROM THE EASTERN BUSHVELD AND RHUM

	(1)	(2)	(3)	(4)	(5)	(6)
	AP-1	CO-174	326-327			
SiO_2	45,05	45,07	44,81	42,75	42,48	42,36
TiO_2	0,14	0,16	0,11	0,62	0,25	1,03
Al_2O_3	5,18	4,26	4,64	9,01	14,78	8,70
Fe_2O_3	1,64*			1,51	2,05	3,16
FeO	7,53	11,98	8,08	11,59	8,44	9,13
MnO	0,14	0,18	0,14	0,23	0,17	0,21
MgO	31,27	32,92	31,87	22,03	18,56	23,72
CaO	3,01	2,36	2,93	7,21	8,79	6,41
Na_2O	0,42	0,74	0,34	1,14	1,23	1,26
K_2O	0,19	0,67	0,32	0,19	0,08	0,16
P_2O_5	0,03	0,02	0,03	0,06	0,02	0,06
Cr_2O_3	0,83	0,74	0,85			
NiO	0,22	0,25	0,26			
L.O.I.	3,53	0,12	5,59			

1) Aapiesdoorndraai **
2) Zwakwater, ultramafic sill bulk composition**
3) Wimbledon, ultramafic sill **
4) Peridotite variety of harrisite, Rhum ***
5) Olivine-eucrite variety of harrisite, Rhum ***
6) Peridotite variety of harrisite; Rhum***

* calculated
** New analysis, M. Sharpe
*** Donaldson, 1977.

Table 6B MICROPROBE ANALYSES OF MINERALS FROM THE AAPIESDORINGDRAAI SPINIFEX TEXTURED PERIDOTITE

	(1)	(2)	(3)	(4)	(5)	(6)	(7)
SiO_2	40,45	53,57				53,54	55,69
Al_2O_3	0,28	29,30	16,74	22,17	16,24	2,42	1,53
TiO_2	0,10		2,27	0,36	2,49	0,44	0,27
MgO	44,23		5,93	7,19	6,05	17,57	30,60
FeO*	13,90	0,08	26,62	24,04	26,67	4,67	9,23
Fe_2O_3			5,52	2,93	7,55		
MnO	0,23		0,49	0,49	0,49	0,18	0,28
Cr_2O_3	0,14		40,98	41,90	39,50	0,89	0,55
NiO	0,52					0,20	0,22
CaO	0,24	11,54				20,30	1,42
Na_2O	0,04	4,39				0,04	0,07
K_2O	0,05	0,12				0,44	0,05
Total	100,23	99,04	98,56	99,08	98,99	100,69	99,91
$Mg/(Mg+Fe^{2+})$	0,8501		0,2839	0,3473	0,2870	0,8705	0,8551
$Ca/(Ca+Na+K)$		0,5875					
$Cr/(Fe^{2+}+Fe^{3+})$			1,22	1,48	1,14		

1) Olivine
2) Plagioclase
3) Chromite in olivine
4) Chromite in plagioclase
5) Chromite in ortho= pyroxene
6) Clinopyroxene
7) Orthopyroxene

* FeO = total Fe as FeO

Analyses by L. Hulbert

lower zone olivines and 0,09 units higher than the highest values reported for the layered sequence. It must therefore be concluded from mineralogical and thermodynamic data that, although evidence for the presence of ultramafic liquid(s) exist, Sharpe and Hulbert, 1982, these could not have been parental to the lower zone.

The texture of AP-1 probably represents crescumulate growth of olivine. The rock is unique and important in that it represents the first occurrence of olivine crescumulates in the Bushveld Complex. These rocks together with the other ultramafic sills constitute the strongest evidence for the presence of an ultramafic magma in early Bushveld times (Sharpe and Hulbert, 1982) although such a magma could not have contributed in any large measure to the origin of the lower zone.

The question now arises as to which marginal rock type of the layered sequence could be the parental magma from which the lower zone crystallized. The contact relationships of the lower, critical, and main zone with the floor in the eastern Bushveld have been studied in detail by Sharpe in recent years (1980, 1981, and 1982B). He recognized a variety of different marginal rocks, representative samples of which were subsequently used by Cawthorn et al. (1979) in a variety of melting experiments. On the basis of these experiments they suggested two candidates as being possible representatives of the parental magma. The first, their sample number 1, is a fine-grained orthopyroxenite sill with a composition of 53,37; 8,08; 2,02; and 15,41 per cent SiO_2, FeO, Fe_2O_3, and MgO respectively and 1280 ppm Cr. This liquid with a Mg* of 0,773 would be in equilibrium with olivine with a Mg* of 0,935; which is considerably higher than the highest value of 0,872 from the lower zone of the eastern Bushveld Complex (Cameron, 1978). Melting of this sample at 3kb revealed the following crystallization sequence (Cawthorn et al., 1979):

T°C	Mineral Assemblage
1350	L
1325	(ol), L
1300	ol, (opx), L
1250	ol, opx, L
1200	ol, opx, sp, L
1166	ol, opx, (cpx) sp, L
1120	ol, opx, cpx, plag, L

The bracket indicates trace equantities

On the basis of the $K_D^{ol\text{-}lig}_{Mg\text{-}Fe^{2+}}$ relationship and the incorrect crystallization order, in that cpx appears before plagioclase, this rock is an unlikely representative of the parental liquid to the lower zone.

The second candidate proposed by Cawthorn et al., their sample #4 is a quenched textured, fine-grained sill, characterized by long orthopyroxene blades arranged in sheaves, and a few hopper olivines. This unusual type of sill was first identified by Sharpe (1978) in the Eastern and Western Transvaal as well as near the Vredefort Dome. This sample contains 55,70; 12,74; 7,17; 12,44 per cent SiO_2, Al_2O_3, FeO, and MgO respectively and 970 ppm Cr. This proposed parental magma would be in equilibrium with olivine with a Mg* of 0,929 if a $K_D^{ol\text{-}lig}_{Mg\text{-}Fe^{2+}}$ of 0,30 is used.

The crystallization order determined experimentally by Cawthorn et al. (1979) for this sample is:

T°C	Mineral Assemblage
1350	L
1325	L
1300	(ol), L
1250	opx, L
1200	opx, L
1166	opx (plag), L
1150	opx, plag, cpx, L
1120	opx, plag, cpx, (sp) L

As mentioned earlier, chromite would crystallize from a melt of this composition at 1250° C if the fo_2 was greater than $10^{-9,2}$ atm. Also, pressure controlled melting of this sample revealed that, at 1300° C, the ol + L assemblage is only stable at pressures less than 4kb, whereas above this pressure the stable assemblage is opx + L. A similar relationship exists for sample #1 at 1325° C. at a pressure of 5kb, i.e. below 5kb ol + L is stable whereas above 5kb opx + L is the stable assemblage. Davies et al. (1980) also propose that Cawthorn's sample #4 is the parental liquid to the lower zone.

The author considers sample #4 to be the closest candidate proposed to date for the lower zone magma, even though the Mg* of olivines produced from such a magma are higher than those observed in the

lower zone layered sequence from the eastern Bushveld. The lowest portion of the layered suite of the Potgietersrus limb contains olivines as high as 0,900 in rocks with less than 1 per cent chromite, and rocks with olivines that have a higher Mg* may be developed in the unexposed deeper succession closer to the feeder of the essentially funnel-shaped intrusions.

By employing distribution coefficients an attempt can be made to obtain some indication of the composition of the parent magma(s) that gave rise to the layered suite in the Potgietersrus area. From the electron probe analysis of lower zone olivines, the Mg* was calculated to range from 0,900 to 0,845 with olivines from near the base having the higher values and those from the top the lowest values (Table 7). The magma from which these olivines crystallized must therefore have had Mg* ranging from 0,736 to 0,627.

From the Mg* of the cumulus olivine the weight per cent MgO necessary in the parent magma was calculated, with the aid of data and Figure 7 in Roeder and Emslie (1970), to be on average 9,91 and 11,97 per cent MgO at 1250 and 1300° C respectively. Comparison of the compositions of the Potgietersrus lower zone olivine and chromite with those from the Kilauea and Makaopuhi eruptions in Hawaii (Evans and Wright, 1972) reveal that the range and mean values of the Mg* of the olivines and chromites is very similar, especially those from Kilauea (Table 8). Even the modal chromite content in these rocks are very much alike, and thus allows comparison of the MgO content of the respective magmas. Ejected pumice samples from Kilauea quenched at 1225° C from a melt that contained 10,2 per cent MgO. The lower temperatures and less magnesian nature of the Makaopuhi magma yielded correspondingly less magnesian olivines (Table 8). This leads to the conclusion that the inferred MgO content of 9,91 per cent and a temperature of 1250° C probably is a close approximation of the actual MgO content and crystallization temperature of the lower zone magma.

TABLE 7 CALCULATED MgO CONTENT OF THE PARENTAL LOWER ZONE LIQUID, AT VARIOUS STRATIGRAPHIC HORIZONS, SOUTH OF POTGIETERSRUS

Sample #	Modal % CHROMITE	$\frac{Mg}{(Mg+Fe^{2+})}$ Olivine	Wt. % MgO @ 1250°C	Wt. % MgO @ 1300°C	Wt % Cr_2O_3 in Chromite	Relative STRATIGRAPHIC LEVEL
3-2395	1,63	0,845	9,55	11,50	43,24	TOP OF LOWER ZONE
3-2485	2,05	0,879	10,00	12,05	39,78	
3-2500	0,64	0,870	9,85	11,90	37,70	
3-3027	1,99	0,879	10,00	12,05	39,38	
3-3766	2,99	0,879	10,00	12,05	33,85	
3-3819	trace	0,872	9,85	11,90	39,27	
3-4002	1,13	0,879	10,00	12,05	39,17	
1-50	3,80	0,890	10,10	12,20	40,35	UPPER CHROMITE LAYER
1-80,5	1,85	0,873	9,85	11,90	41,49	
GV-1	1,12	0,896	10,18	12,25	42,52	LOWER CHROMITE LAYER
1-219	2,00	0,861	9,65	11,75	32,36	
1-223	3,91	0,867	9,75	11,85	38,24	
1-240,9	3,10	0,850	9,60	11,55	35,23	
1-244	1,21	0,865	9,70	11,80	40,12	
1-253,5	1,61	0,870	9,85	11,90	48,35	
6A-259	0,92	0,879	10,00	12,05	37,61	
6A-296,7	1,14	0,883	10,05	12,10	40,84	
X-10	2,28	0,879	10,00	12,05	39,44	
X-21	1,66	0,871	9,85	11,90	47,18	
X-31	0,95	0,895	10,18	12,25	42,07	
A-3	0,55	0,899	10,10	12,20	42,35	
A-9	1,15	0,853	9,65	11,70	40,09	
A-16	0,75	0,900	10,13	12,40	42,48 ←	LOWEST OBSERVED STRAT. LEVEL OF THE LOWER ZONE

TABLE 8 COMPARISON OF MINERAL AND MELT (MgO) COMPOSITIONS FROM THE LOWER ZONE AT POTGIETERSRUS WITH KILAUEA AND MAKAOPUHI VOLCANICS, HAWAII (EVANS AND WRIGHT, 1972)

Locality		Potgietersrus LOWER ZONE	Kilauea Iki (1959)	Makaopuhi (1965)
Olivine:				
$\frac{Mg}{(Mg+Fe^{2+})}$	RANGE	0,900 - 0,845	0,880 - 0,840	0,846 - 0,816
$\frac{Mg}{(Mg+Fe^{2+})}$	MEAN	0,875	0,863	0,840
Chromite:				
Wt. % Cr_2O_3	RANGE	48,3 - 32,3	40 - 60	35 - 43
Wt. % Cr_2O_3	MEAN	40,17	43	38
Volume %		1,67	1,2	1,5
Weight % MgO in liquid at given temperature		9,91% @ 1250°C	10,2 quenching temp = 1225°C	8,3% (bulk) quenching temp = 1205°C - 1170°C
Type of material		harzburgite & olivine pyroxenites	glass (majority of samples are ejected pumice)	ejected pumice & lava quenched in water

It was calculated that the lower zone magma had a Cr_2O_3 content that ranged from 0,06 to 0,09 per cent (Chapter 5.2.5.2). From the composition of the chromite and the Mg* of the associated olivine in the lowermost sample in the stratigraphy (A-16), the composition of the liquid from which this sample crystallized is inferred to have contained 12,40; 9,67; 0,058 per cent MgO, Al_2O_3, and Cr_2O_3 respectively at 1300° C. The Cr_2O_3 content of the melt was calculated from a $D^{ol\text{-}liq}_{Cr_2O_3} \approx 0,85$ given by Huebner et al (1976) whereas the Al_2O_3 content was calculated for $D^{sp\text{-}liq}_{Al}$ of 1,80 (Fisk and Bence, 1980). The Cr_2O_3 can also be calculated by using the Cr_2O_3 content of the the orthopyroxene and a $D^{opx\text{-}liq}_{Cr_2O_3}$ of 6,8 at 1300° C and a fo_2 of $10^{-5,5}$ atm. A Cr_2O_3 content of 0,44 per cent in the orthopyroxene from sample A-16 yields a value of 0,064 per cent Cr_2O_3 in the magma which

agrees well with the previous calculations of 0,058 (0,06) per cent Cr_2O_3.

The Ni content of the melt from which the lowest cumulates in the investigated sequence crystallized, was calculated as being 232 ppm based on D_{Ni}^{ol-liq} of 124/MgO-0,9 (Hart and Davis, 1978), for a melt with 12,40 per cent MgO and a NiO content of 0,27 per cent for the olivine from this horizon.

Although the above calculations place some constraints on the composition of the parental magma of the lower zone at Potgietersrus, it must be stressed that the evidence at hand suggests that at least one major influx of magma took place, during crystallization of the lower zone. This influx is postulated to have taken place immediately prior to the crystallization of the Drummondlea Harzburgite-Chromitite subzone. It is however possible that several smaller influxes into the system took place from time to time. The numerous small reversals in compositional trends of the minerals with increasing stratigraphic height in the study area, as well as the consistancies and gradual reversals in the composition of orthopyroxene and olivine in the entire lower zone and parts of the critical zone in the eastern portion of the Bushveld Complex (Cameron, 1977, 1978, 1980) suggests that new magma was continuously being introduced into the magma chamber during the better part of the evolution of the lower and critical zones.

6.3.2 Critical Zone

The magma that was emplaced prior to the onset of crystallization of the critical zone is envisaged to have been a normal tholeiitic basalt (sample 78-53). It is considered to have been emplaced along the top of the lower zone cumulate pile displacing, the less dense and still more magnesian residual lower zone liquid. As this new magma transgressed the lower zone cumulates and intruded cooler Pretoria Group sedments it quenched against the contact to give rise to the M.Mb./P.G. Where this magma was in contact with the lower zone it mixed with the residual magma and subsequently undercooled and thus a thin envelope of fine-grained rocks (M.Mb./L.Z.) developed. Whole rock major and trace element analyses of the rock types within this marginal member are given in Appendix 8.

Most of the samples from the M.Mb./P.G. are high in silica due to contamination from the Pretoria Group sediments, however the composition of sample 78-53 is believed to represent most closely the composition of this new influx. It is interesting to note that this sample has a composition almost identical to a fine-grained marginal rock considered by Sharpe (1980, p. 40, no. 11) to represent the composition of a major new influx before onset of crystallization of the anorthositic subzone of the critical zone in the eastern Bushveld. Sample 78-53 in the Potgietersrus area was found to be very weakly olivine normative, to have a Mg* of 0,60, Cr and Ni content of 396 and 184 ppm respectively, a Rb/Sr ratio of 0,056 and a Zr/Y ratio of 1,57. The effect of contamination by the country rock arenites can be seen by comparing the Zr/Y ratios of the contaminated samples GR1-88,48 to 109,50 with that of 78-53 (Appendix 8). This affect can also be seen in the Rb/Sr ratio. Noteworthy is also the variation of the S content of these marginal rocks. The uncontaminated fine-grained marginal rock (78-53) contains 90 ppm S compared to other M.Mb./P.G. samples in which the S content ranges from 10 to 900 ppm S. It is believed that extraneous S from the arenites has contaminated the rocks.

Roeder and Emslie (1970) calculated that the $K_D^{\text{opx-liq}}_{\text{Mg-Fe}^{2+}} = 0,23$ based on the reaction:
$Mg^{2+}(opx) + Fe^{2+}(liq) \rightleftharpoons Mg^{2+}(liq) + Fe^{2+}(opx)$. Therefore using a K_D value of 0,23 it was calculated that the initial liquid with a Mg* of 0,60 could give rise to cumulates containing orthopyroxene with a Mg* of 0,872 whereas a $K_D^{\text{ol-liq}}_{\text{Mg-Fe}^{2+}} = 0,30$ dictates the olivines crystallizing from such a liquid have a Mg* of 0,832. This magma therefore contains sufficient MgO to give rise to the cumulates of the critical zone, but the olivine cumulates of the lower zone could not have crystallized from it.

After crystallization of the M.Mb./P.G. this new injection of more dense and cooler magma gradually mixed with the residual lower zone liquid, and as a result of blending of these two contrasting melts, undercooling occurred to give rise to a fairly fine-grained pigeonite gabbronorite (M.Mb./L.Z.) more magnesian (higher Mg* for the Ca-poor pyroxene) than the initial influx (78-53). It is furthermore considered that blending of the two liquids lowered the solubility of S in the residual liquid and

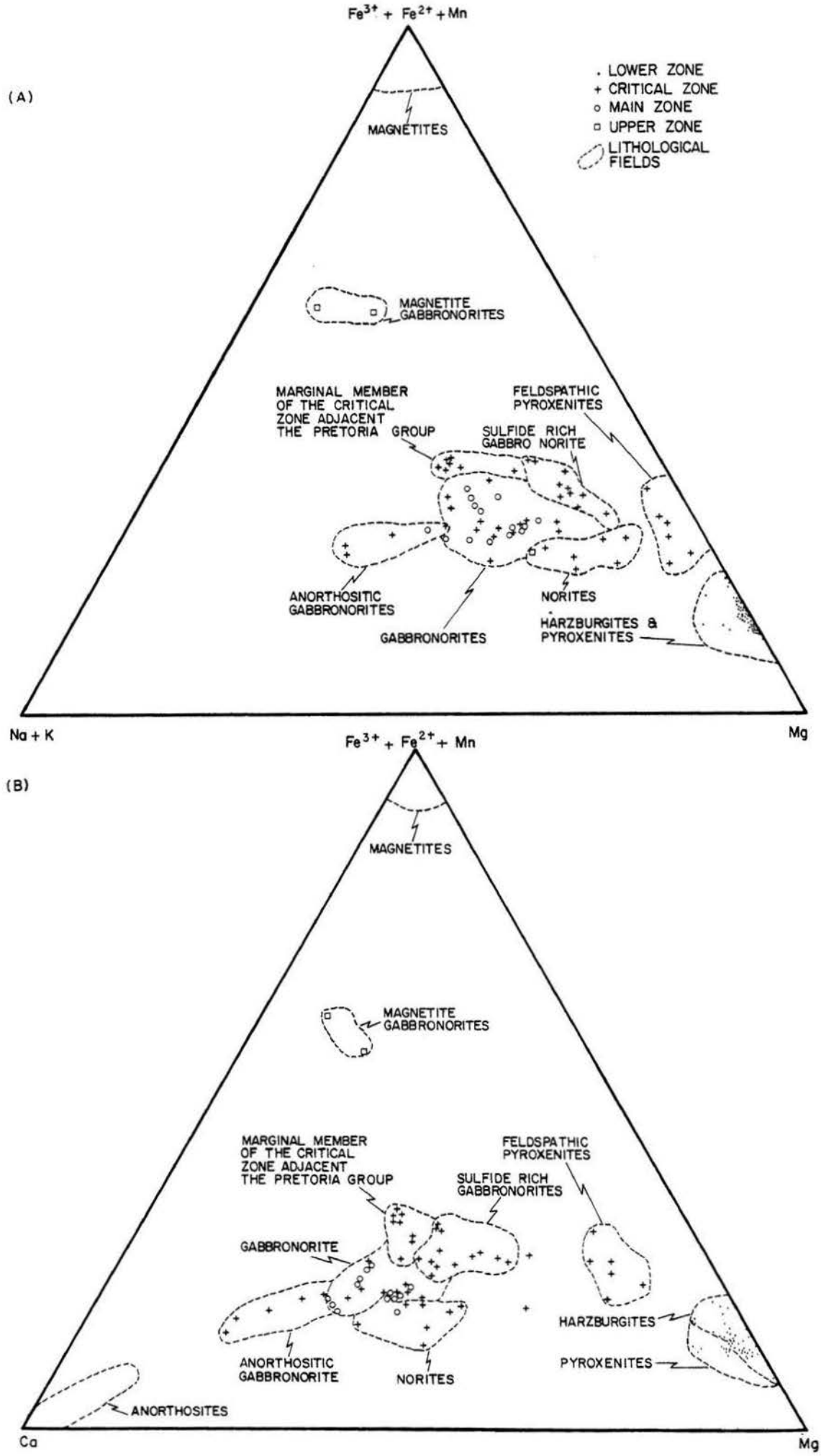

Fig. 62 Cation plot of rocks from the Potgietersrus limb of the Bushveld Complex, south of Potgietersrus in terms of (A) $Fe^{3+}+Fe^{2+}+Mn$: Na+K : Mg and (B) $Fe^{3+}+Fe^{2+}+Mn$: Ca : Mg

caused the separation of immiscible sulfide liquid during crystallization of the gabbronorite. Emplacement of new magma seems to have taken place in a number of successive pulses, which resulted in a cyclic pattern of sulfide separation during crystallization of fine-grained gabbronorites. This feature will be dealt with in more detail in Chapter 8.

6.3.3 Main Zone

The postulated composition of the magma emplaced prior to crystallization of the main zone (Appendix 8, sample 78-92) differs from the previous magma in that it is more aluminous, calcic and magnesian. The rock has a Mg* of 0,71, contains 317 ppm Cr, 128 ppm Ni, 23 ppm Cu and 90 ppm S. Sharpe (1980) also found that the equivalent fine-grained marginal rock in the eastern Bushveld to have a higher Mg* and lower Ni and Cr content than the critical zone equivalent.

Emplacement of this magma and mixing with the residual liquid in the chamber gave rise to the succession of gabbronorites in the main zone up to the inferred level of the pyroxenite marker. These rocks have Mg* that range from 0,75 to 0,62. From this level to the top of the upper zone the Mg* systematically decreases from a value of 0,70 to 0,61. All these main zone gabbronorites have a fairly uniform composition (Fig. 60) and it is considered that the average composition of these gabbronorites is fairly close to that of the magma from which they crystallized.

6.3.4 Origin of the Initial Magmas

It is generally accepted that basaltic magmas result from partial melting of peridotitic upper mantle, and the diversity in basaltic magmas is related to varying degrees of partial melting of different peridotite compositions under different conditions of pressure and temperature as well as volatile content.

MacGregor (1969) found from experiments conducted in the system MgO-SiO_2-TiO_2 that the TiO_2 content of partial melts increases with increasing pressure, suggesting a qualitative analogy in nature that the TiO_2 content of basaltic magmas is indicative of the

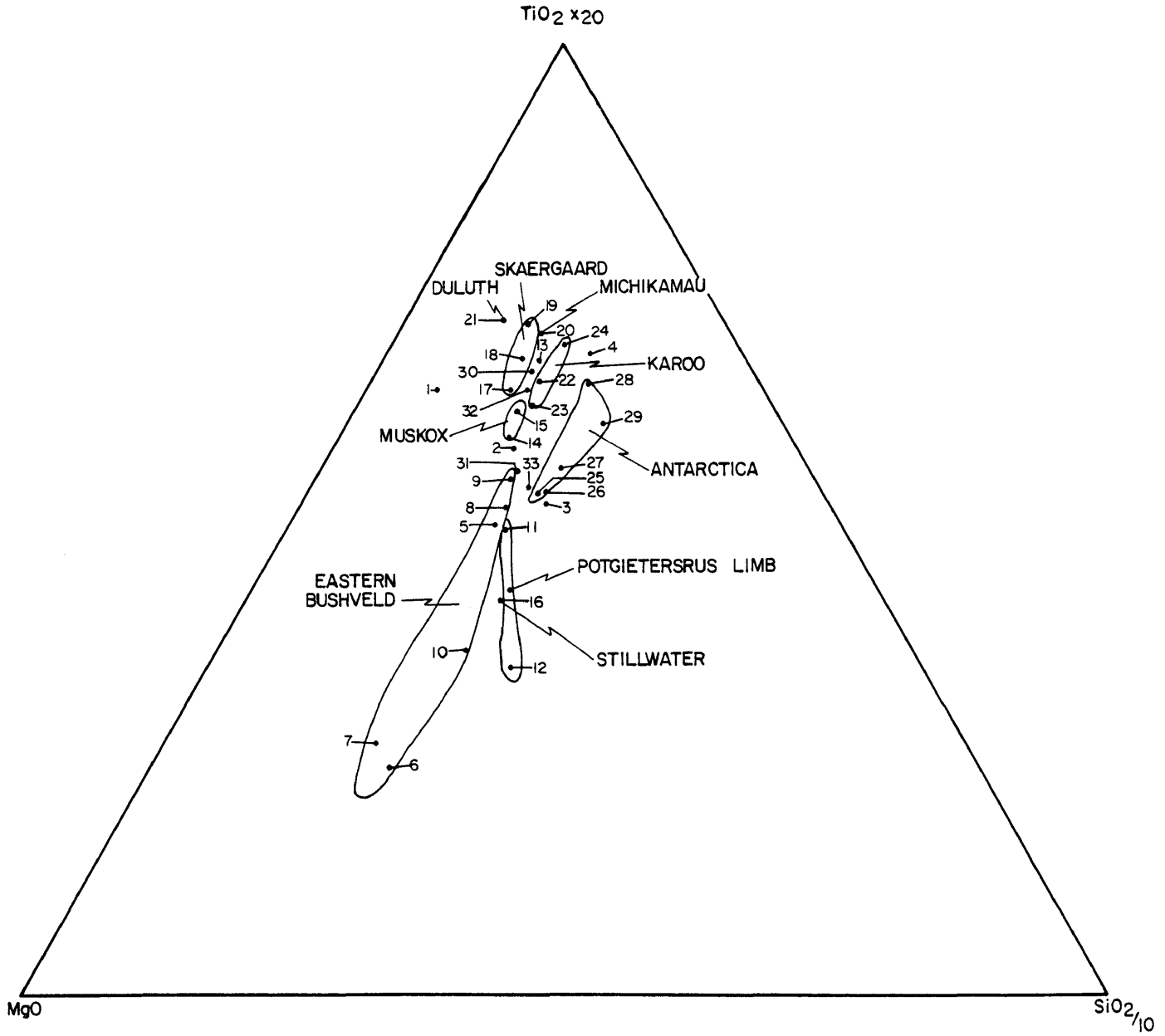

1) VENTERSDORP LAVAS (0.96) - SHARPE, 1980
2) MACHADODORP VOLCANICS (0.88) - BUTTON, 1974
3) HEKPOORT VOLCANICS (0.65)
4) DULLSTROOM VOLCANICS (1.06)
5) PRE-BUSHVELD SILLS (0.72)
6) SYN-BUSHVELD SILLS (0.31)
7) AVERAGE BUSHVELD B_1 CHILL (0.36)
8) AVERAGE BUSHVELD N CHILL (0.68)
9) AVERAGE BUSHVELD B_2 CHILL (0.75)
10) AVERAGE BUSHVELD B_3 CHILL (0.45)

} SHARPE, 1980

11) 78-53 CRITICAL ZONE CHILL (0.62)
12) 78-92 MAIN ZONE CHILL (0.34)

} THIS STUDY

13) WATERBERG SILLS (1.25) - SHARPE, 1980
14) MX_1, MUSKOX CHILL (1.01)
15) MX_2, MUSKOX CHILL (1.11)
16) ST_1, STILLWATER CHILL (0.45)
17) SK_1, SKAERGAARD CHILL (1.17)
18) SK_2, SKAERGAARD CHILL (1.29)
19) SK_3, SKAERGAARD CHILL (1.51)

} IRVINE, 1970

20) MK, MICHIKAMAU CHILL (1.24) - BIGGAR, 1974
21) AUGITE-PORPHYRITIC BASALT FLOW (1.93) POSSIBLE PARENTAL MAGMA TO DULUTH COMPLEX (WEIBLEN & MOREY, 1980)
22) INGELI CHILL (1.1)
23) AVERAGE KAROO DOLERITE (1.0)

} MASKE, 1966

24) CHILLED MARGIN, HENQUEST TYPE KAROO SILL (1.18), WALKER & POLDERUARDT, 1949
25) F_1 CHILLED DIABASE, FERRAR (0.67)
26) F_2 DOLERITES, ANTARCTICA (0.66)
27) F_3 DOLERITES, ANTARCTICA (0.70)
28) F_4 DOLERITES, ANTARCTICA (0.87)
29) F_5 DOLERITES, ANTARCTICA (0.72)

} IRVINE, 1970

30) CHILLED DIABASE - PALISADE SILL (1.21) WALKER, 1969A
31) LOW TiO_2 Q-NORMATIVE LATE TRIASSIC DIABASE (0.76), EAST NORTH AMERICA WEIGAND & RAGLAND, 1970
32) HIGH TiO_2 Q-NORMATIVE LATE TRIASSIC DIABASE (1.12), EAST NORTH AMERICA WEIGAND & RAGLAND, 1970
33) CHILLED DIABASE - GREAT LAKE SHEET, TASMANIA (0.70), McDOUGAL, 1964

( ) = Wt. % TiO_2

Fig. 63 TiO_2-MgO-SiO_2 plot of postulated initial magma compositions for for various stratiform intrusions.

depth of origin. By using this line of reasoning, postulated parental liquids of the Bushveld Complex as well as other intrusions were plotted on a SiO_2, TiO_2, MgO diagram (Fig. 63) in order to evaluate the usefulness of TiO_2 as an indicator of the depth of origin of these parental magmas. Apart from defining distinctive fields for the postulated initial liquids of the various intrusions it also suggests that the initial magmas of the Skaergaard, Duluth, Karoo, and Michikamau were derived from higher pressure regimes in the mantle than those of the Muskox, Bushveld, and Ferrar dolerites of Anarctica. The titanium enrichment in the parental magmas to stratiform anorthositic intrusions (Duluth, Michikamau) tends to confirm the belief that these magmas are generated under high pressure conditions. It is also of interest that petrologically similar stratiform intrusions like the Bushveld Complex and the Stillwater Intrusion plot in TiO_2 depleted regions of the diagram. The Ferrar dolerites with which the stratiform Dufek Intrusion is associated also occupies a field close to the Bushveld - Stillwater region of Figure 63.

The mean composition of the Ventersdorp, Machadodorp, Hekpoort, and Dullstroom volcanics have also been plotted to illustrate the variation in the TiO_2 content of these magmas and to demonstrate that the comparatively low TiO_2 content of the postulated Bushveld magmas is not controlled by regional constraints in the TiO_2 content of the source region.

The higher TiO_2 content of the critical zone chill (#11, Fig. 63) suggests that the magma was derived from deeper levels in the mantle than the magma from which the main zone chill crystallized (#12, Fig. 63). The two chills also differ in that the initial $^{87}Sr/^{86}Sr$ ratio of the main zone is higher (0,70598). Presuming that both magmas were derived from approximately the same source locality or position in the earths mantle, one would speculate that the more primitive critical zone sample was derived from a deeper zone within the mantle.

A somewhat similar situation occurs with respect to Sharpe's (1980) eastern Bushveld samples. The marginal rocks "N" and "B_2" (8 and 9 respectively, Fig. 63) of the upper critical zone have high TiO_2

values whereas his "B_3" main zone chill (#10) plots in the more TiO_2 depleted portion of the Bushveld field. Note the similarity of the TiO_2 content of the main zone sample #10 of the eastern Bushveld and #12 from the Potgietersrus area and how close the marginal rocks of the critical zone, samples #8 and #11 plot together.

The abnormally low TiO_2 content of samples 6 and 7 in Figure 63 are difficult to evaluate, and, the low TiO_2 content could possibly be due to a higher degree of partial melting and resulting dilution of TiO_2 values in these magnesium-rich samples.

Since the postulated B_2 and B_3 magmas (Sharpe, 1980) are very similar to the chills adjacent to the critical and main zone from Potgietersrus with respect to their TiO_2 and major element chemistry, as well as structural setting, it is felt that any genetic interpretation put forward for the eastern Bushveld compartment should also apply to the Potgietersrus compartment. Unpublished REE data of the respective marginal rocks of the eastern Bushveld (Sharpe, unpublished data) (Fig. 64) show that the three basic magma types of Sharpe are all enriched in light REE in the order $B_1 > B_2 > B_3$, yet the envelopes for the middle and heavy rare earth elements tend to overlap with the absolute abundance in the order $B_2 > B_1 > B_3$. Although the B_1, B_2, and B_3 trends are enriched in light rare earths and show unfractionated slopes, additional information on the genesis of the various magma types can be obtained from these trends.

Analyses of the rocks confined to the B_1 envelope belong to a unique type of magma that is rich in SiO_2 and MgO and, on a world wide scale it is volumetrically rather insignificant with respect to other magma types. Outside the Bushveld, the closest analogue to these rocks are what Cameron et al. (1979) refer to as Boninites. The B_1 magma is characterized by having the greatest absolute abundance and enrichment in LREE. Sharpe (personal communication) suggests that it is a primary melt and that the REE pattern reflects that of the mantle source. Seeing that the fractional crystallization of olivine, orthopyroxene, clinopyroxene, garnet and plagioclase in ultramafic and mafic melts are not able to significantly alter the light REE pattern, it must be inherent of a melt derived from a particular source.

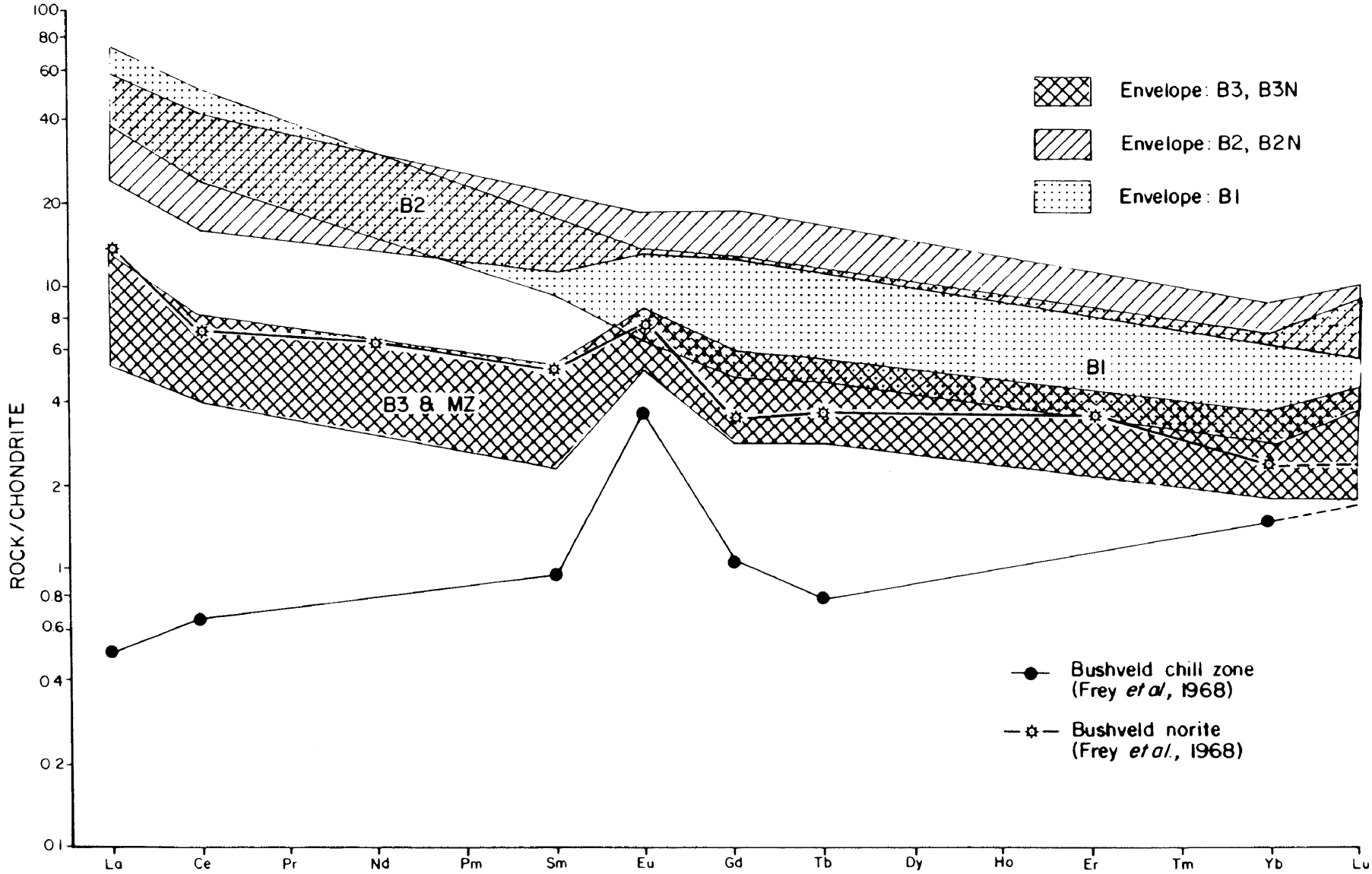

Fig. 64 Chondrite normalized plot of rare earth element data from B1, B2, and B3 initial magmas in the eastern portion of the Bushveld Complex (unpublished data kindly provided by M.R. Sharpe).

Since continued or repeated melting of the same mantle source to form basalts leads to relative depletion of the LREE compared to the middle and heavy REE, the evolving mantle which gave rise to successive melts should become depleted in the LREE. It is envisaged that the early B_1 melt represents a partial melt of a parental peridotite source in the upper mantle. Twenty-eight per cent partial melting of pyrolite in the stability field of spinel peridotite under anhydrous conditions at 10kb pressure will yield an olivine tholeiite with 12 per cent normative olivine and 50 weight per cent SiO_2 (Jaques and Green, 1980). However, if the same amount of melting of pyrolite occurred at 10 kb under water saturated conditions, a siliceous ($\approx$56 per cent SiO_2) magnesian tholeiite will evolve (Jaques and Green, 1980). It is envisaged that segregation of the melt and upward migration through the upper mantle could cause depletion of the mantle, in the immediate surroundings of the melt, in LREE. Subsequently B_2 melting of pyrolite still in the stability field of spinel peridotite, yet at a higher level of the upper mantle, would give rise to melts depleted in LREE if the previously ascending B_1melts scavanged this portion of the mantle in LREE. A similar interpretation of the LREE for the B_3 magma is assumed, yet generation of this magma is inferred to have taken place at higher levels in the upper mantle. This is indicated amongst others by the presence of the Eu anomaly in the B_3 suite of rocks which suggests generation of this melt in lower pressure regimes where plagioclase peridotite is stable.

This therefore substantiates the previous suggestion, based on the low TiO_2 contents, that the main zone melt was derived from a lower pressure regime than the critical zone magma.

6.4 Differentiation within a Lower Zone Cyclic Unit

Since cumulate members within a cyclic unit define solidus trends, plus 30-40 per cent intercumulus liquid, the composition of the cumulate is dictated by the liquidus path during the course of differentiation, it may prove useful to examine the whole rock chemical variation within a cyclic unit to see how it compares with the differentiation trends established from the mineral chemistry. In order to facilitate such a comparison, the 53 metre thick cyclic unit #21 was chosen (Fig. 65B). A liquid that would produce the observed crystallization order in cyclic

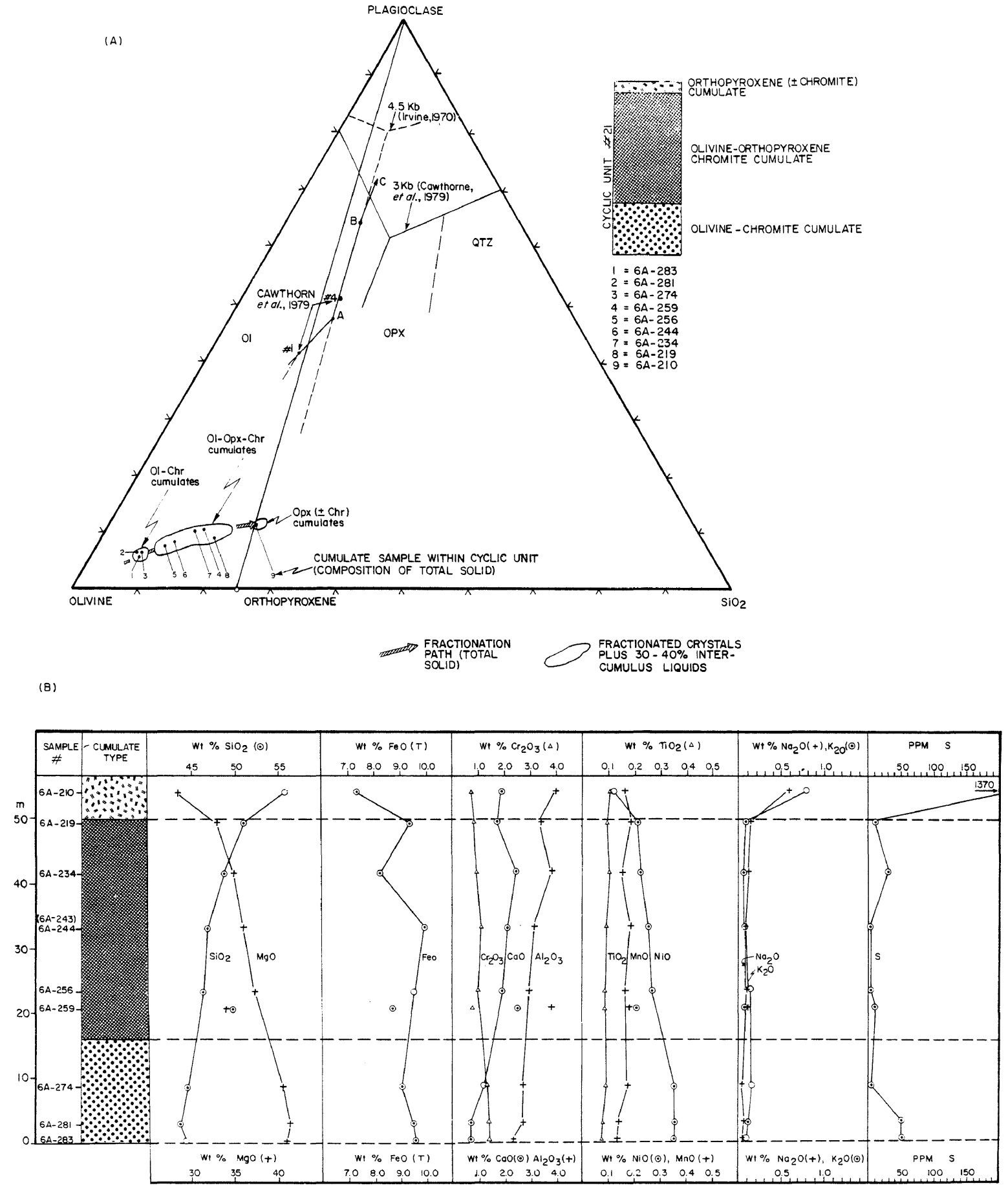

Fig. 65 (A) Pseudoternary system olivine-plagioclase-SiO_2 (after Irvine, 1970), illustrating the postulated liquidus and solidus path of the melt from which cyclic unit 21 crystallized. Solidus compositions represent recalculated normative mineral proportions. (B) Columnar section of cyclic unit 21 showing vertical compositional variations in the constituting rock types.

unit #21 would have a composition close to #1 in the ol-plag-SiO_2 system (Fig. 65A), a composition very similar to Cawthorn et al's. (1979) sample #1.

The melt contributing cumulus crystals to the olivine-chromite cumulate member at the base of cyclic unit 21 is situated within the olivine volume at the position designated #1 (Cawthorn et al's., sample 1). Crystallization of olivine (+/- chromite) could produce the ol-chr cumulates and with continued fractional crystallization the liquid would migrate from point 1 to A giving rise to the observed cumulates 1, 2, and 3 (Fig. 65A). Further crystallization along curve AB would produce the ol-opx (±chr) cumulates 4, 5, 6, 7, and 8. With continued fractionation the liquid will leave the reaction curve and change in composition along BC with precipitation of opx cumulates similar to sample 9. The plagioclase boundary was, however, never reached during crystallization of the lower zone, as processes such as convective overturn or new magma injection brought fresh magma into the zone of crystallization. As a result of this the composition of the crystallizing liquid returned to the olivine field and crystallization of the olivine cumulate at the base of the following cyclic unit commenced.

Within cyclic unit 21, MgO, FeO, Cr_2O_3 and NiO decrease systematically whereas SiO_2, Al_2O_3, and CaO increase with differentiation (Fig. 65B). Na_2O and K_2O remain fairly constant throughout the lower two members but increase in the opx cumulate by a factor of 6 to 8. Sulfur behaves differently to any other element in that it decreases from 50 ppm near the base of the cycle to less than 10 ppm throughout the ol-chr and ol-opx-chr cumulate and then increases again to a value of 1370 ppm in the opx cumulate near the top of the unit. The trace elements Co, V, Zr, and Y increase fairly systematically from the base to the top of this cyclic unit (Appendix 8).

It is evident from the above that cumulate rock types show differentiation trends that agree closely with those inferred on the basis of microprobe analyses (Fig. 36). In fact, the trends shown by the major and, to a lesser extent, the trace elements are better defined and in certain respects more informative than those based on the mineral analyses.

An intriguing question is how much parent liquid was required to give rise to the 53 m of cumulates in cyclic unit #21. This question can be approached by using the Rayleigh fractionation law for trace element abundances in the solid phases:

$$\frac{C_{Tr}}{C^{\circ}_{Tr}} = (F)^{D-1}$$

where C°_{Tr} = initial concentration
C_{Tr} = final concentration
F = fraction of liquid remaining
D = partition coefficient
(Wood and Fraser, 1976).

If the NiO content of the olivine at the base of cyclic unit 21 and at the top of the ol-opx-chr member is known an idea of the amount of parent magma involved to produce these two members of the unit can be obtained. Unfortunately, only the olivines within the ol-opx-chr cumulates were analysed, but they can be of some use in calculating the amount of magma from which they crystallized. The two samples used (6A-259 and 6A-243) are approximately 13 m apart, are barren of sulfides (10 ppm S) and contain approximately equal amounts of olivine and orthopyroxene. Employing a $D^{ol\text{-}liq}_{Ni} = 9,1$ and an initial concentration of 0,22 per cent NiO in olivine (6A-259) and a final concentration of 0,16 per cent NiO (6A-243) it was calculated that 3,84 per cent of the parental magma would have had to fractionate, if the cumulate had consisted entirely of olivine. Seeing that about 50 per cent of the cumulate is orthopyroxene, which contains about half as much Ni as olivine and a correspondingly lower partition coefficient, the amount of crystallization would easily decrease to about 2,9 per cent for this 13 m interval.

6.5 Computer Modelled Differentiation Trends

"Determination of the original composition of the parental magmas of layered intrusions formed by cumulus processes is notoriously difficult due to the lateral transgression, contamination and other factors" (Jackson, 1971, p. 130). Such a calculation is even further complicated by intermittent influxes of new magma of unknown composition and volume that mixes with the residual magma in the chamber. An excellent example of this problem is seen in the Ingeli Intrusion in the Northern Transkei (Maske, 1966) which is extremely well exposed and has been studied

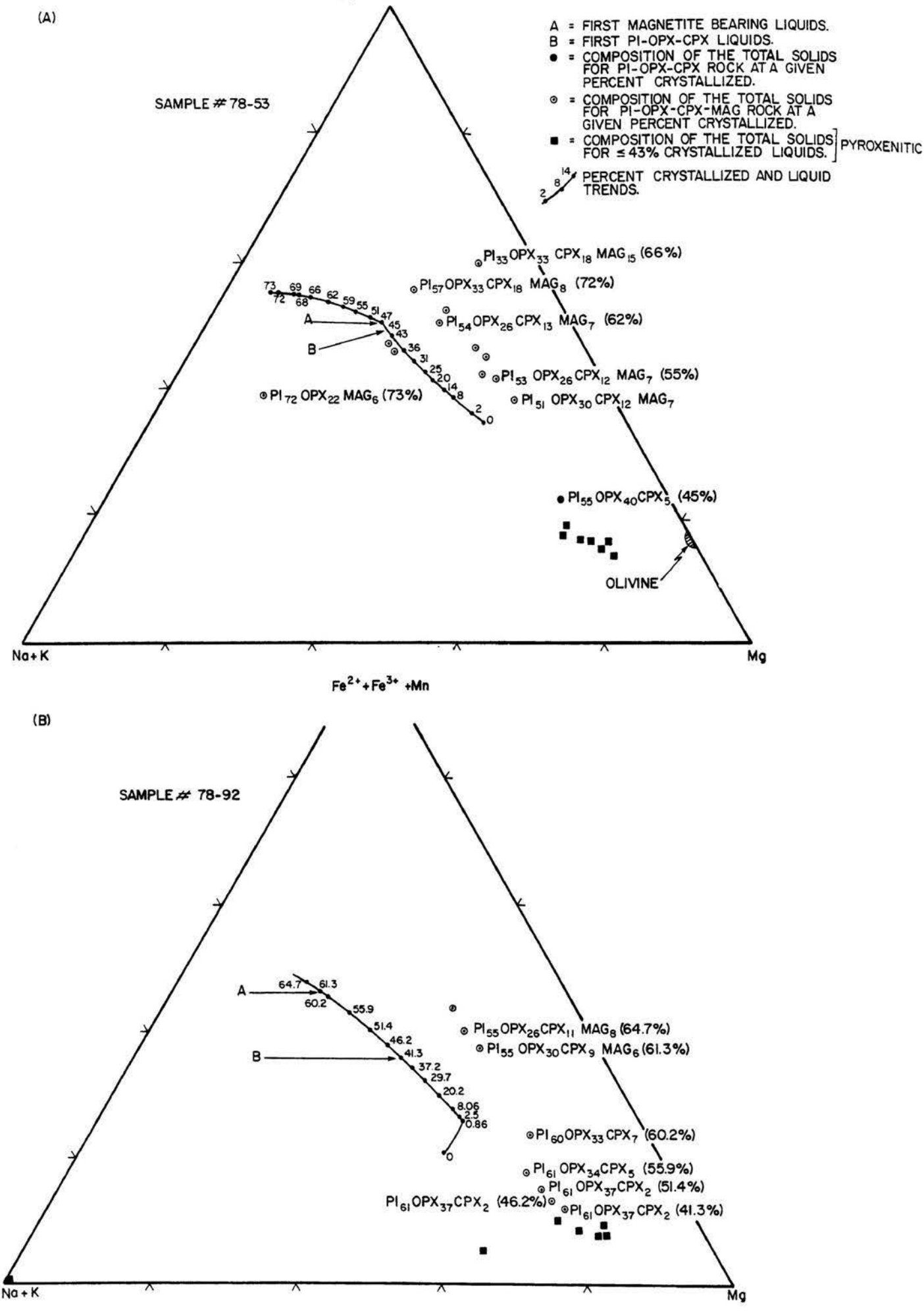

Fig. 66 Cation plot of computer modelled differentiation trends for the postulated initial liquid of (A) the critical zone (78-53) and (B) main zone (78-92) from the southern portion of the Potgietersrus limb of the Bushveld Complex.

in detail. The chilled margin of this intrusion contains 52,9; 9,1; and 6,9 per cent SiO_2, FeO, and MgO respectively, yet the bulk composition of the intrusion is 49,2; 7,1; and 13,3 per cent SiO_2, FeO, and MgO respectively. Evidently, a major discrepancy exists between the bulk and the initial compositions of this intrusion. From this it must be concluded that the chilled margins of intrusions only provide an indication of the chemical and mineralogical character of the initial magma, as the composition of the magma may change due to subsequent mixing of magmas. Such mixing has definitely been the case in the Potgietersrus limb as is indicated by comparing the cyclic nature of the fine-grained rocks of the M.Mb./L.Z. and the uncontaminated chilled rocks of the M.Mb./P.G.

Although the bulk and initial compositions may differ, the initial composition may be most informative regarding the course that such a magma should follow during fractionation. This was determined for the postulated initial critical and main zone magmas, as deduced from the respective chills, and a computer modelled fractionation program by Nathan and van Kirk (1978). This program traces the liquid line of the descent and the possible rock sequences produced by fractionation of the respective magmas. The computer based model simulates closed system fractional crystallization at one atmosphere pressure. The model is meant only to be an aid to a better understanding of the sequence of minerals produced, and their respective compositions, upon fractional crystallization of a magma with a particular initial composition. The model is not meant to reproduce the cumulate stratigraphy within a given zone, but instead, it should simulate the sequence of cumulus minerals and the composition of the total solids and the liquid that evolves with fractional crystallization.

The two initial compositions fractionated with the aid of this program are 78-53 and 78-92 which represent the postulated initial magmas of the critical and main zones (Fig. 66). A surprising feature of the simulated fractionation is that the first differentiate from sample 78-92 (main zone) is plagioclase as is shown by the composition of the total solids (Fig. 66B) in the Na + K corner. The next assemblage to crystallize consists virtually solely of clinopyroxene, which is subsequently followed by ortho-

pyroxene. Continued fractionation of this magma sees the introduction of magnetite after 64,7 per cent crystallization of the initial liquid. This simulated crystallization order coincides with the observed cumulate sequence for the main zone, viz pl, pl-cpx, pl-cpx-opx. The lack of clinopyroxenite cumulates in the main zone as predicted by the 41,3 per cent crystallization products has yet to be resolved.

7 INTENSIVE PARAMETERS OF THE MAGMA(S)

The Rustenburg Layered Suite south of Potgietersrus contains a variety of mineral assemblages that are suited to estimate the intensive parameters of the magma from which these minerals crystallized. On the basis of textural and chemical data it is assumed, except where stated to the contrary, that the coexisting minerals crystallized together from the magma and that they are in equilibrium.

By employing the composition of coexisting phases, the best available thermodynamic data and the appropriate crystalline solution models, the following equilibria reactions can be used to calculate the indicated intensive parameters of the magma:

$Mg_2Si_2O_6$ opx			$\rightleftharpoons$	$Mg_2Si_2O_6$ cpx			(T)
$CaAl_2SiO_6$ cpx	+	SiO_2 melt	$\rightleftharpoons$	$CaAl_2Si_2O_8$ plag			(T-P-$a^{melt}_{SiO_2}$)
Mg_2SiO_4 ol	+	SiO_2 melt	$\rightleftharpoons$	$Mg_2Si_2O_6$ opx			(T-P-$a^{melt}_{SiO_2}$)
$1/3Fe_3O_4$ spinel	+	SiO_2 melt	$\rightleftharpoons$	$FeSiO_3$ opx	+	$1/6\ O_2$ gas	(T-P-$a^{melt}_{SiO_2}$)
$3FeSiO_3$ opx	+	Fe_3O_4 spinel	$\rightleftharpoons$	$3Fe_2SiO_4$ ol	+	$1/2\ O_2$ gas	(T-P-fo_2)
$6Fe_2TiO_4$ titanium-spinel	+	O_2 gas	$\rightleftharpoons$	$2Fe_3O_4$ spinel	+	$6FeTiO_3$ ilmenite	(T-fo_2)

An attempt was made to derive acceptable values from the various methods by employing all available crystalline solution models, and by comparing the calculated parameters with the results of recent experiments on systems with similar phases.

Because of the present re-evaluation of crystallization processes in cumulates, the viscosity and density of the initial magmas of the main and critical zones were also calculated in an effort to determine whether the cumulates of these two zones originated by crystal settling or by crystallization in place.

7.1 Pressure

Compelling petrological evidence is now at hand which shows that the layered rocks of the Bushveld Complex crystallized under relatively high pressure. This was first recognized by Atkins (1969) who used thermodynamic considerations to show that the Bushveld magma crystallized at significantly higher pressures than the

Skaergaard Intrusion. In order to account for the difference in $K_D^{cpx-opx}_{Mg-Fe^{2+}}$ of the two intrusions he calculated that the pressure difference, at constant temperature, was about 5,75 kb. Similarily, Cawthorn (1977) found that the only acceptable way of explaining the observed pyroxene relationships in the Bushveld with the aid of the system Forsterite-Diopside-Quartz, was to assume a pressure of greater than 5kb during crystallization of liquids crystallizing cumulus clinopyroxene. In addition, he also pointed out that the spectacular metamorphic mineral assemblages in the floor, i.e. cordierite-garnet, together with either biotite, quartz, sillimanite or orthopyroxene, as described by Humphrey (1910); Hall (1932); Liebenberg (1942) and Vermaak (1970), suggest relatively high pressures during the evolution of the Bushveld magma.

Due to the need of placing constraints on the operative pressure during the crystallization of the layered suite an investigation of the mineral assemblages in the metamorphic aureole of the Eastern Transvaal was initiated (Hulbert and Sharpe, 1981; Hulbert and Sharpe, research in progress). It is beyond the scope of this treatise to discuss all the findings of these investigations and only those results pertinent to the pressure calculations will briefly be presented here.

The rocks within the aureole and included xenoliths range in metamorphic grade from the albite-epidote hornfels facies to sanidinite hornfels facies. The high-grade metamorphic mineral assemblages are developed in rocks of the northeastern metamorphic aureole (X on Fig. 67A). These rocks appear schistose to hornfelsic and have previously attracted the attention of Hall (1908) and Harker (1932). At locality X in Fig. 67A the stable assemblage staurolite-plagioclase-andalusite-garnet-biotite, which marks the iso-reaction grad where chloritoid breaks down to staurolite and garnet, is developed. This mineral assemblage is ideally suited for determining temperature and pressure conditions during metamorphism. Ghent (1976) formulated the following pressure dependent expression:

$$0 = \frac{-2817,2}{T} + 7,4351 - \frac{0,2678(P-1)}{T} + \log a^{gt}_{gross} - 3 \log a^{plag}_{An}$$

from the reaction:

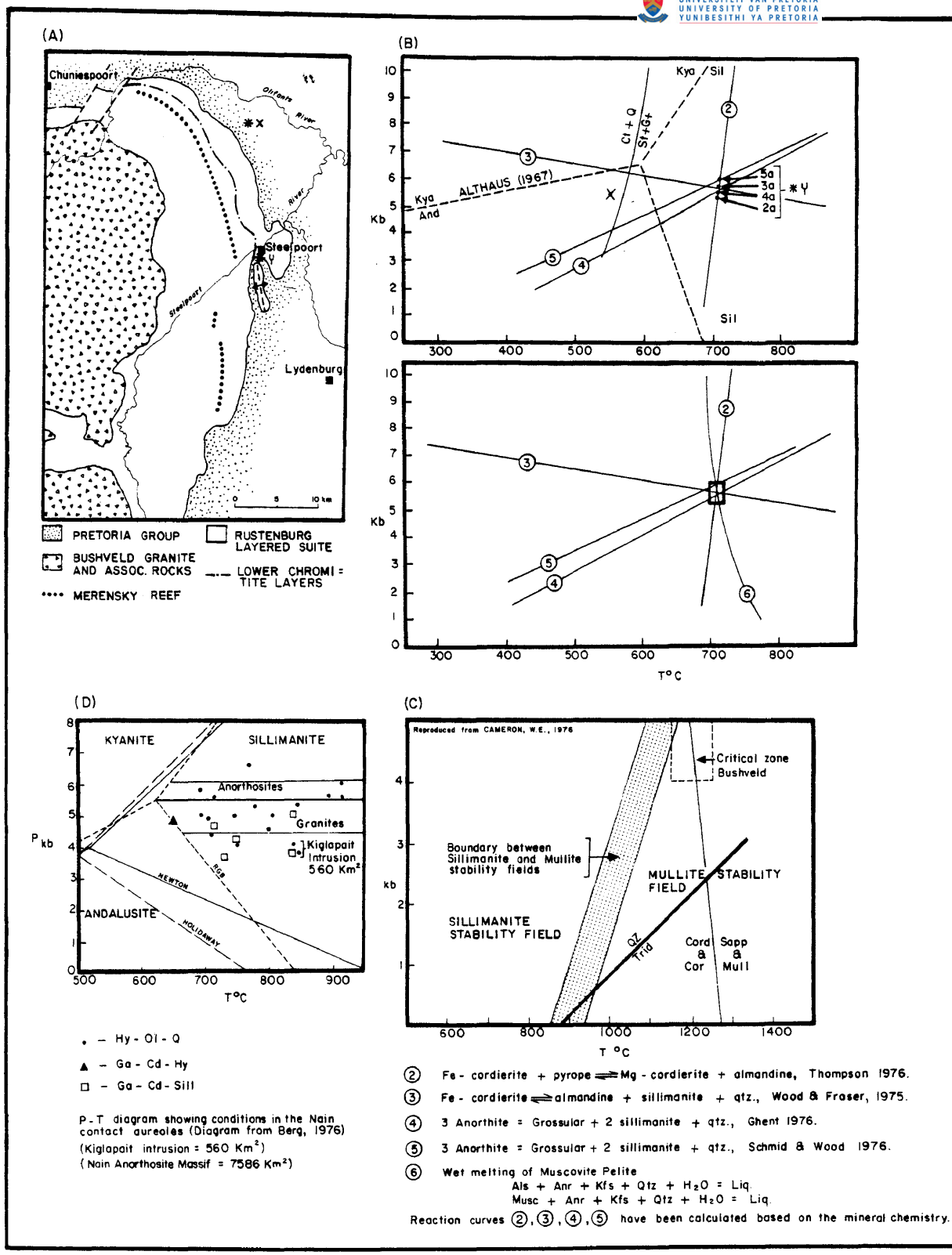

Fig. 67 Pressure-temperature conditions within the Bushveld thermal aureole.

(A) locality of the two study areas X and Y
(B) Conditions for the formation of the metamorphic assemblage of locality X and Y
(C) conditions for the formation of sanidinite facies hornfels xenolith within the middle group chromitite layers
(D) P-T conditions in the contact aureole of the Nain Anorthosite Massif.

3 Anorthite $\rightleftarrows$ Grossular + 2 Andalusite + Quartz and

where $a^{plag}_{An} = X^{plag}_{An} \cdot \gamma$

$a^{gt}_{gross} = X^{gt}_{gross} \cdot \gamma$

P = bars

T = °K

By substituting in this equation results of mineral analyses from the area (Table 9) an operative pressure of 5288 bars was obtained at a temperature of 549°C. The temperature calculation is based on the partitioning of Fe-Mg between coexisting garnet and biotite (Ferry and Spear, 1978).

Spectacular examples of biotite-garnet-cordierite-sillimanite-plagioclase hornfels are developed within the sillimanite zone (locality Y, Fig. 67A). Here the products of the reaction:

$$3Fe_2Al_4Si_5O_{18} \rightleftarrows 2Fe_3Al_2Si_3O_{12} + 4Al_2SiO_5 + 5SiO_2$$
cordierite — garnet — sillimanite — quartz

are developed, which can be equated to P-T conditions by employing the equation:

$$\Delta G° = -RT \ln \left(\frac{a^{gt^2}_{Fe_3Al_2Si_3O_{12}} \cdot a^{sill^4}_{Al_2SiO_5} \cdot a^{qtz^5}_{SiO_2}}{a^{cord^3}_{Fe_2Al_4Si_5O_{18}}} \right)$$

of Wood and Fraser (1976) where

$$\Delta G° = \Delta H_{1\ bar} - T\Delta S° + (P-1)\Delta V°$$

$$\Delta G° = 38250 - T(26,2) + (P-1)\Delta V°$$

$$-RT \ln \frac{(a^{gt}_{alman})^2}{(a^{cord}_{Fe\text{-}cord})^3} = 38250 - T(26,2) + (P-1)\Delta V°$$

A temperature of 709°C was calculated for this locality with the aid of the geothermometer of Ferry and Spear (1978). This temperature, in conjunction with the mineral compositions in Table 9, yield a total pressure of 5494 bars according to the above pressure dependent reaction. This value was verified by employing the equation:

$$\ln \left(\frac{X^{gt}_{gross} \cdot \gamma^{gt}_{gross}}{X^{plag}_{An} \cdot \gamma^{plag}_{An}} \right) = \frac{5123}{T} - 16,02 + 0,6565\frac{(P-1)}{T},$$

which gave a pressure of 5472 bars. This method was formulated by Schmid and Wood (1976) and is based on the partitioning of Ca between garnet and plagioclase in the reaction:

$$3CaAl_2Si_2O_8 \rightleftarrows Ca_3Al_2Si_3O_{12} + 2Al_2SiO_5 + SiO_2$$
plagioclase — garnet — sillimanite — quartz

TABLE 9 REPRESENTATIVE ELECTRON MICROPROBE ANALYSES OF METAMORPHIC MINERALS FROM THE BUSHVELD AUREOLE.

	Locality 4D					Locality 7					
	Bt-4	Gt-4	Cd-4	Pl-4	Mu-4	Gt-7	Bt-7	Pl-7	Mu-7	St-7	And-7
SiO_2	35,48	36,17	48,53	46,48	45,84	36,49	33,58	56,59	46,19	27,67	37,33
Al_2O_3	17,89	22,09	32,81	34,74	35,06	21,42	20,48	27,69	34,81	55,55	62,64
TiO_2	2,75	0,16	0,15		0,16	0,18	1,90		0,50	0,57	0,13
MgO	10,59	4,58	8,20		0,49	1,93	6,75		0,50	1,09	
FeO*	19,04	33,22	8,42	0,26	0,91	38,19	22,46	0,11	0,83	14,92	0,29
MnO	0,13	1,37	0,26		0,16	0,34	0,07		0,09	0,18	
NiO											
CaO	0,07	2,53	0,07	17,68	0,05	2,23	0,12	9,83	0,05		
Na_2O	0,23		0,21	1,32	1,04		0,23	5,82	1,05		
K_2O	9,44		0,07	0,08	10,20		9,44	0,06	10,17		
Cr	0,25	0,20									
Total	95,87	100,32	98,72	100,56	93,91	100,78	95,03	100,10	94,19	99,98	100,39
$\frac{Mg}{Mg+Fe}$	0,497	0,197	0,634			0,082	0,348			0,115	
$\frac{Ca}{Ca+Na+K}$				0,880				0,483			

* total Fe as FeO

Bt = biotite

Gt = garnet

Cd = cordierite

Pl = plagioclase

Mu = muscovite

St = staurolite

And= andalusite

Locality 4D = *Y,

Locality 7 = *X,

An additional, yet less accurate, indication of the pressure can be obtained by employing the method of Thompson (1976B), which is based on the partitioning of Mg-Fe between cordierite and garnet in the exchange reaction:

$$3(\underset{\text{Fe-cord}}{Fe_2Al_4Si_5O_{18}}) + 2(\underset{\text{pyrope}}{Mg_3Al_2Si_3O_{12}}) \rightleftharpoons 3(\underset{\text{Mg-cord}}{Mg_2Al_4Si_5O_{18}}) + 2(\underset{\text{almandine}}{Fe_3Al_2Si_3O_{12}})$$

Although this reaction and the associated equation:

$$\Delta G^\circ = -33428 + 12{,}09T - 0{,}1814(P-1) + 6RT \ln \left(\frac{X_{Fe}^{gt} \cdot X_{Mg}^{cord}}{X_{Fe}^{cord} \cdot X_{Mg}^{gt}}\right)$$

is usually used to calculate the temperature at a given or assumed pressure, it is used here to calculate the pressure. In such pressure calculations the estimated temperature must be very accurate, as this reaction is very sensitive to changes in pressure with slight changes in temperature (Fig. 67B, reaction curve 2). From the above equation a pressure of 5111 bars is indicated at 709°C.

From all available calculations the mean total pressure operative at locality Y was 5484 ±400 bars. The error bracket is well within the limits ascribed to each method. The correctness of these calculations is substantiated by a P-T plot of the above exchange reactions (Fig. 67B) which shows that the observed metamorphic mineral assemblage at locality Y has a very restricted stability field at the intersection of the various reaction curves.

Well developed leucosomes in the rocks at locality Y place a further constraint on the prevailing P and T conditions during metamorphism. This is deduced from the position of the melting curve for muscovite pelite (curve 6, Fig. 67B) which intersects the regime of the calculated P-T conditions.

Also shown in Fig. 67B is the experimentally determined chloritoid + quartz $\rightleftharpoons$ staurolite + garnet reaction curve (Hoschek, 1969), as well as the calculated P-T conditions for locality X. The calculated temperature is only 15° lower than the experimental value.

Cameron (1976) studied a spectacular metamorphic assemblage in inclusions of a sedimentary origin at the level of the middle group chromitite layers in the critical zone of the eastern Bushveld. The assemblage consists of Mg-cordierite, mullite, corundum, Al-spinel, plagioclase and sapphirine. Based on the relevant phase

equilibria, Cameron estimated the P-T bracket for the metamorphic rocks to lie between 1150 to 1250°C and 4,0 to 5,0 kb respectively (Fig. 67C). If a pressure of 4,5 kb for this horizon is assumed, the operative pressure at the base of the lower zone could easily have been 5,1 kb.

Berg (1977) used a similar thermodynamic approach to calculate the P-T conditions during emplacement of the Kiglapait Intrusion and the Nain Anorthosite Massif (Fig. 67D). His calculations, for these mineralogically similar stratiform anorthosite complexes, gave values similar to those calculated for the Bushveld Complex.

The compositional range of the garnets in terms of pyrope, almandine, spessartine, and grossularite from locality X and Y are shown in Fig. 68A. It can be seen that the garnets from locality X are enriched in the almandine and to a certain extent spessartine + grossularite components compared to those from locality Y. Locality X samples fall in the compositional field similar to garnets in upper amphibolite facies rocks from the regional metamorphic terrane of the Front Range, Colarado (Gable and Sims, 1969). The somewhat higher pressure and temperature samples from locality Y fall within the compositional field of garnets from the granulite facies terrane of the Westport area of Ontario, Canada (Edwards and Hays, 1963). According to Fig. 68B the co-existing cordierite-garnet pairs plot well into the field of regional metamorphism as defined by Dallmeyer and Dodd (1971). The above deliberation leaves little doubt that the garnets from the thermal aureole of the eastern Bushveld formed under conditions of medium to high pressure, not unlike that of regional metamorphism.

In the Potgietersrus limb the spectacular metamorphic mineral assemblages are also indicative of relatively high pressures. This was first noted by Hall and Gardthausen (1911, p. 77) who described the presence of disthene (kyanite) in the "contact belt of the Bushveld Complex." Van Rooyen (1950) noted the occurrence of the high pressure metamorphic assemblage biotite-garnet-cordierite-sillimanite in hornfels from the metamorphic aureole about 7-8km north of Potgietersrus. Recently, Nel (personal communication) has calculated the operative pressure in the Potgietersrus thermal aureole at the level where the base of

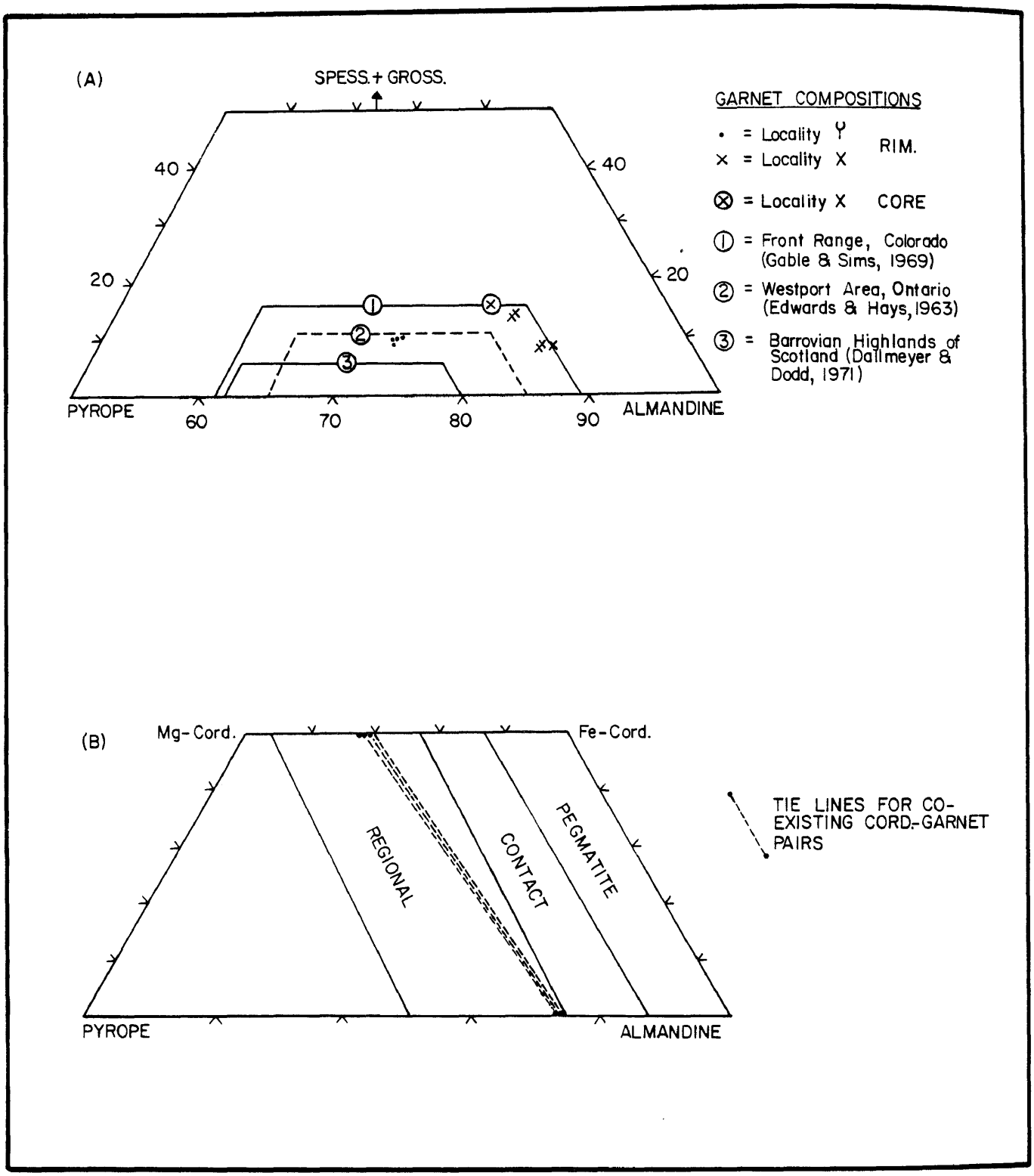

Fig. 68 (A) Compositional range of garnets from the Bushveld termal aureole. Note how the samples from locality X fall in the same compositional field as garnets from the upper amphibolite facies of the Front Range, Colorado; whereas those from locality Y occupy the same field as garnets from the granulite facies terraine of Westport, Ontario.
(B) Cordierite-garnet compositional plane of Dallmeyer and Dodd, 1971, showing the range of compositions of coexisting cordierite and garnet from different metamorphic environments and from the Bushveld thermal aureole.

the main zone is in contact with country rock sediments. Based on samples with suitable mineral assemblages from six different localities he calculated a mean pressure of 4,3 kb, with a range of 3,9 to 4,5 kb.

The presence of the large scale folding in the floor rocks south of Potgietersrus (Truter, 1947) also suggests that directed pressures were operative in these rocks prior to or during emplacement of the Bushveld rocks. This is of importance as the lithostatic pressure alone can under no circumstances account for the high mean calculated value of 4,3 kb. The maximum stratigraphic thickness of the adjacent main and upper zone rock is 2,1 km (van der Merwe, 1976) to which at the most a further 5 km thick succession of Rooiberg Felsite can be added. The lithostatic pressure would therefore, at the most, only account for slightly more than 2 kb pressure. The high pressure metamorphic mineral assemblage in the aureole of the Potgietersrus area and the Eastern Transvaal could therefore only have developed if the country rocks were subjected to stresses during emplacement and crystallization of the mafic rocks. Additional evidence for considerable tectonic stresses during the development of the Transvaal Basin and emplacement of the Bushveld Complex has been documented by Bastin (1968), Hunter (1975) as well as by Sharpe and Chadwick (1981).

7.2 Temperature

The goal of every petrological investigation, whether of igneous or metamorphic rocks, should be to establish the temperature of crystallization of the phases in the rock, as this knowledge is essential to draw sound petrogenetic conclusions. Accurate temperatures are also essential in the calculation of other intensive parameters, i.e. $^{a}SiO_2$, fo_2, fs_2 as most of the crystalline solution models used to calculate these parameters assume a precise knowledge of the prevailing temperature at the time of crystallization.

Both orthopyroxene and clinopyroxene coexist in rocks of the critical, main, and upper zones, and the temperatures of crystallization of these rocks can therefore be calculated according to the methods of Wood and Banno (1973) and of Wells (1977). These investigators have used the composition of coexisting orthopyroxene and clino-

pyroxene as a geothermometer, because these two pyroxenes are immiscible over a wide range of temperatures and compositions, and because the immisciblity gap is relatively unaffected by pressure (Davis and Boyd, 1966). The temperature dependent exchange reaction is:

$$\underset{\text{En-Di(opx)}_{ss}}{Mg_2Si_2O_6} \rightleftharpoons \underset{\text{Di-En(cpx)}_{ss}}{Mg_2Si_2O_6}$$

One of the assumptions made by Wood and Banno was that both orthopyroxene and clinopyroxene phases behave as ideal two site solutions of $CaMgSi_2O_6$ and $Mg_2Si_2O_6$ components, so that the relationship between activity and composition is:

$$a^{cpx}_{Mg_2Si_2O_6} = (X^{M2}_{Mg} \cdot X^{M1}_{Mg})\,cpx$$

$$a^{opx}_{Mg_2Si_2O_6} = (X^{M2}_{Mg} \cdot X^{M1}_{Mg})\,opx$$

and that at equilibrium conditions:

$$\Delta G^\circ_{P,T} = -RT \ln \left[\frac{a^{cpx}_{Mg_2Si_2O_6}}{a^{opx}_{Mg_2Si_2O_6}} \right]$$

Using the activity composition relationship and the experimental data of Davis and Boyd (1966), Wood and Banno (1973) formulated the component activities in terms of temperature and found that the data points plotted close to a straight line. A least squares fit of their data yielded the following relationship between activity ratio and temperature:

$$\ln \left(\frac{a^{cpx}_{Mg_2Si_2O_6}}{a^{opx}_{Mg_2Si_2O_6}} \right) = -\frac{\Delta H^\circ}{RT} + \frac{\Delta S^\circ}{R} = \frac{-10202}{T} + 5{,}35$$

where ΔH° and ΔS° refer to a standard state of the pure phases at 30kb pressure. These authors also found that addition of Fe^{2+} to a system crystallizing two pyroxenes markedly increases the solubility of the $Mg_2Si_2O_6$ and $Fe_2Si_2O_6$ components in the clinopyroxene phase and therefore substituted experimental data on more complex iron-rich systems into the above equation. By doing so they showed that temperature (T, °K) was related to the composition of the coexisting pyroxenes by the equation:

$$T = \frac{-10202}{\ln\left(\frac{a^{cpx}_{Mg_2Si_2O_6}}{a^{opx}_{Mg_2Si_2O_6}}\right) - 7{,}65\ (X^{opx}_{Fe}) + 3{,}88\ (X^{opx}_{Fe})^2 - 4{,}6}$$

They found that extrapolation of the data from 30kb to 1 bar results in a temperature change of less than 50°C. The authors also point out that when total iron in the pyroxene analyses is expressed at FeO, as for instance in microprobe analyses, 30°C should be added to the calculated values to account for the affects of Fe^{3+}.

Wells (1977) updated the Wood-Banno thermometer by incorporating considerably more experimental data on the diopside-enstatite miscibility gap, especially for more iron rich systems. By substituting new values of $\Delta H°$ and $\Delta S°$ he formulated the relationship between temperature and composition of coexisting pyroxenes as:

$$T = \frac{7341}{3{,}355 + 2{,}44\ (X^{opx}_{Fe}) - \ln K}$$

where K is the equilibrium constant. This new calibration gives greater consistency for the more iron-rich systems. Wells (1977) also showed that the pyroxenes with up to 12 per cent Al_2O_3 will not affect the ln K relationship and therefore will not significantly affect the temperature calculations.

The above two pyroxene geothermomenters were used to calculate equilibrium temperatures from all available chemically analysed pyroxene pairs in the Bushveld Complex. Analyses were obtained from Atkins (1969); Markgraaff (1976); Marais (1977); Buchanan et al. (1980); and Gain (1982). As pointed out by Wells (1977), the calculated Wood-Banno temperatures gave inconsistent results for the more iron-rich pyroxene pairs whereas consistent values were obtained for the more Mg-rich phases. Wells' (1977) geothermometer gave reasonably consistent results in the more iron-rich phases as well as for the pigeonite-clinopyroxene pairs, but the values of the more Mg-rich members were a bit lower than the Wood-Banno values. Since both methods are based on the same principles, the Wood-Banno (1973) geothermometer was used for pyroxene pairs in which the $Fe^{2+}/(Fe^{2+}+Mg)$ ratio of the Ca-poor pyroxenes was $\leq 0{,}25$ and the Wells' (1977) method for pyroxenes

pairs in which the ratio for Ca-poor pyroxene was ≧0,25.

The computed temperatures for the critical, main and upper zone of the study area are shown in Table 10, along with their respective activities of $Mg_2Si_2O_6$ and the $Fe^{2+}/(Fe^{2+}+Mg)$ values for the Ca-poor pyroxene (opx(Fe)). Apart from the Wood-Banno (2) and Wells (1) values listed, a third temperature calculation was employed for comparative purposes. This method was proposed by Buchanan (1976) and calculates the $a_{Mg_2Si_2O_6}$ in inverted pigeonite based on the composition of the matrix orthopyroxene, rather than on the bulk composition of the inverted pigeonite. This method gives temperature values of 40°C lower than those based on the bulk composition. For this reason Buchanan's modifiication is not favoured, although it does provide a lower temperature limit as bulk analyses of inverted pigeonites are often difficult to obtain with electron microprobe techniques.

The temperature calculations reveal that the lower portion of the upper zone crystallized over a temperature interval from 1022°C to 1063°C, whereas computed temperatures from the main zone range from 1013 to 1142°C. Higher temperatures of 1124 and 1207°C were obtained on pyroxene pairs from the critical zone. Unfortunately only one sample of lower zone rock from Potgietersrus contained both orthopyroxene and clinopyroxene for which bulk compositions could be obtained. This sample (3-2395) is from a harzburgite xenolith from the top of the lower zone at the -110 m level in the critical zone. The calculated temperatures obtained from this sample is 1201°C, which is very close to the value of 1204°C obtained by employing the Mg* of the orthopyroxene in conjunction with the method of Nathan and van Kirk (1978). The only other suitable lower zone type material is sample AP-1 from the eastern Bushveld which yielded a temperature of 1200°C.

The quenched samples from the M.Mb./P.G. gives temperatures between 1030°C and 917°C with a mean value of 972°C. The 113°C range in temperature and the low mean value is considered to be due to the effects of contamination of the magma with sedimentary material from the Pretoria Group. Temperatures calculated with the Fe-Ti oxide geothermometer of Buddington-Lindsley (1964) gave values similar to the two pyroxene method, thus confirming the low quenching temperatures of these rocks. Further evidence for the low equili-

Table: 10

CALCULATED EQUILIBRIUM TEMPERATURES FOR COEXISTING PYROXENES FROM THE GRASVALLY AREA BASED ON THE WOOD-BANNO GEOTHERMOMETER

	Sample No.	OPX(Fe)	$a^{CPX}_{Mg_2Si_2O_6}$	$a^{OPX}_{Mg_2Si_2O_6}$	T°C	
UPPER ZONE	5-124-1&-2	0,5419	0,0528	0,1896	989*	(1)
	5-124-1&-C	0,5310	0,0528	0,1667	1022	(1)
	5-233-1&-2	0,5284	0,0651	0,2024	1027*	(1)
	5-233-1&-C	0,5157	0,0651	0,1778	1063	(1)
MAIN ZONE	5-640-3A&-1	0,4443	0,0909	0,2704	1084	(1)
	5-640-3A&-C	0,4339	0,0909	0,2432	1116	(1)
	5-935-3A&-1	0,4294	0,0932	0,2885	1056*	(1)
	5-935-3A&-C	0,4196	0,0832	0,2541	1092	(1)
	78-127-1&-2	0,3450	0,0757	0,3927	1013	(1)
	78-125-A&-3	0,4451	0,0967	0,2637	1105*	(1)
	78-125-A&-C	0,4341	0,0967	0,2380	1138	(1)
	78-122-A&-2	0,4105	0,0940	0,2769	1107*	(1)
	78-122-A&-3	0,4226	0,0940	0,2481	1127	(1)
	78-350-1&-2	0,3907	0,0650	0,3306	993*	(1)
	78-350-1&-C	0,3849	0,0650	0,2899	1025	(1)
	78-192-1&-2	0,3517	0,1078	0,3780	1099*	(1)
	78-192-1&-C	0,3428	0,1078	0,3455	1127	(1)
	78-189-1&-2	0,3584	0,1009	0,3643	1088*	(1)
	78-189-1&-C	0,3489	0,1009	0,3391	1111	(1)
	78-207-1&-2	0,3087	0,1094	0,4280	1102	(1)
	78-76B-1&-2	0,3259	0,0860	0,4156	1039	(1)
	78-92-1&-2	0,3481	0,1113	0,3914	1100*	(1)
	78-92-1&-C	0,3398	0,1113	0,3390	1142	(1)
CRITICAL ZONE	78-145-1&-2	0,2997	0,1641	0,4576	1193	(1)
	78-481-1&-2	0,2337	0,0986	0,5427	1158	(2)
	GP3-241-1&-2	0,2609	0,1436	0,4906	1163	(1)
	78-365-1&-2	0,3047	0,1186	0,4226	1124	(1)
	78-403C1&C2	0,2229	0,0880	0,5493	1136	(2)
	78-404-1&-2	0,2411	0,0836	0,5159	1136	(2)
	78-413B1&B2	0,2263	0,1250	0,5426	1207	(2)
	78-431-1&-2	0,3118	0,0871	0,4249	1044	(1)
	3-2370-1&-2	0,2440	0,0721	0,5191	1108	(2)
	3-2395-1&-2	0,1590	0,1192	0,6044	1201	(2)
	3-2455-1&-2	0,2880	0,1328	0,4406	1152	(1)
	GR4-1-A&-B	0,2868	0,0601	0,4569	1101	(2)

	Sample No.	OPX(Fe)	a $Mg_2Si_2O_6$ CPX	a $Mg_2Si_2O_6$ OPX	T°C	
*** M.Mb L.Z.	GR4-3B-A&-B	0,2804	0,0638	0,4585	1110	(2)
	GR4-5-A&B	0,3265	0,0744	0,4118	1172	(2)
	GR4-5-A&C	0,3273	0,0744	0,3647	1192	(2)
	GR4-6-A&B	0,3174	0,0425	0,4126	1066	(2)
	GR1-44-1&-3	0,4143	0,0662	0,2674	1030	(1)
	GR1-69-1&-2	0,4312	0,0562	0,2953	967	(1)
	GR1-88,48-1&-2	0,4123	0,0672	0,3113	1002	(1)
	GR1-93,26-1&-2	0,4463	0,0615	0,2755	992	(1)
** M.Mb P.G.	GR1-97,89-1&-2	0,4494	0,0431	0,2714	923	(1)
	GR1-98,2-1&-2	0,4666	0,0519	0,2601	959	(1)
	GR1-100A&B	0,4223	0,0509	0,2952	951	(1)
	GR1-102,5A&B	0,4180	0,0518	0,3046	951	(1)
	GR1-105A&B	0,4309	0,0603	0,2921	983	(1)
	GR1-107,2A&B	0,3225	0,0659	0,4176	982	(1)
	GR1-109,5A&B	0,4264	0,0683	0,3005	1005	(1)
	78-374-1&-2	0,3409	0,0477	0,4049	917	(1)
	78-53-1&-2	0,3820	0,0585	0,3429	969	(1)
	78-72-1&-2	0,3402	0,1161	0,3910	1116	(1)
	AP -1&-2	0,1448	0,1226	0,6516	1200	(2)

** $\frac{M.Mb}{P.G.}$ = MARGINAL MEMBER OF CRITICAL ZONE ADJACENT THE PRETORIA GROUP

*** $\frac{M.Mb}{L.Z.}$ = MARGINAL MEMBER OF CRITICAL ZONE OVERLYING THE LOWER ZONE

If OPX(Fe) <,25 used (2)
If OPX(Fe) >,25 used (1)

(1) = Wells modification of the Wood-Banno thermometer

(2) = Wood-Banno thermometer

* = Buchanan Method for a $Mg_2Si_2O_6$ OPX

in inverted pigeonite (uses the composition of the matrix orthopyroxene only).

30°C has been added to the calculated temperature to compensate for Fe^{3+}

brium temperatures is the high $MnTiO_3$ (pyrophanite) component of the ilmenites in these rocks. The primary ilmenites contain between 1,34 and 4,66 per cent MnO with a mean value of 2,68 per cent. According to Haggerty (1967, Fig. Hg-41B) such high values indicate low temperatures of crystallization, and according to his diagram 2,0 per cent MnO in the primary ilmenite indicates temperatures of crystallization as low as 850°C. It is to be concluded, therefore, that the liquidus temperatures of the initial critical zone magma was drastically lowered upon emplacement into the hydrous and siliceous country rocks.

Away from the contact, towards the main mass of the intrusive body, yet still in the M.Mb./P.G. the calculated equilibrium temperature rises gradually from 917°C (sample 78-374) at the contact to 969°C (78-53) some 25 m from the contact to 1116°C (78-72) approximately 180 m from the contact. A similar rise in temperature is recorded from coexisting pyroxenes in the M.Mb/L.Z (Table 10, Fig. 12) in that the calculated temperature systematically increases from 1101°C for sample GR4-1 to 1110°C for GR4-3 and to a maximum of 1172°C for GR4-5. However, in the overlying pegmatitic gabbronorite (sample GR4-6) the recorded temperature drops to 1066°C. It is of interest to note here that these lower temperature rocks contain significant amounts of sulfides. In fact traces of sulfides already become apparent in the underlying rocks represented by sample GR4-5. The correctness of the calculated temperatures were verified with the aid of sample GR4-5C, which contains inverted pigeonite. According to the relationship between temperature and composition of pigeonites (Ishii, 1975) this pigeonite (Mg* of 0,672) could have crystallized from a magma at a temperature of 1151°C ± 20°C at a pressure of 4540 bars. This temperature agrees fairly well with the Wood-Banno method especially when the ± 30°C error is taken into account.

The calculated two pyroxene temperatures from all available analyses of pyroxene pairs from the study area as well as from the eastern and western Bushveld were also used to determine the correlation between the Mg* of orthopyroxene and computed temperature of r = 0,731. Similarily, the correlation coefficient for 21 pyroxene pairs from the layered suite in the study area was found to be r = 0,800. The data for the respective marginal members have been excluded. The data from both the study area as well as the eastern

and western Bushveld Complex have been plotted on a temperature vs Mg* (opx) diagram and a curves fitted by the method of least squares. According to these curves, the relationship between temperature and Mg* (opx) is:

$T°C = 333,46\ (X_{Mg}^{opx}) + 907,76$ for the Potgietersrus area and

$T°C = 245,99\ (X_{Mg}^{opx}) + 946,00$ for the eastern and western Bushveld. X_{Mg}^{opx} is the $Mg/Mg+Fe^{2+}$ in the orthopyroxene. From this relationship it would appear as if temperature in the eastern and western Bushveld dropped less per unit value of the Mg* for the orthopyroxene than in the Potgietersrus area.

The hazards of relying on one method of calculation was pointed out earlier, as was the need to verify the correctness of the various calculated intensive parameters wherever possible. In order to verify some of the calculated pyroxene temperatures and to provide temperature calculations for rocks which do not contain coexisting Ca-rich and Ca-poor pyroxenes, the fractionation model of Nathan and van Kirk (1978), hereafter referred to as the N.& V.K. method, was employed. The crystallization temperature of each mineral on the liquidus in this model is considered to be a function of the composition of the melt. These mineral temperature equations are obtained by linear regression analyses of information from published silicate systems and rock melting experiments. This model has the most application in the critical and lower zone assemblages, where clinopyroxene is generally absent. This method will therefore only be used to infer temperatures from orthopyroxenes with Mg* $\geq 0,700$.

After fractionating the lower and critical zone magmas according to the N.& V.K. model, the temperatures for respective compositions of crystallizing olivine and orthopyroxene were fitted to regression curves (Fig. 69). From the regression curve (3) in Fig. 69A the orthopyroxene composition was equated to temperature according to the relationship:

$$T°C = 826,48\, e^{0,4476\ (X_{Mg}^{opx})}$$

The correlation between temperature and X_{Mg}^{opx} is $r = 0,900$. A similar relationship has been formulated for the composition of the crystallizing olivine and temperature as shown in Fig. 69B. Here the relationship between temperature and composition can be

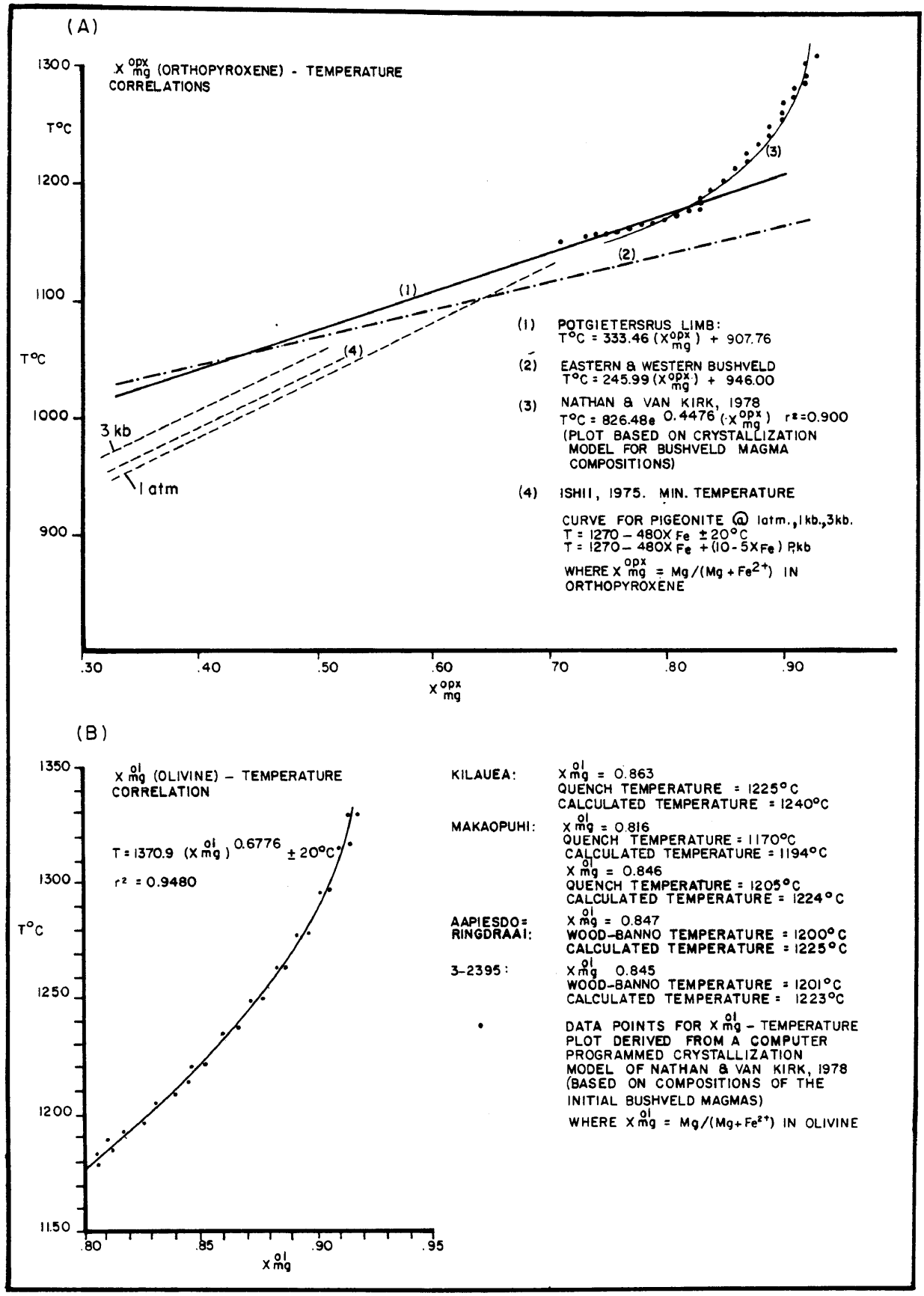

Fig. 69 Temperature vs X_{mg} for (A) Ca-poor pyroxenes and (B) olivine from the Rustenburg Layered Suite south of Potgietersrus. The curves 1 to 4 in Figure 69A were constructed according to the indicated methods of temperature calculation.

expressed as:

$T°C = 1370,9\ (X^{ol}_{Mg})^{0,6776}$ with a correlation of r = 0,948.

Although the above N. & V.K. method is not as appealing as the other procedures used to estimate crystallization temperatures, it is the only available way of placing temperature constraints on the lower zone assemblages, since the extrapolation of curves 1 and 2, in Figure 69A, beyond a Mg* of 0,850 is not adviseable due to the non-linear behaviour of the relationship beyond 0,850.

The composition-temperature relationship for olivines based on the Nathan and van Kirk program, was tested against olivines of known composition and crystallization temperatures reported by Evans and Wright (1972). The results are summarized in Figure 69B. In all cases, including the comparison with the crystallization temperature of the Aapiesdoringdraai peridotite based on the Wood-Banno geothermometer, the values calculated according to the equation $T = 1370,9\ (X^{ol}_{Mg})^{0,6776}$ were within 25°C of the reported value.

A method of verifying the calculated temperatures in rocks containing inverted pigeonite is by employing the method of Ishii (1975). Ishii found that the Fe content of the pigeonite could be related to the temperature of the magma from which it crystallized. His temperature dependent equations and graphical representations are shown in Figure 69A where:

$T = 1270 - 480\ X_{Fe} \pm 20°C$, where $X_{Fe} = Fe^{2+}/(Fe^{2+} + Mg)$ of the pigeonite. This expression can be corrected for pressure effects by the expression:

$T = 1270 - 480\ X_{Fe} + (10 - 5\ X_{Fe}) \cdot P$, where P is the pressure in kilobars.

The results of all various methods of temperature calculations are listed in Table 11 and are represented graphically in Figure 70. It is of interest to note how well the method of Ishii (1975) and the regression based on the Nathan and van Kirk (1978) crystallization model agree with the calculations based on the expression:

$T = 333,46\ (X^{opx}_{Mg}) + 907,6$ (this study). This bracketing method allows one to account for anomalous values as being due to analyitical error or assemblages not in equilibrium unless petrological evidence suggests otherwise. From the calculated temperatures

TABLE 11 MINIMUM EQUILIBRIATION TEMPERATURES FOR A GIVEN STRATIGRAPHIC LEVEL IN THE RUSTENBURG LAYERED SUITE SOUTH OF POTGIETERSRUS

Sample #	Strati= graphic Level	T°C (W-B)	T°C (Ishii) @ 4 Kb	T°C (T.S.)	T°C(N.&.V.K.) OPX
5-124-1&-C	+1480m	1022(1)	1045	1064	
5-233-1&-C	+1446m	1063(1)	1052	1069	
5-640-3A&-C	+1324m	1116(1)	1091	1097	
5-935-3A&-C	+1240m	1092m	1098	1101	
5-1100	+1190m		1103	1104	
78-127-1&-2	+1067m	1013(1)		1130	1114
78-125-A&-C	+ 940m	1138(1)	1092	1096	
78-122-A&-C	+ 850m	1127(1)	1097	1100	
78-350-1&-C	+ 724m	1025(1)	1115	1130	1114
78-192-1&-C	+ 566m	1127(1)	1143	1127	1109
78-189-1&-C	+ 410m	1111(1)	1132	1125	1106
78-207-1&-2	+ 250m	1102(1)		1138	1126
78-76B-1&-2	+ 205m	1039(1)		1132	1118
78-92-1&-C	+ 198m	1142(1)	1136	1128	1111
78-145-1&-2	+ 180m	1193(1)		1141	1131
78-60A	+ 128m			1169	1174
78-128D	+ 123m		1107	1104	
78-481-1&-2	+ 76m	1158(2)		1163	1165
GP3-241-1&-2	+ 56m	1166(1)		1154	1151
78-365-1&-2	+ 48m	1124(1)		1140	1128
78-403-C1&C2	+ 19m	1136(2)		1167	1170
78-404-1&-2	+ 5m	1136(2)		1161	1161
78-424	- 22m			1168	1172
78-413B1&B2	- 61m	1207(2)		1166	1168
78-160A	- 86m			1188	1203
78-431-1&-2	- 94m	1044(1)		1137	1125
78-422	- 95m			1163	1164
78-154	- 100m		1126	1120	1099
3-2370-1&-2	- 104m	1108(2)		1160	1159

Sample ##	Strati= graphic Level	T°C (W-B)	T°C (Ishii)	T°C (T.S.)	T°C(N.&.V.K.)	
					OPX	ol
3-2395-1&-2	- 110m	1201(2)		1188	1204	1223
3-2455-1&-2	- 121m	1152(2)		1145	1136	
3-2485	- 136m			1201	1225	1256
3-2500	- 141m			1199	1221	1247
3-2805	- 230m			1191	1209	
3-2830	- 238m			1190	1207	
3-2940	- 276m			1203	1228	
3-2950	- 280m			1201	1225	
3-3027	- 300m			1200	1224	1257
3-3349	- 402m			1190	1207	
3-3402	- 416m			1192	1210	1229
3-3494	- 446m			1197	1218	
3-3563	- 465m			1192	1211	
3-3764	- 524m			1198	1220	
3-3766	- 530m			1204	1231	1256
3-3819	- 544m			1198	1220	1250
3-3927	- 577m			1203	1228	
3-4002	- 587m			1202	1227	1256
1-50	- 620m			1206	1233	1267
1-67	- 634m			1200	1223	
1-80,5	- 647m			1203	1228	1251
1-123	- 680m			1206	1234	1278
GV-1	- 689m			1211	1242	1273
1-148	- 704m			1205	1232	
1-179	- 726m			1208	1237	1272
1-209	- 747m			1206	1233	1267
1-213	- 750m			1199	1221	
1-219	- 753m			1194	1213	1240
1-223	- 758m			1201	1224	1245
1-223,1	- 765m			1198	1221	
1-240,95	- 772m			1193	1212	1228

Sample ##	Strati= grahpic Level	T°C (W-B)	T°C (Ishii)	T°C (T.S.)	T°C(N.&.V.K.)	
					OPX	ol
1-244	-776m			1199	1222	1243
1-253,5	-782m			1201	1226	1248
6A-243	-784m			1202	1227	1260
6A-259	-797m			1201	1226	1256
6A-286	-817m			1201	1225	
X-1	-958m			1185	1199	
X-3	-984m			1179	1189	
X-5	-1032m			1193	1213	
X-10	-1058m			1200	1223	1256
X-13	-1068m			1196	1216	
X-15	-1089m			1193	1212	
X-18	-1120m			1199	1222	
X-21	-1165m			1199	1221	1249
X-23	-1176m			1196	1217	
X-25	-1190m			1192	1210	
X-27	-1220m			1185	1199	
X-31	-1250m			1205	1232	1272
X-41	-1302m			1207	1235	1270
A-1	-1368m			1201	1225	
A-3	-1408m			1204	1230	1266
A-4	-1434m			1204	1229	
A-7	-1456m			1200	1223	
A-9	-1484m			1200	1223	1232
A-10	-1490m			1192	1211	
A-12	-1530m			1201	1225	
A-13	-1582m			1203	1228	
A-15	-1610m			1207	1234	
A-16	-1640m			1209	1239	1276

Geothermometers:

T°C (W-B) = Wood-Banno Geothermometer

(1) = Wells Modification (1977)

(2) = Wood Banno (1973)

$$(1)T = \frac{7341}{3,35 + 2,44 \times X_{Fe}^{opx} - \ell n\, K} - 273$$

$$(2)T = \frac{-10202}{\ell n\, K - 7,65 \times X_{Fe}^{opx} + 3,88 (X_{Fe}^{opx})^2 - 4,6}$$

where $\ell n\, K = \frac{a^{cpx}_{Mg_2Si_2O_6}}{a^{opx}_{Mg_2Si_2O_6}}$

T°C (Ishii)= Minimum Temperature for Pigeonite

$T = 1270 - 480\, X_{Fe}^{Pig} \pm 20°C$ @ 1 bar.

$T = 1270 - 480\, X_{Fe}^{Pig} + (10 - 5\, x_{Fe}).P_{kb}$

T°C (T.S.)= Potgietersrus Limb, this study.

$T = 333,46\, (X_{Mg}^{opx}) + 907,76$

T°C(N.&.V.K.) = Nathan and Van Kirk, 1978

$OPX = 826,48e^{0,4476(X_{Mg}^{opx})}$ for $X_{Mg}^{opx} \geq ,600$

$ol = 1370,9\, (X_{Mg}^{ol})^{0,6776} \pm 20°C$ for $X_{Mg}^{ol} \geq ,800$

(Fig. 70) it can be seen that the layered rocks in the Potgietersrus area crystallized over a temperature interval of about 175°C.

Although most of the features in Fig. 70 are self-explanatory, certain temperature anomalies warrant further discussion. The N. & V.K. temperature profile shows that after emplacement, cooling and fractionation resulted in an Fe enrichment trend up to the -1490 m level in the intrusion. Up to this point the rate of temperature change is approximately 12°C/100 m. The lowest temperature horizon is associated with the highest concentration of sulfides in this stratigraphic interval and this drop in temperature probably caused a drop in the sulfide carrying capacity of the melt. This decreasing temperature with fractionation was probably accompanied by a decrease in the fo_2, as this parameter is known to decrease with fractionation in tholeiitic melts (Thompson, 1975). Similarly, a large temperature drop (33°C) is associated with anomalous sulfide crystallization at approximately the -1220 m level.

Temperature calculations indicate that the magma that gave rise to the Drummondlea Harzburgite-Chromitite had a higher temperature and was possibly more oxygenated than that which gave rise to the upper Volspruit cumulates. After crystallization of the upper chromitite, the recorded decrease in temperature is accompanied by a normal Fe enrichment trend up to approximately the -400 m level in the intrusion. The slightly higher temperature recorded toward the top of the lower zone could suggest emplacement of new magma into the chamber.

The introduction of the new critical zone liquid into the magma chamber is marked by a drop in temperature of between 100 and 125°C. This drastic drop in the recorded temperature is accompanied by the development of abundant sulfides in the rocks, probably unequalled anywhere else in the Bushveld Complex. From the level of the UG2-like chromitite layer the temperature of the magma decreases up to the +56 m level and from here increases again up to the +128 m level where values of 1169 and 1174°C were recorded. There is strong evidence to suggest that this increase in temperature is due to the introduction of new, more metal (Ni, Cu, and Co)-rich magma at this level, because the associated sulfides have some of the highest pentlandite to pyrrhotite ratios in the complex.

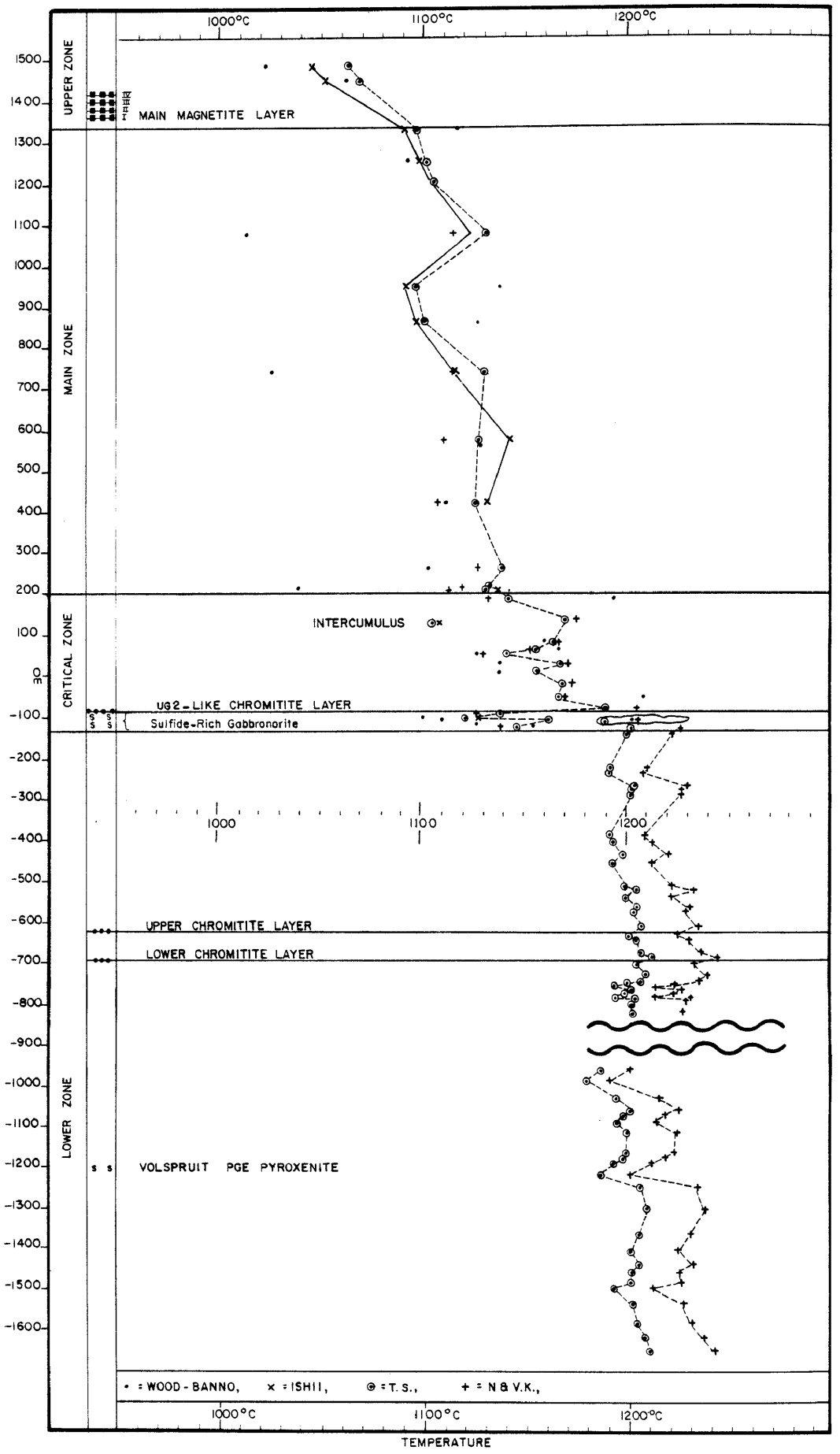

Fig. 70 A temperature profile through the Rustenburg Layered Suite south of Potgietersrus. N. & V.K. and T.S. refer to temperature calculations based on the method of Nathan and Van Kirk (1978) and the method of this study (T°C vs X_{mg}^{opx}).

Within the main zone, recorded temperatures decrease up to the approximate level of the "pyroxenite marker" where a temperature increase of 40°C is indicated. In conjunction with other petrological and geochemical data this increase in temperature is believed to be due to the introduction of a new batch of more primitive magma. From here onwards the crystallization temperature of the magma decreased from about 1130°C to 1064°C above the main magnetitite layer in the upper zone. It is estimated that the main magnetitite layer formed at about 1080°C.

The ultimate test of any temperature calculation in igneous rocks is the temperature at which these phases appear on the liquidus in melting experiments conducted on samples representative of the magma. Cawthorn et al. (1979) determined experimentally the crystallization order and the associated temperature of sample #4. This information is tabulated in section 6.3.1. Since the temperature at which the first opx+pl and pl+opx+cpx cumulates appear in the layered sequence has been calculated, it would be of interest to compare these calculated temperatures with the temperatures recorded for the first opx+pl and pl+opx+cpx bearing assemblages from the melting experiments of Cawthorn et al. (1979). Their experiments at 4kb pressure showed the first opx-pl to crystallize at a temperature of 1166°C and to continue to crystallize to 1155°C. The spotted norite (pl+opx cumulate, #78-365) in the critical zone was calculated to have crystallized at 1140°C, whereas the more mafic melanorite to feldspathic pyroxenite, #78-60A, which is an opx cumulate, was calculated to have crystallized at 1169°C (Table 11). Similarly, sample 78-481 and 78-404, which are orthopyroxene cumulates with abundant intercumulus plagioclase (≈20 per cent) and which are intimately associated with the spotted norites, have calculated crystallization temperatures of 1163 and 1161°C respectively.

The first true pl-opx-cpx cumulates in the study area occur at the +56 m level and are represented by sample GP3-241. This sample was calculated to have crystallized from a magma at a temperature of 1154°C (Table 11). Cawthorn et al. (1979) recorded the first pl+opx+cpx+liq assemblage at a temperature of 1155°C. From the above it can be seen that there is little discrepancy between calculated temperatures based on pyroxene geothermometry and

the experimentally determined temperatures for the same phases. Pyroxene geothermometry can therefore be considered as a powerful tool in deciphering the thermal history of the layered sequence of the Potgietersrus limb of the Bushveld Complex.

Cawthorn et al. (1979) found that sample #4 was totally liquid at 1325°C and that olivine was a liquidus phase at 1300°C. From this it can be inferred that the first olivine cumulates in the layered sequence at Potgietersrus could have crystallized from the melt at about 1300°C. This is further strengthened by the fact that the Mg* of sample #4 is such that it should have crystallized olivine with a $Mg/(Mg+Fe^{2+})$ ratio of 0,929. By employing the olivine thermometer ($T°C = 1370,9\,(X^{ol}_{Mg})^{0,6776}$) the earliest olivines would have crystallized at a temperature of 1305°C, which agrees exceptionally well with the experimentally determined value. Because of the good correlation between the calculated and the experimentally determined values, the calculated crystallization temperature of 1276°C (Table 11, olivine method) for the lowest known stratigraphic horizon seems very realistic. It is therefore considered that the temperatures derived from the olivine thermometer (Table 11) represent the liquidus conditions in the magma that give rise to this sequence of ultramafic cumulates more closely in absolute terms than the orthopyroxene cumulates. Although the olivine and orthopyroxene methods of calculating the temperature differ by a maximum of 40°C, the orthopyroxene method was used in Figure 70 for comparative purposes, since this mineral is present throughout the entire layered sequence, and because it is of greater interest to study the relative changes rather than absolute temperatures when trying to apply genetic interpretations to the phenomena observed in the layered sequence. Extrapolation of the temperature gradient in the Volspruit subzone to 1300°C indicates that a sequence of ol-rich cumulates in excess of 500 m thickness could be developed below this subzone.

The calculated temperatures for the main zone have been compared with the 4kb solidus temperatures of the Ca-poor pyroxenes in the binary T-X diagram (Fig. 26). Sample 5-124 from the +1480 m level was calculated by the method of Ishii (1975) and the method devised in this study to have crystallized at a temperature of 1045°C and 1064°C respectively. According to Fig. 26 the Ca-poor pyroxenes

of this sample should have crystallized at 1025°C. The Ca-poor pyroxene of sample 78-125, on the other hand, crystallized at 1056°C according to Figure 26, whereas the above two methods of calculation suggest crystallization temperatures of 1092 and 1096°C respectively. The corresponding values for sample 78-189 are 1090°C, 1132°C and 1125°C respectively. The mean deviation between the graphical method (Fig. 26) and the calculated values is 37°C. This comparatively small difference between these two methods is probably within the limit of uncertainty of the respective geothermometers, so that the graphical method (Fig. 26) could be used to obtain a minimum temperature for the various main zone horizons.

Ross and Huebner (1975) proposed an approximate geothermometer based on the composition of the clinopyroxene, coexisting with orthopyroxene. The temperature of crystallization is determined by relating the composition of the clinopyroxene to a series of isotherms plotted onto the pyroxene quadrilateral. Fleet (1974B) proposed a similar geothermometer based on the relationship along the augite limb of the pyroxene solvus. The isotherms on Figures 19A and B show that most of the main zone pyroxenes plot between the 1000 and 1100°C contours. In Figure 21A the contours within the pyroxene quadrilateral suggest that the quenched M.Mb./P.G. samples have had their primary liquidus temperatures reduced considerably due to crystallization in a volatile-rich environment. Although temperature estimates based on the pyroxene quadrilateral are very qualitative, they were useful to confirm the low temperatures previously calculated for the marginal member. Anhydrous liquidus temperatures in the M.Mb./P.G. may be approximated by using the pigeonite bearing sample GR1-44. The composition of the coexisting pyroxenes in this sample suggest a temperature of crystallization of 1030°C, based on the Wells (1977) method, whereas the graphical method (Figure 16) and the Ishii method suggest temperatures of 1058 and 1078°C respectively. Crystallization can therefore be assumed within the temperature range of 1030 to 1078°C.

In conclusion, the findings of this study show that pyroxene-, as well as olivine geothermometers can be very useful in the interpretation of the thermal history of a layered intrusion.

7.3 Silica Activity

7.3.1 Theoretical Considerations

Significant in the determination of the a_{SiO_2} of fractionated magmas are the reactions:

$$Fe_2SiO_4 + SiO_2 \rightleftarrows 2FeSiO_3 \qquad (7.3.1)$$
ol liq opx

$$Mg_2SiO_4 + SiO_2 \rightleftarrows 2MgSiO_3 \qquad (7.3.2)$$
ol liq opx

particularly in the Bushveld Complex as olivine is an important constituent in many of the upper and lower zone rocks. The change in a_{SiO_2} caused by crystallization of a weight fraction olivine (F_{ol}) from a melt can, according to Green et al. (1971 A and B), be approximated by:

$$\log a_{SiO_2} \approx \log (1-F_{ol}) \qquad (7.3.3)$$

The extraction of olivine will result in a gradual increase of the a_{SiO_2} in the melt, to the point where orthopyroxene commences to crystallize as well. Upon further fractional crystallization the proportion of olivine should decrease and that of orthopyroxene increase to give rise to the mineral graded nature of the ol-opx-chr cumulate within a cyclic unit, e.g. unit 21. With crystallization of the orthopyroxene cumulates the a_{SiO_2} of the melt increased to such an extent that the melt no longer crystallized olivine. Any of the previously crystallized olivine that comes into contact with the more siliceous melt will be in a reaction relationship with this liquid.

Although equation 7.3.2 has wide application to explain many of the features seen in the lower zone, the Fe-rich analogue, eq. 7.3.1, has yet to be confirmed as an important reaction in the upper zone. In theory, however, it could be important in controlling the extent of the stability field of the Ca-poor pyroxene, the reappearance of Fe-rich olivine in the sequence and also influence the crystallization of the Fe-Ti oxides from the magma. Lindsley and Munoz (1969) propose that the stability field of Ca-poor pyroxene is expanded in magmas with higher a_{SiO_2}, because an increase in the a_{SiO_2} would drive the reactions 7.3.1 and 7.3.2 to the right. The maximum persistence of Ca-poor pyroxenes will therefore occur in systems with an $a_{SiO_2} = 1$ where primary quartz crystallized from the magma, as for instance in quartz monzonites from Quebec and Labrador Canada (Morse, 1980A). Con-

versely, a decrease in the activity of silica in the melt should drive the reaction to the left, causing the disappearance of Ca-poor pyroxene in favour of olivine. The best evidence for such a reaction in the upper zone would be resorbed orthopyroxenes within olivine crystals. Although Von Gruenewaldt (1971) and Molyneux (1970) have studied the upper zone in detail and have demarcated the approximate level where Ca-poor pyroxene disappears, the exact cause of the disappearance of the Ca-poor pyroxene is not known. Although numerous hypothesis have been put forward to explain this, i.e. Walker (1969A); Read et al. (1961); Campbell and Nolan (1974); Danchin and Ferguson (1970) and Brown (1957) the possibility of decreasing a_{SiO_2} caused by the effect of Fe enrichment during fractionation of the Bushveld magma cannot be overlooked as this is known to favour the replacement of Ca-poor pyroxene by Fe-rich olivine according to the reaction:

$$\underset{\text{opx}}{FeSiO_3} + \underset{\text{liq}}{FeO} \rightleftharpoons \underset{\text{olivine}}{Fe_2SiO_4} \qquad (7.3.4)$$

(Campbell and Nolan, 1974).

The a_{SiO_2} in the magma also seems to have a pronounced influence on the mineral assemblages in the lower and upper parts of the upper zone, as can be seen from the following reactions:

$$\underset{\text{opx}}{FeSiO_3} + 1/6\, O_2 \rightleftharpoons 1/3\, \underset{\text{magnetite}}{FeO\cdot Fe_2O_3} + \underset{\text{liq}}{SiO_2} \qquad (7.3.5)$$

and

$$\underset{\text{olivine}}{Fe_2SiO_4} + 1/3\, O_2 \rightleftharpoons 2/3\, \underset{\text{magnetite}}{FeO\cdot Fe_2O_3} + \underset{\text{liq}}{SiO_2} \qquad (7.3.6)$$

It is of interest to note that both these reactions can actually be observed in the upper zone of the eastern Bushveld (Von Gruenewaldt, 1972). In the lower half of the upper zone, symplectic intergrowths of magnetite and orthopyroxene evidently represents a reaction similar to (7.3.5), whereas abundant symplectic intergrowths of magnetite and olivine surrounding early magnetite evidently represent reaction 7.3.6. From these two reactions it can be seen that an increase in fo_2 would drive the above reaction to the right, giving rise to enhanced crystallization of magnetite, whereas an increase in the a_{SiO_2} would drive the reaction to the left, inhibiting the crystallization of spinel and thus give rise to more Fe-rich pyroxene or olivine.

The absence of olivine and the prevalence of Ca-poor pyroxene in

the main and critical zones in the study area suggests that the silica activity was constantly high enough to drive reaction (7.3.1) and (7.3.2) to the right, so that the composition of the crystallizing magma remained in the stability field of orthopyroxene. In these two zones, as well as the upper zone, the assemblage plagioclase and clinopyroxene must be used to calculate the a_{SiO_2} in the melt on the basis of the reaction:

$$\underset{\text{Ca-Tschermak's component in cpx}}{CaAl_2SiO_6} + \underset{liq}{SiO_2} \rightleftharpoons \underset{plag}{CaAl_2Si_2O_8} \qquad (7.3.7)$$

(Bacon and Carmichael, 1973).

7.3.2 Silica Activity Calculations

The variation of the activity of component i with temperature and pressure may be expressed in the general form:

$$(\log a_i)^{P,T} = \frac{A}{T} + B + \frac{C}{T}(P-1) + \log a_{products} - a_{reactants} \qquad (7.3.8)$$

(Wood and Fraser, 1976; Powell, 1978 and Carmichael et al., 1970)

In the case of rocks containing Mg-rich orthopyroxene and olivine, the $a^{melt}_{SiO_2}$ was calculated from the expression:

$$(\log a_{SiO_2})^{P,T} = \frac{A}{T} + B + \frac{C}{T}(P-1) + 2(\log a^{opx}_{MgSiO_3}) - \log {}^{ol}_{Mg_2SiO_4} \qquad (7.3.9)$$

where $\frac{A}{T} + B = \frac{\Delta G^\circ \text{ reaction}}{2{,}303\ RT}$

$$\frac{C}{T}(P-1) = \frac{\Delta V^\circ \text{ reaction}}{2{,}303\ RT}$$

The activity of the components Mg_2SiO_4 and $MgSiO_3$ in the above expression was calculated according to the conventions of Williams (1971A). For rocks without olivine the silica activity was calculated from reaction (7.3.7) by the expression:

$$(\log a_{SiO_2})^{P,T} = \frac{A}{T} + B + \frac{C}{T}(P-1) + \log a^{plag}_{CaAl_2Si_2O_8} - \log a^{cpx}_{CaAl_2SiO_6} \qquad (7.3.10)$$

where the $\log a^{plag}_{CaAl_2Si_2O_8}$ was calculated with the aid of the activity expression of Orville (1972):

$$a^{plag}_{An} = \gamma \cdot X^{plag}_{An} \qquad (7.3.11)$$

where γ is the activity coefficient.

The $\log a^{cpx}_{CaAl_2SiO_6} = X^{M_1}_{Ca} \cdot X^{M_2}_{Al}$ (7.3.12)

and was calculated by using the procedure of Powell and Powell (1974) as well as the mixing model proposed by Wood as outlined by Buchanan (1976).

TABLE 12 SILICA ACTIVITY CALCULATIONS FOR THE REACTION:

$Mg_2SiO_4 + SiO_2 \rightleftharpoons 2\ MgSiO_3$

ol liquid opx

Sample #	Strat. Level	Temp. °C	Pressure (bars)	Log a Mg_2SiO_4	Log a $MgSiO_3$	1 bar Log a SiO_2	* Log a SiO_2	** Log a Mg_2SiO_4	*** Log a SiO_2
3-2485	-136m	1225	4544	-0,1252	-0,0521	-0,0722	-0,2007	-0,1072	-0,2188
3-2500	-141m	1221	4545	-0,1339	-0,0556	-0,0724	-0,2013	-0,1156	-0,2197
3-2940	-276m	1228	4584	-0,1204	-0,0501	-0,0717	-0,2011		
3-3402	-416m	1210	4625	-0,1569	-0,0649	-0,0731	-0,2053	-0,1329	-0,2293
3-4002	-587m	1227	4676	-0,1221	-0,0508	-0,0718	-0,2040	-0,1072	-0,2189
GV-1	-689m	1242	4706	-0,0933	-0,0390	-0,0702	-0,2018	-0,0914	-0,2037
GV-22	-690m	1250	4706	-0,0768	-0,0323	-0,0696	-0,2006		
1-219	-753m	1213	4725	-0,1505	-0,0623	-0,0729	-0,2077	-0,1237	-0,2345
1-223	-758m	1224	4727	-0,1279	-0,0532	-0,0722	-0,2060	-0,1182	-0,2157
1-240,95	-772m	1212	4736	-0,1524	-0,0631	-0,0730	-0,2082	-0,1336	-0,2270
1-244	-776m	1222	4737	-0,1332	-0,0553	-0,0721	-0,2064	-0,1195	-0,2201
1-253,5	-782m	1226	4739	-0,1252	-0,0521	-0,0717	-0,2057	-0,1147	-0,2162
6A-243	-784m	1227	4739	-0,1229	-0,0512	-0,0717	-0,2056	-0,1036	-0,2249
6A-259	-797m	1226	4743	-0,0628	-0,0523	-0,0716	-0,2057	-0,1073	-0,2240
X-10	-1058m	1223	4821	-0,1308	-0,0544	-0,0721	-0,2086	-0,1072	-0,2322
X-13	-1068m	1216	4824	-0,1438	-0,0596	-0,0727	-0,2101		
X-21	-1165	1221	4851	-0,1339	-0,0556	-0,0724	-0,2100	-0,1140	-0,2299
A-3	-1408	1230	4923	-0,1156	-0,0486	-0,0724	-0,2112	-0,0982	-0,2287
A-9	-1484	1223	4945	-0,1306	-0,0543	-0,0721	-0,2122	-0,1304	-0,2124
A-16	-1640	1239	5000	-0,0992	-0,0415	-0,0705	-0,2107	-0,0882	-0,2217
AP-1****		1200	5484		-0,0634	-0,0978	-0,2503	-0,1339	-0,2503

$$\log a\ SiO_2 = \frac{-1034}{T} + 0{,}597 - \frac{0{,}0410(P-1)}{T} + 2 \log a^{opx}_{MgSiO_3} - \log a^{ol}_{Mg_2SiO_4}$$

* $\log a\ SiO_2$ calculated at the given pressure with the Forsterite component of the olivine calculated from the equation

$$\frac{X_{en} - 0{,}15}{0{,}85} = X_{FO}$$

** $\log a\ Mg_2SiO_4$ from probe compositions of olivine

*** $\log a\ SiO_2$ calculated from (**)

**** AP-1 = Aapiesdoringdraai Peridotite, E. Bushveld

TABLE 13 SILICA ACTIVITY CALCULATIONS FOR THE REACTION:

$CaAl_2SiO_6 + SiO_2 \rightleftharpoons CaAl_2Si_2O_8$

pyroxene liquid plagioclase

Sample #	Strat. Level	Temp. (°C)	Pressure (bars)	Plag. X_{an}	Plag. log a an	Cpx log a cats	1 bar log a SiO_2	* log a SiO_2
5-124	+1480	1064	4064	49,01	-0,2039	1)-1,5787	-0,2117	-0,0537
						2)-1,5191	-0,2713	-0,1133
5-233	+1446m	1069	4074	52,35	-0,1752	1)-1,7123	-0,0455	0,1123
		(UPPER ZONE)				2)-1,6359	-0,1219	0,0359
5-640	+1324m	1097	4110	55,26	-0,1561	1)-1,5146	-0,2026	-0,0467
						2)-1,5524	-0,1648	-0,0089
5-935	+1240m	1101	4135	58,69	-0,1424	1)-1,5492	-0,1513	0,0052
						2)-1,5609	-0,1395	0,0169
78-127	+1067m	1130	4187	69,52	-0,1076	1)-1,6045	-0,0400	0,1151
						2)-1,5048	-0,1397	0,0154
78-125	+ 940m	1096	4225	60,43	-0,1361	1)-1,7484	0,0505	0,2109
						2)-1,7657	0,0678	0,2283
78-122	+ 850m	1100	4252	52,91	-0,1706	1)-1,7761	0,0467	0,2077
						2)-1,7761	0,0467	0,2077
78-350	+ 724m	1130	4290	58,73	-0,1422	1)-1,6728	-0,0063	0,1527
						2)-1,6812	0,0021	0,1611
78-192	+ 566m	1143	4337	60,86	-0,1346	1)-1,6926	0,0304	0,1896
						2)-1,6771	0,0149	0,1741
78-189	+ 410m	1132	4384	63,46	-0,1259	1)-1,6154	-0,0460	0,1162
						2)-1,5770	-0,0843	0,0779
78-207	+ 250m	1138	4432	69,63	-0,1073	1)-1,5333	-0,1052	0,0581
						2)-1,5116	-0,1269	0,0364
78-76B	+ 205m	1132	4446	70,33	-0,1052	1)-1,6904	0,0497	0,2142
						2)-1,6576	0,0169	0,1814
78-92	+ 198m	1136	4448	58,10	-0,1446	1)-1,6950	0,0178	0,1819
		(MAIN ZONE)				2)-1,6795	0,0023	0,1664
78-145	+ 180m	1141	4453	74,55	-0,0932	1)-1,5039	-0,1184	0,0453
						2)-1,4767	-0,1455	0,0182
GP3-241	+ 56m	1154	4491	77,37	-0,0852	1)-1,4955	-0,1097	0,0539
						2)-1,4321	-0,1731	-0,0095

Sample ##	Strat. Level	Temp. (°C)	Pressure (bars)	Plag. X_{an}	Plag. log a an	Cpx log a cats	1 bar log a SiO_2	* log a SiO_2
78-365	+ 48m	1140	4493	67,46	-0,1136	1)-1,5023	-0,1411	0,0242
						2)-1,4534	-0,1900	-0,0247
78-403	+ 19m	1167	4501	69,38	-0,1080	1)-1,5542	-0,0649	0,0976
						2)-1,4136	-0,2055	-0,0430
78-404	+ 5m	1161	4505	66,21	-0,1174	1)-1,5489	-0,0836	0,0797
						2)-1,4010	-0,2316	-0,0683
78-413	- 61m	1166	4524	72,06	-0,1003	1)-1,5724	-0,0396	0,1238
						2)-1,4369	-0,1751	-0,0117
78-431	- 94m	1125	4533	64,12	-0,1238	1)-1,4344	-0,2299	-0,0614
						2)-1,3273	-0,3370	-0,1684

(CRITICAL ZONE, LAYERED MEMBER)

GR1-44	M.Mb. / P.G.	1030	4540	66,05	-0,1179	1)-1,8137	0,0819	0,2630
						2)-1,6416	-0,0903	0,0909
GR1-69	"	967	4540	49,22	-0,2020	1)-1,9118	0,0408	0,2311
						2)-1,7407	-0,1303	0,0601
GR1-88,48	"	1002	4540	70,93	-0,1035	1)-1,5943	-0,1470	0,0381
						2)-1,5805	-0,1608	0,0243
GR1-93,26	"	992	4540	49,27	-0,2016	1)-1,8474	-0,0007	0,1859
						2)-1,6672	-0,1809	0,0057
GR1-97,89	"	923	4540	49,25	-0,2017	1)-1,7719	-0,1406	0,0567
						2)-1,6387	-0,2738	-0,0765
GR1-98,20	"	959	4540	52,39	-0,1749	1)-1,9945	0,1432	0,3348
						2)-1,8432	-0,0080	0,1835
GR1-100	"	951	4540	46,67	-0,2251	1)-1,9372	0,0283	0,2211
						2)-1,6784	-0,2306	-0,0378
GR1-102,5	"	951	4540	45,50	-0,2361	1)-1,9716	0,0517	0,2445
						2)-1,6975	-0,2225	-0,0297

Sample ##	Strat. Level	Temp. (°C)	Pressure (bars)	Plag. Xan	Plag. log a an	Plag. log a cats	1 bar log a SiO_2	* log a SiO_2
GR1-105	M.Mb / P.G.	983	4540	57,31	-0,1477	1)-1,8890	0,0869	0,2748
						2)-1,7469	-0,0552	0,1327
GR1-107,2	"	982	4540	52,57	-0,1734	1)-1,9062	0,0774	0,2654
						2)-1,7351	-0,0937	0,0943
GR1-109,5	"	1005	4540	51,30	-0,1840	1)-1,8735	0,0543	0,2390
						2)-1,8009	-0,0183	0,1664
78-374	"	917	4540	75,65	-0,0901	1)-1,7333	-0,0735	0,1248
						2)-1,6576	-0,1492	0,0491
78-53	"	969	4540	57,88	-0,1454	1)-1,5450	-0,2675	-0,0775
						2)-1,5450	-0,2675	-0,0775
GR4-1	M.Mb / L.Z.	1101	4540	65,67	-0,1190	1)-1,6178	-0.0593	0,1125
						2)-1,4852	-0,1919	-0,0201
GR4-3	"	1110	4540	69,36	-0,1080	1)-1,6362	-0,0233	0,1473
						2)-1,5112	-0,1482	0,0224
GR4-5	"	1172	4540	62,19	-0,1301	1)-1,6598	0,0220	0,1854
						2)-1,6282	-0,0096	0,1538
GR4-6	"	1066	4540	67,41	-0,1138	1)-1,4805	-0,2182	-0,0419
						2)-1,3871	-0,3116	-0,1354

* $\log_{10}$ a SiO_2 at the given pressure.

1) = Wood Mixing Model

2) = Powell Mixing Model

$$\log a\, SiO_2 = \frac{-1410}{T} - 0{,}532 + \frac{0{,}052(P-1)}{T} + \log a\, {}^{plag.}_{CaAl_2Si_2O_8} - \log a\, {}^{cpx}_{CaAl_2SiO_6}$$

Following the conventions laid down by Carmichael et al., 1970; the silica activities were calculated from the analytical data of mineral compositions, temperature and pressure given in Table 12 and 13. Silica glass, rather than quartz was taken as the standard state of silica. The coefficients A, B, and C for the appropriate reactions are given in Table 14.

TABLE 14 COEFFICIENTS A, B, AND C FOR THE EQUATION:

$$\text{LOG } a_{SiO_2} = \frac{A}{T} + B + \frac{C(P-1)}{T}$$

Reaction	A	B	C	Reference
$Mg_2SiO_4 + SiO_2(gl) \rightleftarrows 2MgSiO_3$	-1034	+0,597	-0,0424	Nicholls et al., 1971
$Fe_2SiO_4 + SiO_2(gl) \rightleftarrows 2FeSiO_3$	66	-0,46	-0,0406	Nicholls et al., 1971
$CaAl_2SiO_6 + SiO_2(gl) \rightleftarrows CaAl_2Si_2O_8$	-1410	-0,53	+0,052	Bacon and Carmichael, 1973
$FeSiO_3 + 1/6\ O_2 \rightleftarrows 1/3\ Fe_3O_4 + SiO_2(gl)$	4467	-1,63	-0,0479	Nicholls et al., 1971

It can be seen from Table 12 that the pressure corrected $\log_{10} a_{SiO_2}$ values calculated for the lower zone range from -0,2345 to -0,2037. The calculations indicate a fairly restricted range in the a_{SiO_2} in the lower zone magma during crystallization of the olivine-orthopyroxene bearing layers.

In horizons above the lower zone the calculated a_{SiO_2} reveals that the lowest values occur in the upper zone and in the lower to middle parts of the critical zone. Very high values are encountered in the middle portions of the main zone as well as in the M.Mb./P.G. Although many of the calculated silica activity values are high in absolute terms, due to the influence of Ti on the Powell and Powell (1974) and Wood (Buchanan, 1976) mixing models for Al in clinopyroxene, there are systematic trends within the main, critical, and to a lesser extent upper zone that reflect the changing $a^{melt}_{SiO_2}$ as the magma evolved. These changes are in most cases also reflected in the character of the various rock types.

The high $\log_{10} a_{SiO_2}$ values of $\geqq 0,00$, calculated according to the Powell mixing model, for the M.Mb./P.G. rocks indicates that the magma from which these rocks crystallized was saturated in silica. Most of the investigated samples contain abundant free quartz. Exceptions are samples 78-53, 78,374, and GR1-44 and, although they contain no free quartz, they crystallizedin an environment that is considered to have become enriched in silica by contamination

of country rocks. The high and erratic nature of the a_{SiO_2} values from the M.Mb./P.G. rocks can also be ascribed to the variable Ca* of the feldspars, i.e., 0,75 to 0,45; although the high a_{SiO_2} in these rocks are confirmed by the extremely low Al_2O_3 content of the clinopyroxenes (Figure 23), as well as by the high MnO content of the ilmenites and the spinels (Lipman, 1971).

Calculated a_{SiO_2} values of samples from the 450 mm thick interval of mafic rocks from the M.Mb./L.Z. (Fig. 12) were found to increase in a linear fashion from -0,021 to +0,1538 in samples GR4-1 to GR4-5 respectively. In comparison, sample GR4-6, which contains significant amounts of sulfides, yielded the lowest a_{SiO_2} value of -0,1354. It is felt that the solubility of S in the successive, melts was gradually decreasing with increasing silica activity until it reached saturation, whereupon separation of an immiscible sulfide liquid took place to give rise to the horizon represented by sample GR4-6. It is of interest to note that the clinopyroxenes GR4 -1, -3, -5 have amongst the lowest concentration of Al_2O_3 of all the clinopyroxenes in the study area which substantiates a high a_{SiO_2} in the magma from which these rocks crystallized.

The calculated a_{SiO_2} listed in Table 12 and 13 have been plotted against stratigraphic height in Fig. 71. From this figure it can be seen that the a_{SiO_2} in the magma that gave rise to the lower zone ol-opx-chr cumulates was fairly constant. The lowest value of silica activity in the critical zone occurs in the mineralized gabbronorite in the immediate foot-wall sequence to the UG2-like chromitite. Low a_{SiO_2} will undoubtedly also have prevailed during crystallization of the UG2-like chromitite and its hanging-wall opx-chr±cpx cumulates in the lower subzone (1) of the critical zone, due to the prevailing high fo_2. Although limited in number the clinopyroxenes from this subzone appear to contain more Al_2O_3 than those from the overlying subzone 2, suggesting a lower a_{SiO_2} in the lower half of the critical zone.

From about the "0" datum where a sulfide-bearing feldspathic pyroxenite with traces of chromite is developed, the silica activity increases towards the top of the critical zone. This increase in

the a_{SiO_2} in the magma took place during crystallization of the anorthositic subzone (1) of the critical zone and is reflected by relatively high concentrations of quartz in the norm, as well as by the presence of intercumulus modal quartz and by the absence of chromite in the rocks.

Some of the highest silica activites were recorded from norites and gabbronorites at the base of the main zone. After emplacement, the a_{SiO_2} of the magma dropped to a relatively low value of 0,0364 at the +250 m level. This decrease in the a_{SiO_2} could have come about by the crystallization of quartz and more albitic plagioclase at the base of the main zone (Fig. 71). With continued fractionation the residual magma became increasingly siliceous as demonstrated by the increasing a_{SiO_2} in the magma up to the +940 m level in the intrusion. This increasing a_{SiO_2} coincides with a decrease in the Mg* and the Ca* of pyroxene and plagioclase respectively, as well as the normative An/(An+Ab) ratio of the rock. This increase in the a_{SiO_2} is also accompanied by increases in the concentrations of Y and Zr in the rocks, suggesting gradual fractionation of the magma.

From the +940 m level the calculated a_{SiO_2} values decrease through the remaining portion of the main zone and into the upper zone. The low value above the magnetitite layers in the upper zone is considered to reflect the relatively high fo_2 conditions that evidently prevailed during crystallization of these magnetite-rich rocks and therefore reflects conditions similar to those which prevailed during crystallization of the chromite bearing sequence of the critical zone.

The high normative quartz values and the higher than normal amounts of interstitial quartz combined with the upward increasing a_{SiO_2} and the associated low Al_2O_3 content of the clinopyroxenes in the rocks of the main zone below the inferred level of the pyroxenite marker, indicate that the magma was fractionated to such an extent that it could have precipitated cumulus quartz. Although no cumulus quartz was observed in the rocks, it would, in all likelihood have floated off and subsequently have been resorbed by the magma. Mixing of the residual main zone magma with large quantities of new undifferentiated magma at about the level of the pyroxenite

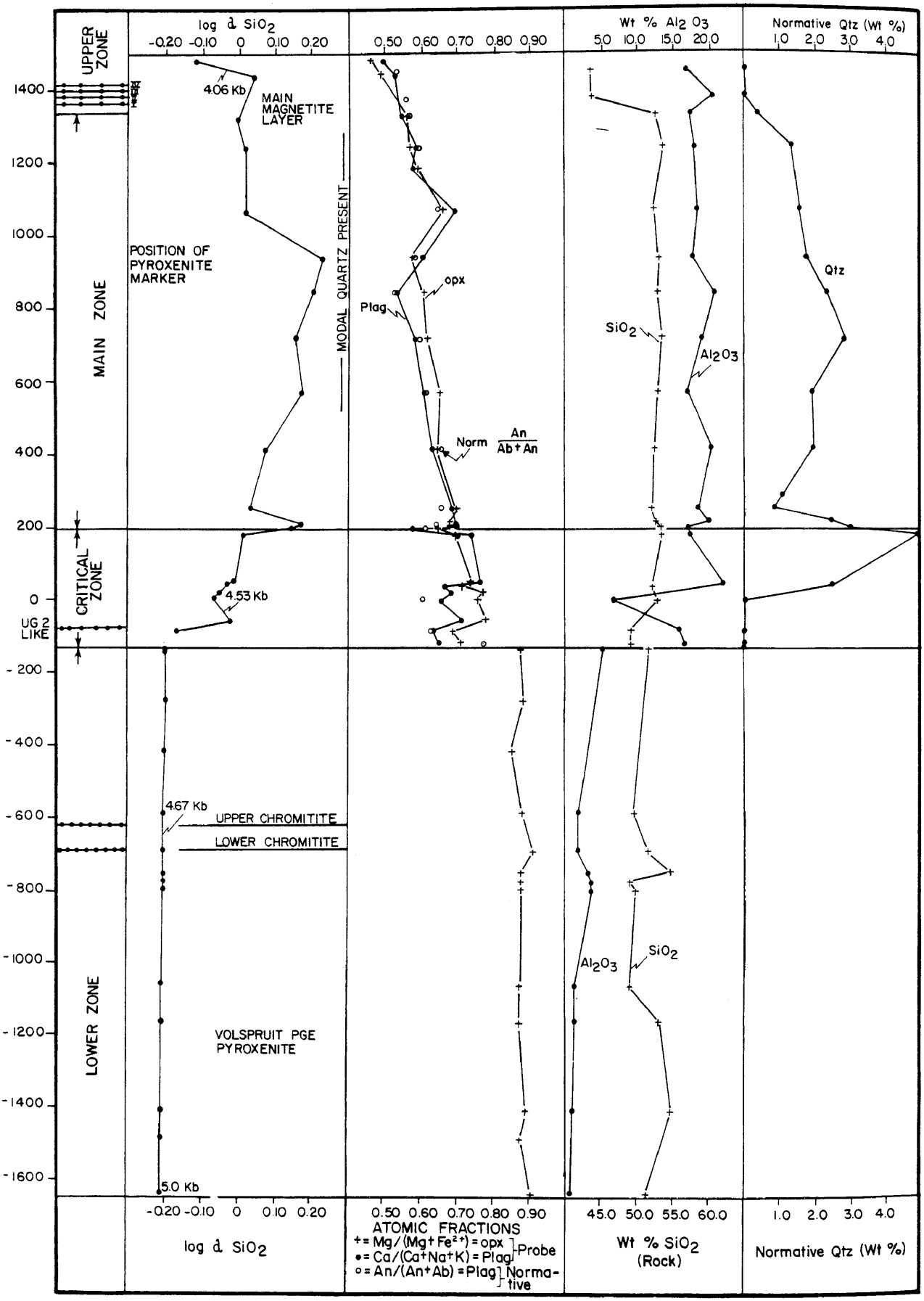

Fig. 71 A silica activity profile through the layered sequence, plotted in conjunction with compositional trends for the normative and atomic fractions anorthite, the $Mg/(Mg+Fe^{2+})$ ratio in orthopyroxene, the weight per cent SiO_2 and the normative per cent quartz in the rocks.

marker probably resulted in the upward decreasing a_{SiO_2} trend (Fig. 71) toward the top of the main zone. Although the exact position of the pyroxenite marker is not known, the influence of this new magma on the intensive parameters of the later magma from which the upper part of the main and upper zone crystallized is most apparent.

For the present, the a_{SiO_2} values based on reaction (7.3.7) will have to be considered as being relative rather than absolute, as neither the Powell nor the Wood mixing model used to calculate the a^{cpx}_{CATS} is absolutely correct and is subject to error when TiO_2 concentrations in clinopyroxene are high, i.e. ≥0,50 per cent. Further work is necessary to solve this mixing model problem. Once this problem is overcome, it should be possible to calculate operative pressures fairly accurately from the a_{SiO_2} calculations of igneous rocks that contain combinations of the assemblages plagioclase, clinopyroxene, orthopyroxene, olivine and magnetite. It is evident from Table 14 that the pressure dependent expression C(P-1)/T will result in a decrease in the calculated a_{SiO_2} with increasing pressure when the olivine-orthopyroxene or the orthopyroxene-magnetite reaction is used, in contrast to an increase for the calculation based on the reaction (7.3.7) (CATS-Anorthite). Since many upper zone layers are made up of plagioclase-clinopyroxene-orthopyroxene-magnetite cumulates, these assemblages should define the pressure. This relationship is shown graphically in Figure 72 from which it can be seen that for a specific composition of the coexisting minerals pressure and a_{SiO_2} are fixed.

7.4 Oxygen Fugacity

7.4.1 fo_2 Calculations Involving Fe-Ti Oxides

Probably the most precise method presently available for estimating magmatic temperatures and oxygen fugacity is that of the Buddington and Lindsley (1964) based on the exchange reaction:

$$XFe_2TiO_4 + (1-X)Fe_3O_4 + 1/4\,O_2 \rightleftarrows XFeTiO_3 + (3/2-X)Fe_2O_3$$

(Wright and Weibien, 1968; Helz, 1973; Luhr and Carmichael, 1980).

Ideally, the composition of grains of unexsolved titaniferous magnetite coexisting with separate primary ilmenite grains, as is commonly the case in quenched volcanic rocks, should be used. Unfortunately, in slowly cooled intrusions the original magnetite-

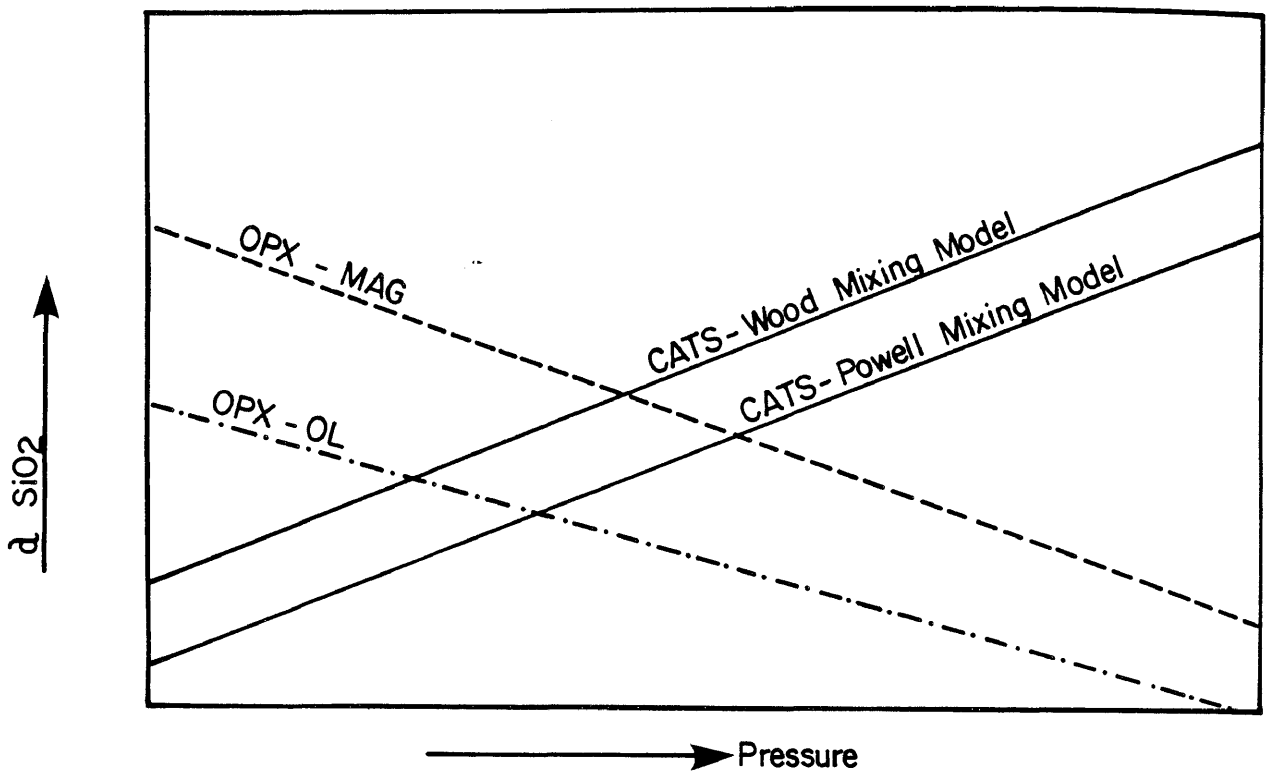

Fig. 72 Variation of silica activity with pressure for various reactions. The diagram also illustrates how this dependancy can be used to calculate operative pressure during crystallization of the magma.

ulvöspinel solid solution has unmixed to give rise to magnetite-ulvöspinel and/or magnetite-ilmenite intergrowths. This is also the case for the Fe-Ti oxides from the upper zone and to a lesser extent the M.Mb./P.G. The nearest to the ideal situation was found in the rocks from the quenched M.Mb./P.G. Here, as mentioned before, discrete grains of exsolved mixtures of magnetite and ilmenite occur together with primary laths of ilmenite that are physically separate from the composite grains. By measuring the modal proportions of the exsolved phases in the composite grains and recasting the microprobe analyses on the basis of the proportions of the exsolved phases, the original bulk composition of the titaniferous magnetite (magnetite-ulvöspinel solid solution) can be ascertained. The bulk composition of this titaniferous magnetite in conjunction with that of the primary ilmenite was then used to calculate the fo_2 - temperature conditions of the magma from which these phases crystallized (method 3, Table 15A). Although this method (Buddington-Lindsley, 1964) is a powerful tool in determining T-fo_2 conditions, the above method of calculating the bulk composition is subject to error. For this reason Himmelberg and Ford (1977) suggested that a better estimate of the oxygen fugacity during crystallization of a magma is obtained by combining the composition of the discrete, unexsolved primary ilmenite grains with the temperature of crystallization calculated from pyroxene thermometry. The fo_2 values calculated in this way for 1 bar and 4540 bars pressure (method 1, Table 15A), as well as fo_2 values calculated from the bulk composition of the titaniferous magnetite and the pyroxene temperatures (method 1) are presented in Table 15A. There is favourable agreement between the results calculated according to methods (1) and (2) which indicates that the estimated bulk composition of the titaniferous magnetite are fairly accurate. The mean difference between the two methods is 0,31 log units at 1 bar. Calculations according to the method of Buddington -Lindsley (method 3, Table 15A) agree reasonably well with those calculated according to the method suggested by Himmelberg and Ford (1977). The discrepancy in fo_2 value calculated for GR1-102,5 according to method 1 and 3 probably reflects an inaccurate assessment of the bulk composition of the primary titaniferous magnetite. The results employing method 2 are considered to be the most accurate indication of fo_2 conditions for the M.Mb./P.G., i.e. $10^{-10,25}$ to $10^{-10,35}$ atm over the temperature range 1002 to 951°C.

TABLE 15A fo_2 CALCULATIONS FOR IRON-TITANIUM OXIDE BEARING ASSEMBLAGES FROM THE MARGINAL MEMBER OF THE CRITICAL ZONE

Method (1) Two Pyroxene Temperature: Primary Composition of Titaniferous Magnetite

Sample #	T°C	1 bar $-\log_{10} fo_2$	4540 bars $-\log_{10} fo_2$
GR1-69	967*	10,90	10,64
GR1-88	1002*	10,25	10,00
GR1-100	951*	11,15	10,88
GR1-102,5	951*	11,50	11,23
GR1-107,2	982*	10,35	10,09

Method (2) Two Pyroxene Temperature : Primary Composition of Ilmenite.

Sample #	T°C	1 bar $-\log_{10} fo_2$	4540 bars $-\log_{10} fo_2$
GR1-69	967*	10,80	10,53
GR1-88	1002*	10,50	10,25
GR1-100	951*	11,00	10,72
GR1-102,5	951*	10,80	10,52
GR1-107,2	982*	10,70	10,43

Method (3) Buddington-Linsley Geothermometer/Geobarometer

Sample #	T°C	1 bar $-\log_{10} fo_2$	4540 bars $-\log_{10} fo_2$
GR1-69	992	10,50	10,24
GR1-88	958	11,50	11,24
GR1-100	1028	9,80	9,55
GR1-102,5	1058	9,60	9,36
GR1-107,2	998	10,60	10,35
78-360	970	10,50	10,24

TABLE 15B fo_2 CALCULATIONS FOR IRON-TITANIUM OXIDE BEARING ASSEMBLAGES FROM THE UPPER ZONE

Method (1) Two Pyroxene Temperature : Primary Composition of Titanferous Magnetite

Sample #	T°C	@ 1 bar $-\log_{10} fo_2$	(bars) Pressure	@ given pressure $-\log_{10} fo_2$
5-124	1064**	9,50	4064	9,26
5-195	1069**	9,40	4074	9,16
5-508	1080**	9,25	4094	9,01

Method (4) fo_2 based on a SiO_2 (Williams, 1971)

$$: -\log_{10} fo_2 = \frac{26802}{T°K} - 9,78 + 6 \log a\, FeSiO_3 - 6 \log a\, SiO_2 - 2 \log a^{spinel}_{Fe_3O_4}$$

Sample #	T°C	$\log_{10} a\, FeSiO_3$	$a^{spinel}_{Fe_3O_4}$	bars Pressure	@ 4064 bars $\log_{10} SiO_2$	@ 4064 bars $-\log_{10} fo_2$
5-124	1064	-0,2264	0,3720	4064	-0,1133	10,44

* Wood-Banno (Wells Modification)
** Method of this study (T.S.)

fo_2 Pressure Correction of Eugster and Wones (1962)

QFM : fo_2 (x bars) = fo_2 (1 bar) + $\frac{0,092\ (P_{bars} - 1)}{T°K}$

Ni-NiO: fo_2 (x bars) = fo_2 (1 bar) + $\frac{0,046\ (P_{bars} - 1)}{T°K}$

A major question concerning these fo_2 calculations in the M.Mb./P.G. is whether the equilibria conditions were determined by the bulk composition of the magma or by the volatile components? The modal proportions of biotite (phlogopite) in samples GR1 -69; -100; -102,5; -107,2; are 0,99; 2,88; 5,75; and 2,82 per cent respectively, which suggests that there is no direct relationship between the amount of mica present and the calculated fo_2. In fact, sample 78-360, which shows no signs of contamination, yields virtually the same T-fo_2 values as the other samples. It would seem, therefore, as if the bulk composition of the melt, rather than the volatile component, exerted the major influence on the "frozen in" fo_2 conditions now present in these phases.

The results of method (1) and (2) are displayed graphically in Figure 73A and B. From these it can be seen that the data plot on a fairly well defined buffer trend as is also shown in Figure 74A and B, so that these curves could be used to infer, by extrapolation, the fo_2 conditions at higher temperatures in the more anhydrous, uncontaminated portion of the M.Mb./P.G.

Estimates of the fo_2 in the upper zone rocks are based on the recast bulk composition of the titaniferous magnetite and the temperature derived from the pyroxene geothermometer (Table 15B, method 1). In an attempt to verify the obtained values, the a_{SiO_2} for sample 5-124 calculated by the CATS/Anorthite method was used, and the fo_2 calculated on the basis of the reaction:

$$FeSiO_3 + 1/6\ O_2 \rightleftharpoons 1/3 FeO \cdot Fe_2O_3 + SiO_2$$

(Table 15B, method 4). This method (4) gave an fo_2 value of about 1,18 log units lower than that calculated according to method 1. Similarly, calculations of fo_2 according to method 4 (Table 15B) for the Skaergaard Intrusion always gave lower fo_2 values than the values obtained with the Buddington - Lindsley method (Fig. 75B). According to the above calculations the magnetite gabbronorites from the basal protion of the upper zone yield values for fo_2 of $10^{-9,4}$ to $10^{-9,5}$ atm at temperatures of 1064 and 1069°C at 1 bar. A fo_2 value of $10^{-9,25}$ atm was calculated for the main magnetitite layer at 1080°C and 1 bar pressure. A correction for prevailing pressures of 4064 and 4094 bars would increase the fo_2 values by 0,24 log units to $10^{-9,16}$ to $10^{-9,26}$ atm for the magnetite gabbronorites and to $10^{-9,01}$ atm for the main magnetitite layer.

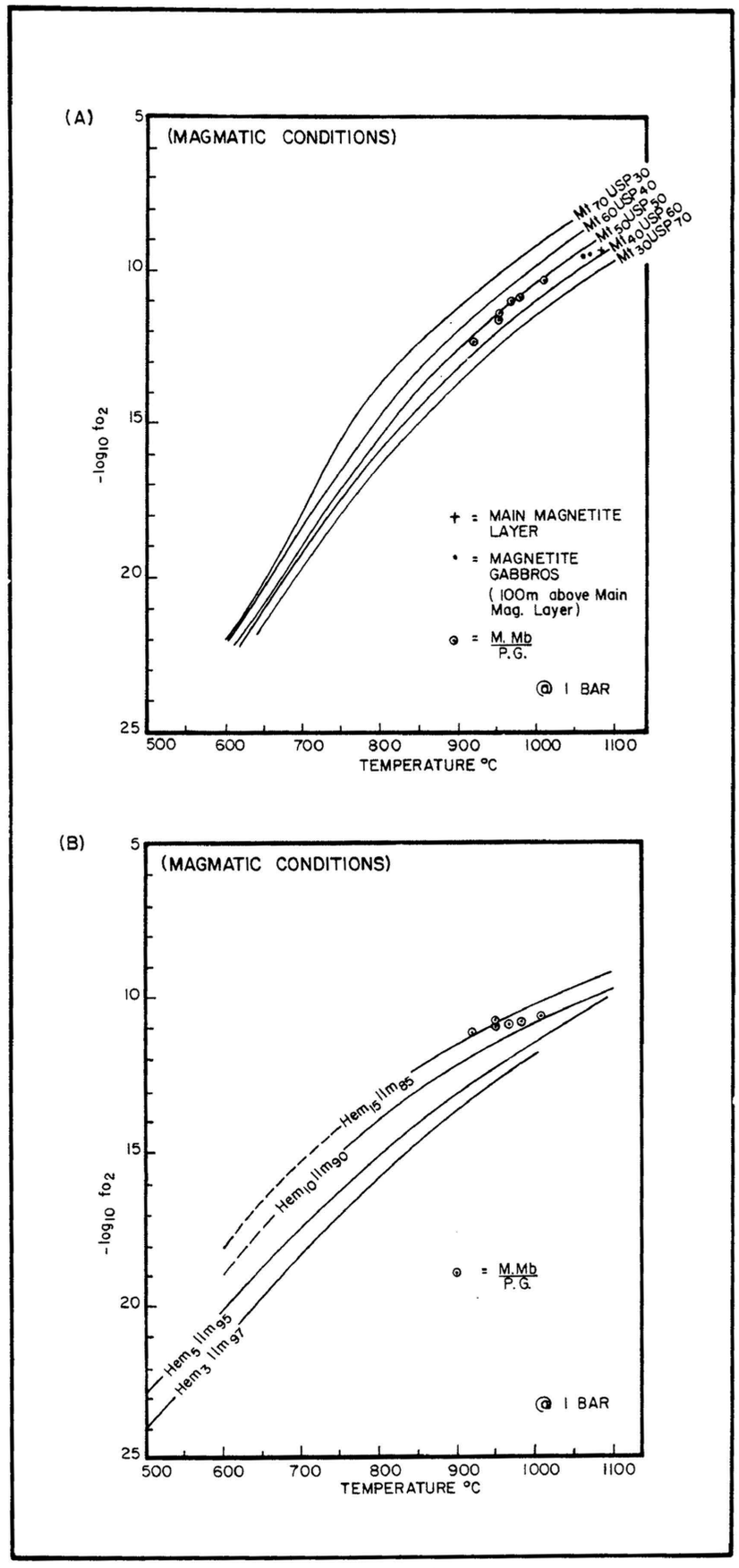

Fig. 73 fo_2 conditions for the formation of (A) titaniferous magnetite calculated according to method 1 (Table 15) and (B) ilmenite calculated according to method 2 (Table 15) for a known composition at a given temperature. Calibration curves from Buddington and Lindsley (1964).

It is of interest to note that the 1 bar fo_2 values from the M.Mb./P.G. and the upper zone samples are confined to a buffer curve mid-way between the QFM and the Ni-NiO buffer which would seem to imply that the initial critical zone magma and that which gave rise to the basal portion of the upper zone, crystallized along the same curve.

From Figure 75A it can be seen that the T-fo_2 conditions recorded for the M.Mb./P.G. specimens plot on the trend for Hawaiian volcanics, designated Hawaii and DH#9, which represent in situ determinations by Peck and Wright (1966) and Sato and Wright (1966) respectively. Fudali (1965) experimentally determined the oxygen fugacity on olivine basalt, olivine andesite, and two pyroxene andesite from Mt. Hood by reproducing naturally occurring Fe^{3+}/Fe^{2+} ratios at 1200°C. These fo_2 determinations ranged from $10^{-8,5}$ to 10^{-7} atm, defining an area straddling the Ni-NiO buffer by approximately 0,7 log units. A very similar relationship was established by Nelson (1979) for andesites from Volcán Ceburuco using the method of Buddington - Lindsley (1964). He found that the fo_2 ≈ Ni-NiO buffer +/- 0,7 atm. Carmichael (1967) found that salic volcanics from California, with olivine phenocrysts, yielded fo_2 values close to the QFM buffer curve, those with orthopyroxene phenocrysts plotted above the QFM curve, whereas those that contain biotite or amphibole plot about one log unit above the Ni-NiO buffer. This, as well as earlier considerations, suggests that the local influence of volatiles in the environment to produce biotite was not as important as originally suspected. Recently Carmichael and Ghiorso (in press) confirmed that the T-fo_2 curves for siliceous magmas containing orthopyroxene coincide with the Ni-NiO buffer.

It is interesting to note that the andesites from the Colima Volcanic Complex, Mexico (Luhr and Carmichael, 1980) contain plagioclase crystals with Ca* similar to that of the M.Mb./P.G., although their orthopyroxene, with an average Mg* of 0,710, are more magnesian. They calculated temperatures of crystallization using the Wood-Banno and Wells (1977) geothermometer and obtained values that ranged from 963 to 1023°C for the hornblende andesites and 1017 to 1056°C for the olivine andesites. The low temperatures ranging from 963 to 1056°C in these siliceous andesites seems to suggest that the similarity in calculated temperatures in the M.Mb./P.G. is more a function of the siliceous nature of the magma, rather than the fluxing influence

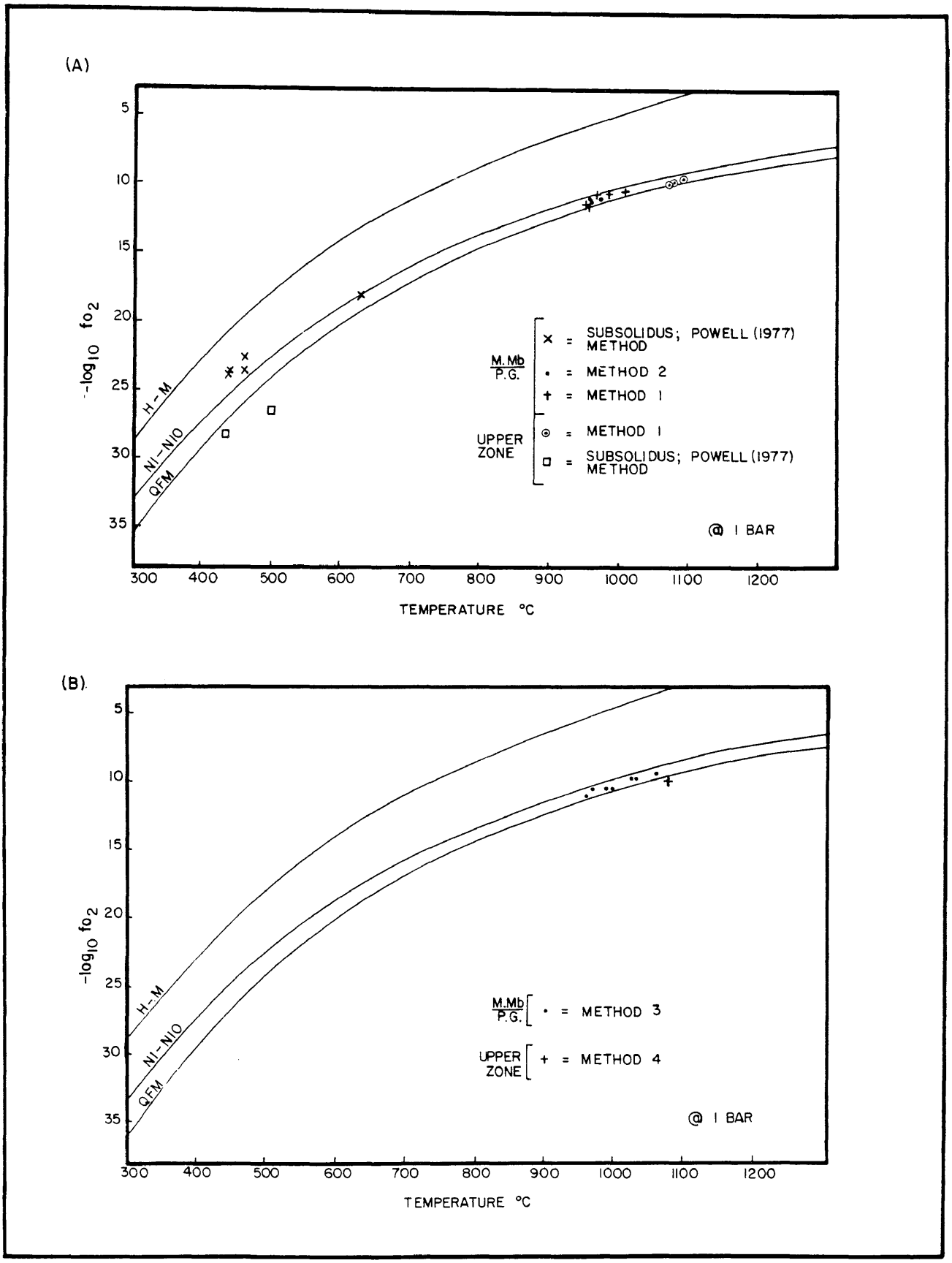

Fig. 74 T-fo_2 conditions for the formation of Fe-Ti oxide pairs based on (A) methods 1 and 2 (Table 15A and B) and (B) methods 3 and 4 (Table 15A and B) and their position relative to the QFM, Ni-NiO, and H-M buffer curves. Also shown are the estimated subsolidus T-fo_2 conditions based on the composition of the exsolved phases.

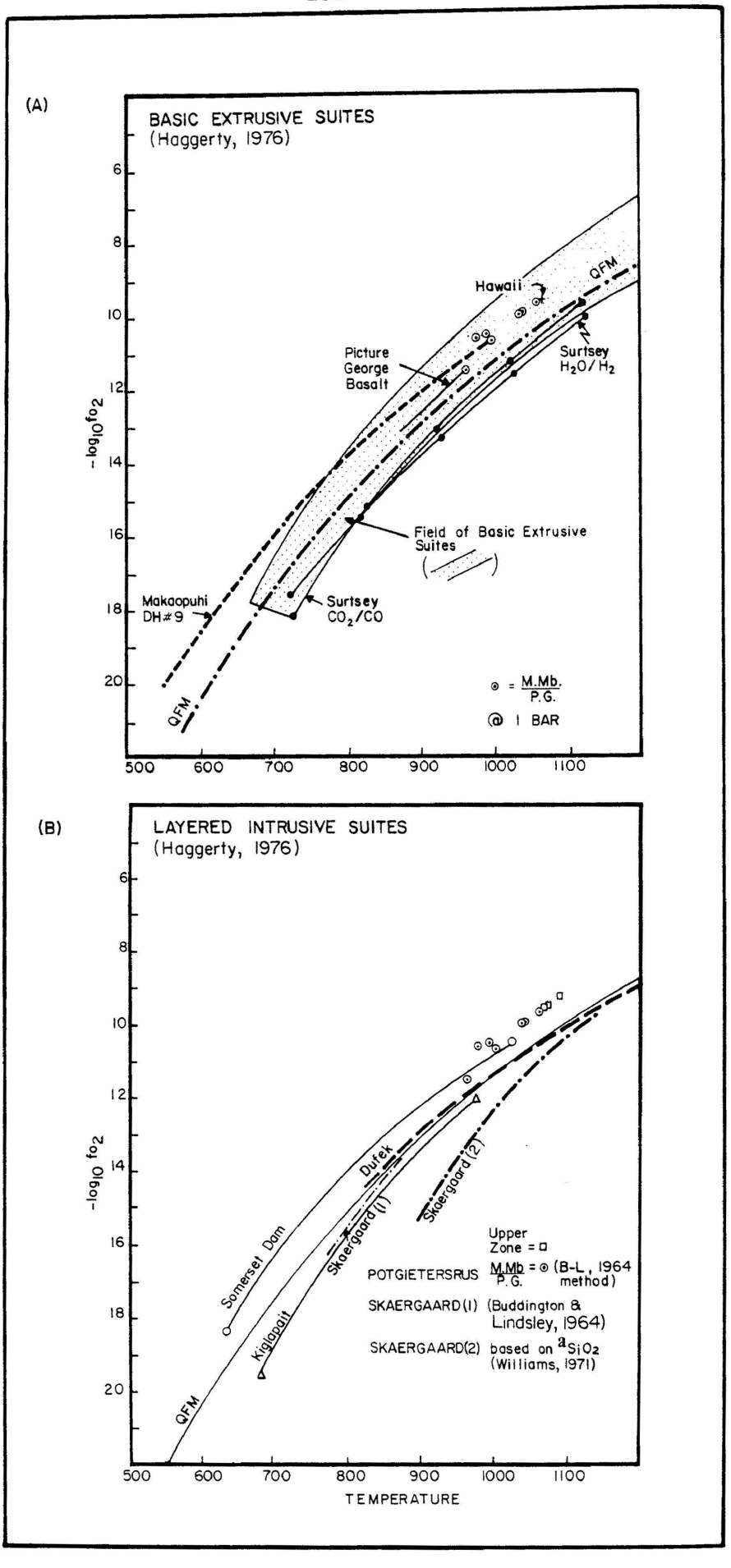

Fig. 75 Comparison of T-fo_2 conditions of crystallization of
(A) basic extrusive suites and
(B) layered intrusive suites, including the study area, based on the method of Buddington and Lindsley (1964).

of water.

T-fo_2 trends from other layered intrusions are shown in Figure 75B. The Somerset Dam Intrusion, as described by Mathison (1975), for instance was buffered under conditions very similar to the magma that gave rise to the layered mafic suite at Potgietersrus. Furthermore, the magma of the Somerset Dam, Dufek and the Potgietersrus layered intrusion have been buffered above the QFM buffer, thus accounting for the similarities in their silicate mineralogy, whereas the olivine bearing Kiglapait and Skaergaard intrusions were buffered slightly below the QFM. Recent data on the Skaergaard Intrusion (Morse et al., 1980B) has revealed that the lower zone crystallized at a temperature of about 1250°C and at a fo_2 of approximately $10^{-7,7}$ atm, whereas the final liquids near the top of the upper zone crystallized at 950°C and a fo_2 of $10^{-13,3}$ atm. Similar values for the lower and upper zones of the Kiglapait Intrusion (Morse, 1980C) are approximately 1250°C at an fo_2 of $10^{-8,1}$ and 960°C at an fo_2 of $10^{-12,2}$ atm respectively. Morse (1980C) also calculated the T-fo_2 conditions in the magma during crystallization of the main magnetitite layer in the Kiglapait Intrusion to be 1094°C at $10^{-9,65}$ atm at 1 bar total pressure. These values agree closely with those of 1080°C at $10^{-9,25}$ atm at 1 bar calculated for the main magnetitite at Potgietersrus.

T-fo_2 conditions of the magmas cooling history can be calculated by using the composition of the exsolved ilmenite and magnetite within the composite magnetite-ilmenite intergrowths of the various rock types (Fig. 74A). This diagram also shows that the T-fo_2 conditions during postcumulus re-equilibriation are usually no longer confined to the vicinity of the Ni-NiO buffer curve.

7.4.2 fo_2 Calculations Involving Chromite

In an earlier discussion concerning the origin of chromite, emphasis was placed on the role of the operative oxygen fugacity during crystallization and how it could have influenced the distribution of chromite in the lower and critical zones.

The method used to calculate the fo_2 in the lower and critical zone

is based on the reaction:

$$3Fe_2SiO_4 + 1/2\,O_2 \rightleftharpoons 3FeSiO_3 + Fe_3O_4$$
olivine gas orthopyroxene spinel

so that under equilibrium conditions:

$$\log_{10} fo_2 = 2\left[-\frac{11411}{T°K} + 3{,}54 + \frac{0{,}0227(P-1)}{T} - \log\left(a^{ol}_{Fe_2SiO_4}\right)^3 + \log\left(a^{opx}_{FeSiO_3}\right)^3 + \log a^{spinel}_{Fe_3O_4}\right]$$

(Williams, 1971A; Arculus and Wills, 1980)

The fo_2 calculations from the lower zone samples are listed in Table 16 where it can be seen that values range from $10^{-6,21}$ to $10^{-4,77}$ atm. The high value was calculated for the foot-wall of the lower chromitite whereas the unmineralized hanging-wall portion of this chromitite was calculated to have crystallized at an fo_2 of $10^{-4,89}$ atm. By using the $D^{opx\text{-}ol}_{Cr}$: fo_2 relationship of Schreiber and Haskins (1976), a calculated $D^{opx\text{-}ol}_{Cr}$ of about 6,40 for this hanging-wall section indicates an fo_2 of 10^{-5} atm at 1300°C. If the chromite rich horizons are excluded, the calculation of the fo_2 on the ol-opx-chr cumulates of the lower zone indicate that they crystallized over a fo_2 interval from $10^{-5,02}$ to $10^{-6,21}$ atm, with a mean value of $10^{-5,48}$ atm.

Snethlage and Klemm (1978) and Snethlage and Von Gruenewaldt (1977) calculated that an increase of between 0,5 to 1,0 log units was sufficient to considerably have enhanced the crystallization of chromite. Therefore, an increase from a mean value of $10^{-5,48}$ atm to $10^{-4,77}$ to $10^{-4,98}$ atm may have been all that was required to give rise to the chromitite layers in the lower zone sequence. These authors also showed that chromite-rich intervals in olivine bearing horizons tend to yield higher fo_2 values than those associated with the pyroxene-rich environments.

The accuracy of the fo_2 calculations employed in this study was tested by calculating the fo_2 for samples LG4+6 and LG4-75 which Snethlage and Von Gruenewaldt (1977) used amongst others for intrinsic fo_2 measurements. By using the composition of the chromite, olivine and orthopyroxene from these silicate-rich samples, the fo_2 was calculated with the aid of the reaction:

$$3Fe_2SiO_4 + 1/2\,O_2 \rightleftharpoons 3FeSiO_3 + Fe_3O_4$$

fo_2 values of $10^{-5,52}$ and $10^{-5,65}$ atm respectively at 1200°C were obtained. Intrinsic oxygen fugacity measurements, on the other

TABLE 16 fo_2 CALCULATIONS OF OLIVINE-ORTHOPYROXENE-CHROMITE CUMULATES FROM THE LOWER ZONE

Reaction: $3\ Fe_2SiO_4 + \frac{1}{2}\ O_2 \rightleftharpoons 3\ FeSiO_3 + Fe_3O_4$

olivine gas orthopyroxene spinel

$$\log_{10} fo_2 = 2\left[\frac{-11411}{T°K} + 3{,}54 + \frac{0{,}0227(P-1)}{T} - \log\left(a^{ol}_{Fe_2SiO_4}\right)^3 + \log\left(a^{opx}_{FeSiO_3}\right)^3 + \log a^{spinel}_{Fe_3O_4}\right]$$

Sample #	T°C	log $a^{ol}_{Fe_2SiO_4}$	log $a^{opx}_{FeSiO_3}$	$a^{Spinel}_{Fe_3O_4}$	bars Pressure	$\log_{10} fo_2$	
3-2500	1221	-1,4171	-0,7273	0,1635	4545	-5,49	
3-2940	1228	-1,4981	-0,7670	0,1652	4584	-5,16	
3-4002	1227	-1,4877	-0,7619	0,1475	4676	-5,30	
GV-1	1242	-1,6975	-0,8653	0,0856	4706	-4,98	
GV-22	1250	-1,8523	-0,9410	0,0579	4706	-4,77	
1-219	1213	-1,3288	-0,6842	0,2331	4725	-5,53	
1-223	1224	-1,4521	-0,7444	0,1393	4727	-5,48	
1-240,95	1212	-1,3196	-0,6796	0,1973	4736	-5,71	
1-244	1222	-1,4208	-0,7291	0,1560	4737	-5,50	
1-253,5	1226	-1,4683	-0,7524	0,1329	4739	-5,47	
6A-259	1226	-1,4654	-0,7511	0,1900	4743	-5,15	
X-10	1223	-1,4347	-0,7359	0,1118	4821	-5,72	
X-13	1216	-1,3630	-0-7011	0,1033	4824	6,10	
X-21	1221	-1,4171	-0,7273	0,0704	4851	-6,21	
A-3	1230	-1,5293	-0,7794	0,1574	4923	-5,06	
A-9	1223	-1,4358	-0,7365	0,1770	4945	-5,33	
A-16	1239	-1,6492	-0,8413	0,0989	5000	-5,02	
* AP-1	1200	-1,4171	-0,6781	0,0730	5300	-6,07	
* LG4+6	1200	-1,5160	-0,7739	0,1407	4500	-5,52	-7,30**
* LG4-75	1200	-1,5740	-0,8041	0,1011	4500	-5,65	-7,00**

* Calculated fo_2 values from other areas of the Bushveld Complex.

** fo_2 values measured by Snethlage and von Gruenewaldt (1977) in silicate fraction.

hand, yielded values of $10^{-7,30}$ and $10^{-7,00}$ atm for the same two samples respectively. The intrinsic oxygen fugacity values are considered to be lower than the actual magmatic conditions due to possible effects of postcumulus re-equilibriation. Examination of Snethlage and Von Gruenewaldt's(1977) Figure 4 shows that the top portion of the LG4 chromitite layer contains as much as 85 per cent modal chromite which suggests that the massive portion of the chromitite layer could have undergone sintering during the postcumulus stage. Even in the silicate-rich rocks LG4-75 and LG4+6, slight subsolidus effects can be seen in that some of the small chromite grains in mutual contact display triple point junctions.

The advantage in calculating fo_2 is that such re-equilibriation affects can be avoided to some extent by analyzing only the cores of olivine, chromite and orthopyroxene grains, as such analyses would most closely reflect magmatic conditions. Although the discrepancy between the calculated and the measured fo_2 for these two samples is 1,56 log units, both methods can be used to place an upper and lower limit on the fo_2 conditions at 1200°C.

A considerably greater discrepancy between the intrinsic fo_2 measurements and calculated fo_2 values was found by Sato and Valenza (1980) for oxides in the Skaergaard Intrusion. They found that the measured fo_2 values were always at least two, and in some cases three, log units lower than those calculated according to the method of Buddington and Lindsley, by Lindsley, et al. (1969) and Morse, et al. (1980B). These lower values are undoubtedly due to incorporation of subsolidus re-equilibriation affects in the intrinsic fo_2 measurements on mineral separates.

7.4.3 Crystallization Path of the Bushveld Magma in Terms of T and fo_2

All the calculated T-fo_2 values for spinel bearing assemblages from the lower, critical and upper zone are plotted in Figure 76. This diagram shows that over the temperature range 1150 to 950°C all these pressure corrected fo_2 values are confined to the proximity of or above the Ni-NiO buffer. However, at higher temperatures, the melt was not confined to the Ni-NiO buffer, for the fo_2 values define a much steeper trend. It is of interest to note that the T-fo_2 values based on intrinsic oxygen fugacity measurements on chromites from the critical zone of the eastern and western Bushveld (Snethlage

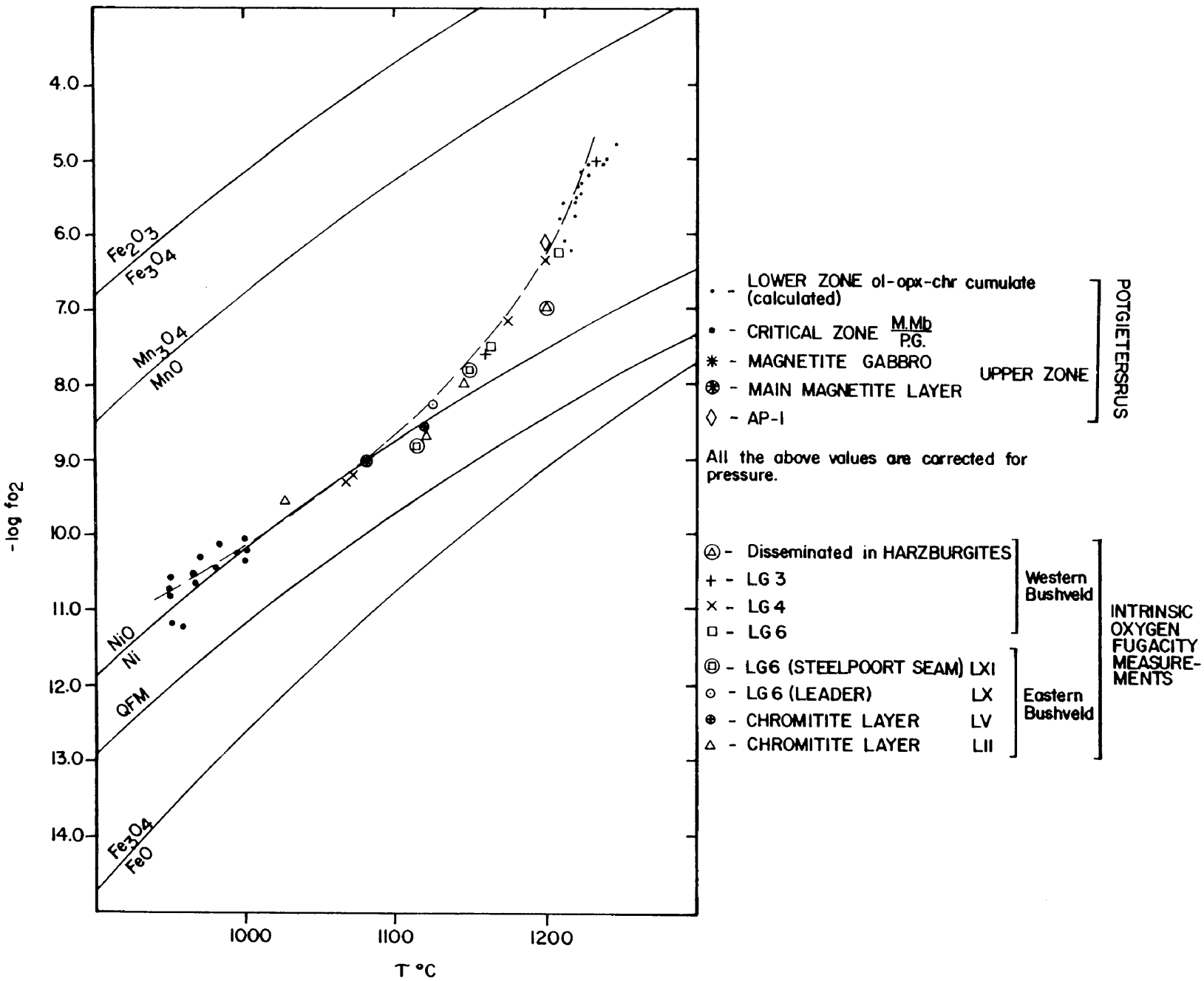

Fig. 76 T-fo_2 conditions for the Potgietersrus limb and the eastern and western sectors of the Bushveld Complex. Data of intrinsic oxygen fugacity measurements is from Snethlage and Von Gruenewaldt (1977) and Snethlage and Klemm (1978).

and Von Gruenewaldt, 1977; Snethlage and Klemm, 1978) also plot on this steeper trend.

Absence of spinels in rocks of the main zone made direct calculation of the fo_2 not possible. However once the mixing model problems are overcome with respect to a $^{cpx}_{CATS}$ the silica activity calculations should be able to provide indirect measurements of fo_2.

Buchanan (1976) and Marais (1977) have compared fractionation trends in different parts of the Bushveld Complex by plotting compositional variation of plagioclase against that of coexisting orthopyroxene. Their diagrams, on which the Potgietersrus trend has been added, are reproduced here as Figure 77. The observed differences in the trends of the composition of coexisting orthopyroxene and plagioclase can probably be ascribed to differing fo_2 conditions. Speidel and Osborne (1967); Sack, et al. (1980); Roeder and Emslie (1970) and Roeder (1974) have shown that relative increases in the oxygen fugacity results in an increase in the magnesium component of pyroxenes and olivines. In the upper zone the reaction:

$$\underset{\text{liquid}}{3FeO} + 1/2\,O_2 \rightleftharpoons \underset{\text{magnetite}}{FeO \cdot Fe_2O_3}$$

is particularly relevant, as a change to a high fo_2 buffer trend during crystallization would result in the FeO extraction from the magma and consequently cause an enrichment of MgO in coprecipitating silicate. The curves in Figure 77A, therefore suggests that in the Bethal area (Buchanan, 1976) the Ongezien section crystallized under higher fo_2 conditions than the Kaallaagte section whereas the UC361 section would have crystallized under conditions intermediate between the two. The higher fo_2 in the Ongezien section would explain the higher percentage of modal Fe-Ti oxides in this area. The position of the curves furthermore suggest that the main and upper zone section studied by Von Gruenewaldt (1971) crystallized under lower fo_2 conditions than did the magma which gave rise to the equivalent section studied by Molyneux (1970) further to the north. Marais (1977) investigated the same compositional relationship across the pyroxenite marker in the main zone along four sections designated from north to south as Thornhill, Steelpoort Park, Galgstroom, and Tonteldoos. It can be seen on Figure 77B that for a certain plagioclase composition the Mg content of the orthopyroxene increases from south towards north in the order Tonteldoos, Galgstroom,

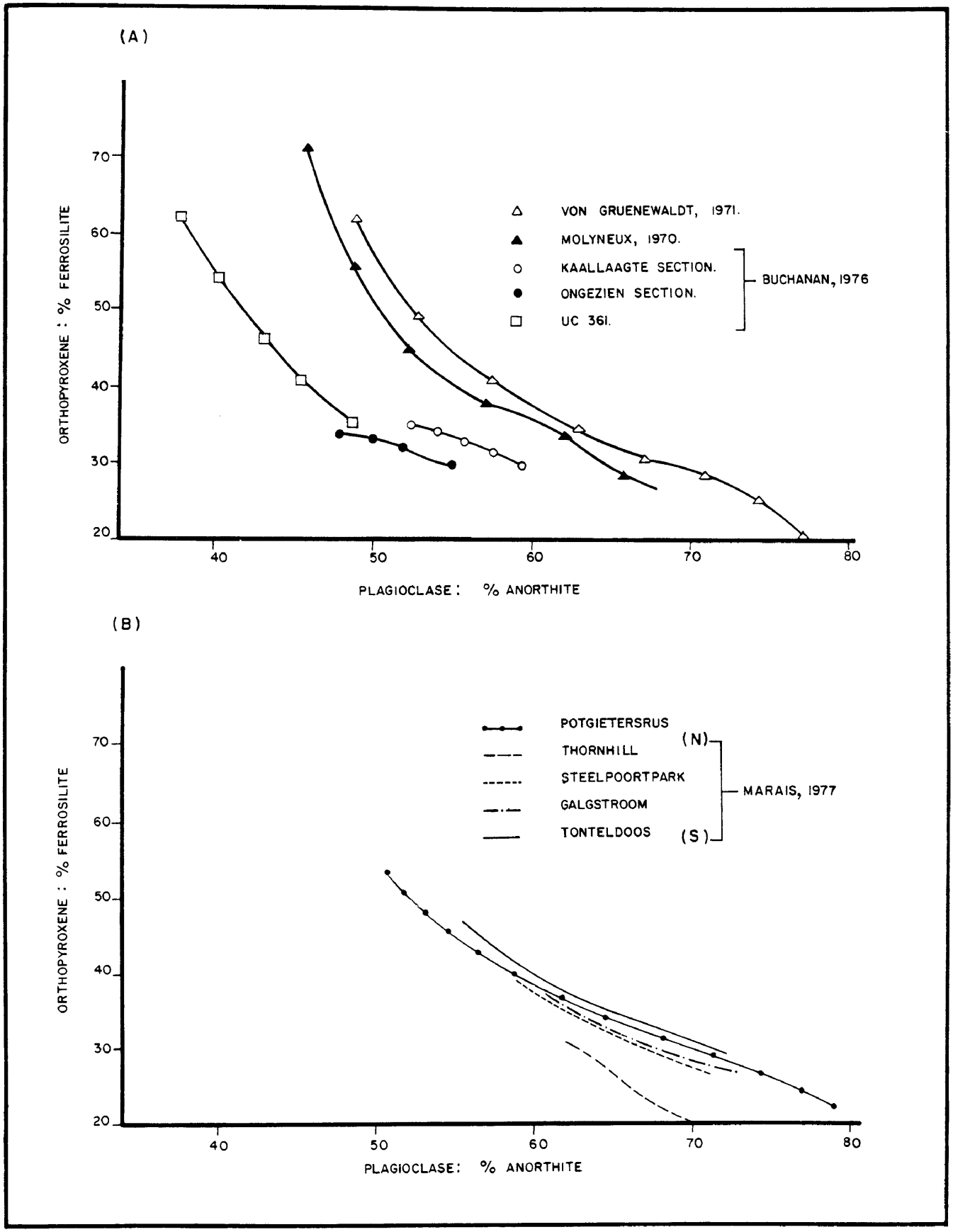

Fig. 77 Variation of the ferrosilite component in orthopyroxene with the anorthite component of plagioclase for:
(A) the eastern Bushveld and the Bethal area, and
(B) the Potgietersrus limb and the four sections across the pyroxenite marker.

Steelpoort Park, Thornhill suggesting increasing fo_2 conditions towards the north during crystallization of the magma. The same trend could be due to a lateral temperature gradient along strike, with the temperature increasing towards the north. Seeing that the cooling curve of magmas tends to parallel buffer curves (Figure 73, 74, and 75) any increase in temperature will normally be accompanied by an increase in fo_2.

Comparison of the Potgietersrus trend with the other Bushveld trends reveal that the Potgietersrus trend is almost identical to that established by Von Gruenewaldt (1971). This would also suggest that these two coincident trends were buffered under the lowest fo_2 conditions relative to those established by Buchanan (1976), Molyneux (1970) and Marais (1977), with the exception of the Tonteldoos section. This implies considerable lateral differences in temperature and consequently also fo_2 during crystallization of the main and upper zones of the Bushveld Complex.

7.5 Density and Viscosity of the Initial Magmas

A question that has received the attention of igneous petrologists in recent years is whether or not the density contrast of liquids and the phases that crystallize from them is sufficiently large to allow settling of crystals, especially plagioclase. Although the exact changes in the composition of the melt with fractionation is not known, the respective composition of the postulated initial main and critical zone magmas can be used to infer whether or not cumulus plagioclase could settle through the magma to accumulate as a crystal pile on the floor of the magma chamber.

The density of the two melts was calculated according to the method of Bottinga and Weill (1970) which is based on published density measurements of the partial molar volumes of the major oxide components in binary and ternary silicate melts. The densities for the postulated liquids in the study area were originally calculated over the interval 1200 to 1500°C and these results were then used to extrapolate to lower temperatures. The density results calculated over the temperature range of 900 to 1300°C are shown in Table 17B. The samples of most immediate interest are 78-53 and 78-92, which are considered to approximate the initial critical and main zone magma compositions respectively. Since all of the critical

TABLE 17 VISCOSITY AND DENSITY CALCULATIONS FOR THE POSTULATED [illegible] LIQUIDS FOR THE POTGIETERSRUS AREA

(A) Viscosity

Sample ##	@ *		1000°C	1100°C	1200°C	1300°C	1400°C	1500°C
GR4-4ε5	1170°C ,	1391 η	-	3381 η	1076 η	272 η	94 η	43 η
78-53	969°C ,	13960 η	8946 η	2321 η	788 η	186 η	65 η	34 η
78-374	1050°C ,	3321 η		1694 η	562 η	127 η	43 η	23 η
GR1-88.48	1002°C ,	28767 η		6850 η	2007 η	462 η	147 η	69 η
GR1-98.2	959°C ,	54176 η	28998 η	6988 η	2124 η	504 η	172 η	80 η
GR1-98.5	959°C ,	53852 η	28882 η	6995 η	2160 η	515 η	178 η	82 η
GR1-99.5	959°C ,	66237 η	35348 η	8476 η	2544 η	607 η	209 η	94 η
GR1-100	951°C ,	63006 η	29792 η	7186 η	2183 η	518 η	179 η	83 η
GR1-102.5	951°C ,	74682 η	35031 η	8341 η	2493 η	590 η	201 η	92 η
GR1-109.5	1005°C ,	26822 η	28882 η	6974 η	2121 η	502 η	173 η	80 η
78-72	1116°C ,	5819 η	29971 η	7222 η	2121 η	541 η	185 η	79 η
78-71	1105°C ,	5756 η		6155 η	1878 η	465 η	162 η	73 η
78-359B	1103 °C,	7101 η		7398 η	2203 η	543 η	188 η	82 η
78-431B	1137°C ,	1128 η		1806 η	607 η	142 η	50 η	27 η
78-170A	1137°C ,	1074 η		1726 η	569 η	136 η	46 η	24 η
78-170B	1137°C ,	1694 η		2716 η	873 η	224 η	77 η	36 η
78-92	1136°C ,	3005 η		4817 η	1488 η	371 η	127 η	57 η

η = Poise, calculated by the method of Bottinga and Weill (1972)
* = Two pyroxene geothermometer

(B) Density

Sample ##	900°C	1000°C	1100°C	1200°C	1300°C
GR4-4ε5	2,668	2,654	2,640	2,625	2,610
78-53	2,728	2,712	2,696	2,680	2,665
78-374	2,770	2,754	2,738	2,722	2,706
GR1-88.48	2,659	2,646	2,633	2,620	2,607
GR1-98.2	2,644	2,631	2,618	2,605	2,592
GR1-98.5	2,644	2,630	2,616	2,603	2,590
GR1-99.5	2,630	2,617	2,604	2,591	2,579
GR1-100	2,643	2,630	2,617	2,604	2,591
GR1-102.5	2,636	2,622	2,608	2,595	2,583
GR1-109.5	2,647	2,634	2,621	2,607	2,594
78-72	2,630	2,617	2,604	2,590	2,577
78-71	2,644	2,630	2,616	2,602	2,589
78-359B	2,645	2,623	2,610	2,596	2,583
78-431B	2,759	2,743	2,727	2,711	2,695
78-170A	2,745	2,729	2,713	2,697	2,681
78-170B	2,678	2,662	2,646	2,631	2,616
78-92	2,651	2,636	2,621	2,607	2,593

Density = $g.cm^{-3}$, calculated by the method of Bottinga and Weill (1970).

zone plagioclase falls within the compositional range An_{60} to An_{80} their densities will range between 2,70 and 2,73 g.cm.$^{-3}$ At 1100°C the postulated critical zone magma (78-53) would have had a density of 2,69 g.cm.$^{-3}$ so that purely on the bases of a density contrast, crystal settling could theoretically have taken place. In contrast, 78-374 which is a sample of an uncontaminated rock from the M.Mb./P.G. and which was once considered to be representative of the initial critical zone magma, yielded a density of 2,73 and 2,75 g.cm.$^{-3}$ at 1100°C and 1000°C respectively. Plagioclase crystals would not have settled through such a liquid. However, at 1200°C the density of the liquid, 2,72 g.cm.$^{-3}$, would allow the most calcic and thus densest plagioclases to settle. Samples GR1-88,48 to 78-359B represent contaminated M.Mb./P.G. samples. Siliceous contamination has reduced the density by about 0,07 g.cm.$^{-3}$, but on the other hand it has increased the viscosity sufficiently to impede settling of plagioclase crystals.

Liquids corresponding in composition to the fine-grained pigeonite gabbros at the base of the critical zone (samples 78-170B and GR4-4 and 5) have densities of about 2,64 g.cm.$^{-3}$ at 1100°C. The large density contrast would have allowed settling of plagioclase crystals in the magma chamber if it is assumed that the compositions of the pigeonite gabbronorite was similar to that of the original magma as is believed to have been the case. The density calculations of the mineralized equivalent of these two samples (78-170A and 78-431B) yielded values of 2,71 and 2,72 g.cm.$^{-3}$ respectively at 1100°C whereas at 1200°C the densities were calculated to be 2,69 and 2,71 g.cm.$^{-3}$ respectively. These samples contain between 4 and 5 weight per cent sulfides which makes exact determination of the density of the corresponding liquid difficult. However if it is assumed that the calculations are correct, then the associated plagioclase (An_{64}) in this sulfide-rich rock would have a negligible if not negative density contrast and thus would float.

The density of the postulated initial main zone magma (sample 78-92) was calculated to be 2,62 and 2,60 g.cm.$^{-3}$ at 1100 and 1200°C respectively. Since all of the plagioclases within this zone have a density of between 2,68 and 2,72 g.cm.$^{-3}$, the density contrast is sufficient to allow crystal settling of plagioclase.

There are very few processes during cooling and crystallization of a magma that are not in some way or other related to the viscosity of the melt. A method to calculate the viscosity was devised by Bottinga and Weill (1972) based on the composition of the melt. This method was used to calculate the viscosity of the respective samples at temperatures ranging from 951 to 1500°C (Table 17A). At 1100°C a liquid with the composition of sample 78-53 has a viscosity of 2321 η which is almost identical to that of a high alumina basalt from Lassen, California (Fig. 78A and B). In comparison, the contaminated samples GR1-88,48 to 78-359B yield viscosities of about three times as high as that of 78-53 at 1100°C. Such high values give melts of this composition properties of a magma close to that of a phonolitic trachyte lava (Fig. 78A). Such a high viscosity would increase the buoyancy of the crystals and prevent crystal settling. This would become even more pronounced at lower temperatures. The high viscosity in these contaminated liquids would have been counteracted to some extent by the simultaneous addition of water during contamination. Shaw (1965) has, for instance, shown in this regard that the concentration of water from 0,5 to 4 weight per cent at 1000°C lowers the viscosity from $\log_{10}\eta = 8$ to 5 in acid magmas. The increased viscosity of the contaminated melt would prevent this liquid from mixing with the bulk of the magma in the chamber, as well as inhibit diffusion of elements. The generally decreasing viscosity away from the contact in conjunction with an increase in temperature also allowed for the gradual coarsening in grain size away from the contact.

Viscosity calculations of postulated liquid compositions in the study area are compared with published values in Figure 78. The postulated initial main zone magma (78-92) had a viscosity of about twice that of the postulated critical zone liquid (78-53). The high viscosity of the main zone sample places it close to the phonolitic trachyte in Figure 78A. Its higher viscosity may be ascribed to the higher a_{SiO_2} calculated for this sample. For comparison, the calculated viscosity of a granitic melt (GR1-75), based on the composition of a granitoid floor melt encountered in the M.Mb./P.G. is shown. The viscosity is very similar to that of a rhyolite from Mono Crater, California (Fig. 78A).

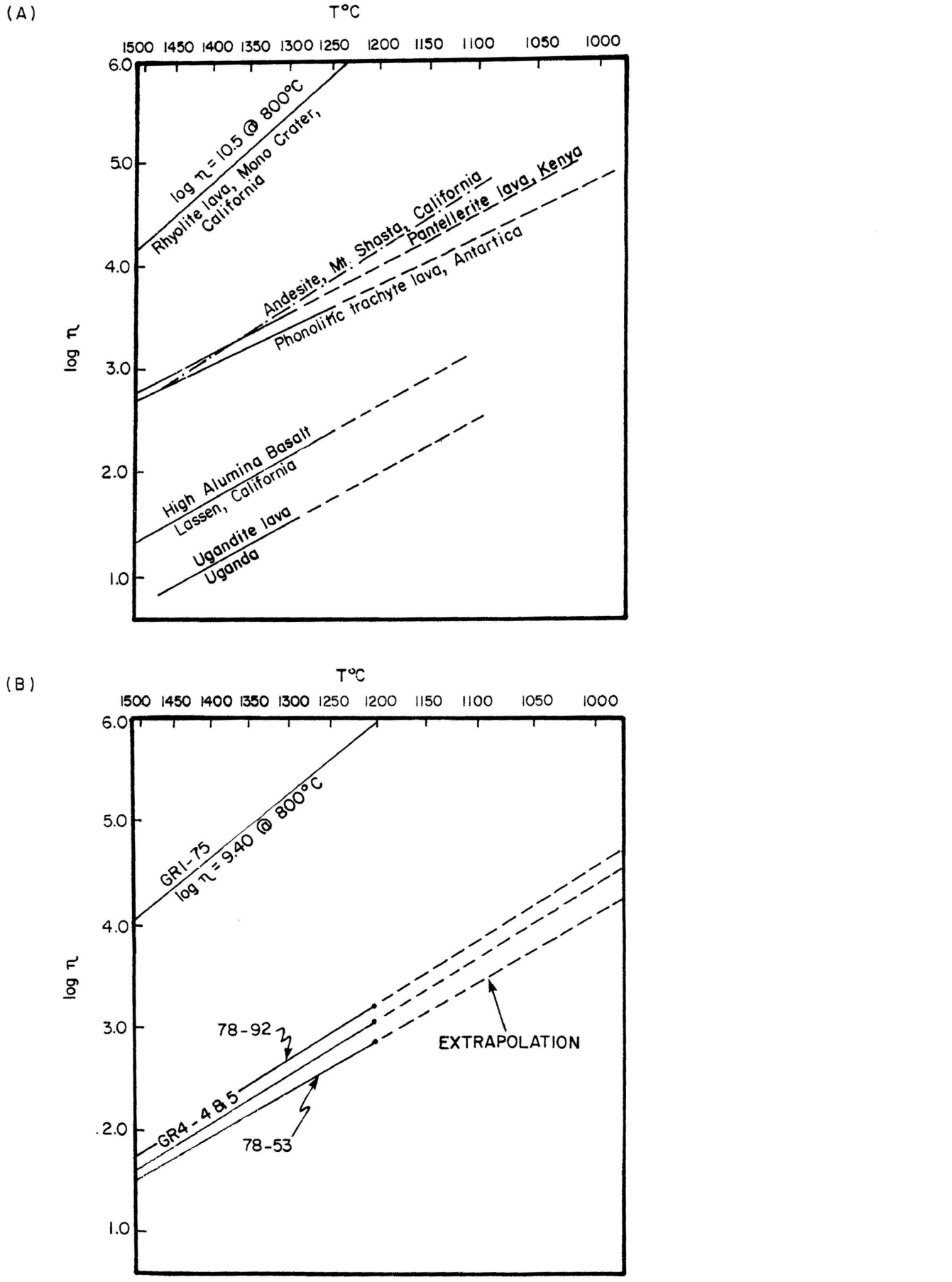

Fig. 78 Logarithms of calculated viscosities at a variety of temperatures for: (A) various lava types from Carmichael, Turner, and Verhoogen (1974) and (B) proposed initial liquids (78-92, 78-53, and GR4-4 and 5) of the critical and main zones of the Potgietersrus limb. Also shown is the calculated viscosity-temperature plot for the granitoid rock GR1-75.

8 SULFIDE AND PGE MINERALIZATION

Ni-Cu sulfides and associated PGE mineralization in the Potgietersrus limb of the Bushveld Complex has attracted the attention of exploration companies intermittently ever since their discovery in 1924 (Wagner, 1929). The principle exploration efforts have been confined for many years to the so-called "Platreef" in the area situated 25 km N.N.W. of the town of Potgietersrus. This platiniferous zone occurs at the base of the Rustenburg Layered Suite and is generally considered to be part of the critical zone (van der Merwe, 1976).

The present investigation has shown sulfide mineralization in the area south of Potgietersrus to be considerably more widespread than previously appreciated, and above average concentrations of sulfides have been found to occur at at least 14 different levels in the succession investigated. By far the most striking of these is a 30 to 40 m thick mineralized gabbronorite at the base of the critical zone, and judging from its thickness and lateral continuity it can be considered one of the more spectacular concentrations of orthomagmatic stratiform sulfide mineralization.

8.1 Sulfides in the Lower Zone

8.1.1 The Volspruit Pyroxenite

During the investigation of the extensive laterite Ni mineralization on the farm Volspruit in 1970, Rio Tinto Exploration Ltd. intersected significant concentrations of Ni-Cu and PGE mineralization in harzburgites, dunites and pyroxenites of the Volspruit Pyroxenite subzone.

The assay data of rocks from the Volspruit subzone for Ni, Cu, Pt and Pd on Figure 79 and 80 was obtained from the diamond drill hole records of Rio Tinto Exploration Ltd. Each of the assay data points on these Figures represent total Ni, Cu, Pt, and Pd values obtained on a two metre split of core.

The lower part of the Volspruit subzone (Fig. 79) contains cyclic units 1 to 9 and consists of alternating opx-ol-chr cumulates and opx cumulates. The high Ni values of the opx-ol-chr cumulates is due to the high modal olivine content and not due to the presence of sulfides. The Cu content on the other hand is a very useful in-

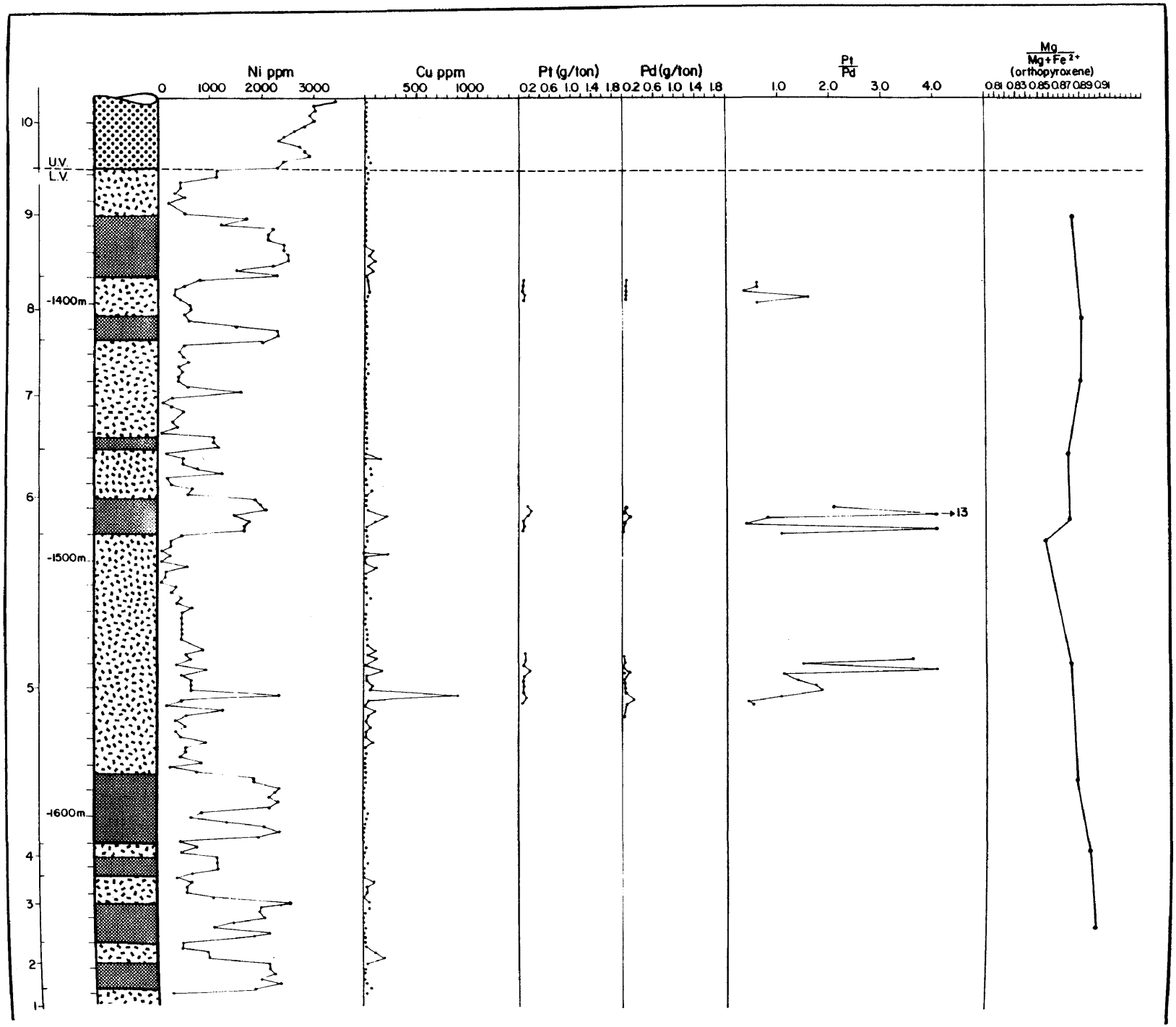

Fig. 79 Variation in Ni, Cu, Pt, and Pd through the lower Volspruit subzone.

dicator of the tenure of sulfide mineralization and from this it is evident that abnormal sulfide concentrations are only developed at the -1550 m and -1485 m levels (Fig. 79). The presence of sulfide mineralization is also indicated by higher Pt and Pd values. The average Mg* of the orthopyroxene for this subzone (Fig. 79) is 0,890 with the maximum value of 0,905 occurring near the base. The only significant drop in the Mg* (0,878 to 0,850) occurs near the base of the weakly mineralized zone at -1485 m. The drop in the Mg* is a feature commonly associated with sulfide-rich horizons. Closer spacing of the analysed orthopyroxenes would probably have revealed a drop in the Mg* near the base of the weakly mineralized horizon at the -1550 m level.

The upper part of the Volspruit subzone (cyclic units 10 to 19) is characterized by a pronounced decrease in the amount of opx-ol-chr cumulate, an increase in the amount of orthopyroxene and opx-chr cumulates, as well as the first appearance of ol-chr cumulates. The Cu content rises noticeably towards the top of the thick ol-chr cumulate at the base of cyclic unit 10, and increases irregularly to peak values near the top of the opx cumulate of this unit (Fig. 80). From here to the top of the overlying 20 m thick unit 11, the Cu, Pt, and Pd values decrease systematically. The highest values are always found in the basal six metres of the mineralized zone where sulfides constitute about 3 weight per cent of the rock and where the average grades are in the order of 0,24 per cent Ni, 0,11 per cent Cu, 1,39 g/ton Pt and 1,73 g/ton Pd. Here the sulfides form drop-like to interstitial patches similar to that shown in Figure 84B. The first noticeable sulfides in the upper Volspruit subzone occur as interstitial to net-textured grains in an ol-chr cumulate at the -1250 m level (Fig. 84A).

The sulfide mineralization for this subzone consists, in decreasing order of abundance, of pyrrhotite, pentlandite, chalcopyrite and cubanite, and is distinct from mineralization elsewhere in the lower zone in that troilite, hexagonal pyrrhotite and cubanite have been noted. The only platinum group mineral observed was sperrylite.

One of the more informative chemical variables shown in Figure 80 is the Mg* of the orthopyroxene, in that it decreases considerably

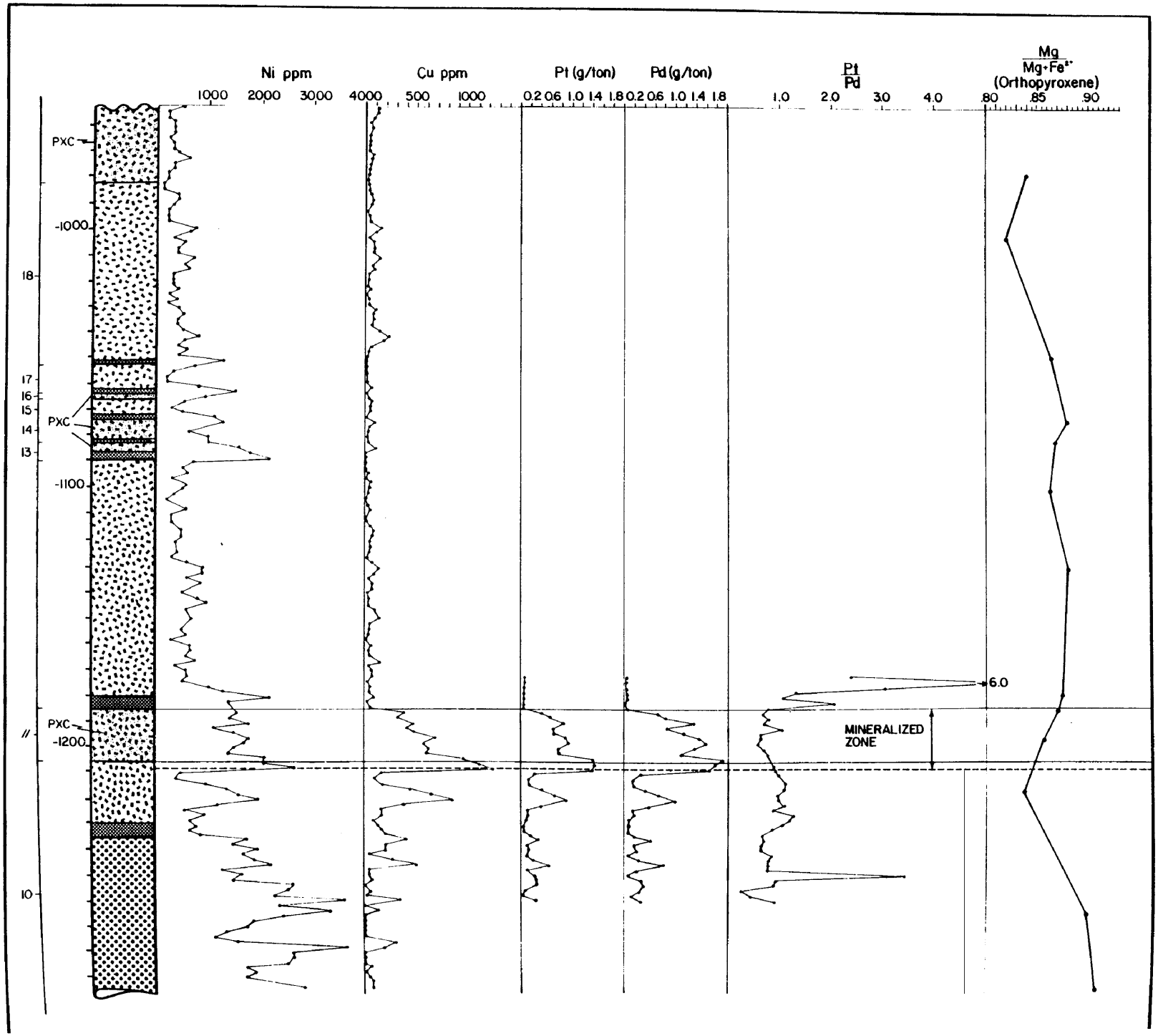

Fig. 80 Variation of Ni, Cu, Pt and Pd through the upper Volspruit subzone.

to as low as 0,830 in the immediate, unmineralized foot-wall pyroxenite. The more closely spaced major element whole rock data (Chapter 6) showed that the MgO content sytematically decreased from about the -1250 m level to the -1200 m level, i.e. slightly into the base of the mineralized zone, and then increases upward through the remainder of this zone, thereby confirming the trend established by microprobe analyses. The Mg* of the orthopyroxene at the -1270 m level is about 0,894, and similar values prevail through the unmineralized cyclic units 1 to 9 of the lower Volspruit subzone. This leads to the conclusion that the rapid Fe enrichment of the pyroxenes directly below, as well as at the base of the mineralized zone, reflects some strong control on the magma that triggered the precipitation of the sulfides. As mentioned previously, such rapid Fe enrichment could not have been due to normal processes of fractional crystallization in a closed system. It is furthermore of interest to note that from the -1220 m level, where the pyroxene has the lowest Mg*, upwards through the mineralized zone to the -1180 m level the sequence changes from a normal, almost chromite-free (0,5 volume per cent), pyroxenite at the top of unit 10 to the orthopyroxene-chromite cumulate of unit 11 which contains 3 per cent chromite at the base, 6 per cent chromite in the middle and up to 9 per cent chromite at the top. The increased modal proportions of chromite towards the top of this unit is accompanied by an increase in the Mg* of the pyroxene (Fig. 80) and, although not as evident from the limited analytical data available, also for the chromite (Fig. 7B). As suggested by Arculus and Osborn (1975), such an increase in the Mg* of the chromite and the coexisting mafic silicate can be ascribed to an increase in fo_2.

The sections illustrated in Figure 79 and 80 are located about 1000 m away from the eastern contact of the Complex. Extensive reverse block-faulting has resulted in large down-dip blocks being uplifted so that this mineralized zone was also intersected by diamond drilling in areas up to 3000 m away from the contact of the intrusion, i.e. closer to the centre of the intrusion. From the study of numerous shallow boreholes drilled in the area, it is evident that the thickness and lateral continuity of individual layers varies considerably and that, in many instances, only the large units can be traced for significant distances.

The down-dip intersection of the mineralization and the associated units is a case in hand (Fig. 81). Here the ol-chr and opx-ol-chr cumulate of cyclic unit 10 were intersected at the base of the hole, but the amount of chromite in the opx-chr cumulate of unit 11 has decreased to such an extent that it has become impossible to distinguish this unit from the opx cumulate at the top of the cyclic unit 10. Similarly, the base of the overlying cyclic unit 12 cannot be defined with certainty as the intersected opx-ol-chr cumulates in the down-dip section tend to be inconsistent along strike.

Of considerable importance, however, is the pronounced increase in the amount of sulfide in the down-dip section and the associated increase in the grade of mineralization. This is especially the case for Pt and Pd values which are, on average, about 1,8 times higher and Cu values which are up to 1,7 times higher. Ni on the other hand only increases marginally. Typical values for the lower 6 m of the mineralized zone are in the order of 0,27 per cent Ni; 0,19 per cent Cu; 3,09 g/ton Pt and 2,56 g/ton Pd. A simplified respresentation of the down-dip enrichment, especially for Pt and Pd, is given in Figure 82, which also illustrates the tremendous increase in thickness of the mineralized zone. As in the up-dip section, Cu, Ni, Pt, and Pd also decrease systematically upwards, although the depletion in the crystallizing magma of both Cu and Pt seems to have been more rapid than Ni and Pd, as is indicated by the increasing Ni:Cu and Pt:Pd ratios (Fig. 81).

Statistical treatment of associated Ni, Cu, Pt, and Pd values from this mineralized zone has shown some very strong inter-element correlations. The high correlation coefficient between Ni and Cu ($r = 0,944$) clearly indicates that virtually all the Ni is in the sulfide form. Both Pt and Pd have correlation coefficients of 0,890 for Ni and 0,930 for Cu which clearly indicates that the PGE were collected by the immiscible sulfide liquid. The low total concentration of chromite (<3 per cent) at the base of this mineralized zone would testify against any significant amount of PGE being derived from the spinels at high temperature, as has been suggested, amongst others, by Naldrett and Cabri (1976).

Whole rock assay data for Ni, Cu, Pt, and Pd from 975 mineralized and unmineralized samples from the Volspruit subzone were evaluated

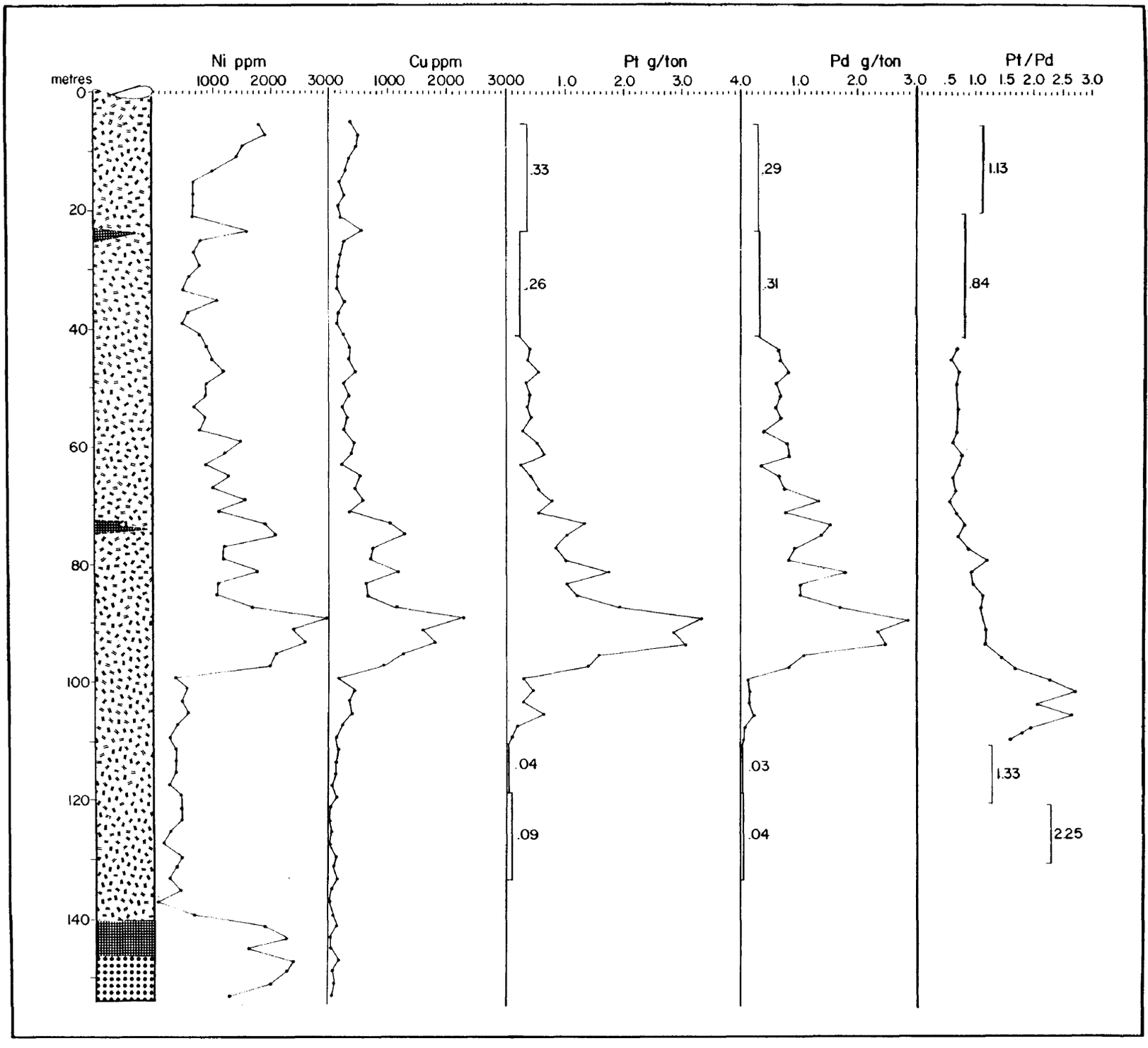

Fig. 81 Down-dip columnar section and Ni, Cu, Pt and Pd variation through the mineralized zone on Volspruit.

statistically (Tables 18 and 19). Table 18 shows that the pyroxenites are substantially enriched in Cu, Pt, and Pd compared to the olivine-bearing rocks. Mean concentration values for Cu, Pt, and Pd in the pyroxenites are 379; 0,46; and 0,53 ppm respectively and for the harzburgites 200; 0,16 and 0,19 ppm respectively. Comparison of Ni values is not possible due to the high silicate Ni contribution of olivine which is also reflected by the low correlation coefficient between Ni, and Cu, Pt, Pd for the harzburgites (Table 19). The higher correlation coefficient between Ni and these elements in the pyroxenite suggests that a substantial amount of the Ni in these rocks is present as sulfide Ni. High correlation coefficients between Cu on the one hand and Pt and Pd on the other hand prevail, irrespective of the rock type, which suggests that the PGE are in the sulfide phase. Unfortunately, insufficient sulfide Ni assays are available from the mineralized zone to determine whether the PGE are preferentially associated with the Ni or with the Cu. Microscopic investigations of the sulfides, however, suggest that the minerals of the PGE are preferentially associated with chalcopyrite.

From the available data it is concluded that crystallization of the lower Volspurit subzone resulted in a gradual enrichment of sulfur in the magma and possibly even reached saturation during cyrstallization of cyclic unit 10. Towards the end of crystallization of this cyclic unit a volumetrically smaller quantity of denser, cooler and less primitive basaltic liquid was emplaced, that spread laterally below the crystallizing hotter and less dense lower zone magma in the chamber. From this basaltic liquid the iron enriched orthopyroxene directly below the mineralized zone separated. Gradual mixing of the lower zone magma with this basaltic liquid could have resulted; first, in oversaturation of the lower zone magma in sulfur and the separation of an immiscible sulfide liquid and, secondly, in the precipitation of some chromite. The reason for the increase in the modal proportion of chromite and the upward increase in the Mg* of coexisting orthopyroxene and chromite can possibly be the result of mixing of two magmas, especially if the fo_2 of the denser and cooler liquid was higher. Although no chromite crystallized from the cooler magma, the effect of gradually contaminating the overlying lower zone liquid with Fe_2O_3 could have resulted in the enlargement of the primary phase volume of spinel (Osborn, 1978) and the onset of the precipitation of chromite together with orthopyroxene

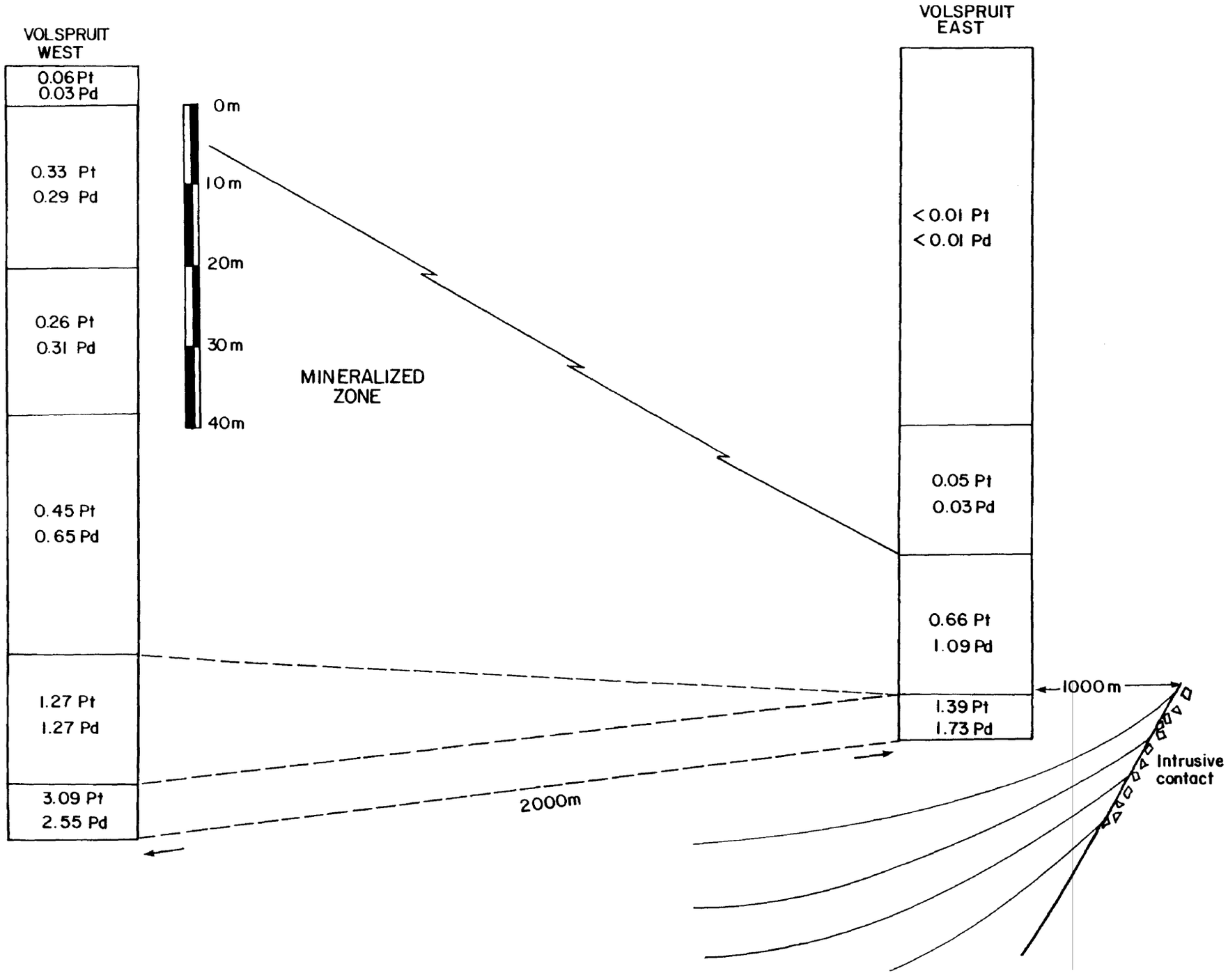

Fig. 82 Schematic representation of the differences in thickness and Pt and Pd values between the up-dip and down-dip sections through the mineralized zone on Volspruit.

to give rise to the orthopyroxene-chromite cumulates of cyclic unit 11. As contamination of the lower zone magma increased on further mixing, the fo_2 gradually increased in the lower zone magma to give rise to the maximum modal proportions of chromite and the relatively high $Mg/(Mg+Fe^{2+})$ ratios for both chromite and orthopyroxene that precipitated from this magma to form the top of cyclic unit 11.

That separation of a sulfide-liquid promotes the crystallization of orthopyroxene rather than olivine in a magma is evident from the following relationship proposed by Marakushev (1979):

$$MgFeSiO_4 + H_2S \rightleftharpoons MgSiO_3 + FeS + H_2O$$

However, since $SO_2^{=}$ is the dominant gaseous species of S at high temperatures, rather than H_2S (Carmichael, Turner and Verhogen, 1974) the following reaction is proposed:

$$MgFeSiO_4 + SO_2 \rightleftharpoons MgSiO_3 + FeS + 1{,}5\ O_2$$

This reaction could also explain the petrographic as well as chemical features seen within cyclic unit 11, i.e. the upward increase in the Mg* of the pyroxenes and chromite, as well as the increased modal concentration of chromite towards the top of this unit.

The release of oxygen would certainly explain the upward increasing Mg* of chromite and opx and the increasing modal proportions of this spinel, for an increase in fo_2 would oxidize $FeO \rightarrow Fe_2O_3$ and thus enlarge the primary phase volume of spinel (Osborn, 1978) and decrease the available FeO that could be taken up by the orthopyroxene.

The upward decrease in Cu, Pt and Pd values also indicates a systematic depletion of these elements as sulfide liquid continued to precipitate. A fresh batch of lower zone magma was subsequently brought into the zone of crystallization at the bottom of the magma chamber and commenced with crystallization of cyclic unit 12.

Unfortunately no analytical data on compositional variation of coexisting silicates and oxides is available for the down-dip section, and the explanation for the observed differences in the two sections must be considered as very tentative at this stage. The only reasonable explanation that can be put forward at this stage for the observed differences between these two sections is proxi-

TABLE 18 Ni, Cu, Pt, and Pd STATISTICS FOR THE VOLSPRUIT SUBZONE

1) HARZBURGITES AND PYROXENITES

Population = 975

	Ni	Cu	Pt	Pd	Pt+Pd	$\frac{Pt}{Pt+Pd}$	$\frac{Cu}{Cu+Ni}$	$\frac{Ni}{Cu}$	$\frac{Pt}{Pd}$
Mean	1345,12	352,72	0,41	0,48	0,90	0,47	0,19	16,95	1,12
Variance	518336,09	96982,55	0,27	0,31	1,15	0,01	0,01	22040,39	3,33
Range	4800,00	2280,00	4,82	4,60	9,41	0,96	0,72	2799,61	41,98
STD Error	23,05	9,97	0,01	0,01	0,03	0,00	0,00	4,75	0,05
Kurtosis	1,36	3,58	11,84	5,21	8,12	1,87	-0,03	315,61	342,67
Min.	100,00	1,00	0,00	0,00	0,00	0,01	0,00	0,38	0,01
Max.	4900,00	2281,00	4,82	4,60	9,42	0,97	0,72	2800,00	42,00
STD DEV.	719,95	311,42	0,52	0,56	1,07	0,12	0,10	148,46	1,82
Skewness	1,02	1,66	2,77	1,91	2,29	0,17	0,13	17,67	16,98

2) PYROXENITES

Population = 830

Mean	1215,84	379,27	0,46	0,53	0,99	0,46	0,21	5,18	0,99
Variance	407339,15	101012,75	0,30	0,33	1,25	0,01	0,00	32,10	2,26
Range	4300,00	2272,00	4,82	4,60	9,41	0,96	0,71	95,06	41,98
STD Error	22,15	11,03	0,01	0,02	0,03	0,00	0,00	0,19	0,05
Kurtosis	1,77	3,39	10,52	4,85	7,40	2,45	0,37	84,68	668,05
Min.	200,00	9,00	0,00	0,00	0,00	0,01	0,01	0,38	0,01
Max.	4500,00	2281,00	4,82	4,60	9,42	0,97	0,72	95,45	42,00
STD. DEV.	638,23	317,82	0,55	0,58	1,11	0,11	0,09	5,66	1,50
Skewness	1,16	1,62	2,61	1,83	2,18	-0,12	0,20	6,89	24,56

3) HARZBURGITES

Population = 145

	Ni	Cu	Pt	Pd	Pt+Pd	$\frac{Pt}{Pt+Pd}$	$\frac{Cu}{Cu+Ni}$	$\frac{Ni}{Cu}$	$\frac{Pt}{Pd}$
Mean	2085,17	200,74	0,16	0,19	0,36	0,54	0,09	84,26	1,84
Variance	513129,31	47134,66	0,04	0,11	0,29	0,02	0,00	143533,61	8,92
Range	4800,00	1029,00	1,18	1,63	2,52	0,87	0,55	2799,19	31,90
STD Error	59,48	18,03	0,01	0,02	0,04	0,01	0,00	31,46	0,24
Kurtosis	2,57	2,82	5,27	5,87	5,08	0,06	3,66	44,47	73,77
Min.	100,00	1,00	0,00	0,00	0,00	0,09	0,00	0,80	0,10
Max.	4900,00	1030,00	1,18	1,63	2,53	0,97	0,55	2800,00	32,00
STD. DEV.	716,33	217,10	0,21	0,34	0,54	0,16	0,09	378,85	2,98
Skewness	0,56	1,77	2,25	2,53	2,38	-0,11	1,72	6,73	7,77

TABLE 19 CORRELATION MATRIX FOR VARIOUS ROCK TYPES FROM THE)NE

(A) (Harzburgites and Pyroxenites (975 samples))

	Ni	Cu	Pt	Pd	Pt+Pd	$\frac{Pt}{Pt+Pd}$	$\frac{Cu}{Cu+Ni}$	$\frac{Ni}{Cu}$	$\frac{Pt}{Pd}$
Ni	1,000								
Cu	0,485	1,000							
Pt	0,400	0,854	1,000						
Pd	0,408	0,847	0,944	1,000					
Pt+Pd	0,410	0,863	0,984	0,986	1,000				
$\frac{Pt}{Pt+Pd}$	0,086	-0,064	0,016	-0,159	-0,076	1,000			
$\frac{Cu}{Cu+Ni}$	-0,101	0,730	0,614	0,617	0,624	-0,094	1,000		
$\frac{Ni}{Cu}$	0,131	-0,100	-0,069	-0,076	-0,074	0,069	-0,170	1,000	
$\frac{Pt}{Pd}$	0,040	-0,074	-0,038	-0,120	-0,082	0,506	-0,104	0,021	1,000

(B) (Harzburgites (145 samples))

	Ni	Cu	Pt	Pd	Pt+Pd	$\frac{Pt}{Pt+Pd}$	$\frac{Cu}{Cu+Ni}$	$\frac{Ni}{Cu}$	$\frac{Pt}{Pd}$
Ni	1,000								
Cu	0,086	1,000							
Pt	0,083	0,826	1,000						
Pd	0,049	0,849	0,921	1,000					
Pt+Pd	0,063	0,857	0,969	0,988	1,000				
$\frac{Pt}{Pt+Pd}$	0,033	-0,359	-0,248	-0,438	-0,373	1,000			
$\frac{Cu}{Cu+Ni}$	-0,413	0,745	0,616	0,610	0,624	-0,253	1,000		
$\frac{Ni}{Cu}$	0,140	-0,181	-0,131	-0,107	-0,118	0,043	-0,194	1,000	
$\frac{Pt}{Pd}$	-0,060	-0,167	-0,059	-0,194	-0,145	0,584	-0,131	-0,017	1,000

(C) (Pyroxenites (830 samples))

	Ni	Cu	Pt	Pd	Pt+Pd	$\frac{Pt}{Pt+Pd}$	$\frac{Cu}{Cu+Ni}$	$\frac{Ni}{Cu}$	$\frac{Pt}{Pd}$
Ni	1,000								
Cu	0,732	1,000							
Pt	0,608	0,855	1,000						
Pd	0,638	0,840	0,946	1,000					
Pt+Pd	0,631	0,859	0,985	0,987	1,000				
$\frac{Pt}{Pt+Pd}$	-0,043	0,047	0,107	-0,068	0,017	1,000			
$\frac{Cu}{Cu+Ni}$	0,210	0,732	0,617	0,605	0,619	0,090	1,000		
$\frac{Ni}{Cu}$	-0,090	-0,418	-0,329	-0,350	-0,344	0,001	-0,668	1,000	
$\frac{Pt}{Pd}$	-0,026	-0,016	0,000	-0,078	-0,040	0,442	-0,004	0,026	1,000

mity of the up-dip section to the contact of the intrusion. More effective heat-loss close to the contact, as well as steepening of the initial layering towards the edge of the intrusion (Fig. 82), could result, first, in the observed down-dip thickening of the rock units; secondly, in slightly lower overall temperatures which could have enhanced chromite precipitation close to the edge and; thirdly, more effective and more rapid mixing of the quantitatively small batch of fresh magma with a larger volume of lower zone magma in the central parts of the intrusion. The latter process could have resulted in larger quantities of sulfide liquid to be extracted from a larger volume of magma, whereas the fo_2 increase, as a result of mixing, was probably not sufficient to noticeably enhance crystallization of chromite.

The absence of Ni enrichment in the down-dip section could possibly indicate that relatively more olivine precipitated from the lower zone magma during crystallization of cyclic unit 10 in the central part of the intrusion and consequently resulted in a relative depletion of Ni in the overlying magma.

Orthopyroxene-chromite cumulates without sulfide mineralization are amongst others also developed within cyclic units 13, 14, and 16, and the question may be raised why these should be barren of sulfides? This may be due to two reasons. Firstly, the presence of orthopyroxene-chromite cumulates within these cyclic units can be ascribed to a change in the succession of rock types within the cycles from a sequence orthopyroxene-olivine-chromite to orthopyroxene cumulates in the lower Volspruit subzone to a sequence of orthopyroxene-olivine-chromite to orthopyroxene-chromite cumulates in the upper Volspruit subzone. Secondly, units 13, 14 and 16 referred to here are very thin and their crystallization could scarcely have resulted in any significant increase in the sulphur content of the magma within the zone of crystallization at the base of the intrusion.

The orthopyroxene-chromite cumulates of unit 19, on the other hand, show a remarkable similarity to those of unit 11, in that they are overlain by orthopyroxene cumulates and in that the $Mg/(Mg+Fe^{2+})$ ratio of the orthopyroxene displays a very similar trend (Fig. 7B).

It is unfortunate that the available borehole intersections do not provide a complete succession of lower zone lithologies as poor outcrops and laterization also prevent reconstruction of the complete succession. The succession of rock types missing between units 19 and 20 is therefore not known, and discussions on the similarities or differences between units 11 and 19 will therefore have to be kept in abeyance until such time as more information becomes available on the missing portions between units 19 and 20.

8.1.2 The Drummondlea Harzburgite-Chromitite

The only occurrence of significant sulfide mineralization in this subzone is associated with the upper and lower chromitite layers. The analytical data for Ni, Cu and S shown in Figure 83 was obtained from 3 to 6 kg of representative material from the indicated intervals.

Primary magmatic sulfides and associated textures were only found within the lower chromitite and associated rocks. Here, weak disseminations occur near the base of the layer and gradually increase towards the top. Well preserved net-textured sulfides are developed in the top 7 cm of the chromitite layer. At the contact between the chromitite and the hanging-wall pyroxenite, small droplets, 1 to 2 mm in diameter, can be observed, which increase in size and frequency upwards in the hanging-wall pyroxenite. Spherical to ovoid blebs ranging from 5 to 10 mm are common, particularly in the lowermost 10 cm of the pyroxenite.

In the top portion of the chromitite and the overlying pyroxenite the sulfide Ni content ranges from approximately 1400 to 6150 ppm with an average value of 2000 ppm. Cu values are considerably lower and average about 250 ppm, whereas S values range from 3520 to 10170 ppm (Fig. 83).

Pentlandite, pyrrhotite and chalcopyrite are the most common sulfides. Cubanite was observed only in one section.

The modal proportion of sulfides increase upwards within the chromitite layer, and the highest concentration is found in the immediate hanging-wall pyroxenite. This would suggest that sulfide precipi-

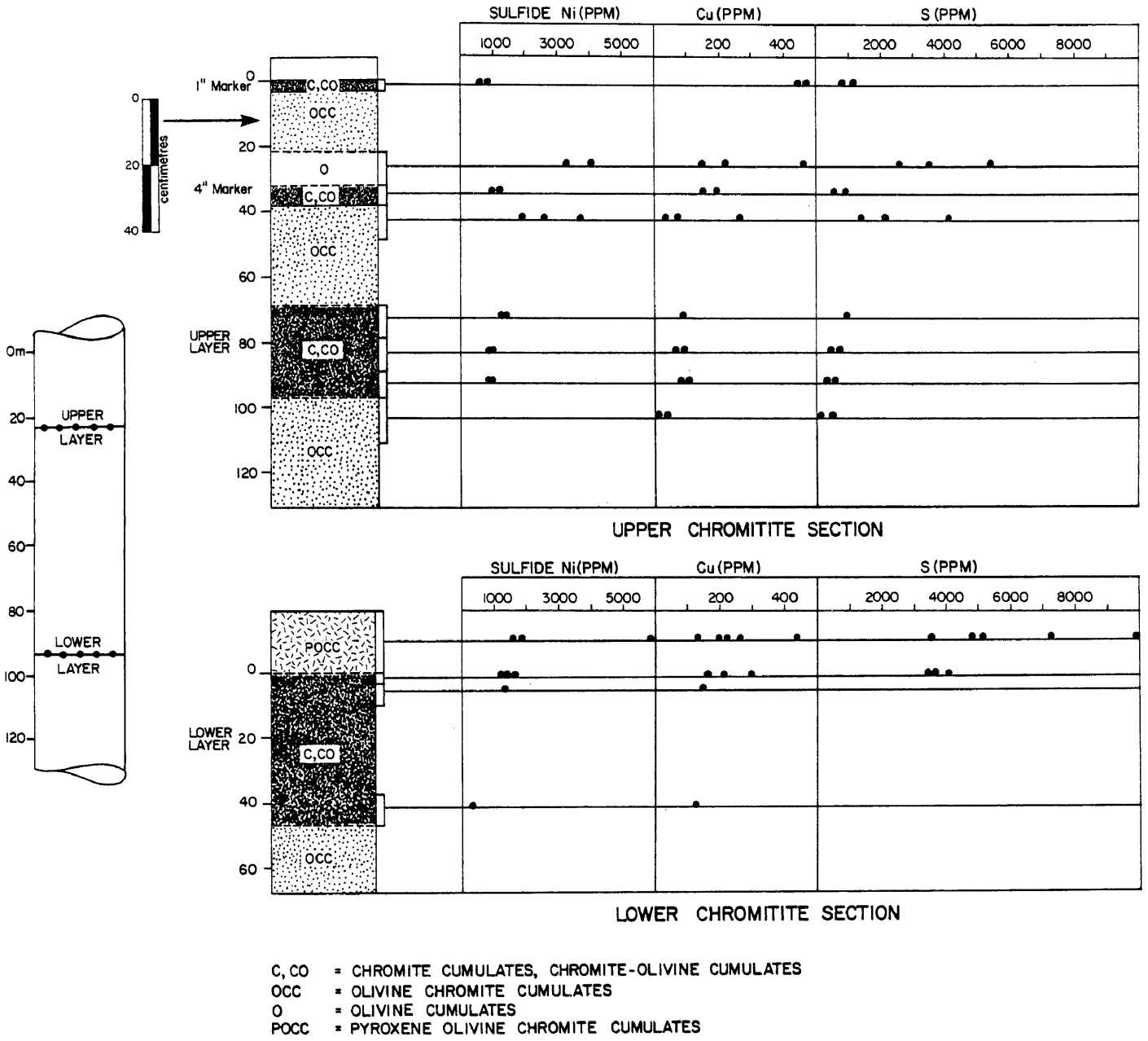

Fig. 83 Sulfide Ni, Cu and S concentration in rocks of the upper and lower chromitite sections. G66,6 level Crasvally Mine.

tation did not take place in response to a rise in the fo_2, which is considered to have resulted in the crystallization of chromite. Instead, the preferential top loaded nature of the sulfides suggests that the solubility of sulfur in the melt was lowered progressively during chromite crystallization, and sulfide crystallization is therefore a direct result of the lowering of the FeO content of the melt (MacLean, 1969; Haughton et al., 1974). Page (1971) also suggested that the sulfide mineralization in the H chromitite zone of the Stillwater Complex was not caused by increased oxygen fugacity or by temperature changes, but due to depletion of FeO in the magma.

In contrast, the sulfide associated with the upper chromitite layers are of a secondary nature and consist of pentlandite, bornite, ± galena and digenite. Secondary minerals observed in the interval between the upper and lower chromitite layers are native Cu, cobaltian pentlandite, and awaruite. In all samples studied pentlandite constitutes 93 to 97 per cent of the sulfides. Modal concentrations of sulfides range from 0,00 to 1,23 weight per cent with a mean of ≤0,01 per cent.

All of these secondary assemblages are considered to have formed from primary magmatic assemblages during the serpentinization of the olivine-rich cumulates. The chemical trends in terms of sulfide Ni, total Cu and S (Fig. 83) suggest, apart from a Ni enrichment, also a pronounced de-sulfurization during serpentinization.

The Cu values seem to have remained fairly constant. This is evident when these values are compared with those of the lower section (Fig. 83), which contains, on average, higher S values and lower Ni values, although the Cu values are very similar.

Apart from the 1" marker, the upper chromitite section also displays upward increasing trends for S, Cu, and Ni which probably reflects the primary modal proportions of the original sulfides. The 1" marker contains the highest Cu values, but low Ni and S values. The high Cu values could reflect initially high Cu sulfide concentration in this marker or secondary enrichment.

The hanging-wall and foot-wall serpentinites of the 4" marker

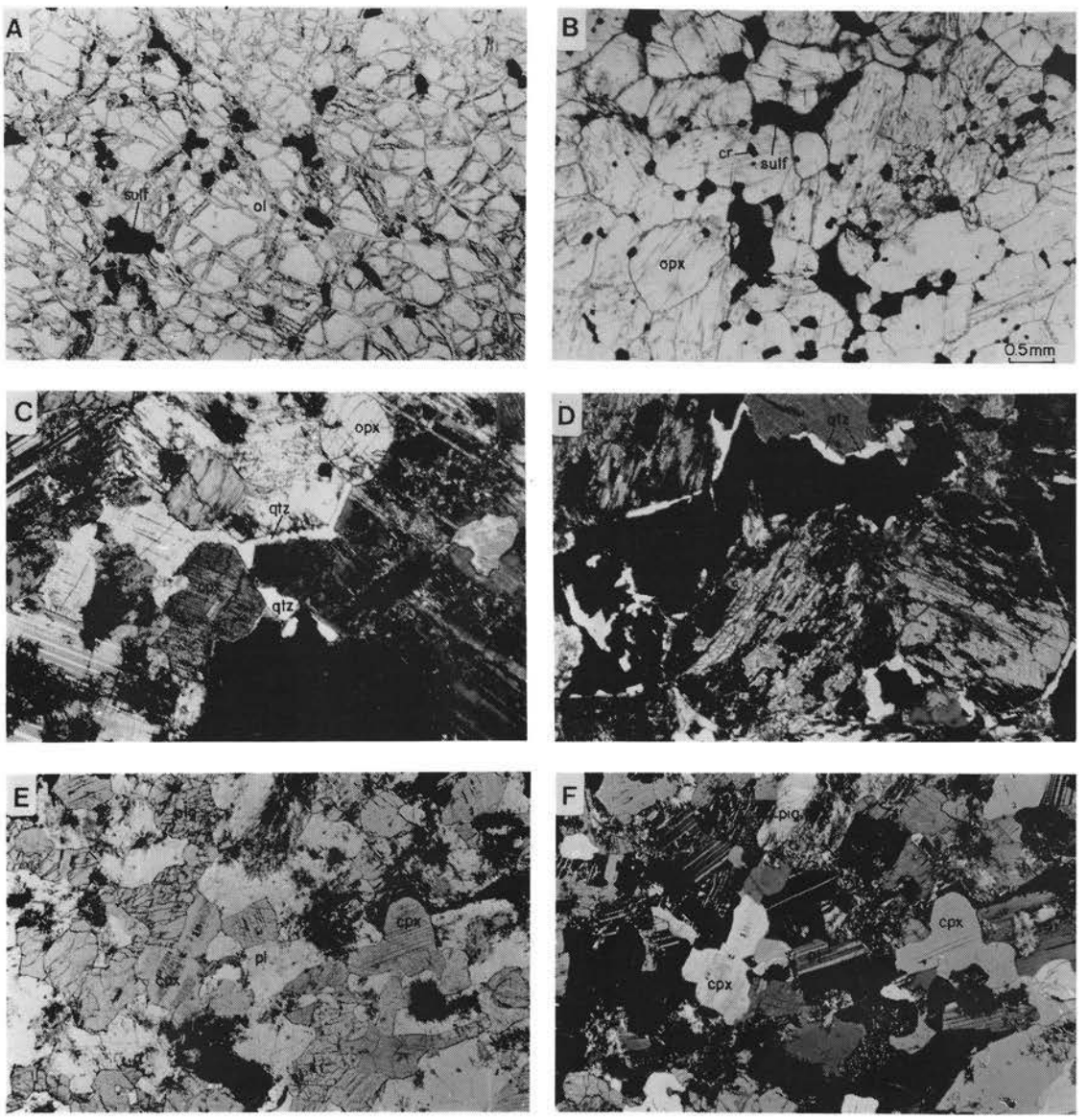

Fig. 84

Figure 84. Photomicrographs of sulfide-rich lithologies in the lower and critical zone of the study area. ol = olivine; sulf = sulfide; cr = chromite; opx = orthopyroxene; qtz = quartz; cpx = clinopyroxene; pl = plagioclase; pig = inverted pigeonite. Sample number in brackets. Scale is the same as for Figure 84B. Figure 84A, B, E have been photographed in plane light whereas C, D, and F - crossed nicols.

(A) Mineralized dunite from the upper Volspruit subzone that contain interstitial patches of sulfide (black). (X-23)

(B) Orthopyroxene-chromite cumulate from the mineralized Volspruit Pyroxenite. Note the disseminated chromite and the large interstitial sulfide grains draped around the orthopyroxenes. (X-25)

(C) Sulfide mineralization in a pegmatitic gabbronorite from mineralized section #1 of the critical zone. Sulfides occur as irregular opaque areas within intercumulus plagioclase and as opaque blebs adjacent to cumulus orthopyroxene. The pegmatitic samples commonly contain intercumulus quartz. (GR-6)

(D) A very coarse variety of the mineralized pegmatitic gabbronorite showing late stage deuteric alteration. Pyroxenes are usually altered to amphiboles and plagioclase is saussuritized. Intercumulus quartz is abundant. (3-2452B)

(E) Pigeonite gabbro from mineralized section #1 of the critical zone. The opaque to dark patches and dustings in the feldspars are sulfides. (78-178)

(F) The same mineralized pigeonite gabbro as in (E). Note the abundance of inverted pigeonite. (78-178)

(stringer) are considerably enriched in sulfide Ni and in S, but not in Cu, relative to the chromitite.

Although the disseminated nature of the sulfides suggests retention of the primary fabric, there is little doubt that considerable Ni enrichment of the sulfides in the serpentinite has occurred during serpentinization. This enrichment can be ascribed to the release of Ni from olivine during the process of serpentinization (Eckstrand, 1975).

Sulfides of a hydrothermal nature occur as fracture infillings on the farm Grasvally. These sulfides occur as "fist size" pods within the fractures and consist, in decreasing order of abundance, of chalcopyrite, cubanite, pentlandite, magnetite and a Pb-telluride. These fracture infillings are commonly associated with intrusive granitoid dikes.

At present only a limited number of PGE assays are available from the upper and lower chromitite horizons within the Drummondlea Harzburgite-Chromitite subzone (Table 20). These assays were unfortunately determined on rather small samples taken from the G66-6 level of the chrome mine on Grasvally, and they cannot be considered as being very representative. More representative values for total PGE in the chromitite horizons are also given in Figure 38, 39, and 40. These show that total PGE in the lower chromitite layer ranges from about 0,25 to 0,85 ppm, whereas the upper chromitite layer averages about 0,35 ppm. The silicate-rich hanging and foot-wall sequence of the upper chromitite layer can contain values of up to 0,30 and 0,60 ppm respectively, whereas the equivalent horizons associated with the lower chromitite layer contain up to 0,50 ppm (g/ton) over 24 cm (Fig. 39). The only other layer known to contain PGE in concentrations $\geqq$0,20 ppm is the "magnetic seam" (Fig. 38) for which a value of 0,90 ppm was recorded.

8.1.3 The Moorddrift Harzburgite-Pyroxenite

Only sporadic sulfide and PGE mineralization was encountered in this portion of the lower zone and the highest sulfide concentration occurs in cyclic unit 31 and 36 (Fig. 7A).

TABLE 20 Cu, Ni, Cr_2O_3, Au, Ag, Pt, AND Pd CONCENTRATIONS FROM VARIOUS HORIZONS IN THE RUSTENBURG LAYERED SUITE SOUTH OF POTGIETERSRUS

Cu	Ni	Cr_2O_3**	Au	Ag	Pt	Pd	Pt/Pd	
			UG2 - LIKE CHROMITITE LAYER					
136	1047	23,38	0,15	0,20	2,05	1,45	1,41	
695	800	20,46	0,10	0,10	1,60	1,05	1,52	
449	1321	17,53	0,05	0,05	1,90	0,65	2,92	
694	495	10,66	0,05	0,10	1,30	0,80	1,62	
560	1100	21,41			2,50	1,00	2,50	
960	1380	23,47			3,30	1,70	1,94	
1560	1530	19,55			1,90	1,30	1,46	
730	1200	19,60			2,80	2,30	1,21	
480	990				1,50	0,60	2,50	
			CHROMITIC GABBRONORITE (C.Z.)					
240	7300				1,2	0,2	6,00	
			MOTTLED ANORTHOSITE (C.Z.)					
1700	6000				1,0	2,7	0,37	
			MAIN MAGNETITE LAYER (U.Z.)					
900	420				0,30	0,10	3,00	
			MAGNETITE GABBRONORITE (U.Z.)					
180	200				0,20	0,10	2,00	
			CRITICAL ZONE (CHILL)					
305	205		35*		47*	37*	1,27	
			TOP OF LOWER ZONE (MINERALIZED PYROXENITE, CYCLIC UNIT # 36)					
Cu	Ni	Cr_2O_3	Au	Ag	Pt	Pd	Pt/Pd	
760	930				0,40	0,70	0,57	
3100	2200				0,80	0,70	1,14	
2300	1500				0,30	0,90	0,33	
1300	1200				0,20	0,60	0,33	
3400	2800				0,40	1,20	0,33	
3800	4100				0,40	1,40	0,29	
2000	2000				0,20	0,90	0,22	
			DRUMMONDLEA CHROMITITE HORIZONS					
110	1200				0,50	0,10	5,00	(1)
140	1700				0,10	0,10	1,00	(2)
210	3400				0,40	0,10	4,00	(3)
120	2400				0,30	0,20	1,50	(4)
180	5100				0,30	0,10	3,00	(5)

1) Bottom of lower chromitite layer
2) 8 centimeters from top of lower chromitite layer
3) 4" marker
4) Hanging-wall pyroxenite for lower chromitite layer
5) Foot-wall of the 4" marker

Concentrations are in ppm unless otherwise designated

* Parts per billion
** wt. per cent
U.Z. = Upper zone
C.Z. = Critical zone

Within cyclic unit 31 rare specks and blebs of sulfides are associated with three thin chromitite layers in a coarse-grained pyroxenite.

The orthopyroxene cumulate of cyclic unit 36 contains zones of disseminated sulfide and PGE mineralization (Table 20). The mean modal sulfide content of this horizon is 4,89 weight per cent, however the high values are confined to an area less than half a metre in thickness. The mean Pt/Pd ratio of all the analysed samples in the unit average 0,45. If, however, the abnormally high value of 1,14 is excluded from the calculation, a mean value of 0,34 is obtained. It is of interest to note that this value is close to 3 times lower than the mean of 830 samples from the Volspruit pyroxenites (Table 18). This is probably a fairly good indication of the fractionated nature of the melt from which this mineralized horizon has crystallized even though the Mg* of the cumulus orthopyroxene from this mineralized horizon is about 0,03 units (≈3 mole per cent enstatite) higher than that of equivalent chromite-poor pyroxenites from the Volspruit subzone. This is also substantiated by the high Cu/Cu + Ni value of 0,526 compared to an average of 0,217 for the Volspruit Pyroxenite.

The overlying harzburgite in cyclic unit 37 is also enriched in sulfides compared to other portions of the Moorddrift subzone, in that it contains 0,92 weight per cent sulfides. For example, a sample for the -141 m level contains 650 ppm sulfide Ni and 47 ppm Cu. This tendency suggests sulfide enrichment near the top portion of the lower zone.

Recognition of these mineralized horizons in the lower zone is of considerable importance, because firstly it opens up this zone, which was previously thought to be barren of sulfides and PGE, as a new exploration target, and secondly, it has a pronounced influence on any further petrogenetic models formulated for the origin of the Merensky Reef and the UG2 platinum group element mineralization, as most of the previous models assume that the UG2 and the Merensky Reef are the first mineralized horizons in the Rustenburg Layered Suite.

8.2 Sulfides in the Critical Zone

Nine mineralized horizons have been encountered in the critical zone.

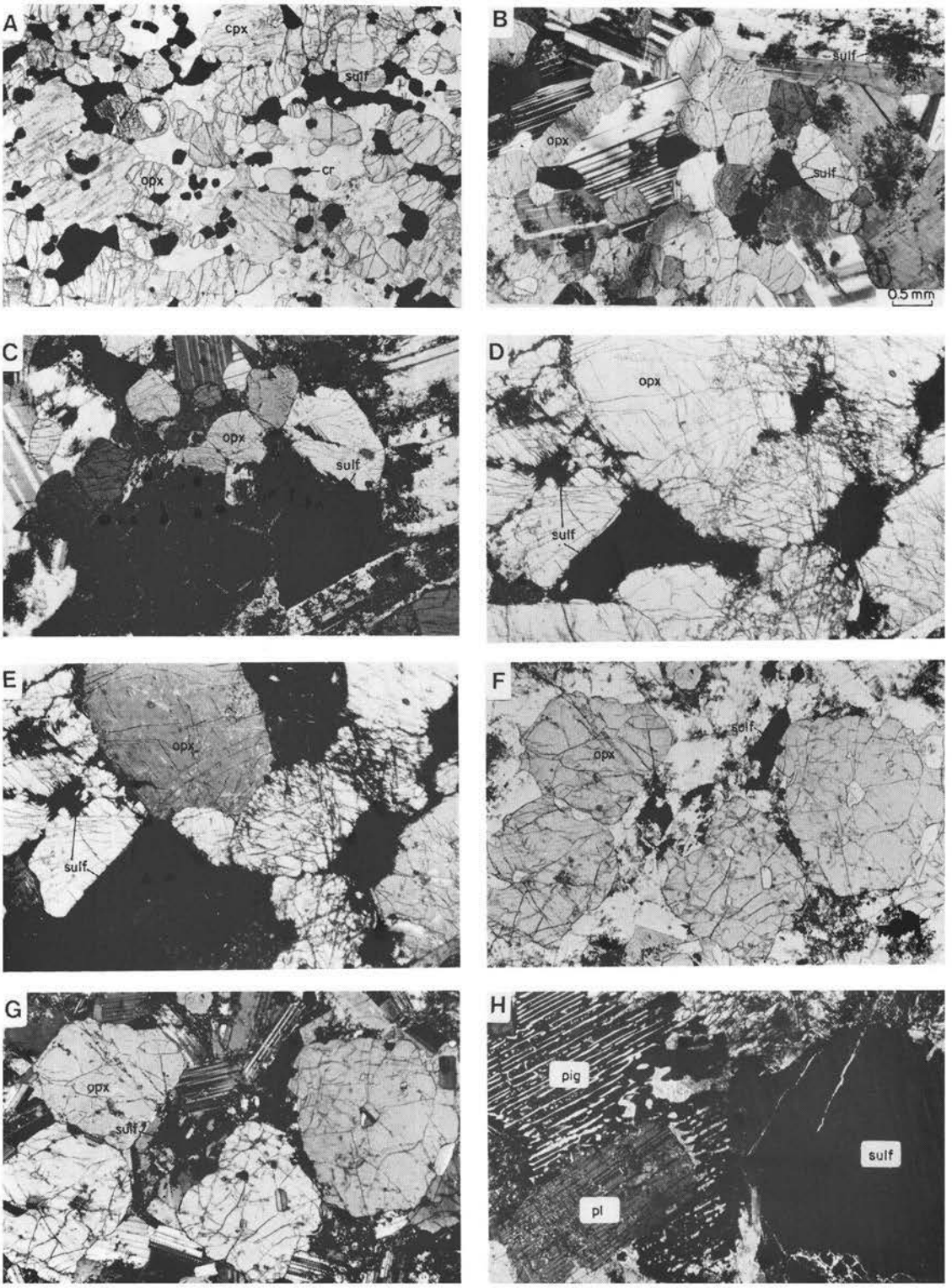

Fig. 85

Figure 85. Photomicrographs of sulfide bearing lithologies from the critical zone. opx = orthopyroxene; sulf = sulfide; cpx = clinopyroxene; pl = plagioclase; pig = inverted pigeonite. Sample number in brackets. Scale is the same as for Figure 85B. Figure 85A, D, F, have been photographed in plane light whereas B, C, E, G, and H - crossed nicols.

(A) Orthopyroxene-chromite cumulate from the hanging-wall of the UG2-like chromitite. The sulfides tend to be draped around cumulus orthopyroxene grains. (78-413)

(B) Plagioclase-orthopyroxene cumulate in the hanging-wall of the above sample. The opaque patches and dustings in the plagioclase are sulfides. (78-416)

(C) Sulfide-rich opx-pl cumulate from the same horizon as above. (78-414)

(D) Mineralized orthopyroxenite from the "O" datum horizon. The coarse sulfide grains form a net-textured relationship with the cumulus ortho-pyroxene. (78-405)

(E) Same as above - crossed nicols. (78-405)

(F) Spotted norite from mineralized section #6. The finely divided sulfides (black) are very pentlandite - rich and make this the most Ni-rich horizon in the critical zone. (78-399)

(G) Same as above - crossed nicols. (78-399)

(H) Mineralized hybrid pegmatitic gabbronorite from the spherical aggregate horizon. Note the spherical sulfide bleb and the altered primary plagioclase crystal enclosed poikiliti-cally by a large oikocryst of inverted pigeonite. (78-142)

Of these, two belong to the marginal members and the remaining seven to the cumulate sequence. A number has been assigned to each horizon (Fig. 86) and these will be referred to as mineralized sections in the ensuing discussions.

8.2.1 Mineralized Section #1

The sequence between the lower zone and the base of the foot-wall pyroxenite of the UG2-like chromitite layer is usually some 30 m thick and consists of fine-grained, sulfide-rich gabbronorites (Fig. 86). Elsewhere along strike this layer may attain a thickness of up to 50 m, and can be traced along strike for 6,5 km in the study area (Fig. 4). This mineralized horizon has also been intersected in diamond drill holes close to the town of Potgietersrus and its strike length therefore seems to be about three times that observed in the study area. One of the most noteworthy features is that this mineralization is only developed where the fine-grained gabbronorites overly lower zone lithologies.

The common mineral assemblage is pyrrhotite (71,09 per cent) chalcopyrite (16,59 per cent) and pentlandite (12,77 per cent). The average sulfide content of surface samples is 5,16 weight per cent.

Mineralization is usually associated with two different rock types. The first type of mineralization is in medium- to coarse-grained and in some cases even pegmatitic gabbronorites (Fig. 84C and D). The pegmatitic fraction may either be pl-opx-(sulfide liquid) or pl-opx-cpx-(sulfide liquid) cumulates although the former cumulate assemblage is more common. Most of the rocks are orthocumulates and contain intercumulus quartz (Fig. 84C and D). The sulfide usually occur as blebs, as fine dustings within the silicates, and as coarse, net-textured sulfide patches engulfing the silicates. The second rock type within this mineralized zone are fine- to medium-grained pigeonite gabbro and gabbronorites (Fig. 84E and F). This rock type can either be a pl-cpx-inv. pigeonite-(sulfide liquid) cumulate or a pl-cpx-(sulfide liquid) cumulate. In some cases the inverted pigeonite is intercumulus, whereas in others it forms discrete cumulus grains. Pl-opx-cpx cumulates with interstial inverted pigeonite are developed in places, usually associated with normal gabbronorites, although this rarer type is commonly devoid of sulfides.

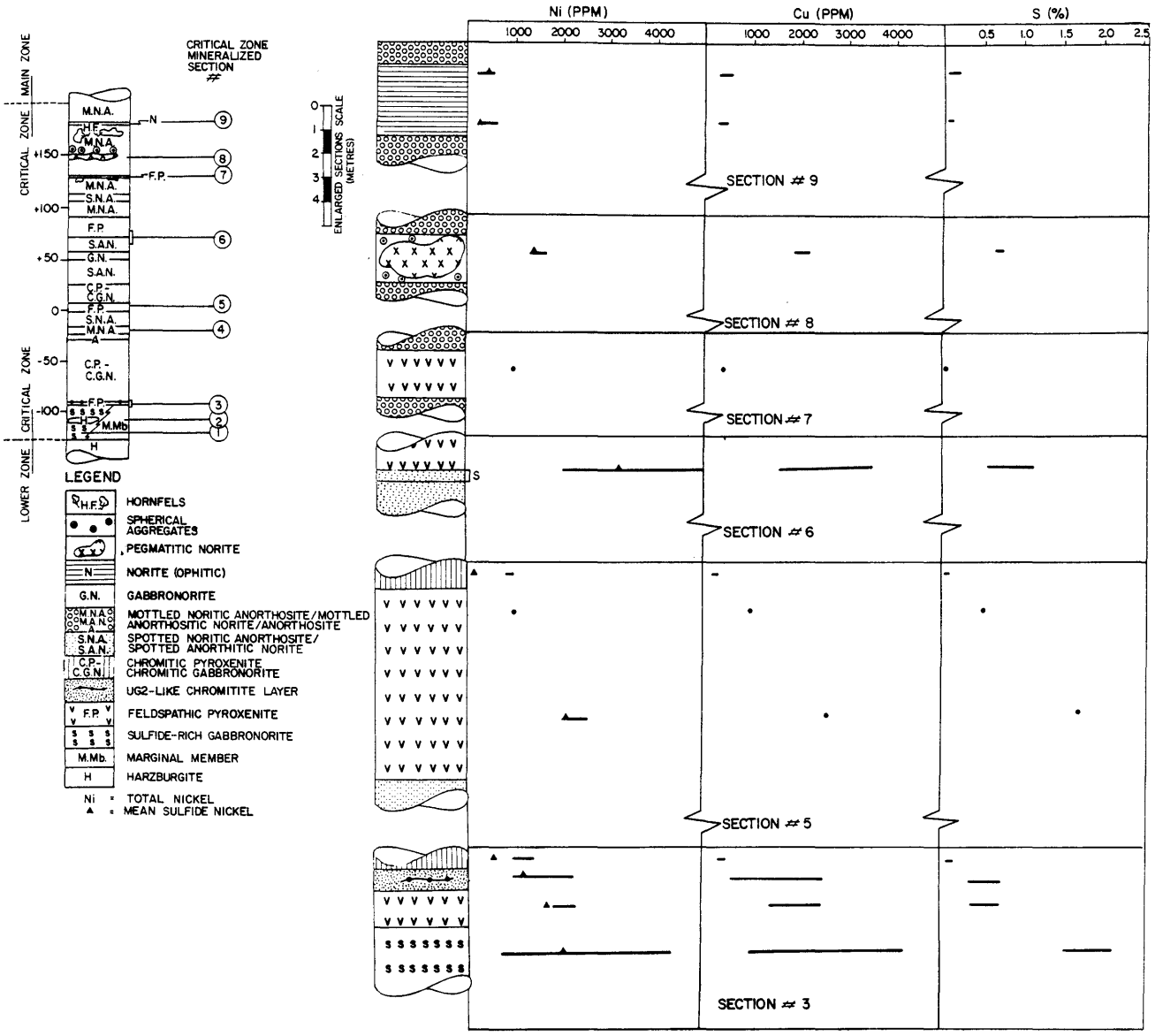

Fig. 86 Diagramatic representation of the distribution, rock types as well as Ni, Cu, and S values of the mineralized sections within the layered member of the critical zone.

Billiton Exploration made available the core of a borehole drilled during the early half of 1981. The intersected stratigraphic sequence (Fig. 87) can be subdivided on the basis of grain size into a number of cycles. Each of these cycles consists of a relatively fine-grained basal gabbronorite member that passes upwards into a coarser grained gabbronorite member. Three different types of cycles seem to be developed on the basis of grain size (Fig. 87), i.e. fine-grained gabbronorite to pegmatitic gabbronorite; medium-grained gabbronorite to pegmatitic gabbronorite and fine-grained gabbronorite to medium-grained gabbronorite. In most cases the medium-grained members consist of a fine-grained gabbronorite at the base which grades upward into a coarser grained pigeonite gabbro which may be pegmatitic at the top. The lowermost and thinnest cycle (Figure 12) consists of a fine-grained gabbronorite that passes upwards into a pegmatitic member.

Any realistic genetic interpretation of the sulfide mineralization encountered in these gabbronorites must explain the following features:

1) The absolute amounts of Cu, Ni, Pt and Pd systematically increase upwards in the mineralized section.

2) The Pt/Pd ratio increases with increasing height.

3) The Pd/Cu ratio decreases with increasing height.

4) A comparatively fine-grained member forms the base of each cycle.

5) The Mg* of the orthopyroxene increases by about 0,10 units (10 mole per cent enstatite) from the base of the section to the top.

6) The mineralization appears to terminate at the UG2-like chromitite layer.

7) The lateral extent of the mineralization seems to be restricted to the lateral extent of the directly underlying lower zone lithologies, i.e. similar rock types as well as mineralization are not developed where the critical zone transgresses onto the sedimentary country rocks.

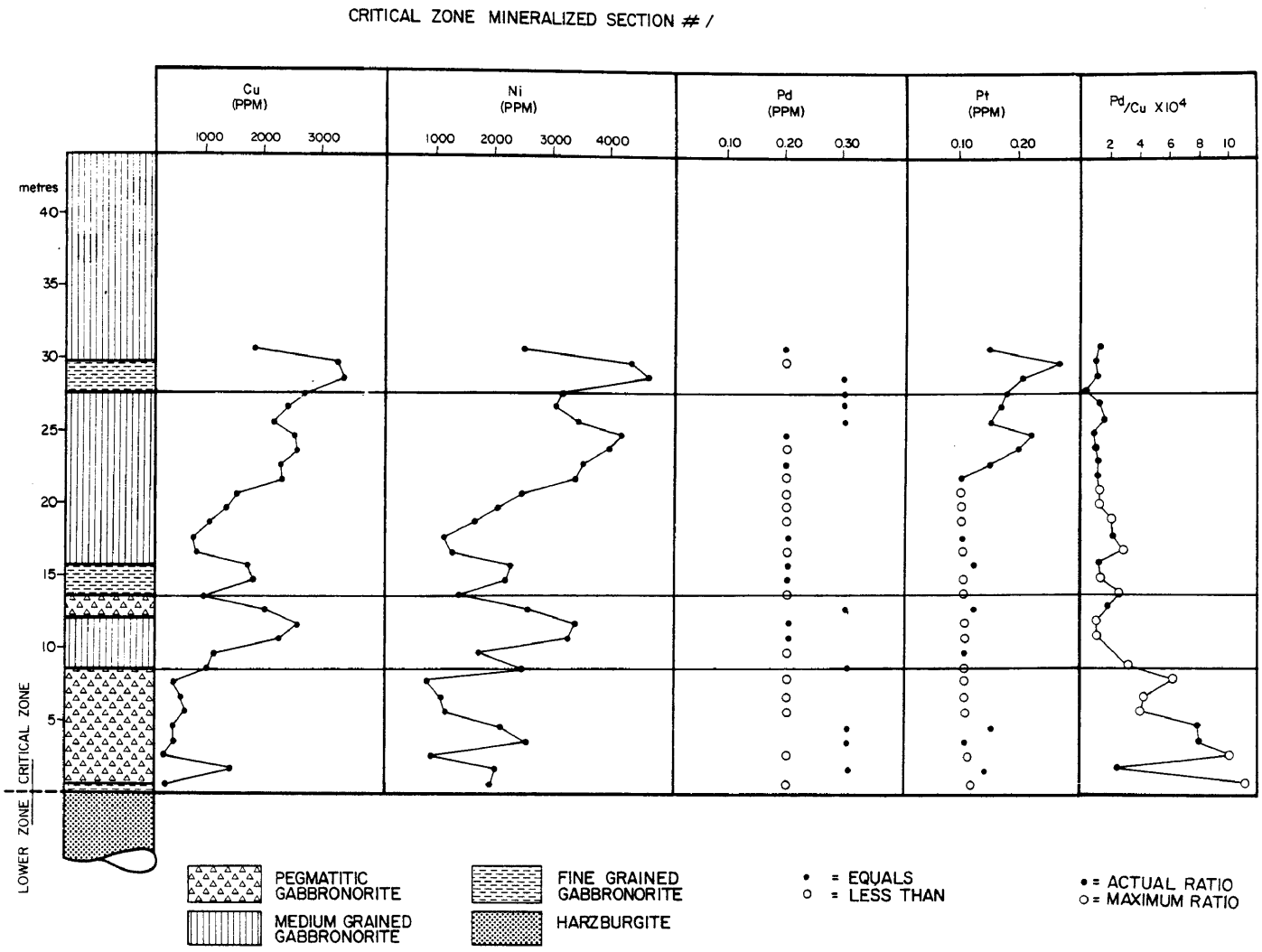

Fig. 87 Columnar section and Ni, Cu, Pt, Pd and Pd/Cu x 10^4 values for mineralized section # 1. Ni values are total Ni in the rock. Diamond drill core and assay values by courtesy of Billiton Exploration Ltd.

Information on the chemical composition of the individual members and the intensive parameters of the magma from which they crystallized is presented for the lower most cycle in Figure 88A and B. Although Al_2O_3, FeO, MgO, CaO, and Cr_2O_3 are rather uninformative, the increasing TiO_2, SiO_2, and alkalis toward the pigeonite gabbro suggest that it is more fractionated than the finer grained underlying gabbronorite. This is also borne out by the decrease in the $Mg/(Mg+Fe^{2+})$ ratio of about 0,04 units for both the ortho- and the clinopyroxene (Fig. 12). The S content of the pigeonite gabbro is also higher than the underlying gabbronorite.

Calculations of the a_{SiO_2} from coexisting clinopyroxene and plagioclase suggest that the a_{SiO_2} of the magma increased during crystallization to culminate during the formation of the pigeonite gabbro (Fig. 88B). This is confirmed by the decreasing bulk Al_2O_3 content of the clinopyroxenes for samples GR4-1 to GR4-3 (Fig. 23). The drop in the a_{SiO_2} during crystallization of the overlying mineralized pegmatitic gabbronorite is associated with a 33 fold increase in the amount of sulfur. Since there is an inverse relationship between the a_{SiO_2} and fo_2 it could be inferred that the separation of sulfides was in response to an increase in the fo_2 of the magma. The increase in the Mg* from 0,673 in the pigeonite gabbro to 0,682 in the pegmatitic gabbronorite also indicates that such an increase in the fo_2 of the magma could have taken place (Sack et al., 1980; Roeder and Emslie, 1970; and Roeder, 1974).

From the above considerations and the information presented in Fig. 87, the best explanation to account for the observed features is that of blending of two liquids of different composition, as was also proposed for the mineralization in the Volspruit Pyroxenite subzone. It is felt that the first influx of critical zone magma was volumetrically relatively small and took place some time after crystallization of the immediately underlying lower zone lithologies. Undercooling during fractionation of this magma in the contact zone produced the 35 cm thick fine-grained layer at the base of the sequence (Fig. 88). Emplacement of a more voluminous quantity of primitive more oxygenated magma, and gradual mixing with the residual melt of the previous influx could have resulted in the separation of immiscible sulfide liquid during crystallization of the pegmatitic gabbronorite. Subsequent emplacements of magma and their mixing with the respective residual liquids could produce the observed sequence of

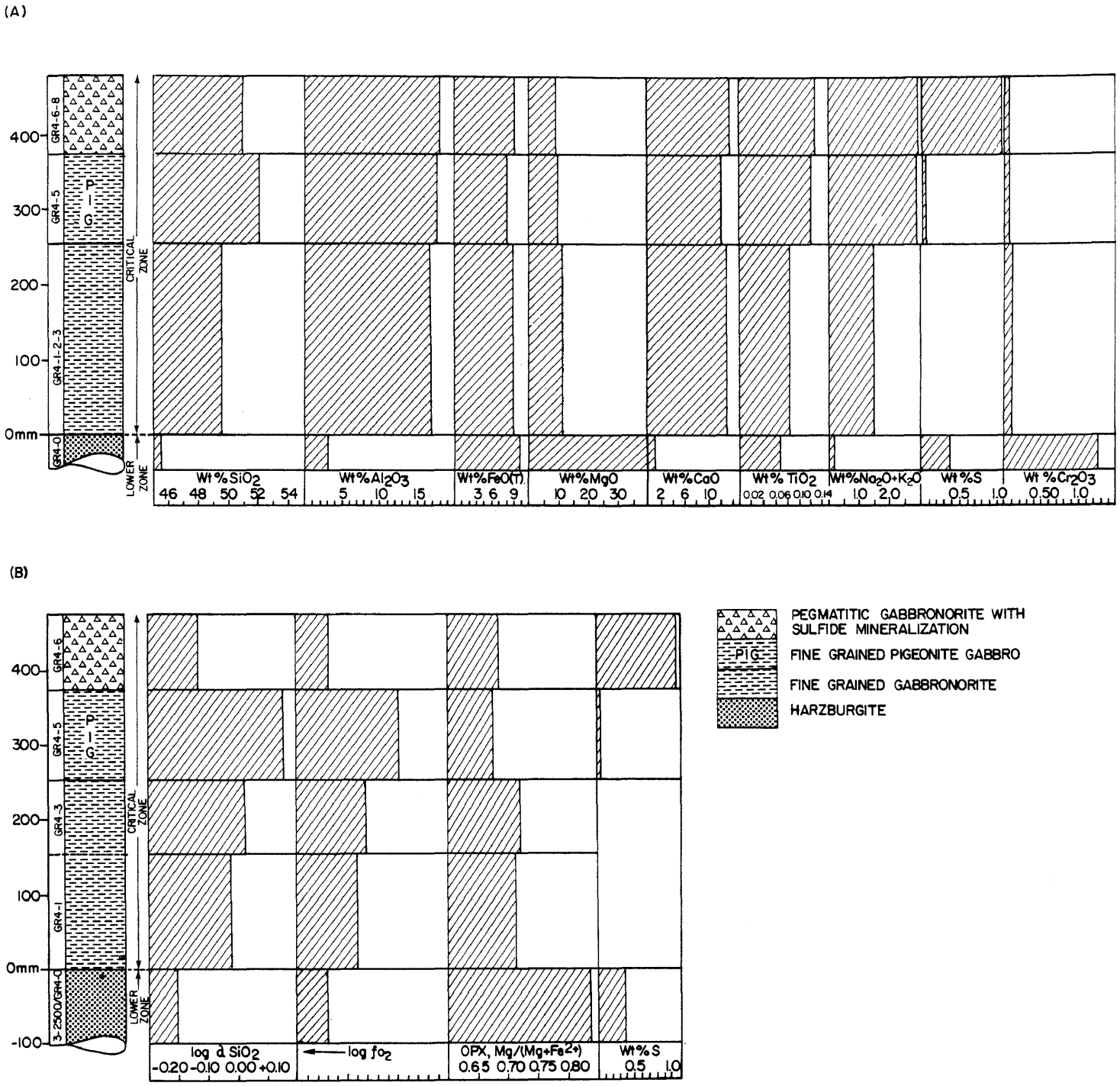

Fig. 88 (A) Chemical composition and
(B) calculated intensive parameters for a cycle in the M.Mb./L.Z. This interval is the lowermost cycle of mineralized section #1 of the critical zone. The $\log_{10} fo_2$ and a_{SiO2} values are only relative. The arrow in the fo_2 column indicates increasing conditions. All calculations were made on the assumption that the pressure during crystallization was 4540 bars.

mineralized cycles at the base of the critical zone (Fig. 87). The fine-grained horizon at the 15 and 28 m levels (Fig. 87) are associated with enhanced concentrations of sulfides. Apart from a finer grain size, undercooling would also have contributed towards a lowering of the solubility of S in the melt.

It is uncertain whether any residual lower zone liquids contributed in any way to the magmas from which these cycles crystallized. The comparatively high sulfide content of these cycles, and the pronounced difference between the M.Mb./L.Z. and M.Mb./P.G. lithologies suggests that some lower zone liquids were involved. Further evidence for undercooling and rapid precipitation of the silicates and sulfides is indicated by the Pd/Cu ratios for the respective horizons in Figure 87. The Pd content of many of the samples is below the detection limit of 0,20 ppm. Consequently, the corresponding Pd/Cu ratios are maximum values. Notice how the two fine-grained horizons at 15 and 28 m have depleted Pd/Cu ratio relative to the surrounding samples. Campbell and Naldrett (1979) and Keays and Campbell (1981) have shown that rapid precipitation of the sulfide liquid results in low "R" values (ratio of the mass of the silicate liquid in effective equilibrium with the sulfide liquid) and consequently a low precious-metal content. The pegmatitic gabbronorites, even though they may contain lower absolute amounts of sulfides and Pt and Pd, have the highest Pd/Cu ratios. This would suggest that the pegmatitic layers crystallized at a slower rate than the others and that the separated sulfide liquid could conceivably have equilibrated with a much larger volume of silicate magma. The Pd/Cu ratio of the medium-grained gabbronorite above the fine-grained horizon at the 15 m level suggests that the sulfide liquid also equilibriated with a comparatively small volume of silicate melt.

The increasing concentration of sulfides from the 18 to 27 m level suggests a constant introduction of new metal-rich liquid. This is indicated by the upward enrichment of Ni, Cu, Pt and Pd of the rocks, coupled with a increase in the Pt/Pd ratios as well as the progressively more magnesium-rich character of the later differentiates. The increasing Pt/Pd ratios towards the top of this mineralized section and the even higher values (3,5 fold) in the directly overlying UG2-like chromitite layer also strengthens the argument

for the continued introduction of more primitive magma (Naldrett and Cabri, 1976).

It would appear that a liquid of a fractionated nature blended with a new one of more primitive composition is much more effective in causing sulfide immiscibility than is local country-rock contamination. The inferred magma mixing rather than local contamination suggests that thorough mixing of contrasting basaltic melts is necessary before sulfide separation will occur. Such mixing and the required periodic influxes could only occur in a magma chamber.

8.2.2 Mineralized Section #2

Analytical data for Ni, Cu, Pt, Pd, Zn and S within core of a borehole drilled by Billiton Exploration, through the M.Mb./P.G. is shown in Fig. 89. The average Cu, Ni, and Zn values of 68, 101, and 88 ppm respectively for the lower 12 samples shown in Figure 89 are considered to be fairly representative of the postulated initial critical zone magma. The mean S value of 216 ppm is however more difficult to evaluate because the metasedimentary country-rocks contain abundant pyrite in places.

The sulfide mineralogy of these rocks is distinct from that of other sections in that it consists predominantly of the assemblage pyrite-chalcopyrite. Pyrrhotite and pentlandite have not been found in these rocks, yet numerous analyses indicate that 16 to 20 per cent of the total Ni is present as sulfide Ni. Microscopic and microprobe examination of these rocks reveals that virtually all of the sulfide Ni is in the form of what appears to be magmatic vaesite and millerite. The pyrite was found to be devoid of Ni.

The top third of DDH-GR1 (Fig. 89) contains higher sulfide concentrations than the rest of the borehole intersection. All of the samples enriched in sulfides are confined to the coarser-grained rocks. Some of the mineralization is restricted to the more fractured portions of the rock, suggesting that some of the sulfides are remobilized. Although most of the Pt and Pd assays are below the detection limit of 0,20 ppm, one sample was found to contain values as high as 0,40 ppm Pt and 0,50 ppm Pd. The frequency of these high values seem to increase towards the top of the borehole (Fig. 89) and are also associated with the coarser grained samples,

CRITICAL ZONE MINERALIZED SECTION #2

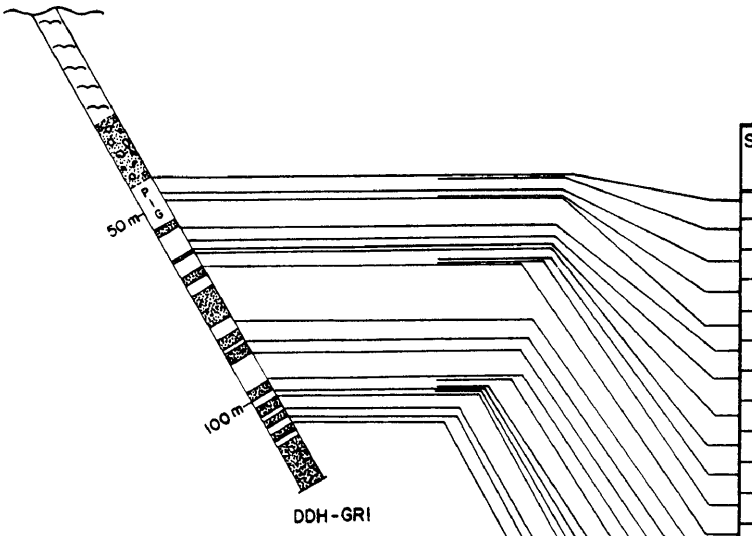

SAMPLE WIDTH (m)	CU (PPM)	NI (PPM)	PT (PPM)	PD (PPM)	S (PPM)	ZN (PPM)	
0.25	2100	3300	0.40	0.30			*
0.25							***
0.42	1200	1200	<0.20	<0.20			*
0.08	800	1300	<0.20	<0.20			*
0.08	1900	2800	0.40	0.50			*
0.25	2000	300	<0.20	<0.20			*
1.53	1200	250	0.20	0.30			*
0.03	4600	800	<0.20	<0.20			*
2.57	1100	1700	<0.20	<0.20			*
0.33	500	4500	<0.20	<0.20			*
0.52	20	100	<0.20	<0.20			*
0.48	300	800	0.20	<0.20			*
0.10	64	101			440	90	
0.10	47	153			310	86	
0.10	50	102			100	91	
0.10	55	113				83	
0.10	36	93			30	82	
0.10	39	101			380	87	
0.10	73	98			520	110	
0.10	69	119			330	107	
0.10	69	122			170	104	
0.10	14	36			20	38	
0.10	223	48			610	62	
0.10	80	122			220	119	

* ANALYSES BY COURTESY OF SHELL SOUTH AFRICA
*** PT = 47 PPB BY COURTESY OF J.C.I.
PD = 37 PPB " " " "
AU = 35 PPB " " " "

Fig. 89 Borehole section and Cu, Ni, Pt, Pd, S, and Zn values for mineralized section #2 of the critical zone. This section is from the lower half of the M.Mb./P.G. Ni is expressed as total Ni.

as was the case for mineralized section 1. This tends to suggest that the sulfides in this coarser grained rock equilibriated with a larger volume of silicate liquid from which the PGE were extracted.

A fine-grained unmineralized sample from near the top of the bore-hole contains 47, 37, and 35 ppb, Pt, Pd and Au respectively, values which could be representative of the concentration of these elements in the initial critical zone magma. Similar and even higher values were recorded by Sharpe (1982A) from fine-grained marginal rocks considered to be representative of quenched initial liquids in the eastern Bushveld Complex.

8.2.3 Mineralized Section #3

This section consists of the UG2-like chromitite and its foot-wall pyroxenite. Ni, Cu, Pt and Pd, as well as some Co, Cr_2O_3, Au and Ag values for this layer and its associated rocks are shown in Figures 86 and 90. Analytical data for the UG2-like chromitite from the northern portion of Grasvally shows that Cu, Ni, Cr_2O_3 and Co values are higher in the bottom half of the layer, whereas the top half contains the higher Pt values (Fig. 90A). This inter-section was found to contain abnormally low Pt and Pd values. The underlying foot-wall pyroxenite is considerably enriched in Ni and Cu and contains values similar to the foot-wall gabbronorite of section #1. Figure 90B is a composite of all assay values available for the UG2-like chromitite from the northern portion of the farm Grasvally, as supplied by Mnr. S.P. Rautenbach. The diagram indi-cates, with the exception of the two closely spaced central data points, that the highest values for Pt, Pd, Au, and Ag occur at the bottom of the layer and decrease in abundance upwards.

The most abundant sulfides in the UG2-like layer are pentlandite (36,60%), chalcopyrite (40,92%) and pyrrhotite (22,46%) with a mean sulfide concentration of about 1,30 weight per cent. In com-parison, the foot-wall pyroxenite contains on average 3,14 weight per cent sulfides of which 15,06 per cent is pentlandite, 20,21 per cent is chalcopyrite and 65,33 per cent is pyrrhotite. The only platinum group minerals found within the chromitite was a Pt-Bi-telluride, and a Pt-Bi-Fe alloy. Galena was noted in a few samples.

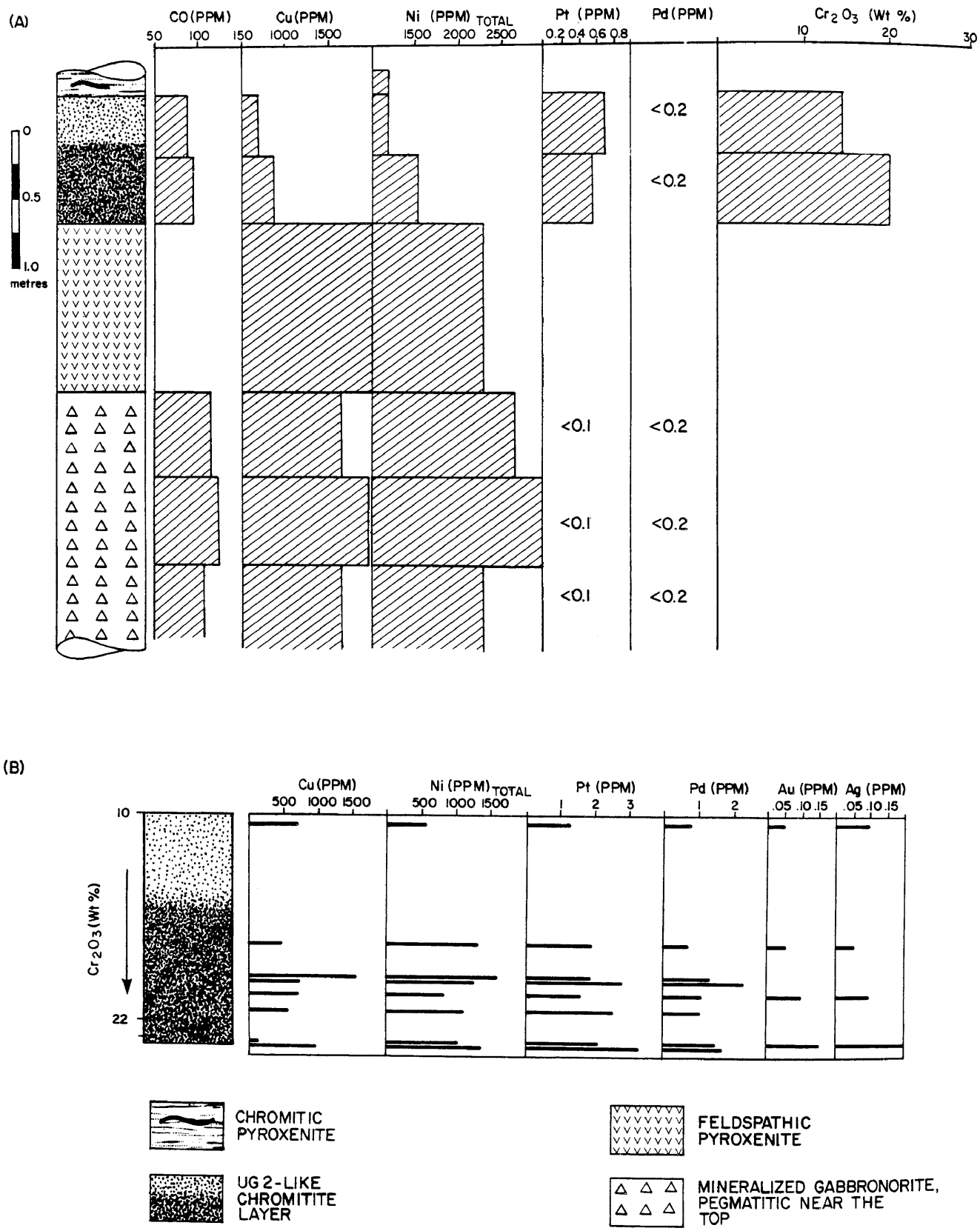

Fig. 90 Mineralized section #3 of the critical zone.

(A) Columnar section of the UG2-like chromitite layer and associated hanging- and foot-wall lithologies, as well as a schematic representation of the variations in Co, Ni, Cu, Pt, Pd, and Cr_2O_3.

(B) Compilation of available Cu, Ni, Pt, Pd, Au and Ag values in the UG2-like chromitite layer from the northern part of Grasvally.

The chromitic pyroxenite and gabbronorite (opx-chr ± cpx cumulate) in the hanging-wall of the UG2-like chromitite layer can contain very weak sulfide and PGE mineralization in places. A weakly mineralized sample from the immediate hanging-wall of the chromitite layer was found to contain 39,70 per cent pentlandite, 25,90 per cent chalcopyrite, and 34,40 per cent pyrrhotite. Modal concentrations seldom exceed 0,28 weight per cent (Fig. 85A). Assay values of 240 ppm Cu, 1300 ppm Ni (total), and 1,20 and 0,20 ppm Pt and Pd have been recorded in this rock type. This rock type usually grades upwards into a chromite- and clinopyroxene-poor rock with slightly less sulfides (Fig. 85B and C).

The more metal-rich nature of the sulfides and the higher Pt/Pd values strongly suggest that the UG2-like chromitite layer crystallized from a more primitive magma than the underlying, fine-grained marginal rocks of the critical zone. The enhanced crystallization of chromite also points to more oxidizing conditions within this new magma.

8.2.4 Mineralized Section #5

This horizon occurs close to the "0" datum and consists primarily of feldspathic pyroxenite, although part of the overlying thin layer of chromitic pyroxenite (opx-chr ± cpx cumulate) has been included because it also contains sporadic patches of sulfides. Ni, Cu, and S values seem to decrease towards the top of this section (Fig. 86). Most of the sulfides from this horizon occur as large interstitial patches (Fig. 85D and E). Modal concentrations of sulfides in the well mineralized portions average 4,65 weight per cent; with 12,72; 14,84; and 72,85 per cent of the sulfides consisting of pentlandite, chalcopyrite, and pyrrhotite respectively.

8.2.5 Mineralized Section #6

This mineralization is confined to a 43 to 50 cm thick horizon at the top of a layer of spotted norite to anorthosite norite (Fig. 86) some 200 m above the base of the critical zone. The sulfides are so finely disseminated that the presence of mineralization could easily be overlooked in the field. All of the rock types of this section are either orthopyroxene cumulates or plagioclase-orthopyroxene cumu-

lates (Fig. 85F and G).

Total Ni values range between 2401 and 5098 ppm, whereas the mean sulfide Ni value for this section is 3200 ppm. Cu values range from 1521 to 5037 ppm. The sulfide content of this horizon is approximately 2,68 weight per cent; of which 33,52 per cent 33,64 per cent; 21,37 per cent; and 11,44 per cent of the total sulfides consist of pentlandite, chalcopyrite, pyrrhotite and pyrite respectively. This is the first occurrence of pyrite in the layered sequence. With the exception of the sulfide mineralization associated with the lower chromitite layer and that in the lower two thirds of the lower Volspruit subzone, this horizon contains the most Ni-rich sulfides in the layered suite.

The only plausible explanation for the high Ni content of the sulfides at this level in the critical zone is that the Ni was introduced into the chamber by a new influx of magma more primitive than the residual liquid in the chamber. As a result of the rapid initial mixing, separation of a sulfide liquid occurred and accumulated together with the last products of crystallization of the old liquid. The immediately overlying pyroxenite layer then crystallized from the reconstituted magma in the chamber. S-isotope data rules out the possibility that the sulfides precipitated in response to contamination of the magma by S of a sedimentary origin.

8.2.6 Mineralized Section #8

Although this horizon is only of a very localized nature, it is of considerable interest because of the associated rock types. The host rock of the sulfide mineralization is a hybrid pegmatitic gabbronorite. Some of these pegmatitic rocks contain large interstitial inverted pigeonite grains with which coarse blebs and dustings of sulfides are associated (Fig. 85H).

The sulfides in these pegmatitic rocks occur mainly as sporadic thumb nail size blebs which consist mainly of pyrrhotite (44,07 per cent); chalcopyrite (37,15 per cent); pentlandite (19,63 per cent); and pyrite (4,15 per cent). On average, the sulfides constitute about 1,89 weight per cent. Sulfide Ni and Cu values are about 1300 and 2000 ppm respectively.

The mineralized pegmatitic layer occurs as discontinuous zones in the upper portion of the critical zone. Their patchy distribution is believed to be due to a variable volatile content of the magma caused by the assimilation and or degasing of the carbonate xenoliths. The release of H_2O and CO_2 during thermal metamorphism probably caused a localized increase in the fo_2 of the magma and triggered the precipitation of sulfides from the melt. The presence of quartz in the pegmatitic rocks and the development of spherical aggregates of pyroxene, similar to those described by Lee and Sharpe (1979) from the eastern Bushveld, in anorthositic rocks, indicates that siliceous sediments were also assimilated by the magma at this level in the intrusion. It is of interest to note here that S-isotope data, to be discussed later, shows that S from the sedimentary source was not responsible for sulfide precipitation, as is believed to be the case for the Platreef by Buchanan et al. (1981).

8.2.7 Mineralized Section #9

This mineralization is developed in a 3 m thick norite layer within a sequence of mottled anorthosites. Although this layer only contains about 0,41 weight per cent sulfides and is therefore of no economic significance, it is worthy of note since the sulfides consist only of pentlandite (30 per cent); chalcopyrite (38,26 per cent); and pyrite 31 (per cent). As a result of surface weathering much of the pentlandite has been altered to violarite. This horizon is significant in that it is the first occurrence in the layered sequence where pyrrhotite is completely absent in the sulfide assemblage.

8.2.8 Other Mineralized Horizons

Minor sulfide mineralization has been encountered at two other levels in the critical zone. These are indicated as sections 4 and 7 in Figure 86. Section 4 is a mottled noritic anorthosite at the -20 m level and contains specks of sulfide mineralization. Section 7 consists of a 2 m thick melanorite or feldspathic pyroxenite that contains 952 ppm total Ni, 271 ppm Cu and 120 ppm S. Small malachite stains have been observed on this rock in outcrops.

No sulfide concentrations were found in the overlying main zone,

although small sulfide grains are present which are usually only visible under the microscope.

8.3 Sulfides in the Upper Zone

Sulfides are common constituents of the upper zone lithologies, and the highest concentrations are usually found to be associated with the main magnetitite layer.

Due to the limited amount of material and assay information on the upper zone in the study area, some data on the lower half of the upper zone is presented from the farm Molendraai northwest of Potgietersrus (Fig. 91). Seeing that the investigation of the sulfides in this area has only recently commenced as a separate project, polished sections are not yet available, the distribution of sulfides are therefore based on available whole-rock analytical data for Cu and sulfide Ni kindly made available to the author by Mining Corporation.

The upward decreasing Cu values in the lower 20 m of this intersection probably reflects normal fractionation conditions of a magma from which small amounts of Cu-rich sulfide liquids separated during crystallization. The reversal at the 260 m level is probably brought about by increased oxidizing conditions before and during crystallization of the magnetite-rich gabbronorite layer. The enhanced crystallization of Fe-Ti oxides resulted in a lowering of the FeO content of the melt and thus also a lowering of the solubility of sulfur in the magma (Haughton et al., 1974). The larger modal sulfide content of these rocks is indicated by the higher Cu and Ni values in this layer.

From the top of the lower magnetite-rich gabbronorite to the middle of the mottled foot-wall anorthosite of the main magnetitite layer a normal depletionary trend in terms of sulfide Ni and Cu is observed with only minor irregularities. This trend is to be expected if fractionation of a liquid took place in a closed system. Under such circumstances the sulfur content of the melt is continuously depleted due to progressive separation of small amounts of sulfide liquid from the crystallizing magma. The increased concentration of Cu and to a lesser extent Ni from the middle to the foot-wall mottled anorthosite through the base and into the middle of the main magnetitite layer is considered to

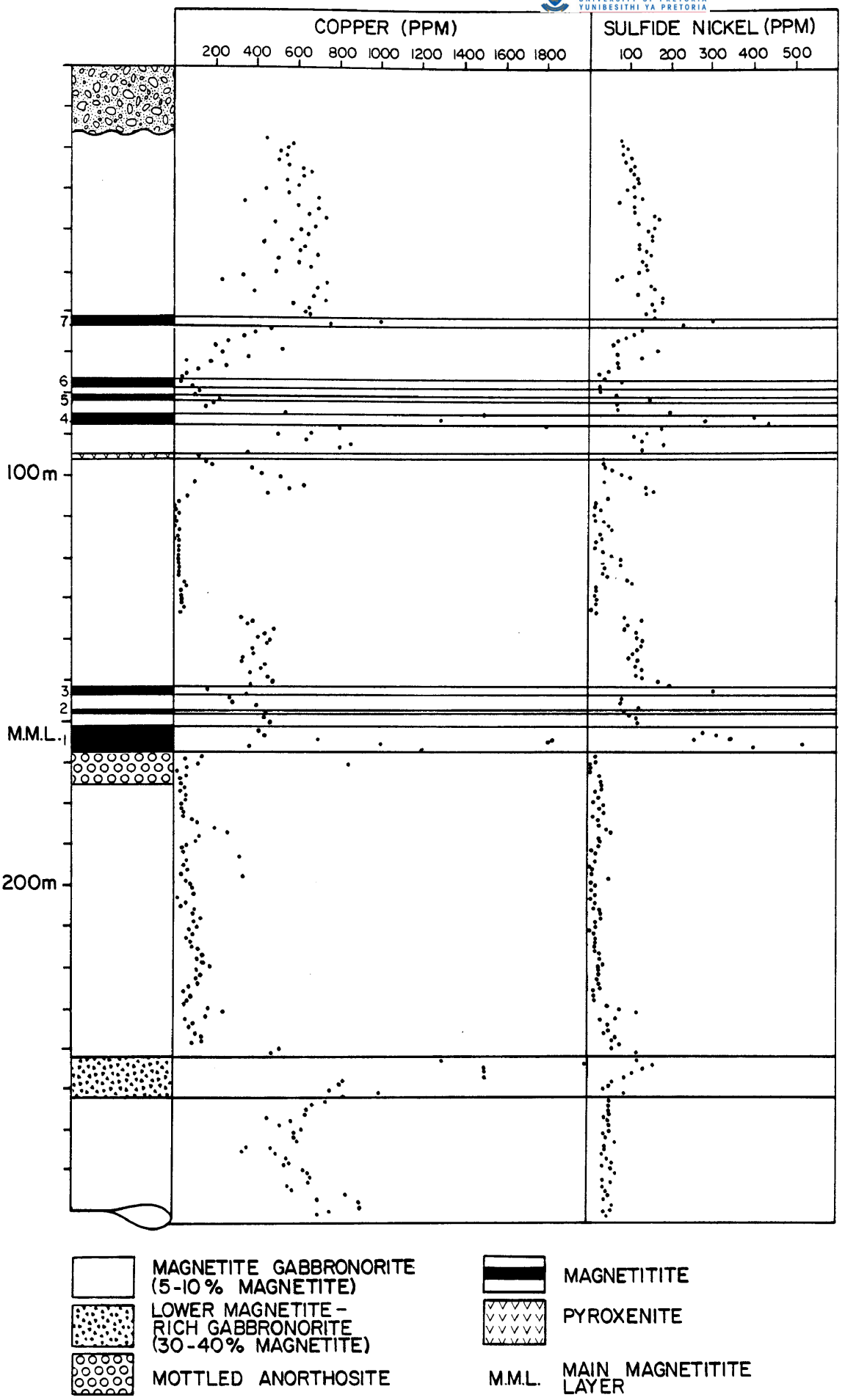

Fig. 91 Generalized columnar section and variations in sulfide Ni and Cu through the lower portion of the upper zone on Molendraai 311LR, northwest of Potgietersrus.

reflect a rise in the fo_2 which resulted in the enhanced crystallization of Fe-Ti oxides to give rise to the main magnetitite layer.

From the 152 m to 136 m level there was a period of rather uniform sulfide crystallization whereas after that sulfide precipitation from the magma dropped and remained at very low levels up to the pyroxenite at the 95 m level. The increased amounts of Ni sulfide, although showing an overall decreasing trend towards the pyroxenite, suggest a more primitive parent magma with a lower Cu/Cu+Ni ratio than its predecessor, which gave rise to the stratigraphic sequence below the main magnetitite layer. It is of interest to note that the consistently low Cu values associated with relatively high and in some cases fluctuating Ni values between the 135 and 95 m levels is a persistent feature found in six diamond drill hole intersections over a strike length of 15 km. The increasing proportion of disseminated magnetite through this interval, coupled with this trend, may suggest the introduction of more oxygenated and primitive magma but any interpretation will have to await further petrographic studies on this interval.

Increasing fo_2 conditions again seems to have enhanced sulfide separation and high Cu and Ni values in the foot-wall of and within magnetitite layer 4. This again caused a depletion of these constituents in the crystallizing magma so that the Ni and Cu values of the rocks directly overlying this layer and in association with magnetitite layers 5 and 6 are low. The very pronounced increasing trend for Cu and Ni above these layers is considered to be due to some replenishment of these elements as a result of a new influx of magma, which culminated with the crystallization of magnetitite layer 7. From here onwards the gradually decreasing Cu and Ni values probably reflect conditions of a normally fractionating magma.

The most noteworthy concentration of sulfides described from the upper zone is mineralization in the immediate foot-wall anorthosite of the main magnetitite layer (Liebenberg, 1970) and within an anorthosite associated with lower magnetitite layer 2 (Von Gruenewaldt, 1976). Von Gruenewaldt (1976) reported average

Cu and Ni values of 0,96 and 0,15 per cent, which are considerably higher than the values in the foot-wall anorthosite in Figure 91. However, all values in this diagram represent averages of one metre of core, so that any higher grades over shorter intervals have been diluted. The highest concentration of sulfides was observed within the lowermost 1 m of the main magnetitite layer where dispersed blebs of sulfides, 5 to 10 mm in diameter, are developed. Small sulfide grains were also noted to occur disseminated through the magnetitite layer.

The main sulfide minerals in the foot-wall anorthosite and the main magnetitite layer are pentlandite, chalcopyrite, cubanite, hexagonal pyrrhotite, ± troilite. The anorthosite contains these minerals in the following proportions: 7,19; 32,38; 3,80 and 57,14 weight per cent respectively, whereas in the magnetitite layers the proportions are 7,00; 14,58; 7,68; and 71,22 per cent. Locally ($\leq$ 1 m) the sulfide content at the bottom of the magnetite layer can be as high as 3,20 weight per cent, however it is usually about 1,57 weight per cent. Other minerals observed were bornite, galena, and gersdorffite.

The main magnetitite layer and the overlying magnetitite layers in the study area south of Potgietersrus differ from those on the farm Molendraai, in that no pyrrhotite is developed. The dominant mineral assemblage here is chalcopyrite and pyrite. Some galena has also been observed. The difference in mineralogy is considered to be due to a late stage sulfidization process which will be discribed below (Section 8.5.1.4). Magnetite gabbronorites from the study area contain on average 0,32 weight per cent sulfides of which 16 per cent is chalcopyrite and the remaining 84 per cent is pyrite.

Only a very limited amount of information is at present available on the Pt and Pd distribution in the upper zone lithologies. Assayed samples from the study area suggest that the magnetite gabbronorites contain <0,20 and <0,10 ppm Pt and Pd respectively, whereas the main magnetitite layer was found to contain 0,30 ppm Pt and 0,10 ppm Pd.

8.4 Chemical Characteristics of the Mineralized Horizons

8.4.1 Cu : Ni Ratio of Sulfides as an Indicator of the Basicity of the Parental Magma

One of the most frequently employed chemical parameter used to classify Ni, Cu and PGE ores is the Cu:Ni ratio of the sulfides. Naldrett and Cabri (1976) have shown that the Cu/(Cu+Ni) ratio increases with progressive differentiation of the host silicate magma, whereas Maclean and Shimazaki (1976) also stated that the Cu:Ni ratio of the sulfides is a good indicator of the basicity of the corresponding silicate magma. This also seems to hold true for the fractionating Bushveld magma as can be seen from Figure 92A. The Cu:Ni ratio for sulfide bearing Bushveld rocks ranges from 1:14 in the lower zone to 13:1 in the upper zone.

The lowest Cu:Ni values have been recorded in samples from the hanging-wall pyroxenite of the lower chromitite layer and from the upper chromitite layer. Secondary sulfides occur in serpentinites associated with the upper chromitite. The low Cu:Ni ratios are therefore not indicative of magmatic conditions, but these values illustrate how low the Cu:Ni ratios of sulfides can get as a result of serpentinization. Samples more indicative of magmatic conditions are those from the fresh and unserpentinized hanging-wall pyroxenite of the lower chromitite. These samples have an average Cu:Ni ratio of 1:7,19. Comparison with Figure 92B suggests a magma with a basicity intermediate between that of the komatiites that produced the Lunnon ore and the most basic noritic magma that gave rise to the Strathcona ore at Sudbury.

The Cu:Ni ratio can also be used to infer the basicity of the parental magma (Maclean and Shimazaki's, 1976, Fig. 6, p. 1055). According to their diagram the likely parent magma to the hanging-wall pyroxenite was basaltic in composition with about eleven per cent normative olivine. This agrees reasonably well with earlier estimates of the character of the parental magma of the lower zone.

The Cu:Ni values in the Volspruit Pyroxenite subzone vary considerably from 0,95:1 to 1:7,19. High sulfide Ni values are recorded from the dunite whereas the lower 6 m of the mineralized interval

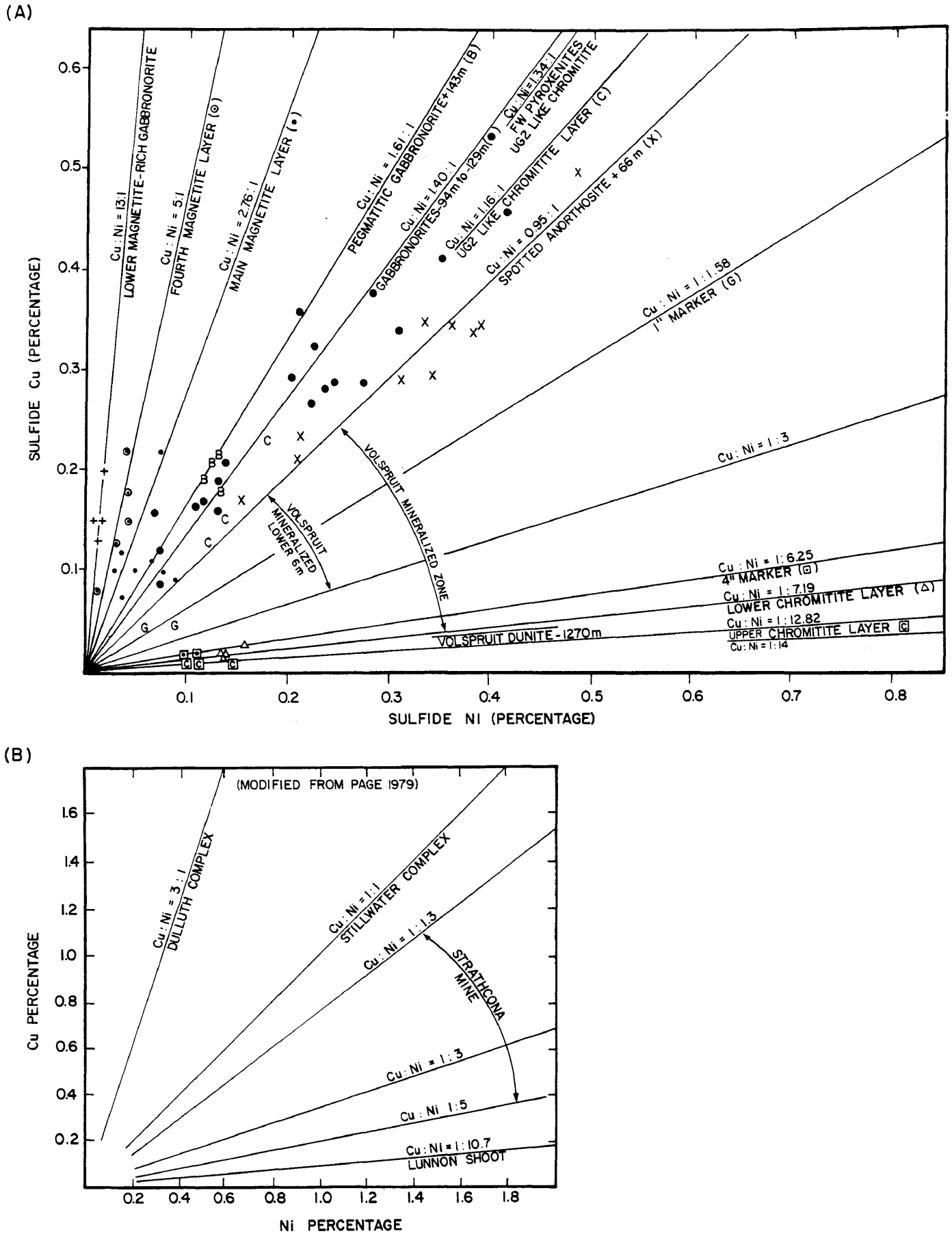

Fig. 92 Cu:Ni ratios for sulfides in:
(A) various horizons in the layered sequence of the Potgietersrus limb and
(B) in other mafic-ultramafic complexes.

is characterized by high Cu values. The values of 0,95:1 for the spotted anorthosite (anorthositic norite) and 1,16:1 for the UG2-like chromitite are very similar to the mean value given by Page (1979) for the basal Stillwater ore. The Cu:Ni values of 1,24:1 to 1,40:1 for the mineralized gabbronorites and the foot-wall pyroxenites of the UG2-like chromitite layer also suggest derivation from a fairly evolved parental magma, somewhat more fractionated than that which gave rise to the mineralized spotted anorthosite at the +66 m level and to the Stillwater ores.

The upper zone Cu:Ni values are found to range from 2,76:1 to 13:1. The Cu:Ni ratios clearly show that the liquid from which the main magnetitite layer crystallized was more basic than that which gave rise to the magnetite-rich gabbronorite which occurs 80 m below the main magnetitite layer. Comparison with Figure 92B shows that the Cu:Ni ratios of the sulfides from the main magnetitite layer are very similar to those of the mineralization near the basal contact of the Duluth Complex.

From the above discussion it appears that the Cu:Ni ratios of the sulfides in a rock give a fairly good indication of the basicity of the magma. Fluctuations of this ratio can be used in conjunction with the stratigraphic column to indicate at what levels in the intrusion the crystallizing magma was replenished by more basic magma.

The sulfide Ni and Cu as well as total Ni and S values used in this study are tabulated in Table 21 together with the respective stratigraphic level from which the samples were taken.

8.4.2 The Influence of Bulk Composition on the Solubility of Sulfur in the Melt

When the major element analyses of each rock type are plotted in terms of the end members $TiO_2+FeO_{(T)}+MgO+CaO+P_2O_5$, SiO_2, and $Al_2O_3+Na_2O+K_2O$, as shown in Figure 93, an apparent trend evolves for the mineralized samples, which distinguishes them from their unmineralized equivalents. The mineralized samples in Figure 93B define a chemical trend of continuously decreasing SiO_2 and increasing Al_2O_3, Na_2O, and K_2O with fractionation from the most

TABLE 21 NICKEL, COPPER AND SULFUR CONCENTRATIONS (PPM) IN THE RUSTENBURG LAYERED SUITE SOUTH OF POTGIETERSRUS

STRAT. LEVEL (m)	Ni (TOTAL)	Ni (SULFIDE)	Cu	S	STRAT. LEVEL (m)	Ni (TOTAL)	Ni (SULFIDE)	Cu	S
1479	200	40	18		179*	183		195	290
1458	66		326	1550	179*	483		452	930
1380	139		477	1021	148	61		35	30
1366	420	110	900		143	1477	1297	2093	7130
1332	57	10	63	530	143*	1646	1350	1824	6370
1324	111		8	40	143*	1623	1340	2145	6880
1240	103		74	50	143*	1364	1180	1913	6050
1190	99		61	60	123	75		27	<10
1131	160	10	50		76	553	60	15	90
1130	117		65	20	66	4000	3600	3500	
1067	119		16	20	66*	3445	3150	3437	11300
940	97		20	40	66*	2027	1740	1521	5560
868*	108		18	10	66*	4142	3855	3473	11410
868*	107		18	190	66*	3698	3400	2968	10100
850	97		13	70	66*	322		19	30
782*	111		14	20	66*	2401	2110	2121	7360
782*	118	40	16	190	66*	3388	3120	2971	8910
724	101		22	20	66*	4085	3790	3423	10780
622	103		27	<10	66*	3602	3302	3531	10110
566	152		35	100	66*	2403	2115	2352	6850
470	173		31	<10	66*	5098	4810	5037	16040
410	123		22	<10	19	788		97	60
392*	160	20	20	300	19*	918	120	136	80
392*	167		24	100	19*	841		160	10
392*	169		27	90	19	730	140	240	
250	208		26	220	6	995	500	915	4990
205	180	30	60		5	2451	2080	2478	16700
205*	162		33	130	-8	233		64	<10
205*	146		40	130	-22	34		10	50
205*	145		37	30	-34	680	130	140	
205*	158		38	20	-34	643		151	460
198	128		23	90	-84,5*	1337	610	385	870
198*	143		30	110	-84,5*	1044	410	261	990
198*	146		38	110	-84,5*	1318	610	324	770
180	525		417	700	-85,5	900	110	480	
180*	358		307	770	-85,5*	2220	1770	2373	6760
180*	514	280	438	710	-85,5*	1762	1230	1279	3260
180*	312		268	270	-85,5*	1949	1380	1536	3610
179*	569	450	550	1660	-86*	2292	1720	2322	10630

STRAT. LEVEL (m)	Ni (TOTAL)	Ni (SULFIDE)	Cu	S	STRAT. LEVEL (m)	Ni (TOTAL)	Ni (SULFIDE)	Cu	S
-86*	2436	1800	1829	12060	M.Mb P.G.	93		36	30
-86*	2274	1710	2637	11890	"	101		39	380
-86	1834	1334	1988	10410	"	98		73	520
-91*	2266	2050	3512	21190	"	100	16	65	
-91*	1582	1360	2133	15570	"	119		69	330
-94	2636	2400	2880	21770	"	99		69	170
-94	1355	1100	1692	20630	"	125	25	78	
-94	1281	1050	1671	9070	"	122		80	220
-94	2227	2000	2962	24600	-141	2151	650	47	560
-94	2556	2300	2829	21350	-180	3110		2238	17580
-94	4269	4050	4622	20280	-280	1020	240	20	100
-94	3027	2800	3803	20370	-299	2131	470	5	210
-94	941	700	870	7980	-402	489	170	39	40
-94	3657	3430	4146	26660	-446	2076		4	30
-94*	2909	2700	2909	18410	-510	2417		7	10
-94*	3256	3010	3438	20070	-524	2078	610	4	<10
-94*	2462	2190	3281	17060	-544	1581	400	7	120
-94*	2425	2200	2702	14080	-577	1065		45	<10
-96	1600	1300	1600		-587	2320	360	16	120
-97	1577	1320	1780	17400					
-110	1628	810	402	3270	-608	2363	380	29	<10
-120	2385		3180	18380					
-128,5	1516		1904	10550	-616	964		5	<10
-128,6	184		75	320	-668	2459		19	100
-128,8	251		235	30	-685	2617		7	470
-129	2274		17	3690	-718	2464	790	1	60
M.Mb P.G.	140		39	110	-735	2417		8	30
"	121		135	150	-765	1162		13	130
"	136		64	<10	-772	925	180	1	1370
"	109		55	10	-780	1571		9	10
"	184		120	90	-785	1609	280	9	30
"	161		56	<10	-790	1908	360	6	110
"	142		33	80	-791	1857		14	<10
"	190	84	138		-792	1547		12	10
"	210	110	130		-810	2350		7	<10
"	230		155	10	-820	2398	470	15	50
"	205	29	305		-825	2460		13	<10
"	107	30	35		-970	852	110	17	440
"	101		64	440	-980	982	170	17	150
"	153		47	310	-982	489	90	13	<10
"	102		50	100	-1032	1099	120	6	40

STRAT. LEVEL (m)	Ni (TOTAL)	Ni (SULFIDE)	Cu	S
-1036*	1069	110	12	100
-1052	980	270	37	480
-1060	1889		3	
-1063	1158	410	30	350
-1074	2732		4	<10
-1100*	763	230	27	430
-1116	1470	1120	233	5330
-1122*	1038	480	46	590
-1130	676	230	27	80
-1142*	1085	280	23	1300
-1163	1300	460	40	10
-1171*	1991	1380	478	4660
-1172	1974	1420	233	5557
-1173	1289	889	293	3950
-1180*	1320	1380	59	8110
-1181*	2233	1420	138	3630
-1188	1652		645	9670
-1208	2403		1333	13390
-1209*	1943		231	1470
-1220	2022		632	11970
-1224*	1480	1070	139	5760
-1233	7449	450	37	950
-1250	4901	980	1	<10
-1270	2151	1250	134	3900
-1275	2969		9	310
-1278	1922		49	910
-1370	1519		4	<10
-1385	1546		145	1010
-1410	1127	120	4	40
-1430	923	60	6	290
-1460*	822	280	18	60
-1478	878	120	16	30
-1498	781		75	1000
-1508	1031	100	10	120
-1533	1015	440	105	830
-1587*	752		28	230
-1594	1777	410	8	380
-1606	1656	570	17	810
-1627*	950	390	20	210
-1644	1414	230	3	<10
-1660*	1594	1080	384	580

STRAT. LEVEL	Ni (TOTAL)	Ni (SULFIDE)	Cu	S
1" MARKER	1710	910	476	114(
1" MARKER	1388	610	453	80(
4" MARKER(H.W.)	4127	3300	147	259(
" " "	6441	6000	466	539(
" " "	4806	4050	226	350(
4" MARKER	1660	1000	149	59(
4" MARKER	1704	1110	190	92(
4" MARKER(F.W.)	4547	3800	262	402(
" " "	3849	2600	70	208(
" " "	3605	1900	33	129(
" " "	5100	4300	180	
UPPER LAYER (T)	1893	1450	93	93(
" " (M)	1438	1130	87	58(
" " (M)	1592	1130	77	54(
" " (B)	1386	1020	89	57(
" " (B)	1463	1030	99	300
UPPER LAYER (F.W.)	3487		18	430
" " (F.W.)	3406		4	100
HW PYROXENITE	2808	1850	132	3590
	6793	6150	436	10170
	2538	1670	193	5140
	3333		263	7330
	3634		216	4850
LOWER LAYER (T)	2882	1400	159	3520
" " (T)				
" " (T)	3198	1390	208	4060
" " (T)	3676	1580	295	3660
" " (B)	1200	270	110	

* = BULK SAMPLE (3-6 KILOGRAMS)

$\frac{M.Mb}{P.G.}$ = MARGINAL MEMBER ADJACENT THE PTA GRP

HW = HANGING-WALL

FW = FOOT-WALL

T = TOP

M = MIDDLE

B = BOTTOM

HW PYROXENITE = HANGING-WALL PYROXENITE FOR THE LOWER CHROMITITE LAYER

UPPER LAYER, LOWER LAYER = CHROMITITE LAYERS

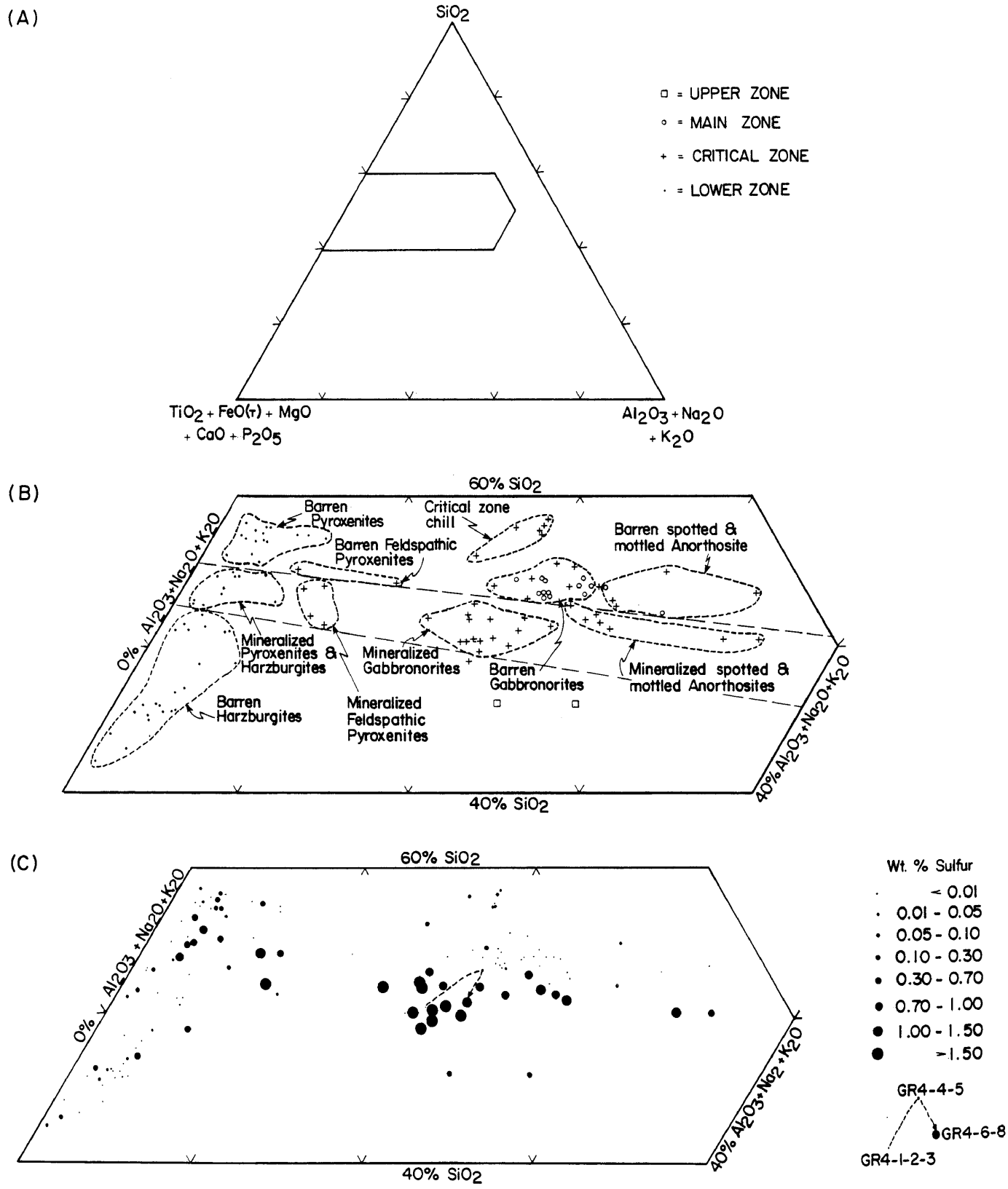

Fig. 93 (A) The ternary system SiO_2-TiO_2+$FeO_{(T)}$+MgO+CaO+P_2O_5-Al_2O_3+Na_2O+K_2O showing the area enlarged in B and C.

(B) Plots of mineralized and unmineralized upper, main, critical and lower zone samples. The mineralized samples define a specific field within this diagram.

(C) Graphic representation of S content of the mineralized samples.

primitive harzburgites and pyroxenites to the gabbronorites and norites. On Figure 93C, the same field as shown in Figure 93B, the weight per cent sulfur for each sample is illustrated graphically. The arrowed broken line connects unmineralized samples GR4-1,2 and 3 that contain 0,01 weight per cent S with samples GR4-4 and 5 that contain between 0,01 to 0,05 per cent sulfur and samples GR4-6 and 8 with between 1,00 to 1,50 weight per cent S. This illustrates that even though certain samples are not mineralized they still plot into this field if they are associated with sulfide mineralization. No explanation can be offered for the reason why the mineralized samples as well as the non-mineralized samples from the same horizon plot within this field.

This ternary plot is commonly used to demonstrate the compositional relationship between immiscible liquids. Lee and Sharpe (1979 and 1980), for instance, used this diagram to illustrate that a special case of liquid immiscibility was operative during formation of the spherical aggregates, the boulder bed and the Merensky Reef. The tie-lines established by them between aggregates and matrix, boulders and matrix, as well as for Merensky Reef samples, occupies an identical field to that defined by the mineralized samples in Figure 93B. They also demonstrated a relative enrichment in normative orthoclase and quartz in the boulders, aggregates and Merensky Reef material relative to their respective matrices. The significance of the above-mentioned coincidence between the field of aggregation of pyroxenes and mineralization in Figure 93B is not clear at this stage. It may however be related in both cases to an increase in alkalis in the liquid, as this would seem to promote boulder aggregation as well as the formation of immiscible sulfide liquid. The bulk composition of mineralized rocks and aggregate-matrix pairs plots in an alkali and femic enriched zone in Figure 93B, compared to their respective unmineralized and aggregate free counterparts.

8.4.3 Pt and Pd Characteristics of the Parental Magma(s)

In the sulfide ores from the Merensky Reef, Pechenga, Sudbury, and Norilsk the Pt/(Pt+Pd) ratio decreases systematically with an increase in the Cu/(Cu+Ni) ratios. From this it can be inferred that the Pt/(Pt+Pd) ratio decreases with increasing fractionation

of the host silicate magma (Naldrett and Cabri, 1976). Although only a limited number of Pt and Pd analyses are available these can be used to comment on the nature of the host silicate melt.

The lower 6 metres of the Volspruit mineralized zone has a Cu/(Cu+Ni) ratio of 0,31 and a Pt/(Pt+Pd) ratio of 0,44 in the up-dip section, whereas the down-dip section gives values of 0,41 and 0,54 respectively. Such values fall within the tholeiite field as defined by Naldrett (1981). Similarly, the mineralized pyroxenite at the top of the lower zone has a Cu/(Cu+Ni) value of 0,53 and a Pt/(Pt+Pd) value of 0,29. These values also suggest a magma of tholeiitic parentage, in composition intermediate between that of Sudbury norites and the flood basalts of Norilsk - Talnakh, but more fractionated than that which gave rise to the Volspruit section. Samples from the UG2-like chromitite layer have a Cu/(Cu+Ni) ratio of 0,54 and a Pt/(Pt+Pd) ratio of 0,63. This value falls outside the tholeiite field, and the Pt/(Pt+Pd) ratio is the highest of all samples.

8.5 Sulfide Mineralogy

This study is based on systematic sampling and microscopic investigations of over 300 polished sections prepared by the author. The normative amount of sulfides in the rocks is based on whole-rock Cu, S, and sulfide Ni values as this was found to be more accurate and a more rapid estimate of the individual sulfide proportions and concentrations than point counting techniques. Where two iron sulfides like pyrite and pyrrhotite or two copper-iron sulfides like chalcopyrite and cubanite coexist in the same rock, a combination of normative and point counting techniques was employed to determine the proportion of sulfide minerals in the rocks. The results are presented in Figure 94.

An energy dispersive analyser attached to a Joel scanning electron microscope was used to assist in the identification of sulfides in polished section. Representative chemical analyses of certain sulfides were also obtained by using energy dispersive analysis and natural standards.

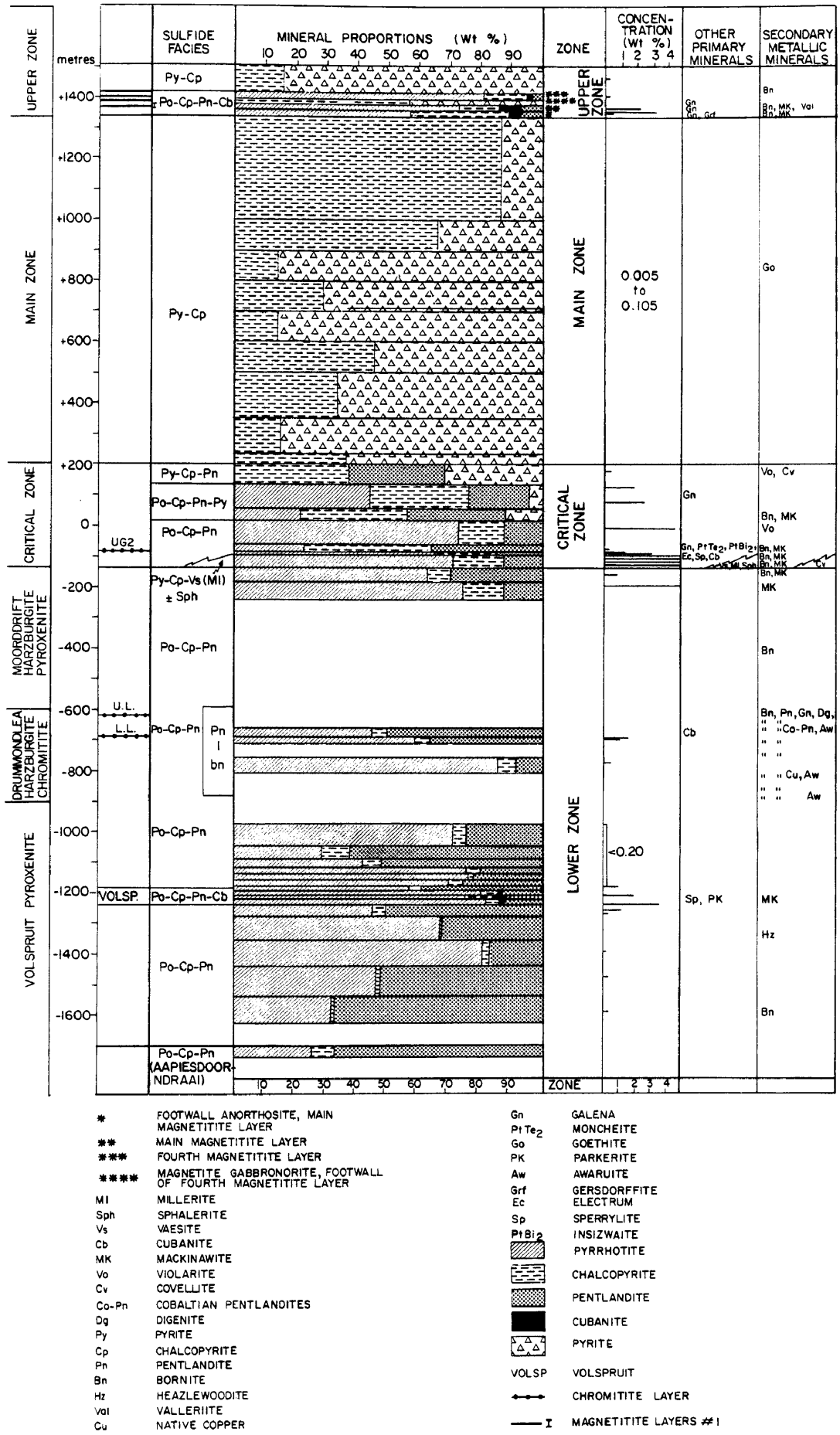

*	FOOTWALL ANORTHOSITE, MAIN MAGNETITITE LAYER
**	MAIN MAGNETITITE LAYER
***	FOURTH MAGNETITITE LAYER
****	MAGNETITE GABBRONORITE, FOOTWALL OF FOURTH MAGNETITITE LAYER
MI	MILLERITE
Sph	SPHALERITE
Vs	VAESITE
Cb	CUBANITE
MK	MACKINAWITE
Vo	VIOLARITE
Cv	COVELLITE
Co-Pn	COBALTIAN PENTLANDITES
Dg	DIGENITE
Py	PYRITE
Cp	CHALCOPYRITE
Pn	PENTLANDITE
Bn	BORNITE
Hz	HEAZLEWOODITE
Val	VALLERIITE
Cu	NATIVE COPPER

Gn	GALENA
$PtTe_2$	MONCHEITE
Go	GOETHITE
PK	PARKERITE
Aw	AWARUITE
Grf	GERSDORFFITE
Ec	ELECTRUM
Sp	SPERRYLITE
$PtBi_2$	INSIZWAITE
	PYRRHOTITE
	CHALCOPYRITE
	PENTLANDITE
	CUBANITE
	PYRITE
VOLSP	VOLSPRUIT
	CHROMITITE LAYER
I	MAGNETITITE LAYERS #1

Fig. 94 Normative variation of the main constituents of the sulfide assemblages in the layered sequence south of Potgietersrus. The sulfur-poor assemblages shown for the upper zone comes from the farm Molendraai.

8.5.1 Distribution of Primary and Secondary Sulfides

8.5.1.1 Lower Zone

From the -1620 m to -1230 m level in the lower zone the sulfide assemblage consists of pyrrhotite, chalcopyrite, and pentlandite. This interval is also the one with the highest proportion of pentlandite in the layered sequence. The samples from the lowest level have a pentlandite to pyrrhotite ratio similar to that reported by Liebenberg (1970) for the Aapiesdoorndraai ultramafic body, which has the highest ratio of all the samples he investigated in the Bushveld Complex. The sulfide concentration in this lower Volspruit section ranges between 0,10 to 0,23 weight per cent (Table 22). Secondary sulfide minerals, when encountered in this interval, are usually bornite and heazlewoodite. Heazlewoodite (Fig. 95A) is confined to serpentinized olivine-rich rocks, and formed from pentlandite during serpentinization. Secondary magnetite is always associated with this heazlewoodite. Since heazlewoodite has a thermal maximum of 556°C (Kullerud et al., 1969) formation of this mineral and the serpentinization process seems to have taken place below this temperature.

Cubanite is a primary phase in the mineralized pyroxenites stradling cyclic units 10 and 11 of the Volspruit subzone. The cubanite bearing assemblage is confined to the lower two-thirds of the mineralized interval. This mineral occurs as exsolution lamellae within chalcopyrite (Fig. 95B) or as irregular grains near the pyrrhotite-silicate contact. The pyrrhotite associated with the cubanite is of the hexagonal variety and contains exsolution lamellae of troilite (Fig. 95E). Typical pentlandite exsolution in pyrrhotite are shown in Figure 95F. Typical sulfide concentrations average about 3 weight per cent but range between 2,00 to 3,60 per cent. Mineral proportions are shown in Figure 94. Other primary metallic minerals in this zone are sperrylite and an unknown Bi-Ni alloy, which on occasion was found to contain traces of iron. This alloy occurs associated with chalcopyrite and both are included in pyrrhotite (Fig. 95C). Idiomorphic crystals of sperrylite, when present, are usually found on the margins of chalcopyrite grains (Fig. 95D).

Cubanite is absent from the upper third of the mineralized pyroxenite. The only secondary mineral observed in the upper

TABLE 22 SULFIDE MINERAL PROPORTIONS, AND CONCENTRATION ASSOCIATED WITH THE RUSTENBURG LAYERED SUITE SOUTH OF POTGIETERSRUS

ZONE	STRAT. LEVEL		MINERAL PROPORTIONS (%) Pn	Cp	Cb	Po	Py	Wt. % Sulfides
U.Z.	+1458	Magnetite gabbronorite		16,00			84,00	0,32
	+1360	Main magnetite layer	7,17	13,29	7,21	72,83		1,57
	+1360	Main magnetite layer, bottom concentration	7,00	14,58	7,68	71,22		3,20
	+1359	Foot-wall anorthosite to the main magnetite layer	7,19	32,38	3,80	57,14		0,11
M.Z.		Main zone gabbronorites (range)		16,00			84,00	
				37,00			63,00	0,005
				46,00			54,00	to
				66,00			34,00	0,015
				83,00			17,00	
		Main zone gabbronorites (mean)		39,00			61,00	
C.Z.								
	+ 180	Gabbronorite	30,03	38,26			31,70	0,41
	+ 143	Pegmatitic gabbronorite	19,63	32,15		44,07	4,15	1,84
	+ 66	Spotted norite and anorthositic norite	33,52	33,64		21,37	11,44	2,68
	+ 5	Feldspathic pyroxenite	12,72	14,84		72,85		4,65
	- 84	Hanging-wall chromitic gabbronorite to UG2-like chromitite	39,70	25,90		34,40		0,28
	- 85.5	UG2-like chromitite layer	36,60	40,92		22,46		1,30
	- 86	Foot-wall feldspathic pyroxenite to UG2-like chromitite	15,06	20,21		65,23		3,14
	- 87 to -129	Mean of the mineralized gabbronorite interval studied between -87 to -129 m level.	12,77	16,59		71,09		5,16
	M.Mb / P.G.	Mean of the fine-to medium-grained gabbronorites	*12,00	14,80		73,20		0,25
L.Z.								
	-141	Harzburgite	22,32	12,45		65,16		0,92
	-180	Pyroxenite	12,83	13,18		74,46		4,89
	-686	Hanging-wall pyroxenite to the lower chromitite layer	50,88	5,13		44,00		1,53
	-686.6	Lower chromitite layer	37,63	4,90		57,47		1,03
	-772	Pyroxenite	13,13	0,52		86,54		0,38
		Mean of the upper Volspruit section excluding the mineralized zone.	24,76	5,66		69,58		<0,20
	≈-1185	Top 1/3 of the Volspruit mineralized zone	39,80	3,87		56,33		1,03
	≈-1220	Lower 2/3 of the Volspruit mineralized zone	12,84	6,74	1,80	78,62		2,00 -3,60
	-1270	Mineralized dunite	39,92	2,18		58,00		0,27-1,11
	-1350 to -1430	Top 1/3 of the Lower Volspruit subzone	17,14	2,06		81,00		0-0,10
	-1430 to 1620	Lower 2/3 of the Lower Volspruit subzone	59,25	1,27		39,49		0-0,23
	**	Upper chromitite	95,74	4,26				0,32
		4" marker layer	93,00	7,00				0,33
		Foot-wall of 4" marker layer	98,00	2,00				0,77
		Hanging-wall of 4" marker layer	97,00	3,00				1,23

* All soluble Ni calculated as pentlandite

** Secondary pentlandite and bornite in serpentinized horizons associated with the upper chromitite.

\- All values are in weight per cent.

part of the mineralized zone is mackinawite after pentlandite.

Sulfides in the Drummondlea Harzburgite-Chromitite subzone consisted of the po-cp-pn assemblage prior to serpentinization. The best preserved primary mineral assemblages and textures are encountered in the pyroxenite at the -772 m level, in the lower chromitite layer at the -686,6 m level and in its hanging-wall pyroxenite (Fig. 94). All other levels within this section contain sulfides in far too low concentrations to allow for accurate estimation of their mineral proportions. The pyroxenite at the -772 m level contains 0,38 weight per cent sulfides, which increase to 1,03 per cent in the lower chromitite and culminate at about 1,53 per cent in the hanging-wall pyroxenite. The increase in sulfides is accompanied by an increase in the pentlandite content from 13,13 per cent at -772 m to more than 50 per cent in the hanging-wall pyroxenite. The chalcopyrite content remains constant (Fig. 94).

The sulfide assemblage associated with the chromitite layers usually occurs as drop-like aggregates of pn, po, and cp (Fig. 95G). Net textured and cusp shaped sulfides draped around cumulus chromite grains (Fig. 95H) are common textural features of sulfides in the chromitite layers. Pentlandite in some samples is extensively replaced by mackinawite (Fig. 98I).

The most common sulfide assemblage in serpentinized rocks of the Drummondlea Harzburgite-Chromitite subzone consists of pentlandite and bornite (Fig. 96A). Most of the pentlandite is considered to have formed during serpentinization as a result of which the original po-pn-cp assemblage was reconstituted, by the addition of Ni from the olivine, to a pentlandite-bornite assemblage. Chalcopyrite of the original Ni-Fe-Cu sulfide aggregates is altered to assemblages containing bornite and digenite (Fig. 96B). The presence of digenite suggests that sulfide phases were still forming at very low temperature, as this mineral is not stable at temperatures above 83°C (Craig, 1974, cg-59). Although unexpected, galena was found to occur associated with secondary pentlandite in places (Fig. 96C). Grains of cobaltian pentlandite and native Cu are extremely rare and associated with the Ni-Fe alloy awaruite (Fig. 96D). This mineral was, however, also found on rare occasions to be associated

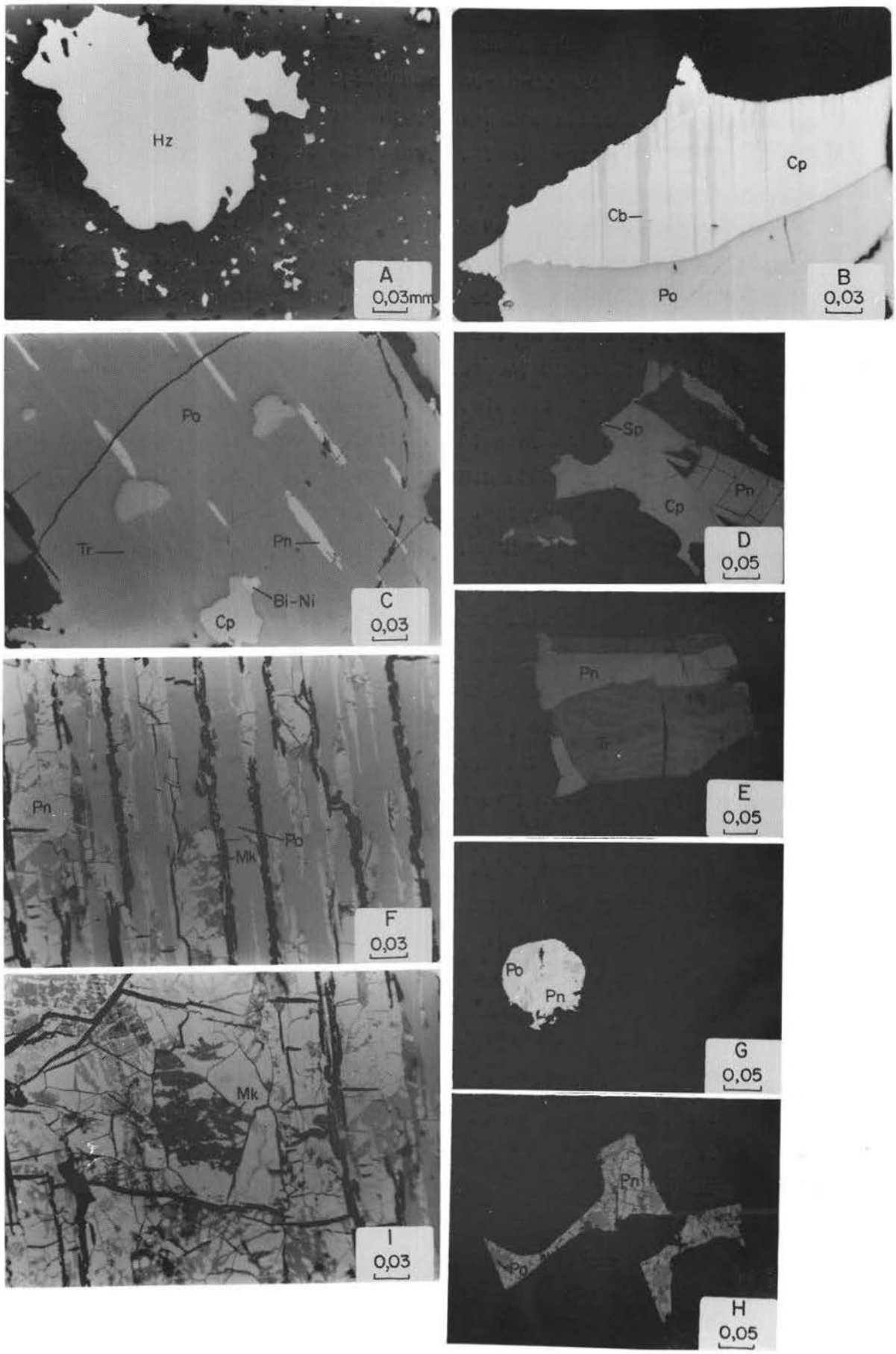

Fig. 95

Figure 95. Textural features of sulfides and other metallic phases in rocks from the lower zone. Hz = healzlewoodite Cp = chalcopyrite; Cb = cubanite; Po = pyrrhotite; Tr = troilite; Pn = pentlandite; Bi-Ni = bismuth-nickel alloy; Sp = sperrylite; Mk = mackinawite. Reflected light - oil immersion. Sample number in brackets.

(A) A large grain of heazlewoodite enclosed in magnetite from a serpentinite in the Volspruit subzone. (VSZ-135)

(B) Exsolved lamellae of cubanite in chalcopyrite from the Volspruit mineralized zone. (32-255)

(C) Bi-Ni alloy in mutual contact with chalcopyrite and pyrrhotite. Volspruit subzone. (32-941)

(D) Idiomorphic crystal of sperrylite at the margin of a chalcopyrite grain. Volspruit subzone. (32-841)

(E) Troilite lamellae in hexagonal pyrrhotite. Volspruit subzone. (32-255)

(F) Coarse lamellae of pentlandite exsolved from pyrrhotite. Drummondlea Harzburgite-Chromitite subzone. (3-103)

(G) Sulfide sphere consisting of pyrrhotite and pentlandite in the lower chromitite. (LL-1)

(H) Net-textured or cusp-shaped sulfides draped around cumulus chromite in the lower chromitite layer. (LL-2)

(I) Pentlandite replaced by mackinawite. Drummondlea Harzburgite-Chromitite subzone. (3-103)

with the more sulfur-rich assemblage pentlandite-bornite. These secondary assemblages are usually associated with secondary magnetite.

It was previously mentioned that concentrations of massive sulfides are locally found as infillings of fractures in the vicinity of the upper chromitite layer. These samples consist of chalcopyrite, cubanite and pentlandite and a Pb-telluride. Textural relationships between cubanite, chalcopyrite and pentlandite are shown in Figure 96E and F. Primary magnetite tends to be associated with the sulfides in all these samples. The Pb-telluride (altaite) occurs as rounded to avoid shaped grains in the chalcopyrite (Fig. 96G).

Except for some mineralization at the top of the Moorddrift Harzburgite-Pyroxenite subzone, lower zone rocks above the upper chromitite are generally very poorly mineralized. Where sulfides are present they consist of the secondary assemblage pentlandite-bornite. The sulfides encountered at the top of the lower zone range in concentration from 0,92 to 4,89 weight per cent in the harzburgite and the pyroxenite respectively. The respective proportions of pn, cp, and po are shown in Figure 94. The decreased pentlandite and increased chalcopyrite component of the sulfides in these samples, relative to the rest of the lower zone, testifies to the more fractionated nature of the magma from which these sulfides have separated. Also, the highest proportion of chalcopyrite observed in any olivine-bearing lower zone horizon occurs in the harzburgites at the top of the lower zone.

8.5.1.2 Critical Zone

The largest variety of primary sulfide assemblages is developed in the critical zone (Fig. 94). Varying proportions of po, cp, and pn abound in the lower half of this zone, with the highest proportion of pentlandite as well as chalcopyrite being associated with the UG2-like chromitite layer. The highest concentration of sulfides occur in the mineralized gabbronorite (5,16 per cent) and in the feldspathic pyroxenite at the +5 m level. Although these samples have the highest sulfide concentration, their grade is comparatively low because 71 to 73 per cent of all the sulfides consist of pyrrhotite. Figure 96H is a typical composite pentlan-

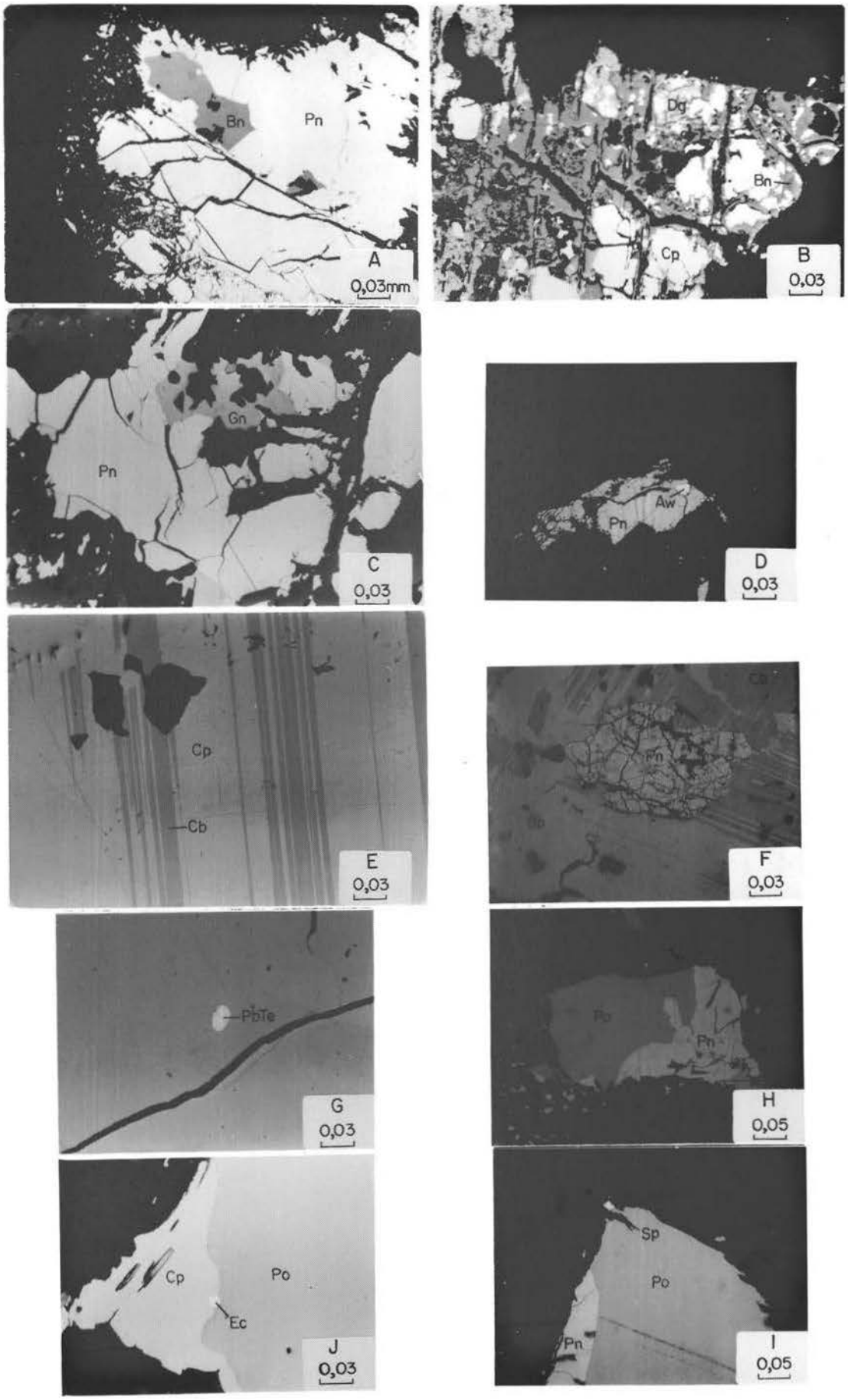

Fig. 96

Figure 96. Textural features of sulfides and other metallic phases in the lower and critical zone lithologies. Pn = pentlandite; Bn = bornite; Cp = chalcopyrite; Dg = digenite; Gn = galena; Aw = awaruite; Cb = cubanite; PbTe = lead-telluride; Ec = electrum; Sp = sperrylite. Reflected light - oil immersion. Sample number in brackets.

(A) Typical pentlandite-bornite assemblage in the Drummondlea Harzburgite-Chromitite subzone (3-103)

(B) Chalcopyrite breaking down to bornite and digenite. Drummondlea Harzburgite-Chromitite subzone.

(C) An unusual pentlandite-galena assemblage found in a serpentinite of the Drummondlea Harzburgite-Chromitite subzone. (U.G.-3,1)

(D) Pentlandite-awaruite assemblage from a serpentinite of the Drummondlea Harzburgite-Chromitite subzone. (6A-244A)

(E) Exsolved cubanite lamellae in chalcopyrite. Massive sulfides in fracture infillings in the Drummondlea Harzburgite-Chromitite subzone. (Dup.-1)

(F) Coarse pentlandite "eyes" in chalcopyrite and cubanite. (Dup.-1)

(G) Pb-telluride (altaite) enclosed in chalcopyrite. (Dup.-1)

(H) Composite pyrrhotite-pentlandite aggregate from mineralized gabbronorite in the basal portion of the critical zone. (78-418A)

(I) Sperrylite grain sitting at the margin of a pyrrhotite grain. Mineralized gabbronorite in the basal portion of the critical zone. (78-418A)

(J) Electrum at the contact between chalcopyrite and pyrrhotite. Mineralized gabbronorite from the basal portion of the critical zone. (78-156B)

dite-pyrrhotite grain in the mineralized gabbronorite. Precious metal values in these mineralized rocks are accounted for by the presence of minerals like sperrylite and electrum. The sperrylite occurs as tiny grains on the margin of composite sulfide grains (Fig. 96I), whereas the electrum tends to occur as rounded grains at the contact between chalcopyrite and pyrrhotite (Fig. 96J). Cubanite has only been observed on one occasion as an irregular, granular exsolution within pyrrhotite. Bornite after chalcopyrite and mackinawite after pentlandite were also noted.

The platinum group minerals associated with the UG2-like chromitite layer seem different from those encountered elsewhere in the layered suite. Only moncheite ($PtTe_2$) and insizwaite ($PtBi_2$) were observed. The moncheite was noted to occur as a xenomorphic greyish-white highly reflecting mineral between two pyrrhotite grains (Fig. 97A). Insizwaite was observed at the triple junction of three chromite grains and is associated with both pyrrhotite and chalcopyrite (Fig. 97B).

Galena is also associated with some of the sulfides in the UG2-like chromitite layer. When found, it is always confined to silicates within or adjacent to the sulfide grains(Fig. 97C).

The only secondary sulfides associated with the UG2-like chromitite layer are bornite and mackinawite.

Rocks of the M.Mb./L.Z. contain the sulfide association po-cp-pn, which differs radically from the sulfide assemblage in their quenched analogue adjacent to the Pretoria Group (M.Mb./P.G.). The typical association in this member is pyrite-chalcopyrite with millerite and vaesite (NiS_2) as the Ni-bearing sulfides. Although vaesite, the Ni analogue of pyrite, was only found on two occasions, the main source of the sulfide Ni is considered to stem from this mineral because pentlandite is not present and because the pyrite in these rocks contains no nickel. In order to allow direct comparison with the estimated mineral proportions of other mineralized layers (Fig. 94), all the sulfide Ni was allocated to pentlandite. According to these calculations the sulfide concentrations in these fine-grained, quenched rocks range from 0,08 to 0,36 weight per cent with a mean value of

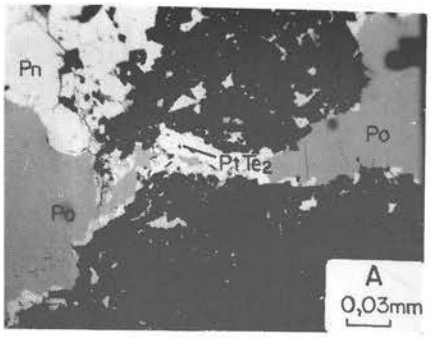

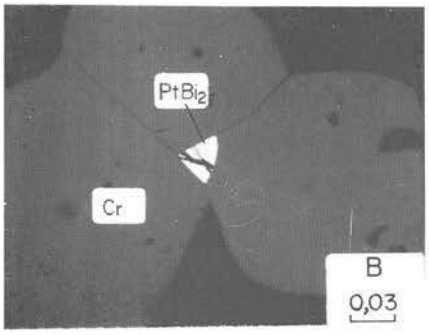

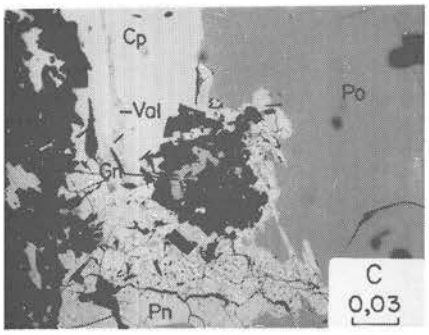

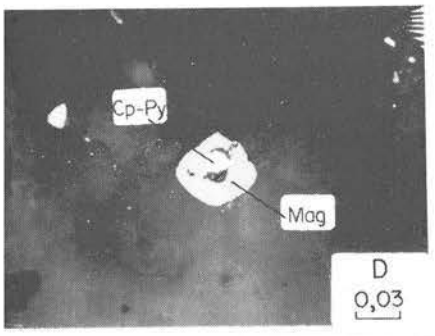

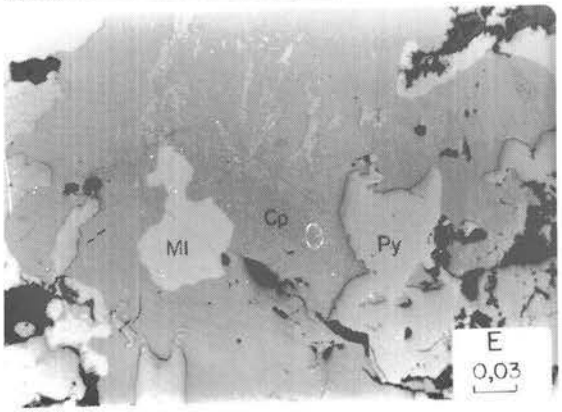

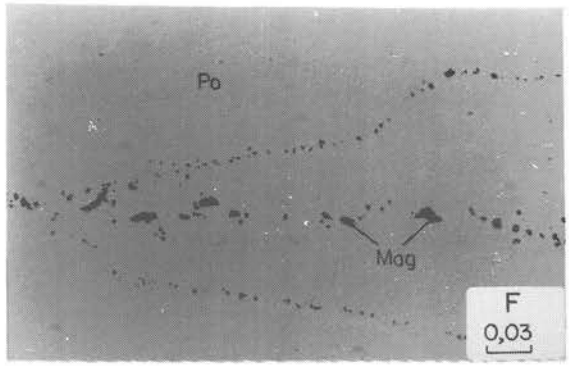

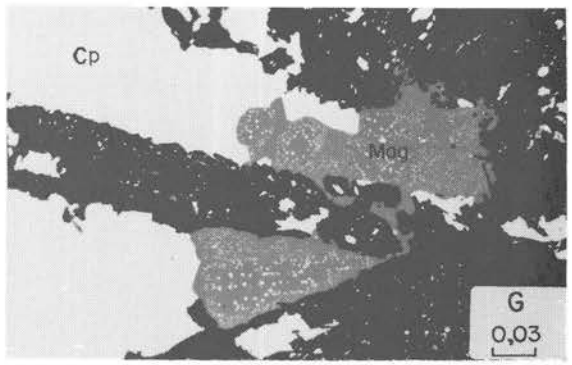

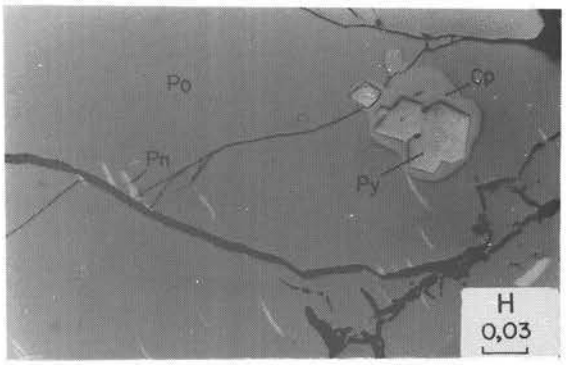

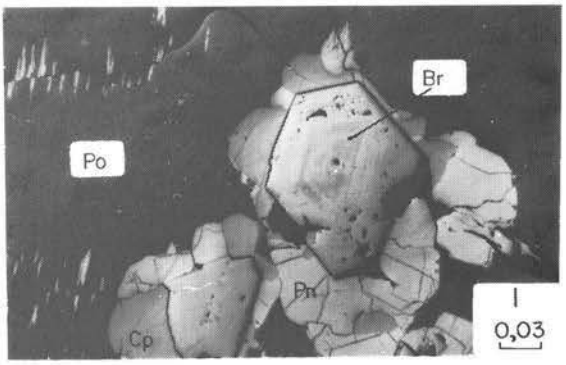

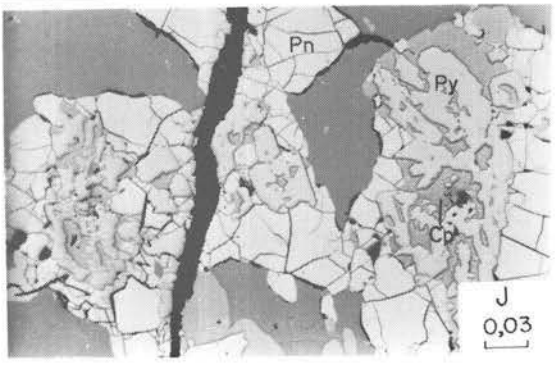

Fig. 97

Figure 97. Textural features of sulfides and other metallic phases in rocks of the critical zone. Pn = pentlandite; Po = pyrrhotite; $PtTe_2$ = moncheite; Mag = magnetite; Cr = chromite; $PtBi_2$ = insizwaite; Cp = chalcopyrite; Val = valleriite; Py = pyrite; Br = bravoite; Ml = millerite; Gn = gablena. Reflected light - oil immersion. Sample number in brackets.

(A) A grain of moncheite ($PtTe_2$) from the UG-2 like chromitite layer on Grasvally. (UG2-11)

(B) Insizwaite ($PtBi_2$) in sulfide at the triple point of three chromite grains in the UG2-like chromitite. (UG2-6)

(C) Galena in silicate fraction associated with sulfides in the UG2-like chromitite. (UG2-11)

(D) Pyrite-chalcopyrite sphere enclosed in magnetite in the M.Mb./P.G. Very fine-grained gabbronorite. (GR1-88,48)

(E) Exsolved blebs of millerite in chalcopyrite from the M.Mb./P.G. Fine-to medium-grained gabbronorite. (78-361A)

(F) Pyrrhotite with trains of magnetite (Ti-poor) believed to represent original oxide from the sulfide-oxide melt. Pegmatitic gabbronorite. (78-42)

(G) Magnetite grain (Ti-poor) with heavy disseminations of sulfides. Both are believed to have crystallized from a sulfide-oxide melt. (78-142)

(H) Euhedral pyrite grains surrounded by chalcopyrite and enclosed in a large pyrrhotite grain. (78-142)

(I) Zoned pyrite (bravoite) crystal enclosed in granular pentlandite. (78-399E)

(J) Graphic intergrowth between pyrite and chalcopyrite in a spotted anorthositic norite in the upper half of the critical zone. (78-399E)

0,25 per cent. Of this approximately 12 per cent is pentlandite, 14,80 per cent chalcopyrite, and 73,20 per cent pyrite. Had the sulfide Ni been calculated as vaesite, the total concentration of sulfides would have been considerably less.

Because of the low concentration of vaesite and its grey colour, its presence in these fine-grained rocks was nearly overlooked, and it was discovered by accident while probing what was originally thought to be sphalerite. To the best of the author's knowledge, this is the first time that vaesite has been encountered in quenched basaltic rocks. Although the vaesite is very rare, its mere presence is petrologically significant in that it provides an upper limit to the temperature and fs_2 conditions of the magma from which these rocks crystallized. The presence of this mineral suggests a temperature maximum of 1007°C (Craig, 1974, p. cg-77) and a fs_2 of $\log_{10}{}^{+1,7}$ according to the plots of Barton and Skinner (1967). The vaesite was typically found to occur as minute grains, together with pyrite and chalcopyrite, enclosed in magnetite (Fig. 97D), or ilmenite. Under high magnification most of the pyrite-chalcopyrite is seen to be graphically intergrown.

Sphalerite was only encountered once within the assemblage py-cp-vs (vaesite). It also occurs within a sulfide sphere inside a magnetite grain, and was found to be a zinc-rich variety with 62,4 per cent zinc or 93 mole per cent ZnS (Table 23).

Away from the very fine-grained chilled marginal rocks, in the medium-grained ophitic to subophitic gabbronorite of the M.Mb./P.G. the sulfide association pyrite-chalcopyrite prevails. Vaesite was not observed and its place is taken by primary millerite. The millerite commonly occurs as irregular straw-yellow exsolved blebs within chalcopyrite (Fig. 97E).

In the upper half of the critical zone the sulfide assemblages are progressively more S-rich, as can be seen by the upward increasing amounts of pyrite (Fig. 94). The po-cp-pn-py assemblage in the spotted anorthositic norites and pegmatitic gabbronorite contain on average 11,44 and 4,15 per cent pyrite respectively, with corresponding average sulfide concentrations of 2,68 and 1,84 per cent. These sulfides appear to have crystallized from immiscible sulfide-oxide liquids as can be seen by the presence

TABLE 23 CHEMICAL COMPOSITION OF SULFIDES IN THE RUSTENBURG LAYERED SUITE SOUTH OF POTGIETERSRUS

Highest Level	Ni	Fe	S	Co	Cu	Zn	As	Total
11) Pentlandite	32,00	31,60	33,00	3,37				99,97
11) Pyrrhotite	0,13	61,32	38,10					99,55
11) Cubanite		40,07	35,20		24,6			99,87
10) Pyrite	3,91	42,44	53,60					99,95
9) Pentlandite	35,50	30,80	33,20	0,07				99,57
9) Pyrrhotite	0,69	59,61	39,08					99,38
8) Pentlandite	32,12	33,47	33,03	1,43			0,02	100,07
8) Pyrrhotite	0,25	61,42	37,95	0,02	0,03		0,02	99,69
8) Chalcopyrite	0,03	30,71	35,23	0,03	34,73		0,03	100,76
7) Pentlandite	34,14	32,41	32,83	0,30				99,68
7) Pyrrhotite	0,20	61,20	38,00					99,40
6) Pentlandite	32,87	31,68	32,97	2,74				100,26
6) Pyrrhotite	0,10	60,96	39,49					100,55
5) Vaesite	46,39	0,50	53,00					99,89
4) Sphalerite		8,32	30,00			62,40		100,72
3) Cobalt pentlandite	19,20	5,31	32,50	42,00				99,01
2) Pentlandite	29,92	36,00	32,32	1,27				99,51
2) Troilite	0,20	64,28	34,82					99,30
2) Cubanite		37,61	41,00		20,29			98,90
1) Heazlewoodite	72,83	0,09	26,65	0,02			0,18	99,77

Lowest Level

Key

11) = Po Cp-Pn-Cb	assemblage from main magnetitite
10) = Py-Cp	assemblage from the main zone
9) = Po-Cp-Pn-Py	assemblage from the spotted norite in the critical zone
8) = Po-Cp-Pn	assemblage from critical zone pyroxenite (+ 5 m)
7) = Po-Cp-Pn	assemblage from the UG2-like chromitite layer
6) = Po-Cp-Pn	assemblage from the mineralized gabbronorite near the base of the critical zone
5) = Py-Cp-Vs	assemblage from the critical zone chill
4) = Py-Cp-Vs-Sph	assemblage from the critical zone chill
3) = Co-Pn-Hz	assemblage consisting of cobalt pentlandite-heazlewoodite from the Drummondlea-Harzburgite-Chromitite
2) = Po-Cp-Pn-Cb	assemblage from the Volspruit mineralized zone
1) = Hz	associated with magnetite in a Volspruit serpentinite

of titanium poor magnetite within the sulfides (Fig. 97F).

Closely associated with some of these sulfide grains are large crystals of ilmenite. This ilmenite may have formed as a result of reaction between oxygen from the immiscible sulfide-oxide liquid and the TiO_2 in the adjoining silicate melt. Ripley (1979) noted a similar feature in the Deer Lake Complex, Minnesota. Spatially associated with the sulfides are also large non-titaniferous magnetite grains with heavy disseminations of sulfides (Fig. 97G). Another interesting texture displayed by the sulfides in these rocks is formed by euhedral pyrite crystals within chalcopyrite, which, in turn, is enclosed in a much larger pyrrhotite grain (Fig. 97H). Pyrite, zoned with respect to Ni (bravoite) was occasionally observed (Fig. 97I).

The mineralized spotted anorthositic norites and spotted norites contain considerably more pentlandite (33,52%) than the pegmatitic gabbronorite. The distinctive graphic intergrowth between pyrite and chalcopyrite, commonly observed in the upper half of the critical zone, is illustrated in Figure 97J.

This po-cp-pn-py assemblage gives way to a py-cp-pn assemblage at the top of the critical zone (Fig. 94). Most of the samples from this part of the sequence are from surface outcrop and consequently the pentlandite has broken down to violarite as a result of surfical weathering (Fig. 98A). Although this thiospinel is stable up to 461°C (Craig, 1971) it is generally considered that most violarites have formed at lower temperatures under normal weathering conditions. The octahedral cleavage of the original pentlandite is usually still visible and in some cases syneresis cracks can be seen.

8.5.1.3 Main Zone

The S enrichment trend of the sulfide assemblages upward in the critical zone continues into and through the main zone to the inferred level of the pyroxenite marker. At this level the composition of the sulfide phase changes from pyrite-rich (85py : 65cp) below to pyrite poor (35py : 56cp) above (Fig. 94).

The sulfide concentration in the main zone is very low and was found to range from 0,005 to 0,105 weight per cent. The mean

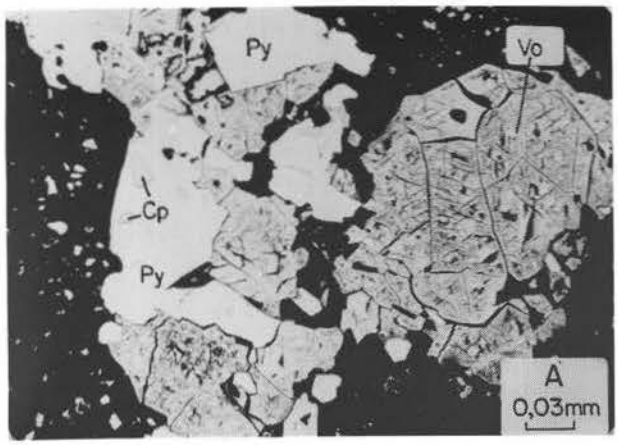

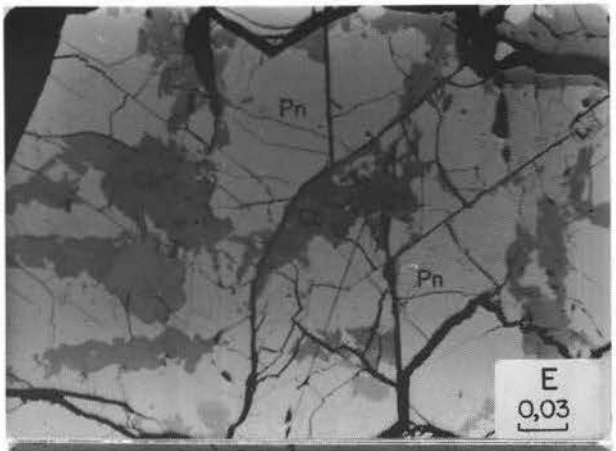

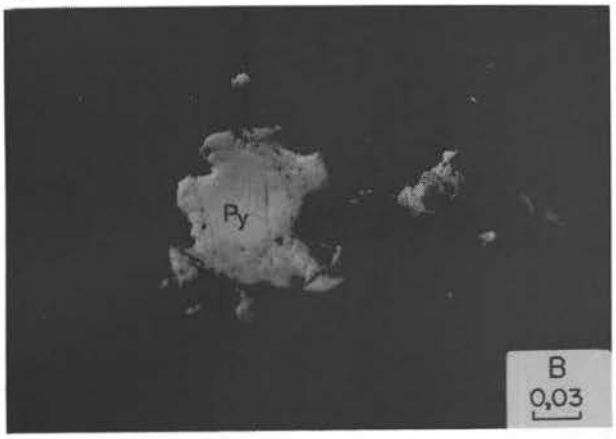

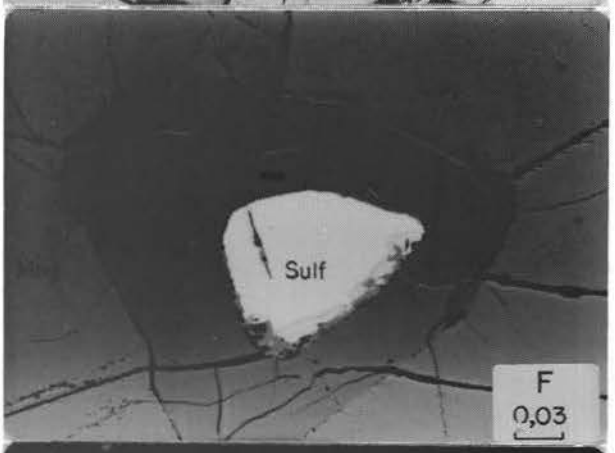

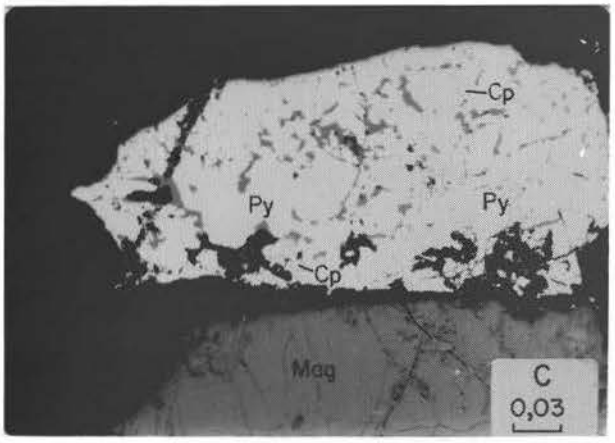

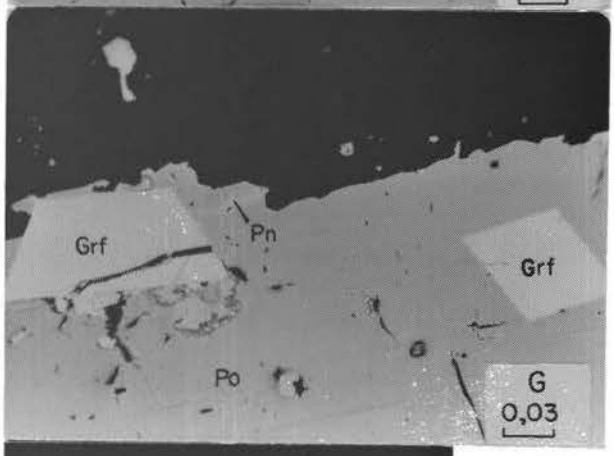

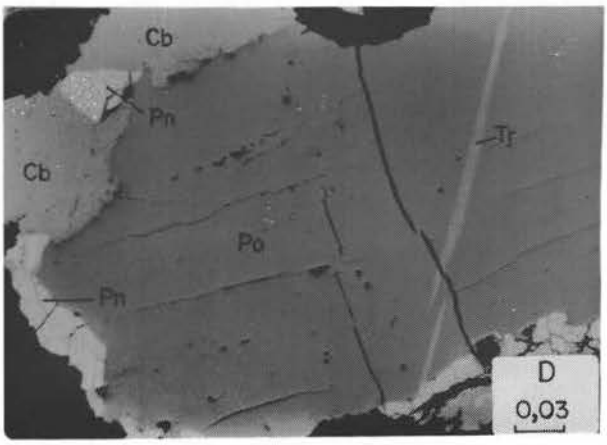

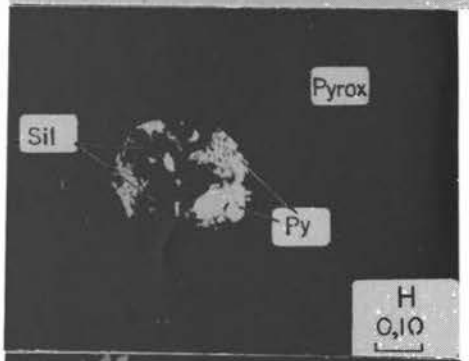

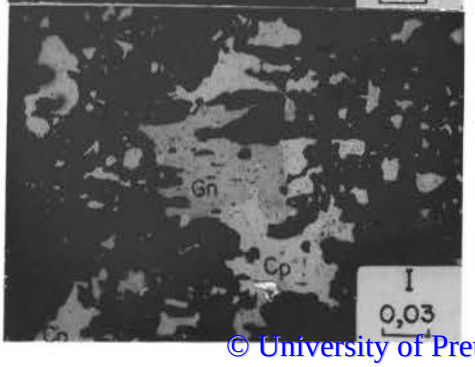

Fig. 98

Figure 98. Textural relationship of sulfides and other metallic phases in the upper critical zone, main zone, and upper zone samples. Py = pyrite; Cp = chalcopyrite; Vo = violarite; Cb = cubanite; Sulf = sulfide; Mag = magnetite; Grf = gersdorffite; Po = pyrrhotite; Tr = triolite; Sil = silicate; Pyrox = pyroxene; Gn = galena. Reflected light - oil immersion. Sample number in brackets.

(A) Py-cp-pn assemblage from the top of the critical zone. Most of the original pentlandite has been replaced by violarite. (78-145)

(B) Typical zoned pyrite crystal from the main zone. The lighter core is enriched in Ni relative to the rim. (78-102)

(C) Pyrite-chalcopyrite association from the main zone. The chalcopyrite is usually graphically intergrown with pyrite. (78-351)

(D) Coarse sulfide droplet in the main magnetitite layer on the farm Molendraai. (M5-39,4(2))

(E) Pentlandite and cubanite within the main magnetitite layer on the farm Molendraai. (M5-39,4 (1))

(F) A sulfide grain in ilmenite, which is in turn enclosed in magnetite. (M5-39,4)

(G) Euhedral gersdorffite crystals in hexagonal pyrrhotite in the foot-wall anorthosite of the main magnetitite layer. (M2-51,5)

(H) A silicate-pyrite sphere enclosed in cumulus clinopyroxene in a magnetite gabbronorite from the study area south of Potgietersrus. (5-124)

(I) A galena-chalcopyrite intergrowth in magnetite gabbronorite from the study area. (5-440)

proportions of py:cp is estimated to be 61:39. Figure 98C is a photomicrograph of a typical pyrite-chalcopyrite association. No pyrrhotite or pentlandite was found in the sulfide assemblage of the main zone, yet the scanning electron microscopic study did reveal that some of the pyrites are zoned and have cores with about 1 per cent Ni (Fig. 98B), whereas the same element was not detected in the rim. Some samples were found to contain up to 3,91 per cent Ni. In the chalcopyrite-rich portions of the main zone chalcopyrite occurs as small grains dispersed throughout the silicates. Most of these grains are not in mutual contact and it appears as if they were originally tiny chalcopyrite droplets suspended in the silicate magma.

It must be pointed out again that country-rock xenoliths have never been observed in the main zone, and it is therefore unlikely that the high fs_2 conditions can be ascribed to sedimentary derived sulfur.

8.5.1.4 Upper Zone

Two sulfide facies seem to be developed in the upper zone. In the study area the main sulfide assemblage is py-cp, whereas north of the town of Potgietersrus the sulfide assemblage is po-cp-pn-cb. The northerly facies will be described first as this seems to be the typical assemblage also found elsewhere in the upper zone of the Bushveld Complex (Von Gruenewaldt, 1976).

Concentrations of sulfides at the bottom of the main magnetitite layer average 3,20 weight per cent compared to 1,57 per cent for the layer as a whole and to 0,11 per cent for the underlying mottled anorthosite. The relative overall proportions of the various phases through these layers is presented in Table 22.

In the eastern portion of the Bushveld Complex most of the sulfides at the equivalent horizon occur at the top of the mottled anorthosite directly underlying the main magnetitite layer (Von Gruenewaldt, 1976). Concentrations are in the order of 2 to 3 per cent and the assemblage here contains pyrite which was never observed in this study. Figure 98D illustrates the textural relationship between pn, po, cb, and tr (troilite) in the main magnetitite layer north of Potgietersrus. Unlike the sem-

blage suggests final equilibrium at temperatures below 139°C (Craig and Kullerud, 1969). Considerable localized concentrations of pentlandite and cubanite are developed in places (Fig. 98E). Postcumulus enlargement of primary titaniferous magnetite grains has, on a few occasions, been noted to include sulfide grains (Fig. 98F). Trace amounts of gersdorffite occur within hexagonal pyrrhotite in the foot-wall anorthosite (Fig. 98G). Some galena is also associated with the gersdorffite.

In the study area south of Potgietersrus the sulfide assemblage py-cp dominates. Here the textural relations are more complex than those observed north of Potgietersrus, because of the presence of two generations of sulfides. The oldest generation of sulfides is the py-cp association which seems to have crystallized from an immiscible sulfide-silicate melt. Evidence for such a melt is suggested by the presence of a composite sulfide-silicate sphere enclosed in silicate (Fig. 98H). The silicate fraction of the sphere has a peculiar composition in that it is Ca and Fe rich, and always poor in TiO_2 (sample 4, Appendix 5). The only reasonable interpretation of this texture is that it represents an immiscible sulfide-silicate droplet trapped in an early crystallizing phase, and, unlike some other samples in the upper zone horizons, it has not been subjected to postcumulus modification. The high CaO and FeO content combined with the extremely low SiO_2 content would significantly increase the sulfur carrying capacity of this liquid, compared to the surrounding upper zone liquid. Preservation of this S-rich silicate liquid sphere would require it to be suspended in a liquid and to be subsequently enclosed by a cumulus phase, in this case clinopyroxene, before separation of the sulfide within the sphere. This texture presents strong evidence that some of the sulfides could have originated from an early immiscible sulfide-silicate melt. The inclusion of this sulfide sphere in cumulus clinopyroxene does suggest early separation of sulfur-rich liquids at temperatures $\geq$1064°C.

Galena was also encountered in the study area in the py-cp assemblage of the magnetite gabbronorites below the second magnetitite layer. The galena occurs associated with, and in some cases seems to have exsolved from, the chalcopyrite (Fig. 98I).

A younger generation of sulfide, evidently related to post-cumulus sulfidation is present in some of the upper zone horizons. Convincing evidence for this is seen in the replacement of (001) and (010) exsolution lamellae of augite in inverted pigeonite by pyrite (Fig. 99A). A similar sulfidation feature is seen where pyrite is replacing granular ilmenite (Fig. 99B and 99C) in titaniferous magnetite. The existence of exsolution textures in these natural titaniferous magnetites indicates the presence of a miscibility gap in the titaniferous magnetite solid solution series. Lindsley (1981) assumes the miscibility gap in the magnetite-ilmenite system to have a consolution temperature of 565 ±15°C, whereas Price (1981) states it to be 490°C on the basis of homogenization temperatures. Where it was possible to measure the equilibrium temperature conditions of these coexisting oxides in the upper zone it was found that the temperature conditions of these coexisting oxides ranged from 470 to 510°C. Seeing that these equilibriation temperatures agree well with data in the literature this suggests that the sulfidation process was active at very low temperatures and that sulfur-rich liquid was present in the postcumulus stages.

The formation of sulfides by reaction of S with Fe-rich silicates has been shown to occur experimentally by Kullerud and Yoder (1963) according to the reaction:

$$2Fe_2SiO_4 + S \rightleftharpoons FeS + Fe_3O_4 + 2SiO_2$$

Similarly, a reaction involving pyroxenes could be expressed as follows:

$$4FeSiO_3 + S \rightleftharpoons FeS + Fe_3O_4 + 4SiO_2$$

This study of the sulfide assemblages in the layered sequence leaves little doubt that successive sulfide liquids became more Fe, Cu, and S-rich with differentiation of the magma. Intrusions like the Muskox (Chamberlain, 1967) and the Skaergaard (Wager et al., 1957) display similar trends. Chamberlain (1967), for example, showed that the abundance of Cu and S in the sulfide fraction increased from 0 to 18 per cent and 33 to 37 per cent respectively during the course of 93 per cent fractionation of the Muskox Intrusion. An important difference between these intrusions is, however, that pyrite, rather than pyrrhotite is the major Fe sulfide in the upper half of the sequence south of Potgietersrus.

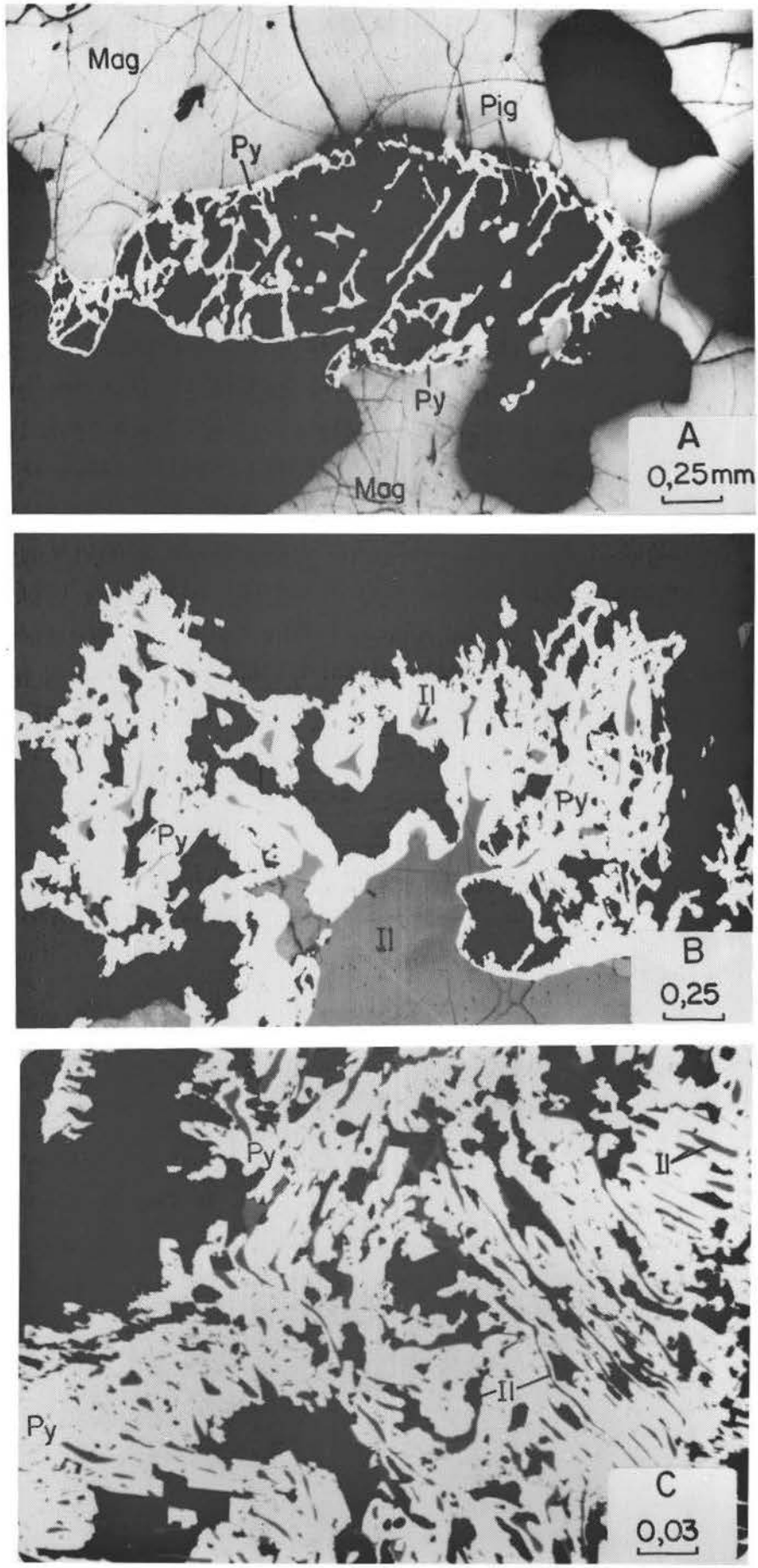

Fig. 99

Figure 99. Replacement textures ascribed to sulfidation in a upper zone sample. Mag = magnetite, Py = pyrite; Pig = inverted pigeonite, Il = ilmenite. Reflected light - oil immersion. Sample number in brackets.

(A) Pyrite replacing (001) and (010) exsolution lamellae of augite in inverted pigeonite. (5-124)

(B) Pyrite replacing coarse granular ilmenite in a magnetite gabbronorite. (5-124)

(C) Advanced sulfidation process where the pyrite contains numerous very thin ribbons of ilmenite. (5-124)

Since the layered sequence containing the sulfide assemblage py-cp is virtually devoid of sedimentary inclusions and the sulfur isotope data suggests a mantle source for the S, a magmatic control has to be called upon to account for the abundance of pyrite in the southern portion of the Potgietersrus limb, and its absence at the equivalent levels in the northern portion of the limb. This difference may be ascribed to a higher prevailing fs_2 in the magma of the southern portion. The only feasible explanation that can be put forward at stage is proximity of the study area to the feeder of the Potgietersrus magma chamber. The fs_2 could be expected to decrease gradually away from the feeder, due to a gradual loss of SO_2, and result in comparatively low fs_2 of the magma north of Potgietersrus. It is well known that high activity of sulfur exists around recent volcanoes and that this is related to the presence of SO_2 and H_2S. Similar situations could have prevailed in subterranean feeders of intrusions. The fs_2 around such a centre would not necessarily have to be high during the early stages, but it could build up considerably in more fractionated liquids. Craig and Kullerud (1969) and Kullerud et al. (1969) have shown that small variations in the metal: sulfur ratios have a considerable effect on the resulting stable sulfide assemblages in the Ni-Fe-S and Cu-Fe-S systems. For example, an increase in the amount of S by a few tenths of one weight per cent could result in a change of the normal assemblage pyrrhotite plus pentlandite to monoclinic pyrrhotite plus pyrite plus pentlandite.

The primary and secondary sulfide assemblages found in the Rustenburg Layered Suite south of Potgietersrus are summarized graphically in Figures 100 and 101. Although the proportions of the major sulfides in the various rock units vary considerably (Fig. 102) the sulfides in certain rock units occupy well defined fields and may, in certain instances, display well defined trends. It is furthermore apparent that some fields are continuous with others, e.g., the mineralized gabbronorites with the UG2-like chromitite and the associated foot-wall pyroxenite.

8.5.2 Nature of the High Temperature (≥700°C) Sulfide Liquid)

The estimated bulk composition of the initial sulfide liquid can be used to infer sulfide phase relations within the (Fe+Ni)-Cu-S

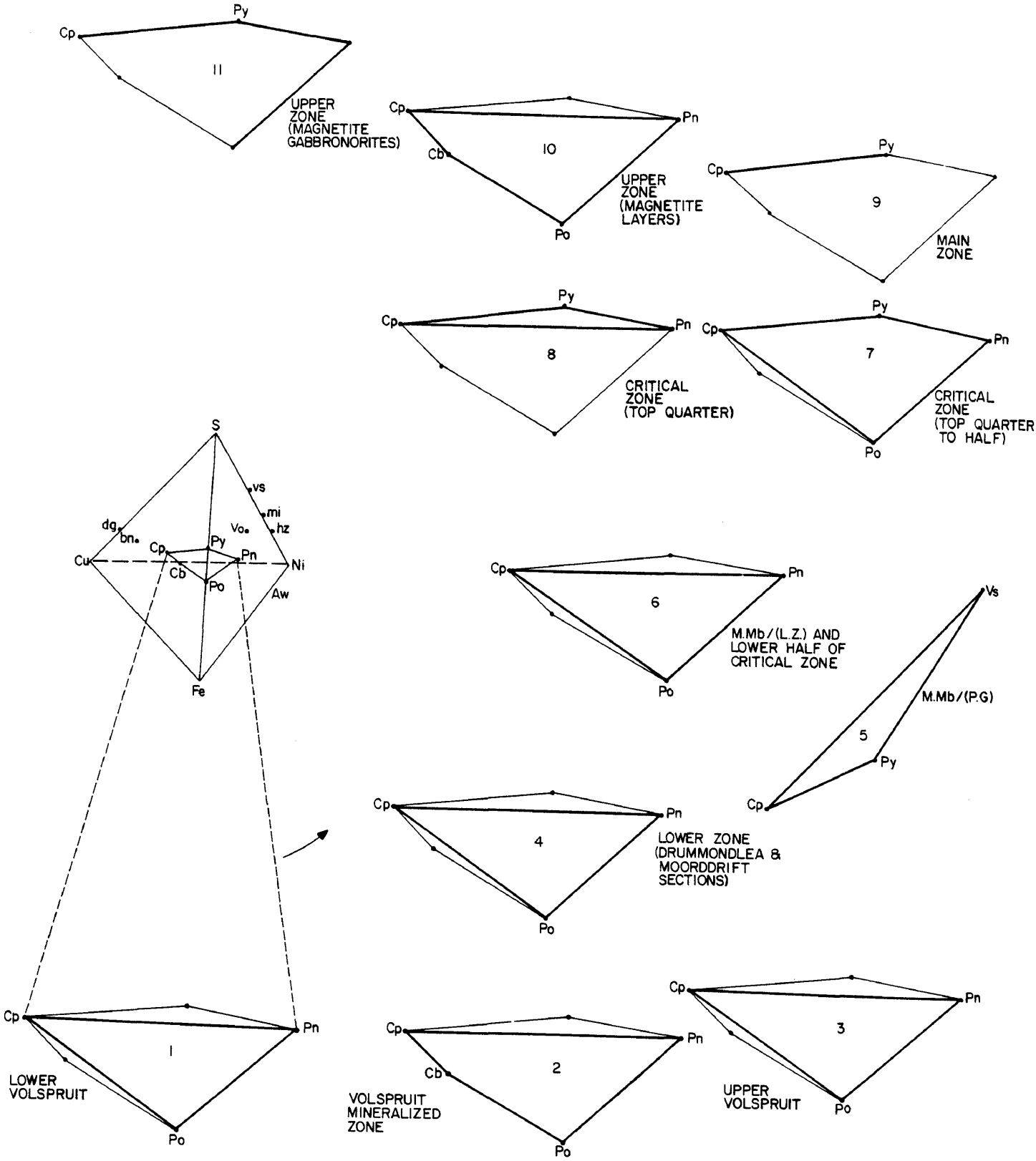

Fig. 100 Summary of sulfide assemblages in terms of phases in the Cu-Fe-Ni-S system observed in the Rustenburg Layered Suite of the Potgietersrus limb of the Bushveld Complex. The assemblages are numbered chronologically as they occur in the stratigraphic column.

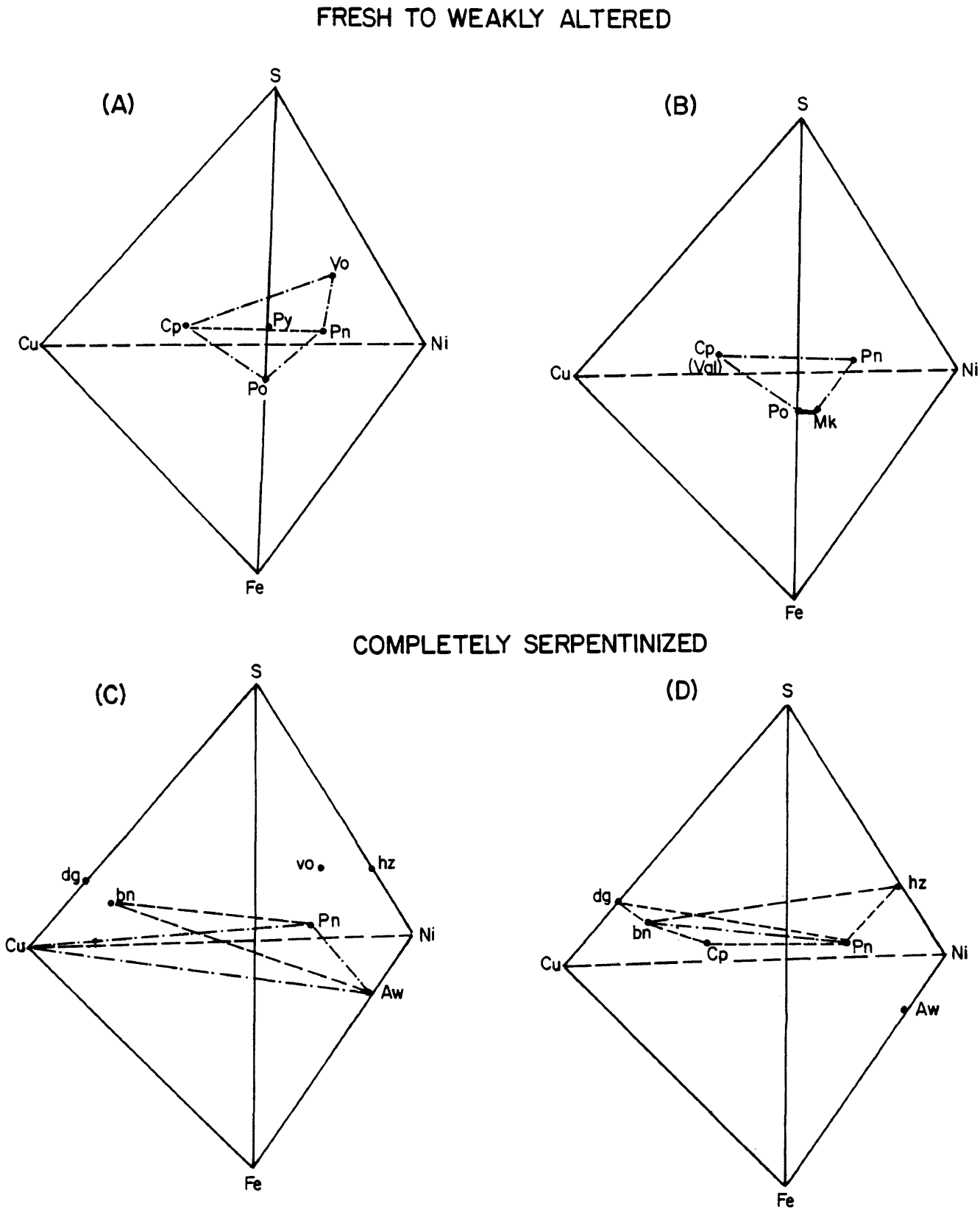

Fig. 101 Sulfide assemblages commonly encountered in weakly and highly altered rocks in the study area. (A) Pentlandite is usually the first sulfide affected and alters to violarite (B) Valleriite after chalcopyrite and mackinawite after either pentlandite or pyrrhotite can be present in weakly altered rocks that contain the primary sulfide assemblage pyrrhotite-chalcopyrite-pentlandite. (C) Completely serpentinized samples containing the assemblage pentlandite-bornite +/- native copper-awaruite or (D) pentlandite-bornite-digenite, or pentlandite-bornite-heazlewoodite. Chalcopyrite in the assemblage pentlandite-bornite appears to be a relict of primary chalcopyrite.

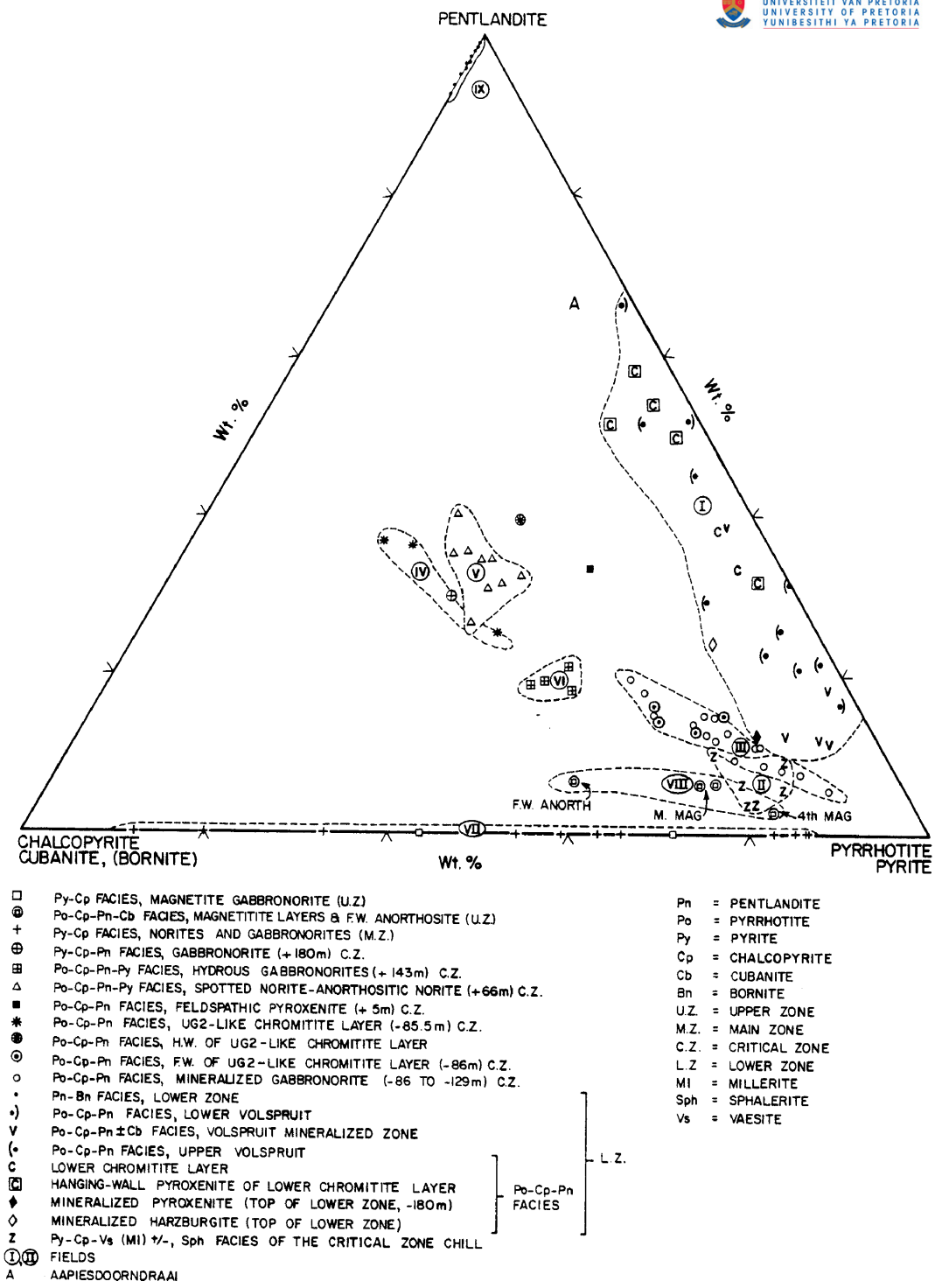

□ Py-Cp FACIES, MAGNETITE GABBRONORITE (U.Z)
⊡ Po-Cp-Pn-Cb FACIES, MAGNETITITE LAYERS & F.W. ANORTHOSITE (U.Z)
+ Py-Cp FACIES, NORITES AND GABBRONORITES (M.Z.)
⊕ Py-Cp-Pn FACIES, GABBRONORITE (+180m) C.Z.
⊞ Po-Cp-Pn-Py FACIES, HYDROUS GABBRONORITES (+143m) C.Z.
△ Po-Cp-Pn-Py FACIES, SPOTTED NORITE-ANORTHOSITIC NORITE (+66m) C.Z.
■ Po-Cp-Pn FACIES, FELDSPATHIC PYROXENITE (+5m) C.Z.
✱ Po-Cp-Pn FACIES, UG2-LIKE CHROMITITE LAYER (-85.5m) C.Z.
◉ Po-Cp-Pn FACIES, H.W. OF UG2-LIKE CHROMITITE LAYER
⊙ Po-Cp-Pn FACIES, F.W. OF UG2-LIKE CHROMITITE LAYER (-86m) C.Z.
○ Po-Cp-Pn FACIES, MINERALIZED GABBRONORITE (-86 TO -129m) C.Z.
• Pn-Bn FACIES, LOWER ZONE
•) Po-Cp-Pn FACIES, LOWER VOLSPRUIT
V Po-Cp-Pn ± Cb FACIES, VOLSPRUIT MINERALIZED ZONE
(• Po-Cp-Pn FACIES, UPPER VOLSPRUIT
C LOWER CHROMITITE LAYER
⊡ HANGING-WALL PYROXENITE OF LOWER CHROMITITE LAYER
♦ MINERALIZED PYROXENITE (TOP OF LOWER ZONE, -180m)
◇ MINERALIZED HARZBURGITE (TOP OF LOWER ZONE)
Z Py-Cp-Vs (MI) +/-, Sph FACIES OF THE CRITICAL ZONE CHILL
Ⓘ Ⓘ FIELDS
A AAPIESDOORNDRAAI

Po-Cp-Pn FACIES
L.Z.

Pn = PENTLANDITE
Po = PYRRHOTITE
Py = PYRITE
Cp = CHALCOPYRITE
Cb = CUBANITE
Bn = BORNITE
U.Z. = UPPER ZONE
M.Z. = MAIN ZONE
C.Z. = CRITICAL ZONE
L.Z = LOWER ZONE
MI = MILLERITE
Sph = SPHALERITE
Vs = VAESITE

Fig. 102 Normative variation of sulfide assemblages within the layered sequence. Note the well established and continuous trends for the critical zone horizons (Field II, II, IV, V, and VI) and the pentlandite enriched nature of some of the later differentiates within this zone (Field V). Also note the atypical secondary pentlandite-bornite facies (Field IX) and its relationship to the other primary sulfide fields. The diagram also clearly illustrates that the sulfides of the hanging-wall pyroxenite to the lower chromitite layer and the Aapiesdoorndraai body are by far the most pentlandite-rich samples encountered in this study. Lower zone sulfides occupy a distinct field (I) along the po-pn leg of the variation diagram whereas the main zone and upper zone sulfides of the study area plot along the cp-py leg (Field VII). In comparison the sulfides from the upper zone at Molendraai are enriched in pentlandite (Field VIII).

system of Kullerud et al., 1969 (Fig. 103).

The bulk composition of the lower zone sulfide liquids, in terms of (Fe+Ni)-Cu-S, plot within the pyrrhotite solid solution (po_{ss}) field at 1000°C or just outside it on the S-poor side. These latter samples 1, 2, 5, 6, 7 and 10 are all Ni-rich and would all plot in the Mss. of the Fe-Ni-S system. The phase relations in Figure 103A illustrate that most of the lower zone sulfides were originally po_{ss} containing between 0 to 4,7 per cent Cu. The sample designated 19 is the mineralized spotted anorthositic norite at the +66 m level in the critical zone. At 1000°C this sample would consist of Cu-rich liuqid and a po_{ss} carrying about 5,2 per cent Cu, which would exsolve from the pyrrhotite at lower temperatures. Most of the remaining critical zone samples plot in the same two phase volume and would consist of po_{ss} and a Cu-rich liquid at 1000°C. The experimental work of Cabri (1973) suggests that these Cu-rich sulfide liquids crystallize to a Cu-rich solid solution known as the intermediate solid solution (iss.).

The projected compositions of the py-cp bearing assemblages of the critical, main and upper zones at 1000, 900, and 700°C are shown in Figure 103B, C, and D. It can be seen from Figure 103C that, at 900°C, a large proportion of the py-cp assemblages plot within the po_{ss} + S liquid + sulfide liquid. A po_{ss} + a Cu-rich liquid would be the stable assemblage at temperatures greater than 900°C. The Cu-rich sulfide liquid becomes, upon cooling, part of an extensive solid solution (iss) field. An excess of sulfur could be responsible for the late stage sulfurization observed in many of the upper zone rocks.

8.5.3 Sulfide Chemistry

A limited number of sulfides from the study area have been analysed as part of a reconnaissance investigation of the sulfide chemistry. With the exception of the two samples (assemblage #1 and #8, Table 23) analysed by E.A. Viljoen of the Council for Mineral Technology, all samples were analysed by the author with the aid of an energy dispersive system attached to a Joel scanning electron microscope. Natural pyrrhotite, pendlandite, chalcopyrite, and heazlewoodite were used as standards. Good reproducibility of the data was obtained for the heavy elements Ni, Fe, Cu, and Co, yet greater variation was noted for S. The analyses should

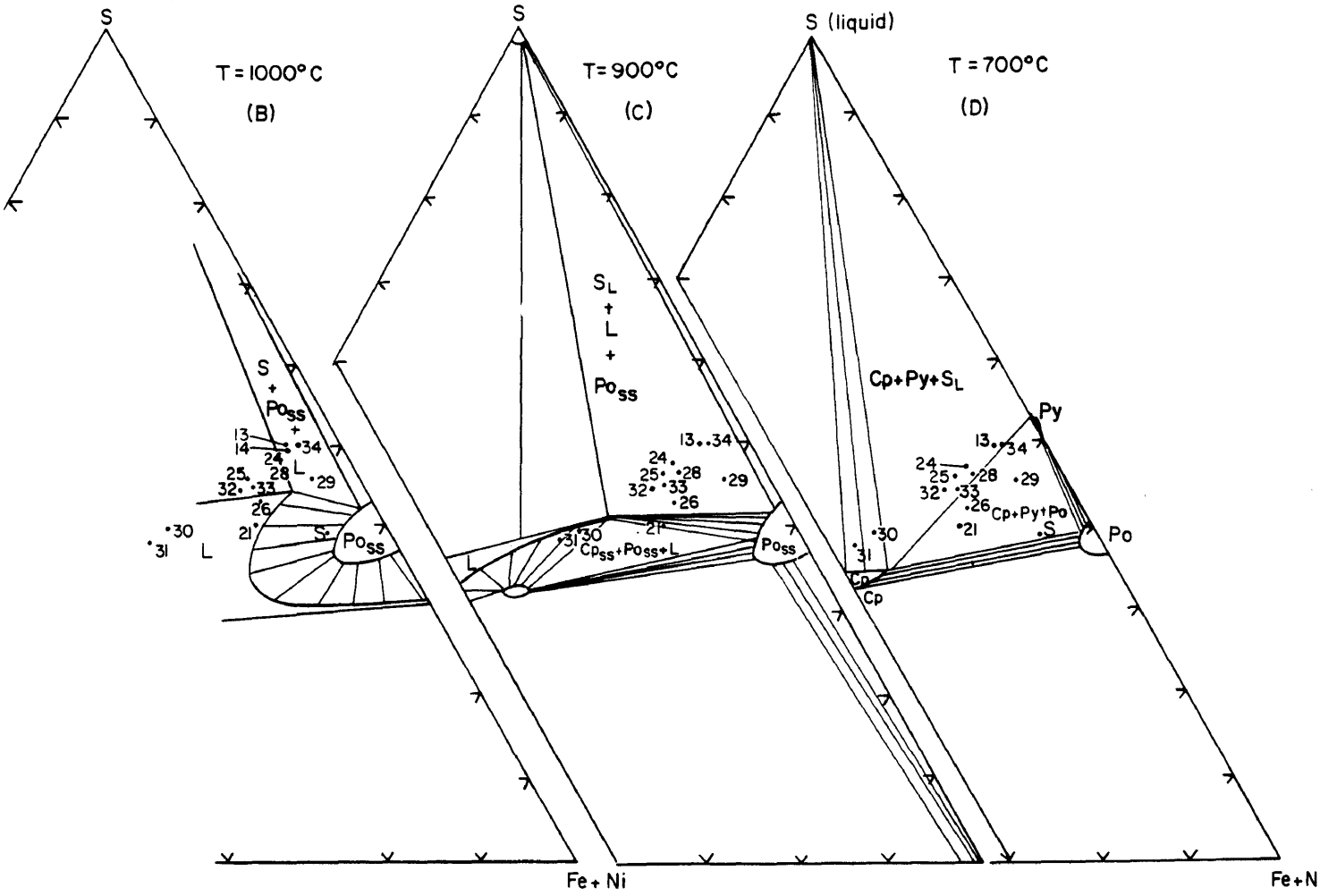

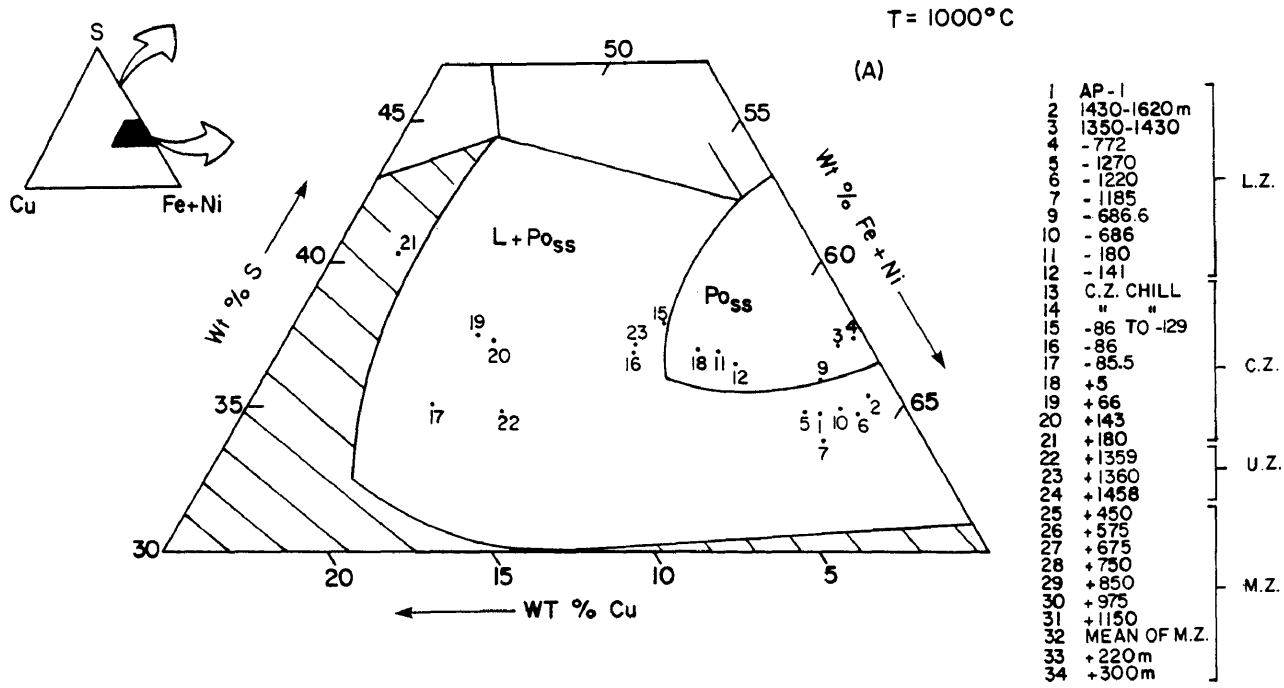

1	AP-1	
2	1430-1620m	
3	1350-1430	
4	-772	
5	-1270	
6	-1220	L.Z.
7	-1185	
9	-686.6	
10	-686	
11	-180	
12	-141	
13	C.Z. CHILL	
14	" "	
15	-86 TO -129	
16	-86	
17	-85.5	C.Z.
18	+5	
19	+66	
20	+143	
21	+180	
22	+1359	U.Z.
23	+1360	
24	+1458	
25	+450	
26	+575	
27	+675	
28	+750	
29	+850	M.Z.
30	+975	
31	+1150	
32	MEAN OF M.Z.	
33	+220m	
34	+300m	

Fig. 103 Portion of the (Fe-Ni)-Cu-S system showing the bulk composition of initial sulfide liquids and the position of the primary phase volumes at (A) 1000°C (B) 1000°C (C) 900°C, and (D) 700°C. Only the sulfur-rich samples have been plotted on the latter three diagrams to illustrate the generation of the py-cp assemblages as observed in the critical, main and upper zones of the study area.

therefore be regarded as being of a semi-quantitative nature with respect to S.

Pentlandite from the Volspruit mineralized zone (Table 23) has a Ni content of 29,92 per cent, which seems low in terms of the expected Ni content for pentlandites low in the layered sequence. This pentlandite coexists with hexagonal pyrrhotite and troilite, as well as cubanite. A survey of pentlandite compositions by Harris and Nickel (1972) reveals that pentlandites in association with troilite have low Ni contents. They have, for example, recorded Ni values of 15,2; 26,5; and 28,1 per cent for the pentlandite associated with troilite in the Muskox Intrusion. Samples from the Mooihoek pipe were found to contain as little as 23,7 per cent Ni. The Ni-poor nature of the pentlandite is also reflected in the low Ni content in 100 per cent sulfides (Table 24). This low Ni content in the pentlandite, combined with the low proportion of pentlandite, probably accounts for the Ni-poor nature of this mineralized horizon.

Most of the remaining pentlandite in the layered sequence was found to contain between 32,00 to 34,14 weight per cent Ni, which is in good accord with the values given by Harris and Nickel for the other pn-po bearing assemblages. The one sample to fall outside this range has a Ni content of 35,5 per cent is from the spotted norite at the +66 m level (No. 9, Table 23). This pentlandite forms part of the assemblage po-cp-pn-py. Such assemblages should contain, according to Harris and Nickel (1972), Ni-enriched pentlandites compared to those of other primary associations.

The pentlandite with the lowest measured Ni content is a cobalt-pentlandite (19,2 per cent Ni) associated with sparse grains of heazlewoodite in a harzburgite from the Drummondlea Harzburgite-Chromitite. Trace amounts of cobalt-poor pentlandites associated with heazlewoodite in the serpentinized Volspruit dunite are inferred to be Ni-rich on the basis of data provided by Harris and Nickel (1972) who found that pentlandite of this association usually contains between 41,2 and 44,2 per cent Ni.

A noteworthy observation that arose from this study is that the cobalt content of normal pentlandite appears to increase with fractionation. The highest cobalt content in pentlandite

observed in the samples from the main magnetitite layer, where a value of 3,37 per cent was recorded. Wager and Brown (1968) and Wager et al. (1957) showed that cobalt tends to build up in the liquid with fractionation. This is in agreement with the data of MacLean and Schimazaki (1976) who showed that $D_{Co}^{sulf-liq} = 7$. This element is therefore not as effectively scavanged by the sulfide liquid as Ni and Cu. The Co enters pentlandite by substituting for Fe in the structure (Riley, 1977).

Another feature seemingly related to fractionation warrants comment. Cubanite in the Volspruit samples is strongly anisotropic, bireflectant, and has a much lighter colour and higher reflectivity than that encountered in the upper zone. The upper zone samples have a darker, red to pinkish tint, and commonly occur in coarse clusters, which appear to be isotropic. It would seem that the upper zone material is predominantly cubic cubanite whereas that encountered in the Volspurit section is orthorhombic. Also, the upper zone cubanite contains more Fe and Cu than that from the Volspruit subzone (Table 23).

Heazlewoodite was only encountered on two occasions in this study and a superior quality analyses is given in Table 23 where it is seen to consist almost entirely of Ni and S. The metal to sulfur ratio for this sample is 2,989:2 which is very close to a theoretical value of 3:2. The small amount of Co that was originally present in the pentlandite is now in the form of minute lath like inclusions of linnaeite in the heazlewoodite.

8.6 Compositional Relationship between the Immiscible Sulfide Liquid and the Host Magma

Information on the Ni, Cu, Fe, and S content of the sulfide melt is useful in obtaining an indication of the amount of Ni, Fe, and Cu in the parental melt, the fs_2 of the magma and the ratio of sulfide liquid in equilibrium with silicate magma (R). For this reason the bulk composition of 100 per cent sulfide was calculated for a number of stratigraphic horizons (Table 24). Data for samples from the +1360 and +1359 m levels are based on values obtained from the po-cp-pn-cb facies north of Potgietersrus, whereas the composition of the remaining upper zone sample was calculated from the py-cp facies in the study area. Low concentrations of

TABLE 24 Ni, Cu, Fe, S, and MOLE FRACTION FeS IN 100% SULFIDE FROM THE RUSTENBURG LAYERED SUITE SOUTH OF POTGIETERSRUS

	STRAT. LEVEL	DESCRIPTION	Ni (Ni+Cu)	PERCENT ELEMENT IN 100% SULFIDES Ni	Cu	Fe	S	TOTAL METAL	MOLE Fraction FeS
U.Z.	+1458	Magnetite gabbronorite	0,09	0,99	9,80	41,56	47,64	52,35	0,824
	+1360	Main magnetite layer	0,25	2,34	6,88	53,55	37,23	62,77	0,988
	+1359	Foot-wall anorthosite to the main magnetitite	0,15	2,25	12,16	50,78	34,79	65,19	?
	+1150	Gabbronorite		<0,99	28,04	33,05	37,91	62,08	0,977
	+ 950	Gabbronorite		<0,99	22,91	35,40	40,60	59,30	0,933
	+ 850	Gabbronorite		<0,99	5,14	43,78	46,10	49,91	0,785
	+ 750	Gabbronorite		<0,99	9,95	41,49	47,56	52,43	0,825
M.Z.	+ 675	Gabbronorite		<0,99	5,14	43,78	46,10	49,91	0,785
	+ 575	Gabbronorite		<0,99	15,76	38,78	44,46	56,52	0,889
	+ 450	Gabbronorite		<0,99	11,66	40,70	46,65	53,35	0,839
	+ 300	Gabbronorite		<0,99	5,14	43,78	50,07	49,91	0,785
	+ 220	Gabbronorite		<0,99	12,69	40,21	46,10	53,89	0,848
C.Z.	+ 180	Gabbronorite	0,47	11,89	13,25	34,63	40,21	59,77	0,941
	+ 143	Pegmatitic gabbronorite	0,39	7,18	11,21	44,24	37,35	62,63	0,986
	+ 66	Spotted norite and anorthositic norite	0,50	12,04	11,69	38,77	37,47	62,40	0,984
	+ 5	Feldspathic pyroxenite	0,45	4,27	5,18	53,53	37,01	62,98	0,991
	-85.5	UG2-like chromitite layer	0,45	11,84	14,26	38,74	35,14	64,84	*1,020
	- 86	Foot-wall feldspathic pyroxenite to the UG2-like chromititie	0,41	5,01	7,03	51,22	36,73	63,26	0,996
	- 87 to - 129	Mean of the mineralized Gabbronorite interval studied	0,43	4,25	5,74	52,16	37,84	62,15	0.978
	M.Mb / P.G.	Mean of the fine-to medium-grained gabbronorites (Chill)	0,45	5,22	6,29	38,36	50,18	49,87	0,785
L.Z.	- 141	Harzburgite	0,65	8,31	4,33	50,88	36,47	63,52	1,00
	- 180	Pyroxenite	0,48	4,31	4,58	54,04	37,06	62,93	0,990
	- 686	Hanging-wall pyroxenite to the lower chromitite	0,90	17,41	1,77	45,88	34,92	65,06	*1,02
	-686.6	Lower chromitite layer	0,88	12,97	1,70	49,33	35,99	64,00	1,00
		Mean of the upper Volspruit section	0,80	8,12	1,94	53,19	36,72	63,25	0,995
	≈-1185	Top 1/3 of the Volspruit mineralized zone	0,89	12,09	1,35	52,47	34,08	65,91	1,03
	≈-1220	Bottom 2/3 of the Volspruit mineralized zone	0,57	3,85	2,87	58,54	34,72	65,26	1,02
	-1350-1430	Top 1/3 of the Lower Volspruit subzone	0,89	5,73	0,71	56,36	37,19	62,80	0,998
	-1430-1620	Lower 2/3 of the Lower Volspruit subzone	0,97	19,85	0,44	44,38	35,32	64,67	*1,01

*** $Log_{10} f_{S_2}$ = +4,84 @ 1064°C for sample @ +1458 m level
= -3,85 @ 1080°C for sample @ +1360 m level
= -2,14 @ 1160°C for sample @ +66 m level
= -3,35 @ 1161°C for sample @ +5 m level
= -5,38 @ 1166°C for sample @ -85,5 m level
= -4,15 @ 1166°C for sample @ -86,0 m level
= -1,84 @ 1137°C for sample @ -87,60-129 m level
= +5,73 @ 1050°C for sample @ M.Mb./P.G.
= -4,85 @ 1242°C for sample @ -686,6 m level
= -5,14 @ 1199°C for sample @ -1220 m level

*** after the method of Toulmin and Barton (1964)
* if >1,00 it is considered ≈1,00 for calculation purposes

sulfides in the main zone make an accurate estimate of the Ni, Fe, Cu, and S content difficult, although the proportions given in Table 24 were calculated from analyses of representative samples, 3 to 6 kg in mass.

Naldrett (1979) suggested that the Ni/(Ni+Fe) ratio of the sulfides is a fairly effective measure of the ratio of silicate magma in equilibrium with sulfide magma (R) when comparing magmas of a similar composition. This ratio suggests that the sulfides in spotted anorthositic norite (+66 m level) and the gabbronorite (+180 m level) in the top portion of the critical zone equilibriated with a considerably larger volume of silicate melt than the sulfides in the mineralized gabbronorite in the lower portion of the critical zone. The latter has a Ni/(Ni+Fe) ratio of 0,073 which is about 1/3 that found in the top portion of the critical zone. High Ni/(Ni+Fe) values in the UG2-like chromitite layer (0,234) and in the lower chromitite (0,208) also suggest large R-values.

Another interesting feature is that the bottom 2/3 of the Volspruit mineralized zone has a Ni/(Ni+Fe) value of 0,061 whereas the top 1/3 has a value of 0,187. The higher values associated with the top 1/3 and the correspondingly higher Pd/Cu ratios for this interval suggest that these sulfides equilibriated with a larger volume of silicate magma than did those from the lower portion of the mineralized zone.

Maclean and Shimazaki (1976) derived the expression:

$K_{metal} \cdot$ wt.% metal in magma = % metal in sulfide liquid,

which is an expression of the relationship between the metal content of a sulfide liquid and that of the parental magma. From this an estimate of the Ni and Cu content of the magma can be made, assuming values of $D_{Cu}^{sulf\text{-}liq} \approx 250$ and $D_{Ni}^{sulf\text{-}liq} \approx 275$ for the gabbroic rocks of the critical, main and upper zone (Naldrett, 1979). Using these D values the Ni and Cu content in the magma that gave rise to the main magnetitite layer was calculated as being 85 and 275 ppm respectively. The parent magma to the spotted anorthositic norite at the +66 m level contained 437 ppm Ni and 467 ppm Cu whereas the magma from which the UG2-like chromitite layer crystallized could have contained 430 ppm Ni and 570 ppm Cu. Similar calculations for the mineralized gabbronorite interval

from the -87 to -129 m level suggests values of 155 ppm Ni and 252 ppm Cu. The value of $D_{Ni}^{sulf\text{-}liq}$ for the more magnesian liquids from which the lower zone lithologies crystallized is unfortunately not known, although it is probably lower than the value used above for the higher levels of the intrusion. The $D_{Cu}^{sulf\text{-}liq}$ value, however, does not seem to change significantly with magma composition (Naldrett, 1979). By using the same value for Cu it was calculated that the magma that gave rise to the lower chromitite contained as little as 54 ppm Cu, but that the Cu content of the magma had increased to 173 ppm during crystallization of the mineralized horizons at the top of the lower zone.

The percentages of Ni, Cu, Fe, and S in 100 per cent sulfides can also be used to infer fs_2 conditions within the host magma. If the mole fraction FeS in the monosulfide and the temperature of sulfide crystallization are known, the $\log_{10} fs_2$ conditions at 1 bar can be calculated using the equation of Toulmin and Barton (1964):

$$\log_{10} fs_2 = (70{,}03 - 85{,}83N)(1000/T-1) + 39{,}30\sqrt{1-0{,}9981N} - 11{,}91 \quad (1)$$

where N = the mole fraction FeS in monosulfide (M_{SS}).

T = absolute temperature.

Toulmin and Barton (1964) were able to relate the fs_2 to the composition of the pyrrhotite over a range of temperatures. In the present study the bulk composition of the sulfides was treated as if it were a high temperature pyrrhotite solid solution from which the mole fraction Fe(+Ni+Cu)S was calculated. The validity of this method is based on the fact that a similar approach was employed by Heming and Carmichael (1973) for quenched pyrrhotite ($\approx M_{SS}$) with noteable amounts of Cu and Ni from volcanic material. Toulmin and Burton (1964) calculated that a pressure increase from 1 bar to 5kb would increase the $\log_{10} fs_2$ by about two orders of magnitude. Scott (1974), however, re-evaluated this relationship and found that the correction should be about one order of magnitude. Information on the Pt-PtS equilibria (Barin and Knacke, 1973) also indicates that a pressure change from 1 bar to 5kb increases the fs_2 values by about one order of magnitude. A pressure correction should therefore be applied to the calculated 1 bar values in order to reflect more closely the actual conditions at

(1) In order to facilitate comparisons, on a relative scale, of fs_2 within the intrusion it was found necessary in certain cases to extrapolate the above equation beyond the liquidus temperature for FeS.

the time of crystallization. The corrections increase the fs_2 by about one order of magnitude for critical and lower zone samples which are inferred to have crystallized at pressures between 4448 to 4540 bars and 4540 to 5000 bars respectively.

It was calculated that a $\log_{10}fs_2$ value of about -5,14 (-4,14) prevailed in the magma at 1199°C during crystallization of the lower portion of the Volspruit mineralized zone (Fig. 104). The given values refer to conditions at 1 bar and those in brackets to conditions at approximately 5kb. Similar, yet slightly higher values of -4,85 (-3,85) were calculated for the magma during crystallization of the lower chromitite layer and its hanging-wall pyroxenite. At 1166°C the UG2-like chromitite layer and its foot-wall pyroxenite would have crystallized under fs_2 conditions of -5,38 (-4,48) and -4,15 (-3,25) atm respectively (Table 24).

The mineralized feldspathic pyroxenite at the +5 m level was calculated to have crystallized at -1161°C at fs_2 conditions of -3,35 (-2,45) atm.

The S-poor assemblage cubanite, troilite, and hexagonal pyrrhotite in the main magnetitite layer indicates that low fs_2 conditions also prevailed in the magma at this level. The calculations suggest that the $\log_{10}fs_2$ at 1080°C was -3,45 (-2,65) atm (Fig. 104).

Higher fs_2 conditions prevailed during crystallization of the upper half of the critical zone, particularily where pyrite forms part of the stable sulfide assemblages. This corresponds to the first occurrence of spotted norites and anorthositic norites at the +66 m level. The near identical mole fraction FeS in the sulfides from the hybrid pegmatitic gabbronorite at the +143 m level implies a similar fs_2 value in the magma at the same temperature.

Apart from the M.Mb./P.G., the mineralized gabbronorite from the -87 to -129 m level yielded the highest calculated fs_2 value for the critical zone. Here, $\log_{10}fs_2$ conditions at 1137°C were calculated to be -1,84 (-0,94) atm.

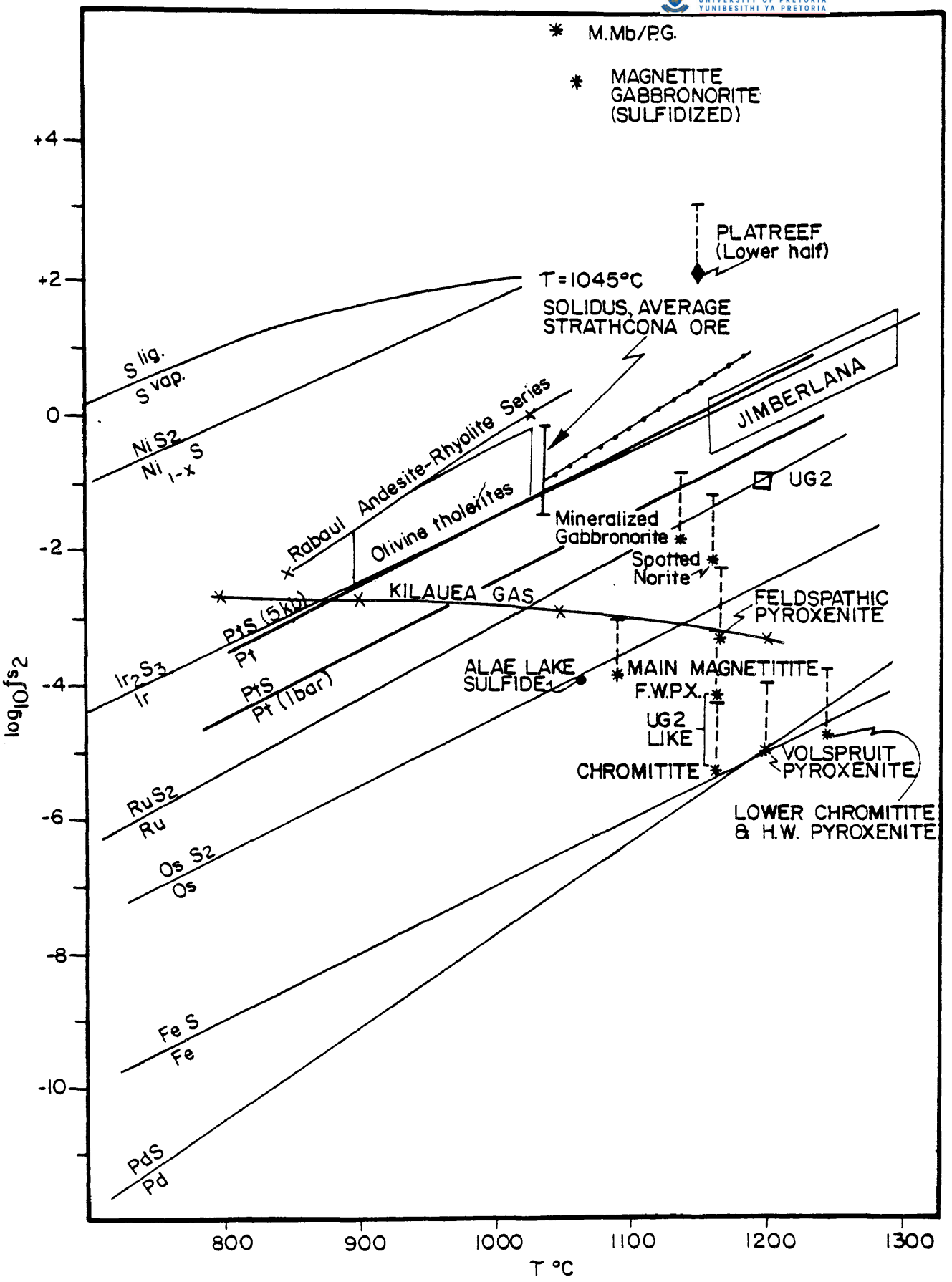

Fig. 104 Calculated T-fs_2 conditions during separation of sulfide liquids from the Potgietersrus magma. The lower fs_2 values (*) represent conditions at one bar whereas the higher values represent conditions under the inferred operative pressure at time of crystallization. Also shown are T-fs_2 conditions for the Rabauel caldera (Heming and Carmichael, 1973), Kilauea gas field (Nordlie, 1971), Alae lake sulfide (Carmichael et al., 1974), Jimberlana Intrusion (Keays and Campbell, 1981), average Strathcona ore (Keays and Crocket, 1970), UG2 chromitite (McLaren and De Villiers, 1982) and for the Platreef (Gain and Mostert, 1981). The Fe-FeS and $Ni_{1-x}S$-NiS_2 curves are taken from Barton and Skinner (1967) whereas the Ir, Ru, Os and Pd curves are from Keays and Crocket (1970).

The sulfur fugacities of the magma that gave rise to the M.Mb./P.G. of the critical zone was, as previously mentioned, inferred to have been very high, a conclusion based on the the assemblage pyrite-chalcopyrite ± vaesite. The 1 bar stability field of vaesite (NiS_2) shown in Figure 104 also confirms this suggestion. For comparison, data for the lower half of the Platreef is also included in Figure 104. The modal proportions of the sulfide assemblages for calculation of the mole fraction FeS in the Platreef sulfides, as well as compositional data of the pyroxenes for temperature calculations were taken from Gain and Mostert (1981). A temperature of 1150°C and a fs_2 of +2,12 (+3,00) were calculated in this way.

fs_2 data on natural magmas is very limited (Fig. 104). Available data does, however, provide a comparison between calculated fs_2 conditions of the Potgietersrus liquids and those from other bodies.

The stabilities of the metals Pd, Fe, Os, Ru, Ir, and Pt and their respective sulfides as a function of temperature and fs_2 is also shown in Figure 104. This information can be used to bracket the fs_2 conditions in the crystalizing magma. The recorded PGM in the mineralized layers south of Potgietersrus are unfortunately of no use to bracket the prevailing fs_2 conditions. However, mineralogical investigations of the Platreef sulfides (Lee, 1981 and Kinloch, 1982) showed that the Pt and Pd sulfides cooperite, braggite, and vysotskite predominate. This implies that the Platreef sulfides crystallized at fs_2 and T conditions within the stability field of PtS (Fig. 104). From the inferred T conditions of crystallization of the Platreef and the 5kb Pt-PtS equilibrium curve (Fig. 104), the minimum $\log_{10} fs_2$ value of the Platreef magma could have been about 0 atm. From this diagram it is also evident that the fs_2 conditions during crystallization of most of the mineralized layers in the study area appear to have been too low to allow Pt-sulfide or even Ru-sulfide to be stable. It is of interest to note that Kinloch (1982) found the Pt and Pd alloys to increase and the Pt and Pd sulfides to decrease towards the south in the Platreef which points to a decrease in the fs_2 in a southerly direction. The low fs_2 values in the lower and critical zone horizons in the study area seem to substantiate this

trend. This condition, however, does not hold for later differentials of the main and upper zones in the study area.

MacLaren and De Villiers (1982) pointed out that the PGM in the UG2 layer in the eastern and western portions of the Bushveld Complex are mainly laurite, cooperite and braggite. This would suggest that the lower fs_2 limit is defined by the Ru-RuS_2 equilibrium curve (Fig. 104), although they present evidence that at most localities prevailing fs_2 conditions were closer to the Pt-PtS equilibria. If pressure is also taken into consideration, the UG2 chromitite layer seems to have crystallized under higher fs_2 conditions (Fig. 104) than the UG2-like chromitite in the study area. The presence of pyrite in the UG2 chromitite layer (Maclaren and De Villiers, 1982) and its absence in the equivalent layer in the study area leads to the same conclusion.

The method employed here to infer fs_2 conditions (Fig. 104) can only be regarded as a relative measure of variation of the fs_2 conditions. Although the main errors in these fs_2 calculations are introduced through estimation of the bulk composition of the sulfide liquid and in the pressure corrections, this is a first attempt at calculating magmatic fs_2 conditions where temperature of crystallization is fairly well known. The presented values are therefore considered to be more accurate than the estimated fs_2 based solely on the PGE buffer curves.

8.7 Sulfur Isotope Investigation

Knowledge of the source of the sulfur necessary to produce Ni, Cu, and PGE mineralization in mafic to ultramafic intrusions is of considerable economic and academic importance. For this reason sulfide mineralization from twelve different stratigraphic horizons were submitted for sulfur isotope determination. An interpretation of the S-isotope data requires a sound knowledge of the petrology and geochemistry of the mineralized layers, as was stressed by Schneider (1970), in order to avoid eroneous interpretations. Consequently, such an approach was adopted for this investigation. The principal objective of this S-isotope investigation was to obtain a better understanding of the origin and conditions of formation of the mineralization within the Rustenburg Layered Suite in the Potgietersrus area.

8.7.1 Collection and Preparation of Material

Fresh sulfide bearing material was obtained form twelve stratigraphic horizons within the layered sequence. All of the samples were examined under reflected light and were found to be devoid of secondary alteration. Sulfides were concentrated by heavy liquid separation and hand picking to between 80 to 100 per cent purity. Two samples from each of the horizons were submitted for S-isotope analyses. For three of these 22 samples insufficient sulfide was available for analysis. The sulfur isotopic composition of the sulfide concentrates is expressed in terms of $\delta^{34}S$, which is defined as:

$$\delta^{34}S = \frac{(\frac{^{34}S}{^{32}S})_{\text{sample}} - (\frac{^{34}S}{^{32}S})_{\text{standard}}}{(\frac{^{34}S}{^{32}S})_{\text{standard}}} \times 10^3 \text{ 0/00}$$

where the standard is sulfur from the troilite of the Canyon Diablo meteorite. Analyses were determined by Dr. C. Rees, McMaster Isotopic Nuclear and Geochemical Study Group, Department of Physics, McMaster University, Hamilton, Ontario, Canada. The instrumentation, preparation and sample gas used are outlined in Thode and Rees (1971) and Rees (1978). Sulfur isotope data of sample pairs from the layered sequence showed the mean spread of $\delta^{34}S$ values to be 0,43 per mil. This suggests that the variation caused by separation of sulfides that have undergone isotopic fractionation is limited.

8.7.2 Previous Work

As part of his classic study on the sulfides in the layered sequence of the Bushveld Complex, Liebenberg (1968) had a variety of mineralized horizons both within the mafic layered sequence of the Bushveld Complex and in the Transvaal sediments analysed for sulfur isotopes. A histogram of the various $\delta^{34}S$ per mil values are shown in Figure 105A. Liebenberg found that the values in the basal zone harzburgites and pyroxenites in the western Bushveld have large positive values of +7,8 and +7,5 per mil. He also found that rocks of the late hypabyssal phase have high positive values of +7,8 and +10,3 per mil. These plutonic rocks are mostly, but not always, in contact with the metasedimentary rocks above the Magaliesberg Quartzite Formation which have $\delta^{34}S$ values between +8,0 and +9,2 per mil.

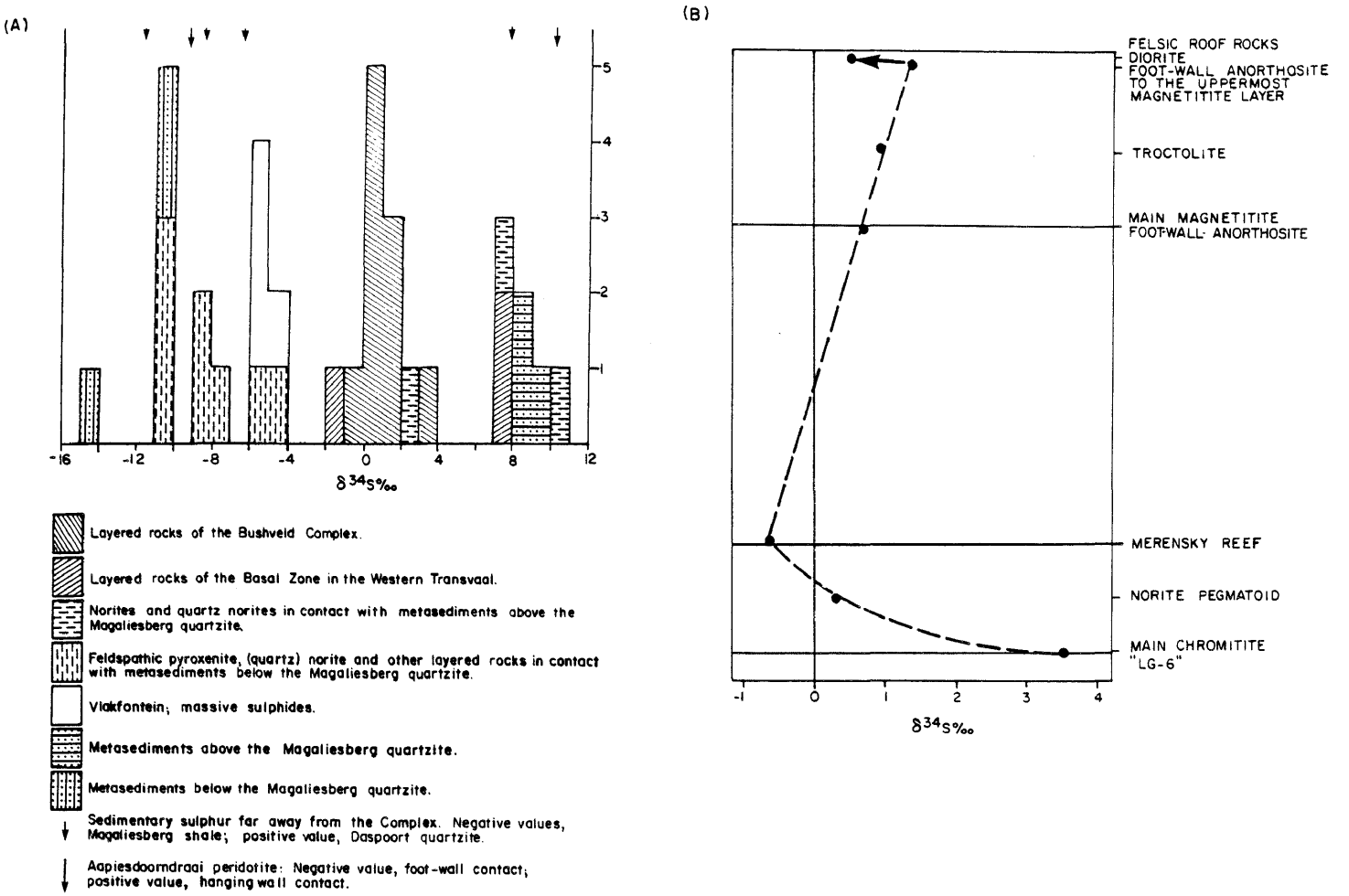

Fig. 105 A summary of the sulfur isotope data of Liebenberg (1968).

(A) A histogram of the $\delta^{34}S$ values of the rocks of the Bushveld Complex and the Pretoria Group, showing the relationship between the values of some rocks of the basal zone, the late hypabyssal phase and the hornfels and the sediments.

(B) Variation of the $\delta^{34}S$ values through the layered sequence.

In contrast, plutonic rocks (i.e. feldspathic pyroxenites, harzburgites, and quartz norites) which intrude or cut across sediments below the Magaliesberg Quartzite have relatively large negative values, ranging from -4,3 to 11,7 per mil. The metasediments in contact with these plutonic rocks have comparable values of between -10,7 and -15,3 per mil. Liebenberg (1968) also investigated unmetamorphosed Magaliesberg shales from the same stratigraphic horizon some distance from the complex and found similar values of -8,5; -11,6; and -6,4 per mil. From this Liebenberg concluded that the sulfur isotope study indicates that assimilation of sedimentary S by the magma was partly responsible for the concentrations of sulfide in the basal zone of the Bushveld Complex in the Western Transvaal.

It would, however, be of considerable interest to know how much external S was assimilated and the reason for the contrasting $\delta^{34}S$ values in the sedimentary horizons above and below the Magaliesberg Quartzite. This data is, therefore, used with due acknowledgement, in an effort to answer the above questions.

The difference in the $\delta^{34}S$ values between the layered rocks of the basal zone in the western sector of the Complex and the metasedimentary sulfides above the Magaliesberg Quartzite indicates that approximately 91 per cent of the sulfur in the basal zone could have been derived from the sediments. Comparison with the values found in the late hypabyssal phase indicates that virtually all the sulfur present in these rocks could have been derived from the sediments above the Magaliesberg Quartzite.

Assuming that the metasedimentary rocks below the Magaliesberg Quartzite in the western sector of the Bushveld Complex have a value of -10,7 per mil, then the feldspathic pyroxenites, quartz norites, and other layered rocks in contact with these sediments could have derived approximately 65 per cent of their sulfur from an external source.

Of interest also is the source of S in the massive sulfides of the Vlakfontein Nickel pipes. De Waal (1977) proposed that these Ni-pipes are centered over carbon dioxide water fluid fountains, whose localization was controlled by active fracture zones in the floor of the complex. Liberation of carbon dioxide and water is related

to metamorphic reactions during emplacement of the complex such as the dissociation of carbonates and clay minerals. This metamorphism could also have released S from the sulfides and sulfates in the sediments and transported them as H_2S, HS^-, SO_4^{2-}, HSO_4^- in hydrothermal solutions. A mean $\delta^{34}S$ value of -4,8 per mil for the Vlakfontein ores indicates that approximately 45 per cent of the S in these ores could have been derived from the sediments, on the assumption that the value for the sediments is -10,7 per mil. This is a minimum estimate, and if a mean value between -8,5 and -6,4 per mil is taken for the sedimentary sulfide samples (samples L3-5 and L3-27, Liebenberg, 1968, p. 195) as much as 65 per cent of all the sulfur could have been derived from the sediments.

Since Liebenberg's research on the S-isotope variation within the layered sequence and the Transvaal sediments, considerable advances have been made in the understanding of the factors which control the $\delta^{34}S$ variation within sedimentary environments. The main factors that control the values of $\delta^{34}S$ in various sediments is the rate of sulfate reduction, which is proportional to the sedimentation rates (Goldhaber and Kaplan, 1975). These authors have shown that the higher the rate of sulfate reduction (R) the more positive the $\delta^{34}S$ values become. This can be expressed by the relationship

$$\log R = 0{,}084\,\delta^{34}S - 1{,}32$$

Hartman and Nielsen (1968) also reported a qualitative relationship between $\delta^{34}S$ and sedimentation rate in the Baltic Sea. They found that in areas with a high sedimentation rate of 0,25 cm/year the $\delta^{34}S$ values average -21 per mil, whereas those with low rates of 0,10 cm/year average -31 per mil. Ronov et al. (1974) have reported a similar control of the sedimentation rate on the isotopic composition of S from Mesozoic sedimentary rocks. Based on data from sulfide ore bodies Schwarz and Burnie (1973) argue that sulfide deposits formed in open systems, i.e., those open to seawater $SO_4^=$, should have more negative $\delta^{34}S$ values compared to those formed in closed systems, which should have more positive values. They believe that closed systems are to be found primarily in near-shore environments, such as lagoons or estuaries where bodies of water are isolated from free exchange with seawater. Vinogradov et al. (1962, p. 983-85) have shown that sulfides in more oxygenated sediments have more positive $\delta^{34}S$ values,

because they formed in a sulfate-free system. This they illustrated by showing that the sediments from deep euxinic portions (2000 m) of the Black Sea have $\delta^{34}S$ values of -29,2 per mil, whereas the shallower (<200 m) oxygenated areas have values of -16,7 per mil.

From the foregoing discussion it is apparent that the lighter (more negative) $\delta^{34}S$ values of the metasediments below the Magaliesberg Quartzite implies a slow sedimentation rate in a reduced environment open to seawater $SO_4^{=}$. In contrast, the positive isotopic composition of the S of the sulfides in sediments above the Magaliesberg Quartzite suggests a much more rapid sedimentation rate in an oxygenated environment. The relative sedimentation rate for these ancient sediments can be inferred by employing the equation of Maynard, 1980, p. 774:

$$\log W = 1{,}33 - 0{,}042\ \Delta\delta^{34}S$$

where log W is the sedimentation rate and $\Delta\delta^{34}S$ is the difference between $\delta^{34}S$ of the $SO_4^{=}$ and the resulting sulfides. Using a Precambrian marine sulfate value of +15 per mil (Holoster and Kaplan, 1966) and the sulfur isotope data on sulfides from a borehole drilled north of Potchefstroom (Liebenberg, 1968, p. 195) a measure of the sedimentation rate of the host sediments can be inferred, as well as the oxidation state of the environment.

Sample L3-5 is an impure quartzite from the Magaliesberg Formation, containing pyrrhotite, chalcopyrite and sphalerite. It has a $\delta^{34}S$ value of -8,5 per mil, whereas sulfide from the underlying shale (L3-25) has a value of -11,6 per mil. The sedimentation rate for L3-5 was calculated at 2,20 cm / year and the rate for L3-25 at 1,65 cm / year . Similarly, pyrite from a sample of the Strubenkop Shale Formation (L3-27) with a $\delta^{34}S$ value of -6,4 per mil gave a sedimentation rate of 2,7 cm / year, whereas pyrite in a Daspoort quartzite (L4-7) with a much more positive value of +7,8 per mil evidently formed in a very high energy environment as it yielded a sedimentation rate of 10,65 cm / year. These values can only be considered as relative values since the exact $\delta^{34}S$ value of seawater sulfate is not known for this period of time. Nevertheless, these calculations do serve to illustrate the influence the sedimentation rate, which in turn controls the rate of sulfate reduction, has upon the resulting $\delta^{34}S$ values. It would appear that the host rock to the sulfides with negative $\delta^{34}S$ values from

below the Magaliesberg Quartzite Formation formed at considerably slower sedimentation rates and under more reducing conditions than those above the Magaliesberg Quartzites.

Although this sedimentary control on the isotopic composition of the sulfides may at first glance appear to be only an academic curiousity, it will be proposed in the discussions to follow that some of these principles may be extended to magmatic sediments (cumulates) to explain certain of the observed $\delta^{34}S$ variations.

The highest $\delta^{34}S$ values from seemingly uncontaminated rocks of the layered sequence is from a noritic pegmatite (+3,5 per mil) which forms the hanging-wall of the main chromitite layer (LG6) at the Groethoek Chrome Mine (Fig. 105B). From the $\delta^{34}S$ values shown in Figure 105B it seems as if the sulfides are becoming lighter or more enriched in ^{32}S with fractionation up to the level of the Merensky Reef. Although data points are limited, the $\delta^{34}S$ values of sulfides in the upper zone are higher than Merensky Reef values and seem to increase upwards to a maximum value in a mineralized anorthosite immediately below the uppermost magnetitite layer. A drop in the $\delta^{34}S$ values to +0,5 per mil is recorded in the more siliceous diorites near the roof of the Complex.

Examination of the limited $\delta^{34}S$ values with fractionation in Fig. 105B suggests that there may be a relationship between the isotopic composition of S in the sulfides and the oxidation state of the magma from which these sulfides crystallized. The highest $\delta^{34}S$ values in the layered sequence are associated with the LG6 chromitite layer. This horizon has a foot-wall sequence of at least 1900 m of cumulates in which there are few signs of contamination from sediments. It is interesting to note that the sulfides associated with the lower chromitite layer and the UG2-like chromitite layer in the study area are also enriched in ^{34}S. The ^{34}S enriched nature of the sulfides associated with the LG6 chromitite are therefore considered to have formed in a more oxygenated environment than those of the Merensky Reef. This is also substantiated by the intrinsic oxygen fugacity measurements of Elliot et al. (1982) who have shown that the fo_2 decreases by about five orders of magnitude from the LG6 chromitite layer to the Merensky Reef.

It is known from mineral assemblages that the magma that gave rise to the lower half of the upper zone was comparatively more silica rich than that from which the olivine-rich upper half, except the diorites near the roof, crystallized. The anorthositic foot-wall of the main magnetitite layer has a $\delta^{34}S$ value of +0,7 per mil (Fig. 105B) whereas the more silica undersaturated troctolite (higher fo_2) has a value of +0,9 per mil. Sulfides in the anorthosite below the uppermost magnetitite have the highest value of +1,4 per mil, which is twice that found in the foot-wall of the main magnetitite layer. In the more siliceous diorites near the roof, the sulfides are more enriched in ^{32}S, as is indicated by the drop to a value of +0,50 per mil. Again, the more siliceous parent melts (lower fo_2) produced more reduced sulfides which is reflected in the lower $\delta^{34}S$ values.

Buchanan et al. (1981) conducted a limited S-isotope investigation on the Platreef horizon. Their results will be discussed below, in conjunction with the findings of this study.

8.7.3 New Isotopic Data : Results and Discussion

In the Potgietersrus limb it is important both from a theoretical and practical point of view to distinguish sulfides formed as a result of purely igneous activity with a mantle source from the sulfur from sulfides formed as a result of the assimilation of sedimentary derived sulfur during emplacement of the magma.

A starting point in any sulfur isotope investigation of magmatic rocks is to determine from available published information the isotopic composition of the sulfur in the mantle in the same geographic area as the study in question. In many cases where this is not possible, one has to assume that the sulfur associated with igneous rocks derived from the upper mantle is isotopically similar to that of meteorites, i.e., a $\delta^{34}S$ value close to zero. The data of Tsai et al. (1979) however, reveals that this assumption is not necessarily always correct, and his work on sulfides from eclogites and associated kimberlites from the Premier and Roberts Victor mines showed that values can range from +0,2 to +2,1 per mil. Similarly, Grinenko and Ukhanov (1977) found values ranging from -0,5 to +2,1 per mil in garnet pyroxenites from Obnazhennaya, and values of +0,5 to 1,8 per mil in eclogites from

the same locality. It can therefore be assumed that primary, mantle derived sulfides could have $\delta^{34}S$ values as high as +2,1 per mil.

The results of the sulfur isotope investigation are listed in Table 25 and diagrammatically summarized in the form of a histogram of $\delta^{34}S$ values in Figure 106. It is interesting to note that the highest $\delta^{34}S$ values are from sulfides associated with chromitite layers, whereas the pyroxenites, which also display high values, are either associated with chromitite layers or contain disseminated chromite. The remaining magmatic rock types, i.e., gabbronorites, norites (spotted) and anorthosites fall within the range 0 to 3,0 per mil. The samples designated "hydrothermal veins" is from a massive chalcopyrite-cubanite-pentlandite vein in the Drummondlea Harzburgite-Chromitite. The values range from +7,30 to +7,54 per mil and fall midway between values given for sulfides from granites and modern hydrothermal environments (Nielsen, 1979), which suggests that this mineralization is of a hydrothermal origin. Included in Figure 106 are $\delta^{34}S$ values from four samples given by Buchanan et al. (1981) including the two skarn values and two samples from Liebenberg (1968) for the Platreef.

The mean $\delta^{34}S$ value of all samples is 3,78 per mil whereas the mean of all the magmatic samples from Potgietersrus is 3,00 per mil and the mean of the magmatic samples from this study is 3,16 per mil. If the values from chromitite associated sulfide mineralization are excluded a considerable lower mean value is obtained. The variation of $\delta^{34}S$ with stratigraphic height is illustrated in Fig. 107.

Immiscible sulfide droplets in a dunite and in the mineralized pyroxenite from the Volspruit subzone have $\delta^{34}S$ values of 4,32 and 3,38 per mil respectively (Table 25). Two samples from each of these horizons were submitted for analyses. Unfortunately, because of insufficient material only one value for each of these two horizons is available. The similarity suggest however, that the values are a fairly reliable indicator of the $\delta^{34}S$ for the sulfides from this level in the intrusion. The sulfides in the hanging-wall pyroxenite immediately above the lower chromitite layer, yielded

Table 25 ISOTOPIC COMPOSITION OF S IN SULFIDES FROM THE RUSTENBURG LAYERED SUITE, POTGIETERSRUS

	$\sigma^{34}S$(°/oo)	DESCRIPTION	STRAT. LEVEL
1)	+ 2,17	Basal concentrations of sulfides in main magnetitite layer (Molendraai)	≈ + 1360 m
1)	+ 2,07		
2)	+ 0,91	Foot-wall anorthosite to the main magnetitite layer (Molendraai)	≈ + 1359 m
3)	+ 1,28	Pegmatitic gabbronorite associated with the spheri= cal aggregate horizon	+ 143 m
3)	+ 0,96		
4)	+ 2,75	Spotted norite	+ 66 m
4)	+ 1,78	Spotted anorthositic norite	+ 66 m
5)	+ 4,02	UG 2-like chromitite	- 85.5 m
5)	+ 3,81	layer	"
5)	+ 3,77		"
6)	+ 4,20	Foot-wall pyroxenite to the UG2-like chromitite	- 86 m
6)	+ 3,76	layer	"
7)	+ 4,47	Gabbronorite (pegmatitic)	≈ - 88 m
8)	+ 2,37	Fine-to medium-grained gabbronorite (± pigeonite)	≈ - 100 m
9)	+ 5,37	Hanging-wall pyroxenite to the lower chromitite	- 686 m
9)	+ 4,63		"
10)	+ 7,54	Massive sulfides infilling fractures	Drummondlea-Harzburgite-Chromitite
10)	+ 7,30		
11)	+ 3,83	Basal portion of mineralized Volspruit pyroxenite.	-1210 m
12)	+ 4,32	Mineralized dunite	-1250 m
		From Liebenberg 1968	
13)	+ 1,9	Norite pegmatoid in contact with Dolomite, Zwartfontein 818 LR.	
14)	+ 0,7	Diopside hornfels on Zwartfontein 818 LR.	
		From Buchanan et al., 1981	
15)	+ 8,44	Pyrrhotite from calc-silicate hornfels on Tweefontein (## 1191,93)	
16)	+ 9,15	Chalcopyrite from calc-silicate hornfels on Tweefontein (## 1191,93)	
17)	+ 6,25	Pyrrhotite from pyroxenitic norite in close spatial relationship with sample ## 1191,93 (## 1193,90)	
18)	+ 2,74	Pyrrhotite from coarse-grained pegmatoidal pyroxenite (## 1295,28)	
19)	+ 3,69	" " " " " "	(## 1352)

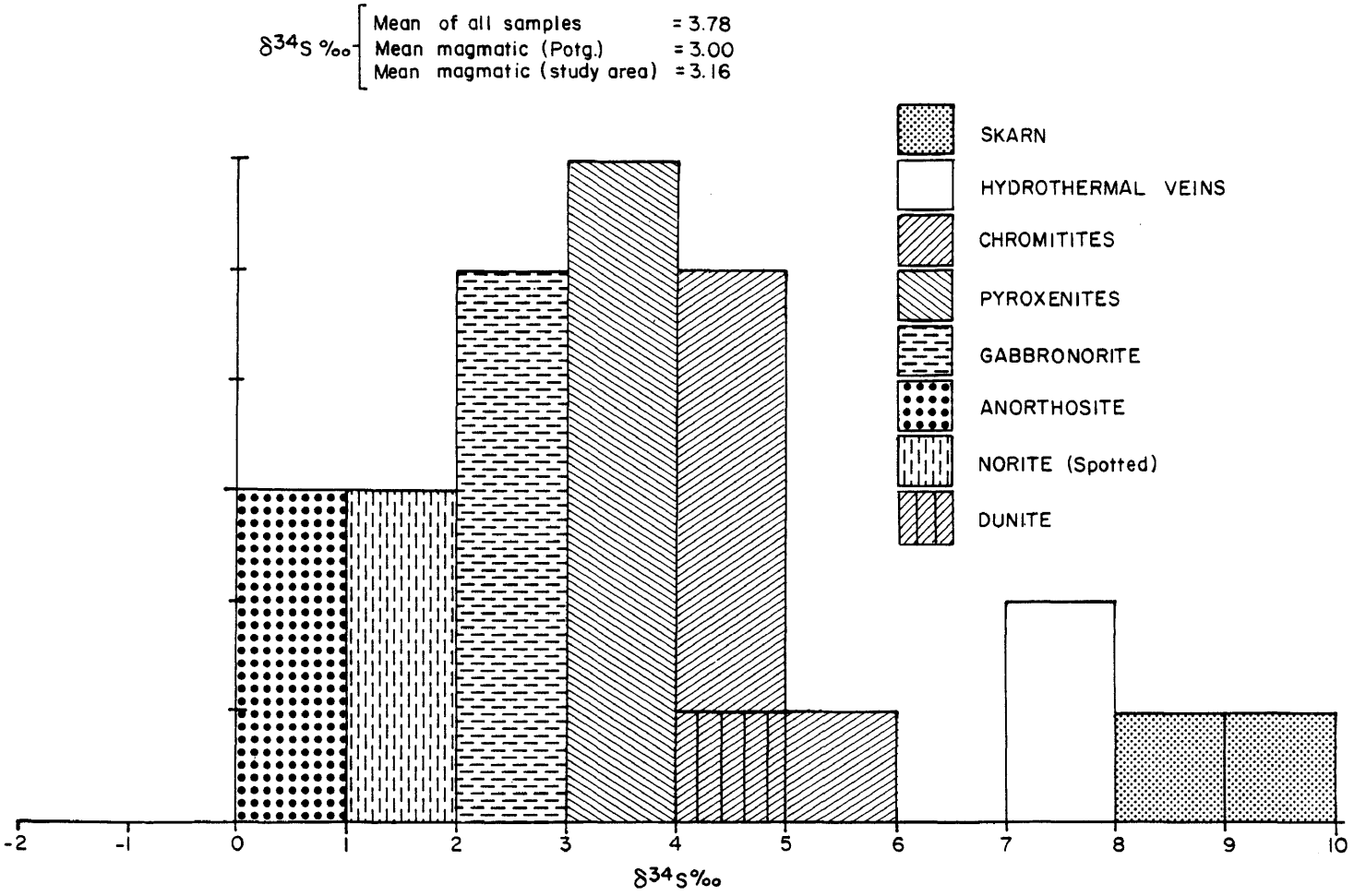

Fig. 106 A histogram of $\delta^{34}S$ values of sulfides from the Potgietersrus area.

$\delta^{34}S$ values of 4,63 and 5,37 per mil, which are by far the highest in the layered sequence. Surface and underground geological observations, as well as examination of all available diamond drill core from the lower zone showed no signs of country rock contamination in this or any other lower zone horizons that could be held responsible for the relatively high $\delta^{34}S$ values.

The next level for which S-isotopic data is available is the medium-grained mineralized pigeonite gabbro at the base of the critical zone (Fig. 107). Here a value of +2,37 per mil was obtained. Associated pegmatitic gabbronorite from higher in the sequence, close to the UG2-like chromitite layer, was found to have a value of +4,47 per mil. The felspathic pyroxenite in the footwall of the UG2-like chromitite yielded values of +3,76 and +4,20 per mil, whereas three samples from the overlying chromitite layer yielded values of 3,77; 3,81; and 4,02 per mil. This isotopic composition of S in and associated with this chromitite layer is comparatively heavy, and again there is no sign of contamination by sedimentary material.

The sulfides in the overlying horizons of the critical zone display a progressive upward enrichment in ^{32}S. The mineralized spotted norite and anorthositic norites at the +66 m level yielded values of 1,78 and 2,75 per mil respectively. This horizon has a strike length of at least 3,5 km and absence of sedimentary inclusions tends to rule out the possibility that contamination of the magma produced this mineralization. The $\delta^{34}S$ values are also too low to be sedimentary derived.

Of considerable interest is the overlying mineralization in the hybrid pegmatitic gabbronorite with which spherical aggregates are associated. The localized hydrous and pegmatitic character of this gabbronorite, as well as the presence of numerous xenoliths of metamorphosed carbonate-rich sediments, leaves little doubt that the precipitation of sulfides at this level of the intrusion resulted from the assimilation of sedimentary material. The S-isotope data from sulfides in this Platreef-type rock are therefore of particular importance as this data would show to what extent the magma was contaminated by sedimentary sulfur. Interestingly enough, amongst the lowest $\delta^{34}S$ values recorded in

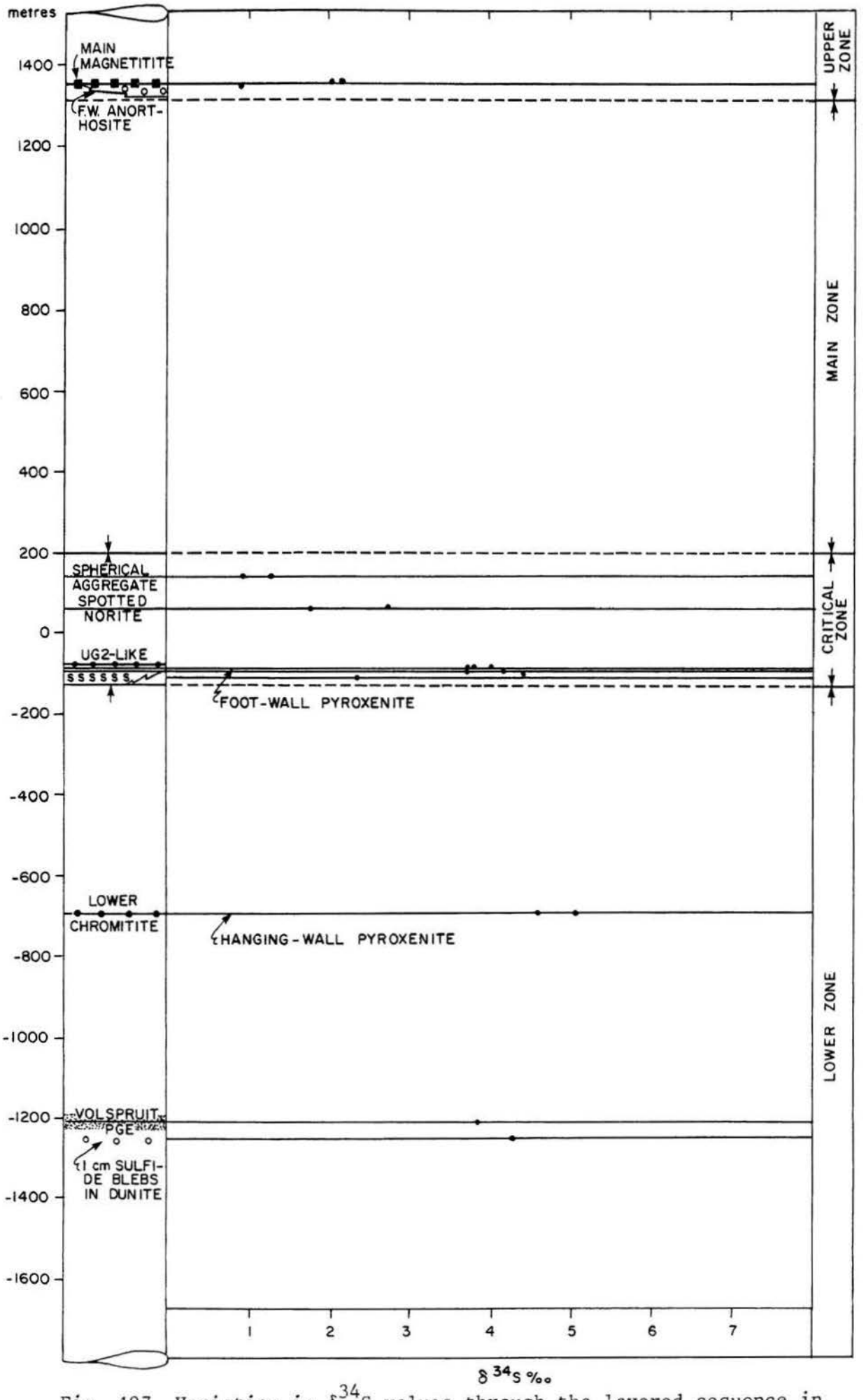

Fig. 107 Variation in $\delta^{34}S$ values through the layered sequence in the study area and in the upper zone on the farm Molendraai.

this study were derived from the sulfides of this contaminated horizon. Values of 0,96 to 1,28 per mil in these sulfides leave little doubt that virtually all of the sulfur is of magmatic origin.

The dearth of sulfides in the main zone unfortunately prevented determination of the isotopic composition of the sulfur in these rocks. The sulfides in the foot-wall anorthosite of the main magnetite layer have a $\delta^{34}S$ value of 0,91 per mil. This value does not differ much from that recorded by Liebenberg (1968) for the equivalent horizon in the eastern Bushveld (Fig. 105), and the similarity of the two values suggests that the magma in both areas was equally reduced during crystallization ofthe anorthositic foot-wall of the main magnetitite layer. The sulfides in the main magnetitite layer north of Potgietersrus contain $\delta^{34}S$ values of 2,07 and 2,17 per mil. Once again, the oxide-rich layers are considerably enriched in ^{34}S compared to the oxide poor layers, even if they are separated by less than one metre.

In every instance where calculations of fo_2 or a_{SiO_2} indicate more reducing conditions during crystallization of the magma, the $\delta^{34}S$ values of the associated sulfides decrease and vice versa. This is more than fortuitous and it is therefore concluded that the oxidation state of the magma influences the $\delta^{34}S$ composition of the precipitating sulfide liquid in a similar way as has been recorded for sedimentary environments. This close relationship between the isotopic data and the oxidation state of the magma was recognized because of the previously calculated intensive parameters and illustrates the ease with which $\delta^{34}S$ values greater than 2 per mil can be ascribed erroneously to contamination of the magma with sedimentary derived sulfur. It is therefore not surprising that a plot of fo_2 vs $\delta^{34}S$ of rocks for which both these parameters have been determined display a strong positive correlation (Fig. 108A). The fo_2 value for the Merensky Reef was taken from Elliot et al. (1982), whereas the $\delta^{34}S$ value for sulfides associated with the LG6 chromitite layer of Groethoek (Liebenberg, 1968) when plotted against the intrinsic fo_2 measured at 1200°C for the LG6 layer close-by (Maandagshoek, Snethlage and Klemm, 1978) falls almost on the regression line shown in Figure 108. The extremely low fo_2 and $\delta^{34}S$ values for the Merensky

Reef probably reflect the extremely reducing conditions during postcumulus re-equilibriation.

From this rather conclusive relationship, further constraints can be placed on the prevailing fo_2 conditions during crystallization of mineralized layers for which only $\delta^{34}S$ values are known. For instance, the observed relationship (Fig. 108) implies that the anorthosite in the foot-wall of the main magnetitite layer, which yielded a $\delta^{34}S$ value of 0,91 per mil, could have crystallized at an fo_2 of about $10^{-10,75}$ atm. In comparison, the overlying main magnetitite layer crystallized at an estimated fo_2 of 10^{-9} atm, which implies that an increase of 1,75 log units in fo_2 of the crystallizaing magma was required to enhance crystallization of magnetite to produce this layer. Along the same lines of evidence it could be inferred that the pegmatitic gabbronorite associated with the spherical aggregates crystallized under fo_2 conditions in the order of $10^{-10,70}$ to $10^{-10,25}$ atm. A $\delta^{34}S$ value of +1,78 per mil for the anorthositic norite horizon (+66m) indicates crystallization at fo_2 conditions of $10^{-9,75}$ atm, whereas the more noritic member with a $\delta^{34}S$ value of +2,75 per mil could have crystallized under conditons of $10^{-8,70}$ atm. The foot-wall pyroxenite of the UG2-like chromitite layer yielded $\delta^{34}S$ values of +3,76 and +4,20 per mil suggesting fo_2 conditions of $10^{-7,0}$ and $10^{-6,40}$ atm, whereas the underlying mineralized gabbronorite is, on the same basis, inferred to have crystallized at $10^{-8,70}$ atm.

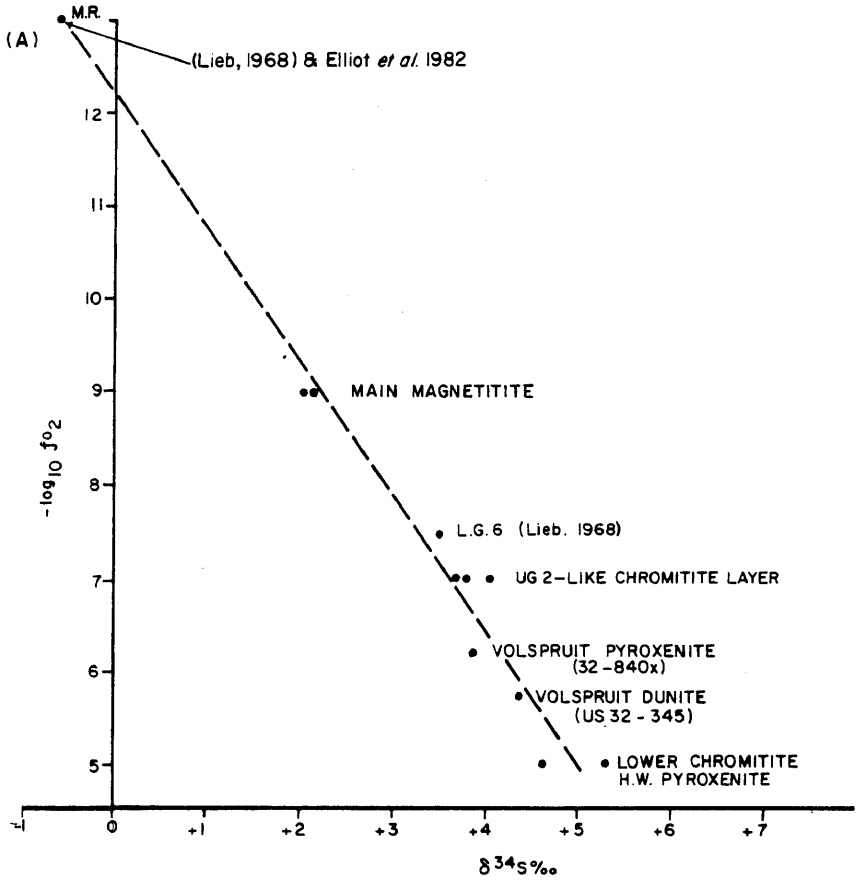

Fig. 108 fo_2-$\delta^{34}S$ plot based on intrinsic and calculated fo_2 values for sulfides from the Bushveld Complex. The $\delta^{34}S$ values for the LG6 chromitite and the Merensky Reef sulfides are from Liebenberg (1968).

A similar study to this one was conducted by Schneider (1970) who determined the sulfur isotope composition on a variety of basalts from North Hessia and Southern Lower Saxony. He also found that the more oxygenated the magma the more positive the $\delta^{34}S$ values for both sulfate and sulfide sulfur in the rock.

With this information on how the fo_2 conditions within the magma can control the isotopic composition of S, the evidence provided by Buchanan et al. (1981) for an external sedimentary source of sulfur for the Platreef sulfides can be reviewed.

Buchanan et al. (1981) presented five $\delta^{34}S$ values for samples from the Platreef and associated rocks. Unfortunately, two of

these samples, i.e., chalcopyrite and pyrrhotite are from the same sample, whereas the remaining three are determinations of pyrrhotite samples rather than bulk sulfide separates. The pyrrhotite and chalcopyrite was derived from a inclusion of calc-silicate hornfels of the Malmani dolomite and gave values of +8,44 and +9,15 per mil respectively. A second sample of pyrrhotite from an igneous rock in close spatial relationship with the above mentioned calc-silicate hornfels gave $\delta^{34}S$ values of 6,25 per mil. The high $\delta^{34}S$ values in the calc-silicate inclusion are to be expected, regardless of whether it is an inclusion or in situ. The close spatial relationship with the calc-silicate hornfels of the second sample does suggest that this particular sample contains some sedimentary sulfur. The remaining two samples, however, have values of 1,74 and 3,69 per mil and are derived from pegmatitic pyroxenites. Investigation of the basal portion of Platreef during a recent underground visit of this reef showed this pegmatitic portion of the reef to contain disseminated chromite as well as thin intermittent layers of fine- to medium-grained opx ± cpx-chr cumulates. The presence of chromite implies high fo_2 conditions, i.e., $>10^{-8}$ atm and the high $\delta^{34}S$ value recorded for these rocks by Buchanan et al. (1981) probably again reflects comparatively high fo_2 conditions during crystallization. Although Buchanan et al. (1981) considered the sulfides in the Platreef to have formed by a process of sulfidation of the magma they concede that these values are not related to sedimentary derived sulfur because they are not far enough removed from the range of values established for the magmatic sulfides of the Bushveld by Liebenberg (1968).

Liebenberg records a $\delta^{34}S$ value of +1,9 per mil in sulfides from a norite near the base of the Platreef, close to the contact with the Malmani dolomite on the farm Zwartfontein 818LR, and a value of 0,7 per mil in a diopside hornfels from Zwartfontein. These values are unquestionably of a magmatic origin, even though one sample is from an inclusion of Malmani dolomite. Therefore, for all the samples where a clear-cut magmatic origin is indicated, the sulfur is clearly of magmatic origin and that only in very localized areas in close proximity to inclusions is some contamination of sedimentary sulfur indicated.

In conclusion, the presently available S-isotope data from Platreef and the study area suggests that virtually all of the sulfur associated with the sulfides in the igneous layered suite in the Potgietersrus area is of a mantle origin. Although the bulk of the S is not of sedimentary origin it is considered that volatiles liberated by the metamorphosed and assimilated sedimentary material, firstly, enhanced the precipitation of sulfides from the Platreef magma, and secondly, altered the oxidation state of the magma which in turn influenced the isotopic composition of the separating sulfide liquid.

9. CONCLUSIONS

9.1. The Rustenburg Layered Suite south of Potgietersrus is at least 3250 m thick and can be divided on the basis of lithology into a lower, critical, main and upper zone. The lower zone consists of at least 37 well defined cyclic units and therefore differs from the equivalent zone elsewhere in the Bushveld Complex. In comparison to its counterparts in the eastern and western Bushveld, the critical zone is extremely thin. It can be divided into two subzones. The 1120 m thick sequence of the main zone also consist of a cyclic sequence of rock units unlike its counterpart in the other sectors of the Complex.

9.2. Structural, chemical, and petrographic data confirms that influx of new magma occurred at the base of the critical and main zone.

9.3. Four episodes of faulting have deformed the area. This has upfaulted a thick sequence of the earliest differentiates including two chromitite layers. These two layers consist of the best metallurgical grade chromite in the Bushveld and are presently being exploited in the area.

9.4. The Mg:Fe:Ca ratio of the Ca-poor pyroxenes ranges from 89,5:8,8:1,6 in the lower zone to 44,2:52,3:3,37 in the upper zone. Similarly, the composition of the Ca-rich pyroxenes range from 46,4:6,0:47,5 to 31,5:22,1:46,4 over the same stratigraphic interval. Textural evidence suggests that the termination of the two pyroxene limit is due to a peritectic reaction between Ca-poor pyroxene and melt.

The mean $K_D^{\text{opx-cpx}}_{\text{Mg-Fe}_T}$ for cumulates from the study area is 0,822 compared to 0,782 from other sectors of the Bushveld Complex. This suggests higher crystallization temperatures in the study area. It was found that the $K_D^{\text{opx-cpx}}_{\text{Mg-Fe}_T}$ is the same irregardless of whether the pyroxene is cumulus or intercumulus. The Al:Si ratio in the Ca-rich pyroxene is a useful measure of the relative a_{SiO_2} of the melt.

Available chemical data on Ca-rich pyroxenes from the Potgietersrus limb suggest a Ca depletion and Fe enrichment fractionation trend unlike most other tholeiitic intrusions.

9.5. The V_2O_5 content in the main magnetitite layer and the Cr_2O_3 and $Cr/Fe^{2+}+Fe^{3+}$ values for the upper and lower chromitite in the study area are the highest encountered in the Bushveld Complex. Textural evidence in especially the chromitite layers suggests the formation of massive, monomineralic layers from chromite- or magnetite-rich cumulates is by a postcumulus process analogous to sintering. Thermodynamic calculations indicate that the main magnetitite layer formed at 1080°C at an fo_2 10^{-9} atm, compared to the lower chromitite layer which crystallized at 1242°C and a fo_2 of $\approx 10^{-5}$ atm in the magma.

9.6. Density calculations based on the composition of the postulated main and critical zone magmas show that gravitative crystal settling could have taken place purely on the basis of density contrast.

9.7. The chemical composition of coexisting cumulus phases were used to determine the intensive parameters of the crystallizing magam. From the $K_D{}^{ol\text{-}liq}_{Mg\text{-}Fe^{2+}}$ relationship it could be illustrated that the parental magma of the lower zone could not have been ultrabasic in character. Pressure calculations, based on the chemical composition of diagnostic pressure sensitive assemblages in the thermal aureole of the eastern Bushveld indicate that the pressure during crystallization of the lower zone could have been as high as 5484 ±400 bars. Calculations also indicate that the Potgietersrus magma crystallized over a temperature interval ranging from 1276°C in the lower zone to 1022°C in the basal portion of the upper zone. Similarly, oxygen fugacity conditions in the lower zone were calculated to be in the order of $10^{-6,21}$ to $10^{-4,98}$ atm, whereas values of 10^{-11} to 10^{-9} atm were operative in the upper zone.

9.8. Significant sulfide and PGE mineralization occurs in the lower part of the lower zone which opens up this zone as a new target area for exploration. Within this zone, increased thickness and grade of Ni, Cu, and PGE mineralization was found to occur away from the intrusive contact towards the centre of the intrusion. Mineralization is commonly associated with a drop in the $Mg/(Mg+Fe^{2+})$ ratio of orthopyroxene and can in most cases be related to new influxes of metal-rich magma. In contrast, sulfide mineralization associated with the chromitite layers is considered to have formed in direct response to chromite crystal-

lization. Chromite crystallization reduced the solubility of S in the magma and caused an immisible sulfide liquid to separate.

Several sulfide facies exist within the layered sequence and suggest progressively more S-rich assemblages with fractionation. The M.Mb./P.G. contains the sulfide assemblage pyrite-chalcopyrite ± vaesite and millerite to the total exclusion of the phases pyrrhotite and pentlandite. Evidence for late stage sulfidation exists in the upper zone.

Magmatic Cu:Ni ratios range from 1:7 in the lower zone to 13:1 in the upper zone and reflect the basicity of the parental magma. Both the Co content of pentlandite and the Fe content of cubanite were found to increase with differentiation.

9.9. fo_2 conditions were too low in the lower and critical zones south of Potgietersrus, to give rise to Pt and Ru sulfides. fs_2 calculations and sulfide mineral assemblages indicate that the sulfur fugacity in the main and upper zone appears to decrease towards the north.

9.10. Sulfur isotope data indicate that all the sulfur in the magma is of a mantle origin, and that the isotopic composition was strongly influenced by the prevailing oxygen fugacity conditions during crystallization.

ACKNOWLEDGEMENTS

The author would like to thank the Institute for Geological Research on the Bushveld Complex and the Council for Scientific and Industrial Research for sponsoring this study.

Sincere thanks are due to Dr. C. Frick of the Geological Survey of South Africa. Had it not been for his generous microprobe facilities and granting of untold requests for sulfide Ni and S analyses many aspects of this study would not have been possible.

Mnr. S.P. Rautenbach, Grasvally, is gratefully acknowledged for providing the only available diamond drill core of the chromitite horizons. His foresight in preserving the core has made part of this study possible. Also, the many hours of stimulating conversation and the wealth of geological information is greatly appreciated.

I would also like to express my sincere gratitude to Mr. and Mrs. J.J.H. Strauss of Grasvally for their generous hospitality and friendship during the course of this study.

Billiton Exploration (Pty.) Ltd. and Rio Tinto Exploration (Pty.) Ltd. kindly allowed access to substantial amounts of borehole information that proved to be invaluable in this study. The management and staff of SAMANCOR at the Grasvally Mine are thanked for assisting in the underground sampling.

I am indebted to Dr. M.R. Sharpe of the Institute for Geological Research on the Bushveld Complex for his assistance in the statistical treatment of some of the data and to his continued interest, friendship, and morale boosting during a few of the "down" moments of this lengthy study.

Prof. G. Von Gruenewaldt is deeply thanked for proposing and supervising the project. Also, he must be commended for his continued good patience and humour during the reading of the early voluminous drafts of the manuscript.

I am also indebted to Mrs. M. Potgieter for drafting of the many diagrams, and to Mrs J.D. Schmidt and my wife Diana for typing of the tables and manuscript.

REFERENCES

AKELLA, J., WILLIAMS, R.J. and MULLINS, O., 1976.
Solubility of Cr, Ti, and Al in coexisting olivine, spinel and liquid at 1 atm. Proc. 7th. Lunar Sci. Conf., 1179-94.

ALTHAUS, E., 1976
The triple point, andalusite-sillimanite-kyanite. Contrib. Mineral. Petrol., v. 16, 19-47.

ARCULUS, R.J., GILLBERG, M.E. and Osborn, E.F., 1974.
The system MgO-Iron Oxide-Cr_2O_3-SiO_2: phase relations among olivine, pyroxene, silica and spinel in air at 1 atm. Carnegie Inst. Wash., Yb. 73, 317-322.

ARCULUS, R.J. and OSBORN, E.F., 1975.
Phase relations in the system MgO-Iron Oxides-Cr_2O_3-SiO_2. Carnegie Inst. Wash., Yb. 74, 507-512.

ARCULUS, R.J. and WILLS, K.J.A., 1980.
The petrology of plutonic blocks and inclusions from the Lesser Antilles Island Arc. J. Petrol., v. 21, part 4, 774-799.

ARCULUS, R.J. and DELANO, J.W., 1980.
Implications for the primitive atmosphere of the oxidation state of the earth's upper mantle. Nature, V. 288, 72-74.

ARMBRUSTMACHER, T.J. and BANKS, N.G., 1974.
Clouded plagioclase in metadolerite dikes, southeastern Bighorn Mountains, Wyoming, Am. Mineral, v. 59, 656-665.

ATKINS, F.B., 1969.
Pyroxenes of the Bushveld Intrusion, South Africa. J. Petrol., v. 10, 222-249.

BACON, C.R. and CARMICHAEL, I.S.E., 1973.
Stages in the P-T path of ascending basalt magma: an example from San Quintin Baja, California. Contrib. Mineral. Petrol., v. 41, 1-22

BARIN, I. and KNACKE, O., 1973.
Thermochemical properties of inorganic substances. Springer-Verlag, New York, 921p.

BARRETT, D.M., JACOBSEN, B.L., McCARTHY, T.S. and CAWTHORN, R.G., 1978.
The structure of the Bushveld Complex south of Potgietersrus as revealed by a gravity survey. Trans. Geol. Soc. S. Africa, v. 81, 271-276.

BARTON, P.B. and SKINNER, B.J., 1967.
Sulfide mineral stabilities, 236-333. In, Barnes, H.L. (Ed.), Geochemistry of hydrothermal ore deposits. Holt, Rinehart and Winston Inc., New York.

BAS, M.J. LE, 1962.
The role of alumina in igneous clinopyroxenes with relation to their parentage. Am. J. Sci., v. 260, 267-288.

BASTIN, H.A., 1968.
Zur tektonik and stratigraphic am nordöstlichen Bushveld - Rand. Ph.D. thesis (unpublished). Technische Hochschule, Aachen, 52p.

BEESON, M.H. and JACKSON, E.D., 1969.
Chemical composition of altered chromites from the Stillwater Complex, Montana. Am. Mineral., v. 54, 1084-1100.

BENCE, A.E. and ALBEE, A.L., 1968.
Empirical correction factors for the electron microanalysis of silicates and oxides. J. Geol., v. 76, 382-403.

BENDER, J.F., HODGES, F.N. and BENCE, A.E., 1978.
Petrogenesis of basalts from the project "Famous" area: experimental study from 0-15 kilobars. Earth Planet. Sci. Lett., v. 41, 277-302.

BERG, J., 1977.
Regional geobarometry in the contact aureoles of the anorthositic Nain Complex, Labrador. J. Petrol., v. 18, part 3, 399-430.

BIGGAR, G.M., 1974.
Phase equilibrium studies of the chilled margines of some layered intrusions. Contrib. Mineral. Petrol., v. 46, 159-67.

BOTTINGA, Y., KUDO, A. and WEILL, D., 1966.
Some observations on oscillatory zoning and crystallization of magmatic plagioclase. Am. Mineral., v. 5, 792-806.

BOTTINGA, Y.A. and WEILL, D.F., 1970.
Densities of liquid silicate systems calculated from partial molar volumes of oxide components. Am. J. Sci., v. 269, 169-182.

BOTTINGA, Y.A. and WEILL, D.F., 1972.
The viscosity of magmatic silicate liquids: a model for calculation. Am. J. Sci., v. 272, 438-75.

BOWEN, N.L., 1922.
The behaviour of inclusions in igneous magmas. J. Geol., v. 30, 513-570.

BOWES, D.R., SKINNER, W.R. and SKINNER, D.L., 1973.
Petrochemistry of the Stillwater Igneous Complex, Montana. Trans. Geol. Soc. S. Afr., v. 76, 153-163.

BOWLES, J.F.W., 1976.
Distinct cooling histories of troctolites from the Freetown layered gabbro. Mineral. Mag., v. 40, 703-714.

BOWLES, J.F.W., 1977.
A method of tracing the temperature and oxygen fugacity histories of complex magnetite-ilmenite grains. Mineral. Mag., v. 41, 103-109.

BOYD, F.R. and BROWN, G.M., 1969.
Electron-probe study of pyroxene exsolution. Min. Soc. Am., Spec. Paper 2, 211-216.

BROWN, G.M., 1957.
Pyroxenes from the early and middle stages of fractionation of the Skaergaard Intrusion, East Greenland. Mineral. Mag., v. 31, 511-543.

BROWN, G.M. and VINCENT, E.A., 1963.
Pyroxenes from late stages of fractionation of the Skaergaard Intrusion, East Greenland. J. Petrol., v. 4, 175-197.

BROWN, G.M., 1967.
Experimental studies on inversion relations in natural pyroxenes. Carnegie Inst. Wash., Yb. 66, 347-53.

BRYNARD, H.J., DE VILLIERS, J.P.R., and VILJOEN, A.E., 1976.
A mineralogical investigation of the Merensky Reef at Western Platinum Mine near Marikana, South Africa. Econ. Geol., v. 71, 1299-1307.

BUCHANAN, D.L., 1976.
The phase chemistry of the Bushveld Complex in the Bethal area. Ph.D. thesis (unpublished) Imperial College of Science and Technology, London. 163p.

BUCHANAN, D.L., 1979.
A combined transmission electron microprobe and electron microprobe study of Bushveld pyroxenes from the Bethal area. J. Petrol., v. 20, 327-354.

BUCHANAN, D.L., NOLAN, J., and VILJOEN, E.A., 1980.
Determination of silica activity in Bushveld rocks. Contrib. Mineral. Petrol., v. 73, 311-319.

BUCHANAN, D.L., NOLAN, J., SUDDABY, P., ROUSE, J.E., VILJOEN, M.J. and DAVENPORT, J.W.J., 1981.
The genesis of sulfide mineralization in a portion of the Potgietersrus limb of the Bushveld Complex. Econ. Geol., v. 76, 568-579.

BUENING, D.K. and BUSECK, P.R., 1973.
Fe-Mg lattice diffusion in olivine. J. Geophys. Res., v. 78, 6852-6862.

BUDDINGTON, A.F. and LINDSLEY, D.H., 1964.
Iron-titanium oxide minerals and synthetic equivalents. J. Petrol., v. 5, 310-357.

BUDWORTH, D.W., 1970A.
An introduction to ceramic science. Pergamon Press. 287p.

BUDWORTH, D.W., 1970B.
The selection of grain growth control additives for the sintering of ceramics. Mineral. Mag., v. 37, no. 271, 833-838.

BURNHAM, C.W., 1972.
Magmas and hydrothermal fluids, 71-136. In, Barnes, H.L. (Ed.), Geochemistry of hydrothermal ore deposits, second edition. John Wiley, New York.

BURNHAM, C.W., 1979.
The importance of volatile constituents, 439-478. In, Yoder, H.S. Jr. (Ed.). The evolution of the igneous rocks: fiftieth anniversary perspectives, Princeton University Press.

BURNS, R.G., 1970.
Mineralogical applications of crystal field theory. Cambridge University Press, London. 244p.

BUTTON, A., 1974.
Low potash pillow basalts in the Pretoria Group, Transvaal Supergroup. Trans. Geol. Soc. S. Afr., v. 77, 99-104.

CABRI, L., 1973.
New data on phase relations in the Cu-Fe-S system. Econ. Geol., v. 68, 443-454.

CAMERON, E.N. and EMERSON, M.E., 1959.
The origin of certain chromite deposits of the eastern part of the Bushveld Complex. Econ. Geol., v. 54, 1151-1213.

CAMERON, E.N. and DESBOROUGH, G.A., 1969.
Occurrence and characteristics of chromite deposits - eastern Bushveld Complex. Econ. Geol. Monogr. 4, 23-40.

CAMERON, E.N., 1969.
Postcumulus changes in the eastern Bushveld Complex. Am. Mineral., v. 54, 754-779.

CAMERON, E.N., 1977.
Chromite in the central sector of the eastern Bushveld Complex, South Africa. Am. Mineral., v. 62, 1082-1096.

CAMERON, E.N., 1978.
The lower zone of the eastern Bushveld Complex in the Olifants River Trough. J. Petrol., v. 19, 437-462.

CAMERON, E.N., 1980.
Evolution of the lower critical zone, central sector, eastern Bushveld Complex, and its chromite deposits. Econ. Geol., v. 75, 845-871.

CAMERON, W.E., 1976.
Coexisting sillimanite and mullite. Geol. Mag., v. 113, 497-514.

CAMERON, W.E., NISBET, E.G. and DIETRICH, V.J., 1979.
Boninites, komatiites and ophiolitic basalts. Nature, v. 280, 550-553.

CAMPBELL, I.H., 1973.
Aspects of the petrology of the Jimberlana Layered Intrusion of Western Australia. Ph.D. thesis (unpublished) University of London.

CAMPBELL, I.H. and NOLAN, J., 1974.
Factors affecting the stability field of Ca-poor pyroxene and the origin of the Ca-poor minimum in Ca-rich pyroxenes from tholeiitic intrusions. Contrib. Mineral. Petrol., v. 48, 205-219.

CAMPBELL, I.H., 1977.
A study of macro-rhythmic layering and cumulate processes in the Jimberlana Intrusion, Western Australia, Part I: The Upper Layered Series. J. Petrol., vol. 18, 183-215.

CAMPBELL, I.H., 1978.
Some problems with the cumulus theory. Lithos, v. 11, 311-323.

CAMPBELL, I.H. and NALDRETT, A.J., 1979.
The influence of silicate: sulfide ratios on the geochemistry of magmatic sulfides. Econ. Geol., v. 74, 1503-1506.

CARMICHAEL, I.S.E., 1967.
The iron-titanium oxides of salic volcanic rocks and their associated ferromagnesium silicates. Contrib. Mineral. Petrol., v. 14, 36-64.

CARMICHAEL, I.S.E., NICHOLLS, E.J., and SMITH, A.L., 1970.
Silica activity in igneous rocks. Am. Mineral., v. 55, 246-263.

CARMICHAEL, I.S.E., TURNER, F.J. and VERHOOGEN, J., 1974.
Igneous petrology. McGraw-Hill, New York, 739p.

CARMICHAEL, I.S.E. and GHIORSO, M.S., (in press)
Intensive variables in siliceous magmas. Contrib. Mineral. Petrol., in press.

CAWTHORN, R.G., 1977.
Pyroxene compositions, reaction relations and the lack of silica enrichment in the eastern Bushveld Complex. Trans. Geol. Soc. S. Afr., v. 80, 139-144.

CAWTHORN, R.G., BIGGAR, G.M., GRAHAM, C.M., GRAHAM, A., FORD, C.E., SHARPE, M. and DAVIES, G., 1979.
Experimental petrological data on the parental magmas to the Bushveld Complex. Inst. Geol. Res. Bushveld Complex, Univ. Pretoria, Res. Rept. 18, 1-27.

CHAMBERLAIN, J.A., 1967.
Sulfides in the Muskox Intrusion. Can. J. Earth Sci., v. 4, 105-153.

CHAYES, F., 1956.
Petrographic modal analyses. An elementary statistical appraisal. J. Wiley and Sons. Inc., New York, 113p.

CLARKE, D.B. and BIGGAR, G.M., 1972A.
Calcium-poor pyroxenes in the system $CaO-MgO-Al_2O_3-SiO_2$ $Fe-O_2$. Lithos, v. 5, 203-216.

COBLE, R.L., 1961.
Sintering crystalline solids. II. Experimental tests of diffusion models in powdered compacts. J. Appl. Physc., v. 32, 793-799.

CONRAD, H., 1961.
The role of grain boundaries in creep and stress rupture, 218-268. In Dorn, J.E. (Ed.), Mechanical behaviour of materials at elevated temperature. McGraw-Hill, New York.

COUSINS, C.A., 1959.
The structure of the mafic portion of the Bushveld Complex Trans. Geol. Soc. S. Afr., v. 62, 179-189.

CRAIG, J.R. and KULLERUD, G., 1969.
Phase relations in the Cu-Fe-Ni-S system and their application to magmatic ore deposits, Econ. Geol. Monog. 4, 344-358.

CRAIG, J.R., 1971.
Violarite stability relations. Am. Mineral., v. 56, 1303-1311.

CRAIG, J.R., 1974.
The Cu-S and Cu-Fe-S system, 58-74. In, Ribbe, P.H. (Ed.), Sulfide mineralogy. Mineral. Soc. Am. short course notes.

CZAMANSKE, G.K. and MIHÁLIK, P., 1972.
Oxidation during magmatic differentiation, Finnmarka Complex, Oslo area, Norway: part 1. The opaque oxides. J. Petrol., v. 13, 493-509.

DALLMEYER, R.D. and DODD, R.T., 1971.
Distribution and significance of cordierite in paragneisses of the Hudson Highlands, south eastern New York. Contrib. Mineral. Petrol., v. 33, 289-308.

DANCHIN, R.V. and FERGUSON, J., 1970.
The geochemistry of the Losberg Intrusion, Fochville, Transvaal. Geol. Soc. S. Afr., Spec. Publ. 1, 689-714.

DAY, R.B. and STOKES, R.J., 1966.
Mechanical behaviour of polycrystalline magnesium oxide at high temperature. J. Am. Ceram. Soc., v. 49, 345-354.

DALLMEYER, R.D. and DODD, R.T., 1971.
Distribution and significance of cordierite in paragneisses of the Hudson Highlands, south eastern New York. Contrib. Mineral. Petrol., v 33, 289-308.

DANCHIN, R.V. and FERGUSON, J., 1970.
The geochemistry of the Losberg Intrusion, Fochville, Transvaal. Geol. Soc. S. Afr., Spec. Publ. 1, 689-714.

DAVIES, G., CAWTHORN, R.G., BARTON, J.M.Jr. and MORTON, M., 1980.
Parental magma to the Bushveld Complex. Nature, v. 287, 33-35.

DAVIS, B.T. and BOYD, F.R., 1966.
The join $Mg_2Si_2O_6$ - $CaMgSi_2O_6$ at 30 kb pressure and its application to pyroxenes from kimberlites. J. Geophys. Res., v. 71, 3567-3576.

DEER, W.A., HOWIE, R.A. and ZUSSMAN, J., 1966.
An introduction to rock forming minerals. Longmans, Green and Co. Ltd., London, 528p.

DONALDSON, C.H., 1977.
Laboratory duplication of comb layering in the Rhum pluton. Mineral. Mag., v. 41, 323-336.

DRAKE, M.J. and WEILL, D.F., 1975.
Partition of Sr, Ba, Ca, Y, Eu^{2+}, Eu^{3+} and other REE between plagioclase feldspar and magmatic liquid: An experimental study. Geochim. Cosmochim. Acta, v. 39, 689-712.

DRAKE, M.J., 1976.
Plagioclase-melt equilibria. Geochim. Cosmochim. Acta., v. 40, 457-465.

DUCHESNE, J.C., 1972A.
Iron-titanium oxide minerals in the Bjerkrem-Sogndal Massif, South-Western Norway. J. Petrol., v. 13, 57-58.

DUCHESNE, J.C., 1972B.
Pyroxenes et olivines dans le massit de Bjerkrem-Songndal (Norvege meridionate) Contribution a l'etude de la serie anorthosite-mangerite. Rept. 24th. Inst. Geol. Congr. Section 2, 320-328.

DUCHESNE, J.C., 1978.
Quantitative modeling of Sr, Ca, Rb, and K in the Bjerkrem-Sogndal layered lopolith (S.W. Norway). Contrib. Mineral Petrol., v. 66, 175-184.

DUKE, M.J., 1976.
Distribution of the period four transition elements among olivine, calcic clinopyroxene and mafic silicate liquid: experimental results. J. Petrol., v. 17, 499-521.

EALES, H.V. and REYNOLDS, I.M., 1981.
Factors influencing the composition of chromite and magnetite in some southern African rocks. ICAM, Johannesburg, 1-49.

ECKSTRAND, O.R., 1975.
The Dumont serpentinite: a model for control of nickeliferous opaque mineral assemblages by alteration reactions in ultramafic rocks. Econ. Geol., v. 70, 183-201.

EDWARDS, H.R. WYNNE and HAY, P.W., 1963.
Coexisting cordierite and garnet in regionally metamorphosed rocks from the Westport area, Ontario. Can. Mineral., v. 7, part 3, 453-478.

ELLIOTT, W.C., GRANDSTAFF, D.E., ULMER, G.C. and BUNTIN, T., 1982.
An intrinsic oxygen fugacity study of platinum-carbon associations in layered intrusions. Econ. Geol., v. 77, 1493-1510.

EVANS, B.W. and WRIGHT, T.L., 1972.
Composition of liquidus chromite from the 1959 (Kilauea Iki) and the 1965 (Makaopuhi) eruptions of Kilauea, volcano, Hawaii. Am. Mineral., v. 57, 217-230.

FERRY, M. and SPEAR, F.S., 1978.
Experimental calibration of the partitioning of Fe and Mg between biotite and garnet. Contrib. Mineral. Petrol., v. 66, 113-117.

FINGER, L.W., 1972.
The uncertainty in the calculated ferric iron content of a microprobe analysis. Carnegie Inst. Wash., Yb. 71, 600-603.

FISK, M.R. and BENCE, A.E., 1980.
Experimental crystallization of chrome spinel in "Famous" basalt 527-1. Earth Planet. Sci. Lett., v. 48, 111-123.

FLANAGAN, F.J., 1969.
U.S. Geological Survey Standards II. First compilation of data for the new U.S.G.S. rocks. Geochim. Cosmochim. Acta, v. 33, 81-120.

FLEET, M.E., 1974A.
Partion of major and minor elements and equilibriation in coexisting pyroxenes. Contrib. Mineral. Petrol., v. 44, 259-273.

FLEET, M.E., 1974B.
Mg, Fe^{2+} site occupancies in coexisting pyroxenes. Contrib. Mineral. Petrol., v. 47, 207-214.

FREER, R., 1981.
Diffusion in silicate minerals and glasses: a data digest and quide to the literature. Contrib. Mineral. Petrol., v. 76, 440-454.

FROHBERG, M.G. and RICHTER, K., 1968.
Reduction and oxidation equilibria between divalent and trivalent chromium in molten calcium oxide-silicon dioxide-chromium oxide slags. Arch. Eisenhuettenw, v. 39, 779-802.

FUDALI, R.F., 1965.
Oxygen fugacities of basaltic and andesitic magmas. Geochim. Cosmochim. Acta, v. 29, 1063-1075.

GABLE, D.J. and SIMS, P.K., 1969.
Geology and regional metamorphism of some high grade cordierite gneisses, Front Range Colorado. Geol. Soc. Amer., Spec. Paper 128, 87p.

GAIN, S.B. and MOSTERT, A.B., 1981.
The geological setting of the platinoid and base metal sulfide mineralization in the Platreef of the Bushveld Complex on Drenthe, north of Potgietersrus. Inst. Geol. Res. Bushveld Complex, Univ. Pretoria, Res. Rept. 28, 22p.

GAIN, S.B., 1982.
The cyclic units of the upper critical zone on Maandagshoek 254KT, eastern Bushveld Complex. M.Sc. thesis (unpublished) Univ. of Pretoria, 155p.

GASPARRINI, E. and NALDRETT, A.J., 1972.
Magnetite and ilmenite in the Sudbury Nickel Irruptive. Econ. Geol., v. 67, 605-621.

GHENT, E.D., 1976.
Plagioclase-garnet-Al_2SiO_5-quartz: a potential geobarometer-geothermometer. Am. Mineral., v. 61, 710-714.

GOLDHABER, M.B. and KAPLAN, I.R., 1975.
Controls and consequences of sulfate reduction rates in recent marine sediments. Soil Sci., v. 119, 42-55.

GOLDING, H.G., 1975.
Relict textures of chromitites from New South Wales. J. Geol. Soc. Australia, v. 22, part 4, 397-412.

GORESY, A., EL., PRINZ, M. and RAMDOHR, P., 1976.
Zoning in spinels as an indicator of crystallization histories of mare basalts. Proc. 7th Lunar Sci. Conf., 1261-1279.

GREEN, D.H., RINGWOOD, A.E., WARE, N.G., HIBBERSON, W.O., MAJOR, A., and KISS, A., 1971A.
Experimental petrology and petrogenesis of Apollo 12 basalts. Proc. Lunar Sci., Conf., v. 1, 601-615.

GREEN, D.H., WARE, N.G., HIBBERSON, W.V., and MAJOR, A., 1971B.
Experimental petrology of Appollo 12 basalts: part 1, sample 12009. Earth Planet Sci. Lett., v. 13, 85-96.

GRINENKO, L.N. and UKHANOV, A.V., 1977.
Sulfur levels and isotopic compositions in the upper mantle xenoliths from the Obnazhennaya, Kimberlite pipe. Geochem. Inter., v. 14, 169-171.

GRUENEWALDT, G., VON, 1971.
A petrological and mineralogical investigation of the rocks of the Bushveld Igneous Complex in the Tauteshooste-Roossenekal area of the Transvaal. D.Sc. thesis (unpublished) Univ. of Pretoria. 228p.

GRUENEWALDT, G., VON, 1973.
The main and upper zones of the Bushveld Complex in the Roossenekal area, Eastern Transvaal. Trans. Geol. Soc. S. Afr., v. 76, 207-227.

GRUENEWALDT, G., VON, 1976.
Sulfides in the upper zone of the eastern Bushveld Complex. Econ. Geol., v. 71, 1324-1336.

GRUENEWALDT, G., VON and WEBER-DIEFFENBACH, K., 1977.
Coexisting Ca-poor pyroxenes in the main zone of the Bushveld Complex. Contrib. Mineral. Petrol., v. 65, 11-18.

GUPTA, A.K., KOSUKE, O., KENZO, Y. and LIDIAK, E., 1973.
Effect of silica concentration on the diopsidic pyroxenes in the system diopside-$CaTiAl_2O_6SiO_2$. Contrib. Mineral. Petrol., v. 41, 333-344.

HAGGERTY, S.E., 1976.
Opaque mineral oxides in terrestial igneous rocks, Hg-101-135. In, Rumble, D. (Ed.), Mineral. Soc. Am. short course notes on Oxide Minerals.

HALL, A.L., 1908.
The geology of the country east of Potgietersrus. Rept. Geol. Surv. S. Afr. Trans., 62-102.

HALL, A.L., 1908.
On the contact metamorphism in the Pretoria series of the Lydenburg and Zoutpansberg districts. Trans. Geol. Soc. S. Afr., v. XI, 1-25.

HALL, A.L. and GARDTHAUSEN, C., 1911.
Note on remarkable xenoliths of altered shale from the norite of Potgietersrus and Mapoch's country. Trans. Geol. Soc. S. Afr., v. XIV, 74-78.

HALL, A.L., 1932.
The Bushveld Igneous Complex of the central Transvaal. Dept. of Mines, Geol. Survey of South Africa, Mem. 28, 569p.

HAMILTON, D.L., BURNHAM, C.W. and OSBORN, E.F., 1964.
The solubility of water and effects of oxygen fugacity and water content on crystallization in mafic magmas. J. Petrol., v. 5, part 1, 21-39.

HAMILTON, J., 1977.
Sr isotope and trace element studies of the Great Dyke and Bushveld mafic phase and their relation to early Proterozoic magma genesis in Southern Africa. J. Petrol., v. 18, 24-52.

HARKER, A., 1932.
Metamorphism: A study of the transformation of rock masses. Methuen and Co. Ltd., London. 362p.

HARRIS, D.C. and NICKEL, E.H., 1972.
Pentlandite compositions and associations in some mineral deposits. Can. Mineral., v. 11, 861-877.

HART, S.R. and BROOKS, C., 1974.
Clinopyroxene - matrix partitioning of K, Rb, Cs, Sr and Ba. Geochim. Cosmochim. Acta, v. 38, 1799-1806.

Hart, S.R. and DAVIS, K.E., 1978.
Nickel partitioning between olivine and silicate melt. Earth Planet. Sci. Lett., v. 40, 203-219.

HARTMANN, M., VON and NIELSEN, H., 1968.
$\delta^{34}S$ - Werte in rezentzen Meeressedimenten und ihre deutung am beispiel einiger sediment profile ans der westlichen ostsee. Geol. Rundschau., v. 58, 621-655.

HAUGHTON, D., ROEDER, P.L. and SKINNER, B.J., 1974.
Solubility of sulfur in mafic magmas. Econ. Geol., v. 69, 451-462.

HEALY, G. and SCHOTTMILLER, J.C., 1964.
The chromium oxide-silica system at low oxygen pressures. Trans. Met. Soc. AIMME, v. 230, 420-425.

HELZ, R.T., 1973.
Phase relations of basalts in their melting range at P_{H_2O} = 5kb as a function of oxygen fugacity: part 1, mafic phases. J. Petrol., v. 14, 249-302.

HEMING, R.F. and CARMICHAEL, I.S.E., 1973.
High temperature pumice flows from the Rabaul Caldera, Papua New Guinea. Contrib. Mineral. Petrol. v. 38, 1-20.

HENDERSON, P. and SUDDABY, P., 1971.
The nature and origin of the chrome-spinel of the Rhum Layered Intrusion. Contrib. Mineral. Petrol., v. 33, 21-31.

HESS, G.B., 1972.
Heat and mass transport during crystallization of the Stillwater Complex. Geol. Soc. Am. Mem. 132, 503-520.

HILL, R. and ROEDER, P., 1974.
The crystallization of spinel from basaltic liquid as a fuction of oxygen fugacity. J. Geol., v. 82, 709-729.

HIMMELBERG, G.R. and FORD, A.B., 1976.
Pyroxenes of the Dufek Intrusion, Antarctica. J. Petrol., v. 17, part 2, 219-243.

HIMMELBERG, G.R. and FORD, A.B., 1977.
Iron-titanium oxides of the Dufek Intrusion, Antarctica. Am. Mineral., v. 62, 623-633.

HIRASHIMA, H., TOYODA, H. and YOSHIDA, T., 1974.
Redox equilibria of chromium ions in glass melts, RP_2O_6 (R:Mg, Ca, Ba) with a gas phase. Yogya Kyokai Shi, v. 82, 309-317.

HOLOSTER, W.T. and KAPLAN, I.R., 1966.
Isotope geochemistry of sedimentary sulfates. Chem. Geol., v. 1, 93-135.

HOOVER, J.D., 1978.
Petrologic features of the Skaergaard Marginal Border Group. Carnegi Inst. Wash., Yb. 76. 733-739.

HOSCHEK, Y., 1969.
The stability of staurolite and chloritoid and the significance in metamorphism of pelitic rocks. Contrib. Mineral. Petrol., v. 22, 208-232.

HUEBNER, J.S., LIPIN, B.R. and WIGGENS, L.D., 1976.
Partitioning of chromium between silicate crystals and melts. Proc. 7th Lunar Sci. Conf., 1195-1220.

HUEBNER, J.S. and TURNOCK, A.C., 1980.
The melting relations of 1 bar of pyroxenes composed largely of Ca-Mg- and Fe bearing components. Am. Min., v. 65, 225-271.

HUNTER, D.R., 1975.
The regional geological setting of the Bushveld Complex. (An adjunct to the provisional tectonic map of the Bushveld Complex). Econ. Geol. Res. Unit, Univ. Witwatersrand, Johannesburg, 18p.

HUNTINGTON, H.D., 1979.
Kiglapait mineralogy I: apatite, biotite, and volatiles. J. Petrol., v. 20, 625-652.

HULBERT, L.J. and SHARPE, M.R., 1981.
Stop 1: andalusite-biotite-cordierite-muscovite hornfels, Faugha Ballagh. Third International Platinum Symposium - excursion guidebook, 39-41. ed. Vermaak, C.F. and Von Gruenewaldt, G.

HUMPHREY, W.A., 1910.
The geology of the Rustenburg and Zeerust Bushveld south of Dwarsberg. Dept. of Mines, Geol. Survey of South Africa, Annual Report for 1910, 63-79.

IRVINE, T.N., 1965.
Chromium spinel as a petrogenetic indicator. Part 1, theory. Can. J. Earth Sci., v. 2, 648-671.

IRVINE, T.N., 1967A.
Chromian spinel as a petrogenetic indicator. Part 2, petrological applications. Can. J. Earth Sci., v. 4, 71-103.

IRVINE, T.N., 1967B.
The ultramafic rocks of the Muskox Intrusion, Northwest Territories, Canada, 38-49. In, Wyllie, P.J. (Ed.), Ultramafic and related rocks. John Wiley, New York.

IRVINE, T.N., 1970.
Crystallization sequences in the Muskox Intrusion and other layered intrusions. Part 1, olivine-pyroxene-plagioclase relations. Geol. Soc. S. Afr. Spec. Publ. 1, 441-478.

IRVINE, T.N. and BARAGAR, W.R.A., 1971.
A guide to the classification of common volcanic rocks. Can. J. Earth Sci., v. 8, 523-548.

IRVINE, T.N., 1975.
Crystallization sequences in the Muskox Intrusion and other layered intrusions - II. Origin of chromitite layers and similar deposits of other magmatic ores. Geochim. Cosmochimica Acta, v. 39, 991-1020.

IRVINE, T.N., 1976.
Meta-stable liquid immiscibility and MgO-FeO-SiO_2 fractionation patterns in the system Mg_2SiO_4-Fe_2SiO_4-$CaAl_2Si_2O_6$-SiO_2. Carnegie Inst. Wash., Yb. 75, 597-611.

IRVINE, T.N., 1977.
Chromite crystallization in the join Mg_2SiO_4-$CaMgSi_2O_6$-$CaAl_2Si_2O_8$-$MgCr_2O_4$-SiO_2. Carnegie Inst. Wash., Yb. 76, 465-472.

IRVINE, T.N., 1982.
Terminology for layered intrusions. J. Petrol., v. 23, part 2, 127-162.

ISHII, T., 1975.
The relations between temperature and composition of pigeonite in some lavas and their application to geothermometry. Mineral. J., v. 8, 48-57.

JACKSON, E.D., 1961.
Primary textures and mineral associations in the ultramafic zone of the Stillwater Complex, Montana. U.S. Geol. Surv., Prof. Pap. 358, 106p.

JACKSON, E.D., 1966.
Discussion on a paper by J.A. McDonald, Liquid immiscibility as a factor in chromite seam formation in the Bushveld Igneous Complex. Econ. Geol., v. 61, 777-780.

JACKSON, E.D., 1967.
Ultramafic cumulates in the Stillwater, Great Dyke and Bushveld Intrusions, 20-38. In, Wyllie, P.J. (Ed.), Ultramafic and related rocks. John Wiley, New York.

JACKSON, E.D., 1969.
Chemical variation in coexisting chromite and olivine in the chromitite zones of the Stillwater Complex. Econ. Geol. Monogr. 4, 41-71.

JACKSON, E.D., 1970.
The cyclic units in layered intrusions. A comparison of repetitive stratigraphy in the ultramafic parts of the Stillwater, Muskox, Great Dyke and Bushveld Complexes. Geol. Soc. S. Afr., Spec. Publ. 1, 391-424.

JACKSON, E.D., 1971.
The origin of ultramafic rocks by cumulus processes. Fortschr. Miner., v. 48, 128-174.

JAQUES, A.L. and GREEN, D.H., 1980.
Anhydrous melting of peridotite at 0-15 kb pressure and the genesis of tholeiitic basalts. Contrib. Mineral. Petrol., v. 73, 287-310.

KEAYS, R.R. and CROCKET, J.H., 1970.
A study of precious metals in the Sudbury Nickel Irruptive ores. Econ. Geol., v. 65, 438-450.

KEAYS, R.R. and CAMPBELL, I.H., 1981.
Precious metals in the Jimberlana Intrusion, Western Australia: implications for the genesis of platiniferous ores in layered intrusions. Econ. Geol., v. 76, 1118-1141.

KINGERY, W.D., BOWEN, H.K. and UHLMANN, D.R., 1976.
Introduction to ceramics. John Wiley and Sons, 1032p.

KINLOCH, E.D., 1982.
Regional trends in the platinum group mineralogy of the critical zone of the Bushveld Complex, South Africa. Econ. Geol., v. 77, 1328-1347.

KIRKPATRICK, R.J., 1975.
Crystal growth from the melt: a review. Am. Mineral., v. 60, 798-814.

KOTZE, D.A., 1968.
Mineralogical changes in the magnesite and chrome-magnesite refractories due to variations in the slag composition. M.Sc. thesis (unpublished) Univ. of Pretoria. 56p.

KRETZ, R., 1961.
Some applications of thermodynamics to coexisting minerals of variable composition. Examples: orthopyroxene-clinopyroxene and orthopyroxene-garnet. J. Geol., v. 69, 361-387.

KRETZ, R., 1963.
Distribution of magnesium and iron between orthopyroxene and calcic pyroxene in natural mineral assemblages. J. Geol., v. 71, 773-785.

KRUPARZ, H. and van RENSBURG, W.L., 1965.
The chromite deposits at Nietverdient, Marico district, Transvaal. Ann. Geol. Surv. S. Afr., v. 4, 137-150.

KULLERUD, G. YODER, H.S., 1963.
Sulfide-silicate relations. Carnegie Inst. Wash., Yb. 62, 215-218.

KULLERUD, G., YUND, R.A. and MOH, G.H., 1969.
Phase relations in the Cu-Fe-S and the Cu-Ni-S and Fe-Ni-S system. Econ. Geol. Monogr. 4, 323-343.

KUNO, H., 1950.
Petrology of Hakone volcano and adjacent areas, Japan. Geol. Soc. Am. Bull. 61, 957-1020.

KUSHIRO, I., 1960.
Si-Al relations in clinopyroxenes from igneous rocks. Am. J. Sci., v. 258, 548-554.

KUSHIRO, I., 1969.
The system Forsterite-Diopside-Silica with and without water at high pressure. Am. J. Sci., v. 267A, 295-324.

KYNASTON, H. and MELLOR, E.T., 1905.
On a traverse from Pretoria to Pietersburg. Rept. Geol. Surv. S. Afr. Trans., 11-25.

KYNASTON, H., MELLOR, E.T. and HALL, A.L., 1911.
The geology of the country round Potgietersrus. An explanation of sheet 7, Geol. Survey of South Africa.

LEE, C.A. and SHARPE, M.R., 1979.
Spheroidal pyroxenite aggregates in the Bushveld Complex - a special case of silicate liquid immiscibility. Earth Planet. Sci. Lett., v. 44, 295-310.

LEE, C.A. and SHARPE, M.A., 1980.
Further examples of silicate liquid immiscibility and spherical aggregation in the Bushveld Complex. Earth Planet. Sci. Lett., v. 48, 131-147.

LEE, C.A., 1981.
The Platreef, 26-28. In, Vermaak, C.F and Von Gruenewaldt, G. (Eds.), Third International Platinum Symposium Excursion Guidebook.

LIEBENBERG, W.R., 1942.
The basal rocks of the Bushveld Complex in the Marico district south of Dwarsberg. Trans. Geol. Soc. S. Afr., v. 45, 81-108.

LIEBENBERG, L., 1968.
The sulfides in the layered sequence of the Bushveld Igneous Complex. D.Sc. thesis (unpublished) Univ. Pretoria, 260p.

LIEBENBERG, L., 1970.
The sulfides in the layered sequence of the Bushveld Igneous Complex. Geol. Soc. S. Afr., Spec. Publ. 1, 108-208.

LINDSLEY, D.M., 1964.
Iron-titanium oxides as thermometers and oxygen barometers. Carnegie Inst. Wash., Yb. 63, 60-66.

LINDSLEY, D.H., BROWN, G.M. and MUIR, I.D., 1969.
Conditions of the ferrowollastonite-ferrohedenbergite iversion in the Skaergaard Intrusion, East Greenland, 193-201. In, Papik, J.J. (Ed.). Mineral. Soc. Am., Spec. Paper 2.

LINDSLEY, D.H. and MUNOZ, J.L., 1969.
Subsolidus relations along the join hedenbergite-ferrosilite. Am. J. Sci., v. 267A, 295-324.

LINDSLEY, D.H., 1981.
Some experiments pertaining to the magnetite-ulvöspinel miscibility gap. Am. Mineral., v. 66, 759-762.

LIPMAN, P.W., 1971.
Iron-titanium oxide phenocrysts in compositionally zoned ash-flow sheets from southern Nevada. J. Geol., v. 79, 438-456.

LOFGREN, G., 1974.
An experimental study of plagioclase crystal morphology: isothermal crystallization. Am. J. Sci., v. 274, 243-273.

LOFGREN, G.E. and DONALDSON, C.H., 1975.
Curved branching crystals and differentiation of comb-layered rocks. Contrib. Mineral. Petrol., v. 49, 309-319.

LONGHI, J. and WALKER, D., 1975.
Fe-Mg distribution between olivine and lunar basaltic liquids. EOS, v. 56, 471, (abstract).

LUHR, J. and CARMICHAEL, I.S.E., 1980.
The Colima Volcanic Complex, Mexico I. Post-caldera andesites from Volcán Colima. Contrib. Mineral. Petrol., v. 71, 343-372.

MAALØE, S., 1976.
The zoned plagioclase of the Skaergaard Intrusion, East Greenland. J. Petrol., v. 17, part 3, 398-419.

MacGREGOR, I.D., 1969.
The system $MgO-SiO_2-TiO_2$ and its bearing on the distribution of TiO_2 in basalts. Am. J. Sci., v. 267A, 342-263.

MacLEAN, W.H., 1969.
Liquidus phase relations in the $FeS-FeO-Fe_3O_4-SiO_2$ system, and their application in geology. Econ. Geol., v. 64, 865-884.

MacLEAN, W.H. and SHIMAZAKI, H., 1976.
The partition of Co, Ni, Cu, and Zn between sulfide and silicate liquids. Econ. Geol., v. 71, 1049-1057.

MARAIS, C.L., 1977.
An investigation of the pyroxenite marker and the associated rocks in the main zone of the eastern Bushveld Complex. M.Sc. thesis (unpublished). Univ. Pretoria. 87p.

MARAKUSHEV, A.A., 1979.
Some aspects of ore formation in ultramafics. Mineral. Deposita, v. 14, 81-101.

MARKGRAAFF, J., 1976.
Pyroxenes of the western Bushveld Complex, South Africa. Trans. Geol. Soc. S. Afr., v. 79, 217-224.

MASKE, S., 1966.
The petrology of the Ingeli Mountain Range. Ann. Univ. Stellenbosch, v. 41A, 109p.

MATHISON, C.I., 1975.
Magnetites and ilmenites in the Somerset Dam layered basic Intrusion, Southern Queensland. Lithos, v. 8, 93-111.

MUAN, A. and OSBORNE, E.F., 1956.
Phase equilibria at liquidus temperatures in the system $MgO-FeO-Fe_2O_3-SiO_2$. J. Am. Ceramic Soc., v. 39, 121-140.

MUAN, A., 1957.
Phase equilibrium relationships at liquidus temperatures in the system $FeO-Fe_2O_3-Al_2O_3-SiO_2$. J. Am. Ceramic Soc., v. 40, 420-431.

MAYNARD, J.B., 1980.
Sulfur isotopes of iron sulfides in Devonian-Mississipian shales of the AppalachianBasin: Control by rate of sedimentation. Am. J. Sci., v. 280, 772-786.

McBIRNEY, A. and NOYES, R.M., 1979.
Crystallization and layering of the Skaergaard Intrusion. J. Petrol., v. 20, 487-554.

McCALLUM, I.S., RAEDEKE, L.D. and MATHEZ, E.A., 1980.
Investigations of the Stillwater Complex: Part I. Stratigraphy and structure of the banded zone. Am. J. Sci., v. 280-A, 59-87.

McConnell, R.B., 1974.
Evolution of taphrogenic lineaments in continental platforms. Geol. Rundsch., v. 63, 389-430.

McDONALD, J.A., 1965.
Liquid immiscibility as a factor in chromitite seam formation in the Bushveld Igneous Complex. Econ. Geol., v. 60, 1674-1685.

McDONALD, J.A., 1967A.
Liquid immiscibility in chromitite seam formation. A reply Econ. Geol., v. 62, 288-292.

McDONALD, J.A., 1967B
Evolution of part of the lower critical zone, farm Ruighoek, Western Bushveld. J. Petrol., v. 8, 165-209.

McLAREN, C.H. and De VILLIERS, J.P.R., 1982.
The platinum-group chemistry and mineralogy of the UG-2 chromitite layer of the Bushveld Complex. Econ. Geol., v. 77, 1348-1366.

McSWEEN, H.Y. and NYSTROM, P.G., 1979.
Mineralogy and petrology of the Dutchmans Creek gabbroic Intrusion, South Carolina. Am. Mineral., v. 64, 531-545.

MEDARIS, L.G., 1972.
High-pressure peridotites in South Western Oregon. Bull. Geol. Soc. Am., v. 83, 41-58.

MERWE, M.J., van der, 1976.
The layered sequence of the Potgietersrus limb of the Bushveld Complex. Econ. Geol., v. 71, no. 7, 1337-1352.

MERWE, M.J., van der, 1978.
The geology of the basic and ultramafic rocks of the Potgietersrus limb of the Bushveld Complex. Ph.D. thesis (unpublished) University of the Witwatersrand, Johannesburg. 176p.

MOLENGRAAFF, G.A.F., 1901.
Géologie de la Republique Sud-Africaine du Transvaal. Bull. Soc. Geol. de France, 4 Sēr Tome 1, 13-92.

MOLYNEUX, T.G., 1970.
A geological investigation of the Bushveld Complex in Sekhukhuneland and part of the Steelpoort Valley, Eastern Transvaal, with particular reference to the oxide minerals. D.Sc. thesis (unpublished) Univ. of Pretoria. 125p.

MORSE, S.A., 1969.
The Kiglapait Layered Intrusion, Labrador. Geol. Soc. Am., Mem. 112. 204p.

MORSE, S.A., 1980A.
Basalts and phase diagrams. An introduction to the quantitative use of phase diagrams in igneous petrology. Springer-Verlag, New York. 493p.

MORSE, S.A., LINDSLEY, D.H. and WILLIAMS, R.J., 1980B.
Concerning intensive parameters in the Skaergaard Intrusion. Am. J. Sci., v. 180, 159-170.

MORSE, S.A., 1980C.
Kiglapait mineralogy II: Fe-Ti oxide minerals and the activities of oxygen and silica. J. Petrol., v. 21, part 4, 685-719.

MUIR, I.D., 1954.
Crystallization of pyroxenes in a iron-rich diabase from Minnesota. Mineral. Mag., v. 30, 376-388.

NALDRETT, A.J., BRAY, G., GASPARRINI, E.L., PODOLSKY, T., and RUCKLEDGE, J.C., 1970.
Cryptic variation and the petrology of the Sudbury Nickel Irruptive. Econ. Geol., v. 65, 122-155.

NALDRETT, A.J. and CABRI, L.J., 1976.
Ultramafic and related mafic rocks. Their classification and genesis with special reference to the concentration of nickel sulfides and platinum group elements. Econ. Geol., v. 71, 1131-1158.

NALDRETT, A.J., 1979.
Partitioning of Fe, Co, Ni and Cu between sulfide liquid and basaltic melts and the composition of Ni-Cu sulfide deposits. A reply and further discussion. Econ. Geol., v. 74, 1517-1520.

NALDRETT, A.J., 1981.
Platinum group element deposits - a review, 197-233. In, Cabri, L.J., Platinum-Group Elements: mineralogy, geology, recovery. Can. Inst. Min. Met., special v. 23.

NAKAMURA, V. and KUSHIRO, I., 1970.
Equilibrium relations of hypersthene and pigeonite and augite in crystallizing magmas: microprobe study of a pigeonite andesite from Weiselberg, Germany. Am. Mineral., v. 55, 1999-2015.

NATHAN, H.D. and KIRK, C.K.,van, 1978.
A model of magmatic crystallization. J. Petrol., v. 19, part 1, 66-94.

NELSON, S.A., 1979.
The geology and petrology of Volcán Ceboruco, Nayarite, Mexico. Ph.D. thesis (unpublished). University of California, Berkely. 164p.

NEUMANN, E.R., 1974.
The distribution of Mn^{2+} and Fe^{2+} between ilmenites and magnetites in igneous rocks. Am. J. Sci., v. 274, 1074-1088.

NICHOLLS, J., CARMICHAEL, I.S.E. and STORMER, J., 1971.
Silica activity and Ptotal in igneous rocks. Contrib. Mineral Petrol., v. 33, 1-20.

NIELSEN, H., 1979.
Sulfur isotopes, 283-313. In, Jäger, E. (Ed.), Lectures in isotope geochemistry. Springer Verlag, Berlin.

NORDLIE, B.E., 1971.
The composition of the magmatic gas of Kilauea and its behaviour in the near surface environment. Am. J. Sci., v. 271, 417-463.

NORRISH, K. and HUTTON, J.J., 1969.
An accurate x-ray spectrographic method for analysis of a wide range of geological samples. Geochim. Cosmochim. Acta, v. 33, 431-453.

NWE, YIN YIN and COPLEY, P.A., 1975.
Chemistry, subsolidus relations and electron petrography of pyroxenes from the late stage ferrodiorites of the Skaergaard Intrusion, East Greenland. Contrib. Mineral. Petrol., v. 53, 37-54.

O'HARA, M.J., 1967.
Mineral facies in ultrabasic rocks 7-17. In, Wyllie, P.J. (Ed.), Ultramafic and related rocks. John Wiley, New York.

O'HARA, M.J., SAUNDER, M.J. and MERCY, E.L.P., 1975.
Garnet peridotite primary ultrabasic magma and eclogite; interpretation of upper mantle processes in Kimberlites. Physics and chemistry of the earth, v. 9, 571-604.

ORVILLE, P.M., 1972.
Plagioclase cation exchange equilibria with aqueous chloride solution: results at 700°C and 2000 bars in the presence of quartz. Am. J. Sci., v. 272, 234-272.

OSBORN, E.F. and WATSON, E.B., 1977.
Studies of phase relations in subalkaline volcanic rock series. Carnegie Inst. Wash., Yb. 76, 472-478.

OSBORN, E.F., 1978.
Changes in phase relations in response to change in pressure from 1 atm to 10kb for the system Mg_2SiO_4-Iron Oxide-$CaAl_2SiO_8$-SiO_2. Carnegie Inst. Wash., Yb. 77, 784-790.

PAGE, N.J., 1971.
Comments on the role of oxygen fugacity in the formation of immiscible sulfide liquids in the H chromitite zone of the Stillwater Complex, Montana. Econ. Geol., v. 66, 607-610.

PAGE, N.J., 1979.
Stillwater Complex, Montana - structure, mineralogy and petrology of the basal zone with emphasis on the occurrence of sulfides. U.S. Geol. Surv., Prof. Pap. 1038, 39-61.

PEARCE, J.A. and NORRY, M.J., 1979.
Petrogenetic implications of Ti, Zr, Y, and Nb variations in volcanic rocks. Contrib. Mineral Petrol., v. 69, 33-47.

PECK, D.L. and WRIGHT, T.L., 1966.
Experimental studies of molten basalt in situ: a summary of physical and chemical measurements on recent lava lakes on Kilauea volcanoe, Hawaii. Geol. Soc. Amer., Abs., 101, 158.

PHILPOTTS, J.A. and SCHNETZLER, C.C., 1970.
Phenocryst-matrix partition coefficients for K, Rb, Sr, and Ba with application to anorthosite and basalt genesis. Geochim. Cosmochim. Acta, v. 34, 307-322.

POWELL, M. and POWELL, R., 1974.
An olivine-clinopyroxene geothermometer. Contrib. Mineral. Petrol., v. 48, 249-263.

POWELL, R. and POWELL, M., 1977.
Geothermometry and oxygen barometry using coexisting iron-titanium oxides: a reappraisal. Mineral. Mag., v. 41, 257-263.

POWELL, R., 1978.
Equilibrium thermodynamics in petrology, an introduction. Harper and Row, London, 284p.

PRICE, G.D., 1981.
Subsolidus phase relations in the titanomagnetite solid solution series. Am. Mineral., v. 66, 751-758.

READ, H.H., SADASHIVAIAH, M.S. and HAQ, B.T., 1961.
The hypersthene gabbro of the Insch Complex, Aberdeenshire. Proc. Geol. Ass., v. 76, 1-11.

REES, C.E., 1978.
Sulfur isotope measurements using SO_2 and SF_6. Geochim. Cosmochim. Acta, v. 42, 383-389.

RILEY, J.F., 1977.
The pentlandite group $(Fe, Ni, Co)_9S_8$: new data and an appraisal of structure-composition relationships. Mineral. Mag., v. 41, 345-349.

RIPLEY, E.M., 1979.
Sulfide petrology of basal chilled margins in layered sills of the Archean Deer Lake Complex, Minnesota. Contrib. Mineral. Petrol., v. 69, 345-354.

ROEDER, P.L. and OSBORN, E.F., 1966
Experimental data for the system MgO-FeO-Fe_2O_3-$CaAl_2Si_2O_8$-SiO_2 and their petrological implications. Am. J. Sci., v. 264, 428-480.

ROEDER, P.L. and EMSLIE, R.F., 1970.
Olivine-liquid equilibrium. Contrib. Mineral. Petrol., v. 29, 275-289.

ROEDER, P.L., 1974.
Activity of iron and olivine solubility in basaltic liquids. Earth Planet. Sci. Lett., v. 23, 397-410.

ROEDER, P.L., CAMPBELL, I.H. and JAMIESON, H.E., 1979.
A re-evaluation of the olivine spinel geothermometer. Contrib. Mineral. Petrol., v. 68, 325-334.

ROEX, A.P., LE ERLANK, A.J. and NEEDHAM, H.D., 1981.
Geochemical and mineralogical evidence for the occurrence of at least three distinct magma types in the "Famous" region. Contrib. Mineral. Petrol., v. 77, 24-37.

RONOV, A.B., GRINENKO, V.A., GIRIN, Yu.P., SARINA, L.J., KAZAKOV, G.A. and GRINENKO, L.N., 1974.
Effects of tectonic conditions on the concentration and isotope composition of sulfur in sediments. Geochem. Intern., v. 11, 1246-1272.

ROOYEN, D.P., van, 1950.
The metamorphic rocks constituting the floor of the Bushveld Igneous Complex north of Potgietersrus. Trans. Geol. Soc. S. Afr., v. L111, 65-71.

ROSS, M. and HUEBNER, S., 1975.
Estimation of the minimum temperature for coexist of orthopyroxene, pigeonite, and augite and its application to prediction of temepratures of crystallization of lunar pyroxenes. Proc. of 6th Lunar Sci. Conf., 689-691.

SACK, R.O., CARMICHAEL, I.S.E., RIVERS, M. and GHIORSO, M.S., 1980.
Ferric-ferrous equilibria in natural silicate liquids at 1 bar. Contrib. Mineral. Petrol., v. 75, 369-376.

SATO, M. and WRIGHT, T.L., 1966.
Oxygen fugacities directly measured in volcanic gases. Science, v. 153, 1103-1105.

SATO, M. and VALENZA, M., 1980.
Oxygen fugacity of the layered series of the Skaergaard Intrusion, East Greenland. Am. J. Sci., v. 280-A, 134-158.

SCHMID, R. and WOOD, B.J., 1976.
Phase relationships in granulitic metapelites from the Ivreaverbans Zone (Northern Italy). Contrib. Mineral. Petrol., v. 54, 255-279.

SCHNEIDER, A., 1970.
The sulfur isotope composition of basaltic rocks. Contrib. Mineral. Petrol., v. 25, 95-124.

SCHREIBER, H.D. and HASKINS, L.A., 1976.
Chromium in basalts: experimental determinations of redox states and partitioning among synthetic silicate phases. Proc. 7th Lunar Sci. conf., 1221-1259.

SCHWARZ, H.P. and BURNIE, S.W., 1973.
Influence of sedimentary environments on sulfur isotope ratios in clastic rocks, a review. Mineral Deposita, v. 8, 264-277.

SCOTT, S.D., 1974.
The Fe-S system. Mineral. Soc. Am. Short Course Notes. CS21-CS41.

SHARPE, M.R., 1978.
Cone-type diabases from the Eastern Transvaal - representatives of a quenched magma. Trans. Geol. Soc. S. Afr., v. 81, 373-378.

SHARPE, M.R., 1980.
Evolution of the Bushveld magma chambers. Inst. for Geol. Res. Bushveld Complex, Univ. Pretoria, Res. Rept. 20, 57p.

SHARPE, M.R. and SNYMAN, J.A., 1980.
A model for the emplacement of the eastern compartment of the Bushveld Complex. Techtonophysics, v. 65, 85-110.

SHARPE, M.R., 1981.
The chronology of magma influxes to the eastern compartment of the Bushveld Complex as exemplified by its marginal border groups. J. Geol. Soc. London, v. 138, 307-326.

SHARPE, M.R. and CHADWICK, B., 1981.
The geometry and origina of structures in certain Transvaal Sequence rocks within and adjacent to the eastern compartment of the Bushveld Complex. Inst. Geol. Res. Bushveld Complex, Univ. Pretoria, Res. Rept. 27, 19p.

SHARPE, M., 1982A.
Noble metals in the marginal rocks of the Bushveld Complex. Econ. Geol., v. 77, 1286-1295.

SHARPE, M.R., 1982B.
The floor contact of the eastern Bushveld Complex: field relations and petrography. Inst. Geol. Res. Bushveld Complex. Univ. Pretoria, Res. Dept. 36, 43p.

SHARPE, M.R. and HULBERT, L.J., 1982.
Ultramafic sills from the eastern Bushveld Complex - evidence for peridotitic liquids. Inst. Geol. Res. Bushveld Complex, Univ. Pretoria, Res. Rept. 33, 40p.

SHAW, H.R., 1965.
Comments on viscosity, crystal settling and convection in granitic magmas. Am. J. Sci., v. 263, 120-152.

SINTON, J.M., 1977.
Equilibrium history of the basal alpine-type peridotite, Red Mountain, New Zealand. J. Petrol., v. 18, 216-246.

SMIT, P.J., HALES, A.L. and GOUGH, D.I., 1962.
The gravity survey of the Republic of South Africa. Geol. Surv. S. Afr., Handbook 6, 422p.

SNETHLAGE, R. and VON GRUENEWALDT, G., 1977.
Oxygen fugacity and its bearing on the origin of chromitite layers in the Bushveld Complex, 352-370. In, Klemm, D.D. and Schneider, H.J. (Eds.), Time and stratabound ore deposits. Springer-Verlag, Berlin.

SNETHLAGE, R. and KLEMM, D.D., 1978.
Intrinsic oxygen fugacity measurements on chromites from the Bushveld Complex and their petrogenetic significance. Contrib. Mineral. Petrol., v. 67, 127-138.

SPANGENBERG, K., 1943.
Die chromitlagerstätte von Tampadel in Zobten. Z. Prakt. Geol., v. 51, 13-35.

SPIEDEL, D.H. and OSBORN, E.F., 1967.
Element distribution among coexisting phases in the system $MgO-FeO-Fe_2O_3-SiO_2$ as a function of temperatures and oxygen fugacity. Am. Mineral. v. 52, 1139-1152.

SPRY, A., 1969.
Metamorphic textures. Pergamon Press, New York. 350p.

STRECKEISEN, A., 1967.
Classification and nomenclature of igneous rocks. N. Jb. Mineral., Abh., v. 107, 144-240.

TAYLOR, S.R., 1975.
Lunar science: a post Apollo view, Pergamon Elmsford, New York. 372p.

THODE, H.G. and REES, C.E., 1971.
Measurements of sulfur concentrations and the isotope ratios $^{33}S/^{32}S$, $^{34}S/^{32}S$ and $^{36}S/^{32}S$ in Apollo 12 samples. Earth Planet. Sci. Lett., v. 12, 434-438.

THOMPSON, R.N., 1975.
The 1 atmosphere liquidus oxygen fugacities of some tholeiitic, intermediate, alkalic and ultra-alkalic lavas. Am. J. Sci., v. 275, 1049-1072.

THOMPSON, A.B., 1976B.
Mineral reactions in pelitic rocks: II. Calculations of some P-T-X (Fe-Mg) phase relations. Am. J. Sci., v. 276, 425-454.

TOULMIN, P. and BARTON, P.B., 1964.
A thermodynamic study of pyrite and pyrrhotite. Geochim. Cosmochim. Acta, v. 28, 641-671.

TRUTER, F.C., 1947.
A remarkable transcurrent fault near Potgietersrus, Transvaal. Trans. Geol. Soc. S. Afr., V.L., 1-15.

TSAI, H.M., SHIEH, Y. and MEYER, H.O.A., 1979.
Mineralogy and $S^{34/32}$ratios of sulfides associated with kimberlites, xenoliths, and diamonds, 87-103. In, Boyd, F.R. and Meyer, H.O.A., The mantle sample: inclusions in kimberlites and other volcanics.

TSUSUE, A., 1973.
The distribution of manganese and iron between ilmenite and granitic magma in the Osumi Peninsula, Japan. Contrib. Mineral. Petrol., v. 40, 305-312.

ULMER, G.C., 1969.
Experimental investigation of chromite spinels. Econ. Geol. Monogr. 4, 114-131.

VERMAAK, C.F., 1970.
The geology of the lower portion of the Bushveld Complex and its relationship to the floor rocks in the area west of the Pilansburg, Western Transvaal. Geol. Soc. S. Afr., Spec. Publ. 1, 242-265.

VERMAARK, C.F., 1976.
The Merensky Reef - thoughts on its environment and genesis. Econ. Geol., v. 71, 1270-1298.

VERMAAK, C.F. and HENDRIKS, L.P., 1976.
A review of the mineralogy of the Merensky Reef, with specific reference to new data on the precious metal mineralogy. Econ. Geol., v. 71, 1244-1269.

VILLIERS, J.S., DE, 1967.
The geology of the area south of Potgietersrus, with special reference to the chromite deposits. Ph.D. thesis (unpublished), Univ. of the Witwatersrand, Johannesburg, 124p.

VILLIERS, J.S., DE, 1970.
The structure and petrology of the mafic rocks of the Bushveld Complex south of Potgietersrus. Geol. Soc. S. Afr. Spec. Publ. 1, 23-35.

VINCENT, E.A., 1960.
Ulvöspinel in the Skaergaard Intrusion, Greenland. Neues. Jb. Mineral. Abh. 94, 993-1016.

VINOGRADOV, A.P., GRINENKO, V.A. and USTINOV, V.I., 1962.
Isotopic composition of sulfur compounds in the Black Sea. Geochem. Intern., v. 10, 973-997.

WAAL, S.A., DE and VILJOEN, E.A., 1975.
An electron-microprobe study of the nickel distribution in a serpentinite from Volspruit, Potgietersrus. Nat. Inst. Metall., Rept. 845, 15p.

WAAL, S.A., DE, 1977.
Carbon dioxide and water from metamorphic reactions as agents for sulfide and spinel precipitation in mafic magmas. Trans.Geol. Soc. S. Afr., v. 80, 193-196.

WAGER, L.R., VINCENT, E.A. and SMALES, A.A., 1957.
Sulfides in the Skaergaard Intrusion, East Greenland. Econ. Geol., v. 52, 856-895.

WAGER, L.R., BROWN, G.M. and WADSWORTH, W.J., 1960.
Types of igneous cumulates. J. Petrol., v. 1, 73-85.

WAGER, L.R. and BROWN, G.M., 1968.
Layered igneous rocks. Oliver and Boyd, Edinburgh and London. 588p.

WAGNER, P.A., 1929.
The platinum deposits and mines of South Africa. Oliver and Boyd, Edinburgh. 338p.

WALKER, K.R., 1969A.
A mineralogical, petrological and geochemical investigation of the Palisades Sill, New Jersey. Geol. Soc. Amer., Mem. 115, 175-187.

WALKER, K.R., 1969B.
The Pallisades Sill, New Jersey: a reinvestigation. Geol. Soc. Am., Spec. Pap. 111.

WALKER, K.R., WARE, N.G. and LOVERING, J.R., 1973.
Compositional variations in pyroxenes of the differentiated Palisade Sill, New Jersey. Geol. Soc. Am., v. 84, 89-110.

WALKER, D., KIRKPATRICK, R.J., LONGHI, J. and HAYS, J.F., 1976.
Crystallization history of Lunar picritic basalt sample 12002: phase-equilibria and cooling-rate studies. Bull. Geol. Soc. Am., v. 87, 646-656.

WATSON, E.B., 1976.
Two-liquid partition coefficients: experimental data and geochemical implications. Contrib. Mineral. Petrol., v. 56, 119-134.

WELLS, P.R.A., 1977.
Pyroxene thermometry in simple and complex systems. Contrib. Mineral. Petrol., v. 62, 129-139.

WEISER, T., 1966.
Geochemische untersuchungen an chromites mit det elektron en mikrosoude. Ph.D. thesis. Ludwig-Maximilians Universitat, München.

WILLIAMS, R.J., 1971A.
Reaction constants in the system FeO-MgO-SiO_2-O_2 at 1 atm between 900 and 1300°C: experimental results. Am. J. Sci., v. 270, 334-360.

WILLIAMS, R.J., 1971B.
Reaction constants in the system FeO-MgO-SiO_2-O_2 : intensive parameters in the Skaergaard Intrusion, East Greenland. Am. J. Sci., v. 271, 132-146.

WILSHIRE, H.G., 1967.
The Prospect alkaline diabase picrite intrusion, New South Wales, Australia. J. Petrol., v. 8, 97-163.

WONES, D.R. and DODGE, F.C.W., 1977.
The stability of phlogopite in the presence of quartz and diopside, 229-246. In, Fraser, D.G. (Ed.), Thermodynamics in geology. D. Reidel Publishing Co., Holland.

WOOD, B.J. and BANNO, S., 1973.
Garnet-orthopyroxene and orthopyroxene-clinopyroxene relationships in simple and complex systems. Contrib. Mineral. Petrol., v. 42, 109-124.

WOOD, B.J. and FRASER, D.G., 1976.
Elementary thermodynamics for geologists. Oxford University Press. 303p.

WORST, B.G., 1960.
The Great Dyke of Southern Rhodesia. Bull, Geol. Surv. S. Rhodesia, v. 47, 234p.

WRIGHT, T.L. and WEIBIEN, P.W., 1968.
Mineral compositions and paragenesis in tholeiitic basalt from Makuopuhi lava lake, Hawaii. Geol. Soc. Amer., Spec. Pap. 115, 242-243.

ZUBOKOV, S.M. and YUSUPOVA, E.M., 1964.
Refractories - a translation of Ogneupory, 28-33.

APPENDIX 1

MICROPROBE ANALYSES OF PYROXENES (SUBSOLIDUS COMPOSITIONS)

	Upper Zone							Main Zone				
Sample #	5-124A	5-124B	5-138A	5-195A	5-233A	5-233B	5-233C	5-315A	5-410A	5-440A	5-616A	5-640A	5-640B
SiO_2	51,07	49,77	52,20	51,12	51,76	50,50	50,76	50,90	51,71	50,01	50,68	51,03	50,38
Al_2O_3	1,05	0,63	0,41	1,80	1,30	0,65	1,20	2,18	1,54	1,66	2,28	1,96	0,64
TiO_2	0,47	0,30	0,21	0,56	0,47	0,30	0,37	0,58	0,45	0,46	0,77	0,65	0,42
MgO	11,22	15,01	11,33	10,66	10,67	16,31	11,74	11,47	12,83	10,76	12,26	13,06	19,68
FeO*	15,58	31,64	14,54	13,51	14,16	31,11	14,34	13,46	12,05	13,42	13,03	13,23	27,50
MnO	0,44	0,76	0,22	0,37	0,44	0,64	0,35	0,32	0,30	0,40	0,34	0,34	0,46
NiO	0,09	N.d.	0,05	0,09	0,06	0,08	0,06	N.d.	N.d.	N.d.	0,08	0,07	0,08
CaO	19,91	1,59	21,41	20,74	20,37	0,88	20,73	21,02	21,03	22,04	19,58	18,23	0,85
Na_2O	0,28	0,07	0,11	0,21	0,24	0,07	0,15	0,15	0,20	0,22	0,32	0,32	0,08
K_2O	0,06	0,05	0,04	0,04	0,05	0,06	0,05	0,04	0,06	0,05	0,05	0,04	0,05
Cr_2O_3	0,07	0,05	0,08	0,06	0,09	0,05	0,08	0,07	0,09	0,09	0,13	0,10	0,05
Total	100,24	99,95	100,60	99,16	99,61	100,65	99,83	100,19	100,26	99,11	99,53	99,03	100,19

CATIONS BASED ON 6 OXYGENS

Si	1,956	1,958	1,984	1,962	1,979	1,959	1,945	1,934	1,950	1,933	1,929	1,945	1,932
Al^{iv}	0,044	0,029	0,016	0,038	0,021	0,029	0,054	0,066	0,050	0,067	0,071	0,055	0,028
Al^{vi}	0,003	0,000	0,002	0,043	0,037	0,000	0,000	0,032	0,018	0,009	0,031	0,033	0,000
Ti	0,013	0,008	0,006	0,016	0,013	0,008	0,001	0,017	0,013	0,013	0,022	0,018	0,012
Mg	0,640	0,880	0,642	0,610	0,608	0,943	0,670	0,649	0,721	0,620	0,695	0,742	1,125
Fe^{2+}	0,479	1,041	0,462	0,434	0,452	1,009	0,459	0,428	0,380	0,434	0,414	0,421	0,882
Mn	0,014	0,025	0,007	0,012	0,014	0,021	0,011	0,010	0,010	0,013	0,010	0,010	0,014
Ni	0,002	N.d.	0,002	0,003	0,001	0,002	0,001	N.d.	N.d.	N.d.	0,002	0,002	0,002
Ca	0,817	0,067	0,872	0,853	0,834	0,036	0,851	0,856	0,850	0,913	0,799	0,744	0,034
Na	0,020	0,005	0,008	0,016	0,017	0,005	0,011	0,011	0,015	0,016	0,023	0,023	0,006
K	0,002	0,002	0,002	0,002	0,002	0,003	0,002	0,002	0,003	0,002	0,002	0,002	0,002
Cr^{3+}	0,002	0,001	0,002	0,002	0,002	0,001	0,002	0,002	0,003	0,003	0,004	0,003	0,001
ε	4,012	4,020	4,005	3,991	3,980	4,016	4,007	4,008	4,013	4,023	4,002	3,998	4,038

ATOM PER CENT

Mg	32,71	44,26	32,48	32,15	32,10	47,43	33,83	33,57	36,95	31,52	36,42	38,90	55,12
Fe	25,51	52,36	23,38	22,87	23,86	50,75	23,18	22,14	19,47	22,06	21,69	22,07	43,21
Ca	41,76	3,37	44,12	44,96	44,03	1,81	42,97	44,28	43,56	46,41	41,87	39,01	1,66

* TOTAL IRON AS FeO

N.d. = NOT DETERMINED

MICROPROBE ANALYSES OF PYROXENES (SUBSOLIDUS COMPOSITIONS)

	Main Zone												
Sample #	5-640C	5-935A	5-935B	5-935C	5-1100A	5-1100B	5-1100C	5-1300A	78-127A	78-127B	78-125A	78-125B	78-125C
SiO_2	51,54	50,23	50,84	52,00	51,90	51,46	51,86	50,39	51,12	52,39	50,52	51,72	51,54
Al_2O_3	1,17	1,81	0,73	1,30	1,47	0,69	1,24	1,47	1,88	1,04	1,73	0,62	1,11
TiO_2	0,59	0,59	0,31	0,55	0,68	0,42	0,74	0,71	0,58	0,38	0,79	0,42	0,48
MgO	13,31	12,95	19,81	12,37	12,77	19,94	13,41	12,71	14,54	23,31	13,19	20,02	13,10
FeO*	12,50	11,69	26,94	10,82	10,87	24,74	11,15	11,49	10,33	20,82	12,65	26,24	11,98
MnO	0,35	0,41	0,60	0,31	0,32	0,53	0,29	0,37	0,19	0,61	0,36	0,39	0,26
NiO	0,05	0,07	0,06	0,04	0,08	0,07	0,07	0,07	0,09	0,07	0,09	0,05	0,06
CaO	19,31	21,66	1,16	21,16	20,80	1,08	20,76	20,90	19,84	1,81	19,00	0,98	19,52
Na_2O	0,20	0,34	0,07	0,30	0,33	0,06	0,25	0,24	0,32	0,07	0,34	0,05	0,28
K_2O	0,04	0,05	0,06	0,05	0,05	0,05	0,05	0,06	0,04	0,05	0,05	0,04	0,04
Cr_2O_3	0,08	0,12	0,04	0,05	0,07	0,07	0,07	0,06	0,19	0,09	0,12	0,05	0,12
Total	99,14	99,92	100,62	99,95	99,34	99,11	99,89	98,47	99,12	100,64	98,84	100,53	98,49
CATIONS BASED ON 6 OXYGENS													
Si	1,961	1,911	1,937	1,975	1,963	1,966	1,954	1,937	1,931	1,939	1,933	1,957	1,970
Al^{iv}	0,039	0,081	0,033	0,025	0,037	0,031	0,046	0,063	0,069	0,045	0,067	0,027	0,030
Al^{vi}	0,013	0,000	0,000	0,033	0,028	0,000	0,009	0,004	0,014	0,000	0,011	0,000	0,020
Ti	0,016	0,017	0,009	0,016	0,019	0,012	0,020	0,021	0,016	0,010	0,022	0,011	0,013
Mg_{2+}	0,754	0,734	1,125	0,700	0,719	1,135	0,753	0,728	0,818	1,286	0,752	1,129	0,746
Fe^{2+}	0,397	0,372	0,859	0,344	0,343	0,790	0,351	0,369	0,326	0,644	0,404	0,830	0,383
Mn	0,011	0,013	0,019	0,010	0,010	0,017	0,009	0,012	0,006	0,019	0,011	0,012	0,008
Ni	0,001	0,002	0,002	0,001	0,002	0,002	0,002	0,002	0,003	0,002	0,002	0,001	0,002
Ca	0,787	0,883	0,047	0,861	0,843	0,044	0,838	0,861	0,803	0,071	0,779	0,039	0,799
Na	0,014	0,025	0,005	0,022	0,024	0,004	0,018	0,018	0,023	0,005	0,025	0,003	0,020
K	0,002	0,002	0,003	0,002	0,002	0,002	0,002	0,003	0,002	0,002	0,002	0,002	0,002
Cr^{3+}	0,002	0,004	0,001	0,001	0,002	0,002	0,002	0,002	0,005	0,002	0,003	0,001	0,003
ε	3,997	4,044	4,040	3,990	3,992	4,005	4,004	4,020	4,016	4,025	4,011	4,012	3,996
ATOM PER CENT													
Mg	38,90	36,90	55,39	36,74	37,74	57,64	38,77	37,18	42,01	64,26	38,86	56,50	38,69
Fe	20,48	18,70	42,29	18,05	18,00	40,12	18,07	18,84	16,74	32,18	20,87	41,54	19,86
Ca	40,60	44,39	2,31	45,19	44,25	2,23	43,15	43,97	41,24	3,54	40,25	1,95	41,44

* TOTAL IRON AS FeO

MICROPROBE ANALYSES OF PYROXENES (SUBSOLIDUS COMPOSITIONS)

	Main Zone												
Sample #	78-122A	78-122B	78-122C	78-350A	78-350B	78-192A	78-192B	78-192C	78-189A	78-189B	78-189C	78-207A	78-207B
SiO_2	51,59	51,35	51,83	50,23	51,87	52,54	51,73	51,42	51,37	52,49	52,00	52,37	52,50
Al_2O_3	1,46	0,83	0,71	1,63	0,77	1,37	0,75	0,95	1,43	0,78	0,79	1,55	0,74
TiO_2	0,76	0,41	0,45	0,76	0,45	0,48	0,40	0,41	0,66	0,48	0,44	0,71	0,38
MgO	13,78	21,05	21,49	13,78	21,02	14,40	22,67	23,01	13,96	22,88	23,61	16,35	25,54
FeO*	10,45	24,45	23,77	10,37	22,96	9,63	21,44	21,06	9,86	22,29	21,84	9,45	19,41
MnO	0,27	0,52	0,66	0,30	0,55	0,40	0,28	0,32	0,43	0,37	0,45	0,27	0,55
NiO	0,07	0,06	0,07	0,10	0,07	0,08	0,11	0,06	0,06	0,09	0,07	0,07	0,07
CaO	20,54	1,88	1,74	21,26	1,59	20,32	1,61	1,54	21,12	1,03	1,03	20,52	1,61
Na_2O	0,29	0,10	0,06	0,31	0,05	0,19	0,06	0,07	0,12	0,06	0,05	0,31	0,06
K_2O	0,05	0,05	0,05	0,06	0,04	0,03	0,05	0,05	0,06	0,05	0,04	0,04	0,05
Cr_2O_3	0,08	0,04	0,07	0,15	0,13	0,12	0,09	0,10	0,04	0,05	0,05	0,16	0,18
Total	99,34	100,74	100,84	98,95	99,50	99,56	99,19	98,99	99,11	100,51	100,37	100,80	101,09
CATIONS BASED ON 6 OXYGENS													
Si	1,948	1,934	1,942	1,915	1,960	1,967	1,947	1,937	1,944	1,950	1,935	1,907	1,923
Al^{iv}	0,052	0,036	0,031	0,073	0,034	0,033	0,032	0,042	0,056	0,034	0,034	0,067	0,031
Al^{vi}	0,012	0,000	0,000	0,000	0,000	0,027	0,000	0,000	0,007	0,000	0,000	0,000	0,000
Ti	0,021	0,011	0,012	0,021	0,012	0,013	0,011	0,011	0,018	0,013	0,012	0,020	0,010
Mg	0,775	1,180	1,200	0,783	1,183	0,803	1,272	1,292	0,787	1,267	1,309	0,904	1,395
Fe^{2+}	0,330	0,770	0,745	0,330	0,725	0,301	0,675	0,663	0,312	0,692	0,679	0,293	0,594
Mn	0,008	0,016	0,020	0,009	0,017	0,012	0,008	0,010	0,013	0,011	0,014	0,008	0,017
Ni	0,002	0,002	0,002	0,003	0,002	0,002	0,003	0,002	0,002	0,002	0,002	0,002	0,002
Ca	0,831	0,075	0,069	0,868	0,064	0,815	0,064	0,062	0,856	0,041	0,041	0,816	0,063
Na	0,021	0,007	0,004	0,002	0,003	0,013	0,004	0,005	0,008	0,004	0,003	0,022	0,004
K	0,002	0,002	0,002	0,003	0,002	0,001	0,002	0,002	0,003	0,002	0,002	0,002	0,002
Cr^{3+}	0,002	0,001	0,002	0,004	0,004	0,003	0,002	0,003	0,001	0,001	0,001	0,004	0,005
ε	4,004	4,034	4,029	4,011	4,006	3,990	4,020	4,029	4,007	4,017	4,032	4,045	4,050
ATOM PER CENT													
Mg	40,03	58,27	59,58	39,52	59,98	41,79	63,25	64,05	40,07	63,35	64,51	44,90	67,98
Fe	17,04	38,02	36,99	16,65	36,76	15,68	33,56	32,87	15,88	34,60	33,46	14,55	28,94
Ca	42,92	3,70	3,42	43,81	3,24	42,47	3,18	3,07	43,58	2,05	2,02	40,53	3,07

* TOTAL IRON AS FeO

MICROPROBE ANALYSES OF PYROXENES (SUBSOLIDUS COMPOSITIONS)

	Main Zone					Critical Zone							
Sample #	78-76B-A	78-76B-B	78-92A	78-92B	78-92C	78-145A	78-145B	78-60A	78-128D-A	78-128D-B	78-128D-C	78-481A	78-481B
SiO_2	51,96	52,94	51,30	51,79	51,45	52,00	52,63	54,29	50,99	51,31	51,05	53,96	53,17
Al_2O_3	1,72	0,79	1,38	0,68	0,69	1,75	0,79	1,29	1,60	0,65	0,91	0,44	1,12
TiO_2	0,68	0,41	0,51	0,44	0,54	0,60	0,43	0,27	0,62	0,40	0,26	0,20	0,43
MgO	14,68	23,73	14,85	23,57	23,72	15,80	25,25	27,53	14,09	19,88	21,33	16,45	27,43
FeO*	9,18	19,77	9,57	22,42	21,59	9,08	17,71	13,53	11,13	24,69	23,02	4,69	14,94
MnO	0,18	0,48	0,33	0,46	0,47	0,30	0,55	0,38	0,24	0,51	0,48	0,25	0,42
NiO	0,11	0,09	0,06	0,09	0,08	0,07	0,09	0,10	0,07	0,07	0,09	0,05	0,06
CaO	20,53	1,84	20,61	1,00	1,29	20,97	1,26	1,65	20,63	1,17	1,71	23,94	1,24
Na_2O	0,36	0,05	0,28	0,04	0,06	0,29	0,07	0,06	0,25	0,03	0,09	0,13	0,03
K_2O	0,06	0,05	0,05	0,05	0,04	0,05	0,04	0,04	0,06	0,05	0,05	0,06	0,04
Cr_2O_3	0,25	0,18	0,12	0,16	0,10	0,17	0,16	0,37	0,17	0,13	0,24	0,15	0,38
Total	99,71	100,33	99,06	100,70	100,03	101,08	98,98	99,51	99,85	98,89	99,23	100,32	99,26
CATIONS BASED ON 6 OXYGENS													
Si	1,942	1,954	1,938	1,928	1,924	1,920	1,950	1,958	1,925	1,965	1,940	1,978	1,938
Al^{iv}	0,058	0,034	0,061	0,030	0,030	0,076	0,034	0,042	0,071	0,029	0,040	0,019	0,048
Al^{vi}	0,017	0,000	0,000	0,000	0,000	0,000	0,000	0,012	0,000	0,000	0,000	0,000	0,000
Ti	0,019	0,011	0,014	0,012	0,015	0,016	0,011	0,007	0,017	0,011	0,007	0,006	0,012
Mg_{2+}	0,818	1,305	9,836	1,308	1,322	0,869	1,394	1,480	0,792	1,135	1,208	0,899	1,490
Fe^{2+}	0,287	0,610	0,302	0,698	0,675	0,280	0,548	0,408	0,351	0,791	0,731	0,144	0,456
Mn	0,005	0,015	0,010	0,014	0,014	0,009	0,017	0,011	0,007	0,016	0,015	0,008	0,013
Ni	0,003	0,002	0,002	0,002	0,002	0,002	0,002	0,003	0,002	0,002	0,002	0,001	0,002
Ca	0,822	0,072	0,834	0,040	0,051	0,829	0,050	0,063	0,834	0,048	0,069	0,940	0,048
Na	0,026	0,003	0,002	0,003	0,004	0,020	0,005	0,004	0,003	0,002	0,006	0,009	0,002
K	0,003	0,002	0,002	0,003	0,002	0,002	0,002	0,002	0,002	0,002	0,002	0,003	0,002
Cr^{3+}	0,007	0,005	0,003	0,004	0,003	0,004	0,004	0,010	0,005	0,004	0,007	0,004	0,011
ε	4,007	4,013	4,004	4,042	4,042	4,033	4,017	4,000	4,009	4,005	4,027	4,011	4,022
ATOM PER CENT													
Mg	42,44	65,67	42,39	63,92	64,55	43,93	69,97	75,85	40,06	57,49	60,15	45,33	74,72
Fe	14,89	30,69	15,31	34,11	32,95	14,15	27,51	20,91	17,75	40,07	36,40	7,26	22,86
Ca	42,65	3,62	42,29	1,95	2,49	41,90	2,51	3,22	42,18	2,43	3,43	47,40	2,40

* TOTAL IRON AS FeO

MICROPROBE ANALYSES OF PYROXENES (SUBSOLIDUS COMPOSITIONS)

			Critical Zone										
Sample #	GP3-241A	GP3-241B	78-365A	78-365B	78-403B-A	78-403B-B	78-404A	78-404B	78-424A	78-413A	78-413B	78-160A	78-431A
SiO_2	51,35	53,15	52,00	52,91	52,74	54,25	52,77	53,77	54,42	52,28	55,00	56,49	50,36
Al_2O_3	2,15	0,83	1,55	1,03	2,25	0,87	2,09	1,48	1,03	2,01	1,04	0,97	2,97
TiO_2	0,28	0,34	0,72	0,32	0,41	0,24	0,26	0,32	0,32	0,32	0,28	0,24	0,31
MgO	15,25	26,62	15,74	25,50	16,45	27,80	15,55	27,01	27,86	16,19	27,91	30,71	14,08
FeO*	6,12	16,47	7,41	18,24	6,15	14,47	7,17	15,04	13,92	6,26	13,92	10,48	9,14
MnO	0,26	0,39	0,28	0,43	0,27	0,42	0,30	0,18	0,38	0,31	0,32	0,22	0,34
NiO	0,07	0,06	0,06	0,07	0,06	0,11	0,06	0,08	0,08	0,09	0,07	0,07	0,04
CaO	23,26	1,18	20,70	1,00	20,23	0,88	20,96	1,39	1,04	20,62	1,20	1,11	21,45
Na_2O	0,25	0,04	0,25	0,08	0,36	0,07	0,54	0,08	0,03	0,36	0,06	0,04	0,33
K_2O	0,04	0,04	0,05	0,05	0,04	0,05	0,05	0,04	0,04	0,04	0,03	0,04	0,04
Cr_2O_3	0,28	0,26	0,26	0,29	0,89	0,24	0,90	0,30	0,48	0,39	0,41	0,44	0,21
Total	99,31	99,38	99,02	99,92	99,85	99,40	100,65	99,71	99,80	98,87	100,67	100,81	99,27
CATIONS BASED ON 6 OXYGENS													
Si	1,918	1,947	1,943	1,943	1,939	1,964	1,940	1,947	1,961	1,945	1,953	1,975	1,900
Al^{iv}	0,082	0,035	0,057	0,044	0,061	0,036	0,060	0,053	0,039	0,055	0,027	0,025	0,100
Al^{vi}	0,012	0,000	0,011	0,000	0,036	0,001	0,030	0,010	0,004	0,033	0,016	0,014	0,032
Ti	0,007	0,009	0,020	0,008	0,011	0,006	0,007	0,008	0,008	0,008	0,074	0,006	0,004
Mg	0,849	1,453	0,876	1,396	0,901	1,500	0,851	1,458	1,496	0,897	1,480	1,600	0,792
Fe^{2+}	0,191	0,504	0,231	0,560	0,189	0,438	0,220	0,455	0,419	0,194	0,414	0,306	0,288
Mn	0,008	0,012	0,008	0,013	0,008	0,012	0,009	0,002	0,011	0,009	0,009	0,006	0,010
Ni	0,002	0,002	0,002	0,002	0,002	0,003	0,001	0,006	0,002	0,002	0,002	0,002	0,001
Ca	0,931	0,046	0,829	0,039	0,797	0,034	0,825	0,054	0,040	0,822	0,045	0,041	0,867
Na	0,018	0,003	0,018	0,005	0,025	0,005	0,038	0,005	0,002	0,025	0,004	0,002	0,024
K	0,002	0,002	0,002	0,002	0,002	0,002	0,002	0,002	0,002	0,002	0,001	0,002	0,002
Cr^{3+}	0,008	0,007	0,007	0,008	0,025	0,007	0,026	0,008	0,001	0,014	0,011	0,012	0,006
ε	4,029	4,020	4,004	4,020	3,996	4,008	4,009	4,008	3,985	4,006	4,036	3,991	4,026
ATOM PER CENT													
Mg	43,07	72,54	45,24	69,97	47,74	76,06	44,88	74,12	76,52	46,88	76,32	82,17	40,67
Fe	9,69	25,16	11,93	28,07	10,01	22,21	11,60	23,13	21,43	10,14	21,35	15,71	14,79
Ca	47,23	2,29	42,82	1,95	42,23	1,72	43,51	2,74	2,04	42,96	2,32	2,10	44,53

* TOTAL IRON AS FeO

MICROPROBE ANALYSES OF PYROXENES (SUBSOLIDUS COMPOSITIONS)

	CRITICAL ZONE					MARGINAL MEMBER (CRITICAL ZONE)					
Sample #	78-431B	78-422A	78-422B	3-2370A	3-2370B	3-2455A	3-2455B	78-53A	78-53B	78-359B-A	78-359B-B	78-361B-A	78-361B-B
SiO_2	51,96	52,03	53,47	51,08	52,46	50,82	51,87	52,83	50,70	51,50	51,30	51,52	52,30
Al_2O_3	1,06	1,72	0,96	1,79	1,10	2,14	1,08	1,49	0,61	0,85	0,89	1,76	0,77
TiO_2	0,28	0,42	0,32	0,42	0,33	0,46	0,43	0,42	0,25	0,28	0,26	0,51	0,42
MgO	24,71	16,20	27,71	16,28	27,49	15,41	25,45	14,79	22,41	13,78	20,25	13,81	21,47
FeO*	19,50	7,54	15,20	7,03	15,78	9,05	18,18	9,50	23,20	11,23	25,34	9,83	23,58
MnO	0,53	0,22	0,34	0,18	0,29	0,27	0,37	0,43	0,44	0,34	0,61	0,27	0,41
NiO	0,06	0,06	0,06	0,08	0,10	0,10	0,07	0,08	0,06	0,05	0,07	0,07	0,07
CaO	1,25	20,32	1,26	21,09	1,12	20,16	1,44	20,19	0,76	22,51	1,12	21,09	1,14
Na_2O	0,07	0,36	0,07	0,37	0,05	0,41	0,05	0,34	0,07	0,23	0,05	0,31	0,05
K_2O	0,05	0,04	0,05	0,05	0,04	0,05	0,04	0,05	0,05	0,06	0,05	0,05	0,04
Cr_2O_3	0,06	0,54	0,28	0,61	0,33	0,56	0,30	0,08	0,07	0,10	0,13	0,25	0,14
Total	99,53	99,45	99,72	98,98	99,09	99,43	99,19	100,20	98,84	100,58	100,07	99,47	100,39
CATIONS BASED ON 6 OXYGENS													
Si	1,932	1,936	1,941	1,915	1,924	1,909	1,922	1,963	1,930	1,930	1,949	1,941	1,959
Al^{iv}	0,046	0,064	0,041	0,079	0,047	0,091	0,047	0,037	0,027	0,038	0,040	0,059	0,034
Al^{vi}	0,000	0,011	0,000	0,000	0,000	0,003	0,000	0,028	0,000	0,000	0,000	0,019	0,000
Ti	0,007	0,011	0,008	0,011	0,009	0,013	0,012	0,011	0,007	0,008	0,007	0,014	0,011
Mg_{2+}	1,369	0,898	1,499	0,909	1,503	0,863	1,408	0,819	1,274	0,775	1,146	0,775	1,198
Fe^{2+}	0,606	0,234	0,461	0,220	0,484	0,284	0,564	0,295	0,740	0,354	0,805	0,309	0,738
Mn	0,016	0,007	0,010	0,005	0,009	0,008	0,011	0,013	0,014	0,011	0,020	0,008	0,013
Ni	0,002	0,002	0,002	0,002	0,003	0,003	0,002	0,002	0,002	0,002	0,002	0,002	0,002
Ca	0,049	0,810	0,049	0,847	0,044	0,811	0,057	0,804	0,031	0,910	0,046	0,851	0,045
Na	0,005	0,025	0,005	0,026	0,003	0,029	0,003	0,024	0,005	0,017	0,004	0,022	0,003
K	0,002	0,002	0,002	0,002	0,001	0,002	0,001	0,002	0,002	0,003	0,002	0,002	0,002
Cr^{3+}	0,002	0,015	0,008	0,018	0,009	0,016	0,008	0,002	0,002	0,003	0,004	0,007	0,004
ε	4,036	4,015	4,026	4,034	4,036	4,032	4,035	4,000	4,038	4,040	4,025	4,009	4,009
ATOM PER CENT													
Mg	67,63	46,24	74,61	46,00	74,00	44,07	59,39	42,70	62,29	38,00	57,38	40,05	60,47
Fe	29,94	12,04	22,94	11,13	23,83	14,50	27,79	15,38	36,18	17,36	40,31	15,96	37,25
Ca	2,42	41,70	2,43	42,86	2,16	41,42	2,80	41,91	1,51	44,62	2,30	43,97	2,27

* TOTAL IRON AS FeO

MICROPROBE ANALYSES OF PYROXENES (SUBSOLIDUS COMPOSITIONS)

	MARGINAL MEMBER (CRITICAL ZONE)						LOWER ZONE					
Sample #	78-360A-A	78-360A-B	78-72A	78-72B	78-154A	78-154B	78-154C	3-2395	3-2485	3-2500	3-2805	3-2830	3-2940
SiO_2	52,00	51,38	51,65	53,16	52,74	51,79	50,93	55,49	55,32	55,50	55,46	54,95	55,23
Al_2O_3	1,98	0,85	1,43	0,77	1,58	0,79	1,35	1,62	1,39	1,76	1,26	1,30	1,48
TiO_2	0,48	0,40	0,61	0,50	0,51	0,28	0,42	0,29	0,30	0,37	0,25	0,14	0,23
MgO	13,73	22,44	14,43	22,43	13,33	22,39	13,84	29,88	32,31	30,99	31,74	30,50	32,54
FeO*	8,35	22,37	9,62	20,26	9,82	22,69	10,21	9,67	7,82	8,06	9,92	9,89	7,53
MnO	0,35	0,51	0,33	0,40	0,41	0,51	0,40	0,18	0,13	0,17	0,28	0,18	0,22
NiO	0,05	0,06	0,09	0,07	0,06	0,07	0,04	0,08	0,09	0,13	0,07	0,09	0,09
CaO	21,49	1,16	21,45	1,32	21,60	1,39	20,45	1,57	0,99	1,13	0,90	1,66	0,99
Na_2O	0,38	0,06	0,28	0,06	0,19	0,05	0,28	0,05	0,05	0,07	0,05	0,06	0,07
K_2O	0,04	0,05	0,05	0,04	0,04	0,05	0,04	0,05	0,04	0,05	0,05	0,06	0,03
Cr_2O_3	0,42	0,12	0,39	0,18	0,12	0,13	0,15	0,35	0,54	0,56	0,44	0,48	0,39
Total	99,27	99,40	100,33	99,19	100,41	100,14	98,11	99,23	98,98	98,79	100,42	99,31	98,80
CATIONS BASED ON 6 OXYGENS													
Si	1,951	1,939	1,932	1,982	1,965	1,942	1,948	1,966	1,950	1,961	1,946	1,953	1,948
Al^{iv}	0,049	0,038	0,063	0,014	0,035	0,034	0,052	0,034	0,050	0,039	0,052	0,047	0,052
Al^{vi}	0,038	0,000	0,000	0,000	0,034	0,000	0,008	0,033	0,007	0,034	0,000	0,007	0,009
Ti	0,014	0,011	0,017	0,033	0,014	0,007	0,012	0,007	0,008	0,009	0,006	0,003	0,006
Mg_{2+}	0,768	1,262	0,804	1,256	0,740	1,251	0,789	1,578	1,697	1,631	1,659	1,615	1,710
Fe^{2+}	0,262	0,706	0,300	0,631	0,306	0,711	0,326	0,286	0,230	0,238	0,291	0,293	0,222
Mn	0,011	0,016	0,010	0,012	0,012	0,016	0,012	0,005	0,003	0,005	0,008	0,005	0,006
Ni	0,002	0,002	0,002	0,002	0,001	0,002	0,001	0,002	0,002	0,003	0,002	0,002	0,002
Ca	0,864	0,047	0,859	0,052	0,862	0,055	0,838	0,059	0,037	0,042	0,033	0,063	0,037
Na	0,028	0,004	0,020	0,004	0,013	0,003	0,020	0,003	0,003	0,004	0,003	0,004	0,004
K	0,002	0,002	0,002	0,002	0,002	0,002	0,002	0,002	0,001	0,002	0,002	0,002	0,001
Cr^{3+}	0,012	0,004	0,011	0,005	0,003	0,003	0,004	0,009	0,015	0,015	0,012	0,013	0,010
ε	4,001	4,031	4,020	3,983	3,987	4,026	4,012	3,984	4,003	3,983	4,014	4,007	4,007
ATOM PER CENT													
Mg	40,54	62,63	40,95	64,59	38,78	62,02	40,39	82,05	86,40	85,34	83,66	81,93	86,84
Fe	13,83	35,03	15,28	32,71	16,03	35,25	16,69	14,87	11,71	12,45	14,67	14,86	11,27
Ca	45,61	2,33	43,75	2,69	45,17	2,72	42,90	3,06	1,88	2,19	1,66	3,19	1,88

* TOTAL IRON AS FeO

MICROPROBE ANALYSES OF PYROXENES (SUBSOLIDUS COMPOSITIONS)

LOWER ZONE

Sample #	3-2950	3-3027	3-3349	3-3402	3-3494	3-3563	3-3764	3-3766	3-3819	3-3927	3-4002	1-50	1-67
SiO_2	55,36	55,20	56,27	55,50	56,06	55,06	55,15	55,72	54,60	55,60	55,84	56,14	55,80
Al_2O_3	1,37	1,41	1,11	2,38	1,53	1,33	1,28	1,64	1,56	1,12	1,58	1,28	1,21
TiO_2	0,20	0,29	0,24	0,20	0,26	0,24	0,17	0,14	0,16	0,20	0,14	0,17	0,13
MgO	31,98	32,34	30,98	30,54	31,35	31,87	32,07	32,81	32,91	32,28	32,25	32,85	31,96
FeO*	7,82	8,11	10,11	9,49	8,58	9,81	8,48	7,28	8,75	7,58	7,59	6,95	8,07
MnO	0,20	0,23	0,27	0,25	0,24	0,28	0,11	0,19	0,20	0,13	0,23	0,18	0,22
NiO	0,07	0,11	0,08	0,07	0,07	0,12	0,15	0,09	0,11	0,35	0,14	0,09	0,10
CaO	0,92	1,09	1,01	0,67	0,87	0,89	0,85	0,95	0,94	0,89	1,08	1,39	1,00
Na_2O	0,05	0,05	0,05	0,03	0,05	0,04	0,05	0,04	0,06	0,05	0,06	0,04	0,04
K_2O	0,04	0,04	0,06	0,04	0,03	0,05	0,04	0,05	0,04	0,03	0,05	0,03	0,04
Cr_2O_3	0,58	0,44	0,41	0,38	0,44	0,35	0,41	0,48	0,36	0,44	0,45	0,32	0,46
Total	98,59	99,31	100,59	99,55	99,48	100,04	98,76	99,39	99,69	98,67	99,41	99,44	99,03

CATIONS BASED ON 6 OXYGENS

Si	1,958	1,944	1,969	1,953	1,968	1,939	1,953	1,950	1,923	1,963	1,957	1,961	1,966
Al^{iv}	0,042	0,056	0,031	0,047	0,032	0,055	0,047	0,050	0,064	0,037	0,043	0,039	0,034
Al^{vi}	0,015	0,002	0,014	0,046	0,031	0,000	0,006	0,017	0,000	0,019	0,022	0,013	0,016
Ti	0,005	0,007	0,006	0,005	0,006	0,006	0,004	0,003	0,004	0,005	0,003	0,004	0,003
Mg_{2+}	1,685	1,697	1,615	1,602	1,640	1,673	1,692	1,711	1,727	1,699	1,684	1,710	1,678
Fe^{2+}	0,231	0,238	0,295	0,279	0,251	0,289	0,251	0,213	0,257	0,223	0,222	0,203	0,237
Mn	0,005	0,006	0,008	0,007	0,007	0,008	0,003	0,005	0,005	0,003	0,006	0,005	0,006
Ni	0,002	0,003	0,002	0,002	0,002	0,003	0,004	0,002	0,003	0,009	0,004	0,002	0,003
Ca	0,034	0,041	0,037	0,025	0,032	0,033	0,032	0,035	0,035	0,033	0,040	0,052	0,037
Na	0,003	0,003	0,003	0,002	0,003	0,002	0,003	0,002	0,004	0,003	0,004	0,002	0,002
K	0,001	0,001	0,002	0,001	0,001	0,002	0,001	0,002	0,001	0,001	0,002	0,001	0,001
Cr^{3+}	0,016	0,012	0,011	0,010	0,012	0,009	0,011	0,013	0,010	0,012	0,012	0,008	0,012
ε	3,997	4,010	3,993	3,979	3,985	4,019	4,007	4,003	4,033	3,997	3,999	4,000	3,995

ATOM PER CENT

Mg	86,41	85,88	82,94	84,05	85,28	83,85	85,67	87,34	85,53	86,90	86,53	87,02	85,96
Fe	11,84	12,05	15,15	14,63	13,05	14,48	12,70	10,87	12,72	11,40	11,40	10,33	12,14
Ca	1,74	2,07	1,90	1,31	1,66	1,65	1,62	1,78	1,73	1,68	2,05	2,64	1,89

* TOTAL IRON AS FeO

MICROPROBE ANALYSES OF PYROXENES (SUBSOLIDUS COMPOSITIONS)

	LOWER ZONE													
Sample #	1-80,5	1-123	GV-1	1-148	1-179	1-209	1-213	1-219	1-223	1-240,95A	1-240,95B	1-244	1-253,5	6A-243
SiO_2	56,08	55,87	55,51	56,38	55,95	56,35	55,60	54,80	55,44	54,64	52,06	56,16	55,31	56,88
Al_2O_3	1,13	1,19	1,39	1,45	1,23	1,21	1,13	1,31	1,23	1,27	1,83	1,49	1,32	1,61
TiO_2	0,22	0,21	0,16	0,20	0,21	0,19	0,17	0,17	0,19	0,18	0,32	0,18	0,23	0,13
MgO	32,37	32,97	34,91	32,56	33,62	32,64	31,70	31,62	32,23	32,23	16,51	32,19	33,29	32,31
FeO*	7,54	6,87	6,13	7,07	6,65	6,88	8,30	9,40	7,97	9,68	3,84	8,34	8,07	7,65
MnO	0,24	0,21	0,21	0,15	0,21	0,17	0,23	0,20	0,15	0,17	0,21	0,20	0,24	0,31
NiO	0,07	0,10	0,08	0,12	0,10	0,07	0,10	0,09	0,09	0,10	0,09	0,10	0,08	0,07
CaO	0,76	0,85	0,90	0,89	0,86	0,83	1,25	1,01	0,74	0,93	23,50	0,91	0,93	1,09
Na_2O	0,06	0,05	0,05	0,06	0,03	0,05	0,03	0,06	0,04	0,06	0,04	0,05	0,04	0,07
K_2O	0,04	0,04	0,04	0,04	0,04	0,04	0,04	0,05	0,05	0,05	0,03	0,05	0,04	0,04
Cr_2O_3	0,39	0,39	0,32	0,54	0,40	0,52	0,39	0,45	0,26	0,42	0,60	0,33	0,53	0,54
Total	98,90	98,76	99,70	99,46	99,30	98,95	98,94	99,16	98,39	99,73	99,03	100,00	100,08	100,70
CATIONS BASED ON 6 OXYGENS														
Si	1,971	1,963	1,930	1,967	1,954	1,973	1,965	1,944	1,947	1,931	1,927	1,960	1,933	1,966
Al^{iv}	0,029	0,037	0,056	0,033	0,046	0,027	0,035	0,054	0,047	0,052	0,073	0,040	0,054	0,034
Al^{vi}	0,017	0,012	0,000	0,026	0,004	0,022	0,012	0,000	0,000	0,000	0,006	0,021	0,000	0,031
Ti	0,006	0,005	0,004	0,005	0,005	0,005	0,004	0,004	0,006	0,004	0,008	0,004	0,006	0,003
Mg	1,696	1,726	1,809	1,698	1,750	1,703	1,669	1,672	1,713	1,697	0,912	1,674	1,734	1,664
Fe^{2+}	0,221	0,201	0,178	0,206	0,194	0,201	0,245	0,278	0,253	0,286	0,119	0,243	0,235	0,221
Mn	0,007	0,006	0,006	0,004	0,006	0,005	0,006	0,006	0,005	0,006	0,006	0,006	0,007	0,009
Ni	0,002	0,002	0,002	0,003	0,003	0,002	0,002	0,002	0,003	0,003	0,002	0,003	0,002	0,002
Ca	0,028	0,032	0,033	0,033	0,032	0,031	0,047	0,038	0,027	0,035	0,933	0,034	0,034	0,040
Na	0,002	0,003	0,003	0,004	0,002	0,003	0,002	0,004	0,003	0,004	0,002	0,003	0,002	0,004
K	0,002	0,001	0,001	0,001	0,001	0,001	0,002	0,002	0,002	0,002	0,001	0,002	0,001	0,001
Cr^{3+}	0,010	0,010	0,008	0,014	0,011	0,014	0,010	0,012	0,009	0,011	0,017	0,009	0,014	0,014
ε	3,991	3,998	4,030	3,994	4,008	3,987	3,999	4,016	4,015	4,031	4,006	3,999	4,022	3,989
ATOM PER CENT														
Mg	87,19	88,10	89,55	87,66	88,56	88,01	85,10	84,10	85,95	84,09	46,43	85,80	86,57	86,44
Fe	11,36	10,26	8,81	10,63	9,81	10,38	12,49	13,98	12,69	14,17	6,05	12,45	11,73	11,48
Ca	1,43	1,63	1,63	1,70	1,62	1,60	2,39	1,91	1,35	1,73	47,50	1,74	1,69	2,07

* TOTAL IRON AS FeO

MICROPROBE ANALYSES OF PYROXENES (SUBSOLIDUS COMPOSITIONS)

			LOWER ZONE										
Sample #	6A-259	6A-286	X-1	X-3	X-5	X-10	X-13	X-15	X-18	X-21	X-23	X-25	X-27
SiO_2	55,25	55,00	54,22	55,04	55,06	54,78	55,00	55,73	55,34	56,08	55,00	54,36	55,51
Al_2O_3	1,54	1,16	1,70	1,60	1,86	1,79	1,81	1,66	1,48	1,53	0,73	1,18	1,22
TiO_2	0,20	0,15	0,15	0,06	0,06	0,12	0,19	0,13	0,07	0,15	0,14	0,15	0,05
MgO_*	33,60	33,57	30,25	28,93	30,54	31,55	31,82	30,27	32,84	30,93	32,83	31,58	30,11
FeO*	8,15	8,21	10,94	11,83	9,14	8,01	8,99	9,15	8,49	8,07	9,22	9,85	10,96
MnO	0,22	0,18	0,32	0,31	0,19	0,11	0,22	0,19	0,18	0,18	0,22	0,29	0,28
NiO	0,09	0,08	0,08	0,01	0,11	0,08	0,09	0,05	0,03	0,11	0,06	0,08	0,00
CaO	0,99	1,24	1,28	0,97	1,12	2,49	1,43	1,18	0,54	1,16	0,53	1,24	0,92
Na_2O	0,05	0,07	0,05	0,01	0,01	0,05	0,05	0,08	0,00	0,05	0,05	0,07	0,02
K_2O	0,06	0,03	0,04	0,00	0,00	0,04	0,04	0,00	0,00	0,04	0,05	0,05	0,00
Cr_2O_3	0,49	0,60	0,65	0,00	0,59	0,49	0,51	0,68	0,73	0,62	0,22	0,33	0,91
Total	100,64	100,29	99,68	99,68	98,68	99,51	100,15	99,12	99,70	98,92	99,05	99,18	99,98

CATIONS BASED ON 6 OXYGENS

Si	1,922	1,924	1,931	1,960	1,956	1,932	1,931	1,970	1,941	1,976	1,949	1,936	1,963
Al^{iv}	0,063	0,047	0,069	0,040	0,044	0,068	0,069	0,030	0,059	0,024	0,030	0,049	0,037
Al^{vi}	0,000	0,000	0,002	0,027	0,033	0,006	0,006	0,039	0,002	0,039	0,000	0,000	0,013
Ti	0,005	0,003	0,004	0,001	0,001	0,003	0,005	0,003	0,001	0,003	0,003	0,004	0,001
Mg_{2+}	1,742	1,750	1,605	1,535	1,617	1,658	1,664	1,594	1,716	1,624	1,734	1,676	1,587
Fe^{2+}	0,237	0,240	0,325	0,352	0,271	0,236	0,263	0,270	0,249	0,237	0,273	0,293	0,324
Mn	0,006	0,005	0,009	0,009	0,005	0,003	0,006	0,005	0,005	0,005	0,006	0,008	0,008
Ni	0,002	0,002	0,002	0,000	0,003	0,002	0,002	0,001	0,000	0,003	0,001	0,002	0,000
Ca	0,036	0,046	0,048	0,037	0,042	0,094	0,053	0,044	0,020	0,043	0,020	0,047	0,034
Na	0,003	0,004	0,003	0,000	0,000	0,003	0,003	0,005	0,000	0,003	0,003	0,004	0,001
K	0,002	0,001	0,002	0,000	0,000	0,001	0,001	0,000	0,000	0,001	0,002	0,002	0,000
Cr^{3+}	0,013	0,016	0,018	0,026	0,016	0,013	0,014	0,019	0,020	0,017	0,006	0,009	0,025
ε	4,031	4,038	4,018	3,987	3,998	4,019	4,017	3,980	4,013	3,975	4,027	4,030	3,993

ATOM PER CENT

Mg	86,45	85,95	81,14	79,78	83,78	83,40	84,04	83,54	86,44	85,29	85,54	83,13	81,59
Fe	11,76	11,78	16,43	18,29	14,04	11,87	13,28	14,15	12,54	12,44	13,46	14,53	16,65
Ca	1,78	2,25	2,42	1,92	2,17	4,72	2,67	2,30	1,00	2,25	0,98	2,33	1,74

* TOTAL IRON AS FeO

MICROPROBE ANALYSES OF PYROXENES (SUBSOLIDUS COMPOSITIONS)

			LOWER ZONE									
Sample #	X-31	X-41	A-1	A-3	A-4	A-7	A-9	A-10	A-12	A-13	A-15	A-16
SiO_2	56,05	55,94	56,24	55,21	56,29	55,60	55,90	55,82	56,36	56,74	56,35	56,31
Al_2O_3	1,37	1,33	1,08	1,01	1,08	1,52	1,10	1,01	1,02	1,07	1,05	1,04
TiO_2	0,13	0,05	0,07	0,15	0,04	0,06	0,14	0,04	0,05	0,06	0,08	0,14
MgO	33,73	33,41	32,96	34,07	33,70	32,37	32,63	31,56	33,22	32,68	33,98	34,40
FeO*	7,31	6,77	8,07	7,63	7,65	8,22	8,29	9,64	8,13	7,59	7,01	6,46
MnO	0,23	0,15	0,18	0,24	0,17	0,19	0,17	0,22	0,20	0,18	0,17	0,15
NiO	0,07	0,04	0,07	0,10	0,10	0,07	0,12	0,02	0,04	0,07	0,04	0,08
CaO	1,01	1,57	0,84	0,85	0,80	0,81	0,79	0,82	0,82	1,02	0,84	0,65
Na_2O	0,06	0,03	0,00	0,06	0,01	0,01	0,05	0,01	0,00	0,04	0,01	0,07
K_2O	0,05	0,00	0,00	0,05	0,00	0,00	0,04	0,00	0,00	0,00	0,00	0,05
Cr_2O_3	0,30	0,55	0,42	0,24	0,56	0,46	0,44	0,46	0,47	0,55	0,44	0,44
Total	100,31	99,84	99,93	99,61	100,40	99,31	99,67	99,60	100,32	100,00	99,97	99,79
CATIONS BASED ON 6 OXYGENS												
Si	1,945	1,948	1,962	1,935	1,953	1,953	1,959	1,967	1,959	1,973	1,956	1,954
Al^{iv}	0,055	0,052	0,038	0,041	0,044	0,047	0,041	0,033	0,041	0,027	0,042	0,042
Al^{vi}	0,001	0,002	0,006	0,000	0,000	0,015	0,004	0,-08	0,001	0,016	0,000	0,000
Ti	0,003	0,001	0,001	0,004	0,001	0,001	0,003	0,001	0,002	0,001	0,002	0,003
Mg_{2+}	1,744	1,734	1,713	1,779	1,742	1,695	1,704	1,657	1,721	1,693	1,758	1,779
Fe^{2+}	0,212	0,197	0,235	0,223	0,222	0,241	0,242	0,284	0,236	0,220	0,203	0,187
Mn	0,006	0,004	0,005	0,007	0,005	0,005	0,005	0,006	0,005	0,005	0,005	0,004
Ni	0,002	0,001	0,002	0,002	0,002	0,002	0,003	0,000	0,001	0,002	0,001	0,002
Ca	0,037	0,058	0,031	0,031	0,029	0,030	0,029	0,030	0,030	0,038	0,031	0,024
Na	0,004	0,000	0,000	0,002	0,000	0,000	0,003	0,000	0,000	0,002	0,000	0,004
K	0,002	0,002	0,000	0,004	0,000	0,000	0,001	0,000	0,000	0,000	0,000	0,002
Cr^{3+}	0,008	0,015	0,015	0,006	0,015	0,012	0,012	0,012	0,013	0,015	0,012	0,012
ε	4,019	4,014	4,008	4,034	4,013	4,001	4,006	3,998	4,009	3,992	4,010	4,013
ATOM PER CENT												
Mg	87,50	87,17	86,55	87,50	87,40	86,21	86,27	84,06	86,61	86,77	88,25	89,39
Fe	10,63	9,90	11,87	10,96	11,13	12,25	12,25	14,40	11,87	11,27	10,19	9,39
Ca	1,85	2,91	1,56	1,52	1,45	1,52	1,46	1,52	1,50	1,94	1,55	1,20

* TOTAL IRON AS FeO

SAMPLE NO	STRATIGRAPHIC LEVEL	ROCK TYPE	STATUS
5-124A	+1480m	Pl-CPX-OPX-Mag Cumulate	Cumulus CPX
5-124B	+1480m	" " " " "	Cumulus OPX
5-138A	+1475m	" " " " "	Cumulus CPX
5-195A	+1460m	" " " " "	Cumulus CPX
5-233A	+1446m	" " " " "	Cumulus CPX
5-233B	+1446m	" " " " "	Cumulus OPX(Inv.Pig.)
5-233C	+1446m	Pl-CPX-OPX-Mag Cumulate	Exsolved CPX in Inv.Pig.
5-315A	+1424m	" " " " "	Cumulus CPX
5-410A	+1392m	" " " " "	Cumulus CPX
5-440	+1382m	Pl-Mag-CPX-OPX Cumulate	Cumulus CPX
5-616A	+1332m	Pl Cumulate	Intercumulus CPX
5-640A	+1324m	Pl-CPX-OPX Cumulate	Cumulus CPX
5-640B	+1324m	" " " "	Cumulus OPX(Inv.Pig.)
5-640C	+1324m	" " " "	Exsolved CPX in Inv.pig.
5-935A	+1240m	" " " "	Cumulus CPX
5-935B	+1240m	" " " "	Cumulus OPX(Inv.Pig.)
5-935C	+1240m	" " " "	Exsolved CPX in Inv.Pig.
5-1100A	+1190m	" " " "	Cumulus CPX
5-1100B	+1190m	" " " "	Cumulus OPX(Inv.Pig.)
5-1100C	+1190m	" " " "	Exsolved CPX in Inv.Pig.
5-1300A	+1130m	" " " "	Cumulus CPX
78-127A	+1067m	Pl-CPX Cumulate	Cumulus CPX
78-127B	+1067m	" " "	Intercumulus OPX
78-125A	+940m	Pl-CPX-OPX Cumulate	Cumulus CPX
78-125B	+940m	" " " "	Cumulus OPX(Inv.Pig.)
78-125C	+940m	" " " "	Exsolved CPX in Inv.Pig.
78-122A	+850m	" " " "	Cumulus CPX
78-122B	+850m	" " " "	Cumulus OPX(Inv.Pig.)
78-122C	+850m	" " " "	Intercumulus OPX
78-350A	+724m	" " " "	Cumulus CPX
78-350B	+724m	" " " "	Intercumulus OPX
78-192A	+566m	" " " "	Cumulus CPX
78-192B	+566m	" " " "	Cumulus OPX(Inv.Pig.)
78-192C	+566m	" " " "	Intercumulus OPX
78-189A	+410m	" " " "	Cumulus CPX

SAMPLE NO	STRATIGRAPHIC LEVEL	ROCK TYPE	STATUS
78-189B	+410m	Pl-CPX-OPX Cumulate	Cumulus OPX(Inv.Pig.)
78-189C	+410m	" " " "	Intercumulus OPX
78-207A	+250m	" " " "	Cumulus CPX
78-207B	+250m	" " " "	Cumulus OPX
78-76B-A	+205m	Pl-OPX Cumulate	Intercumulus CPX
78-76B-B	+205m	" " "	Cumulus OPX
78-92A	+198m	MAIN ZONE Initial Magma	Primary CPX
78-92B	+198m	" " " "	Primary Inv.Pig.
78-92C	+198m	" " " "	Ophitic OPX
78-145A	+180m	Pl-OPX Cumulate	Intercumulus CPX
78-145B	+180m	" " "	Cumulus OPX
78-60A	+128m	OPX Cumulate	Cumulus OPX
78-128D-A	+123m	Pl-Cumulate	Intercumulus CPX
78-128D-B	+123m	" "	Mantle of Inv.Pig. about
78-128D-C	+123m	" "	Core of Intercumulus OPX
78-481A	+76m	OPX Cumulate	Intercumulus CPX
78-481B	+76m	" "	Cumulus OPX
GP3-241A	+56m	Pl-OPX-CPX Cumulate	Cumulus CPX
GP3-241B	+56m	" " " "	Cumulus OPX
78-365A	+48m	Pl-OPX Cumulate	Intercumulus CPX
78-365B	+48m	" " "	Cumulus OPX
78-403B-A	+19m	Opx-Cpx-Chr-Cumulate	Cumulus CPX
78-403B-B	+19m	" " " "	Cumulus OPX
78-404A	+5m	OPX Cumulate	Intercumulus CPX
78-404B	+5m	" "	Cumulus OPX
78-424	-22m	Pl - Cumulate	Intercumulus OPX
78-413A	-61m	OPX-CPX-Chr Cumulate	Cumulus CPX
78-413B	-61m	" " " "	Cumulus OPX
78-160A	-86m	Chromite Cumulate	Intercumulus OPX
78-431A	-94m	Pl-OPX-CPX Cumulate	Cumulus CPX
78-431B	-94m	" " " "	Cumulus OPX
78-422A	-95m	Pl-OPX Cumulate	Intercumulus CPX
78-422A	-95m	" " "	Cumulus OPX
3-2370A	-104m	fine grained Gabbronorite	Primary CPX
3-2370B	-104m	" " "	Primary OPX
3-2455A	-121m	Pl-CPX-OPX Cumulate	Cumulus CPX
3-2455B	-121m	" " " "	Cumulus OPX

SAMPLE NO	STRATIGRAPHIC LEVEL	ROCK TYPE	STATUS
78-53A	M.Mb/P.G.	Gabbronorite	Primary CPX
78-53B	M.Mb "	"	Primary OPX
78-359B-A	M.Mb "	"	Primary CPX
78-359B-B	M.Mb "	"	Primary OPX(Inv.Pig.)
78-361B-A	M.Mb "	"	Primary CPX
78-361B-B	M.Mb "	"	Primary OPX
78-360A-A	M.Mb "	"	Primary CPX
78-360A-B	M.Mb "	"	Primary OPX
78-72A	M.Mb "	"	Primary OPX
78-72B	M.Mb "	"	Primary CPX
78-154A	M.Mb/L.Z.	"	Primary CPX
78-154B	M.Mb/L.Z.	"	Primary OPX(Inv.Pig.)
78-154C	M.Mb/L.Z.	"	exsolved CPX in Inv.Pig.
3-2395	-110m	Ol-Chr Cumulate	Intercumulus OPX
3-2485	-136m	Ol-OPX-Chr Cumulate	Cumulus OPX
3-2500	-141m	Ol-OPX-Chr Cumulate	Cumulus OPX
3-2805	-230m	Ol-Chr Cumulate	Intercumulus OPX
3-2830	-238m	OPX Cumulate	Cumulus OPX
3-2940	-276m	OPX-Ol-Chr Cumulate	Cumulus OPX
3-2950	-280m	OPX Cumulate	Cumulus OPX
3-3027	-300m	Ol-Chr Cumulate	Intercumulus OPX
3-3349	-402m	OPX-Cumulate	Cumulus OPX
3-3402	-416m	OPX-Ol-Chr Cumulate	Cumulus OPX
3-3494	-446m	OPX Cumulate	Cumulus OPX
3-3563	-465m	" "	Cumulus OPX
3-3764	-524m	OPX-Chr Cumulate	Cumulus OPX
3-3766	-530m	Ol-Chr Cumulate	Intercumulus OPX
3-3819	-544m	OPX Cumulate	Cumulus OPX
3-3927	-577m	OPX Cumulate	Cumulus OPX
3-4002	-587m	OPX-Ol-Chr Cumulate	Cumulus OPX
1-50	-620m	Ol-Chr Cumulate	Intercumulus OPX
1-67	-634m	OPX Cumulate	Cumulus OPX
1-80.5	-647m	Ol-Chr Cumulate	Intercumulus OPX
1-123	-680m	" " "	Intercumulus OPX
GV-1	-689m	OPX-Ol-Chr Cumulate	Cumulus OPX
1-148	-704m	OPX Cumulate	Cumulus OPX

SAMPLE NO	STRATIGRAPHIC LEVEL	ROCK TYPE	STATUS
1-179	-726m	01-Chr Cumulate	Intercumulus OPX
1-209	-747m	01-Chr Cumulate	Intercumulus OPX
1-213	-750m	OPX Cumulate	Cumulus OPX
1-219	-753m	OPX-01-Chr Cumulate	Cumulus OPX
1-223	-758m	" " " "	Cumulus OPX
1-240,95A	-772m	" " " "	Cumulus OPX
1-240,95B	-772m	" " " "	Intercumulus CPX
1-244	-776m	" " " "	Cumulus OPX
1-253,5	-782m	" " " "	Cumulus OPX
6A-243	-784m	" " " "	Cumulus OPX
6A-259	-797m	" " " "	Cumulus OPX
6A-286	-817m	01-Chr Cumulate	Intercumulus OPX
X-1	-958m	OPX-Chr Cumulate	Cumulus OPX
X-3	-984m	OPX-Cumulate	Cumulus OPX
X-5	-1032m	OPX-Cumulate	Cumulus OPX
X-10	-1058m	OPX-01-Chr Cumulate	Cumulus OPX
X-13	-1068m	OPX-Chr Cumulate	Intercumulus OPX
X-15	-1089m	OPX Cumulate	Cumulus OPX
X-18	-1120m	OPX Cumulate	Cumulus OPX
X-21	-1165m	OPX-01-Chr Cumulate	Cumulus OPX
X-23	-1176m	OPX-Chr Cumulate	Cumulus OPX
X-25	-1190m	OPX-Chr Cumulate	Cumulus OPX
X-27	-1220m	OPX Cumulate	Cumulus OPX
X-31	-1250m	01-Chr Cumulate	Intercumulus OPX
X-41	-1302m	01-Chr Cumulate	Intercumulus OPX
A-1	-1368m	OPX-01-Chr Cumulate	Cumulus OPX
A-3	-1408m	OPX-01-Chr Cumulate	Cumulus OPX
A-4	-1434m	OPX Cumulate	Cumulus OPX
A-7	-1456m	OPX Cumulate	Cumulus OPX
A-9	-1484m	OPX-01-Chr Cumulate	Cumulus OPX
A-10	-1490m	OPX Cumulate	Cumulus OPX
A-12	-1530m	OPX Cumulate	Cumulus OPX
A-13	-1582m	OPX Cumulate	Cumulus OPX
A-15	-1610m	OPX Cumulate	Cumulus OPX
A-16	-1640m	OPX-01-Chr Cumulate	Cumulus OPX

OPX = orthopyroxene

Ol = olivine

Chr = chromite

Inv. Pig. = Inverted Pigeonite

CPX = Clinopyroxene

Note: Intercumulus orthopyroxene = intercumulus and reaction orthopyroxene for samples numbered 3 - 2395 to A-16

APPENDIX 2

MICROPROBE ANALYSES OF PYROXENES (BULK COMPOSITIONS)

	UPPER ZONE						MAIN ZONE							
Sample #	5-124-1	5-124-C	5-124-2	5-233-1	5-233-C	5-233-2	5-640-3A	5-640-C	5-640-1	5-935-3A	5-935-C	5-935-1	78-127-1	78-127-2
SiO_2	49,09	49,97	49,77	49,68	49,93	49,78	49,77	54,12	51,05	49,47	51,50	51,42	50,64	51,70
Al_2O_3	1,87	0,69	0,63	1,50	0,73	0,63	2,34	0,73	0,65	2,12	0,79	0,70	1,94	0,90
TiO_2	0,44	0,32	0,30	0,40	0,31	0,30	0,72	0,39	0,36	0,73	0,36	0,33	0,55	0,42
MgO	10,87	14,38	15,01	11,56	14,87	15,49	13,55	17,60	18,45	13,53	17,78	18,84	14,51	23,02
FeO*	17,07	29,01	31,64	17,55	28,22	30,93	1-,67	24,04	26,29	14,69	22,91	25,27	11,27	21,61
MnO	0,39	0,71	0,76	0,30	0,61	0,68	0,47	0,65	0,72	0,26	0,37	0,39	0,45	0,65
NiO	N.d.	N.d.	N.d.	N.d.	N.d.	N.d.	0,03	0,03	0,04	N.d.	N.d.	N.d.	N.d.	N.d.
CaO	18,56	5,16	1,59	17,92	5,32	1,52	17,79	5,16	2,42	18,34	5,07	1,95	19,80	1,83
Na_2O	0,24	0,10	0,07	0,23	0,06	0,05	0,19	0,08	0,06	0,26	0,11	0,08	0,33	0,08
K_2O	0,09	0,05	0,05	0,05	0,06	0,06	0,05	0,06	0,07	0,07	0,03	0,04	0,07	0,06
Cr_2O_3	0,52	0,05	0,05	0,12	0,06	0,06	0,09	0,08	0,09	0,09	0,10	0,12	0,16	0,06
Total	99,14	100,44	99,87	99,31	100,17	99,50	99,67	99,94	100,20	99,56	99,02	99,14	99,72	100,33
CATIONS BASED ON 6 OXYGENS														
Si	1,916	1,951	1,959	1,931	1,948	1,959	1,902	1,957	1,954	1,896	1,973	1,972	1,914	1,930
Al^{iv}	0,084	0,032	0,029	0,069	0,034	0,029	0,098	0,033	0,029	0,096	0,027	0,028	0,086	0,040
Al^{vi}	0,002	0,000	0,000	0,000	0,000	0,000	0,007	0,000	0,000	0,000	0,000	0,004	0,001	0,000
Ti	0,013	0,009	0,009	0,012	0,009	0,009	0,021	0,011	0,010	0,021	0,010	0,010	0,016	0,012
Mg	0,632	0,837	0,880	0,670	0,865	0,909	0,772	1,004	1,053	0,773	1,015	1,077	0,817	1,281
Fe^{2+}	0,557	0,947	1,041	0,570	0,921	1,018	0,469	0,769	0,842	0,471	0,734	0,811	0,356	0,675
Mn	0,013	0,230	0,025	0,010	0,020	0,023	0,015	0,021	0,023	0,008	0,012	0,013	0,014	0,021
Ni	N.d.	N.d.	N.d.	N.d.	N.d.	N.d.	0,001	0,001	0,001	N.d.	N.d.	N.d.	N.d.	N.d.
Ca	0,776	0,216	0,067	0,746	0,222	0,064	0,728	0,212	0,099	0,753	0,208	0,080	0,802	0,073
Na	0,018	0,008	0,005	0,017	0,005	0,004	0,014	0,006	0,004	0,019	0,008	0,006	0,024	0,006
K	0,004	0,002	0,003	0,002	0,003	0,003	0,002	0,003	0,003	0,003	0,001	0,002	0,003	0,003
Cr^{3+}	0,016	0,002	0,002	0,004	0,002	0,002	0,003	0,002	0,003	0,003	0,003	0,004	0,005	0,002
ε	4,032	4,028	4,021	4,031	4,029	4,020	4,032	4,019	4,023	4,044	4,002	4,005	4,038	4,042
ATOM PER CENT														
Mg	32,2	41,8	44,3	33,7	43,1	45,6	39,2	50,6	52,8	38,7	51,9	54,7	41,4	63,1
Fe	28,3	47,4	52,4	28,7	45,9	51,1	23,8	38,3	42,2	23,6	37,5	41,2	18,0	33,3
Ca	39,5	10,8	3,4	37,6	11,1	3,2	37,0	10,7	5,0	37,7	10,6	4,1	40,6	3,6

MICROPROBE ANALYSES OF PYROXENES (BULK COMPOSITIONS)

Sample #	78-125-A	78-125-C	78-125-3	78-122-A	78-122-3	78-122-2	78-350-1	78-350-C	78-350-2	78-189-1	78-189-C	78-189-2	78-192-1
SiO_2	51,54	51,88	51,95	51,50	52,00	52,00	51,43	51,97	52,09	51,78	52,20	52,34	51,45
Al_2O_3	1,62	0,77	0,71	1,45	0,94	0,62	1,64	0,89	0,76	1,96	0,97	0,90	1,61
TiO_2	0,73	0,36	0,35	0,66	0,43	0,43	0,74	0,54	0,50	0,65	0,50	0,43	0,56
MgO	13,51	17,42	18,27	13,42	17,38	18,33	13,31	19,39	20,59	14,71	21,54	21,71	14,85
FeO*	15,38	23,81	26,12	13,48	22,67	22,75	11,90	21,62	23,53	11,74	20,57	21,61	11,85
MnO	0,36	0,56	0,63	0,35	0,66	0,66	0,35	0,49	0,53	0,37	0,36	0,56	0,34
NiO	0,04	0,04	0,04	0,03	0,03	0,04	0,05	0,03	0,03	0,04	0,07	0,04	0,03
CaO	17,36	5,36	2,62	17,87	4,75	3,62	20,21	4,96	1,94	18,63	4,70	2,02	18,25
Na_2O	0,26	0,10	0,07	0,26	0,08	0,08	0,27	0,09	0,06	0,29	0,09	0,04	0,23
K_2O	0,06	0,05	0,06	0,05	0,05	0,05	0,07	0,06	0,06	0,06	0,05	0,05	0,06
Cr_2O_3	0,16	0,13	0,13	0,13	0,07	0,08	0,09	0,07	0,07	0,11	0,06	0,08	0,14
Total	101,02	100,48	100,95	99,20	99,06	98,66	100,06	100,11	100,16	100,34	101,13	99,78	99,37

CATIONS BASED ON 6 OXYGENS

Si	1,939	1,969	1,968	1,959	1,987	1,990	1,940	1,958	1,961	1,942	1,936	1,936	1,961
Al^{iv}	0,061	0,031	0,032	0,041	0,013	0,010	0,060	0,039	0,034	0,058	0,064	0,042	0,039
Al^{vi}	0,011	0,003	0,000	0,024	0,029	0,018	0,013	0,000	0,000	0,014	0,022	0,000	0,001
Ti	0,021	0,010	0,010	0,019	0,012	0,012	0,021	0,015	0,014	0,016	0,018	0,014	0,012
Mg	0,758	0,985	1,031	0,761	0,990	1,046	0,748	1,089	1,155	0,836	0,820	1,190	1,212
Fe^{2+}	0,484	0,756	0,828	0,429	0,724	0,728	0,375	0,681	0,741	0,374	0,367	0,638	0,677
Mn	0,011	0,018	0,020	0,011	0,021	0,021	0,011	0,016	0,017	0,011	0,012	0,011	0,018
Ni	0,001	0,001	0,001	0,001	0,001	0,001	0,002	0,001	0,001	0,001	0,001	0,002	0,001
Ca	0,700	0,218	0,106	0,728	0,194	0,148	0,817	0,200	0,078	0,738	0,746	0,187	0,081
Na	0,019	0,007	0,005	0,019	0,006	0,006	0,020	0,007	0,004	0,017	0,021	0,006	0,003
K	0,003	0,002	0,003	0,002	0,002	0,002	0,003	0,003	0,003	0,003	0,003	0,002	0,002
Cr^{3+}	0,005	0,004	0,004	0,004	0,002	0,002	0,003	0,002	0,002	0,004	0,003	0,002	0,002
ε	4,013	4,006	4,008	3,998	3,983	3,986	4,013	4,011	4,010	4,014	4,013	4,032	4,009

ATOM PER CENT

Mg	39,0	50,3	52,5	39,7	51,9	54,4	38,6	55,3	58,5	42,9	42,4	59,1	61,5
Fe	24,9	38,6	42,1	22,4	38,0	37,9	19,3	34,6	37,5	19,2	19,0	31,7	34,4
Ca	36,1	11,1	5,4	38,0	10,2	7,7	42,1	10,2	4,0	37,9	38,6	9,3	4,1

MICROPROBE ANALYSES OF PYROXENES (BULK COMPOSITIONS)

	MAIN ZONE									CRITICAL ZONE			
Sample #	78-192-C	78-192-2	78-207-1	78-207-2	78-76B-1	78-76B-2	78-92-1	78-92-C	78-92-2	78-145-1	78-145-2	78-481-1	78-481-2
SiO_2	51,67	52,48	51,46	53,72	51,56	52,50	51,56	51,93	52,06	51,70	52,54	51,80	52,57
Al_2O_3	0,88	0,79	2,17	0,79	1,59	0,77	1,64	0,87	0,78	2,45	0,68	1,89	1,12
TiO_2	0,42	0,42	0,57	0,29	0,61	0,41	0,60	0,43	0,42	0,41	0,38	0,88	0,40
MgO	21,38	22,28	14,94	23,64	14,84	23,20	15,10	21,65	22,99	17,51	25,14	15,79	27,30
FeO*	19,87	21,54	10,03	18,81	10,16	19,99	11,71	19,86	21,88	10,48	19,17	6,93	14,84
MnO	0,28	0,53	0,35	0,51	0,32	0,29	0,34	0,45	0,49	0,26	0,50	0,25	0,23
NiO	0,10	0,04	0,04	0,04	N.d.	N.d.	0,04	0,05	0,05	0,05	0,06	N.d.	0,00
CaO	4,64	1,81	18,56	2,02	19,87	1,48	18,22	5,32	1,76	17,00	1,68	20,03	1,64
Na_2O	0,09	0,07	0,24	0,06	0,26	0,05	0,24	0,10	0,08	0,19	0,04	0,34	0,05
K_2O	0,05	0,06	0,06	0,05	0,05	0,05	0,06	0,05	0,05	0,05	0,06	0,12	0,05
Cr_2O_3	0,09	0,11	0,16	0,12	0,26	0,15	0,13	0,12	0,12	0,23	0,21	0,32	0,26
Total	99,47	100,13	98,58	100,05	99,52	98,89	99,64	100,83	100,68	100,34	100,46	98,35	98,46

CATIONS BASED ON 6 OXYGENS

Si	1,943	1,957	1,943	1,976	1,938	1,964	1,940	1,932	1,937	1,913	1,935	1,942	1,933
Al^{iv}	0,039	0,035	0,057	0,024	0,062	0,034	0,060	0,038	0,034	0,087	0,029	0,058	0,049
Al^{vi}	0,000	0,000	0,039	0,010	0,008	0,000	0,013	0,000	0,000	0,020	0,000	0,035	0,000
Ti	0,012	0,012	0,016	0,008	0,017	0,012	0,017	0,012	0,012	0,011	0,011	0,025	0,011
Mg	1,198	1,238	0,840	1,296	0,830	1,294	0,847	1,200	1,275	0,965	1,380	0,882	1,496
Fe^{2+}	0,625	0,672	0,317	0,579	0,319	0,626	0,368	0,618	0,681	0,324	0,590	0,217	0,456
Mn	0,009	0,017	0,011	0,016	0,010	0,009	0,011	0,014	0,015	0,008	0,016	0,008	0,007
Ni	0,003	0,001	0,001	0,001	N.d.	0,000	0,001	0,001	0,001	0,001	0,002	0,000	0,000
Ca	0,187	0,072	0,751	0,080	0,800	0,059	0,734	0,212	0,070	0,674	0,066	0,805	0,065
Na	0,007	0,005	0,018	0,004	0,019	0,004	0,018	0,007	0,006	0,014	0,003	0,025	0,004
K	0,002	0,003	0,003	0,002	0,002	0,002	0,003	0,002	0,002	0,002	0,003	0,006	0,002
Cr^{3+}	0,003	0,003	0,005	0,003	0,008	0,004	0,004	0,004	0,004	0,007	0,006	0,009	0,008
ε	4,028	4,016	4,001	4,000	4,016	4,008	4,015	4,040	4,037	4,027	4,040	4,002	4,031

ATOM PER CENT

Mg	59,6	62,5	44,1	66,3	42,6	65,4	43,4	59,1	62,9	49,2	67,8	46,3	74,2
Fe	31,1	33,9	16,6	29,6	16,4	31,6	18,9	30,4	33,6	16,5	29,0	11,4	22,6
Ca	9,3	3,6	39,3	4,1	41,0	3,0	37,7	10,4	3,5	34,3	3,3	42,3	3,2

MICROPROBE ANALYSES OF PYROXENES (BULK COMPOSITIONS)

	Critical Zone												
Sample #	GP3-241-1	GP3-241-2	78-365-1	78-365-2	78-403C1	78-403C2	78-404-1	78-404-2	78-413B1	78-413B2	78-431-1	78-431-2	3-2455-1
SiO_2	51,85	53,68	51,76	54,06	51,29	54,70	51,55	54,77	51,86	54,41	50,18	52,25	51,09
Al_2O_3	2,47	0,85	2,33	0,96	2,10	1,02	2,13	1,03	2,21	1,21	2,61	1,22	2,47
TiO_2	0,43	0,26	0,45	0,35	0,44	0,29	0,39	0,26	0,45	0,23	0,36	0,28	0,42
MgO	16,76	25,89	16,04	23,59	15,70	27,90	15,28	26,94	16,24	27,52	14,91	23,86	15,83
FeO^*	8,83	16,29	9,62	18,42	6,86	14,26	7,88	15,25	7,44	14,34	10,54	19,26	10,43
MnO	0,21	0,32	0,33	0,41	0,26	0,43	0,25	0,42	0,20	0,43	0,31	0,33	0,28
NiO	0,04	0,04	0,04	0,04	N.d.	N.d.	0,05	0,04	0,04	0,04	N.d.	N.d.	0,04
CaO	18,03	1,96	18,80	1,86	20,40	1,42	20,44	1,83	18,84	1,24	19,49	2,04	17,50
Na_2O	0,26	0,05	0,25	0,05	0,35	0,06	0,35	0,03	0,36	0,08	0,31	0,07	0,28
K_2O	0,05	0,04	0,05	0,06	0,06	0,05	0,05	0,06	0,06	0,04	0,05	0,04	0,06
Cr_2O_3	0,47	0,30	0,37	0,25	1,06	0,38	0,96	0,24	0,91	0,46	0,38	0,15	0,51
Total	99,40	99,68	100,04	100,05	98,52	100,51	99,33	100,87	98,61	100,00	99,14	99,50	98,91

CATIONS BASED ON 6 OXYGENS

Si	1,927	1,940	1,924	1,982	1,926	1,959	1,927	1,964	1,938	1,959	1,900	1,941	1,923
Al^{iv}	0,073	0,037	0,076	0,018	0,074	0,041	0,073	0,036	0,062	0,041	0,100	0,053	0,077
Al^{vi}	0,035	0,000	0,026	0,023	0,019	0,002	0,021	0,007	0,035	0,010	0,016	0,000	0,032
Ti	0,012	0,007	0,013	0,010	0,012	0,008	0,011	0,007	0,013	0,006	0,010	0,008	0,012
Mg	0,928	1,409	0,888	1,289	0,879	1,489	0,851	1,439	0,904	1,476	0,841	1,321	0,888
Fe^{2+}	0,274	0,498	0,299	0,565	0,215	0,427	0,246	0,457	0,232	0,432	0,334	0,598	0,328
Mn	0,007	0,010	0,010	0,013	0,008	0,013	0,008	0,013	0,006	0,013	0,010	0,010	0,009
Ni	0,001	0,001	0,001	0,001	N.d.	N.d.	0,002	0,001	0,001	0,001	N.d.	N.d.	0,001
Ca	0,718	0,077	0,749	0,073	0,821	0,054	0,819	0,070	0,754	0,048	0,791	0,081	0,706
Na	0,019	0,004	0,018	0,004	0,025	0,004	0,025	0,002	0,026	0,006	0,023	0,005	0,020
K	0,002	0,002	0,002	0,003	0,003	0,002	0,002	0,003	0,003	0,002	0,002	0,002	0,003
Cr^{3+}	0,014	0,009	0,011	0,007	0,031	0,011	0,028	0,007	0,027	0,013	0,011	0,004	0,015
ε	4,010	4,013	4,017	3,987	4,014	4,010	4,014	4,007	4,002	4,007	4,039	4,025	4,015

ATOM PER CENT

Mg	48,3	71,0	45,9	66,9	45,9	75,6	44,4	73,2	47,8	75,5	42,8	66,0	46,2
Fe	14,3	25,1	15,4	29,3	11,3	21,7	12,9	23,2	12,3	22,1	17,0	29,9	17,1
Ca	37,4	3,9	38,7	3,8	42,9	2,8	42,7	3,6	39,7	2,4	40,2	4,1	36,7

MICROPROBE ANALYSES OF PYROXENES (BULK COMPOSITIONS)

	Critical Zone					Critical Zone				Marginal Member Adjacent The Pretoria Group			
Sample#	3-2455-2	3-2370-1	3-2370-2	3-2395-1	3-2395-2	GR1-44-1	GR1-44-3	GR1-69-1	GR1-69-2	GR1-88,48-1	GR1-88,48-2	GR1-93,26-3	GR1-93,26-1
SiO_2	53,84	53,00	54,27	53,02	54,89	53,14	51,81	52,32	50,95	52,47	52,73	51,97	52,54
Al_2O_3	1,16	1,16	1,07	2,45	1,66	1,27	1,25	1,05	0,93	1,72	0,77	1,24	0,63
TiO_2	0,36	0,44	0,29	0,50	0,27	0,35	0,36	0,37	0,27	0,48	0,31	0,42	0,30
MgO	24,35	14,97	26,47	17,24	28,96	13,59	18,14	12,90	19,01	12,57	19,66	12,58	18,50
FeO*	17,62	6,55	15,22	4,95	9,76	10,07	22,87	10,80	25,68	10,11	24,58	12,26	26,57
MnO	0,44	0,25	0,33	0,27	0,26	0,36	0,54	0,32	0,83	0,30	0,54	0,42	0,83
NiO	0,04	0,04	0,05	0,05	0,03	0,03	0,04	0,03	0,04	0,04	0,04	0,03	0,04
CaO	2,07	21,29	1,09	20,32	2,18	20,75	3,89	20,81	1,01	20,24	1,10	19,96	1,20
Na_2O	0,07	0,30	0,04	0,32	0,05	0,26	0,12	0,24	0,06	0,20	0,06	0,28	0,05
K_2O	0,06	0,04	0,04	0,04	0,06	0,06	0,06	0,04	0,04	0,06	0,05	0,06	0,06
Cr_2O_3	0,23	0,84	0,45	0,97	0,54	0,19	0,07	0,13	0,09	0,18	0,13	0,07	0,08
Total	100,24	98,88	99,32	100,13	98,66	100,07	99,15	99,01	98,91	98,40	99,97	99,29	100,80
CATIONS BASED ON 6 OXYGENS													
Si	1,966	1,977	1,972	1,934	1,963	1,983	1,975	1,983	1,963	1,987	1,988	1,973	1,986
Al^{iv}	0,034	0,023	0,028	0,066	0,037	0,017	0,025	0,017	0,037	0,013	0,012	0,027	0,014
Al^{vi}	0,016	0,028	0,018	0,039	0,033	0,039	0,031	0,030	0,005	0,064	0,022	0,029	0,014
Ti	0,010	0,012	0,008	0,014	0,007	0,010	0,010	0,011	0,008	0,014	0,009	0,012	0,009
Mg_{2+}	1,325	0,832	1,433	0,937	1,544	0,756	1,030	0,729	1,091	0,709	1,105	0,712	1,042
Fe^{2+}	0,538	0,204	0,462	0,151	0,292	0,314	0,729	0,342	0,827	0,320	0,775	0,389	0,840
Mn	0,014	0,008	0,010	0,008	0,008	0,011	0,017	0,010	0,027	0,010	0,017	0,014	0,027
Ni	0,001	0,001	0,001	0,001	0,001	0,001	0,001	0,001	0,001	0,001	0,001	0,001	0,001
Ca	0,081	0,851	0,042	0,794	0,084	0,830	0,159	0,845	0,042	0,821	0,044	0,812	0,049
Na	0,005	0,022	0,003	0,023	0,003	0,019	0,009	0,018	0,004	0,015	0,004	0,021	0,004
K^{3+}	0,003	0,002	0,002	0,002	0,003	0,003	0,003	0,002	0,002	0,003	0,002	0,003	0,003
Cr	0,007	0,025	0,013	0,028	0,015	0,006	0,002	0,004	0,003	0,005	0,004	0,002	0,002
ε	3,999	3,985	3,993	3,998	3,990	3,987	3,992	3,991	4,010	3,962	3,984	3,994	3,990
ATOM PER CENT													
Mg	68,2	44,1	73,9	49,8	80,4	39,8	53,7	38,0	55,7	38,3	57,4	37,2	54,0
Fe	27,7	10,8	23,9	8,0	15,2	16,5	38,0	17,9	42,2	17,3	40,3	20,3	43,5
Ca	4,2	45,1	2,2	42,2	4,4	43,7	8,3	44,1	2,1	44,4	2,3	42,4	2,5

MICROPROBE ANALYSES OF PYROXENES (BULK COMPOSITIONS)

	Critical Zone - Marginal Member adjacent the Pretoria Group												
Sample#	GR1-97,89-2	GR1-97,89-1	GR1-98,2-2	GR1-98,2-1	GR1-100A	GR1-100B	GR1-102,5A	GR1-102,5B	GR1-105A	GR1-105B	GR1-107,2A	GR1-107,2B	109,5A
SiO_2	52,11	51,94	52,53	51,63	52,12	52,90	51,51	51,69	52,02	52,56	51,87	52,88	52,32
Al_2O_3	1,05	0,97	0,85	0,70	1,01	0,66	1,00	0,61	1,10	0,64	1,08	0,81	1,07
TiO_2	0,38	0,29	0,32	0,31	0,26	0,30	0,31	0,33	0,41	0,24	0,42	0,27	0,43
MgO	12,39	18,34	12,16	17,97	12,74	19,08	13,21	19,38	13,39	19,11	14,31	22,86	13,27
FeO*	11,51	26,68	12,26	28,01	10,90	24,85	10,85	24,80	11,56	25,78	7,99	19,39	11,96
MnO	0,36	0,71	0,31	0,70	0,32	0,68	0,38	0,75	0,39	0,77	0,18	0,50	0,45
NiO	0,04	0,06	0,07	0,07	0,08	0,07	0,04	0,04	0,03	0,04	0,03	0,04	0,03
CaO	21,37	1,31	20,79	1,22	21,01	1,36	20,89	1,41	20,60	1,17	20,96	0,92	20,07
Na_2O	0,25	0,05	0,19	0,03	0,25	0,08	0,27	0,06	0,25	0,05	0,26	0,04	0,20
K_2O	0,04	0,06	0,05	0,05	0,06	0,06	0,05	0,05	0,04	0,05	0,05	0,04	0,04
Cr_2O_3	0,10	0,12	0,07	0,11	0,09	0,07	0,12	0,09	0,09	0,11	0,15	0,15	0,06
Total	99,60	100,53	99,60	100,87	98,84	100,11	98,63	99,21	99,88	100,52	97,30	97,90	99,90
CATIONS BASED ON 6 OXYGENS													
Si	1,973	1,972	1,990	1,968	1,981	1,996	1,976	1,963	1,986	1,977	1,977	1,988	1,972
Al^{iv}	0,027	0,028	0,010	0,031	0,019	0,004	0,034	0,024	0,037	0,014	0,023	0,012	0,028
Al^{vi}	0,020	0,015	0,028	0,000	0,026	0,025	0,011	0,003	0,012	0,014	0,025	0,024	0,020
Ti	0,011	0,008	0,009	0,009	0,007	0,009	0,009	0,009	0,012	0,007	0,012	0,008	0,012
Mg	0,699	1,038	0,686	1,021	0,722	1,073	0,751	1,104	0,753	1,076	0,813	1,281	0,746
Fe^{2+}	0,364	0,847	0,388	0,893	0,346	0,784	0,346	0,793	0,365	0,815	0,255	0,610	0,377
Mn	0,012	0,023	0,010	0,023	0,010	0,022	0,012	0,024	0,012	0,025	0,006	0,016	0,014
Ni	0,001	0,002	0,002	0,002	0,003	0,002	0,001	0,001	0,001	0,001	0,001	0,001	0,001
Ca	0,867	0,053	0,844	0,050	0,856	0,055	0,854	0,058	0,833	0,047	0,856	0,037	0,811
Na	0,018	0,004	0,014	0,002	0,018	0,006	0,020	0,004	0,018	0,004	0,019	0,003	0,015
K	0,002	0,003	0,002	0,002	0,003	0,003	0,002	0,002	0,002	0,002	0,002	0,002	0,002
Cr^{3+}	0,003	0,004	0,002	0,003	0,003	0,002	0,004	0,003	0,003	0,003	0,005	0,004	0,002
ε	3,997	3,996	3,985	4,004	3,994	3,981	4,012	4,003	4,010	3,994	3,995	3,986	3,999
ATOM PER CENT													
Mg	36,2	53,5	35,8	52,0	37,5	56,1	38,5	56,5	38,6	55,5	42,3	66,4	38,6
Fe	18,9	43,7	20,2	45,5	18,0	41,0	17,7	40,6	18,7	42,0	13,2	31,6	19,5
Ca	44,9	2,7	44,0	2,5	44,5	2,9	43,8	3,0	42,7	2,4	44,5	1,9	41,9

MICROPROBE ANALYSES OF PYROXENES (BULK COMPOSITIONS)

M Mb ADJACENT THE PRETORIA GROUP. CRITICAL ZONE - MARGINAL MEMBER OVERLYING LOWER ZONE.

Sample #	GR1-109,5B	78-374-1	78-374-2	78-53-1	78-53-2	78-72-1	78-72-2	GR4-1-A	GR4-1-B	GR4-3B-A	GR4-3B-B	GR4-5-A	GR4-5-C
SiO_2	51,75	52,10	52,71	51,91	53,35	52,19	52,47	52,18	52,34	52,08	53,68	52,26	51,65
Al_2O_3	0,65	1,36	0,71	1,61	0,67	1,94	0,91	1,76	0,85	1,67	0,98	1,53	0,90
TiO_2	0,29	0,49	0,27	0,54	0,32	0,60	0,31	0,41	0,25	0,39	0,26	0,45	0,28
MgO	19,46	14,17	22,82	13,37	20,93	15,05	22,81	14,56	24,55	14,35	24,28	14,29	22,35
FeO*	25,78	9,46	21,03	9,94	23,05	11,86	20,96	7,76	17,59	7,76	16,86	9,47	19,38
MnO	0,67	0,30	0,57	0,35	0,63	0,35	0,50	0,33	0,46	0,28	0,35	0,37	0,50
NiO	0,03	0,03	0,03	0,04	0,04	0,04	0,04	0,04	0,04	0,04	0,04	0,03	N.d.
CaO	1,29	21,99	0,81	21,04	1,29	17,99	1,82	21,46	1,57	21,24	1,36	20,56	4,63
Na_2O	0,08	0,25	0,04	0,20	0,04	0,24	0,08	0,30	0,07	0,27	0,09	0,21	0,09
K_2O	0,03	0,06	0,07	0,08	0,04	0,04	0,02	0,06	0,06	0,06	0,05	0,05	0,06
Cr_2O_3	0,06	0,11	0,10	0,17	0,12	0,39	0,35	0,30	0,23	0,51	0,29	0,24	0,16
Total	100,09	100,32	99,16	99,25	100,48	100,69	100,27	99,16	99,01	98,65	98,24	99,46	100,00

CATIONS BASED ON 6 OXYGENS

Si	1,968	1,946	1,973	1,958	1,988	1,940	1,950	1,953	1,971	1,959	1,988	1,960	1,930
Al^{iv}	0,029	0,054	0,027	0,042	0,012	0,060	0,040	0,047	0,029	0,041	0,012	0,040	0,040
Al^{vi}	0,000	0,006	0,004	0,030	0,017	0,025	0,000	0,031	0,008	0,033	0,031	0,028	0,000
Ti	0,008	0,014	0,008	0,015	0,009	0,017	0,009	0,012	0,007	0,011	0,007	0,013	0,008
Mg	1,103	0,789	1,273	0,752	1,163	0,834	1,263	0,812	1,352	0,804	1,340	0,799	1,245
Fe^{2+}	0,820	0,296	0,658	0,314	0,718	0,369	0,651	0,243	0,544	0,244	0,522	0,297	0,606
Mn	0,022	0,009	0,018	0,011	0,020	0,011	0,016	0,010	0,014	0,009	0,011	0,012	0,016
Ni	0,001	0,001	0,001	0,001	0,001	0,001	0,001	0,001	0,001	0,001	0,001	0,001	N.d.
Ca	0,053	0,880	0,032	0,851	0,052	0,717	0,072	0,861	0,062	0,856	0,054	0,826	0,185
Na	0,006	0,018	0,003	0,015	0,003	0,017	0,006	0,022	0,005	0,020	0,006	0,015	0,007
K	0,001	0,003	0,003	0,004	0,002	0,002	0,001	0,003	0,003	0,003	0,002	0,002	0,003
Cr^{3+}	0,002	0,003	0,003	0,005	0,004	0,011	0,010	0,009	0,007	0,015	0,008	0,007	0,005
ε	4,012	4,019	4,005	3,997	3,989	4,004	4,020	4,004	4,004	3,997	3,984	3,999	4,044

ATOM PER CENT

Mg	55,8	40,2	64,8	39,2	60,2	43,4	63,6	42,4	69,1	42,2	69,9	41,6	61,1
Fe	41,5	15,0	33,5	16,4	37,2	19,2	32,8	12,7	27,8	12,8	27,3	15,5	29,8
Ca	2,7	44,8	1,7	44,4	2,7	37,3	3,6	44,9	3,2	44,9	2,8	43,0	9,1

MICROPROBE ANALYSES OF PYROXENES (BULK COMPOSITIONS)

Sample #	GR4-5-B	GR4-6-A	GR4-6-B	APA-1	APA-2
SiO_2	53,55	50,98	53,49	53,54	55,69
Al_2O_3	1,01	2,18	0,94	2,42	1,53
TiO_2	0,24	0,47	0,35	0,44	0,27
MgO	23,09	13,77	23,10	17,57	30,60
FeO*	19,95	8,98	19,14	4,67	9,23
MnO	0,34	0,41	0,54	0,18	0,28
NiO	0,03	0,03	0,04	0,20	0,22
CaO	1,09	21,79	1,50	20,30	1,42
Na_2O	0,05	0,30	0,05	0,44	0,07
K_2O	0,07	0,05	0,05	0,04	0,05
Cr_2O_3	0,10	0,19	0,20	0,89	0,55
Total	99,52	99,15	99,40	100,69	99,91
CATIONS BASED ON 6 OXYGENS					
Si	1,983	1,926	1,981	1,939	1,960
Al^{iv}	0,017	0,074	0,019	0,061	0,040
Al^{vi}	0,027	0,023	0,022	0,042	0,023
Ti	0,007	0,013	0,010	0,012	0,007
Mg_{2+}	1,274	0,775	1,275	0,948	1,605
Fe^{2+}	0,618	0,284	0,593	0,141	0,272
Mn	0,011	0,013	0,017	0,006	0,008
Ni	0,001	0,001	0,001	0,006	0,006
Ca	0,043	0,882	0,060	0,788	0,054
Na	0,004	0,022	0,004	0,031	0,005
K	0,003	0,002	0,002	0,002	0,002
Cr^{3+}	0,003	0,006	0,006	0,025	0,015
ε	3,990	4,021	3,989	4,001	3,997
ATOM PER CENT					
Mg	65,8	39,9	66,2	50,5	83,2
Fe	31,9	14,6	30,8	7,5	14,1
Ca	2,2	45,4	3,1	42,0	2,8

Sample No.	Stratigraphic Level	Status
5-124-1	+ 1480 m	Cumulus CPX
5-124-C	+ 1480 m	Cumulus OPX (Inv. Pig.)
5-124-2	+ 1480 m	MATRIX OPX in Inv. Pig.
5-233-1	+ 1446 m	Cumulus CPX
5-233-C	+ 1446 m	Cumulus OPX (Inv. Pig.)
5-233-2	+ 1446 m	MATRIX OPX in Inv. Pig.
5-640-3A	+ 1324 m	Cumulus CPX
5-640-C	+ 1324 m	Cumulus OPX (Inv. Pig.)
5-640-1	+ 1324 m	MATRIX OPX in Inv. Pig.
5-935-3A	+ 1240 m	Cumulus CPX
5-935-C	+ 1240 m	Cumulus OPX (Inv. Pig.)
5-935-1	+ 1240 m	Matrix OPX in Inv. Pig.
78-127-1	+ 1067 m	Cumulus CPX
78-127-2	+ 1067 m	Intercumulus OPX
78-125-A	+ 940 m	Cumulus CPX
78-125-C	+ 940 m	Cumulus OPX (Inv. Pig.)
78-125-3	+ 940 m	MATRIX OPX in Inv. Pig.
78-122-A	+ 850 m	Cumulus CPX
78-122-3	+ 850 m	Cumulus OPX (Inv. Pig.)
78-122-2	+ 850 m	MATRIX OPX in Inv. Pig.
78-350-1	+ 724 m	Cumulus CPX
78-350-C	+ 724 m	Cumulus OPX (Inv.Pig.)
78-350-2	+ 724 m	MATRIX OPX in Inv. Pig.
78-192-1	+ 566 m	Cumulus CPX
78-192-C	+ 566 m	Cumulus OPX (Inv. Pig.)
78-192-2	+ 566 m	Intercumulus OPX
78-189-1	+ 410 m	Cumulus CPX
78-189-C	+ 410 m	Cumulus OPX (Inv. Pig.)
78-189-2	+ 410 m	Intercumulus OPX
78-207-1	+ 250 m	Cumulus CPX
78-207-2	+ 250 m	Cumulus OPX
78-76B-1	+ 205 m	Intercumulus CPX
78-76B-2	+ 205 m	Cumulus OPX
78-92-1	+ 198 m	Primary CPX
78-92-C	+ 198 m	Primary Inv. Pig.
78-92-2	+ 198 m	Opnitic OPX
78-145-1	+ 180 m	Intercumulus CPX
78-145-2	+ 180 m	Cumulus OPX

Sample No.	Stratigraphic Level	Status
78-481-1	+ 76 m	Intercumulus CPX
78-481-2	+ 76 m	Cumulus OPX
GP3-241-1	+ 56 m	Cumulus CPX
GP3-241-2	+ 56 m	Cumulus OPX
78-365-1	+ 48 m	Intercumulus CPX
78-365-2	+ 48 m	Cumulus OPX
78-403C1	+ 19 m	Cumulus CPX
78-403C2	+ 19 m	Cumulus OPX
78-404-1	+ 5 m	Intercumulus CPX
78-404-2	+ 5 m	Cumulus OPX
78-413B1	- 61 m	Cumulus CPX
78-413B2	- 61 m	Cumulus OPX
78-431-1	- 94 m	Cumulus CPX
78-431-2	- 94 m	Cumulus OPX
3-2370-1	- 104 m	Primary CPX
3-2370-2	- 104 m	Primary OPX
3-2395-1	- 110 m	Intercumulus CPX
3-2395-2	- 110 m	Intercumulus OPX
3-2455-1	- 121 m	Cumulus CPX
3-2455-2	- 121 m	Cumulus OPX
GR1-44-1	M.Mb./P.G.	Primary CPX
GR1-44.3	M.Mb./P.G.	Primary Inv. Pig.
GR1-69-1	M.Mb./P.G.	Primary CPX
GR1-69-2	M.Mb./P.G.	Primary OPX
GR1-88,48-1	"	Primary CPX
GR1-88,48-2	"	Primary OPX
GR1-93,26-3	"	Primary CPX
GR1-93,26-1	"	Primary OPX
GR1-97,89-2	"	Primary CPX
GR1-97,89-1	"	Primary OPX
GR1-98,2-2	"	Primary CPX
GR1-98,2-1	"	Primary OPX
GR1-100A	"	Primary CPX
GR1-100B	"	Primary OPX
GR1-102,5A	"	Primary CPX
GR1-102,5B	"	Primary OPX
GR1-105A	"	Primary CPX
GR1-105B	"	Primary OPX
GR1-107,2A	"	Primary CPX

Sample No.	Stratigraphic Level	Status
GR1-107,2B	M.Mb.	Primary OPX
GR1-109,5A	"	Primary CPX
GR1-109,5B	"	Primary OPX
78-374-1	"	Primary CPX
78-374-2	"	Primary OPX
78-53-1	"	Primary CPX
78-53-2	"	Primary OPX
78-72-1	"	Primary CPX
78-72-2	"	Primary OPX
GR4-1-A	M.Mb/L.Z.	Primary CPX
GR4-1-B	"	Primary OPX
GR4-3B-A	"	Primary CPX
GR4-3B-B	"	Primary OPX
GR4-5-A	"	Primary CPX
GR4-5-C	"	Primary Inv. Pig.
GR4-5-B	"	Primary OPX
GR4-6-A	"	Primary CPX
GR4-6-B	"	Primary OPX
APA-1	AAPIESDORING=	Primary CPX
APA-2	DRAAI	Primary OPX

* Matrix OPX in Inv. Pig. = BULK COMPOSITION of OPX host in inverted Pigeonite.

APPENDIX 3

MICROPROBE ANALYSES OF OLIVINES

Sample #	3-2395	3-2485	3-2500	3-3027	3-3402	3-3766	3-3819	3-4002	1-50	UGC-1A	UGC-1B	UGC-1C
SiO_2	38,95	40,47	39,45	39,60	39,94	39,15	39,76	39,15	39,72	41,45	40,78	41,45
Al_2O_3	0,13	0,10	0,12	0,11	0,11	0,10	0,11	0,15	0,12	0,09	0,09	0,10
TiO_2	0,09	0,09	0,09	0,09	0,12	0,09	0,13	0,12	0,12	0,10	0,09	0,09
MgO	45,27	47,37	46,04	48,09	44,48	48,09	47,55	47,80	47,58	52,36	52,10	52,40
FeO*	14,77	11,61	12,27	11,73	13,88	11,78	12,38	11,71	10,45	6,04	5,60	5,30
MnO	0,28	0,10	0,20	0,15	0,14	0,21	0,25	0,21	0,11	0,17	0,16	0,22
NiO	0,15	0,26	0,27	0,22	0,26	0,22	0,29	0,32	0,29	0,17	0,20	0,21
CaO	0,08	0,08	0,08	0,09	0,08	0,05	0,08	0,07	0,08	0,08	0,07	0,07
Na_2O	0,05	0,04	0,05	0,04	0,05	0,05	0,04	0,04	0,03	0,04	0,05	0,06
K_2O	0,03	0,04	0,04	0,05	0,04	0,04	0,05	0,05	0,04	0,04	0,04	0,05
Cr_2O_3	0,11	0,09	0,09	0,08	0,05	0,05	0,03	0,05	0,05	0,12	0,13	0,20
Total	99,91	100,25	98,70	100,25	99,15	99,83	100,67	99,67	98,59	100,66	100,31	100,15

CATIONS BASED ON 4 OXYGENS

Si	0,981	0,998	0,993	0,980	1,006	0,974	0,983	0,976	0,992	0,994	0,981	0,996
Al	0,004	0,003	0,003	0,003	0,003	0,003	0,003	0,004	0,003	0,003	0,003	0,003
Ti	0,001	0,001	0,001	0,001	0,002	0,001	0,002	0,002	0,002	0,002	0,002	0,002
Mg_{2+}	1,700	1,741	1,728	1,774	1,670	1,784	1,752	1,776	1,772	1,871	1,904	1,876
Fe^{2+}	0,311	0,239	0,258	0,242	0,292	0,245	0,256	0,244	0,218	0,121	0,113	0,106
Mn	0,006	0,002	0,004	0,003	0,003	0,004	0,005	0,004	0,002	0,003	0,003	0,004
Ni	0,003	0,005	0,005	0,004	0,005	0,004	0,005	0,006	0,006	0,003	0,004	0,004
Ca	0,002	0,002	0,002	0,002	0,002	0,001	0,002	0,001	0,002	0,002	0,002	0,002
Na	0,002	0,002	0,002	0,002	0,002	0,002	0,002	0,002	0,001	0,002	0,002	0,003
K^{3+}	0,001	0,001	0,001	0,001	0,001	0,001	0,001	0,001	0,001	0,001	0,001	0,002
Cr	0,002	0,001	0,001	0,001	0,001	0,001	0,001	0,001	0,001	0,002	0,002	0,004
$\frac{Mg}{(Mg+Fe^{2+})}$	0,8453	0,8792	0,8700	0,8799	0,8511	0,8792	0,8725	0,8792	0,8904	0,9392	0,9439	0,9465
Stratigraphic level (m)	-110	-136	-141	-300	-416	-530	-544	-587	-620	~620	~620	~620

* TOTAL IRON AS FeO

MICROPROBE ANALYSES OF OLIVINES

Sample #	1-80,5	1-123	GV-1	GV-22	1-179	1-209	1-219	1-223	1-240,95	1-244	1-253,5	6A-243
SiO_2	39,77	39,84	39,85	41,05	40,01	39,55	39,89	39,83	39,15	39,66	40,23	39,20
Al_2O_3	0,10	0,10	0,09	0,12	0,09	0,11	0,10	0,09	0,13	0,12	0,11	0,17
TiO_2	0,13	0,11	0,13	0,10	0,11	0,11	0,11	0,10	0,12	0,09	0,12	0,09
MgO	46,19	48,61	48,63	49,00	48,40	47,56	45,71	46,69	45,55	45,83	46,51	48,77
FeO*	11,91	9,52	10,02	8,37	10,03	10,41	13,01	12,77	14,31	12,70	12,32	11,54
MnO	0,20	0,17	0,14	0,13	0,19	0,25	0,26	0,22	0,24	0,22	0,27	0,15
NiO	0,24	0,25	0,24	0,23	0,20	0,28	0,23	0,27	0,25	0,30	0,22	0,16
CaO	0,08	0,06	0,07	0,08	0,09	0,05	0,09	0,08	0,06	0,07	0,09	0,08
Na_2O	0,04	0,04	0,04	0,04	0,03	0,04	0,04	0,05	0,05	0,05	0,03	0,06
K_2O	0,04	0,04	0,04	0,04	0,05	0,05	0,05	0,04	0,04	0,04	0,04	0,04
Cr_2O_3	0,07	0,07	0,05	0,09	0,08	0,08	0,05	0,05	0,05	0,05	0,07	0,07
Total	98,77	98,91	99,30	99,25	99,23	98,49	99,54	100,19	99,95	99,13	100.01	100,33

CATIONS BASED ON 4 OXYGENS

Si	0,998	0,989	0,987	1,007	0,991	0,990	0,998	0,990	0,983	0,996	0,998	0,969
Al	0,003	0,003	0,002	0,003	0,002	0,003	0,003	0,002	0,003	0,003	0,003	0,005
Ti	0,002	0,002	0,002	0,001	0,002	0,002	0,002	0,001	0,002	0,001	0,002	0,001
Mg_{2+}	1,728	1,800	1,795	1,791	1,787	1,775	1,705	1,730	1,706	1,715	1,721	1,798
Fe^{2+}	0,250	0,197	0,207	0,171	0,208	0,218	0,275	0,265	0,300	0,266	0,255	0,238
Mn	0,004	0,003	0,003	0,003	0,004	0,005	0,005	0,004	0,005	0,004	0,005	0,003
Ni	0,005	0,005	0,004	0,004	0,004	0,005	0,004	0,005	0,005	0,006	0,004	0,003
Ca	0,002	0,001	0,002	0,002	0,002	0,001	0,002	0,002	0,001	0,002	0,002	0,002
Na	0,002	0,002	0,002	0,002	0,001	0,002	0,002	0,002	0,002	0,002	0,001	0,003
K	0,001	0,001	0,001	0,001	0,001	0,001	0,001	0,001	0,001	0,001	0,001	0,001
Cr^{3+}	0,001	0,001	0,001	0,001	0,001	0,001	0,001	0,001	0,001	0,001	0,001	0,001
$\frac{Mg}{(Mg+Fe^{2+})}$	0,8736	0,9013	0,8966	0,9128	0,8957	0,8906	0,8611	0,8671	0,8504	0,8657	0,8709	0,8831
Stratigraphic level (m)	-647	-680	-689	-690	-726	-747	-753	-758	-772	-776	-782	-784

MICROPROBE ANALYSES OF OLIVINES

Sample #	6A-259	6A-296,7	X-10	X-21	X-31	X-41	A-3	A-9	A-16
SiO_2	40,17	39,77	39,78	38,93	39,77	39,93	40,69	39,87	40,55
Al_2O_3	0,10	0,14	0,10	0,11	0,07	0,00	0,11	0,10	0,10
TiO_2	0,13	0,12	0,11	0,09	0,12	0,00	0,11	0,11	0,10
MgO	48,08	47,58	47,66	48,04	48,83	48,98	47,50	45,92	49,20
FeO*	11,82	11,20	11,68	12,60	10,15	10,50	10,58	14,01	9,73
MnO	0,28	0,12	0,17	0,15	0,22	0,17	0,17	0,10	0,18
NiO	0,22	0,21	0,23	0,16	0,10	0,23	0,26	0,22	0,27
CaO	0,11	0,08	0,06	0,07	0,03	0,02	0,06	0,07	0,09
Na_2O	0,04	0,04	0,04	0,04	0,05	0,00	0,04	0,04	0,06
K_2O	0,04	0,04	0,03	0,03	0,05	0,00	0,04	0,05	0,04
Cr_2O_3	0,05	0,07	0,11	0,06	0,07	0,02	0,03	0,10	0,05
Total	101,04	99,37	99,97	100,23	99,46	99,85	99,59	100,59	100,37

All olvines are of a cumulus origin except UGC-1B & UGC-1C. UGC-1C olivine is the vein type, and UGC-1B olivine is the spherical type included in chromite

CATIONS BASED ON 4 OXYGENS

Si	0,986	0,989	0,986	0,968	0,984	0,985	1,005	0,992	0,992
Al	0,003	0,004	0,003	0,003	0,002	0,000	0,003	0,003	0,003
Ti	0,002	0,002	0,002	0,001	0,002	0,000	0,002	0,002	0,001
Mg_{2+}	1,759	1,764	1,761	1,781	1,801	1,802	1,749	1,702	1,793
Fe^{2+}	0,242	0,233	0,242	0,262	0,210	0,216	0,218	0,291	0,199
Mn	0,005	0,002	0,003	0,003	0,004	0,003	0,003	0,002	0,003
Ni	0,004	0,004	0,004	0,003	0,002	0,004	0,005	0,004	0,005
Ca	0,003	0,003	0,001	0,001	0,000	0,000	0,001	0,001	0,002
Na	0,002	0,002	0,002	0,002	0,002	0,000	0,002	0,002	0,002
K	0,001	0,001	0,001	0,001	0,001	0,000	0,001	0,001	0,001
Cr^{3+}	0,001	0,001	0,002	0,001	0,001	0,000	0,000	0,002	0,000
$\frac{Mg}{(Mg+Fe^{2+})}$	0,8790	0,8833	0,8791	0,8717	0,8955	0,8929	0,8891	0,8539	0,9001
Stratigraphic level	-797	-826	-1058	-1165	-1250	-1302	-1408	-1484	-1640

APPENDIX 4

MICROPROBE ANALYSES OF PLAGIOCLASE FELDSPARS

	UPPER ZONE									MAIN ZONE		
Sample #	5-124	5-138	5-195	5-233	5-410	5-440	5-508	5-616	5-640	5-935	5-1100	5-1300
SiO_2	55,26	55,00	54,53	55,13	54,81	53,54	54,81	54,49	55,24	52,52	54,31	52,43
Al_2O_3	28,08	28,53	28,67	28,57	27,88	28,95	28,97	28,52	27,93	30,42	28,50	30,57
FeO^*	0,54	0,40	0,37	0,33	0,40	0,39	0,53	0,38	0,40	0,51	0,51	0,46
CaO	9,89	10,45	10,48	10,78	10,92	11,28	10,76	11,43	10,81	12,31	11,99	12,36
Na_2O	5,32	4,97	4,90	5,06	5,11	4,47	5,00	4,72	4,54	4,41	4,61	4,20
K_2O	0,44	0,50	0,43	0,55	0,25	0,50	0,42	0,69	0,45	0,53	0,45	0,46
Total	99,56	99,85	99,38	100,42	99,41	100,16	100,54	100,23	99,37	100,77	100,37	100,52

CATIONS BASED ON 32 OXYGENS

Si	10,008	9,937	9,896	9,918	9,960	9,770	9,855	9,851	10,016	9,488	9,816	9,482
Al	5,994	6,071	6,128	6,059	5,971	6,226	6,140	6,078	5,970	6,478	6,072	6,516
Fe^{2+}	0,083	0,060	0,056	0,049	0,062	0,059	0,081	0,057	0,060	0,077	0,077	0,070
Ca	1,920	2,023	2,038	2,078	2,126	2,205	2,073	2,214	2,100	2,384	2,322	2,395
Na	1,896	1,741	1,724	1,765	1,803	1,582	1,745	1,654	1,596	1,555	1,615	1,472
K	0,101	0,115	0,100	0,126	0,058	0,118	0,098	0,159	0,104	0,123	0,103	0,107
$\frac{Ca}{(Ca+Na+K)}$	0,4901	0,5215	0,5277	0,5235	0,5332	0,5646	0,5293	0,5497	0,5526	0,5869	0,5747	0,6026
Cumulus	x	x	x	x	x	x	x	x	x	x	x	x
Intercumulus												
Stratigraphic level	+1480	+1475	+1460	+1446	+1392	+1382	+1360	+1332	+1324	+1240	+1190	+1130

* TOTAL IRON AS FeO

MICROPROBE ANALYSES OF PLAGIOCLASE FELDSPARS

	MAIN ZONE										CRITICAL ZONE	
Sample #	78-127	78-125	78-122	78-350	78-192	78-189	78-207	78-76B	78-92	78-145-1	78-145-2	78-60A
SiO_2	50,91	52,20	55,25	52,44	52,66	52,03	51,65	50,43	52,55	48,83	49,53	51,35
Al_2O_3	30,41	29,31	27,83	29,38	29,79	29,73	30,46	31,23	29,97	33,10	33,11	31,13
FeO^*	0,46	0,52	0,30	0,29	0,53	0,61	0,32	0,30	0,50	0,33	0,25	0,26
CaO	13,90	12,64	10,75	12,58	12,64	12,80	14,24	14,15	11,88	14,94	13,25	13,10
Na_2O	3,21	4,29	5,02	4,61	4,29	3,91	3,27	3,17	4,50	2,67	3,33	3,68
K_2O	0,24	0,43	0,41	0,42	0,31	0,25	0,25	0,20	0,36	0,23	0,18	0,24
Total	99,13	99,39	99,56	99,72	100,22	99,33	100,19	99,48	99,76	100,15	99,65	99,76

CATIONS BASED ON 32 OXYGENS

Si	9,355	9,564	10,010	9,572	9,555	9,524	9,389	9,237	9,563	8,922	9,038	9,350
Al	6,587	6,330	5,944	6,322	6,372	6,415	6,527	6,743	6,429	7,122	7,122	6,682
Fe^{2+}	0,070	0,079	0,045	0,044	0,080	0,093	0,048	0,045	0,076	0,050	0,038	0,039
Ca	2,736	2,481	2,087	2,460	2,457	2,510	2,773	2,777	2,316	2,922	2,590	2,556
Na	1,143	1,524	1,763	1,631	1,509	1,387	1,152	1,125	1,587	0,944	1,178	1,299
K	0,056	0,100	0,094	0,097	0,071	0,058	0,057	0,043	0,083	0,053	0,041	0,055
$\frac{Ca}{(Ca+Na+K)}$	0,6952	0,6043	0,5291	0,5873	0,6086	0,6346	0,6963	0,7033	0,5810	0,7455	0,6799	0,6537
Cumulus	x	x	x	x	x	x	x	x		x		
Intercumulus											x	x
Stratigraphic level (m)	+1067	+ 940	+ 850	+ 724	+ 566	+ 410	+ 250	+ 205	+ 198	+ 180	+ 180	+ 128

MICROPROBE ANALYSES OF PLAGIOCLASE FELDSPARS

	CRITICAL ZONE										
Sample #	78-128D	78-481	GP3-241-1	GP3-241-2	78-365	78-403B	78-404	78-424	78-413B	78-160 B	78-431-2
SiO_2	50,22	49,10	48,53	50,40	50,30	50,60	51,07	49,14	50,40	51,54	51,60
Al_2O_3	31,30	32,16	33,05	31,14	31,00	30,96	30,70	32,51	31,52	29,66	30,25
FeO^*	0,45	0,33	0,21	0,32	0,51	0,26	0,27	0,48	0,34	0,27	0,57
CaO	14,04	13,98	15,82	14,04	13,69	13,89	13,47	15,72	14,18	13,64	13,31
Na_2O	3,40	3,19	2,46	3,49	3,50	3,27	3,72	2,50	2,92	3,86	3,93
K_2O	0,19	0,25	0,15	0,13	0,23	0,18	0,11	0,16	0,18	0,15	0,28
Total	99,60	99,03	100,27	99,52	99,73	99,16	99,34	100,51	99,54	99,22	99,94

CATIONS BASED ON 32 OXYGENS

Si	9,202	9,051	8,872	9,234	9,286	9,287	9,351	8,957	9,217	9,463	9,412
Al	6,761	6,987	7,115	6,725	6,680	6,699	6,626	6,986	7,795	6,419	6,504
Fe^{2+}	0,068	0,051	0,032	0,049	0,077	0,039	0,041	0,073	0,052	0,041	0,086
Ca	2,756	2,761	3,095	2,756	2,681	2,731	2,642	3,070	2,778	2,683	2,601
Na	1,208	1,143	0,871	1,239	1,240	1,163	1,320	0,883	1,035	1,374	1,390
K	0,044	0,058	0,034	0,030	0,053	0,042	0,025	0,037	0,042	0,058	0,065
$\frac{Ca}{(Ca+Na+K)}$	0,6876	0,6968	0,7737	0,6847	0,6746	0,6938	0,6626	0,7694	0,7206	0,6520	0,6412
Cumulus	x		x		x			x			
Intercumulus		x		x		x	x		x	x	
Stratigraphic level (m)	+ 123	+ 76	+ 56	+ 56	+ 48	+ 19	+ 5	- 22	- 61	- 86	- 94

MICROPROBE ANALYSES OF PLAGIOCLASE FELDSPARS

	CRITICAL ZONE			MARGINAL MEMBER OF CRITICAL ZONE						
Sample #	78-422	3-2370	3-2455	78-374D	78-53	78-359B	78-361	GR1-44	GR1-69	GR1-88,48
SiO_2	52,15	50,37	50,40	49,33	54,15	50,30	50,86	52,01	55,81	50,69
Al_2O_3	30,05	31,22	30,54	31,77	29,18	31,34	31,07	30,73	28,76	31,53
FeO*	0,43	0,54	0,29	0,37	0,41	0,46	0,22	0,38	0,22	0,44
CaO	13,43	13,98	13,29	15,14	12,05	12,69	13,61	13,26	9,93	14,12
Na_2O	3,76	3,93	3,98	2,58	4,64	3,86	3,40	3,55	5,44	2,61
K_2O	0,25	0,21	0,35	0,17	0,31	0,30	0,26	0,32	0,33	0,89
Total	100,07	100,25	98,85	99,38	100,77	99,00	99,42	100,29	100,52	100,28

CATIONS BASED ON 32 OXYGENS

Si	9,482	9,193	9,302	9,073	9,742	9,252	9,305	9,427	9,988	9,230
Al	6,440	6,717	6,644	6,886	6,187	6,795	6,701	6,563	6,066	6,762
Fe^{2+}	0,065	0,082	0,044	0,057	0,062	0,071	0,033	0,058	0,033	0,067
Ca	2,616	2,734	2,628	2,983	2,323	2,501	2,668	2,576	1,904	2,755
Na	1,325	1,390	1,424	0,920	1,619	1,379	1,206	1,250	1,888	0,922
K	0,057	0,043	0,082	0,040	0,071	0,071	0,060	0,074	0,076	0,207
$\frac{Ca}{(Ca+Na+K)}$	0,6543	0,6561	0,6357	0,7565	0,5788	0,6330	0,6781	0,6605	0,4922	0,7093
Cumulus	x									
Intercumulus				**	**	**	**	**	**	**
STRAT. LEVEL	- 95	- 104	- 121	SURFACE SAMPLES				DRILL HOLE INTERSECTION (DDH-GR1)		

** MARGINAL MEMBER OF CRITICAL ZONE ADJACENT THE PRETORIA GROUP
*** MARGINAL MEMBER OF CRITICAL ZONE ADJACENT THE LOWER ZONE

MICROPROBE ANALYSES OF PLAGIOCLASE FELDSPARS

			MARGINAL MEMBER OF CRITICAL ZONE										
Sample #	GR1-93,26	GR1-97,89	GR1-98,2	GR1-100	GR1-102,5	GR1-105	GR1-107,2	GR1-109,57	GR4-1	GR4-3B	GR4-5	GR4-6	78-154A
SiO_2	55,76	56,03	54,39	56,20	55,77	52,61	55,07	54,04	50,60	50,75	52,40	51,96	53,08
Al_2O_3	28,57	28,25	29,49	27,79	27,57	29,33	29,02	29,27	30,95	31,88	30,37	30,96	29,86
FeO^*	0,38	0,34	0,30	0,40	0,58	1,10	0,32	0,31	0,29	0,38	0,43	0,63	0,69
CaO	9,90	10,04	10,75	9,41	9,17	11,93	10,53	10,42	13,30	14,21	12,60	13,35	12,10
Na_2O	5,39	5,49	5,22	5,36	5,45	4,35	4,93	5,19	3,67	3,31	4,03	3,39	4,24
K_2O	0,36	0,33	0,27	0,88	0,93	0,85	0,48	0,41	0,27	0,23	0,30	0,26	0,35
Total	100,39	100,51	100,45	100,08	99,52	100,22	100,39	99,66	99,11	100,78	100,16	100,58	100,32

CATIONS BASED ON 32 OXYGENS

Si	9,999	10,038	9,781	10,118	10,086	9,588	9,893	9,793	9,297	9,186	9,500	9,395	9,605
Al	6,039	5,965	6,250	5,876	6,301	6,145	6,145	6,251	6,702	6,801	6,491	6,599	6,369
Fe^{2+}	0,058	0,051	0,045	0,060	0,086	0,168	0,048	0,047	0,044	0,057	0,066	0,096	0,104
Ca	1,902	1,928	2,071	1,816	1,778	2,330	2,028	2,023	2,618	2,756	2,448	2,586	2,346
Na	1,876	1,909	1,820	1,873	1,913	1,537	1,718	1,825	1,308	1,164	1,419	1,190	1,487
K	0,082	0,077	0,062	0,202	0,216	0,198	0,111	0,095	0,060	0,053	0,069	0,060	0,080
$\frac{Ca}{(Ca+Na+K)}$	0,4927	0,4925	0,5239	0,4667	0,4550	0,5731	0,5257	0,5130	0,6567	0,6936	0,6219	0,6741	0,5995
Cumulus													
Intercumulus	**	**	**	**	**	**	**	**	***	***	***	***	***

APPENDIX 5 PHLOGOPITE, AMPHIBOLE, CHALCEDONY, AND IRON RICH ALTERATION PHASES - MICROPROBE CHEMICAL ANALYSES

Sample #	(1)	(2)	(3)	(4)	(5)	(6)	(7)	(8)	(9)	(10)
SiO_2	37,00	36,43	48,44	36,36	30,89	30,00	28,62	28,50	32,22	95,22
Al_2O_3	13,83	13,88	1,88	18,25	13,09	15,68	15,03	14,93	0,15	0,99
TiO_2	2,56	4,35	0,48	0,13	0,14	0,13	2,47	4,95	0,17	0,12
MgO	18,25	15,92	11,68	1,23	7,97	8,89	9,42	7,69	2,36	0,09
FeO*	14,07	15,43	15,14	19,05	38,89	37,41	28,27	30,28	45,05	0,16
MnO	0,11	0,09	0,35	0,07	0,27	0,27	0,20	0,14	3,35	0,10
NiO	0,28	0,16	0,23	0,82	0,76	0,79	0,90	0,79	1,18	-
CaO	0,10	0,16	18,68	22,00	2,06	1,23	0,68	1,34	0,21	0,07
Na_2O	0,09	0,07	0,12	0,06	0,12	0,10	0,08	0,08	14,41	0,11
K_2O	7,06	8,61	0,04	0,04	0,10	0,09	4,33	2,61	0,06	0,20
Cr_2O_3	0,32	0,60	0,06	0,05	0,10	0,08	0,08	0,11	0,00	0,42
Total	93,67	95,70	97,15	98,09	94,39	94,67	90,08	91,42	99,18	97,47
Si	5,550	5,443	7,341							
Al	2,444	2,443	0,336							
Ti	0,288	0,488	0,055							
Mg	4,080	3,545	2,639							
Fe^{2+}	1,764	1,927	1,919							
Mn	0,013	0,011	0,045							
Ni	0,033	0,019	0,029							
Ca	0,016	0,025	3,033							
Na	0,026	0,020	0,035							
K	1,353	1,644	0,007							
Cr	0,037	0,070	0,008							
Oxygens	22	22	23							

1) 78-72, Phlogopite
2) 78-360A, Biotite adjacent Ilmenite
3) 5-616,5, Amphibole alteration after Augite
4) 5-124-1, Silicate com= position associated with sulfide - silicate droplet
5) 5-138-4, Altered ortho= pyroxene
6) 5-195-1, "
7) 5-440-1, "
8) 5-440-6, "
9) 2A-47-8, ?
10) 78-257, Chalcedony Pseudomorph after Olivine (Fo_{93})

* Total Iron as FeO

APPENDIX 6 MAGNETITE AND ILMENITE ANALYSES FROM THE CRITICAL AND UPPER ZONE, SOUTH OF POTGIETERSRUS

MAGNETITE ANALYSES

Sample #	GR1-69A	GR1-69C	GR1-88A	GR1-88C	GR1-100A	GR1-100C	GR1-102A	GR1-102C	GR1-107A
SiO_2	0,00	0,00	0,00	0,00	0,00	0,00	0,00	0,00	0,00
TiO_2	0,86	17,08	0,69	17,70	0,79	17,28	5,02	19,96	0,77
Al_2O_3	1,04	0,73	0,63	0,47	0,82	0,58	2,94	2,00	0,82
Cr_2O_3	0,79	0,59	3,95	2,72	0,64	0,45	0,77	0,55	0,74
FeO	31,69	45,74	31,13	45,62	31,32	45,24	35,26	47,41	31,38
Fe_2O_3	65,09	33,74	61,97	29,91	65,26	33,42	55,18	27,05	65,48
MnO	0,12	0,76	0,18	1,07	0,21	1,31	0,77	2,02	0,18
MgO	0,04	0,06	0,04	0,07	0,04	0,05	0,10	0,11	0,09
Total	99,64	98,71	98,59	97,56	99,09	98,34	100,02	99,10	99,46
X^{ulv}(Max)	0,024	0,490	0,020	0,513	0,023	0,498	0,142	0,564	0,022
X^{mt}(Min)	0,933	0,450	0,896	0,395	0,939	0,436	0,751	0,312	0,936
X^{mt}(Max)	0,939	0,484	0,904	0,434	0,948	0,482	0,781	0,382	0,947
X^{ulv}(Min)	0,021	0,476	0,016	0,494	0,018	0,475	0,127	0,529	0,016

ILMENITE ANALYSES

Sample #	GR1-69B	GR1-69D	GR1-88B	GR1-88D	GR1-100B	GR1-100D	GR1-102B	GR1-102D	GR1-107B
TiO_2	49,75	49,40	51,96	49,79	50,51	49,08	50,05	49,61	50,51
Al_2O_3	0,13	0,13	0,16	0,15	0,13	0,13	0,13	0,15	0,14
Cr_2O_3	0,17	0,12	0,24	0,48	0,09	0,14	0,12	0,14	0,09
FeO	42,44	41,24	43,57	42,21	41,66	40,57	40,09	39,70	41,66
Fe_2O_3	5,86	6,56	0,20	4,16	4,55	7,29	5,88	5,05	4,41
MnO	2,06	2,93	2,85	2,27	3,52	3,29	4,57	4,66	3,50
MgO	0,08	0,08	0,11	0,11	0,07	0,09	0,12	0,07	0,08
Total	100,49	100,47	99,09	99,17	100,54	100,59	100,97	99,38	100,39
X^{ilm}(Max)	0,894	0,869	0,927	0,899	0,876	0,854	0,840	0,845	0,877
X^{hem}(Min)	0,051	0,059	0,000	0,032	0,040	0,065	0,052	0,044	0,038
X^{hem}(Max)	0,055	0,062	0,002	0,039	0,043	0,068	0,055	0,048	0,041
X^{ilm}(Min)	0,894	0,869	0,927	0,899	0,876	0,854	0,840	0,845	0,877

X^{ulv} (Max) = Maximum ulvöspinel fraction
X^{ulv} (Min) = Minimum " "

X^{mt} (Min) = Minimum magnetite fraction
X^{mt} (Max) = Maximum " "

X^{ilm} (Max) = Maximum ilmenite fraction
X^{ilm} (Min) = Minimum " "

X^{hem} (Min) = Minimum hematite fraction
X^{hem} (Max) = Maximum " "

MAGNETITE ANALYSES

Sample #	GR1-107C	78-374A	78-374C	78-360A	78-360C	5-124-3	5-124-7	5-124-7A	5-124-9
SiO_2	0,00	0,00	0,00	0,00	0,00	0,00	0,00	0,00	0,00
TiO_2	17,28	1,22	18,00	0,68	16,37	16,37	16,19	12,76	13,36
Al_2O_3	0,59	1,22	0,87	1,19	0,76	2,16	2,73	3,22	3,43
Cr_2O_3	0,52	0,94	0,70	4,74	3,27	0,15	0,23	0,16	0,15
FeO	45,28	31,80	46,34	31,83	45,15	44,81	46,27	41,31	42,85
Fe_2O_3	33,51	64,71	31,04	62,20	32,62	32,24	35,48	38,39	37,60
MnO	1,28	0,15	0,68	0,19	0,57	0,40	0,57	0,57	0,40
MgO	0,09	0,09	0,10	0,12	0,22	0,14	0,10	0,34	0,06
Total	98,55	99,16	97,74	100,95	98,97	96,27	101,55	96,76	97,86
X^{ulv}(Max)	0,496	0,035	0,520	0,019	0,467	0,477	0,447	0,369	0,382
X^{mt}(Min)	0,435	0,912	0,421	0,870	0,435	0,449	0,467	0,517	0,522
X^{mt}(Max)	0,482	0,922	0,449	0,883	0,466	0,470	0,490	0,555	0,538
X^{ulv}(Min)	0,473	0,030	0,506	0,012	0,452	0,467	0,435	0,350	0,374

ILMENITE ANALYSES

Sample #	GR1-107D	78-374B	78-374D	78-360B	78-360D	5-124-2	5-124-5
TiO_2	49,43	51,79	46,40	47,98	47,05	52,95	52,25
Al_2O_3	0,15	0,22	0,14	0,19	0,19	0,25	0,17
Cr_2O_3	0,61	0,22	0,16	0,32	0,45	0,12	0,13
FeO	41,77	44,55	39,99	41,47	40,94	45,72	45,40
Fe_2O_3	6,26	0,00	12,04	7,34	10,58	0,00	0,00
MnO	2,38	1,75	1,43	1,34	0,97	1,39	1,33
MgO	0,11	0,13	0,12	0,14	0,18	0,13	0,09
Total	100,72	98,66	100,29	98,79	100,36	100,56	99,37
X^{ilm}(Max)	0,877	0,951	0,846	0,888	0,864	0,962	0,964
X^{hem}(Min)	0,050	0,000	0,110	0,064	0,093	0,000	0,000
X^{hem}(Max)	0,059	0,000	0,114	0,070	0,100	0,000	0,000
X^{ilm}(Min)	0,877	0,951	0,846	0,888	0,864	0,962	0,964

MAGNETITE ANALYSES

Sample #	5-124-X	5-138-2	5-138-3	5-195-1	5-195-2	5-195-9	5-195-7	5-195-X	5-315-1C
SiO_2	0,00	11,43	8,20	0,00	0,00	0,00	0,00	0,00	0,00
TiO_2	19,55	10,93	12,91	14,64	11,49	17,51	14,20	19,37	1,14
Al_2O_3	2,90	8,19	3,20	3,00	2,92	2,78	3,05	2,66	0,70
Cr_2O_3	0,14	0,11	0,12	0,11	0,08	0,11	0,16	0,15	0,11
FeO	48,24	47,52	47,15	43,56	40,95	45,53	43,17	47,73	30,81
Fe_2O_3	26,02	8,50	19,90	35,12	42,34	29,50	35,98	26,41	63,20
MnO	0,45	0,17	0,24	0,57	0,53	0,94	0,60	0,74	0,11
MgO	0,06	1,08	0,49	0,05	0,14	0,12	0,06	0,06	0,03
Total	97,46	*93,58	*96,71	97,05	98,46	96,50	97,22	97,12	96,10
X^{ulv}(Max)	0,559	0,296	0,355	0,422	0,328	0,507	0,409	0,557	0,034
X^{mt}(Min)	0,352	0,000	0,063	0,486	0,580	0,390	0,496	0,352	0,942
X^{mt}(Max)	0,372	0,115	0,274	0,507	0,605	0,427	0,519	0,380	0,947
X^{ulv}(Min)	0,549	0,160	0,250	0,412	0,315	0,488	0,398	0,543	0,031

ILMENITE ANALYSES

Sample #	5-138-1	5-195-8	5-195-3	5-315-1B
TiO_2	53,01	52,73	52,88	52,58
Al_2O_3	0,20	0,18	0,16	0,18
Cr_2O_3	0,09	0,10	0,09	0,09
FeO	45,40	45,44	45,25	45,42
Fe_2O_3	0,00	0,05	0,00	0,00
MnO	1,10	1,70	1,65	1,49
MgO	0,07	0,10	0,10	0,10
Total	99,87	100,30	100,13	99,86
X^{ilm}(Max)	0,977	0,956	0,961	0,962
X^{hem}(Min)	0,000	0,000	0,000	0,000
X^{hem}(Max)	0,000	0,000	0,000	0,000
X^{ilm}(Min)	0,977	0,956	0,961	0,962

* 78-138-2,&3 contain 5,42 & 4,49 Wt. % CaO respectively.

MAGNETITE ANALYSES

Sample #	5-315-X	5-410-5	5-410-6	5-410-X	5-410-Y	5-440-1	5-440-4	5-440-7
SiO_2	0,00	0,00	0,00	0,00	0,00	0,00	0,00	0,00
TiO_2	19,54	18,20	14,86	15,04	17,82	6,03	4,18	7,88
Al_2O_3	0,40	2,83	3,14	3,42	3,25	1,80	2,62	1,16
Cr_2O_3	0,10	0,09	0,10	0,09	0,09	0,12	0,13	0,12
FeO	47,29	46,79	43,05	43,45	45,98	34,17	32,36	36,05
Fe_2O_3	28,00	28,55	32,91	31,80	26,77	53,37	55,48	51,13
MnO	0,60	0,61	0,54	0,12	0,22	0,35	0,29	0,40
MgO	0,05	0,07	0,07	0,09	0,08	0,90	0,03	0,86
Total	95,99	97,14	94,67	94,02	94,22	96,74	95,96	97,60
X^{ulv}(Max)	0,576	0,523	0,439	0,446	0,527	0,176	0,122	0,228
X^{mt}(Min)	0,390	0,387	0,464	0,463	0,384	0,717	0,751	0,680
X^{mt}(Max)	0,413	0,411	0,486	0,472	0,396	0,780	0,814	0,742
X^{ulv}(Min)	0,564	0,511	0,428	0,441	0,521	0,144	0,090	0,197

ILMENITE ANALYSES

Sample #	5-315-1A	5-315-1Y	5-410-2A	5-410-2B	5-440-2
TiO_2	52,90	52,99	52,69	52,65	52,08
Al_2O_3	0,18	0,15	0,13	0,13	0,19
Cr_2O_3	0,11	0,08	0,11	0,11	0,07
FeO	45,23	44,43	45,38	45,36	44,59
Fe_2O_3	0,00	0,00	0,00	0,00	0,95
MnO	1,46	1,49	1,44	1,43	1,93
MgO	0,08	0,07	0,06	0,10	0,12
Total	99,96	99,21	99,81	99,78	99,36
X^{ilm}(Max)	0,967	0,973	0,967	0,965	0,941
X^{hem}(Min)	0,000	0,000	0,000	0,000	0,005
X^{hem}(Max)	0,000	0,000	0,000	0,000	0,009
X^{ilm}(Min)	0,967	0,973	0,967	0,965	0,941

MAGNETITE ANALYSES

Sample ##	5-440-X	5-508-4	5-508-X
SiO_2	0,00	0,00	0,00
TiO_2	26,75	19,37	20,37
Al_2O_3	1,06	3,52	3,42
Cr_2O_3	0,09	0,08	0,08
FeO	52,86	46,05	3,42
Fe_2O_3	14,16	25,86	23,98
MnO	1,05	0,54	0,56
MgO	0,71	1,30	1,26
Total	96,68	96,72	96,66
X^{ulv}(Max)	0,770	0,551	0,580
X^{mt}(Min)	0,129	0,277	0,252
X^{mt}(Max)	0,204	0,368	0,342
X^{ulv}(Min)	0,733	0,506	0,535

ILMENITE ANALYSES

Sample ##	5-508-3
TiO_2	52,62
Al_2O_3	0,19
Cr_2O_3	0,12
FeO	45,40
Fe_2O_3	0,00
MnO	1,29
MgO	0,11
Total	99,73
X^{ilm}(Max)	0,967
X^{hem}(Min)	0,000
X^{hem}(Max)	0,000
X^{ilm}(Min)	0,967

Sample #	Strat. Level	Description
GR1-69A&B	M.Mb / P.G.	Exsolved Magnetite & Ilmenite Resp.
GR1-69C	"	Calculated composition of Primary Titaniferous Magnetite
GR1-69D	"	Primary Ilmenite
GR1-88A&B *	"	Exsolved Magnetite & Ilmenite Resp.
GR1-88C *	"	Calculated Composition of Primary Titaniferous Magnetite
GR1-88D *	"	Primary Ilmenite
GR1-100A&B	"	Exsolved Magnetite & Ilmenite Resp.
GR1-100C	"	Calculated composition of Primary Titaniferous Magnetite
GR1-100D	"	Primary Ilmenite
GR1-102 A&B*	"	Exsolved Magnetite & Ilmenite Resp.
GR1-102C *	"	Calculated Composition of Primary Titaniferous Magnetite
GR1-102D *	"	Primary Ilmenite
GR1-107A&B*	"	Exsolved Magnetite & Ilmenite Resp.
GR1-107C *	"	Calculated Composition of Primary Titaniferous Magnetite
GR1-107D *	"	Primary Ilmenite
78-374 A&B	"	Exsolved Magnetite & Ilmenite Resp.
78-374 C	"	Calculated Composition of Primary Titaniferous Magnetite
78-374 D	"	Primary Ilmenite
78-360 A&B	"	Exsolved Magnetite & Ilmenite Resp.
78-360 C	"	Calculated Composition of Primary Titaniferous Magnetite
78-360 D	"	Primary Ilmenite

Sample ##	Strat. Level	Description
5-124-3&2	+1480m	Exsolved Magnetite & Ilmenite Resp. (2-3 micron beam)
5-124-7&5	+1480m	Exsolved Magnetite & Ilmenite Resp. (2-3 micron beam)
5-124-7A	+1480m	Traverse Composition of Exsolved Magnetite (2-3 micron beam)
5-124-9	+1480m	Bulk Composition of Exsolved Magnetite (25 micron beam)
5-124-X	+1480m	Calculated Composition of Primary Titaniferous Magnetite
5-138-2&1	+1475m	Exsolved Magnetite-silicate phase & Ilmenite Resp. (2-3 micron beam)
5-138-3	+1475m	Exsolved Magnetite-silicate phase (25 micron beam)
5-195-1&8	+1460m	Exsolved Magnetite & Ilmenite Resp. (2-3 micron beam)
5-195-2	+1460m	Exsolved Magnetite (2-3 micron beam)
5-195-9	+1460m	" "
5-195-7	+1460m	Bulk Composition of Exsolved Magnetite (25 micron beam)
5-195-X	+1460m	Calculated Composition of Primary Titaniferous Magnetite
5-195-3	+1460m	Exsolved Ilmenite
5-315-1C	+1424m	Exsolved Magnetite (2-3 micron beam)
5-315-1B	+1424m	Exsolved Trellis Ilmenite
5-315-1A	+1424m	" " "
5-315-1Y	+1424m	Exsolved Granular Ilmenite

Sample ##	Strat. Level	Description
5-315-X	+1424m	Calculated Composition of Primary Titaniferous Magnetite
5-410-5&2A	+1392m	Exsolved Magnetite & Ilmenite Resp. (2-3 micron beam)
5-410-6&2B	+1392m	" " "
5-410-X	+1392m	Bulk Composition of Exsolved Magnetite (25 micron beam)
5-410-Y	+1392m	Calculated Composition of Primary Titaniferous Magnetite
5-440-1	+1382m	Exsolved Magnetite (2-3 micron beam)
5-440-4&2	+1382m	Exsolved Magnetite & Ilmenite Resp. (2-3 micron beam)
5-440-X	+1382m	Calculated Composition of Primary Titaniferous Magnetite
5-508-4&3	+1360m	Exsolved Magnetite & Ilmenite Resp. (2-3 micron beam)
5-508-X	+1360m	Calculated Composition of Primary Titaniferous Magnetite

* GR1-107, 88, 102, and 107 are abbreviations for GR1-107,2; 88,48; 102,5 and 107,2 respectively.

GR1 samples represent Magnetite - Ilmenite pairs from fine to very fine grained gabbronites in $\frac{M.Mb}{P.G.}$

5-124 to 508 represent Magnetite - Ilmenite associations from the upper zone.

APPENDIX 7

CHROMITE ANALYSES FROM THE CRITICAL ZONE AND LOWER ZONE, South of Potgietersrus

Sample #	78-403	78-413	78-160B	3-2395	78-360-1	78-360-2	3-2500	3-2940	3-2950	3-3027	3-3402
TiO_2	3,08	2,80	1,77	0,95	3,78	0,68	2,12	0,88	0,70	1,14	1,09
Al_2O_3	10,28	8,85	13,45	16,41	5,48	1,19	15,13	15,57	13,03	16,57	20,77
Cr_2O_3	36,27	35,03	42,15	43,24	29,43	4,74	37,70	38,95	47,28	39,38	23,18
Fe_2O_3	15,00	19,03	10,13	8,46	26,27	62,20	12,36	12,92	8,49	13,17	22,41
FeO	29,65	27,93	23,70	22,15	31,52	31,83	24,71	24,53	21,88	19,18	25,19
MnO	0,26	0,45	0,25	0,39	0,40	0,19	0,22	0,37	0,45	0,34	0,34
MgO	3,77	4,47	7,38	8,38	2,48	0,12	7,23	6,64	7,99	10,50	6,77
Total	98,31	98,58	98,83	99,98	99,35	100,95	99,47	99,87	99,82	100,28	99,75
CATIONS BASED ON 32 ' OXYGEN											
Ti	0,658	0,599	0,363	0,191	0,829	0,159	0,429	0,180	0,144	0,225	0,218
Al	3,422	2,950	4,269	5,050	1,877	0,428	4,749	4,881	4,087	5,020	6,392
Cr_{3+}	8,096	7,827	8,973	8,925	6,752	1,136	7,936	8,191	9,944	8,003	4,788
Fe^{2+}	3,189	4,048	2,055	1,666	5,736	14,140	2,480	2,589	1,703	2,550	4,406
Fe	7,010	6,610	5,345	4,845	7,658	8,056	5,511	5,466	4,876	4,130	5,509
Mn	0,067	0,112	0,061	0,091	0,103	0,053	0,054	0,088	0,106	0,078	0,080
Mg	1,590	1,886	2,965	3,264	1,076	0,059	2,872	2,635	3,171	4,025	2,638
CATION RATIOS											
$Mg/(Mg+Fe^{2+})$	0,185	0,222	0,357	0,403	0,123	0,007	0,343	0,325	0,394	0,494	0,324
Cr/(Cr+Al)	0,703	0,726	0,678	0,639	0,782	0,726	0,626	0,627	0,709	0,615	0,428
$Al/(Al+Fe^{3+}+Cr)$	0,233	0,199	0,279	0,323	0,131	0,027	0,313	0,312	0,260	0,322	0,410
$Cr/(Cr+Fe^{2+}+Fe^{3+})$	0,443	0,423	0,548	0,578	0,335	0,049	0,498	0,504	0,602	0,545	0,326
$Cr/(Cr+Fe^{3+}+Al)$	0,551	0,528	0,587	0,571	0,470	0,072	0,523	0,523	0,632	0,514	0,307
Fe^{3+}/Fe^{2+}	0,455	0,612	0,385	0,344	0,749	1,755	0,450	0,474	0,349	0,618	0,800
$Fe^{3+}/(Fe^{3+}+Al+Cr)$	0,217	0,273	0,134	0,107	0,399	0,900	0,164	0,165	0,108	0,164	0,483
$Cr/(Fe^{2+}+Fe^{3+})$	0,794	0,734	1,212	1,371	0,504	0,051	0,993	1,017	1,511	1,198	0,483
Rock type	CGN	CGN	C	H	CGN	CGN	H	H	P	H	H
Stratigraphic level (m)	+ 19	- 61	- 86	- 110	M.Mb / P.G.	M.Mb / P.G.	- 141	- 276	- 280	- 300	- 416

CHROMITE ANALYSES FROM THE LOWER ZONE, South of Potgietersrus

Sample #	3-3494	3-3563	3-3651	3-3764	3-3766	3-3772	3-3819	3-3927	3-4002	1-50	1-67
TiO_2	1,16	1,22	0,95	1,01	0,80	0,20	1,14	0,85	0,76	0,79	0,94
Al_2O_3	14,03	13,53	17,25	12,32	20,05	17,31	12,68	10,43	17,18	17,20	14,62
Cr_2O_3	39,27	40,89	37,99	43,82	33,85	42,48	39,27	48,61	39,17	40,35	46,21
Fe_2O_3	14,21	11,89	12,92	11,84	15,35	9,67	14,81	8,38	11,76	9,59	6,58
FeO	24,68	23,11	21,46	20,54	20,78	18,14	22,27	22,83	22,22	21,99	21,39
MnO	0,41	0,39	0,48	0,35	0,40	0,37	0,35	0,37	0,42	0,45	0,42
MgO	6,62	7,22	8,78	8,76	9,68	10,45	7,60	6,95	8,19	8,11	8,39
Total	100,38	98,25	99,83	98,63	100,91	98,72	98,12	98,42	99,70	98,48	98,55
CATIONS BASED ON 32 OXYGEN											
Ti	0,237	0,253	0,190	0,208	0,157	0,063	0,238	0,180	0,154	0,161	0,193
Al	4,412	4,324	5,292	3,902	5,992	5,293	4,067	3,377	5,296	5,358	4,589
Cr_{3+}	8,282	8,764	7,818	9,307	6,787	8,713	8,447	10,551	8,100	8,431	9,727
Fe_{2+}	2,855	2,428	2,533	2,396	2,390	1,891	3,033	1,735	2,318	1,911	1,322
Fe	5,514	5,248	4,680	4,623	4,415	3,943	5,077	5,251	4,870	4,868	4,770
Mn	0,097	0,094	0,110	0,084	0,090	0,086	0,095	0,091	0,098	0,105	0,099
Mg	2,635	2,920	3,409	3,511	3,661	4,043	3,085	2,847	3,196	3,197	3,332
CATION RATIOS											
$Mg/(Mg+Fe^{2+})$	0,323	0,358	0,421	0,432	0,453	0,506	0,378	0,352	0,396	0,397	0,411
Cr/(Cr+Al)	0,652	0,670	0,596	0,705	0,531	0,622	0,675	0,758	0,605	0,611	0,679
$Al/(Al+Fe^{3+}+Cr)$	0,284	0,279	0,338	0,205	0,381	0,333	0,262	0,216	0,337	0,341	0,293
$Cr/(Cr+Fe^{2+}+Fe^{3+})$	0,497	0,533	0,520	0,570	0,480	0,599	0,510	0,602	0,530	0,554	0,615
$Cr/(Cr+Fe^{3+}+Al)$	0,533	0,565	0,500	0,596	0,432	0,548	0,543	0,674	0,516	0,537	0,622
Fe^{3+}/Fe^{2+}	0,518	0,463	0,541	0,518	0,664	0,480	0,598	0,331	0,476	0,393	0,277
$Fe^{3+}/(Fe^{3+}+Al+Cr)$	0,184	0,157	0,162	0,154	0,187	0,119	0,195	0,111	0,148	0,122	0,085
$Cr/(Fe^{2+}+Fe^{3+})$	0,990	1,142	1,084	1,326	0,924	1,493	1,042	1,510	1,127	1,244	1,596
Rock type	P	P	H	P	H	H	P	P	H	H	P
Stratigraphic level (m)	- 446	- 465	- 488	- 524	- 530	- 535	- 544	- 577	- 587	- 620	- 634

CHROMITE ANALYSES FROM THE LOWER ZONE, South of Potgietersrus

Sample #	1-80,5	1-123	1-148	1-179	1-209	1-213	1-219	1-223A	1-233-1	1-240,9	1-244A
TiO_2	0,94	0,78	0,48	0,74	0,51	1,05	1,41	1,01	1,33	1,48	0,56
Al_2O_3	17,51	17,69	17,73	17,62	16,49	15,19	15,79	17,81	13,20	16,04	15,53
Cr_2O_3	41,49	40,92	44,94	42,06	44,00	40,12	32,36	38,24	43,07	35,23	40,12
Fe_2O_3	7,78	10,14	6,71	9,30	8,61	12,30	17,87	11,00	10,010	15,27	12,28
FeO	21,47	18,84	18,05	17,64	17,67	21,60	22,86	22,66	21,72	23,12	23,76
MnO	0,25	0,36	0,33	0,30	0,33	0,36	0,37	0,47	0,37	0,35	0,34
MgO	8,63	10,40	10,78	11,13	10,76	8,47	7,70	7,98	8,12	7,84	6,90
Total	98,08	99,14	99,01	98,80	98,38	99,09	98,37	99,17	97,91	99,39	99,48
CATIONS BASED ON 32 OXYGEN											
Ti	0,191	0,156	0,097	0,148	0,104	0,213	0,288	0,204	0,275	0,299	0,117
Al	5,443	5,383	5,379	5,351	5,062	4,742	4,986	5,508	4,208	5,005	4,876
Cr_{3+}	8,651	8,353	9,145	8,569	9,060	8,400	6,855	6,933	9,207	7,375	8,450
Fe_{2+}	1,548	1,974	1,304	1,807	1,692	2,454	3,605	2,175	2,085	3,045	2,463
Fe	4,745	4,077	3,892	3,810	3,857	4,791	5,131	4,980	4,919	5,129	5,302
Mn	0,060	0,083	0,076	0,070	0,077	0,095	0,088	0,109	0,089	0,083	0,081
Mg	3,395	4,005	4,138	4,277	4,179	3,346	3,078	3,124	3,275	3,097	2,743
CATION RATIOS											
$Mg/(Mg+Fe^{2+})$	0,417	0,496	0,515	0,529	0,520	0,411	0,375	0,386	0,400	0,377	0,341
Cr/(Cr+Al)	0,614	0,608	0,630	0,616	0,642	0,639	0,579	0,590	0,686	0,596	0,634
$Al/(Al+Fe^{3+}+Cr)$	0,348	0,343	0,340	0,340	0,320	0,304	0,323	0,353	0,272	0,325	0,309
$Cr/(Cr+Fe^{2+}+Fe^{3+})$	0,579	0,580	0,638	0,604	0,620	0,537	0,440	0,526	0,569	0,474	0,521
$Cr/(Cr+Fe^{3+}+Al)$	0,553	0,532	0,578	0,545	0,573	0,539	0,444	0,508	0,595	0,478	0,535
Fe^{3+}/Fe^{2+}	0,326	0,484	0,335	0,474	0,439	0,512	0,703	0,437	0,419	0,594	0,465
$Fe^{3+}/(Fe^{3+}+Al+Cr)$	0,099	0,126	0,082	0,115	0,107	0,157	0,233	0,139	0,133	0,197	0,156
$Cr/(Fe^{2+}+Fe^{3+})$	1,375	1,380	1,760	1,525	1,633	1,159	0,785	1,109	1,319	0,902	1,088
Rock type	H	H	P	H	H	P	H	H	P	H	P
Stratigraphic level (m)	- 647	- 680	- 704	- 726	- 747	- 750	- 753	- 758	- 766	- 772	- 776

CHROMITE ANALYSES FROM THE LOWER ZONE, South of Potgietersrus

Sample #	1-253,5	6A-259	6A-286	6A-296-7	X-1	X-10	X-13	X-21	X-23	X-25	X-31
TiO_2	0,37	1,13	0,39	0,92	0,46	0,44	0,61	0,47	0,45	0,45	0,41
Al_2O_3	11,51	14,41	12,56	17,15	18,26	19,65	15,73	10,67	13,27	12,61	15,49
Cr_2O_3	48,35	37,61	51,16	40,84	38,75	39,44	43,82	47,18	47,52	46,61	42,07
Fe_2O_3	10,54	14,55	6,20	9,45	10,07	9,09	8,13	9,83	8,19	9,06	11,00
FeO	20,29	22,66	20,89	22,19	25,19	21,57	22,12	23,70	21,53	23,27	21,33
MnO	0,38	0,41	0,20	0,47	0,35	0,36	0,38	0,35	0,34	0,30	0,43
MgO	8,79	7,52	8,64	8,19	6,15	8,64	7,86	6,17	8,08	6,84	8,24
Total	100,24	98,29	100,04	99,20	99,23	99,19	98,65	98,37	99,38	99,14	98,97

CATIONS BASED ON 32 OXYGEN

Ti	0,078	0,233	0,082	0,186	0,096	0,090	0,126	0,102	0,095	0,096	0,086
Al	3,604	4,581	3,919	5,306	5,702	5,996	4,930	3,474	4,171	4,020	4,839
Cr_{3+}	10,151	8,019	10,702	8,476	8,117	8,073	9,211	10,299	10,016	9,964	8,815
Fe_{2+}	2,110	2,956	1,238	1,869	2,011	1,773	1,629	1,045	1,646	1,846	2,196
Fe	4,515	5,119	4,631	4,879	5,590	4,679	4,928	5,482	4,809	5,272	4,736
Mn	0,090	0,098	0,049	0,109	0,083	0,093	0,090	0,086	0,081	0,073	0,101
Mg	3,482	3,026	3,410	3,207	2,432	3,337	3,118	2,543	3,214	2,760	3,258

CATION RATIOS

$Mg/(Mg+Fe^{2+})$	0,435	0,372	0,424	0,397	0,303	0,416	0,388	0,317	0,401	0,344	0,408
Cr/(Cr+Al)	0,738	0,636	0,732	0,615	0,587	0,574	0,651	0,748	0,706	0,713	0,646
$Al/(Al+Fe^{3+}+Cr)$	0,227	0,295	0,247	0,339	0,360	0,379	0,313	0,220	0,263	0,254	0,305
$Cr/(Cr+Fe^{2+}+Fe^{3+})$	0,605	0,498	0,646	0,557	0,516	0,556	0,584	0,578	0,608	0,583	0,560
$Cr/(Cr+Fe^{3+}+Al)$	0,640	0,516	0,675	0,542	0,513	0,510	0,584	0,651	0,633	0,629	0,556
Fe^{3+}/Fe^{2+}	0,467	0,578	0,267	0,383	0,360	0,379	0,331	0,373	0,342	0,350	0,464
$Fe^{3+}/(Fe^{3+}+Al+Cr)$	0,133	0,190	0,078	0,119	0,127	0,112	0,103	0,129	0,104	0,117	0,139
$Cr/(Fe^{2+}+Fe^{3+})$	1,532	0,993	1,823	1,256	1,068	1,251	1,405	1,368	1,552	1,400	1,271
Rock type	H	H	P	H	P	H	P	P	P	P	D
Stratigraphic level (m)	- 782	- 797	- 817	- 826	- 958	-1058	-1068	-1165	-1176	-1190	-1250

CHROMITE ANALYSES FROM THE LOWER ZONE, South of Potgietersrus

Sample #	A-3	A-9	A-16	GV-7	GV-13	GV-16	GV-9	GV-12	GV-6	GV-23	GV-15
TiO_2	0,47	0,59	0,44	0,42	0,74	0,62	0,46	0,31	0,36	0,22	0,41
Al_2O_3	13,75	13,16	17,41	13,51	17,90	17,56	16,28	11,31	11,00	10,94	12,52
Cr_2O_3	42,35	40,09	43,48	51,15	45,14	43,91	48,48	52,87	55,50	55,15	51,60
Fe_2O_3	12,33	13,49	8,00	5,80	7,12	6,31	5,02	5,52	5,58	6,31	5,94
FeO	20,83	24,98	16,25	17,79	18,96	19,12	19,86	16,39	12,76	11,61	18,53
MnO	0,30	0,26	0,35	0,49	0,35	0,43	0,54	0,47	0,42	0,46	0,47
MgO	8,38	5,65	11,55	10,52	10,74	9,82	9,56	10,72	13,43	13,98	9,87
Total	98,41	98,22	97,48	99,68	100,94	97,77	100,19	97,59	99,05	98,67	99,34

CATIONS BASED ON 32 OXYGEN

Ti	0,099	0,126	0,090	0,087	0,145	0,127	0,094	0,067	0,075	0,047	0,086
Al	4,349	4,264	5,335	4,156	5,340	5,424	4,957	3,574	3,372	3,354	3,897
Cr_{3+}	8,983	8,712	8,938	10,550	9,033	0,098	9,900	11,199	11,406	11,336	10,770
Fe^{2+}	2,493	2,793	1,569	1,143	1,359	1,248	0,979	1,116	1,095	1,237	1,184
Fe	4,682	5,752	3,540	3,890	4,021	4,197	4,297	3,681	2,781	2,531	4,099
Mn	0,073	0,065	0,092	0,113	0,080	0,100	0,123	0,111	0,097	0,106	0,110
Mg	3,354	2,318	4,478	4,093	4,054	3,838	3,683	4,284	5,206	5,420	3,887

CATION RATIOS

$Mg/(Mg+Fe^{2+})$	0,417	0,287	0,559	0,513	0,502	0,478	0,462	0,538	0,652	0,682	0,487
Cr/(Cr+Al)	0,674	0,671	0,626	0,717	0,629	0,627	0,666	0,758	0,772	0,772	0,734
$Al/(Al+Fe^{3+}+Cr)$	0,275	0,270	0,337	0,262	0,339	0,344	0,313	0,225	0,213	0,211	0,246
$Cr/(Cr+Fe^{2+}+Fe^{3+})$	0,556	0,505	0,636	0,677	0,627	0,626	0,652	0,700	0,746	0,751	0,671
$Cr/(Cr+Fe^{3+}+Al)$	0,568	0,553	0,564	0,666	0,574	0,577	0,625	0,705	0,719	0,712	0,679
Fe^{3+}/Fe^{2+}	0,532	0,486	0,443	0,294	0,338	0,297	0,228	0,303	0,394	0,489	0,289
$Fe^{3+}/(Fe^{3+}+Al+Cr)$	0,158	0,177	0,099	0,072	0,086	0,079	0,062	0,070	0,069	0,078	0,075
$Cr/(Fe^{2+}+Fe^{3+})$	1,252	1,020	1,749	2,096	1,679	1,671	1,876	2,334	2,942	3,008	2,039
Rock type	H	H	H	H	H	H	H	H	C	C	H
Stratigraphic level (m)	-1408	-1484	-1640	*	*	*	*	*	*	*	*

* = see key

CHROMITE ANALYSES FROM THE LOWER ZONE, South of Potgietersrus

Sample #	GV-14	GV-18	GV-4	GV-1	GV-20	GV-10	GV 19	GV-22	DV-1	DV-2	78-257
TiO_2	0,29	0,39	0,41	0,51	0,40	0,32	0,39	0,48	0,10	0,15	0,32
Al_2O_3	11,77	12,79	11,94	20,41	12,13	11,50	12,00	18,44	8,95	9,12	11,34
Cr_2O_3	53,16	53,11	54,10	42,52	52,92	55,55	53,17	46,32	57,88	57,11	54,76
Fe_2O_3	6,48	5,49	5,65	7,15	6,05	4,16	6,71	4,76	6,13	6,02	4,89
FeO	13,22	14,60	14,18	14,98	15,91	15,40	13,95	17,89	11,50	13,25	15,66
MnO	0,44	0,31	0,30	0,26	0,25	0,31	0,34	0,36	0,42	0,42	0,48
MgO	13,00	12,54	12,77	13,10	11,68	11,82	12,09	11,00	13,84	12,74	11,49
Total	98,36	99,23	99,34	98,94	99,36	99,06	99,46	99,25	98,82	98,80	98,94
CATIONS BASED ON 32 OXYGEN											
Ti	0,062	0,080	0,084	0,101	0,083	0,068	0,080	0,097	0,024	0,034	0,068
Al	3,630	3,908	3,652	6,034	3,736	3,554	3,665	5,554	2,767	2,839	3,520
Cr_{3+}	10,991	10,880	11,095	8,433	10,928	11,509	10,886	9,357	11,994	11,916	11,395
Fe_{2+}	1,278	1,074	1,106	1,354	1,192	0,824	1,311	0,918	1,213	1,199	0,972
Fe	2,899	3,171	3,083	3,150	3,482	3,384	3,029	3,832	2,527	2,931	3,455
Mn	0,102	0,073	0,070	0,060	0,060	0,073	0,079	0,082	0,098	0,098	0,111
Mg	5,070	4,846	4,940	4,900	4,550	4,620	4,982	4,192	5,409	5,014	4,510
CATION RATIOS											
$Mg/(Mg+Fe^{2+})$	0,636	0,604	0,616	0,609	0,566	0,577	0,622	0,523	0,682	0,631	0,566
Cr/(Cr+Al)	0,752	0,736	0,752	0,583	0,745	0,764	0,748	0,628	0,813	0,808	0,764
$Al/(Al+Fe^{3+}+Cr)$	0,288	0,246	0,230	0,381	0,236	0,224	0,231	0,351	0,173	0,178	0,222
$Cr/(Cr+Fe^{2+}+Fe^{3+})$	0,725	0,719	0,726	0,652	0,700	0,732	0,715	0,663	0,762	0,743	0,720
$Cr/(Cr+Fe^{3+}+Al)$	0,691	0,686	0,700	0,533	0,689	0,724	0,686	0,591	0,751	0,747	0,717
Fe^{3+}/Fe^{2+}	0,441	0,339	0,359	0,430	0,342	0,244	0,433	0,240	0,480	0,409	0,282
$Fe^{3+}/(Fe^{3+}Al+Cr)$	0,080	0,068	0,070	0,086	0,075	0,052	0,083	0,058	0,076	0,075	0,061
$Cr/(Fe^{2+}+Fe^{3+})$	2,631	2,563	2,648	1,872	2,338	2,735	2,508	1,970	3,206	2,885	2,574
Rock type	C	C	C	P	C	C	C	D	C	C	
Stratigraphic level	*	*	*	*	*	*	*	*	*	*	*

CHROMITE ANALYSES FROM THE LOWER ZONE, South of Potgietersrus

Sample #	UGC-1	GVC-F
TiO_2	0,40	0,22
Al_2O_3	12,00	12,30
Cr_2O_3	54,48	54,90
Fe_2O_3	5,78	4,52
FeO	14,21	15,24
MnO	0,48	0,24
MgO	12,80	12,10
Total	100,15	99,87
CATION BASED ON 32 OXYGEN		
Ti	0,082	0,047
Al	3,644	3,755
Cr_{3+}	11,091	11,237
Fe^{3+}	1,124	0,855
Fe^{2+}	3,067	3,309
Mn	0,109	0,057
Mg	4,915	4,671
CATION RATIOS		
$Mg/(Mg+Fe^{2+})$	0,616	0,585
$Cr/(Cr+Al)$	0,753	0,750
$Al/(Al+Fe^{3+}+Cr)$	0,230	0,237
$Cr/(Cr+Fe^{2+}+Fe^{3+})$	0,726	0,728
$Cr/(Cr+Fe^{3+}+Al)$	0,699	0,708
Fe^{3+}/Fe^{2+}	0,367	0,268
$Fe^{3+}/(Fe^{3+}+Al+Cr)$	0,071	0,056
$Cr/(Fe^{2+}+Fe^{3+})$	2,646	2,679
	C	C
	*	*

Sample #	GVC-NIM
TiO_2	0,22
Al_2O_3	12,30
Cr_2O_3	54,90
Fe_2O_3	4,83
FeO	15,00
MnO	0,24
MgO	12,10
SiO_2	<0,20
CaO	0,05
V_2O_3	0,21
ZnO	0,11
NiO	0,09
CoO	0,032
S ppm	< 20
Na ppm	<100
K ppm	< 50
Total	100,04
	*

CHROMITE ANALYSES FROM SAMPLE GTS

Sample #	1	2	3	4	4A	5	6	7	8	9	10
TiO_2	0,33	0,33	0,32	0,29	0,32	0,28	0,40	0,36	0,32	0,28	0,33
Al_2O_3	12,81	12,41	12,35	12,09	12,12	12,73	13,31	13,52	12,82	13,92	14,41
Cr_2O_3	54,51	55,11	55,89	55,53	55,18	54,24	53,70	53,30	52,81	51,97	51,90
Fe_2O_3	3,57	4,48	3,44	3,80	3,84	4,44	3,43	3,03	4,60	5,04	3,75
FeO	15,54	13,92	14,21	14,03	14,27	15,96	16,66	16,90	16,03	16,05	17,35
MnO	0,39	0,24	0,20	0,34	0,32	0,38	0,34	0,27	0,31	0,44	0,28
MgO	11,80	13,03	12,80	12,68	12,52	11,64	11,22	10,96	11,39	11,57	10,83
Total	98,96	99,52	99,20	98,76	98,56	99,67	99,06	98,34	98,31	99,27	98,85

CATIONS BASED ON 32 OXYGEN

Ti	0,069	0,068	0,067	0,061	0,067	0,059	0,083	0,076	0,068	0,059	0,069
Al	3,939	3,774	3,772	3,714	3,733	3,897	4,096	4,190	3,987	4,258	4,434
Cr_{3+}	11,240	11,238	11,443	11,437	11,396	11,135	11,082	11,078	10,985	10,659	10,710
Fe^{2+}	0,705	0,874	0,674	0,748	0,758	0,872	0,678	0,603	0,915	0,987	0,740
Fe^{2+}	3,398	3,009	3,084	3,065	3,124	3,473	3,644	3,723	4,534	3,491	3,796
Mn	0,091	0,057	0,048	0,080	0,075	0,088	0,080	0,065	0,074	0,101	0,066
Mg	4,590	5,012	4,943	4,926	4,877	4,507	4,368	4,297	4,469	4,476	4,216

CATION RATIOS

$Mg/(Mg+Fe^{2+})$	0,571	0,625	0,616	0,617	0,610	0,565	0,545	0,536	0,558	0,562	0,526
Cr/(Cr+Al)	0,741	0,749	0,752	0,755	0,753	0,741	0,730	0,726	0,734	0,715	0,707
$Al/(Al+Fe^{3+}+Cr)$	0,248	0,238	0,237	0,234	0,235	0,245	0,258	0,264	0,251	0,268	0,279
$Cr/(Cr+Fe^{2+}+Fe^{3+})$	0,733	0,743	0,753	0,750	0,746	0,719	0,719	0,719	0,712	0,704	0,703
$Cr/(Cr+Fe^{3+}+Al)$	0,708	0,707	0,720	0,719	0,717	0,700	0,699	0,698	0,691	0,670	0,674
Fe^{3+}/Fe^{2+}	0,208	0,291	0,219	0,244	0,243	0,251	0,186	0,162	0,259	0,283	0,195
$Fe^{3+}/(Fe^{3+}+Al+Cr)$	0,044	0,055	0,042	0,047	0,048	0,055	0,043	0,038	0,058	0,062	0,047
$Cr/(Fe^{2+}+Fe^{3+})$	2,740	2,894	3,044	2,999	2,935	2,562	2,564	2,560	2,469	1,380	2,361

Sample #	11
TiO_2	0,36
Al_2O_3	14,49
Cr_2O_3	51,71
Fe_2O_3	3,97
FeO	16,67
MnO	0,28
MgO	11,28
Total	98,76

CATIONS BASED ON 32 OXYGEN

Ti	0,075
Al	4,447
Cr	10,644
Fe^{3+}	0,782
Fe^{2+}	3,638
Mn	0,066
Mg	4,380

CATION RATIOS

$Mg/(Mg+Fe^{2+})$	0,546
$Cr/(Cr+Al)$	0,705
$Al/(Al+Fe^{3+}+Cr)$	0,280
$Cr/(Cr+Fe^{2+}+Fe^{3+})$	0,707
$Cr/(Cr+Fe^{3+}+Al)$	0,671
Fe^{3+}/Fe^{2+}	0,215
$Fe^{3+}/(Fe^{3+}+Al+Cr)$	0,049
$Cr/(Fe^{2+}+Fe^{3+})$	2,408

KEY

Sample No.	COMMENTS
GV-7	5 m above upper layer
GV-13	2,8 m above upper layer
GV-16	2,0 m above upper layer
GV-9	1,0 m above upper layer
GV-12	0,7 m above upper layer
GV-23	Top third of upper layer
GV-6	Bottom third of upper layer
GV-15	0,6 m below upper layer
GV-14	1,7 m below upper layer
GV-18	3,6 m below upper layer
GV-4	4,0 m below upper layer
GV-1	2 cm above lower chromitite
GV-20	Top of lower chromitite
GV-10	Middle of lower chromitite
GV-19	Bottom of lower chromitite
GV-22	1 m below base of lower chromitite
DV-1	From De Villiers, 1970
DV-2	From De Villiers, 1970
78-257	Chromite from pit on Zoetveld (associated olivine is completely replaced by chalcedony)
UGC-1	Core from 4" chromitite?
GVC-NIM	Grasvally concentrate as analysed by NIM, Fe_2O_3 determined chemically
GVC-F	Same as above except Fe_2O_3 calculated based on stoichiometry

APPENDIX 8

CHEMICAL ANALYSES AND NORM CALCULATIONS OF ROCKS FROM THE RUSTENBURG LAYERED SUITE SOUTH OF POTGIETERSRUS

Sample #	5-200	5-449	5-616.5	5-640	5-935	5-1100	5-1300	78-127	78-125	78-122	78-350	78-193	78-192	78-190	78-189	78-207	78-76B	78-92	78-145
SiO_2	42,85	42,35	50,43	52,31	52,57	53,01	51,77	52,04	53,24	53,55	53,20	53,38	53,01	53,23	52,42	52,17	52,85	53,61	53,19
TiO_2	3,66	3,21	1,17	0,20	0,24	0,20	0,24	0,21	0,26	0,27	0,28	0,27	0,24	0,24	0,20	0,18	0,26	0,34	0,31
Al_2O_3	16,66	19,98	22,54	17,30	18,10	19,29	18,17	18,48	17,59	20,98	19,10	16,10	17,01	17,84	20,24	18,60	20,31	17,36	17,42
Fe_2O_3	5,16	4,71	2,67	1,70	1,74	1,70	1,74	1,71	1,76	1,77	1,78	1,77	1,74	1,74	1,70	1,68	1,76	1,84	1,81
FeO	14,77	13,56	6,37	7,07	5,91	5,40	6,34	5,18	6,55	4,23	4,07	6,03	5,53	6,16	3,95	4,58	4,43	5,13	5,33
MnO	0,17	0,12	0,14	0,17	0,15	0,14	0,14	0,16	0,17	0,11	0,12	0,17	0,15	0,16	0,12	0,15	0,11	0,13	0,14
MgO	3,01	1,31	2,27	6,30	6,15	5,95	6,19	7,37	6,22	4,83	5,30	8,01	7,79	8,04	5,71	7,89	6,56	7,42	8,30
CaO	7,86	7,05	8,52	11,17	12,09	11,88	11,65	12,05	11,53	11,93	12,28	11,41	11,81	9,47	12,62	11,97	10,74	11,58	10,95
Na_2O	2,84	3,48	4,01	2,90	2,73	2,62	2,36	2,38	2,76	2,94	2,81	2,09	2,36	2,39	2,54	2,28	2,59	2,38	1,91
K_2O	1,25	1,16	1,23	0,30	0,29	0,16	0,12	0,32	0,43	0,57	0,58	0,54	0,43	0,53	0,46	0,44	0,51	0,58	0,26
P_2O_5	0,07	0,08	0,03	0,02	0,03	0,03	0,02	0,02	0,04	0,04	0,06	0,06	0,03	0,04	0,04	0,03	0,05	0,04	0,06
L.O.I.	0,58	1,04	1,18	0,91	0,43	0,69	1,75	0,44	0,12	0,29	0,63	0,57	0,32	0,25	0,50	0,43	0,29	0,16	0,61
Total	98,88	98,05	100,56	100,35	100,43	101,07	100,49	100,36	100,67	101,51	100,21	100,40	100,42	100,09	100,50	100,40	100,46	100,57	100,29
S	1550	1021	530	40	50	60	20	20	40	70	20	<10	100	<10	<10	220	130	90	700
Zn	138	141	71	72	60	55	68	72	68	54	50	66	60	69	48	73	55	46	66
Cu	326	477	63	8	74	61	65	16	20	13	22	27	35	31	22	26	33	23	417
Ni	66	139	57	111	103	99	117	119	97	97	101	163	152	173	123	208	162	128	525
Co	178	116	64	83	76	82	82	94	107	106	82	119	135	93	123	91	79	66	108
Cr	0	1	56	35	50	54	59	233	117	32	33	76	58	56	51	325	289	317	582
V	1072	1374	324	179	180	142	183	98	185	186	153	157	151	106	117	123	95	119	119
Zr	47	50	39	10	23	9	16	23	34	34	58	41	32	38	23	19	51	39	42
Y	17	14	12	9	13	10	12	10	13	12	13	14	12	10	10	10	11	13	13
Sr	409	437	467	293	294	325	288	287	287	282	301	224	252	251	293	276	277	275	229
Rb	45	44	43	9	4	5	7	8	15	12	17	14	12	15	11	20	14	13	9
Q				0,40	1,28	2,76	2,70	0,89	1,57	2,14	2,62	3,30	1,82	2,61	1,89	0,86	2,29	2,80	4,71
C		0,45																	
Or	7,88	7,35	7,38	1,80	1,73	0,95	0,77	1,92	2,54	3,36	3,44	3,18	2,55	3,13	2,73	2,57	3,00	3,44	1,57
Ab	26,43	28,81	36,25	26,17	24,45	23,34	21,51	21,28	24,67	25,97	25,21	18,79	21,06	21,39	22,64	20,32	23,02	21,21	17,10
An	30,77	36,71	40,10	33,38	36,15	40,12	39,07	38,48	34,05	41,55	37,72	32,90	34,26	36,14	42,16	38,78	41,77	34,55	38,12
Ne	0,38	2,73																	
Di	2,94		0,85	11,29	12,82	10,15	10,31	12,44	11,87	9,40	13,65	13,63	14,12	6,01	12,05	12,45	6,48	13,42	9,71
He	5,12		0,90	6,36	5,93	4,41	5,13	4,16	6,11	3,62	4,54	4,96	4,79	2,24	3,73	3,38	1,95	4,20	2,88
En			1,71	11,80	10,51	11,24	12,16	13,98	11,12	8,39	7,78	15,28	14,28	19,06	9,64	15,34	14,68	13,58	18,01
Fs			1,80	6,64	4,86	4,88	6,05	4,67	5,73	3,22	2,59	5,56	4,85	7,12	2,98	4,16	4,41	4,25	5,34
Fo	5,51	2,91	3,13																
Fa	9,60	10,77	3,30																
Mt	5,72	5,26	2,81	1,78	1,82	1,76	1,85	1,77	1,83	1,82	1,86	1,84	1,81	1,81	1,76	1,73	1,82	1,90	1,89
Il	5,41	4,78	1,65	0,28	0,34	0,27	0,35	0,29	0,36	0,37	0,40	0,37	0,34	0,33	0,27	0,24	0,37	0,46	0,43
Cr			0,01	0,01	0,01	0,01	0,01	0,39	0,02	0,01	0,01	0,01	0,01	0,01	0,01	0,05	0,05	0,05	0,07
Ap	0,16	0,19	0,07	0,05	0,06	0,06	0,05	0,04	0,09	0,09	0,12	0,12	0,07	0,09	0,09	0,06	0,12	0,09	0,12
C.T.	1	1	3	4	4	4	4	5	4	4	4	4	4	4	4	4	6	7	6
S.L.	+1458	+1380	+1332	+1324	+1240	+1190	+1130	+1067	+ 940	+ 850	+ 724	+ 622	+ 566	+ 470	+ 410	+ 250	+ 205	+ 198	+ 180

Sample #	78-68A	78-142D	78-60A	78-128D	GP3-32	79-481	78-143	78-397	78-398	78-399	78-367E	78-367G	78-365B	78-364B	78-404	78-405A	GP3-446	78-424B	78-411
SiO_2	52,86	50,59	52,96	53,09	52,42	53,62	49,54	49,05	48,66	49,26	49,77	52,42	52,26	52,93	52,38	50,77	51,45	50,30	48,59
TiO_2	0,26	0,33	0,19	0,27	0,19	0,24	0,15	0,09	0,10	0,13	0,15	0,18	0,17	0,27	0,22	0,23	0,09	0,04	0,41
Al_2O_3	24,65	19,70	10,75	20,79	23,08	5,11	20,74	26,77	24,55	22,43	21,77	15,35	22,20	19,28	6,76	7,26	22,33	31,99	8,05
Fe_2O_3	1,76	1,82	1,69	1,77	1,69	1,74	1,65	1,59	1,60	1,63	1,65	1,68	1,67	1,77	1,71	1,73	1,59	0,01	1,91
FeO	2,36	6,20	8,10	4,23	4,29	10,56	5,32	2,27	4,12	4,82	4,77	5,77	3,16	5,15	10,93	14,86	2,72	0,62	11,92
MnO	0,09	0,14	0,19	0,11	0,11	0,25	0,09	0,05	0,06	0,09	0,09	0,15	0,09	0,13	0,25	0,29	0,08	0,01	0,24
MgO	2,63	5,66	18,35	4,83	5,53	22,38	6,96	2,80	4,23	5,68	6,39	12,80	6,02	7,27	19,65	18,31	8,56	0,43	18,32
CaO	12,52	10,81	6,04	11,83	11,66	4,58	10,31	13,73	12,38	11,15	10,80	8,58	11,82	10,47	5,71	5,32	11,30	15,39	6,45
Na_2O	2,94	1,89	1,09	2,55	2,54	0,59	2,09	2,27	2,20	2,27	2,22	1,70	2,43	2,28	0,95	0,79	1,94	2,61	0,83
K_2O	0,57	0,66	0,23	0,58	0,27	0,10	0,50	0,33	0,37	0,57	0,49	0,43	0,41	0,54	0,14	0,11	0,42	0,23	0,09
P_2O_5	0,07	0,03	0,02	0,03	0,04	0,01	0,03	0,03	0,03	0,03	0,03	0,04	0,05	0,06	0,02	0,01	0,01	0,02	0,02
L.O.I.	0,52	2,03	0,03	0,67	0,18	0,41	1,46	0,62	0,77	1,19	0,81	0,76	0,32	0,35	0,05	0,26	0,48	0,46	0,10
Total	101,28	99,86	99,64	100,75	102,00	99,59	98,84	99,60	99,07	99,25	98,94	99,86	100,60	100,50	98,77	99,94	100,97	102,11	96,93
S	30	7130	120	< 10		90	11,300	5560		11410	10,100	30	10	< 10	4990	16700	< 10	50	460
Zn	43	152	97	53	74	114	40	23	27	38	39	65	41	63	113	137	41	8	148
Cu	35	2093	271	27	63	15	3437	1521	3249	3473	2968	19	28	28	915	2478	64	10	151
Ni	61	1477	952	75	164	553	3445	2027	4651	4142	3698	322	133	154	995	2451	233	34	643
Co	98	99	127	70	136	121	131	92	143	119	121	93	127	170	139	188	63	78	143
Cr	81	374	1818	134	260	2201	598	196	337	458	558	1232	487	510	3052	2359	827	131	28454
V	85	110	113	76	80	147	67	43	52	59	63	101	78	103	121	131	49	11	348
Zr	44	46	26	61	21	20	21	9	11	19	22	19	28	43	15	10	9	6	12
Y	10	13	9	10	9	11	7	6	6	8	7	8	9	12	10	10	5	3	10
Sr	351	262	159	330	303	74	307	416	363	324	324	275	368	315	97	112	353	499	116
Rb	18	16	6	19	8	8	18	8	12	21	16	19	9	13	5	7	16	5	4
Q	3,39	2,99	0,53	3,68	1,82	0,91	0,01	0,78				1,21	2,33	2,96			0,99	0,43	
C																			
Or	3,34	4,03	1,36	3,42	1,60	0,58	3,03	1,99	2,23	3,41	2,96	2,54	2,38	3,18	0,87	0,69	2,42	1,32	0,53
Ab	26,05	17,43	9,62	22,86	22,21	5,21	19,09	20,43	19,94	20,52	20,07	15,13	21,54	20,36	8,49	7,04	17,01	22,77	7,35
An	51,66	44,26	23,16	43,37	49,45	10,80	46,33	61,94	56,33	49,66	48,19	32,56	47,74	40,38	13,58	15,82	49,73	72,81	17,70
Ne																			
Di	5,64	5,38	3,88	8,57	3,93	7,34	3,02	3,60	2,67	3,20	3,14	6,09	6,36	6,43	8,87	5,75	3,42	0,55	8,61
He	1,69	2,89	0,87	3,29	1,38	1,79	1,20	1,28	1,61	1,44	1,22	1,32	1,38	2,10	2,57	2,52	0,44	0,42	2,35
En	4,50	13,29	47,53	9,00	12,90	56,94	17,98	5,94	8,18	11,60	15,66	31,89	13,20	16,67	47,66	40,54	21,34	0,87	39,35
Fs	1,34	7,12	10,71	3,46	4,55	13,92	7,17	2,12	5,66	5,25	6,07	6,94	2,87	5,45	13,80	17,77	2,78	0,67	10,76
Fo									0,85	1,95	0,38				1,19	5,09			4,62
Fa									0,65	0,88	0,15				0,34	2,23			1,26
Mt	1,81	1,95	1,72	1,89	1,72	1,78	1,75	1,66	1,68	1,71	1,74	1,73	1,72	1,83	1,77	1,80	1,62	0,01	1,97
Il	0,36	0,47	0,26	0,38	0,26	0,33	0,21	0,13	0,14	0,18	0,21	0,25	0,24	0,37	0,30	0,32	0,12	0,05	0,57
Cr	0,01	0,05	0,25	0,01	0,04	0,32	0,09	0,03	0,06	0,07	0,09	0,18	0,07	0,08	0,47	0,36	0,12		4,83
Ap	0,15	0,08	0,06	0,08	0,08	0,03	0,08	0,06	0,07	0,07	0,07	0,08	0,12	0,14	0,05	0,02	0,04	0,06	0,03
C.T.	3	8	9A	3	3	9A	6	6	6	6	6	6	6	6	9A	9A	6	3	10
S.L.	+148	+143	+128	+123	+112	+76	+66	+66	+66	+66	+66	+66	+48	+44	+6	+5	-8	-22	-34

Sam=	UG 2																		
ple #	F.W.Px.	78-418	78-378	78-414	78-422	78-430C	78-431B	78-431S	78-432B	78-156B	78-156C	78-185A	78-170A	78-170B	78-171B	3-2395	3-2452	3-2500	3-2950
SiO_2	51,99	49,55	48,85	51,14	50,01	47,23	48,77	48,21	51,44	47,85	48,01	47,87	47,87	50,06	45,65	44,97	49,66	50,13	52,43
TiO_2	0,20	0,17	0,12	0,14	0,13	0,13	0,12	0,13	0,24	0,15	0,15	0,15	0,11	0,13	0,12	0,13	0,17	0,15	0,13
Al_2O_3	5,63	12,82	19,36	16,81	14,68	17,21	15,82	14,94	14,81	15,01	15,25	15,90	17,00	17,64	16,01	4,74	14,55	5,12	3,90
Fe_2O_3	1,70	1,67	1,62	1,64	1,63	1,63	1,62	1,63	1,74	1,65	1,65	1,65	1,61	1,63	1,62	1,63	1,67	1,65	1,63
FeO	12,59	9,40	5,12	6,36	9,25	8,01	10,75	10,92	9,10	8,91	8,94	8,70	7,93	4,28	8,88	9,68	8,99	7,38	6,35
MnO	0,25	0,17	0,10	0,13	0,16	0,11	0,15	0,17	0,16	0,13	0,14	0,15	0,11	0,10	0,12	0,19	0,16	0,15	0,17
MgO	20,01	12,82	7,87	11,14	11,49	9,56	8,70	8,87	10,49	9,47	9,70	8,81	9,65	9,63	8,78	29,47	10,20	29,70	28,46
CaO	5,42	9,08	11,55	11,49	8,73	10,05	10,29	10,15	9,11	11,79	11,70	10,29	12,08	12,38	12,17	3,16	9,56	2,07	4,21
Na_2O	0,63	1,54	1,50	1,64	1,97	1,74	2,06	2,03	1,76	1,54	1,50	1,83	1,34	1,76	1,32	0,16	2,02	0,18	0,07
K_2O	0,19	0,32	0,73	0,23	0,34	0,64	0,54	0,59	0,42	0,68	0,59	0,93	0,42	0,77	0,49	0,05	0,33	0,06	0,06
P_2O	0,01	0,02	0,02	0,02	0,01	0,01	0,01	0,03	0,04	0,02	0,02	0,02	0,02	0,02	0,02	0,01	0,02	0,01	0,02
L.O.I.	0,76	1,20	2,31	0,58	0,99	2,13	1,51	1,51	0,24	1,38	1,57	1,23	1,06	0,79	1,90	4,63	1,67	3,33	1,61
Total	99,38	98,76	99,15	101,32	99,39	98,45	100,34	99,18	99,51	98,58	99,22	97,53	99,20	99,19	97,08	98,82	99,00	99,93	99,04
S	10410	17400	9520	8950	15220	21770	20630		9070	24600	21350	20280	20370	7980	26660	3270	18380	560	100
Zn	113	75	58	55	76	54	65	74	81	53	58	58	44	38	147	90	71	75	66
Cu	1988	1780	3439	1261	1605	2880	1692	1719	1671	2962	2829	4622	3803	870	4146	402	3180	47	20
Ni	1834	1577	4356	794	832	2636	1355	1543	1281	2227	2556	4269	3027	941	3657	1628	2385	2151	1020
Co	151	183	176	119	145	164	178	198	136	177	175	174	197	106	205	128	156	121	101
Cr	2635	1956	763	1976	993	1372	511	539	1151	702	706	570	1126	868	452	5500	996	2302	7808
V	132	95	87	78	85	71	75	81	125	95	94	103	92	106	99	89	90	58	98
Zr	18	12	39	11	6	12	7	10	20	13	9	9	6	11	11	9	20	38	21
Y	9	10	7	7	7	7	8	9	11	11	9	8	7	8	8	4	9	6	6
Sr	81	227	301	248	252	256	290	274	262	285	265	294	289	367	287	47	321	59	28
Rb	9	8	33	6	8	20	12	14	11	26	21	44	18	29	16	4	24	6	5
Q									0,43										
C																		1,07	
Or	1,14	1,91	4,43	1,33	2,03	3,88	3,24	3,57	2,54	4,16	3,58	5,70	2,52	4,54	3,04	0,34	1,99	0,39	0,35
Ab	5,69	14,05	13,77	14,44	17,82	16,09	18,70	18,67	15,82	14,21	13,74	16,96	12,17	15,81	12,44	1,50	18,45	1,58	0,61
An	11,87	27,42	44,75	36,99	30,13	38,14	32,68	30,61	31,30	32,75	33,73	33,37	39,52	37,90	37,96	11,93	30,20	9,89	9,78
Ne																			
Di	8,87	10,44	8,00	11,58	7,38	7,13	9,08	9,99	7,56	14,40	13,54	9,89	11,62	15,42	12,92	2,42	9,74		7,40
He	2,98	3,98	2,79	3,30	3,10	3,15	5,98	6,58	3,38	7,18	6,65	5,35	5,08	3,23	7,11	0,40	4,56		0,76
En	48,71	23,40	17,08	21,22	20,35	11,02	8,94	8,41	25,21	8,32	9,80	8,67	11,73	12,86	6,19	37,11	17,86	61,98	66,50
Fs	16,35	8,94	5,96	6,05	8,55	4,87	5,89	5,45	11,27	4,15	4,82	4,69	5,12	2,70	3,41	6,19	8,37	7,92	6,87
Fo	1,39	5,39	0,81	2,30	5,85	9,34	8,11	8,74		8,43	8,01	8,56	7,02	4,47	9,54	31,80	4,45	13,18	4,14
Fa	0,46	2,06	0,28	0,65	2,46	4,13	5,34	5,73		4,20	3,94	4,63	3,06	0,94	5,25	5,31	2,08	1,68	0,42
Mt	1,77	1,76	1,73	1,68	1,71	1,75	1,71	1,74	1,82	1,76	1,76	1,77	1,70	1,70	1,77	1,69	1,78	1,67	1,64
Il	0,27	0,24	0,18	0,20	0,19	0,19	0,17	0,18	0,33	0,21	0,21	0,21	0,16	0,18	0,18	0,18	0,24	0,21	0,17
Cr	0,41	0,31	0,12	0,17	0,15	0,23	0,08	0,08	0,18	0,11	0,11	0,09	0,19	0,13	0,07	1,06	0,16	0,36	1,25
Ap	0,04	0,04	0,06	0,06	0,03	0,03	0,04	0,09	0,09	0,05	0,06	0,05	0,05	0,05	0,05	0,03	0,05	0,02	0,04
C.T.	9A	6	3	6	6	4	4	4	4	4	4	4	4	4	4	11	14	12	9 B
S.L.	-86	*	*	*	*	*	*	*	*	*	*	*	*	*	*	-110	-120	-141	-280

Sample ##	3-3023	3-3349	3-3496	3-3729	3-3764	3-3819	3-3927	3-4002	6A-30	F.W. 1" St	6A-48	6A-80	6A-89	6A-101.5	H.W. Px.LL	6A-124.5	6A-138.1	6A-161	6A-182
SiO_2	40,65	55,27	45,52	35,91	38,00	51,32	56,44	46,89	40,61	37,41	55,12	35,66	40,14	39,33	49,09	54,35	44,50	39,11	39,84
TiO_2	0,06	0,15	0,10	0,05	0,05	0,08	0,08	0,07	0,06	0,02	0,09	0,03	0,04	0,04	0,04	0,08	0,05	0,06	0,04
Al_2O_3	1,84	5,40	3,20	2,40	1,93	2,21	2,35	2,05	2,48	1,27	3,66	1,64	2,12	2,39	1,71	3,07	1,56	3,05	1,82
Fe_2O_3	1,56	1,65	1,60	1,55	1,55	1,58	1,58	1,57	1,56	1,52	1,59	1,53	1,54	1,54	1,54	1,58	1,55	1,56	1,54
FeO	8,47	7,69	7,22	8,68	7,75	7,85	6,39	6,81	7,34	4,31	5,73	7,84	7,04	5,94	6,10	6,56	7,17	7,07	7,89
MnO	0,13	0,19	0,15	0,14	0,15	0,20	0,17	0,15	0,13	0,04	0,15	0,11	0,12	0,12	0,14	0,16	0,12	0,14	0,10
MgO	36,21	24,98	31,72	34,63	36,35	30,81	30,09	34,25	36,06	38,04	28,71	37,28	36,74	35,57	33,40	31,52	38,00	35,66	37,51
CaO	0,79	2,81	1,69	0,17	0,06	1,33	1,51	1,05	1,12	0,01	1,76	0,10	1,06	0,72	1,37	2,01	0,41	1,17	0,39
Na_2O	0,04	0,76	0,07	0,02	0,03	0,16	0,24	0,05	0,04	0,02	0,57	0,04	0,00	0,02	0,07	0,06	0,11	0,01	0,03
K_2O	0,07	0,43	0,15	0,05	0,05	0,10	0,19	0,11	0,05	0,01	0,52	0,12	0,01	0,11	0,25	0,20	0,15	0,11	0,03
P_2O_5	0,02	0,00	0,02	0,00	0,00	0,01	0,00	0,00	0,01	0,00	0,00	0,00	0,00	0,00	0,00	0,00	0,00	0,00	0,00
L.O.I.	8,33	0,59	6,41	10,22	11,00	3,77	0,88	5,00	8,80	12,33	0,82	12,96	9,40	11,23	4,14	1,14	6,51	8,88	11,45
Total	98,17	99,92	97,85	93,82	96,92	99,42	99,92	98,00	98,26	94,98	98,72	97,31	98,21	97,01	97,85	100,73	100,13	96,82	100,64
S	210	40	30	10	<10	120	<10	120	<10	2630	<10		100	470	3590		60	30	470
Zn	74	96	70	82	102	80	65	66	60		74	60	47	41	47	72	72	55	47
Cu	5	39	4	7	4	7	45	16	29		5	5	19	7	132	12	1	8	49
Ni	2131	489	2076	2417	2078	1581	1065	2320	2363	3771	964	2977	2459	2617	2808	980	2464	2417	2387
Co	135	97	119	108	100	116	104	116	113		144	120	121	124	121	124	138	117	127
Cr	4276	2879	3912	53640	9545	2905	3725	5468	4976	25239	5822	3987	5704	3950	6065	6533	4796	10610	2122
V	51	80	56	67	45	59	69	47	47		80	31	43	41	45	77	30	56	31
Zr	30	22	21	5	5	19	8	10	11		16	0	3	4	6	4	11	0	0
Y	5	10	4	3	3	3	3	2	3		3	0	3	0	0	4	4	0	0
Sr	11	130	24	5	3	0	26	11	10		91	0	11	3	18	49	5	21	0
Rb	8	29	11	4	8	14	16	9	5		35	6	2	3	11	15	14	7	2
Q		0,89					1,80												
C	0,33			2,29	1,92				0,35	1,34		1,42	0,16	1,07			0,48	0,85	1,13
Or	0,46	2,46	0,93	0,32	0,34	0,60	1,08	0,65	0,34	0,11	2,98	0,79	0,11	0,69	1,48	1,10	0,88	0,68	0,22
Ab	0,36	6,59	0,71	0,21	0,30	1,45	2,05	0,45	0,40	0,22	4,93	0,44	0,07	0,20	0,61	0,57	1,02	0,09	0,28
An	3,81	9,66	8,01	0,85	0,32	4,88	4,53	4,94	5,55	0,08	5,60	0,54	5,34		3,53	7,01	1,94	5,90	1,95
Ne																			
Di		2,59	0,23			1,07	1,87	0,11			2,03				2,28	1,71			
He		0,40	0,02			0,14	0,19	0,01			0,19				0,20	0,17			
En	27,63	65,01	48,84	24,10	26,79	68,25	77,94	52,74	27,54	29,13	74,05	13,74	26,53	30,48	59,66	73,50	36,82	24,53	25,74
Fs	3,29	10,05	5,61	2,40	2,65	9,02	8,26	5,16	2,80	1,01	6,99	1,48	2,51	2,54	5,41	7,35	3,53	2,21	2,84
Fo	54,77		29,54	56,85	57,69	10,88		30,10	54,56	60,05	0,56	71,10	56,92	54,13	22,04	5,36	48,18	56,41	59,16
Fa	6,52		3,39	5,66	5,71	1,44		2,94	5,56	2,09	0,05	7,67	5,39	4,52	2,00	0,53	4,62	5,08	6,53
Mt	1,65	1,66	1,69	1,69	1,68	1,62	1,57	1,61	1,65	1,66	1,59	1,68	1,63	1,69	1,58	1,54	1,56	1,66	1,62
Il	0,09	0,20	0,14	0,07	0,07	0,12	0,11	0,09	0,09	0,04	0,12	0,04	0,06	0,07	0,06	0,10	0,07	0,09	0,05
Cr	1,00	0,43	0,78	5,49	2,47	0,46	0,55	1,13	1,07	4,22	0,85	1,05	1,24	0,86	1,09	1,00	0,84	2,44	0,42
Ap	0,04	0,01	0,04	0,01	0,00	0,02	0,00	0,01	0,02	0,00	0,00	0,00	0,00	0,02	0,01	0,00	0,00	0,00	0,00
C.T.	11	9B	11	11	11	9B	9B	12	11	11	9B	11	11	11	12	9B	11	11	11
S.L.	-299	-402	-446	-510	-524	-544	-577	-587	-608	-619	-621	-660	-668	-685	-686	-704	-718	-735	-747

Sample #	6A-198.3	6A-210	6A-219	6A-234	6A-244	6A-256	6A-259	6A-274	6A-281	6A-283	6A-286	32-89	32-145	32-318	32-385	32-399	32-416	32-452	32-585
SiO_2	55,05	54,92	50,00	47,61	44,67	43,90	47,91	40,31	39,42	39,44	54,83	55,97	55,44	55,92	55,61	46,82	55,11	39,82	54,76
TiO_2	0,08	0,10	0,08	0,09	0,07	0,07	0,06	0,06	0,06	0,06	0,15	0,06	0,06	0,06	0,07	0,04	0,07	0,02	0,05
Al_2O_3	3,23	3,89	3,23	3,68	2,98	2,74	3,60	2,38	2,33	2,02	4,36	2,55	2,26	1,85	2,57	1,54	2,71	1,04	1,76
Fe_2O_3	1,58	1,60	1,58	1,59	1,57	1,57	1,56	1,56	1,56	1,56	1,65	1,56	1,56	1,56	1,57	1,54	1,58	1,52	1,55
FeO	5,61	5,75	7,75	6,58	7,99	7,54	6,94	6,72	7,13	7,09	5,39	9,24	7,78	7,29	6,75	7,68	6,96	10,04	7,55
MnO	0,16	0,15	0,17	0,14	0,17	0,14	0,16	0,15	0,12	0,11	0,15	0,22	0,20	0,18	0,16	0,14	0,16	0,13	0,17
MgO	30,98	27,99	32,10	33,83	34,06	35,20	32,70	36,62	37,15	36,57	25,95	30,99	30,51	31,44	30,74	35,41	30,34	36,48	31,46
CaO	2,15	1,88	1,64	2,35	1,98	1,79	2,34	1,08	0,53	0,60	3,30	1,22	1,26	1,21	1,50	0,75	1,48	0,28	1,15
Na_2O	0,17	0,56	0,11	0,11	0,06	0,08	0,08	0,03	0,06	0,03	0,87	0,10	0,11	0,06	0,28	0,04	0,38	0,03	0,09
K_2O	0,29	0,77	0,10	0,07	0,07	0,10	0,06	0,14	0,09	0,07	1,18	0,13	0,02	0,01	0,05	0,09	0,05	0,00	0,04
P_2O_5	0,01	0,01	0,01	0,00	0,00	0,01	0,00	0,01	0,02	0,00	0,03	0,00	0,00	0,00	0,00	0,00	0,00	0,00	0,00
L.O.I.	1,08	1,48	2,80	4,05	4,59	6,28	3,23	0,16	9,45	10,14	1,24	0,11	0,21	0,49	0,02	5,13	0,27	9,48	0,51
Total	100,39	99,10	99,57	100,10	98,21	99,42	98,64	98,22	97,92	97,69	99,10	102,15	99,41	100,07	99,32	99,18	99,11	98,84	99,09
S	130	1370	10	30	110	<10	10	<10	50	50	10	440	<10	40	480		350	<10	5330
Zn	64	72	91	55	76	67	62	52	47		60	86	65	65	62	66	63	58	60
Cu	13	1	9	9	6	14	12	7	15		26	17	13	6	37	3	30	4	233
Ni	1162	925	1571	1609	1908	1857	1547	2350	2398	2357	780	852	489	1099	980	1889	1158	2732	1470
Co	135	183	190	125	121	129	117	112	114		129	124	148	127	117	116	109	146	153
Cr	5733	5055	5590	5297	5599	5497	4254	5634	5434	7868	3450	7357	3102	4368	6400	7054	6521	6083	5659
V	81	79	68	73	67	61	64	44	45		84	98	93	79	80	60	83	40	75
Zr	16	19	15	10	7	11	10	6	4		40	0	3	3	7	0	10	0	0
Y	3	3	2	3	3	2	3	0	0		8	0	2	3	3	3	3	0	0
Sr	58	78	20	35	30	23	36	9	7		180	0	3	0	14	0	19	0	0
Rb	26	49	9	5	5	7	5	6	5		68	0	2	0	4	7	7	0	4
Q											0,21		0,60	0,70	0,24				
C								0,25	1,34	0,87		0,01				0,02		0,52	
Or	1,66	4,38	0,58	0,40	0,43	0,62	0,34	0,88	0,54	0,44	3,19	0,71	0,16	0,09	0,29	0,51	0,30		0,24
Ab	1,48	4,88	0,97	0,98	0,58	0,73	0,76	0,30	0,57	0,35	8,10	0,87	0,99	0,50	2,36	0,35	3,30	0,31	0,80
An	6,71	5,59	7,69	8,92	7,45	6,64	8,96	5,31	2,53	3,05	6,01	5,59	5,29	4,47	5,29	3,60	5,21	1,40	4,04
Ne																			
Di	2,41	2,41	0,03	1,62	1,51	1,40	1,61				6,16		0,48	0,87	1,26		1,25		0,98
He	0,20	0,23	0,00	0,15	0,17	0,15	0,17				0,60		0,06	0,10	0,13		0,13		0,12
En	75,58	71,89	59,10	46,18	37,74	33,94	50,10	25,70	25,04	26,96	66,66	76,34	79,88	81,42	79,31	50,11	77,39	26,26	79,82
Fs	6,50	7,04	7,18	5,47	4,44	3,63	5,33	2,32	2,36	2,56	6,54	11,48	10,42	9,56	8,40	5,33	8,60	3,69	9,67
Fo	2,65	0,93	19,45	31,70	40,10	45,27	27,34	57,05	58,96	57,23		1,98				33,47	0,92	56,65	1,62
Fa	0,22	0,09	2,36	3,00	4,71	4,85	2,90	5,14	5,57	5,45		0,29				3,56	0,10	7,97	0,19
Mt	1,56	1,61	1,59	1,59	1,61	1,61	1,58	1,65	1,64	1,66	1,68	1,50	1,55	1,54	1,55	1,56	1,56	1,61	1,54
Il	0,11	0,13	0,11	0,12	0,10	0,10	0,09	0,09	0,08	0,08	0,21	0,08	0,08	0,08	0,10	0,06	0,06	0,03	0,07
Cr	0,85	0,73	0,87	0,91	1,08	0,97	0,75	1,22	1,27	1,29	0,54	1,10	0,44	0,62	1,03	1,38	1,38	1,50	0,86
Ap	0,02	0,02	0,02	0,00	0,01	0,03	0,01	0,02	0,04	0,00	0,04	0,00	0,00	0,00	0,00	0,00	0,00	0,00	0,00
C.T.	9B	9B	12	12	12	12	12	11	11	11	11	9B	9B	9B	9B	12	9B	12	9B
S.L.	-765	-772	-780	-785	-790	-791	-792	-810	-820	-821	-822	-970	-982	-1032	-1052	-1060	-1063	-1074	-1116

Sample #	32-643	32-744	32-790	32-808	32-818	32-890	32-934	32-946	32-1027	32-1104	32-1112	42-48	42-86	42-111	42-155	42-183	42-219	42-259	42-283
SiO_2	56,11	52,66	50,91	50,12	51,79	53,39	50,29	50,30	38,17	36,07	36,74	48,84	53,87	56,44	55,52	55,22	55,66	46,60	45,35
TiO_2	0,06	0,05	0,08	0,06	0,04	0,05	0,05	0,04	0,01	0,01	0,01	0,04	0,05	0,05	0,06	0,06	0,06	0,03	0,03
Al_2O_3	1,86	1,38	2,18	2,00	2,00	2,12	1,73	1,45	0,56	0,49	0,87	0,85	1,12	1,16	1,33	2,22	2,04	0,70	0,90
Fe_2O_3	1,56	1,55	1,58	1,56	1,54	1,55	1,55	1,54	1,51	1,51	1,51	1,54	1,55	1,55	1,56	1,56	1,56	1,53	1,53
FeO	6,41	7,43	9,51	11,04	10,52	8,50	9,08	6,77	7,50	6,94	7,48	6,95	6,37	5,83	8,16	7,22	6,82	6,95	6,57
MnO	0,16	0,17	0,20	0,22	0,23	0,16	0,16	0,15	0,13	0,12	0,15	0,16	0,16	0,16	0,20	0,18	0,17	0,15	0,14
MgO	31,47	33,62	29,13	29,04	29,18	30,74	33,54	35,66	41,38	41,68	40,50	35,03	33,76	32,37	30,73	29,86	30,28	36,62	35,10
CaO	1,25	1,08	1,00	1,10	1,00	1,03	1,37	0,98	0,28	0,25	0,27	0,61	0,84	0,89	1,09	0,91	0,90	0,63	0,29
Na_2O	0,18	0,07	0,12	0,08	0,06	0,19	0,11	0,03	0,03	0,03	0,03	0,05	0,07	0,12	0,13	0,27	0,20	0,04	0,15
K_2O	0,03	0,07	0,09	0,00	0,03	0,08	0,14	0,02	0,03	0,07	0,01	0,03	0,05	0,05	0,11	0,16	0,22	0,04	0,04
P_2O_5	0,00	0,00	0,00	0,00	0,00	0,00	0,01	0,00	0,00	0,00	0,00	0,00	0,00	0,00	0,00	0,00	0,00	0,00	0,00
L.O.I.	0,80	0,87	0,91	0,41	0,31	1,02	0,93	1,52	7,94	8,46	8,12	4,50	1,43	0,96	0,25	1,39	1,35	5,65	7,91
Total	99,89	98,95	95,71	95,63	96,70	98,83	98,96	98,46	97,54	95,63	95,69	98,60	99,27	99,58	99,14	99,05	99,26	98,94	98,01
S	80	10	3950	10000	9670	13390	11970	950	<10	310	910	<10	40	290	30	1000	830	380	810
Zn	58	57	68	76	70	44	57	49	42	33	44	71	60	60	85	71	81	62	57
Cu	27	40	293	736	645	1333	632	37	1	9	49	4	4	6	16	75	105	8	17
Ni	676	1300	1289	2135	1652	2403	2022	1050	2660	2969	1922	1519	1127	923	878	781	1015	1777	1656
Co	109	118	151	171	169	173	175	121	127	127	137	137	120	110	121	116	121	126	128
Cr	4700	6130	22136	22014	14510	4869	6170	7449	8278	9097	12654	3855	4472	3926	4021	5364	3641	4121	4187
V	69	64	134	121	84	110	60	60	23	21	25	36	47	49	53	54	50	32	33
Zr	5	0	6	3	0	3	6	0	0	0	0	3	4	0	0	3	4	0	0
Y	3	3	4	4	3	0	2	2	0	0	0	0	0	0	2	2	0	0	0
Sr	5	4	4	3	0	8	11	0	0	0	0	3	4	0	0	10	12	0	0
Rb	4	6	9	0	0	7	8	2	0	0	0	5	3	5	11	14	15	4	8
Q	0,93													1,34	0,43	1,10	1,36		
C			0,03		0,04						0,31								0,06
Or	0,19	0,42	0,56	0,04	0,17	0,45	0,78	0,13	0,19	0,46	0,10	0,19	0,30	0,29	0,67	0,93	1,27	0,25	0,26
Ab	1,59	0,64	1,07	0,74	0,52	1,63	0,99	0,26	0,31	0,32	0,34	0,43	0,59	1,06	1,16	2,40	1,75	0,42	1,40
An	3,91	3,03	4,85	4,90	4,82	4,50	3,59	3,55	1,26	0,96	1,37	1,96	2,46	2,32	2,55	4,17	3,84	1,53	1,47
Ne																			
Di	1,43	1,47		0,27		0,30	1,95	0,77	0,10	0,20		0,75	1,09	1,33	1,81	0,09	3,12	1,11	
He	0,14	0,16		0,04		0,04	0,27	0,07	0,01	0,01		0,07	0,10	0,11	0,24	0,01	0,03	0,10	
En	81,33	69,51	72,72	67,25	72,47	73,21	55,38	61,15	12,00	4,94	10,35	60,67	77,42	83,87	79,98	79,25	80,09	49,61	51,46
Fs	8,08	7,60	9,88	11,53	12,54	10,55	7,69	5,15	1,09	0,40	0,90	6,11	7,21	7,42	10,87	9,47	9,09	4,75	4,79
Fo		13,06	3,94	7,81	4,23	5,98	23,38	23,49	75,26	82,76	76,26	24,97	7,72					36,29	34,74
Fa		1,43	0,53	1,34	0,73	0,86	3,24	2,11	6,84	6,82	6,68	2,51	0,72					3,47	3,23
Mt	1,54	1,53	1,60	1,58	1,56	1,56	1,53	1,52	1,56	1,58	1,58	1,57	1,54	1,54	1,56	1,57	1,57	1,56	1,62
Il	0,08	0,06	0,11	0,08	0,06	0,07	0,07	0,05	0,02	0,01	0,02	0,05	0,07	0,07	0,09	0,08	0,08	0,04	0,05
Cr	0,73	1,04	4,65	4,35	2,82	0,80	1,06	1,33	1,31	1,47	2,04	0,67	0,73	0,59	0,59	0,88	0,55	0,81	0,87
Ap	0,00	0,00	0,00	0,00	0,00	0,00	0,02	0,00	0,00	0,00	0,00	0,00	0,00	0,01	0,01	0,01	0,16	0,00	0,00
C.T.	9B	9B	9B	9B	9B	9B	9B	9B	11	11	11	12	12	9B	9B	9B	9B	12	12
S.L.	-1130	-1163	-1173	-1185	-1188	-1208	-1220	-1233	-1250	-1275	-1278	-1370	-1410	-1430	-1478	-1498	-1533	-1594	-1606

Sample #	42-322	78-5	78-24	78-47	GR4-0	GR4-1-2-3	GR4-4-5	GR4-6-8	78-72	78-361A	78-71	78-359B	78-53	79-374	GR1-88.48	GR1-98.2	GR1-98.5	GR1-99	GR1-100
SiO_2	48,26	55,98	55,73	79,42	40,48	48,92	52,11	49,68	53,35	53,69	54,68	54,27	49,97	49,72	55,44	56,01	56,34	57,33	55,52
TiO_2	0,03	0,06	0,01	0,01	0,06	0,08	0,10	0,12	0,29	0,30	0,56	0,55	0,62	0,78	0,63	0,71	0,73	0,73	0,72
Al_2O_3	0,89	1,76	1,04	3,10	2,85	16,56	17,31	17,33	19,48	23,08	17,05	17,89	15,67	16,16	14,76	14,86	15,14	15,12	14,90
Fe_2O_3	1,53	1,56	1,51	1,51	1,56	1,58	1,60	1,62	1,79	1,80	2,06	2,05	2,12	2,28	2,13	2,21	2,23	2,23	2,22
FeO	5,86	6,41	6,99	8,26	6,34	6,14	5,34	6,29	4,70	2,49	6,31	6,03	8,82	10,14	7,77	7,55	7,58	7,40	7,68
MnO	0,14	0,16	0,12	0,41	0,10	0,20	0,15	0,14	0,12	0,07	0,15	0,13	0,19	0,20	0,19	0,16	0,16	0,17	0,18
MgO	35,31	31,63	27,38	1,29	34,92	11,10	8,86	7,93	6,68	3,02	6,48	5,58	7,77	8,66	7,18	5,80	5,54	5,32	5,52
CaO	0,70	1,03	0,06	0,05	0,99	12,55	11,66	12,95	10,52	11,13	9,89	10,22	10,91	11,97	8,13	8,91	9,12	8,64	8,67
Na_2O	0,08	0,17	0,02	0,03	0,03	1,17	2,15	2,19	2,55	2,93	2,70	2,66	2,15	1,30	0,87	2,68	2,96	2,93	2,48
K_2O	0,02	0,03	0,04	0,05	0,08	0,26	0,67	0,61	0,57	1,06	0,81	0,85	0,58	0,38	0,87	0,48	0,47	0,56	0,99
P_2O_5	0,00	0,00	0,00	0,00	0,00	0,02	0,02	0,01	0,06	0,07	0,11	0,11	0,10	0,18	0,12	0,13	0,15	0,14	0,15
L.O.I.	5,90	0,19	0,13	2,03	10,98	1,64	0,97	1,70	0,37	1,00	0,24	0,25	0,53	0,01	1,12	0,40	0,02	0,22	0,87
Total	98,72	98,98	93,08	96,16	98,39	100,22	100,94	100,57	100,48	100,64	101,04	100,59	99,43	101,78	99,21	99,90	100,44	100,80	99,90
S	<10				3690	30	320	10550	110	150	<10	10	90	900	310		30	380	520
Zn	48	64	38	45	41	68	49	57	62	48	77	72	94	86	86	83	82	87	110
Cu	3	12	11	8	17	235	75	1904	39	135	64	55	120	132	47	55	36	39	73
Ni	1414	1047	8313	1716	2274	251	184	1516	140	121	136	109	184	184	153	113	93	101	98
Co	117	150	122	396	114	92	80	137	87	123	83	112	88	104	83	100	96	90	87
Cr	5134	6141	29489	19550	5258	708	390	407	493	125	453	360	396	372	351	224	188	180	205
V	36	66	46	74	49	64	90	95	102	70	146	145	232	228	182	171	172	168	186
Zr	0	4	0	11	3	4	6	9	52	82	89	63	30	48	127	145	143	153	141
Y	0	3	0	4	0	4	7	8	13	11	21	19	19	24	21	26	26	29	25
Sr	0	5	0	0	3	297	385	385	330	380	301	315	353	315	294	280	286	294	311
Rb	3	0	0	0	·4	5	30	21	20	40	26	25	20	15	42	14	11	17	43
Q		0,95	9,17	74,09					3,09	4,52	4,24	4,60			14,85	8,97	8,02	9,73	8,52
C			0,92	3,55	1,01														
Or	0,15	0,17	0,24	0,32	0,48	1,54	3,94	3,64	3,38	6,25	4,79	5,07	3,52	2,23	5,35	2,92	2,83	3,33	6,02
Ab	0,73	1,50	0,20	0,31	0,30	10,57	19,07	19,74	22,73	26,32	24,05	23,89	19,61	11,59	8,19	24,48	26,70	26,43	22,76
An	1,96	3,71	0,29	0,28	5,08	39,24	35,19	35,70	39,62	46,56	31,72	34,24	31,82	36,89	35,05	27,46	26,76	26,56	27,16
Ne																			
Di	1,07	0,84				14,38	13,48	16,24	7,08	5,03	9,02	8,45	11,63	10,75	3,17	8,32	8,77	7,66	7,71
He	0,08	0,08				4,03	4,00	6,63	2,23	1,39	3,92	4,03	6,30	6,00	1,59	4,90	5,41	4,78	4,88
En	60,36	82,12	74,70	3,99	33,46	17,77	16,72	4,20	14,73	5,80	13,24	11,15	13,54	18,35	18,99	12,10	10,98	10,93	11,73
Fs	4,81	8,08	8,19	11,46	2,93	4,99	4,96	1,71	4,64	1,60	5,75	5,32	7,34	10,25	9,56	7,12	6,77	6,82	7,42
Fo	26,10				49,34	4,31	0,53	7,20					1,80	0,01					
Fa	2,08				4,32	1,21	0,15	2,94					0,98	0,00					
Mt	1,57	1,54	1,56	1,75	1,68	1,65	1,66	1,69	1,85	1,88	2,13	2,14	2,25	2,37	2,31	2,35	2,34	2,34	2,37
Il	0,05	0,08	0,02	0,02	0,08	0,11	0,14	0,17	0,40	0,42	0,77	0,76	0,87	1,08	0,92	1,01	1,03	1,02	1,03
Cr	0,99	0,90	4,67	4,17	1,27	0,11	0,06	0,06	0,08	0,02	0,07	0,06	0,06	0,07	0,54	0,03	0,03	0,03	0,03
Ap	0,00	0,00	0,00	0,00	0,00	0,04	0,04	0,02	0,14	0,16	0,24	0,24	0,22	0,37	0,28	0,28	0,32	0,30	0,33
C.T.	12	9B			11	14	14	14	14	14	14	14	14	14	14	14	14	14	14
S.L.	-1644	-1116			-129	-128,9	-128,7	-128,6	**	**	**	**	**	**	**	**	**	**	**

Sample #	GR1-102	GR1-107	GR1-109	GR1-X
SiO_2	56,38	55,23	55,13	50,39
TiO_2	0,72	0,32	0,70	0,78
Al_2O_3	14,98	12,59	14,87	16,83
Fe_2O_3	2,22	1,82	2,20	2,47
FeO	7,54	8,51	7,85	8,58
MnO	0,19	0,20	0,21	0,20
MgO	5,30	11,54	5,47	6,45
CaO	8,50	7,07	8,68	9,74
Na_2O	2,34	2,53	2,37	2,66
K_2O	1,08	0,43	1,09	0,88
P_2O_5	0,13	0,06	0,14	0,15
L.O.I.	0,85	0,02	1,00	0,00
Total	100,23	100,32	99,71	99,13
S	170	610	220	
Zn	104	62	119	
Cu	69	48	80	
Ni	99	223	122	
Co	85	89	86	
Cr	206	874	231	
V	180	157	179	
Zr	154	64	146	
Y	27	15	27	
Sr	326	167	319	
Rb	50	26	52	
Q	10,20	2,82	8,30	
C				
Or	6,55	2,52	6,62	
Ab	21,44	22,47	21,84	
An	27,72	21,40	27,40	
Ne				
Di	6,99	7,50	7,62	
He	4,51	2,76	5,04	
En	11,44	27,69	11,69	
Fs	7,38	10,20	7,73	
Fo				
Fa				
Mt	2,37	1,88	2,36	
Il	1,02	0,44	1,00	
Cr	0,03	0,14	0,04	
Ap	0,29	0,13	0,31	
C.T.	14	14	14	
S.L.	**	**	**	

*) Mineralized gabbronorite (pl-cpx-opx cumulate)
- occupies the interval between the base of the critical zone and the UG2 like chromitite layer.

**) Marginal member adjacent the Pretoria Group

C.T.) Cumulate (rock) type

S.L.) Stratigraphic level

- major element analyses are in weight percent
- trace element analyses are in ppm

(1) Plagioclase-clinopyroxene-orthopyroxene-magnetite cumulate.
(3) Plagioclase cumulate.
(4) Plagioclase-clinopyroxene-orthopyroxene cumulate.
(5) Plagioclase-clinopyroxene cumulate.
(6) Plagioclase-orthopyroxene cumulate.
(7) Gabbronorite (initial main zone liquid).
(8) Pegmatitic gabbronorite.
(9A) Orthopyroxene cumualte (critical zone type).
(9B) Orthopyroxene cumulate (lower zone type).
(10) Orthopyroxene (± Clinopyroxene) chromite cumulate.
(11) Olivine-chromite cumulate.
(12) Olivine-orthopyroxene-chromite cumulate.
(14) Gabbronorite.

Analyst; L.J. HULBERT

APPENDIX 9 MAJOR WHOLE ROCK OXIDE AND TRACE ELEMENT STATISTICS

	SiO_2	TiO_2	Al_2O_3	Fe_2O_3	FeO	MnO	MgO	CaO	Na_2O	K_2O	P_2O_5	S	Zn	Cu	Ni	Co	Cr	V	Nb	Zr	Y	Sr	Rb
Plagioclase-clinopyroxene-orthopyroxene-magnetite cumulates (2 samples)																							
$\bar{X}$	43,58	3,52	18,76	5,05	14,49	0,15	2,21	7,62	3,23	1,23	0,08	1285	139	401	102	147		1223		48	15	423	44
Sx																							
Ku																							
Min	43,55	3,31	16,94	4,86	13,96	0,12	1,35	7,26	2,89	1,20	0,07	1021	138	326	66	116	0	1072		47	14	409	44
Max	43,61	3,72	20,58	5,25	15,01	0,17	3,06	7.99	3,58	1,27	0,09	1550	141	477	139	178	1	1374		50	17	437	45
SK																							
Sx																							
Plagioclase cumulates (6 samples)																							
$\bar{X}$	51,16	0,34	23,62	1,84	3,61	0,09	3,95	11,86	2,68	0,60	0,04	1691	51	606	791	103	237	61		35	8	375	21
Sx	0,56	0,17	1,69	0,17	1,03	0,02	1,10	0,85	0,32	0,15	0,01	1567	9	566	713	17	108	13		7	1	35	5
Ku	-1,45	5,13	3,14	5,10	-1,23	3,17	-0,31	2,11	2,08	1,13	4,18	5,94	1,90	5,99	5,98	-0,14	4,53	-0,82		0,09	1,46	-1,56	-0,87
Min	49,38	0,03	19,83	1,51	0,74	0,01	0,42	8,56	1,54	0,22	0,02	10	8	10	34	64	56	11		6	3	301	5
Max	53,00	1,18	31,41	2,69	6,41	0,15	8,07	15,11	4,03	1,24	0,07	9520	74	3439	4356	176	763	87		61	12	499	43
SK	0,12	2,20	1,65	2,18	-1,09	-1,54	0,35	-0,05	0,55	0,99	1,93	2,43	-1,31	2,44	2,44	1,03	2,09	-1,08		-0,37	-1,15	0,83	0,58
Sx	1,39	0,42	4,14	0,42	2,52	0,04	2,71	2,09	0,80	0,37	0,02	3820	24	1387	1746	43	266	32		19	3	86	14
Plagioclase-clinopyroxene-orthopyroxene cumulates (10 samples)																							
$\bar{X}$	49,28	0,14	16,29	1,68	8,82	0,14	9,56	11,23	1,72	0,62	0,03	19371	67	2719	2349	171	799	94		10	8	286	21
Sx	0,35	0,01	0,34	0,01	0,58	0,01	0,16	0,38	0,08	0,05	0,00	1920	9	387	345	9	100	5		1	0	9	3
Ku	1,28	6,43	-1,36	0,75	3,94	-1,09	-0,30	-1,20	-1,10	0,81	3,22	0,74	5,75	-1,07	-0,77	1,40	-0,82	0,39		3,30	-0,16	5,62	2,46
Min	47,65	0,11	14,86	1,63	4,34	0,11	8,78	9,14	1,36	0,42	0,02	7980	38	870	941	106	452	71		6	7	256	11
Max	51,59	0,24	17,87	1,74	11,14	0,18	10,52	12,70	2,07	0,96	0,05	26660	147	4622	4269	205	1372	125		20	11	367	44
SK	1,01	2,37	0,29	0,57	-1,52	-0,12	0,20	-0,31	-0,07	0,85	1,52	-1,24	2,21	0,115	0,44	-1,22	0,73	0,36		1	0,89	2,10	1,47
Sx	1,11	0,03	1,07	0,03	1,85	0,02	0,52	1,20	0,25	0,16	0,01	6074	30	1224	1093	30	317	15		3	1	31	9
Plagioclase-clinopyroxene-orthopyroxene cumulates (12 samples)																							
$\bar{X}$	52,79	0,24	18,35	1,74	5,48	0,15	6,53	11,65	2,56	0,41	0,04	54	61	33	128	98	78	155		28	11	280	11
Sx	0,12	0,01	0,38	0,01	0,30	0,01	0,32	0,22	0,07	0,04	0,00	17	2	6	10	5	23	8		4	0	7	1
Ku	-0,93	-1,06	-0,27	-0,79	-1,27	-1,09	-1,22	5,72	-1,02	-0,56	-0,51	5,94	-1,33	-0,34	0,25	-0,78	9,59	-1,13		0,27	-1,45	0,80	-0,63
Min	52,13	0,18	16,11	1,68	3,95	0,11	4,77	9,48	2,09	0,13	0,02	10	48	8	97	76	32	106		9	9	224	4
Max	53,43	0,29	20,71	1,79	7,10	0,18	8,04	12,61	2,92	0,58	0,06	220	73	74	208	135	325	186		58	14	26	20
SK	0,16	-0,39	0,26	-0,28	-0,24	-0,28	0,23	-2,02	-0,20	-0,73	0,69	2,27	-0,33	0,94	1,11	0,70	3,01	-0,49		0,56	-0,07	-0,71	-0,11
Sx	0,42	0,03	1,33	0,03	1,06	0,02	1,12	0,78	0,26	0,15	0,01	59	8	21	36	19	80	28		14	1	325	4
Plagioclase-orthopyroxene cumulates (14 samples)																							
$\bar{X}$	51,12	0,17	19,92	1,68	5,24	0,11	7,98	10,88	2,09	0,41	0,04	6916	50	1420	1641	120	721	77		21	8	305	12
$S\bar{x}$	0,36	0,02	1,06	0,02	0,57	0,01	0,84	0,37	0,08	0,03	0,00	1803	4	369	444	8	124	6		3	0	15	1
Ku	-1,20	0,08	-0,67	0,01	0,81	-0,99	-0,72	0,62	-0,78	-0,94	-0,84	-1,64	-1,15	-1,46	-1,00	-0,14	2,73	-1,00		-0,16	-0,41	-0,69	-1,23
Min	49,12	0,09	13,07	1,58	2,28	0,05	2,82	8,64	1,57	0,22	0,01	10	23	19	133	63	196	43		6	5	227	6
Max	53,27	0,31	26,95	1,82	9,59	0,18	13,08	13,83	2,58	0,58	0,07	17400	76	3473	4651	183	1956	119		51	13	416	21
SK	0,25	0,92	-0,10	0,60	0,93	0,22	0,33	0,23	-0,34	-0,13	0,42	0,24	0,04	0,42	0,82	0,16	1,54	0,131		0,99	0,73	0,27	0,31
Sx	1,34	0,07	3,98	0,06	2,13	0,04	3,14	1,38	0,30	0,10	0,02	6748	17	1382	1663	33	467	23		14	2	57	4

	SiO_2	TiO_2	Al_2O_3	Fe_2O_3	FeO	MnO	MgO	CaO	Na_2O	K_2O	P_2O_5	S	Zn	Cu	Ni	Co	Cr	V	Nb	Zr	Y	Sr	Rb
					Olivine-chromite cumulates							(19 samples)											
$\bar{X}$	44,83	0,07	2,62	1,72	8,14	0,15	39,43	1,03	0,10	0,12	0,01	Serpentinization	60	35	2255	121	5944	47	0	9	2	18	9
Sx	0,79	0,01	0,24	0,01	0,24	0,01	1,03	0,21	0,05	0,03	0,00		4	20	105	2	818	4	0	2	0	9	3
Ku	5,57	1,61	0,73	0,84	1,03	0,42	3,16	2,01	17,39	11,75	-1,66		0,31	17,86	5,47	-0,23	7,92	0,98	0	2,21	0,09	15,62	15,31
Min	40,45	0,02	0,62	1,64	5,50	0,12	26,57	0,07	0,01	0,02	0,00		41	1	780	100	2122	23	0	0	0	0	0
Max	56,10	0,16	4,97	1,78	10,14	0,20	45,36	3,31	0,95	0,57	0,02		102	4,02	2977	138	536400	89	0	40	8	180	68
SK	1,94	1,08	0,35	-0,59	-0,32	0,45	-1,61	1,47	4,11	3,12	0,37		0,94	4,18	-1,89	-0,07	2,61	1,00	0	1,64	0,75	3,84	3,77
Sx	3,48	0,03	1,05	0,03	1,07	0,02	4,51	0,91	0,21	0,12	0,01		17	89	460	10	3566	17	0	11	2	40	14
					Orthopyroxene-olivine chromite cumulates							(15 samples)											
$\bar{X}$	49,69	0,66	2,24	1,64	7,55	0,16	35,98	1,30	0,09	0,08	0,01	383	64	19	1859	128	4998	51	0	7	1	15	5
Sx	0,66	0,01	0,35	0,01	0,30	0,00	0,64	0,19	0,01	0,01	0,00	237	2	8	121	4	298	3	0	2	0	4	0
Ku	1,38	3,46	-0,29	-0,06	5,76	-1,35	0,25	-1,50	0,89	6,24	-0,03	12,53	1,08	11,18	0,27	8,60	0,98	-1,54	0	6,82	0,75	0,65	0,18
Min	43,71	0,03	0,75	1,57	6,24	0,14	30,53	0,31	0,04	0,00	0,00	10	47	3	1127	116	2302	32	0	0	0	0	0
Max	54,55	0,16	5,26	1,70	11,02	0,18	40,05	0,75	0,18	0,27	0,02	3590	91	132	2808	190	7054	73	0	38	6	59	11
SK	-0,60	1,59	0,76	0,04	2,01	0,23	-0,51	0,24	1,20	2,09	0,88	3,45	0,70	3,26	0,82	2,77	-0,59	0,05	0	2,32	0,95	1,06	-0,10
Sx	2,56	0,03	1,37	0,03	1,15	0,12	2,49	2,43	0,04	0,06	0,01	919	11	33	470	18	1154	14	0	9	1	17	2
					Orthopyroxene cumulates							(26 samples)		"LOWER ZONE TYPE"									
$\bar{X}$	54,34	0,76	2,43	1,58	7,53	0,18	30,71	1,47	0,20	0,15	0,00	2331	67	170	1167	132	6876	78	0	6	2	21	11
Sx	0,38	0,01	0,18	0,01	0,28	0,00	0,41	0,14	0,03	0,04	0,00	807	2	62	92	4	985	4	0	1	0	6	2
Ku	-0,45	3,03	2,42	1,09	0,42	-0,47	2,67	8,39	3,07	5,44	1,69	1,98	0,45	6,56	1,15	-0,78	5,48	0,81	0	-0,38	5,13	3,94	3,17
Min	50,29	0,04	1,17	1,51	5,59	0,15	25,01	0,89	0,03	0,01	0,00	10	44	1	489	97	2879	49	0	0	0	0	0
Max	56,81	0,15	5,41	1,65	11,08	0,23	36,23	4,26	0,76	0,78	0,02	13390	96	1333	2403	183	22136	134	0	22	10	130	49
SK	-0,82	1,61	1,43	0,85	0,91	0,80	0,08	2,65	1,86	2,26	1,35	1,82	0,34	2,52	1,13	0,67	2,43	0,87	0	0,99	1,53	2,06	1,75
Sx	1,94	0,02	0,97	0,03	1,44	0,02	2,08	0,72	0,18	0,18	0,01	4118	11	319	469	25	5024	21	0	7	2	33	11
					Orthopyroxene cumulates							(5 samples)		"Critical zone type"									
$\bar{X}$	52,49	0,22	7,12	1,72	11,44	0,25	19,80	5,43	0,81	0,16	0,02	6462	114	1133	1357	145	2413	128	0	17	9	104	7
Sx	0,53	0,01	0,98	0,01	1,11	0,01	0,77	0,24	0,09	0,02	0,00	3188	6	478	343	11	207	5	0	2	0	15	0
Ku	2,06	-2,08	2,36	0,16	0,23	2,23	0,81	0.97	-1,85	-1,42	-2,33	-0,99	2,29	-2,35	-1,04	1,57	0,03	0,15	0	0,38	-0,61	1,55	-1,20
Min	50,59	0,19	5,14	1,69	8,10	0,20	18,24	4,60	0,59	0,10	0,01	90	97	15	553	121	1818	113	0	10	9	74	5
Max	53,87	0,24	10,75	1,75	14,80	0,29	22,74	6,04	1,09	0,23	0,03	16700	137	2478	2451	188	3052	147	0	26	11	159	9
SK	-1,06	-0,10	1,45	-0,37	0,06	-0,70	0,01	-0,82	0,38	0,49	0,25	0,71	0,75	0,34	0,72	1,29	0,21	0,33	0	0,13	0,51	1,29	0,00
Sx	1,19	0,02	2,19	0,02	2,49	0,03	1,72	0,54	0,21	0,05	0,01	7130	14	1070	769	26	463	12	0	5	9	33	1

$\bar{X}$ = MEAN
Sx = STANDARD ERROR
Ku = KURTOSIS
Min = MINIMUM
Max = MAXIMUM

SK = SKEWNESS
Sx = STANDARD DEVIATION
Nb = BELOW DETECTION LIMIT

APPENDIX 10 CORRELATION MATRIX FOR VARIOUS CUMULATES

CORRELATION MATRIX FOR PLAGIOCLASE CUMULATES

	SiO_2	TiO_2	Al_2O_3	Fe_2O_3	FeO	MnO	MgO	CaO	Na_2O	K_2O	P_2O_5	Cr_2O_3	NiO	S	Zn	Cu	Ni	Co	Cr	V	Nb	Zr	Y	Sr	Rb
SiO_2	1,000																								
TiO_2	0,041	1,000																							
Al_2O_3	-0,473	-0,242	1,000																						
Fe_2O_3	0,032	0,998	-0,276	1,000																					
FeO	0,245	0,625	-0,884	0,652	1,000																				
MnO	0,466	0,647	-0,869	0,664	0,962	1,000																			
MgO	0,149	-0,241	-0,827	-0,201	0,599	0,497	1,000																		
CaO	-0,254	-0,851	0,682	-0,862	-0,924	-0,941	-0,263	1,000																	
Na_2O	0,152	-0,847	0,172	0,819	0,190	0,315	-0,661	-0,543	1,000																
K_2O	0,011	-0,871	-0,489	0,896	0,751	0,698	0,082	-0,830	0,533	1,000															
P_2O_5	0,651	-0,007	-0,080	-0,019	-0,069	0,134	-0,140	-0,052	0,224	-0,023	1,000														
Cr_2O_3	-0,412	-0,356	-0,429	-0,311	0,285	0,070	0,800	0,038	-0,770	0,028	-0,350	1,000													
NiO	-0,388	-0,253	-0,461	-0,202	0,327	0,107	0,757	-0,015	-0,698	0,188	-0,319	0,971	1,000												
S	-0,408	-0,202	-0,455	-0,151	0,345	0,121	0,732	-0,045	-0,656	0,238	-0,332	0,960	0,998	1,000											
Zn	0,351	0,505	-0,833	0,517	0,922	0,943	0,592	-0,873	0,180	0,509	0,071	0,194	0,156	0,158	1,000										
Cu	-0,391	-0,243	-0,456	-0,192	0,328	0,107	0,749	-0,019	-0,688	0,199	-0,319	0,968	0,999	0,998	0,152	1,000									
Ni	-0,386	-0,256	-0,459	-0,205	0,325	0,105	0,758	-0,012	-0,700	0,184	-0,319	0,973	1,000	0,997	0,156	0,999	1,000								
Co	-0,252	-0,466	-0,412	-0,434	0,224	0,081	0,804	0,066	-0,768	-0,179	-0,095	0,912	0,814	0,788	0,290	0,808	0,818	1,000							
Cr	-0,374	-0,384	-0,452	-0,339	0,285	0,074	0,825	0,052	-0,799	0,005	-0,367	0,997	0,968	0,955	0,192	0,965	0,970	0,903	1,000						
V	0,607	-0,304	-0,753	-0,281	0,417	0,473	0,784	-0,186	-0,486	-0,057	0,481	0,429	0,396	0,359	0,523	0,387	0,397	0,606	0,451	1,000					
Nb																									
Zr	0,757	0,274	-0,753	0,298	0,581	0,664	0,396	-0,489	0,072	0,502	0,360	-0,034	0,105	0,106	0,440	0,104	0,101	-0,119	0,002	0,578	0,003	1,000			
Y	0,666	0,703	-0,676	0,704	0,772	0,905	0,176	-0,874	0,562	0,658	0,454	-0,288	-0,224	-0,209	0,788	-0,223	-0,226	-0,215	-0,289	0,400	0,000	0,708	1,000		
Sr	-0,521	0,393	0,749	0,371	-0,408	-0,436	-0,864	0,133	0,600	0,169	-0,282	-0,509	-0,437	-0,394	-0,536	-0,426	-0,439	-0,678	-0,539	-0,967	0,006	-0,474	-0,286	1,000	
Rb	-0,059	0,757	-0,579	0,792	0,791	0,694	0,264	-0,791	0,338	0,975	-0,091	0,246	0,399	0,445	0,531	0,409	0,396	0,021	0,225	0,053	0,002	0,503	0,579	0,039	1,000

CORRELATION MATRIX FOR PLAGIOCLASE - CLINOPYROXENE - ORTHOPYROXENE CUMULATES (MINERALIZED)

	SiO_2	TiO_2	Al_2O_3	Fe_2O_3	FeO	MnO	MgO	CaO	Na_2O	K_2O	P_2O_5	Cr_2O_3	NiO	S	Zn	Cu	Ni	Co	Cr	V	Nb	Zr	Y	Sr	Rb
SiO_2	1,000																								
TiO_2	0,731	1,000																							
Al_2O_3	-0,242	-0,556	1,000																						
Fe_2O_3	0,395	0,859	-0,431	1,000																					
FeO	-0,323	0,036	-0,696	0,081	1,000																				
MnO	0,219	0,434	-0,890	0,371	0,783	1,000																			
MgO	0,514	0,676	-0,042	0,525	-0,432	-0,230	1,000																		
CaO	-0,497	-0,570	0,446	-0,409	-0,475	-0,627	-0,111	1,000																	
Na_2O	0,408	0,054	-0,207	-0,098	0,297	0,508	-0,398	-0,683	1,000																
K_2O	0,066	-0,141	0,235	0,043	-0,293	-0,053	-0,297	0,082	0,338	1,000															
P_2O_5	0,608	0,849	-0,706	0,710	0,189	0,614	0,500	-0,436	0,021	-0,294	1,000														
Cr_2O_3	0,233	0,257	0,391	0,148	-0,395	-0,494	0,737	-0,224	-0,209	-0,253	-0,008	1,000													
NiO	-0,659	-0,247	0,220	0,154	0,138	-0,123	-0,280	0,258	-0,431	0,290	-0,288	-0,113	1,000												
S	-0,924	-0,531	-0,070	-0,190	0,568	0,072	-0,520	0,286	-0,267	-0,014	-0,439	-0,330	0,637	1,000											
Zn	-0,345	0,062	-0,204	0,356	0,388	0,264	-0,238	0,064	-0,242	-0,350	0,239	-0,405	0,322	0,370	1,000										
Cu	-0,662	-0,208	0,143	0,146	0,178	-0,117	-0,204	0,274	-0,522	0,174	-0,239	-0,074	0,978	0,657	0,293	1,000									
Ni	-0,643	-0,233	0,211	0,152	0,126	-0,123	-0,245	0,264	-0,450	0,281	-0,268	-0,103	0,998	0,617	0,297	0,982	1,000								
Co	-0,831	-0,456	-0,218	-0,232	0,714	0,262	-0,525	0,140	-0,234	-0,272	-0,200	-0,346	0,566	0,882	0,435	0,619	0,560	1,000							
Cr	0,306	0,310	0,360	0,177	-0,417	-0,467	0,772	-0,248	-0,185	-0,253	0,050	0,996	-0,169	-0,399	-0,418	-0,131	-0,157	-0,404	1,000						
V	0,613	0,732	-0,252	0,650	-0,355	0,109	0,533	-0,005	-0,290	-0,011	0,725	0,009	-0,058	-0,585	0,154	-0,020	-0,031	-0,472	0,063	1,000					
Nb																									
Zr	0,632	0,873	-0,379	0,852	-0,069	0,251	0,661	-0,447	0,031	-0,153	0,739	0,312	-0,319	-0,458	0,220	-0,306	-0,325	-0,483	0,358	0,610	0,001	1,000			
Y	0,486	0,728	-0,815	0,613	0,242	0,570	0,386	-0,263	0,041	-0,103	0,753	-0,166	-0,372	-0,192	0,082	-0,288	-0,365	-0,193	-0,120	0,525	0,002	0,704	1,000		
Sr	0,264	-0,302	0,502	-0,397	-0,733	-0,477	-0,163	0,515	0,041	0,400	-0,267	-0,219	-0,256	-0,465	-0,260	-0,304	-0,251	-0,529	-0,194	0,239	0,007	-0,220	-0,215	1,000	
Rb	0,011	-0,097	0,301	0,083	-0,409	-0,202	-0,145	0,238	0,014	0,912	-0,254	-0,140	0,491	-0,010	-0,363	0,424	0,499	-0,210	-0,146	0,186	0,002	-0,198	-0,145	0,407	1,000

CORRELATION MATRIX FOR PLAGIOCLASE - CLINOPYROXENE - ORTHOPYROXENE CUMULATES (UNMINERALIZED)

	SiO_2	TiO_2	Al_2O_3	Fe_2O_3	FeO	MnO	MgO	CaO	Na_2O	K_2O	P_2O_5	Cr_2O_3	NiO	S	Zn	Cu	Ni	Co	Cr	V	Nb	Zr	Y	Sr	Rb
SiO_2	1,000																								
TiO_2	0,708	1,000																							
Al_2O_3	-0,311	-0,149	1,000																						
Fe_2O_3	0,666	0,967	-0,228	1,000																					
FeO	0,051	0,019	-0,748	0,111	1,000																				
MnO	0,145	-0,051	-0,903	0,006	0,859	1,000																			
MgO	0,122	-0,206	-0,735	-0,141	0,375	0,674	1,000																		
CaO	0,397	-0,079	0,416	-0,086	-0,555	-0,565	-0,519	1,000																	
Na_2O	0,049	0,141	0,465	0,065	-0,072	-0,332	-0,813	0,182	1,000																
K_2O	0,548	0,418	0,064	0,308	-0,471	-0,142	0,098	-0,140	-0,023	1,000															
P_2O_5	0,788	0,637	-0,063	0,580	-0,343	-0,093	0,000	-0,029	-0,129	0,787	1,000														
Cr_2O_3	-0,482	-0,415	0,104	-0,451	-0,251	0,021	0,269	0,126	-0,243	0,106	-0,223	1,000													
NiO	-0,035	-0,207	-0,495	-0,127	0,012	0,264	0,812	-0,058	-0,838	0,095	-0,005	0,225	1,000												
S	-0,499	-0,490	0,063	-0,540	-0,261	-0,057	0,293	0,203	-0,186	-0,012	-0,417	0,854	0,390	1,000											
Zn	-0,175	-0,214	-0,651	-0,129	0,731	0,805	0,641	-0,568	-0,323	-0,216	-0,370	0,407	0,292	0,300	1,000										
Cu	-0,231	-0,039	-0,054	0,037	0,201	-0,020	0,026	0,127	-0,217	-0,702	-0,440	-0,174	0,057	0,052	-0,042	1,000									
Ni	0,062	-0,342	-0,362	-0,294	-0,028	0,327	0,870	-0,345	-0,786	0,281	0,025	0,556	0,810	0,523	0,506	-0,140	1,000								
Co	0,195	0,103	-0,163	0,007	-0,210	0,033	0,281	0,079	-0,389	0,472	0,394	-0,037	0,471	0,002	-0,195	-0,408	0,263	1,000							
Cr	-0,444	-0,475	-0,085	-0,477	-0,141	0,180	0,457	0,074	-0,413	0,050	-0,214	0,966	0,382	0,832	0,494	-0,098	0,678	-0,024	1,000						
V	0,037	0,464	-0,115	0,447	0,375	0,097	-0,469	0,236	0,494	-0,284	-0,166	-0,207	-0,426	-0,166	0,095	0,103	-0,645	-0,195	-0,310	1,000					
Nb																									
Zr	0,770	0,785	-0,075	0,736	-0,325	-0,130	0,013	-0,094	-0,024	0,809	0,882	-0,152	0,006	-0,274	-0,293	-0,351	0,041	0,266	-0,175	-0,077	1,000				
Y	0,477	0,836	-0,288	0,801	0,002	0,058	-0,062	0,224	-0,109	0,262	0,545	-0,170	0,000	-0,250	-0,159	0,178	-0,213	0,189	-0,174	0,491	0,621	1,000			
Sr	0,420	-0,299	0,612	-0,301	-0,204	-0,481	-0,745	0,460	0,672	-0,512	-0,423	-0,032	-0,679	0,011	-0,388	0,257	-0,660	-0,582	-0,125	0,189	-0,413	-0,326	1,000		
Rb	0,265	0,116	-0,080	0,082	-0,328	0,057	0,355	-0,162	-0,256	0,749	0,525	0,575	0,274	0,362	0,203	-0,671	0,580	0,297	0,567	-0,396	0,587	0,063	-0,436	1,000	

CORRELATION MATRIX FOR PLAGIOCLASE - ORTHOPYROXENE CUMULATES

	SiO_2	TiO_2	Al_2O_3	Fe_2O_3	FeO	MnO	MgO	CaO	Na_2O	K_2O	P_2O_5	Cr_2O_3	NiO	S	Zn	Cu	Ni	Co	Cr	V	Nb	Zr	Y	Sr	Rb
SiO_2	1,000																								
TiO_2	0,842	1,000																							
Al_2O_3	-0,440	-0,401	1,000																						
Fe_2O_3	0,764	0,976	-0,427	1,000																					
FeO	0,017	0,158	-0,859	0,261	1,000																				
MnO	0,472	0,488	-0,980	0,527	0,873	1,000																			
MgO	0,324	0,154	-0,947	0,169	0,780	0,882	1,000																		
CaO	-0,441	-0,323	0,865	-0,388	-0,769	-0,858	-0,854	1,000																	
Na_2O	-0,004	0,108	0,698	0,095	-0,578	-0,598	-0,814	0,468	1,000																
K_2O	0,070	0,071	0,330	0,122	-0,257	-0,287	-0,341	-0,103	0,613	1,000															
P_2O_5	0,682	0,788	0,133	0,728	-0,354	-0,049	-0,341	0,116	0,519	0,319	1,000														
Cr_2O_3	0,003	-0,081	-0,805	-0,025	0,767	0,728	0,883	-0,682	-0,829	-0,345	-0,514	1,000													
NiO	-0,764	-0,484	0,491	-0,354	-0,082	-0,485	-0,462	0,334	0,221	0,311	-0,267	-0,220	1,000												
S	-0,762	-0,475	-0,122	-0,329	0,576	0,119	0,122	-0.092	-0,246	-0,145	-0,629	0,377	0,676	1,000											
Zn	0,574	0,558	-0,954	-0,573	0,801	0,980	0,847	-0,847	-0,529	-0,247	0,026	0,653	-0,598	-0,012	1,000										
Cu	-0,785	-0,482	0,299	-0,332	0,147	-0,300	-0,285	0,186	0,078	0,212	-0,397	-0,057	0,952	0,811	-0,427	1,000									
Ni	-0,759	-0,469	0,475	-0,335	-0,066	-0,468	-0,451	0,327	0,202	0,291	-0,268	-0,206	0,999	0,684	-0,583	0,955	1,000								
Co	-0,165	0,125	-0,369	0,228	0,627	0,418	0,222	-0,288	-0,174	-0,032	0,015	0,407	0,209	0,582	0,356	0,323	0,222	1,000							
Cr	0,053	-0,045	-0,825	0,003	0,760	0,749	0,902	-0,690	-0,854	-0,378	-0,497	0,996	-0,267	0,330	0,681	0,102	-0,251	0,377	1,000						
V	0,826	0,881	-0,756	0,874	0,499	0,815	0,566	-0,636	-0,271	-0,150	0,512	0,322	-0,608	-0,313	0,846	0,532	-0,590	0,261	0,360	1,000					
Nb																									
Zr	0,763	0,899	-0,035	0,854	-0,189	0,122	-0,190	-0.071	0,474	0,360	0,909	-0,395	-0,351	-0,602	0,216	0,428	-0,348	-0,068	-0,375	0,621	1,000				
Y	0,750	0,957	-0,412	0,949	0,223	0,513	0,148	-0,289	0,086	0,045	0,739	0,006	-0,446	-0,368	0,571	0,436	-0,429	0,280	0,038	0,861	0,835	1,000			
Sr	-0,428	-0,534	0,912	-0,568	-0,807	-0,904	-0,801	0,750	0,593	0,308	0,031	-0,623	0,338	-0,161	-0,874	0,147	0,317	-0,278	-0,646	-0,770	-0,203	0,512	1,000		
Rb	0,045	-0,072	0,236	-0,017	-0,256	-0,253	-0,133	-0,190	0,246	0,822	0,087	-0,186	0,373	-0,141	-0,253	0,266	0,360	-0,296	-0,198	-0,186	0,134	0,150	0,182	1,000	

CORRELATION MATRIX FOR OLIVINE - CHROMITE CUMULATES

	SiO_2	TiO_2	Al_2O_3	Fe_2O_3	FeO	MnO	MgO	CaO	Na_2O	K_2O	P_2O_5	Cr_2O_3	NiO	S	Zn	Cu	Ni	Co	Cr	V	Nb	Zr	Y	Sr	Rb
SiO_2	1,000																								
TiO_2	0,832	1,000																							
Al_2O_3	0,645	0,906	1,000																						
Fe_2O_3	-0,207	0,008	0,266	1,000																					
FeO	-0,611	-0,248	-0,160	0,106	1,000																				
MnO	0,169	0,475	0,414	-0,034	0,255	1,000																			
MgO	-0,860	-0,969	-0,882	0,052	0,260	-0,460	1,000																		
CaO	0,776	0,904	0,863	-0,114	-0,253	0,500	-0,896	1,000																	
Na_2O	0,834	0,696	0,493	-0,236	-0,532	0,206	-0,762	0,631	1,000																
K_2O	0,821	0,679	0,496	-0,054	-0,662	0,091	-0,697	0,543	0,907	1,000															
P_2O_5	0,510	0,704	0,532	0,068	-0,070	0,310	-0,579	0,550	0,378	0,433	1,000														
Cr_2O_3	-0,523	-0,238	-0,101	0,186	0,407	0,236	0,173	-0,358	-0,253	-0,288	-0,264	1,000													
NiO	-0,785	-0,797	-0,610	0,319	0,275	-0,509	0,824	-0,807	-0,780	-0,578	-0,508	0,270	1,000												
S	0,094	0,209	0,388	0,076	0,142	0,066	-0,240	0,376	-0,031	-0,186	-0,094	-0,106	-0,264	1,000											
Zn	0,083	0,384	0,298	0,046	0,514	0,582	-0,378	0,154	0,082	0,020	0,240	0,340	-0,244	-0,007	1,000										
Cu	0,163	0,439	0,525	-0,124	0,435	0,555	-0,449	0,613	0,112	0,126	0,194	-0,115	-0,463	0,641	0,348	1,000									
Ni	-0,747	-0,760	-0,577	0,266	0,299	-0,528	0,803	-0,728	-0,817	-0,627	-0,440	0,131	0,976	-0,223	-0,281	-0,376	1,000								
Co	0,256	-0,005	-0,193	-0,622	-0,078	-0,089	-0,061	0,172	0,250	0,137	0,050	-0,460	-0,303	0,088	0,241	0,205	-0,217	1,000							
Cr	-0,435	-0,122	0,021	0,172	0,366	0,284	0,066	-0,253	-0,213	-0,231	0,227	0,980	0,218	-0,099	0,405	-0,068	0,089	-0,500	1,000						
V	0,576	0,881	0,902	0,134	0,009	0,578	-0,899	0,810	0,558	0,463	0,534	0,153	-0,695	0,319	0,481	0,546	-0,693	-0,148	0,259	1,000					
Nb																									
Zr	0,752	0,734	0,450	-0,148	-0,311	0,209	-0,701	0,568	0,697	0,721	0,763	-0,301	-0,683	-0,158	0,290	-0,016	-0,659	0,261	-0,261	0,521	1,000				
Y	0,682	0,717	0,473	-0,266	-0,107	0,347	-0,744	0,568	0,655	0,571	0,577	-0,099	-0,691	-0,116	0,563	0,169	-0,670	0,191	-0,032	0,613	0,873	1,000			
Sr	0,848	0,788	0,621	-0,181	-0,498	0,311	-0,840	0,747	0,975	0,888	0,437	-0,225	-0,826	-0,003	0,114	0,188	-0,849	0,195	-0,163	0,677	0,719	0,685	1,000		
Rb	0,824	0,692	0,477	-0,168	-0,588	0,122	-0,727	0,555	0,956	0,958	0,427	-0,236	-0,690	-0,176	0,116	-0,074	-0,737	0,166	-0,185	0,504	0,782	0,708	0,939	1,000	

CORRELATION MATRIX FOR OLIVINE - ORTHOPYROXENE - CHROMITE CUMULATES

	SiO_2	TiO_2	Al_2O_3	Fe_2O_3	FeO	MnO	MgO	CaO	Na_2O	K_2O	P_2O_5	Cr_2O_3	NiO	S	Zn	Cu	Ni	Co	Cr	V	Nb	Zr	Y	Sr	Rb
SiO_2	1,000																								
TiO_2	0,165	1,000																							
Al_2O_3	0,034	0,926	1,000																						
Fe_2O_3	0,520	0,385	0,365	1,000																					
FeO	-0,811	-0,102	0,006	0,410	1,000																				
MnO	0,285	0,233	0,193	-0,232	-0,056	1,000																			
MgO	-0,554	-0,832	-0,780	0,079	0,361	-0,380	1,000																		
CaO	-0,005	0,752	0,901	0,111	-0,176	0,219	-0,698	1,000																	
Na_2O	0,265	0,652	0,559	0,506	-0,264	-0,048	-0,528	0,359	1,000																
K_2O	0,209	0,133	0,186	-0,123	-0,343	-0,128	-0,305	0,318	0,009	1,000															
P_2O_5	-0,182	0,621	0,662	0,410	0,118	0,263	-0,430	0,624	-0,273	0,374	1,000														
Cr_2O_3	0,639	-0,564	-0,410	0,002	0,527	-0,430	0,644	-0,358	-0,620	0,097	-0,243	1,000													
NiO	-0,455	-0,079	0,003	0,436	0,430	-0,474	0,199	-0,085	-0,142	0,519	0,206	0,487	1,000												
S	0,228	-0,101	-0,079	-0,018	-0,292	-0,359	-0,096	0,000	0,090	0,801	0,042	0,040	0,649	1,000											
Zn	-0,019	0,488	0,448	0,095	0,302	0,759	-0,431	0,289	0,149	-0,098	0,500	-0,270	-0,227	-0,414	1,000										
Cu	0,241	0,119	0,135	0,058	-0,280	-0,323	-0,283	0,176	0,167	0,840	0,222	-0,058	0,671	0,963	-0,314	1,000									
Ni	-0,481	-0,011	0,060	0,462	0,474	-0,419	0,163	-0,049	-0,175	0,469	0,232	0,488	0,986	0,560	-0,164	0,604	1,000								
Co	-0,090	0,033	0,064	-0,050	0,372	0,296	-0,104	-0,043	0,086	-0,068	0,144	0,012	-0,027	-0,148	0,601	-0,145	-0,040	1,000							
Cr	-0,424	-0,438	-0,270	-0,248	0,287	-0,302	0,396	-0,129	-0,584	0,340	-0,130	0,900	0,331	0,104	-0,144	0,027	0,317	0,114	1,000						
V	-0,138	0,653	0,808	-0,005	0,063	0,228	-0,601	0,850	0,204	0,227	0,481	-0,047	-0,139	-0,210	0,462	-0,064	-0,093	0,155	0,218	1,000					
Nb																									
Zr	0,192	0,956	0.869	0,426	-0,050	0,211	-0,822	0,649	0,639	0,170	0,666	-0,603	0,062	0,015	0,481	0,247	0,121	0,094	-0,524	0,491		1,000			
Y	-0,069	0,881	0,905	0,386	0,067	0,183	-0,677	0,739	0,455	0,069	0,546	-0,307	0,027	-0,213	0,480	-0,012	0,054	-0,115	-0,220	0,747		0,805	1,000		
Sr	0,032	0,909	0,966	0,368	-0,076	0,171	-0,783	0,900	0,575	0,221	0,640	-0,512	0,047	0,055	0,329	0,264	0,094	-0,059	-0,398	0,698		0,874	0,845	1,000	
Rb	0,280	0,234	0,230	0,058	-0,399	0,096	-0,333	0,246	0,274	0,811	0,390	-0,086	0,273	0,554	0,191	0,578	0,226	0,095	0,151	0,213		0,252	0,180	0,195	1,000

CORRELATION MATRIX FOR ORTHOPYROXENE CUMULATES (LOWER ZONE TYPE)

	SiO_2	TiO_2	Al_2O_3	Fe_2O_3	FeO	MnO	MgO	CaO	Na_2O	K_2O	P_2O_5	Cr_2O_3	NiO	S	Zn	Cu	Ni	Co	Cr	V	Nb	Zr	Y	Sr	Rb
SiO_2	1,000																								
TiO_2	0,174	1,000																							
Al_2O_3	0,169	0,904	1,000																						
Fe_2O_3	0,072	0,841	0,681	1,000																					
FeO	-0,672	-0,304	-0,287	-0,267	1,000																				
MnO	-0,273	-0,087	-0,124	-0,107	0,786	1,000																			
MgO	-0,246	-0,723	-0,760	-0,474	-0,096	-0,360	1,000																		
CaO	0,017	0,828	0,778	0,644	-0,345	-0,226	-0,472	1,000																	
Na_2O	0,417	0,665	0,746	0,576	-0,330	-0,205	-0,639	0,308	1,000																
K_2O	0,310	0,560	0,682	0,507	-0,408	-0,290	-0,474	0,322	0,778	1,000															
P_2O_5	0,026	0,496	0,323	0,592	-0,240	-0,168	-0,132	0,604	0,117	0,271	1,000														
Cr_2O_3	-0,701	-0,115	-0,139	-0,117	0,674	0,493	-0,151	-0,161	-0,272	-0,244	-0,277	1,000													
NiO	-0,631	-0,339	-0,322	-0,140	0,588	0,113	0,224	-0,246	-0,331	-0,272	-0,037	0,443	1,000												
S	-0,586	-0,341	-0,242	-0,221	0,691	0,197	0,059	-0,258	-0,225	-0,209	-0,090	0,459	0,897	1,000											
Zn	0,185	-0,488	0,463	0,323	0,164	0,555	-0,649	0,211	0,409	0,385	0,198	0,004	-0,398	-0,324	1,000										
Cu	-0,490	-0,298	-0,210	-0,186	0,640	0,194	0,010	-0,248	-0,193	-0,229	-0,165	0,409	0,877	0,953	-0,345	1,000									
Ni	-0,627	-0,346	-0,327	-0,143	0,578	0,128	0,237	-0,242	-0,339	-0,270	-0,032	0,424	0,994	0,866	-0,379	0,852	1,000								
Co	-0,432	-0,300	-0,118	-0,191	0,481	0,129	-0,006	-0,282	-0,082	0,188	-0,142	0,416	0,640	0,758	-0,218	0,665	0,619	1,000							
Cr	-0,696	-0,113	-0,120	-0,138	0,664	0,487	-0,165	-0,135	-0,276	-0,233	-0,276	0,996	0,437	0,455	0,013	0,402	0,422	0,423	1,000						
V	-0,441	0,193	0,245	-0,009	0,473	0,343	-0,429	0,173	-0,051	-0,089	-0,298	0,686	0,333	0,370	-0,032	0,437	0,318	0,405	0,699	1,000					
Nb																									
Zr	0,110	0,893	0,839	0,869	-0,364	-0,205	-0,543	0,762	0,651	0,620	0,583	-0,186	-0,186	-0,269	0,332	-0,257	-0,176	-0,151	-0,183	0,091	1,000				
Y	-0,152	0,787	0,715	0,641	0,000	0,116	-0,580	0,677	0,464	0,269	0,224	0,158	-0,242	-0,204	0,398	-0,197	-0,250	-0,278	0,152	0,244	0,643	1,000			
Sr	0,254	0,781	0,894	0,604	-0,400	-0,290	-0,619	0,592	0,837	0,823	0,216	-0,228	-0,326	-0,246	0,412	-0,229	-0,336	-0,069	-0,216	0,031	0,733	0,640	1,000		
Rb	0,340	0,600	0,667	0,605	-0,477	-0,339	-0,439	0,336	0,777	0,970	0,324	-0,272	-0,258	-0,254	0,343	-0,255	-0,257	-0,112	-0,269	-0,142	0,682	0,302	0,823	1,000	

CORRELATION MATRIX FOR ORTHOPYROXENE CUMULATES (CRITICAL ZONE TYPE)

	SiO_2	TiO_2	Al_2O_3	Fe_2O_3	FeO	MnO	MgO	CaO	Na_2O	K_2O	P_2O_5	Cr_2O_3	NiO	S	Zn	Cu	Ni	Co	Cr	V	Nb	Zr	Y	Sr	Rb
SiO_2	1,000																								
TiO_2	-0,038	1,000																							
Al_2O_3	-0,105	0,630	1,000																						
Fe_2O_3	0,119	0,956	-0,793	1,000																					
FeO	-0,781	0,443	-0,535	0,402	1,000																				
MnO	-0,632	0,686	-0,649	0,657	0,942	1,000																			
MgO	0,710	0,513	-0,746	0,688	-0,125	0,060	1,000																		
CaO	-0,200	0,830	0,774	0,855	-0,345	-0,497	-0,777	1,000																	
Na_2O	-0,053	0,553	0,890	0,652	-0,534	-0,556	-0,698	0,865	1,000																
K_2O	0,105	0,991	0,696	0,965	-0,537	-0,767	-0,498	0,817	0,594	1,000															
P_2O_5	0,405	0,720	0,657	0,656	-0,786	-0,801	-0,301	0,804	0,816	0,751	1,000														
Cr_2O_3	-0,195	0,165	-0,581	0,343	0,485	0,556	0,128	0,013	-0,211	-0,279	-0,066	1,000													
NiO	-0,912	0,061	-0,119	0,139	0,849	0,635	-0,523	0,091	-0,223	-0,030	-0,499	0,283	1,000												
S	-0,934	0,146	-0,230	0,065	0,934	0,791	-0,455	-0,014	-0,259	-0,241	-0,581	0,402	0,968	1,000											
Zn	-0,755	0,658	-0,455	0,550	0,934	0,960	-0,116	-0,440	-0,446	-0,718	-0,823	0,342	0,697	0,836	1,000										
Cu	-0,904	0,003	-0,204	0,054	0,888	0,707	-0,478	0,081	-0,236	-0,100	-0,490	0,432	0,986	0,984	0,734	1,000									
Ni	-0,952	0,030	-0,048	0,140	0,840	0,637	-0,583	0,108	-0,158	-0,052	-0,497	0,225	0,992	0,971	0,726	0,973	1,000								
Co	-0,981	0,176	-0,083	0,039	0,886	0,759	-0,562	0,030	-0,129	-0,252	-0,553	0,276	0,934	0,976	0,852	0,938	0,962	1,000							
Cr	-0,147	0,173	-0,556	0,353	0,427	0,519	0,141	0,029	-0,163	-0,282	-0,014	0,996	0,212	0,340	0,302	0,366	0,159	0,222	1,000						
V	0,174	0,758	-0,846	0,815	0,409	0,525	0,788	-0,984	-0,939	-0,764	-0,821	0,075	-0,001	0,084	0,442	0,012	-0,037	0,006	0,048	1,000					
Nb																									
Zr	0,734	0,561	0,480	0,518	-0,911	-0,961	0,152	0,255	0,317	0,649	0,621	-0,634	-0,671	-0,833	-0,932	-0,757	-0,685	-0,821	-0,606	-0,276	1,000				
Y	0,257	0,950	-0,565	0,939	0,151	0,443	0,655	-0,810	-0,460	-0,914	-0,519	0,074	-0,369	-0,166	0,393	-0,310	-0,340	-0,132	0,103	0,718	-0,312	1,000			
Sr	-0,179	0,583	0,995	0,769	-0,466	-0,586	-0,778	0,742	0,866	0,649	0,584	-0,601	-0,056	-0,162	-0,374	-0,147	0,020	-0,006	-0,580	-0,818	0,421	-0,543	1,000		
Rb	0,015	0,096	-0,567	0,170	0,372	0,230	-0,448	-0,585	-0,850	-0,128	-0,636	-0,086	0,337	0,239	0,188	0,279	0,263	0,107	-0,153	0,691	0,000	0,000	-0,547	1,000	

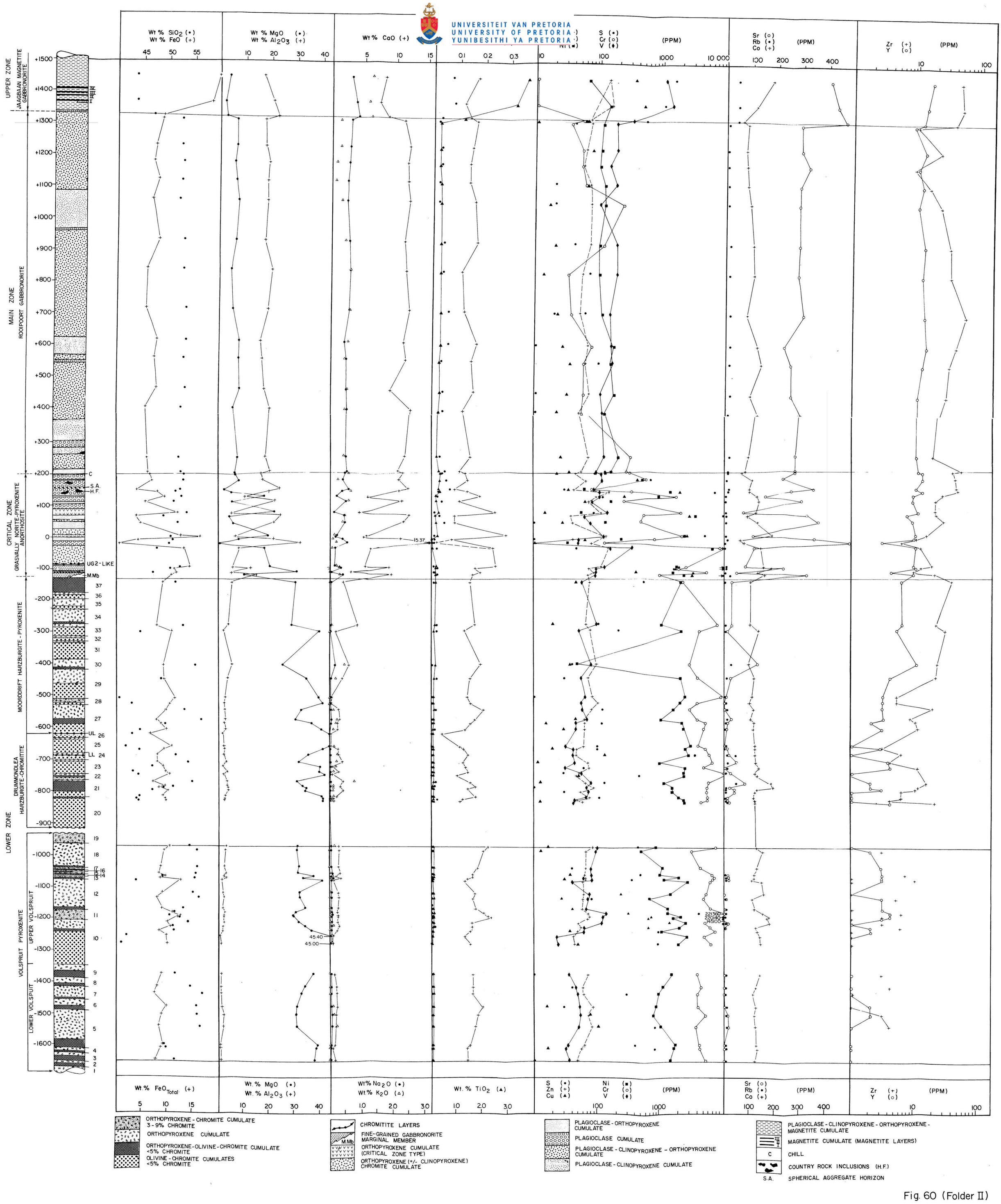

Fig. 60 (Folder II)

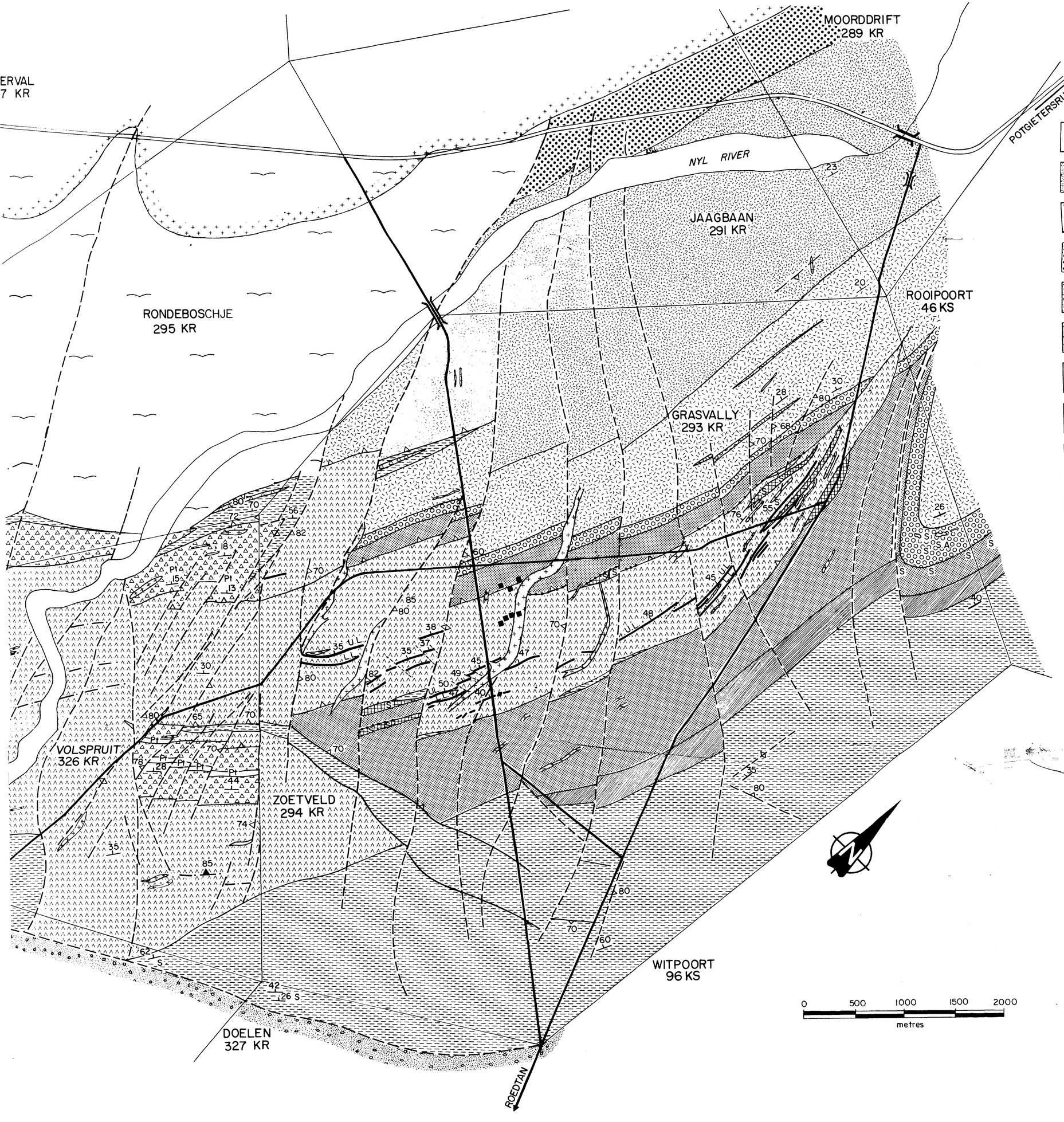

ALLUVIUM

BASALT AND SANDSTONE — KAROO SEQUENCE

GRANITE, GRANOPHYRE & GRANITOID DYKES

MAGNETITE GABBRONORITES, MAGNETITITE, GABBRONORITES — UPPER ZONE

PIGEONITE GABBRONORITE, GABBRO, ANORTHOSITE

GABBRONORITE, GABBRO, NORITE — MAIN ZONE

MOTTLED ANORTHOSITE, NORITIC ANORTHOSITE, ANORTHOSITIC NORITE, NORITE, FELDSPATHIC PYROXENITE, GABBRONORITE — Subzone 2

SPOTTED NORITE & ANORTHOSITIC NORITE, ANORTHOSITE, FELDSPATHIC PYROXENITE, CHROMITIC PYROXENITE — Subzone 1

UG2-LIKE CHROMITITE LAYER — CRITICAL ZONE

FINE-GRAINED GABBRONORITE

FINE-MEDIUM GRAINED GABBRONORITE, VERY FINE GRAINED GABBRONORITE CHILL — Marginal member (M.Mb./P.G.)

HARZBURGITE WITH MINOR PYROXENITE

UPPER AND LOWER CHROMITITE LAYERS — LOWER ZONE

PYROXENITE WITH MINOR HARZBURGITE

QUARTZITE, CONGLOMERATE, MINOR SHALE AND MARL AND HORNFELSIC EQUIVALENTS — PRETORIA GROUP

BUSHVELD COMPLEX

HORNFELSIC INCLUSIONS
S SULFIDES
S.A. SPHERICAL AGGREGATES
Pt VOLSPRUIT PLATINIFEROUS PYROXENITE
FAULT — Post FI
FAULT CONTACT ZONE — FI
TRIG. BEACON
MINE BUILDINGS
BRIDGE
NATIONAL ROAD
SECONDARY ROAD

0 500 1000 1500 2000
metres

THE GEOLOGY OF THE RUSTENBURG LAYERED SUITE SOUTH OF POTGIETERSRUS

by L. HULBERT
1983

Fig. 4 (Folder I)